UNIVERSITY OF SOUTHAMPTON

FACULTY OF SCIENCE

OCEANOGRAPHY

MAGNETOSTRATIGRAPHY OF LOWER CRETACEOUS AND OLIGOCENE FORMATIONS IN THE UK AND NORTHWEST BELGIUM

by

TING FUNG

Submitted for the Degree of

Doctor of Philosophy

AUG 1991

ACKNOWLEDGMENT

My grateful thanks are due to Dr E.A.Hailwood (and his family) for his (and their) great generous help throughout the period of my study, not only in academic aspect but also in showing great consideration towards my family. His great valuable advices in the present study as well in the preliminary draft copy of this thesis have thrown big light on it.

Special thanks are given to my dear wife and my family for their invaluable encouragement during my study.

Many thanks are also given to the CVCP, UK, for the ORS Award financially contributed for three years; and the Education Committee of China for its financial support during my first year of study.

Particular thanks are also given to other people in the Oceanography Department, Dr J.Ali and Dr G.Butcher for their generous help in field work; Mr P.Riddy for his technical and computing advice; Mr K.Padley for his technical support; and many others for their friendly help. Dr N.Hamilton and Dr M.Collins are also tranked for their examination of my Transfer Report and help in other aspects.

UNIVERSITY OF SOUTHAMPTON

ABSTRACT

FACULTY OF SCIENCE

OCEANOGRAPHY

Doctor of Philosophy

MAGNETOSTRATIGRAPHY OF LOWER CRETACEOUS AND OLIGOCENE FORMATIONS IN THE UK AND NORTHWEST BELGIUM

by Ting Fung

The magnetostratigraphy of certain Lower Cretaceous sedimentary sequences (the Wessex and Weald Clay Formations) of southern England and Oligocene sequences of southwest England (the Bovey Formation) and northwest Belgium (the Boom Clay Formation) has been investigated.

Five sections through the Wessex Formation along the coast of southern England are well-correlated using combined geological, sedimentological and magnetic evidence (including NRM intensity variations and magnetic polarity reversals sequences). The results indicate that below the magnetic reversal found in the Vectis Formation by Kerth & Hailwood (1988), four other significant reversed polarity events occur within the Wessex Formation. When combined with available biostratigraphic evidence (pollen palynomorphs, Hughes & McDougall 1989) this magnetic polarity sequence can be correlated with the geomagnetic polarity time scale (GPTS) between Chron CM1 and Chron CM5 (or possibly Chron CM8?). This confirms that the Wessex Formation spans the Barremian and upper Hauterivian stages. The age of the Coarse Quartz Grit (CQG) at Worbarrow Bay can be estimated as 123Ma, using the GPTS. However, the CQG layers at other sections occurring at different positions in the polarity sequence clearly have different (younger) ages than the CQG at Worbarrow.

Preliminary results from two short sections through the Weald Clay Formation of southeast England indicate the presence of a magnetic reversal in Bed 2 of Thurrell *et al* (1978) in this formation.

A reliable magnetic polarity sequence has been obtained for the Oligocene Bovey Formation of SW England, even though this formation is very weakly magnetised. When combined with age constraints based on tectonic controls of the fault basin and limited biostratigraphic evidence, this magnetic polarity sequence can be correlated with Chron C10 to C12 of the Middle to Early Oligocene GPTS, spanning the time interval 30.25 to ~34.0 Ma.

Although serious magnetic overprints, believed to be due to secondary diagenesis, have affected the upper part of the Boom Clay Formation of Belgium, a reasonably reliable magnetic polarity sequence has been defined for its lower part. The reliability is supported by the good repeatability of magnetic polarities within small sampling intervals. When combined with available detailed biostratigraphic evidence, the Boom Clay magnetostratigraphy can be correlated with Chron C11 to C12 on the GPTS of Berggren *et al* (1985), indicating an age range of 30.5 to 33.5Ma.

Finally, magnetic fabric data from the Wessex and Wealden Basins define a depositional style fabric, in which the magnetic lineations generally conform with the depositional environment models proposed by Allen (1975) and Stewart (1983). Magnetic fabric evidence from the Boom Clay Formation suggests a northerly transport direction at the southwestern margin of the North Sea Basin in the Oligocene. Unfortunately, the Bovey Formation did not yield meaningful magnetic fabric data, due to its extremely weak magnetic anisotropy.

CONTENTS

LIST OF ABBREVIATIONS

ACS: Abrook Clay and Sand (sedimentary unit of the Bovey Formation).

a.f.: Alternating field.

α_{95}: 95% confidence angular limit of Fisher statistics.

AMS: Anisotropy of magnetic susceptibility.

BF(1-4): Normal polarity events defined in the Bovey Formation.

BC(1-3): Normal polarity events defined in the Boom Clay Formation.

CGS: Compton Grange Sandstone (the Isle of Wight).

CMD: Characteristic magnetisation direction.

CQG: Coarse quartz grit in the Wessex Formation.

CRM: Chemical remanent magnetisation.

DDRM: Depositional DRM.

Dec: Declination of magnetic vector.

DRM: Detrital remanent magnetisation.

DSDP: Deep Sea Drilling Project.

GPTS: Geomagnetic polarity time scale.

HFTM: High field torque magnetometer.

Inc: Inclination of magnetic vector.

IRM: Isothermal remanent magnetisation.

k: Precision parameter of Fisher statistics.

k_{max}: Maximum principal susceptibility axis.

k_{min}: Minimum principal susceptibility axis.

k_{int}: Intermediate principal susceptibility axis.

LFTM: Low field torque magnetometer.

mA/m: Milliampere per meter.

mT: Millitesla.

NRM: Natural remanent magnetisation.

PDDRM: Post depositional DRM.

Rc: Regression coefficient for straight line fit.

SCL: Southacre Clay and Lignite (sedimentary unit of the Bovey Formation).

SEP: (Magnetic vector) stable end point.

TRM: Thermal remanent magnetisation.

VGP: Virtual geomagnetic pole.

WS(1-4): Reversed polarity events defined in the Wessex Formation.

ZAZ: Azimuth of z-x plane of sample coordinates with respect to north.

ZPL: Angle between z-axis of sample and the vertical.

LIST OF FIGURES AND TABLES

CHAPTER I INTRODUCTION TO PALAEOMAGNETISM AND MAGNETOSTRATIGRAPHY

§1.1 The Magnetic Earth

1.1.1) Main features of the Earth's magnetic field.

The directional properties of the present geomagnetic field may be demonstrated by means of a magnetic compass. The needle of a compass is normally weighted so that it will swing in a horizontal plane, its deviation from geographical north being called the declination, D. If a non-magnetic needle which is balanced horizontally on a pivot, is then magnetised, it becomes inclined to the vertical when exposed to the earth's magnetic field. Over most of the northern hemisphere the north-seeking end of such a magnetised needle will dip downwards, the angle it makes with the horizontal being called the magnetic dip angle or inclination, I. Over most of the southern hemisphere the north seeking end of the needle will dip upwards. The total intensity F, the declination D and the inclination I together completely define the magnetic field at any point on the earth. The horizontal and vertical components of the vector **F** are denoted by H and Z. H may be further resolved into two components X and Y, X being the component along the geographical meridian northward and Y the orthogonal component eastward. They are simply related to one another by the following equations.

$$\left.\begin{array}{lll} H = F\cos I & Z = F\sin I & \tan I = Z/H \\ X = H\cos D & Y = H\sin D & \tan D = Y/X \\ F^2 = H^2 + Z^2 = X^2 + Y^2 + Z^2 & & \end{array}\right\} \quad (1.1.1)$$

The quantities F, D, I, X, Y and Z are called the *magnetic elements*. The relationships between these elements are illustrated in Fig.1.1.1

By means of modern survey techniques, such as large-scale aeromagnetic surveys and satellite surveys, the observations of the geomagnetic field have been extended to the whole of the Earth's surface. The variation of the geomagnetic field over the Earth's surface is best illustrated by means of isomagnetic charts, ie. maps on which lines are drawn through points at which a given magnetic element

has the same value. Contours of equal intensity for any of the elements X, Y, Z, H and F are also called isodynamics. For an example, see Peddie (1982) for the 1980 world isomagnetic charts.

Apart from its spatial variation, the Earth's magnetic field also shows temporal changes ranging from short term variations on timescales of seconds to secular variations on timescales of hundreds to thousands of years and on an even longer timescale to reversals of polarity. The short period, transient, variations are due to external influences and are additional to the earth's main magnetic field, which is of internal origin. Variations on timescales of 10^2 - 10^4 years may be determined from archaeomagnetic and palaeomagnetic studies, particularly of recent sediment cores. These timescales are probably characteristic of motions in the Earth's fluid core (eg see McElhinny 1973).

There have been many attempts to mathematically model the geomagnetic field which is dominated by the dipole component. Consider the field of a uniformly magnetised sphere whose magnetic axis runs north-south (Fig. 1.1.2). Let P be any external point distant r from the centre O and θ the angle NOP, ie. θ is the magnetic co-latitude. If m is the magnetic moment of a geocentric dipole directed along the axis, the potential at P is

$$V = \frac{m}{4\pi} \frac{\cos\theta}{r^2} \qquad (1.1.2)$$

and the inward radial component of force corresponding to the magnetic component Z is given by

$$Z = -\mu_0 \frac{\partial V}{\partial r} = \frac{\mu_0 m}{2\pi} \frac{\cos\theta}{r^3} \qquad (1.1.3)$$

The component at right angles to OP in the direction of decreasing θ, corresponding to the magnetic component H, is given by

$$H = -\frac{\mu_0}{r} \frac{\partial V}{\partial \theta} = \mu_0 \frac{m}{4\pi} \frac{\sin\theta}{r^3} \qquad (1.1.4)$$

where μ_0 is the permeability of free space. The inclination, I, is then given by

$$\tan I = \frac{Z}{H} = 2 \operatorname{cotan} \theta \qquad (1.1.5)$$

If the colatitude θ is replaced by the geographic latitude λ, the relation between I and λ is

$$\tan I = 2 \tan \lambda \qquad (1.1.6)$$

The magnitude of the total field F is given by

$$F = (H^2 + Z^2)^{1/2} = \mu_0 \frac{m}{4\pi} (1 + 3 \cos^2\theta)^{1/2} \qquad (1.1.7)$$

Thus the field intensity is a function of the co-latitude. The geomagnetic poles, ie. the points where the axis of the geocentric dipole which best approximates the earth's field meets the surface of the earth, are currently situated at approximately 79°N, 70°W and 79°S, 110°E. The magnetic axis is thus inclined at about 11° to the geographical axis.

Spherical harmonic analysis has been widely used in the modelling of the earth's magnetic field. If there is no magnetic material near the ground surface, the Earth's magnetic field can be derived from a potential function V which satisfies Laplace's equation:

$$\frac{\partial^2 V}{\partial x^2} + \frac{\partial^2 V}{\partial y^2} + \frac{\partial^2 V}{\partial z^2} = 0 \text{ (outside source)} \qquad (1.1.8)$$

and can thus be represented as a series of spherical harmonics (eg see McElhinny 1973 and Jacobs 1984). The first term (n=1) of the solution corresponds to a geocentric dipole which at present is inclined at about 11.5° to the rotation axis. The second term involving n=2 corresponds to a geocentric quadrupole, the terms n=3 a geocentric octupole etc.. The non-dipole components of the earth's field , though much weaker than the dipole component, show more rapid changes. The time scale of the non-dipole changes is measured in decades and that of the dipole in centuries (McElhinny 1971). However, the internal dipole field is not stable but drifts westward at a fraction of a degree per year. This contributes the main feature of instability of the earth's field, ie. secular variation which makes the virtual magnetic pole positions vary around the geographic north and south pole.

It must be noted that a spherical harmonic analysis is nothing more than a mathematical procedure for representing the field by hypothetical sources at the Earth's centre. Although a number of authors have attempted to carry out spherical harmonic analyses of the palaeomagnetic field of the Earth (eg see Meshcheryakov *et al* 1979, Hoffman 1988), to trace back or predict the geomagnetic field in certain times, none of these attempts have yet given reasonable results.

1.1.2) Reversals of the geomagnetic field.

Besides the secular variation of the earth's magnetic field, on typical timescales of 10^2-10^4 years, a particularly interesting phenomenon is that of geomagnetic polarity reversals which were first identified in the early part of this century (eg see Matuyama 1929). Because these reversals appear to occur synchronously on a world wide scale, they provide a particular useful basis for calibration of the chronology of geological history. Considerable efforts have been put into this research in recent years.

However, before the overwhelming acceptance of the fact the Earth reverses its magnetic field, many attempts were made to prove the occurence of a "self-reversal" mechanism in certain rocks and sediments, as first proposed by Graham (1949). However, studies of reversals in rocks proved that the self-reversal mechanism is very rare in nature (eg see Vlasov & Zvegintsev 1969 and Heller 1980).

In spite of this fact, to prove that a reverse polarity rock sample was magnetised when the Earth's field was in reverse polarity state, it is necessary to confirm the reversal record in rocks of various types of the same age at different sites. Although there is some evidence for a possible relationship between polarity of magnetisation and chemical properties in igneous samples (Johnson *et al* 1975), most researches do not indicate a meaningful relation of this type. It is concluded that most polarity reversal patterns are independent characteristics of the rocks, magnetically printed on the different type of rocks as a result of their formation during

successive normal and reverse polarity periods (an example was demonstrated by Jacobs 1984).

During a polarity inversion, the direction of the geomagnetic field swings through about 180°, the virtual geomagnetic poles (VGP, defined as the poles of the dipolar field which gives the observed direction of magnetisation at the site under consideration) following quite different paths for different transitions.

Some studies have succeeded in identifying a record of the geomagnetic field during a polarity transition (eg Koci 1985, Valet *et al* 1986). It appears that, during a reversal, the intensity of the field first decreases by a factor of three or four for several thousand years while the field direction is maintained. The magnetic vector then usually executes several swings of magnitude about 30°, before moving along an irregular path to the opposite polarity state, the intensity remaining reduced meanwhile and rising to its normal value later. It is not certain whether the field remains dipolar during the transition. Fig. 1.1.3 shows an example of a reversal record given by Dodson *et al* (1978) from the Tatoosh intrusion in Mount Rainier Park, USA. The change in declination was gradual at first but the inclination changed rapidly during this transition. Moreover the dispersion of directions, as measured by the Fisher precision parameter, k, increased markedly during the reversal at sampling site levels, reaching a maximum at the time of minimum intensity of magnetisation.

Patterns of field direction change during reversals are still largely an unsolved question, in particular, whether the magnetic field vector at a given locality tends to move along a similar path during successive polarity transitions. Some analyses have suggested that there may be preferred meridional bands within which most transition pole paths lie. Opdyke *et al* (1973) carried out some detailed palaeomagnetic investigations of high accumulation rate sediment cores, coming from widely separated geographical regions. This study supports a transition model in which a dipolar field is predominant during each of the polarity reversals studied. Hoffman (1986) carried out palaeomagnetic investigations based on Australasian basalts, providing

a view of transtional field behaviour. The results suggested that, during a geomagnetic field reversal, the dipole field executes two actions, from which some unsuccessful reversal attempts (aborted attempts with a similar intermediate field geometry) are made and then completed by successful polarity transition.

Fig.1.1.4 shows the average frequency of reversals over the past 150 m.y. based on the timescale of Heirtzler *et al* (1968) as seen through a sliding window 10 m.y. long (after Cox 1975). During the past 100 m.y. the frequency of reversals has increased from zero to the present frequency of nearly 4 per m.y. in two main steps, one at 75 Ma and one at 45 Ma. The mean frequency of reversals showed no statistically significant changes from about 75 to 45 Ma and then increased rather abruptly by a factor of more than two. It then remained approximately constant until the present. Thus c.45 Ma seems to mark a boundary between two intervals during which the statistical properties of the dynamo, which is believed to generate the main dipole field in the centre of the earth,were distinctly different.

Jacobs (1984) related the major changes in the frequency of reversals over the last 150 m.y. to the heat flow from the earth (Fig.1.1.5), using the heat flow data from Sprague and Pollack (1980). It can be seen that the onset of the Cretaceous normal polarity interval at about 105 Ma, during which there were almost no reversals, coincides with an increase in heat flow. This period of normal polarity lasted until about 85 Ma which is just about the maximum in the heat flow. Further, the sharp increase in the frequency of reversals at about 45 Ma coincides with the reduction in heat flow to low values. This possibly indicates that the heating or cooling from deep mantle convection could cause some fundamental changes in geomagnetic field behaviour.

In addition to polarity change, the earth's magnetic field has often departed for brief periods from its usual near-axial configuration without establishing, and perhaps not even instantaneously approaching, a reversed direction. This type of behaviour has been called a "geomagnetic excursion" (eg see Jacobs 1984). It has been reported from lava flows of various ages in

different part of the world and from some deep-sea and lake sediments. Magnetic excursions are generally observed to commence with a sudden and often fairly smooth movement of the VGP towards equatorial latitudes. The VGP may then return almost immediately, or it may cross the equator and move through latitudes in the opposite hemisphere before swinging back again to resume a near-axial position. Barbetti and McElhinny (1976) define the term "excursion" to describe a VGP movement of more than 40° from the geographical pole. This is differentiated from secular variation (when the VGP colatitude θ remains less than 40°) and from short polarity events (of duration $<10^{4}$ yr). It is possible that excursions represent abortive reversals (Jacobs 1984).

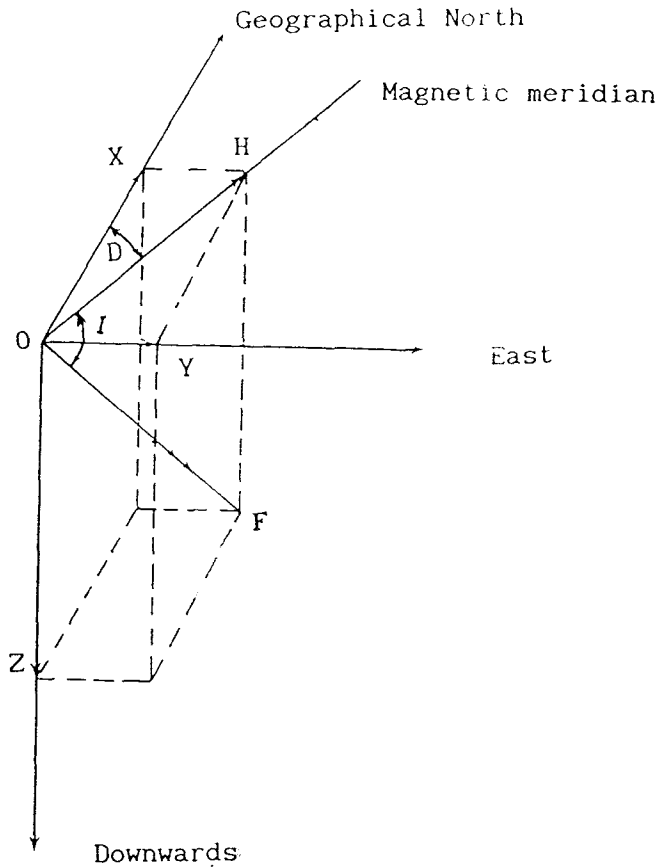

Fig. 1.1.1 Geomagnetic elements in geographic coordinates.

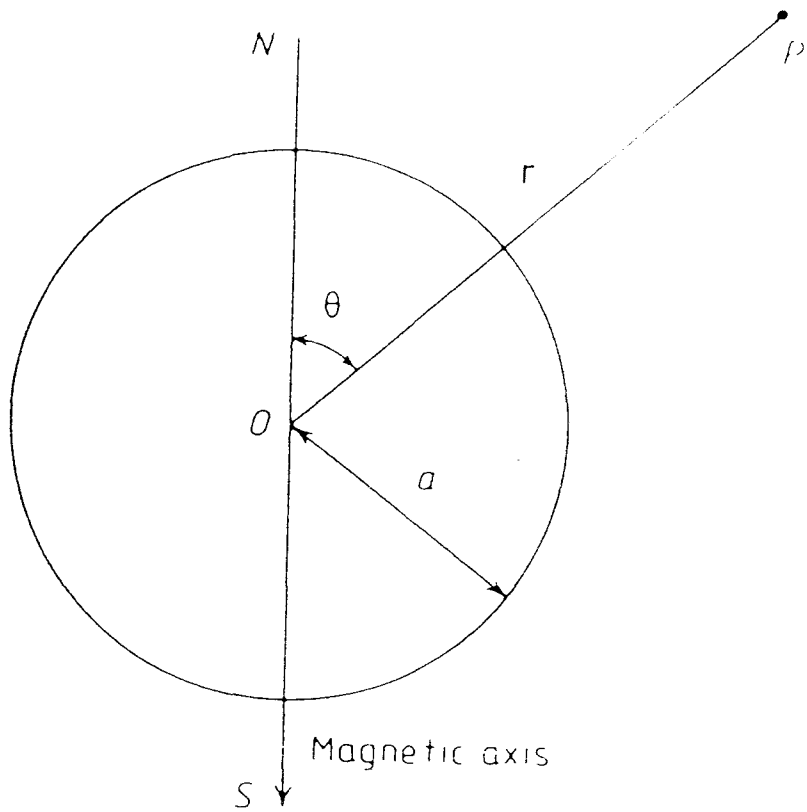

Fig. 1.1.2 Configuration of potential of geomagnetic field. a is the radius of the earth, P is an observing point outside the earth and θ the co-latitude from the north pole. The distance between O and P is r (from Jacobs 1984).

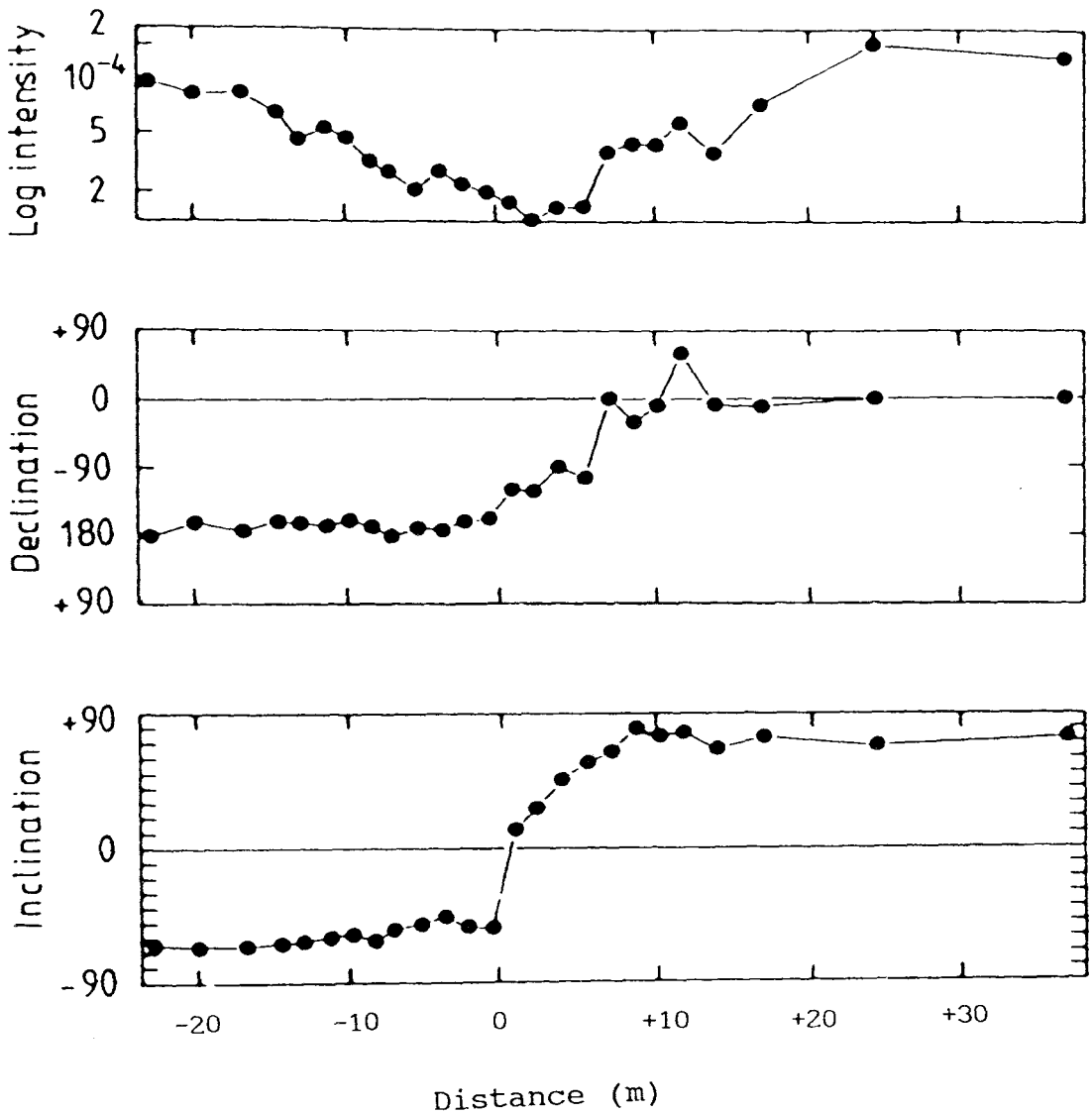

Fig. 1.1.3 Changes in intensity declination and inclination of the geomagnetic field during a polarity reversal recorded in the Tatoosh intrusion, USA. Sampling section is referred to a defined reverse plane in the intrusive rocks (from Dodson *et al* 1978).

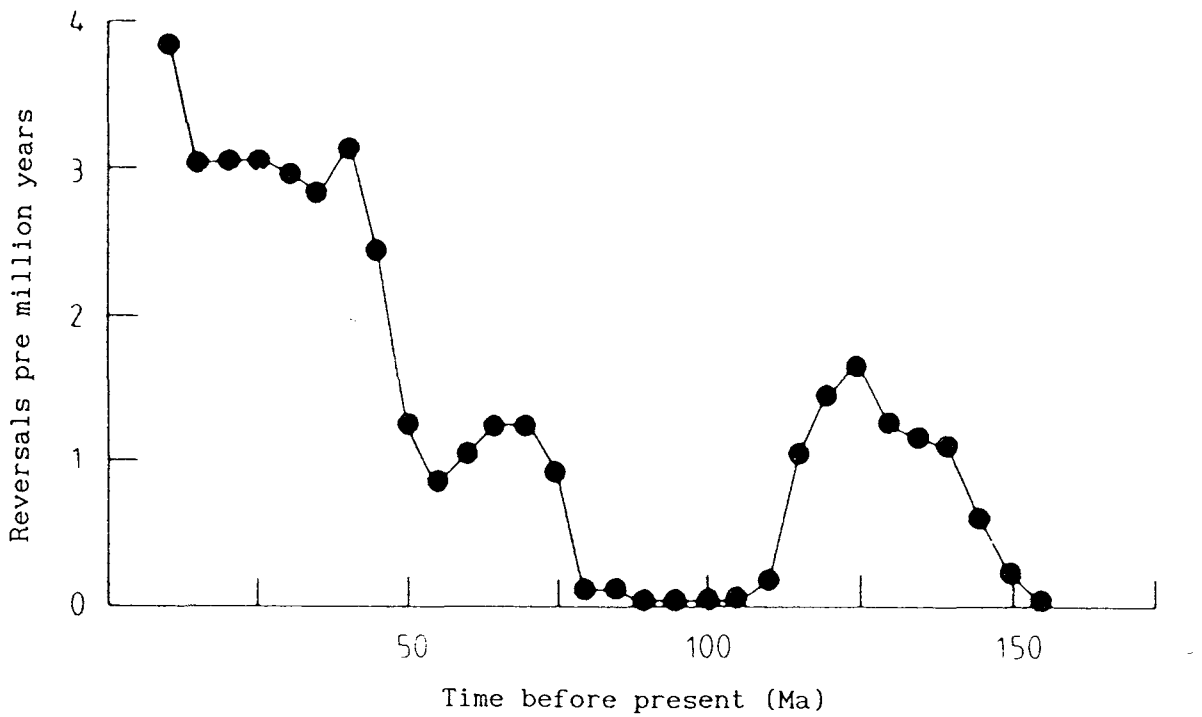

Fig. 1.1.4 Variation in the average frequency of reversals as seen through a sliding window 10 m.y long. From c.76 Ma to the present the rates are from Heirtzler *et al* (1968) and prior to 76 Ma from Larson and Pitman (1972) (from Cox 1975).

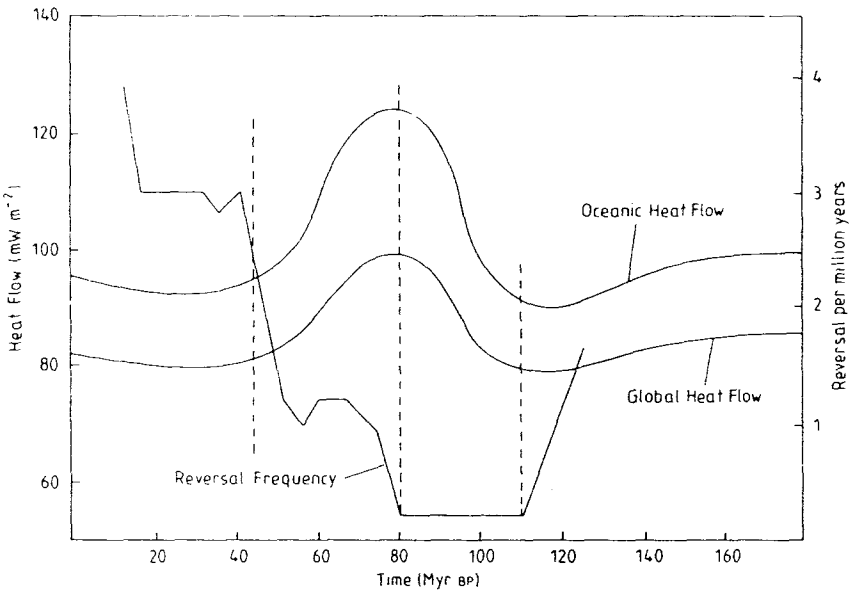

Fig. 1.1.5 Variability of mean oceanic and global heat flow (after Sprague and Pollack 1980) and variations in the average frequency of reversals of the geomagnetic field (from Jacobs 1984).

§1.2 Mineral and rock magnetism

1.2.1) Magnetic minerals.

In the upper part of the Earth iron forms various iron minerals with other elements, eg. sulphides, silicates and oxides. The iron minerals which are responsible for the magnetic remanence in most crustal rocks can be plotted within the ternary system $FeO-TiO_2-Fe_2O_3$ (Fig.1.2.1). The oxides in this system crystallise with the silicate phases at temperatures in the range of 1200-800°C, after which the crystallisation is always complete by 750°C, and some in this system can acquire magnetic remanence. The commonest compositions of natural oxide minerals in igneous rocks are those of the titanomagnetite series, which can be oxidized towards the titanohematite series (or correctly referred to as titanomaghemites) (see Piper 1987).

Any of the oxide phases in igneous rocks may survive as detrital components in sedimentary rocks. In this environment, they are normally metastable and may alter to form new phases controlled by the redox potential (Eh) and the acidity (pH) of the environment. For palaeomagnetism, two series of iron oxides, the titanomagnetite and the ilmeno-hematite series are important.

Members of the titanomagnetite series have cubic symmetry and possess an inverse spinel structure. Because of the atomic structure of the titanomagnetite system, there is a net magnetic moment giving the structure ferrimagnetic properties (Nagata 1953). With a spontaneous magnetisation of 90-93 Am^2/kg (Nagata 1953), magnetite has the strongest magnetic properties of any common crustal mineral. Saturation is commonly achieved in applied fields of 50-150 mT but it may occur at fields higher than this value, depending on the grain size and oxidation.

Magnetite is magnetically anisotropic with "easy" and "hard" directions of magnetisation along the (111) and (100) crystallographic directions, respectively, but this effect is usually weak compared with the anisotropy associated with the shape of the magnetite grains. Coercivity increases with decreasing grain-size, from $3 \cdot 10^3$ A/m for

30μm grains to $1.5 \cdot 10^{-5}$ A/m near the transition size for single-domain and multi-domain grains (O'Reilly, 1983). It seems probable that the stable NRM, which is of principal concern in palaeomagnetism, is commonly carried by elongate or pseudo single domain (PSD) grains (Stacey 1963).

The hematite-ilmenite series (αFe_2O_3-$FeO \cdot TiO_3$) forms solid solutions above 980°C and below this temperature the isolated hematite mainly contributes to the rock magnetisation. The Curie temperature of hematite is commonly as high as 680°C. Magnetic coercivities of this series are much higher than those of the titanomagnetites, and are strongly dependent on grain size, stress and thermal history (Chevallier & Mathieu 1943).

Hematite is a common constituent of many igneous and sedimentary rocks. It occurs in sediments as black, polycrystalline particles, often containing magnetite particles, and in many cases as a fine-grained coating on other particles. If hematite shows evidence of having pseudomorphed magnetite, it is known as *martite*. It is stable as long as organic matter is absent; the latter encourages Fe^{3+} to reduce to Fe^{2+} and is accompanied by a colour change to drab greens and greys. Low Eh and low pH ground waters have the same effect (Piper 1987). Fig.1.2.2 shows the variation of Curie temperature for the range from $\frac{1}{3}Fe_3O_4$ to $\frac{1}{2}Fe_2O_3$.

There are other magnetic minerals which play sub-roles in magnetisation. Goethite belongs to the mineral group of iron hydroxides which normally occurs as a complex of four crystal structures, of which only one, goethite (α-FeOOH), carries a remanent magnetisation with a Curie temperature of 110-120°C. Goethite is formed in the weathering environment and occurs as yellow to brown coloured phases in weathered rocks and soils (Piper 1987).

Pyrrhotite belongs to a series of iron sulphide minerals ($Fe_{1-x}S$). The majority of these species are only slightly ferrimagnetic, but the compositional range x= 0.09 to 0.13 (in the general formula $Fe_{1-x}S$) is strongly ferrimagnetic with a spontaneous magnetisation ranging up to 26 Am^2/kg and a Curie point of 320°C. The remanence of pyrrhotite is

typically soft and comparable to that of low coercivity magnetite (Piper 1987).

1.2.2) Magnetisation of rocks.

Types of Natural Magnetisation in Rocks

There are three main types of natural remanent magnetisation in rocks, namely thermoremanent magnetisation (TRM), chemical remanent magnetisation (CRM) and detrital remanent magnetisation (DRM), of which the latter two types are most relevant to the present study.

1) Chemical Remanent Magnetisation (CRM).

CRM is acquired during the formation of a magnetic mineral at low temperatures (below the Curie point) by chemical or phase change in the presence of an applied field. CRM can be imagined to arise from a process of nucleation. During the early stages the grains of hematite (under the oxidation condition) are small enough that their relaxation time (see Equation 1.2.1) is very short and the grains are superparamagnetic. The spontaneous magnetisation occurs in the presence of an applied field, as the grain grows, so it passes through the critical "blocking diameter" d_B, and the relaxation time increases very rapidly. The remanence magnetisation becomes "frozen in" and subsequent changes in field direction, as the grain grows further, have no effect upon its direction of magnetisation.

CRM is probably the most common origin of the magnetisation of red beds, and there are several quite different circumstances in which it can be produced (Elmore and Van der Voo 1982). Hematite can be formed by chemical precipitation during the consolidation of sediments. The dehydration of iron oxyhydroxide: $2FeOOH \longrightarrow Fe_2O_3 + H_2O$ has been documented in many sedimentary beds (eg Hedley 1968, Strangway *et al* 1968). Other possibilities include the oxidation of titanomagnetites to titanomaghemites or titanohematites. A particular interest in the palaeomagnetism of sedimentary rocks is the CRM of hematite acquired during the consolidation and compaction of sediments which may record the ambient geomagnetic field at some time after deposition.

2) Detrital Remanent Magnetisation (DRM).

DRM is defined as the process of alignment of magnetic particles by an applied field as they fall through a fluid (usually water) and the rotation of such particles in the field direction when they are in the water-filled interstitial pores of a wet sediment. The former magnetisation is termed "depositional DRM" (DDRM), whilst the latter, due to particle rotation after deposition but prior to consolidation, is termed "post-depositional DRM" (PDDRM) (Payne and Verosub 1982).

Two main processes, which are thought to contribute to post-depositional DRM, play an important role in the accurate recording of the geomagnetic field direction during or near the time of deposition of the sediments. Initially, the water-lain sediments have loose packing with minimum grain contact and are completely saturated with water. As sedimentation proceeds the grains are pressed into a tighter configuration and the inter-granular water is progressively expelled. The smaller magnetic grains between the matrix of larger grains are rotated into the direction of the ambient field during this process.

PDDRMs are also acquired in intertidal (littoral) environments over short periods after these sediments are deposited. Since the sediments here are rapidly dried out by intermittent exposure, the burrowing activity of marine organisms (bioturbation) enables the acquisition of PDDRM. In sub-littoral environments, however, bioturbation precludes acquisition of PDDRM near the sediment surface, because it helps to create and maintain a high water content in the sediment (Verosub 1977).

In the present study of Wealden sediments from southern England, red or variegated sediments represent a high proportion of the whole sample set. Sediments broadly grouped as "red" owe their colour to finely-disseminated hematite and generally possess a relatively strong (~1-100 mA/m) NRM. They occur most commonly in arid to semiarid, fluviatile and aeolian sequences, and in certain shallow-marine and near shore environments associated with moist climates. The hematite

occurs as two principal phases, namely detrital and well-crystallised (specularite) grains in the size range 5-500 μm and as a fine-grained diagenetic phase, coating the detrital silicate grains and with a grain-size mostly <2 μm (Collinson, 1965). The magnetic components in red sediments are routinely distinguished by thermal demagnetisation and, in many cases, the pigment is found to have a lower blocking temperature spectrum than the specularite grains and rock as a whole (Piper 1987).

As a result of diagenetiic changes, red sediments may have a very complex magnetic history. Generally, the specularite grains may be linked to primary DRM and PDDRM components, and the secondary pigment or overgrowths to secondary CRMs (Piper 1987), but the distinction may not be as simple as this. Turner (1980) has generalized these considerations in terms of minerological maturity versus diagenetic time, as shown as Fig.1.2.3. Type A sediments contain a predominantly single component DDRM or PDDRM acquired over short time intervals; they are capable of recording secular variation and even, to some extent, geomagnetic polarity transitions. Type B sediments are multicomponent and may carry antiparallel components, which can frequently be demonstrated by a combination of thermal and chemical demagnetisation. Type C sediments have a remanence residing entirely in diagenetic phases which can often be shown to be syn- or post-folding, one single polarity is often present and directions are typically well-grouped throughout a whole formation.

Main physical characteristics of rock magnetisation.

There are three distinctive types of magnetic behaviour depending on magnetic grain size, namely superparamagnetic (SP), single-domain (SD) and multi-domain (MD) (Stacey 1963). It is generally believed that stable remanence resides in SD grains, while the less stable components are located in large MD grains or in hyperfine SD grains in which thermal activation plays a dominant role. Fig.1.2.4 shows the isothermal magnetisation process of a ferromagnetic material with multidomain structure. In practice, when grains of magnetic mineral consist of a randomly-oriented assemblage, they execute the similar hysteresis loops. The main difference between magnetite and hematite

(or equivalent magnetic minerals within the two series) residing in rock samples is that magnetite will reach its saturation much quicker than hematite, so that the magnetisation curve will be steeper before saturation is reached (eg see Tarling 1983). This property has been used for distinction of the major magnetic minerals in rock samples.

Coercivity is a measure of the resistance of the domain structure to changes. Since changes in rock magnetisation result primarily from the motion of domain walls in multi-domain grains, the coercivity is determined by obstructions of the wall motion such as lattice impurities. In single-domain grains the coercivity is dependent on the anisotropy, or directional control, of the magnetic energy of the particle, which has much higher obstructional effect against the directional modification. However, the magnetic field required to demagnetise a magnetic sample is often less than the theoretical coercivity. There are two main reasons which might explain this: 1) the thermal agitation in small grains reduces their effective coercivity near the superparamagnetic field; 2) the effective grain coercivities are affected by interactions between grains. Although this effect cannot be quantified, it probably acts to reduce the effective coercivity (Piper, 1987).

Temperature plays an important role in magnetisation processes. The temperature fluctuations will be able to move the magnetic moment from one "easy" orientation to the other to reduce the "energy state" within the sample to a minimum. This condition depends on a critical value of the grain volume v for a particular temperature value T. The diameter corresponding to this critical volume, d_B, is called the "blocking diameter". For a given v, the crucial temperature T_c which agitates the magnetic moment and allows it to change orientations is called the "blocking temperature", T_B. Thus, if an assemblage of identical grains has an initial moment M_o, then this moment will decay exponentially with time (eg see McElhinny 1973).

An important parameter which defines the decay rate is relaxation time τ, defined as:

$$\tau = \frac{1}{c} \exp\left(\frac{vk}{kT}\right) \qquad (1.2.1)$$

where c is a frequency factor equal to about 10^{10}/s, k is the anisotropy constant, which is related to the coercivity Hc. k is the Boltzmann Constant. Neglecting changes in the anisotropy constant k with temperature (which will be small (McElhinny 1973)), the relaxation time τ_1 at temperature T1 for a grain of fixed volume is simply related to the relaxation time τ_2 at temperature T2:

$$T_1 \ln(c\tau_1) = T_2 \ln(c\tau_2) \qquad (1.2.2)$$

Thus the same effect upon the remanence is obtained either by maintaining the grain at temperature T1 for sufficient time τ_1 or by raising it to a higher temperature T2 and maintaining this for some shorter time τ_2. This forms the basis of the method of thermal demagnetisation. Although this theory of blocking temperatures and relaxation times can qualitatively predict the purely physical effects of prolonged heating or cooling on the magnetic history of a rock, in practice, chemical changes occurring in the rock will cause the destruction of primary magnetic mineral phases and the growth of new phases.

1.2.3) Magnetic units.

In this study, the rationalised Sommerfeld SI (Systéme International) units are used. The units are based on the force between two poles of strengths, m1 and m2, in a vacuum space:

$$F = \frac{m_1 \, m_2}{4\pi\mu_0 r^2} \qquad (1.3.1)$$

where r is the distance between the poles and the constant μ_o is the permeability of free space with an SI value of $4\pi \cdot 10^{-7}$. The SI convention means that both the magnetic field (F) of a material and its intensity of magnetisation (J) are measured in amperes per meter (A/m) and are related to magnetic induction (B) in a magnetised medium, by $B = \mu_o(F+J)$, which is measured in Tesla (T). Magnetic fields will therefore be expressed in terms of Tesla and the intensity of magnetisation per unit volume is expressed in terms of A/m. This

convention means that the susceptibility constant (k), relating the intensity of magnetisation generated by a material to the applied magnetic field, becomes dimensionless, but is 4π greater than it would have been in cgs or MKSA units. Table 1.2.1 lists the SI units, together with the equivalent cgs units (together with conversion factors) since the latter have been used widely in the palaeomagnetic literature in the past.

Table 1.2.1 Magnetic units used in palaeomagnetism (after Hailwood 1989).

Property	SI units		commonly used cgs unit	conversion factor
	unit	commonly used sub-unit		
Intensity of remanent magnetisation of rock	Am^{-1}	mAm^{-1}	Gauss(G)	$1mA/m = 10^{-6}G$
Magnetic moment of rock	Am^2	mAm^2	$G \cdot cm^3$	$1mAm^2 = 1G \cdot cm^3$
Magnetic field	T	mT or nT	Oe or γ	$1mT = 10Oe$ $1nT = 1\gamma = 10^{-5}Oe$
Magnetic susceptibility (per unit volume)	Dimensionless		$(G \cdot Oe^{-1})$	1 SI unit = $4\pi \cdot G \cdot Oe^{-1}$

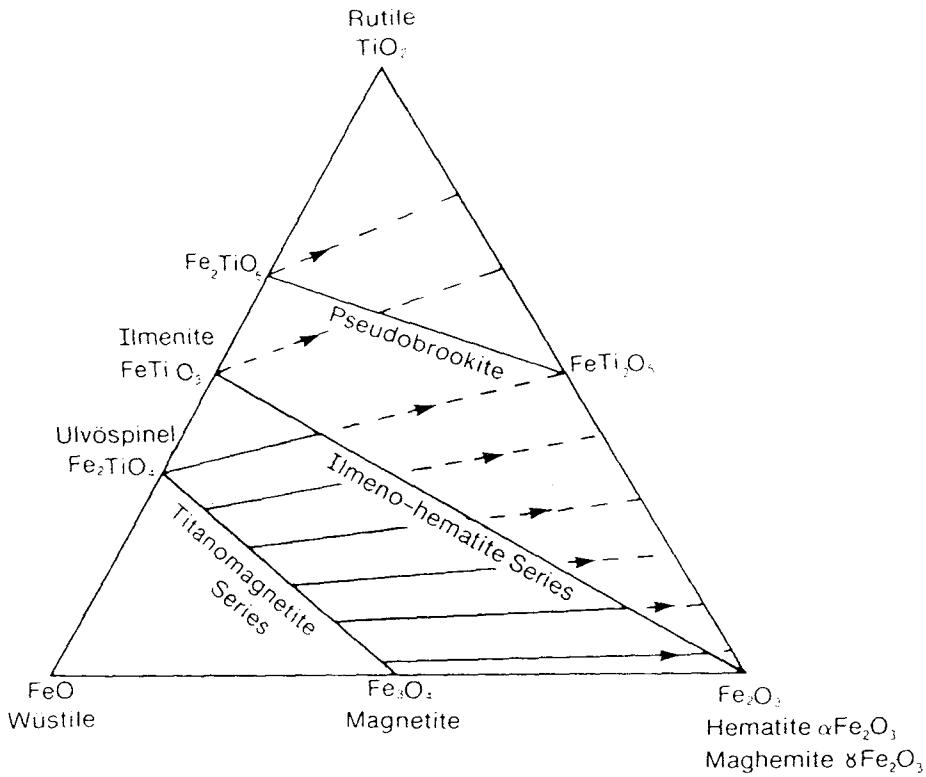

Fig. 1.2.1 The ternary system incorporating the iron-titanium oxides. The directions of increasing oxidation are shown by arrowed lines. The actual oxidation may follow more complex paths. (from Piper 1987).

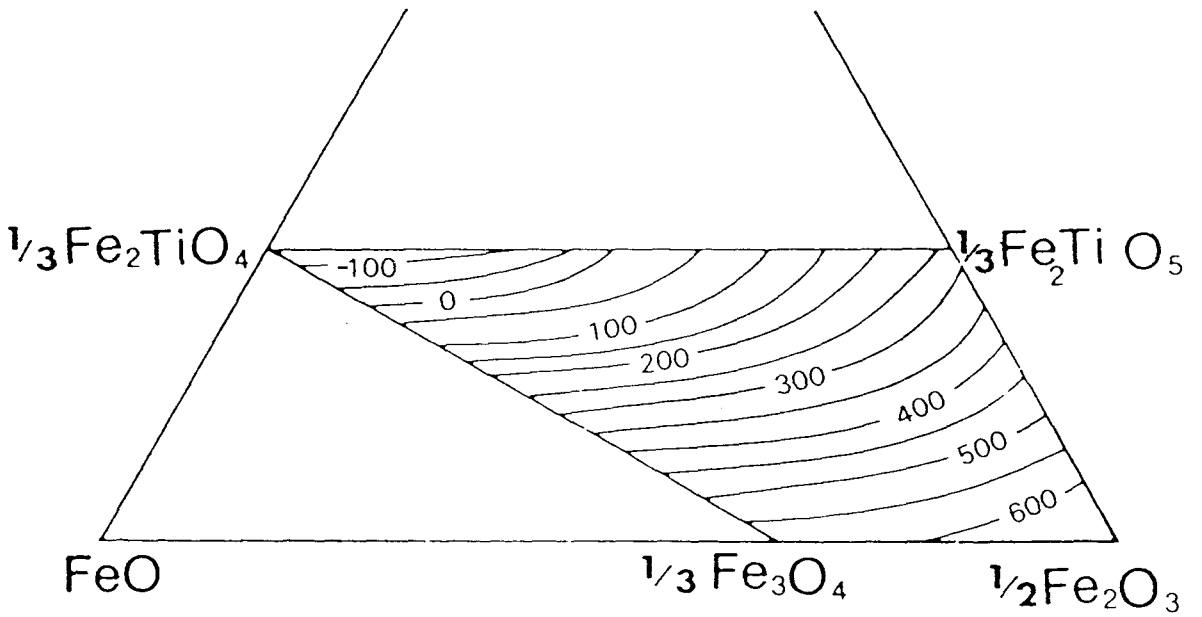

Fig. 1.2.2 Contour diagram showing the variation of Curie temperature for the range from 1/3Fe2TiO4 - 1/3Fe3O4 to 1/2Fe2O3 and its oxidized equivalents. (from Readman and O'Reilly 1972).

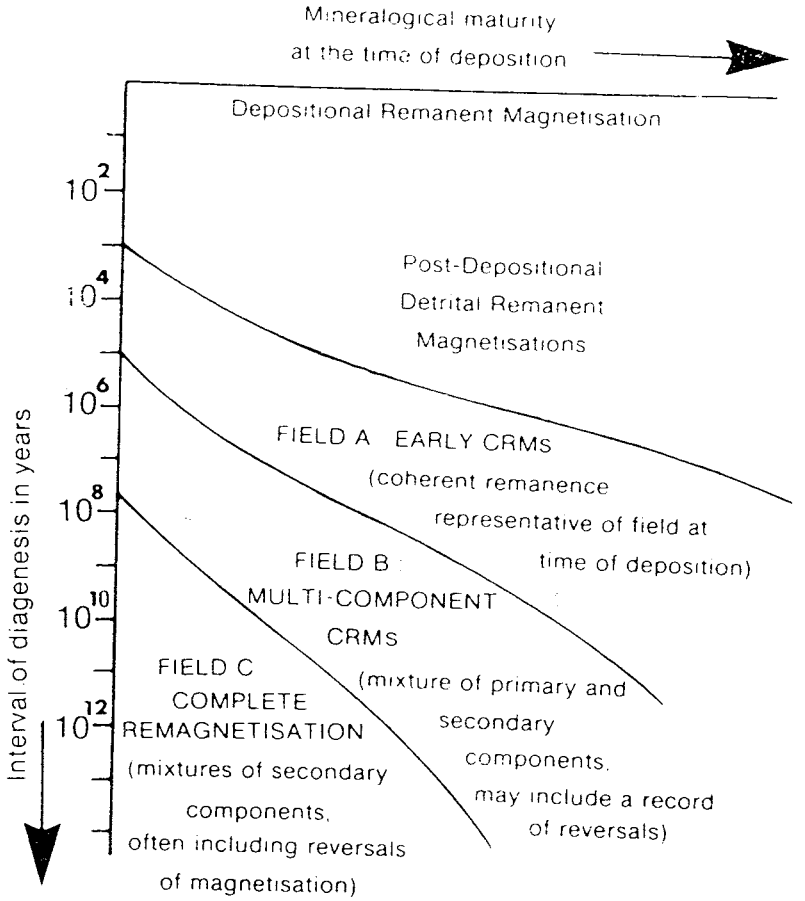

Fig. 1.2.3 The types of magnetism in red sediments as a function of mineralogical maturity and the time period of diagenesis. (from Turner 1980).

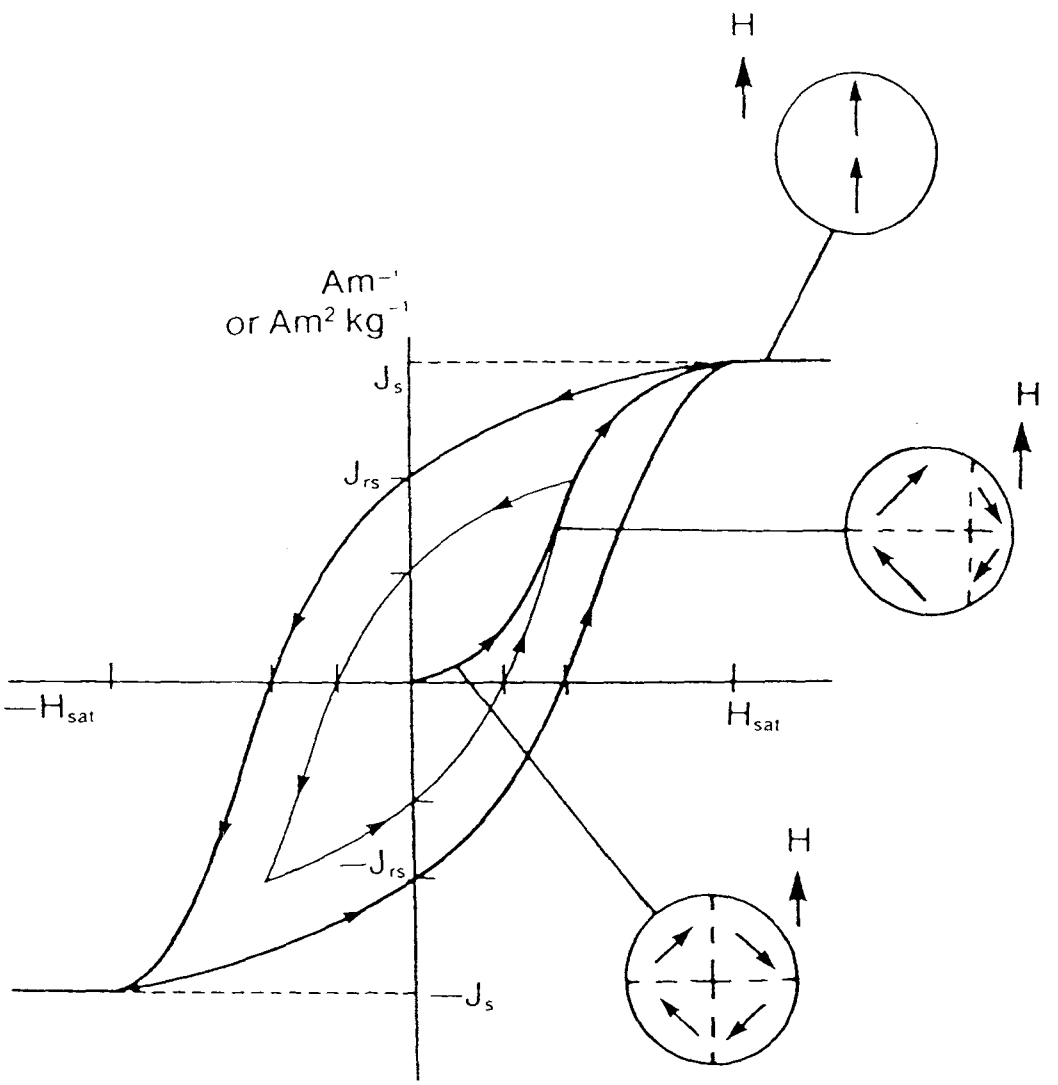

Fig. 1.2.4 Magnetisation, J, as a function of applied field, H, for MD ferromagnetic material. J initially increases linearly with the applied field, and this part of the curve is reversible. If H is increased further the slope of the curve decreases and if the applied field increases beyond the value H_{sat} then it produces no further increase in J. The corresponding value of J is the saturation magnetisation, J_s. If H is reduced to zero, instead of J falling to zero, the material acquires an isothermal remanence J_{rs}. The circles show a schematic representation of domain structures.

§1.3 Principles of magnetostratigraphy

1.3.1) Magnetostratigraphy dating and correlation.

It has been recognized for a long time that palaeomagnetism has value in the subdivision and correlation of sedimentary sequences. However, it was not until it was applied to deep-sea sedimentary sequences in the 1970's that the value of magnetic stratigraphy was fully appreciated. Magnetostratigraphy organizes stratigraphic information according to their magnetic properties acquired at or soon after the time of deposition. The polarity of the earth's magnetic field has reversed repeatedly in the geological past. Because polarity transitions, while lasting only a few thousand years, are synchronous over the entire globe, their records in marine or terrestrial land-based sediments provides isochrons applicable to worldwide correlations.

Dating a geological formation and correlating a group of relevant formations in different areas, from a very local to global scales, by magnetostratigraphy, provides a supplementary technique to conventional biostratigraphy and radiometric dating. In order to do so, the first stage is to carry out palaeomagnetic analysis on samples from regularly spaced sites in a stratigraphic section through a formation or a continuous drilled core through it, using the techniques described in Chapter II. By these means, the polarity of the characteristic remanent magnetisation at each stratigraphical level is defined. The resultant changes in polarity with stratigraphical level in that particular lithostratigraphical section will define a series of normal and reverse magnetozones. Afterwards, available biostratigraphical and other controls (eg lithological and radiometric evidence) are then used to correlate these magnetozones with the corresponding time equivalent magnetic chrons on a standard geomagnetic polarity reversal time scale, which thus enables dating of the magnetozone boundaries in that formation (Hailwood 1989).

Therefore, it is necessary to first establish a standard geomagnetic polarity time scale (GPTS). If a distinctive set of reversals observed in a particular rock sequence can be matched

unambiguously with the appropriate part of this GPTS, then the geological age of each of the beds containing a polarity inversion can be deduced, provided that the approximate age of the sediment unit is known by means of other independent evidence, such as microfossils, tectonic controls, etc. However, a single short reverse polarity interval within an otherwise normal polarity section (or vice reverse) may be sufficiently identified on the GPTS, if 1) a limited amount of biostratigraphical information (normally at the Epoch or Stage level) is available (eg see Townsend and Hailwood 1985), or 2) a unique reversal pattern within an identifiable geological period is revealed, for example, after or before a long period of normal or reverse polarity (eg the middle Cretaceous long normal polarity interval).

The construction and refinement of the GPTS has been a major research objective over the past three decades. The pattern of geomagnetic polarity reversals is now reasonably well established, particularly from studies of marine magnetic anomalies, from the later Jurassic (Oxfordian) to the present. However, a reasonably satisfactory calibration of this pattern of reversals against the biostratigraphical and radiometric time scales has been achieved so far only for the Cenozoic and late Cretaceous. Controversies remain, even for parts of this interval, but the uncertainties are greater for the early Mesozoic, and for most older geological periods. Thus, at present it is still some way from achieving the objective of defining an accurately calibrated standard GPTS, even for the Mesozoic and Tertiary (Hailwood 1989).

1.3.2) Construction of the geomagnetic polarity time scale (GPTS).

The development of fields of investigation, such as biostratigraphy and radiometric dating, and of modern palaeomagnetic analytical instruments, such as the balanced fluxgate spinner magnetometer and the cryogenic magnetometer, have contributed much to the development of magnetostratigraphy. So far, three separate sources of information have been used in the construction of the GPTS. 1) palaeomagnetic data from isotopically-dated igneous rocks, especially basaltic lava sequences, 2) palaeomagnetic data from

biostratigraphically and isotopically-dated sedimentary sequences, and 3) interpretation of lineated marine magnetic anomalies (Hailwood 1989). Many authors have contributed to the construction of the GPTS, from these three aspects. (For example, see Matuyama (1929), Cox *et al* (1963), Opdyke *et al* (1966, 1972), Heirtzler *et al* (1968), Theyer & Hammond (1974), Alvarez *et al* (1977)). The development of magnetic and other time scales has been summarized by, for example, Snelling (1985), Berggren *et al* (1985), Hallam *et al* (1985), and Hailwood (1989).

Of the three information sources used to build the geomagnetic polarity time scale, the third one has played a particularly important role, in which the GPTS is established and tested not only from "vertically" sampled geological section but also from different long "horizontal" magnetic anomaly profiles in different ocean basins.

A comparison of marine magnetic anomaly profiles run approximately perpendicular to the mid-oceanic ridges in different ocean basins shows remarkable general consistency (see Fig.1.3.1). In some cases, parts of the anomaly sequence appear to be missing, or are duplicated due to a small shift in the spreading axis to new positions, but such cases can be identified by comparison with profiles from other ocean basins. In certain regions, such as the south Atlantic, an apparently uninterrupted sequence of marine magnetic anomalies can be identified, which is believed to represent a continuous record of the sequence of polarity reversals over the past 100 m.y. or so. If the rate of sea floor spreading is known in such cases, or can be deduced by some independent method, then the time of each successive reversals can be obtained from the distance of the corresponding anomaly source from the mid-ocean ridge axis. In the case of a relatively slow-spreading ocean basin, such as the Atlantic, the maximum resolution (ie. the duration of the shortest polarity interval that can be detected reliably) is about 0.10 m.y., whereas for parts of the fast-spreading Pacific Ocean basin the resolution may be as high as 0.01 m.y. (Hailwood 1989).

The age calibration of the standard GPTS derived from marine magnetic anomaly data is based on the assumption of uniformity of sea floor spreading rates. Generally, the sea floor spreading rates on either side of the mid-ocean ridge are expected to be nearly constant,

but they involve episodic intrusion and extrusion of basaltic material at the mid-ocean ridge crests. It is to be expected that short-term changes in spreading rate will occur on a local scale (eg Windley 1984). Evidence comes from the comparison of stacked anomaly profiles from different ocean basins. The effects of such local short-term irregularities will tend to cancel out if data from different ridge segments are combined (Blakely 1974). Long-term differences in relative spreading rates between pairs of ridge segments in the same or in different ocean basins can be investigated by plotting the distances of successive anomaly source block boundaries, from the two ridge segments against each other. If the rates of spreading from the different ridge segments were all constant then the sets of points for each ridge segment-pair would lie on straight lines through the origin, and the relative spreading rates could be derived from the gradients of these lines (Heirtzler 1968). Fig.1.3.2 shows some data on sea floor spreading rates.

Although the line for the South Pacific basin shows a change of slope at around Chron 24, the slopes for the other profiles are approximately uniform, which means the spreading rate for each ocean basin satisfies the assumption of constant rate, at least to a first approximation. However the different line slopes for different ocean basins indicates that the spreading rates varied between oceans. This approach allows a comparison of marine magnetic anomaly data from different ocean basin for a particular interval of geological time, and the selection of profiles which show no apparent evidence of spreading rate changes during that interval. However, before the magnetic sequence optimized from different ocean basins can be used to provide a polarity time scale, it must first be biostratigraphically calibrated (eg La Brecque *et al* 1985).

A method to date the magnetic polarity sequences utilizes the fact that when the new ocean crust is first formed at the mid-ocean ridge crest it has no sediment cover. It begins to acquire such cover almost immediately, and as it moves away from the ridge crest so the thickness of overlying sediments increases progressively. The biostratigraphical age of the sediment layer resting directly on the igneous basement can be ascertained by drilling through the overlying deposits and sampling

this layer directly. This should give a close approximation to the age of the underlying igneous basement (see Hailwood 1989). If this drilling is carried out on top of a clearly identified marine magnetic anomaly, then an estimate of the biostratigraphical age of that anomaly is possible. Application of this technique became possible with the advent of the Deep Sea Drilling Project (DSDP), and the first review of results obtained was given by Tarling (1971). This confirmed the general validity of previous studies by Heirtzler *et al* (1968).

Meanwhile, the attention of palaeomagnetic studies of sedimentary sections was turned also to magnetostratigraphical investigations on land. Some of the classic land sections of uplifted marine facies deposits that had excellent biostratigraphical control and spanned various important geological boundaries began to be investigated. The first comprehensive magnetobiostratigraphical investigation of these sediments was reported by Alvarez *et al* (1977), and this provided the first complete biostratigraphical calibration of the sequence of geomagnetic polarity reversals during the late Cretaceous and early Paleocene from a single locality (the Bottaccione Gorge, near Gubbio, northern Italy).

Fig.1.3.3 shows the palaeomagnetic polarity time scale for the interval from the Late Cretaceous to the present based on marine magnetic anomalies from several ocean basins and isotopically calibrated by Heirtzler *et al* (1968) and La Brecque *et al* (1977) respectively. The application of the new K/Ar. constants by Mankinen & Dalrymple (1979) indicates an accumulated discrepancy in ages compared with those based on the older constants. Thus, the age differences between the scales for the Pleistocene stage is less than 0.1 m.y., but it increases to more than 4.5 m.y. in the Maestrichtian.

Fig.1.3.4 displays the biostratigraphically calibrated polarity time scale for the Late Palaeocene to present of Berggren *et al* (1985). The nomenclature used on this GPTS is the revised Chron nomenclature of Tauxe *et al* (1983). Referring to the long period of normal polarity in the middle Cretaceous the nomenclature for Mesozoic anomaly numbers includes the prefix "CM", to distinguish them from the Cenozoic and

late Cretaceous anomaly numbers, (which are prefixed only by the letter C).

1.3.3) Mesozoic polarity time scale

The pattern of geomagnetic polarity reversals throughout the late Jurassic and Cretaceous is relatively well established from both analyses of marine magnetic anomalies and stratigraphic sequences on land. Considerable progress has been made in recent years with the isotopic and biostratigraphical calibration of this sequence. (For example, see Obradovich & Cobban (1975), Kennedy & Odin (1982) and Kent & Gradstein (1985)). The reliability of this calibration is quite good for the late Cretaceous, but is less certain for the early Cretaceous and late Jurassic. Because the oldest sea floor known to exist in the present ocean basins is of Oxfordian age (mid-Jurassic), no marine anomaly record of pre-Oxfordian polarity reversals has yet been identified. Consequently the structure of the GPTS for the early Jurassic and older periods has had to be deduced exclusively from palaeomagnetic studies of land sections (see Channell *et al* 1982).

Larson and Hilde (1975) produced an improved model of the geomagnetic polarity time scale, to compare with others published in the early 1970s, for the early Cretaceous - late Jurassic period. The main source of information was from the "Hawaiian" magnetic lineations identified in the northwest Pacific Ocean. Fig.1.3.5 shows the magnetic survey profiles in the Hawaii area, which were used in the analyses of Larson *et al* (1972) and Hilde (1973). Fig.1.3.6 shows the improved magnetic reversal model, which has been correlated with the Keathley lineations in the western North Atlantic (Larson *et al* 1972). This pattern of magnetic reversals has been placed in a framework of geological time by using two Deep Sea Drilling Project (DSDP) drill holes that reached volcanic basement on two late Mesozoic lineation patterns (DSDP site 166 on the Phoenix lineations and DSDP Site 105 on the Keathly lineations).

Subsequent marine magnetic and DSDP investigations have added considerable information concerning the number, distribution, and age of the early Cretaceous - late Jurassic reversals (Hailwood, 1989).

For the improved magnetic reversal model presented by above authors, a fundamental assumption is that the Hawaiian lineations were generated at a constant spreading rate of the sea floor. All parts of the Hawaiian lineation pattern can be related linearly to at least one other expression of the same reversal sequence at a different location. Thus, unless simultaneous changes in spreading rates occurred on different plate boundaries, the assumption of a constant spreading rate for the Hawaiian lineation sequence is probably a good approximation. The constant spreading rate used for computation purpose in this area was 3.294 cm/yr (Larson & Hilde, 1975).

Larson *et al* (1972) produced an age calibration of the Hawaiian magnetic reversal sequence based on corrected radiometric ages. They argued that the normal interval between Chron CM7 and CM8 (corresponding to the location of DSDP site 166) was late Cretaceous in age, c.120 Ma, and that the approximate age of DSDP site 105 (drilled on the normal interval between Chrons CM24 and CM25) was mid-Oxfordian, c.152 Ma. All magnetic reversal boundaries were then assigned radiometric ages by interpolation and extrapolation from these two points. The authors claimed that, considering all the inaccuracies associated with the exercise, the radiometric calibration of these reversals is good to about 0.01 m.y. Fig.1.3.7 shows the more recent Cretaceous polarity time-scale of Kent & Gradstein (1985).

The GPTS for the Mesozoic has been investigated independently by magnetostratigraphic studies of sediment cores drilled by the DSDP and of pelagic limestone sequences exposed on land. Early Cretaceous magnetostratigraphical sections at Cismon in the southern Alps (Channell *et al* 1979) and at Poggio le Guaime, Valdorbia and Gorgo a Cerbara in Umbria (Lowrie *et al* 1980) indicate that the Cretaceous long normal interval began in the early Aptian and lasted through the Albian, Cenomanian, Turonian, Coniacian and Santonian stages (Fig.1.3.8). There have been several reports of short duration reversed chrons within the quiet interval (eg Keating & Helsley 1978, Hailwood *et al* 1979) but these have not yet been correlated between different magnetostratigraphical sections and appear to have no consistent expression in the oceanic GPTS record.

The youngest anomaly of the M-sequence of marine magnetic anomalies (CM0) is just younger than the Aptian-Barremian boundary. Anomalies CM0 to CM4 can be correlated adequately with magnetostratigraphical results based on land (Hallam *et al* 1985). For older M-sequence reversals there is not an unambiguous correlation with the magnetostratigraphical record in continental outcrops or DSDP cores. Results from DSDP site 534 (Ogg 1983) and from sections in the southern Alps at Foza and San Giorgo (Ogg 1981) could be matched to the anomaly reversal sequence from Chron CM16 to CM22. This locates the position of the Cretaceous-Jurassic boundary (indicated by a sudden increase in abundance of nannofossils) near to the reversal boundary which marks the young end of anomaly CM18. These direct correlations and age determinations for anomalies CM0 to CM4 and CM16 to CM22 have important consequences for the dating of M-sequence anomalies.

1.3.4) Magnetostratigraphic polarity units.

It was recognized during the early development of magnetostratigraphy in the 1960's that a distinction could be made between episodes of dominantly normal or reverse polarity, having a duration of 10^6 yr, and shorter episodes of opposite polarity within these, having a duration of about 10^4-10^5 yr. The former were referred to as magnetic epochs and the latter as magnetic "events" in the early terminology. Subsequent studies have shown that geomagnetic polarity reversals actually occur on a much broader spectrum of time scales ranging from less than 10^4 to greater than 10^7 yr.

The International Subcommision on Stratigraphic Classification of the International Union of Geological Sciences (Anon 1979) attempted to standardize magnetostratigraphic nomenclature. The Subcommision recommended that the term "epoch" be replaced formally by the term "polarity chron" for describing the basic subdivision of time derived from geomagnetic polarity. It was further recommended that the term "magnetic event" be replaced by "polarity subchron" for describing shorter polarity intervals with the chrons, and that the term "polarity superchron" be used to describe longer polarity intervals (such as the long mid-Cretaceous dominantly normal polarity interval). Other chronostratigraphic terms were defined for rockunits (whether or not

they are magnetic), which formed during these time intervals, and magnetic lithostratigraphical-intervals based on the identification of magnetic polarity in rock units. There are: polarity sub-chronozone, polarity chronozone and polarity superchronozone, respectively for chronostratigraphic intervals; and polarity subzone, polarity zone and polarity superzone respectively for lithological units. The terminology is summarized in Table 2.1.1.

Table 2.1.1 Magnetostratigraphic nomenclature (from Hailwood 1989).

Approx. duration of polarity inter.	chronological term proposed by IUGS 1979	equivalent chronstratigraphic term	equivalent lithological term
10^4-10^5 years	polarity subchron	polarity sub-chronozone	polarity sub-zone
10^5-10^6 years	polarity chron	polarity chronozone	polarity zone(=magnetozone)
10^6-10^7 years	polarity super-chron	polarity super-chronozone	polarity super-zone

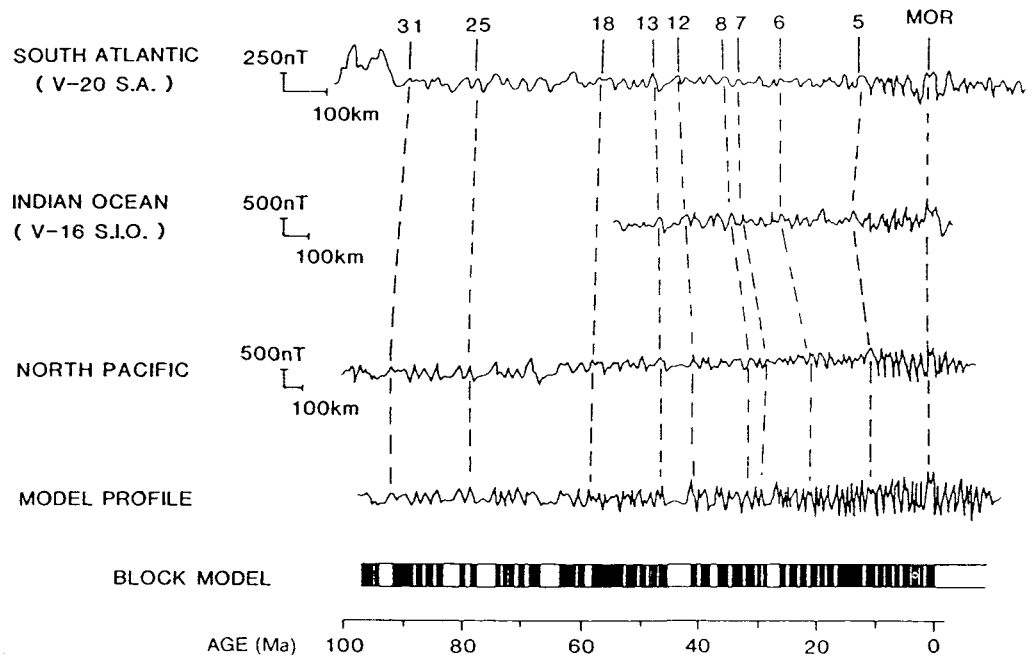

Fig. 1.3.1 Comparison between observed and model marine magnetic anomaly profiles in the south Atlantic, south Indian Ocean and north Pacific, illustrating the high degree of correlation. "Standard" reference numbers for specific anomalies are shown above the top profile (from Hailwood 1979, Heirtzler *et al* 1968). MOR= middle ocean ridges.

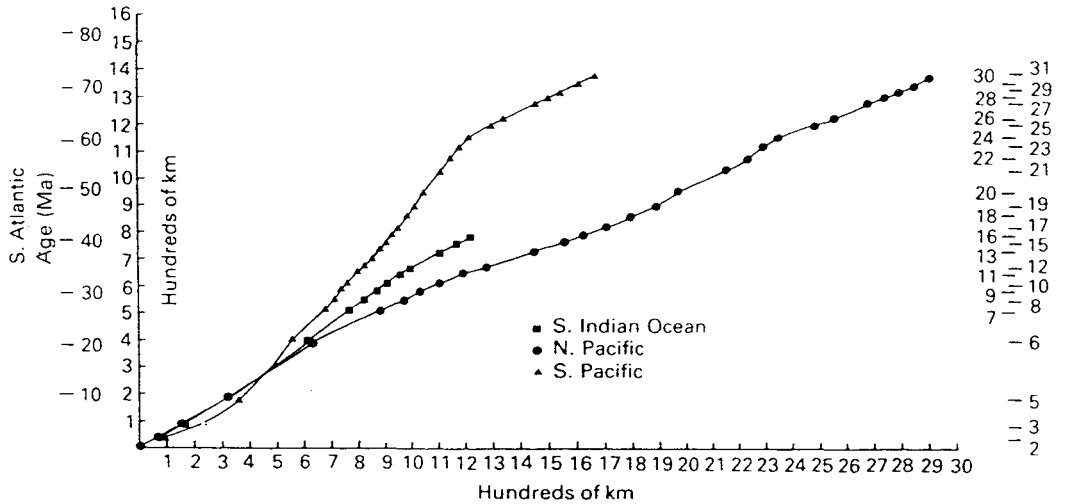

Fig. 1.3.2 The distance of certain magnetic anomalies from mid-ocean ridge crests in different ocean basins (with corresponding age), plotted against distance from crest in the south Atlantic Ocean basin, to display the relative rates of sea floor spreading. Anomaly reference numbers are shown on the right. (from Heirtzler *et al* 1968).

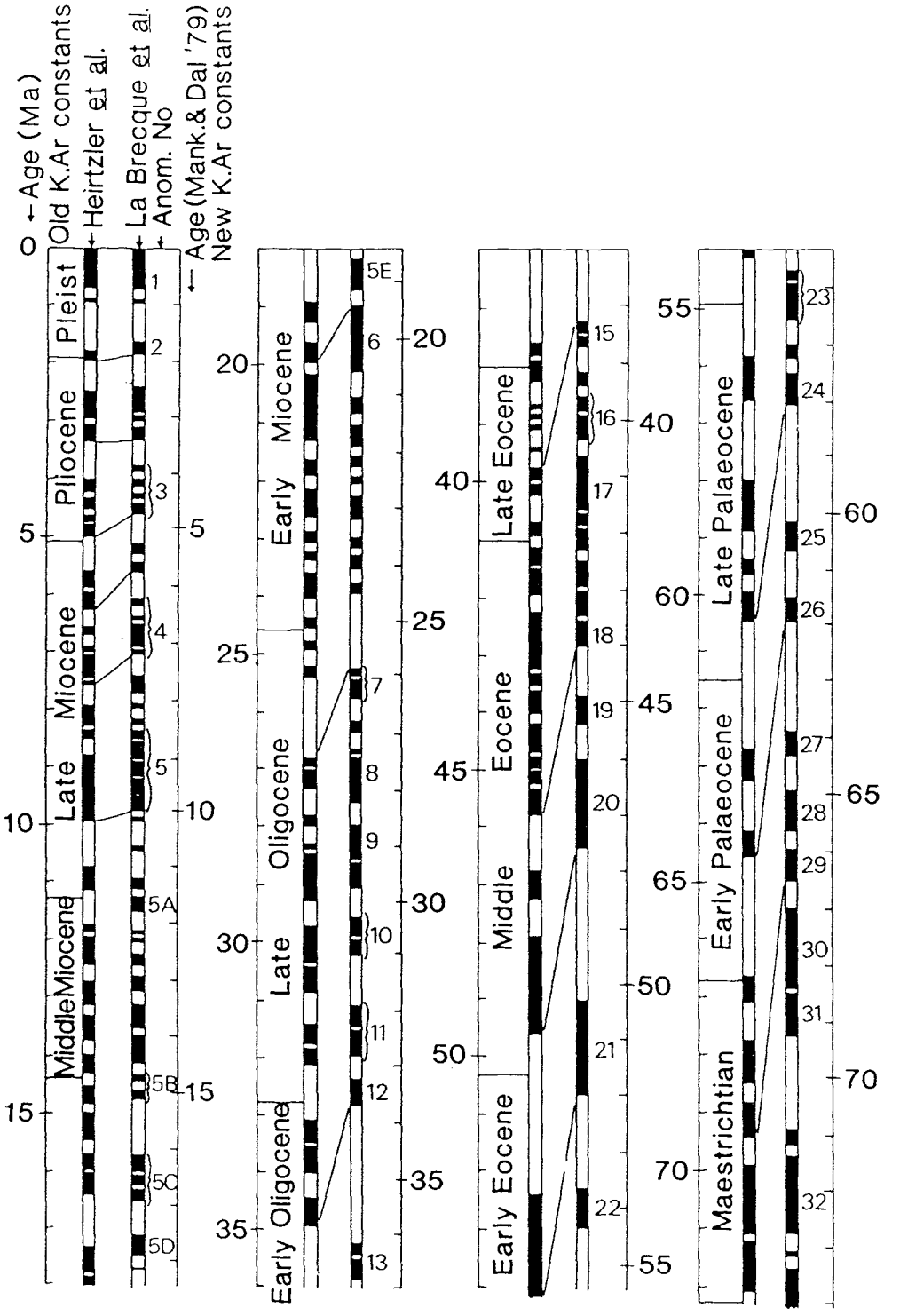

Fig. 1.3.3 Comparison between the Heirtzler *et al* (1968) and the La Brecque *et al* (1977) magnetic polarity time scale, both derived from sea floor spreading magnetic anomalies. Revised numerical ages for the latter time scale are shown. (from Hailwood 1989).

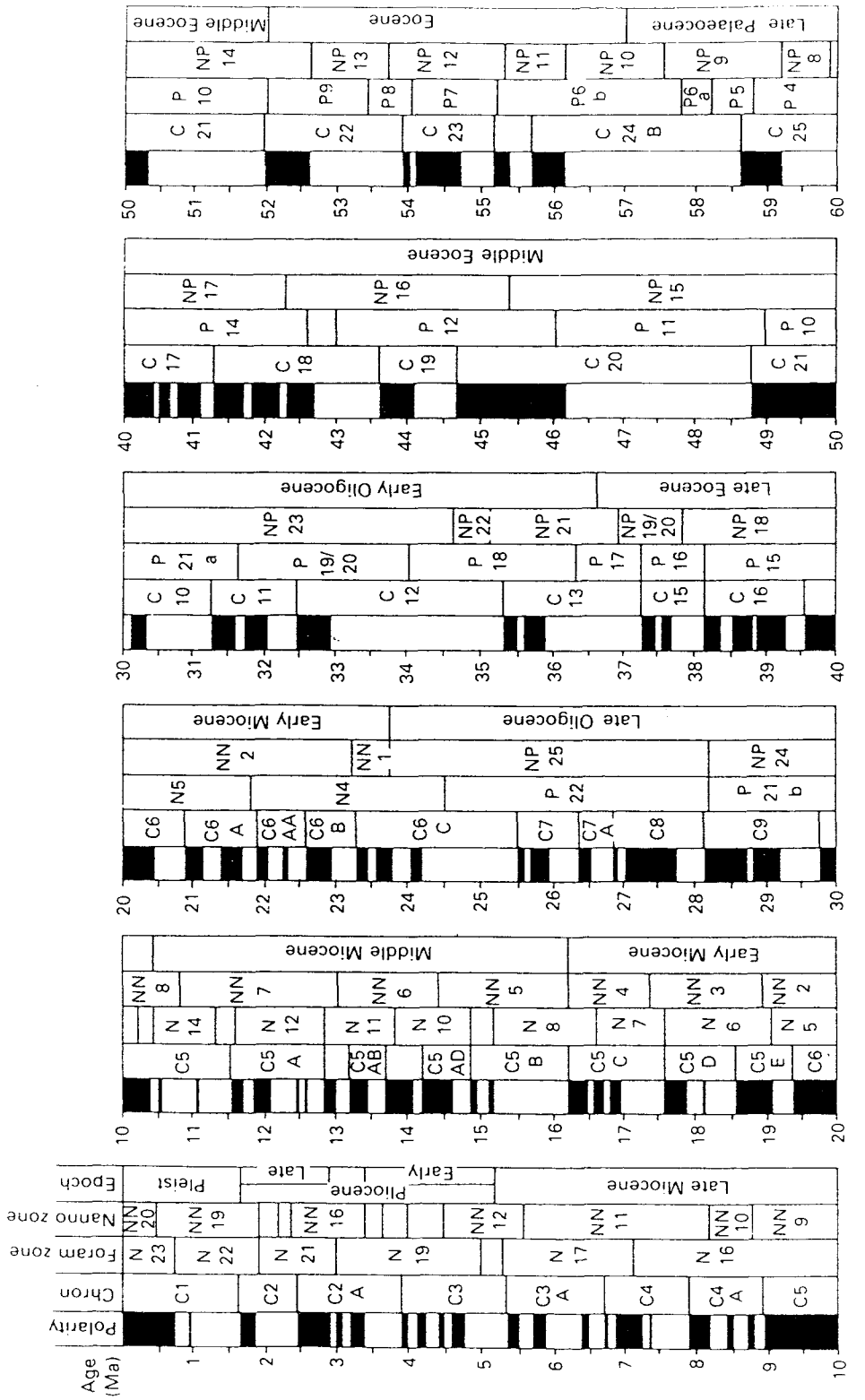

Fig.1.3.4 Cenozoic magnetic polarity timescale biostratigraphically calibrated by Berggren (1985) (from Hallwood 1989).

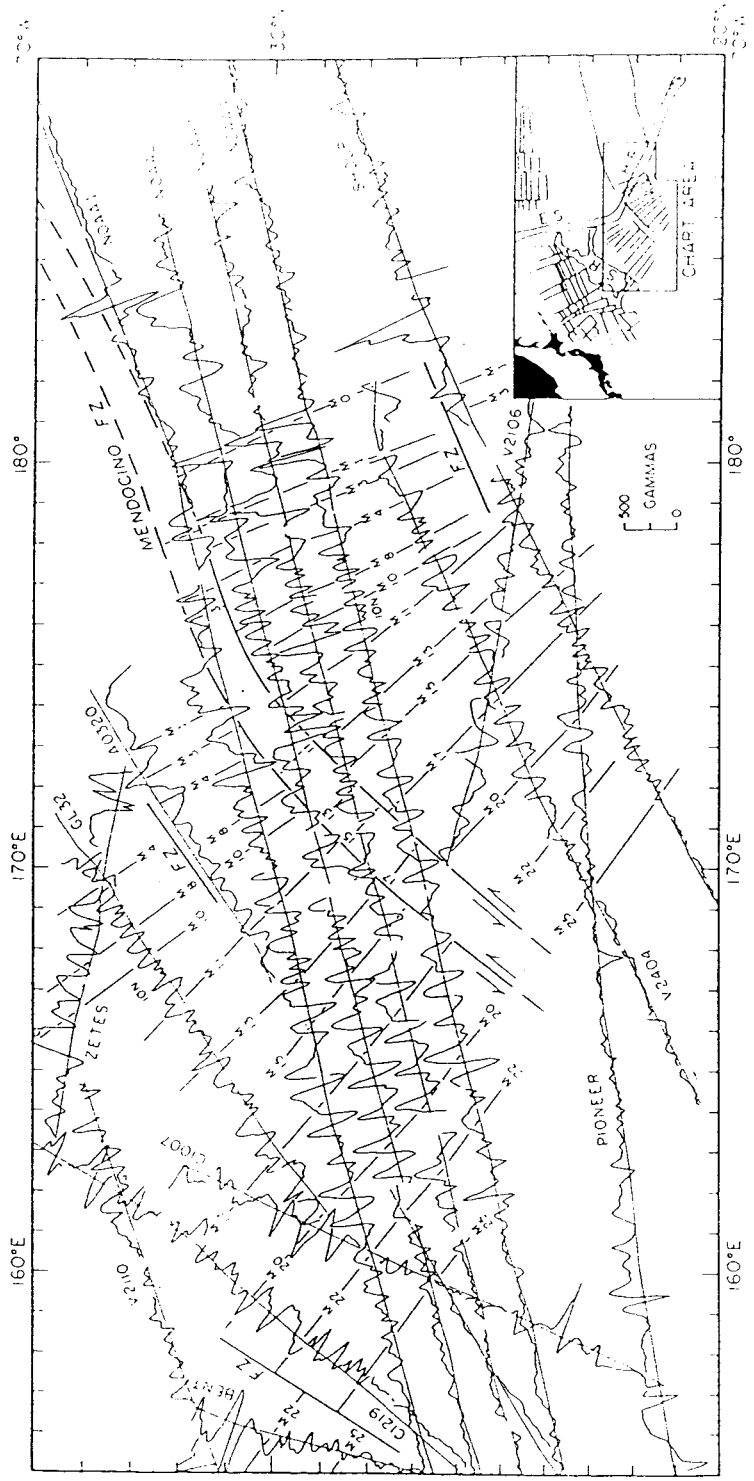

Fig. 1.3.5 Hawaiian magnetic lineation pattern in the northwest Pacific Ocean. The four NOOA profiles are from Hilde (1973). The other profiles, except for GL32, are from Larson and Chase (1972). Magnetic anomaly profiles are plotted along ship or airplane tracks with the track as the zero anomaly value. Heavy lines labeled FZ are fracture zones. The magnetic lineation numbering system is after Larson and Chase (1972). In the index chart insert, SR is Shatsky Rise. ES is the Emperor Seamounts, and HR is the Hawaiian Ridge (from Larson & Hilde 1975).

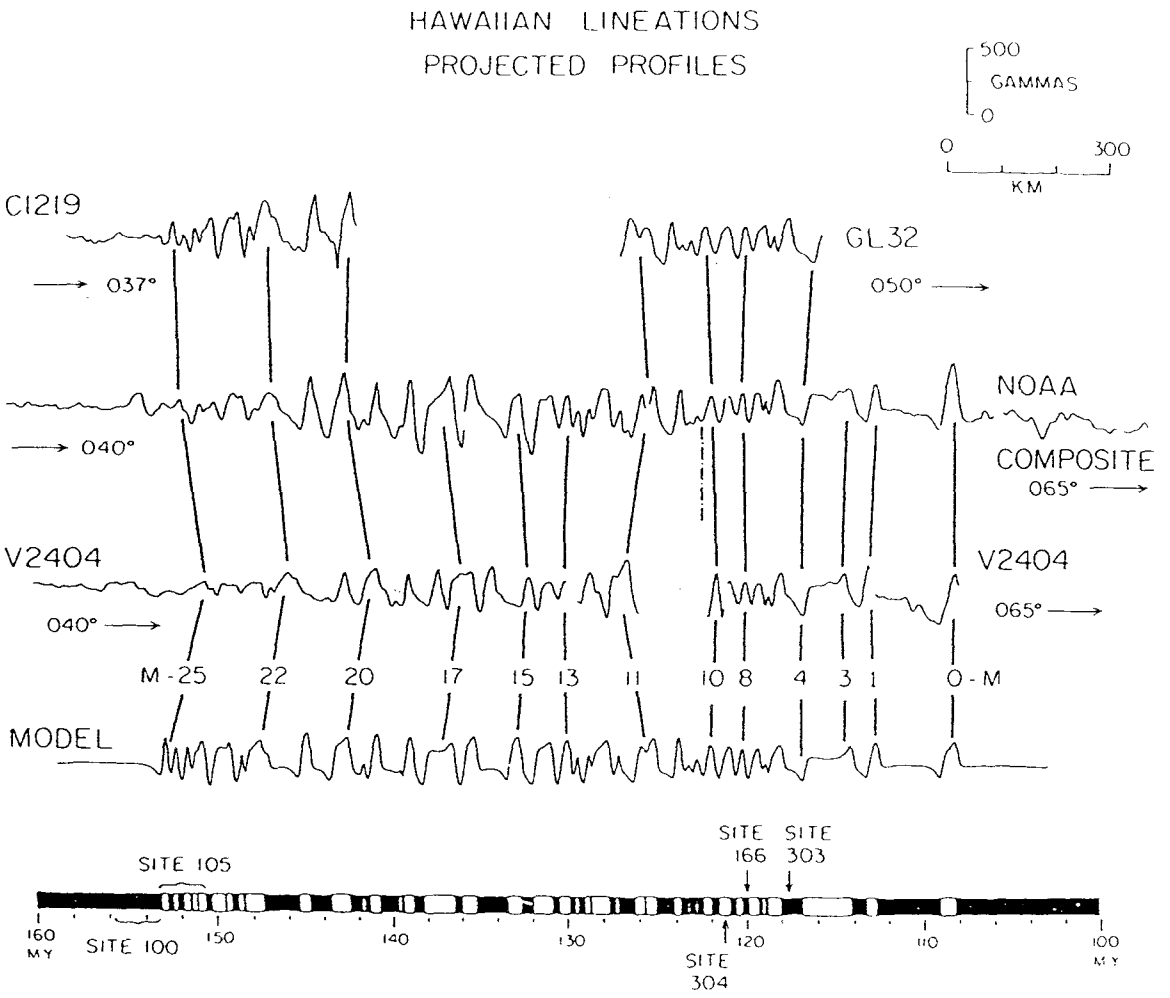

Fig. 1.3.6 The comparison of selected magnetic anomaly profiles for the Jurassic-Cretaceous (showing the Hawaiian lineations) with a synthetic anomaly sequence and corresponding source block model (from Larson *et al* 1972).

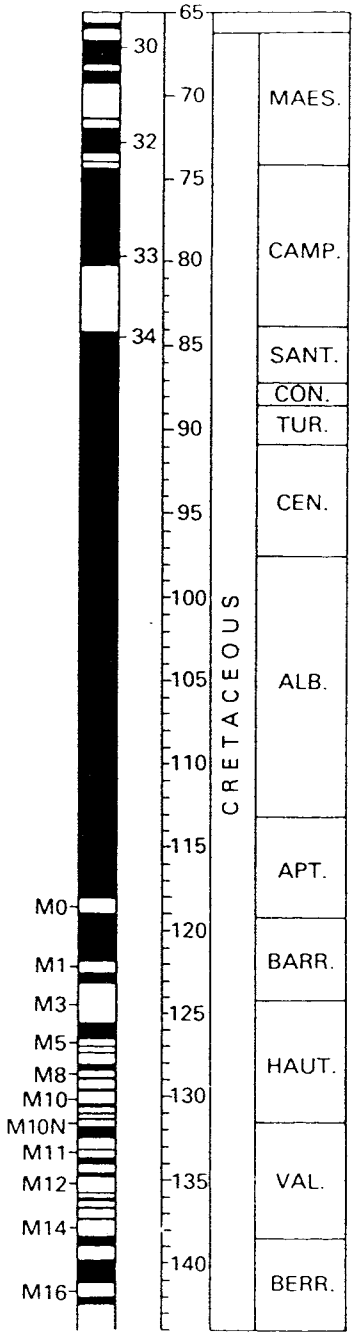

Fig. 1.3.7 Cretaceous polarity timescale (from Kent & Gradstein 1985).

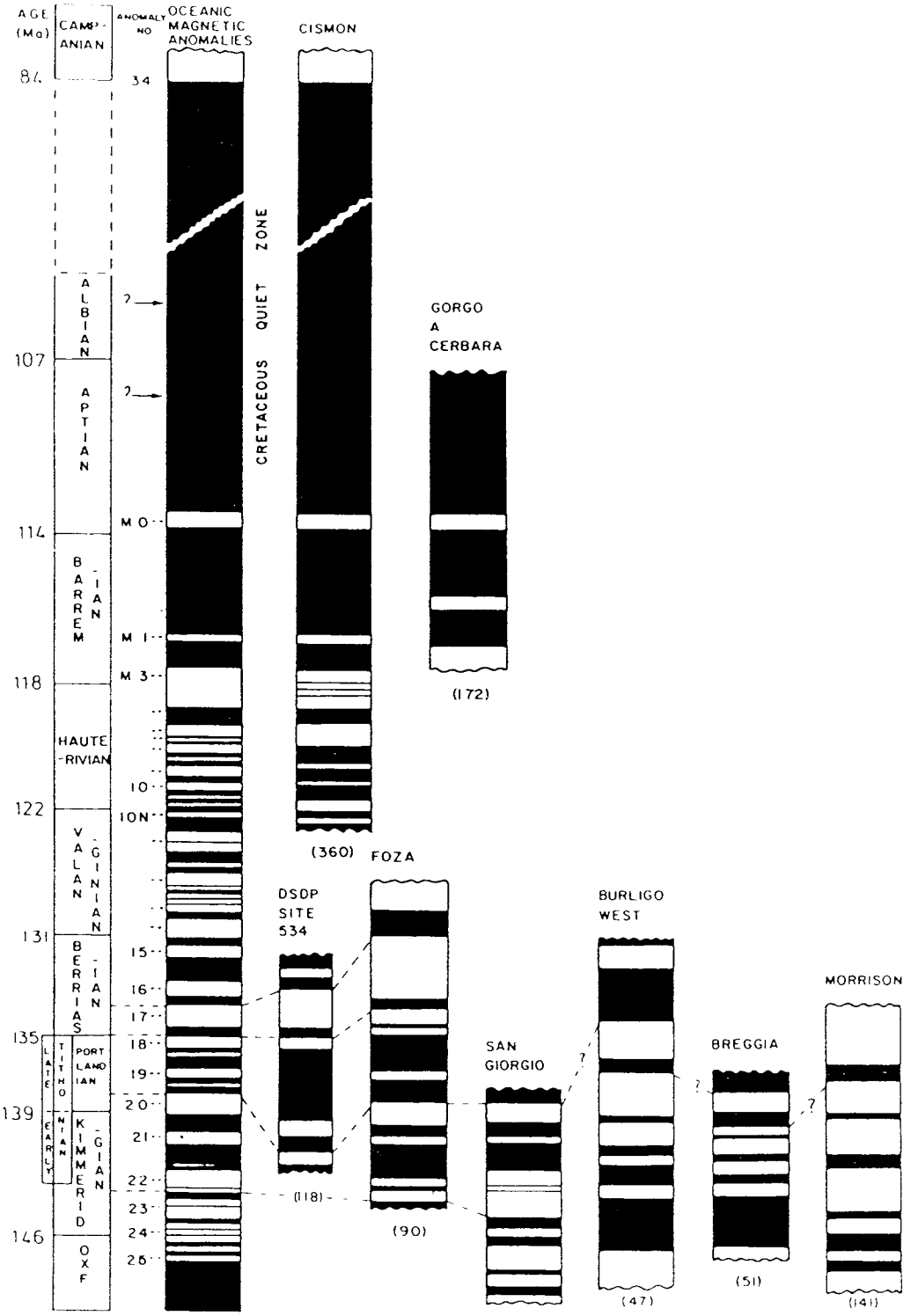

Fig. 1.3.8 Early Cretaceous and late Jurassic magnetostratigraphic sections and their correlation with the geomagnetic polarity interpreted from CM-sequence oceanic magnetic anomalies. The absolute ages associated with stage boundaries are adopted from Van Hinte (1976). The dashed tie lines are primarily biostratigraphic and secondarily magnetostratigraphic and correlate the magnetozones to the oceanic sequences. (from Channell *et al* 1982).

CHAPTER II. TECHNIQUES —— FIELD, LABORATORY AND DATA PROCESSING

§2.1. Field work and preparation of samples.

2.1.1) Principles of palaeomagnetic field work.

The first and critical stage in any magnetostratigraphic study is the collection of oriented samples throughout the selected geological sections. A variety of sampling procedures have been developed and adapted for different purposes in palaeomagnetic studies. Hailwood (1989) summarized previous approaches to palaeomagnetic field work, which failed to produce reliable data in many cases, and strongly recommended that some principles be adopted. In order that the reliability of magnetostratigraphical data can be assessed properly it is essential that the field sampling program should be designed to satisfy, as completely as possible, the recommended objectives. Chan and Alvarez (1983) also make some recommendation for the recording of information in palaeomagnetic field works.

2.1.2) Field work and sample preparation in present study.

The lower Cretaceous sedimentary units of southern England which are the main subject of this study (spanning the Hauterivian, Barremian and Aptian stages) are exposed mainly along the coast of southern Dorset and the southwest coast of the Isle of Wight. These units are well-exposed along the beach cliffs, and previously published detailed geological and lithological accounts (eg Arkell 1947, Stewart 1978 and Thurell *et al* 1968) were used as a basis for the present study. Sampling sites for each section were carefully planned in order to achieve the maximum resolution and to average out the possible effects of secular variation of the geomagnetic field. A typical stratigraphical interval between sampling sites was chosen to be about 2 m and two separate oriented samples were taken at each sampling site. The spacing between the two samples was typically 2-10 cm (vertically or horizontally). Thus, for instance, for the southwestern Isle of Wight section (which extended from between Chron CM0 to near the top of CM1, a total period of 2m.y. and total thickness of this section about 140m (from the boundary between the Vectis and Wessex Formations to

Hanover Point, the lowest outcrop)), the average time span represented by each site was 10^2-10^3 yrs, and that between neighbouring sites was 10^3 -10^4 yrs.

The Lower Cretaceous sediments of southern England are mainly unconsolidated, consisting of shales, marls, silty clay and fine sandstone. Therefore, the sampling method developed by Townsend and Hailwood (1985) could be applied, in which non-magnetic copper tubes were inserted using light hammer blows. The copper tubes were about 300 mm long with a wall thickness of 0.5mm and an inner diameter of about 26 mm. After a fresh exposure in the section had been chosen and weathered materials dug out by spade, two tubes were then carefully hammered into the beds, using a block of wood to protect the tube from the hammer blows. On average the tubes penetrated about 50-70 mm into the sediment, provided that the beds were not too dry or hard.

The great advantage of this method is its speed and convenience in the field. However, under certain circumstances, it may introduce "noise" and errors into the palaeomagnetic results, particularly when the sediments sampled are extremely soft (see discussion of results from the Boom Clay in Chapter VI).

In the laboratory, the palaeomagnetic samples were extruded using an aluminum screw extruder, without disturbing the orientation lines which were transferred from the copper tube to the core samples. Generally, two specimens were then cut from each sample with a height of 22.5 mm (which is thought to reduce the shape anisotropy of the specimen to a minimum, see Chapter VII). The specimens were then wrapped in cling film to protect them from decomposing and drying out. The preparation of two specimens from the core obtained from each copper tube is on the grounds that compaction effects might be greater for the lower part of the core than for the upper part (though the upper part may perhaps have suffered more weathering). If the specimen from lower part of the core showed possible evidence of a compaction effect on its magnetic remanence, then the upper part could be used instead. Compaction effects may be expected to be least in firm, dry sediments and greater in soft, wet sediments.

After inserting the sampling tubes at each site, an orientation table (comprising a magnetic compass combined with a pair of spirit levels for leveling the top of the table and a clinometer) is mounted on the top of the tube. Then, the azimuth of the x-axis (defined as Fig.2.3.1), with respect to geographic north and the dip of the z-axis (measured from the vertical) were measured. A magnetic compass was used exclusively in the present study (rather than a sun compass), since the sections and surrounding areas do not have strong magnetic sources and the sediments themselves are magnetically so weak that they chould not affect the magnetic compass. During field work a detailed record of the geological and lithological features of the section was made, and a meter ruler and 30 m tape measure were used to measure the precise stratigraphical interval between sites, in order to related the sample positions to previously published stratigraphical records for the sections.

§2.2 Laboratory work and instrumentation

All samples were measured by means of the cryogenic magnetometer and subjected to demagnetisation using alternating magnetic field (a.f.) and thermal demagnetisers. Selected samples were then subjected to isothermal remanent magnetisation (IRM) acquisition investigations and magnetic fabric determination.

2.2.1) Cryogenic magnetometer.

A CCL 1-axis cryogenic magnetometer incorporating a SCU500 SQUID system, combined with a stationary sample 3-axis a.f. demagnetiser, was utilized to determine the magnetisation of all samples in the present study. The sensing element of the cryogenic magnetometer is operated at liquid helium temperature (-270°C) in a liquid helium dewer, which is maintained by a surrounding liquid nitrogen (-183°C) dewer. In this state, the sensing element becomes super-conducting. The sensing element comprises a superconducting ring which is made of a metal with perfect diamagnetism. All magnetic flux is expelled from the ring below a certain temperature; this is the Meissner effect. Such a ring has the property that, when an external field is applied to it while it is in the superconducting state, all flux is expelled from the interior of the metal, but not from the hole within the ring. Consequently, an induced current flows in one direction on the outer face of the ring and in the opposite direction on the inner face. If the applied field is removed, the currents on the outside of the ring disappear, but the current on the inside face persists, to maintain the field within the ring at the same value. In this way, the magnetic field in which the ring was originally cooled is effectively trapped within the hole. The ability of the superconductor to trap and maintain the magnetic field presented by a magnetic sample within this ring can be utilized for measurements of the magnetisation.

In principle, the cryogenic magnetometer is perhaps two orders of magnitude more sensitive than the best balanced fluxgate instruments, but in practice instrumental noise often limits the effective sensitivity to about 0.01-0.05 mA/m. However, a major advantage of the cryogenic magnetometer is its more-or-less "instantaneous" response,

compared with the significant time required to measure the magnetisation by other types of magnetometer. Thus, in magnetostratigraphical investigations which commonly involve the measurement of large number of weakly magnetic sedimentary samples, the cryogenic magnetometer has clear advantages over other instruments.

Plate 2.2.1 shows the combined system, comprising the cryogenic magnetometer and the a.f. demagnetiser. The lower metal cylinder contains the cryogenic magnetometer with its sensing element and cooling chambers (for both liquid helium and nitrogen). The 2-axis a.f. demagnetiser is mounted on the top. When in use, the whole system is mounted inside a magnetic shielding chamber, comprising two inner layers of μ-metal and two outer layers of Si-Fe, which can be seen behind the magnetometer system in Plate 2.2.1. The magnetically-shielded space has a minimum axial field of less than 15nT, as measured by a fluxgate magnetometer with its sensor aligned along the cylindrical axis of the magnetometer. Fig.2.2.1 shows the basic configuration of the cryogenic magnetometer. The sample transportation system comprises a moving carriage which is operated by computer. This moves the sample between the magnetometer and the af demagnetiser and rotates it into different orientations for each position.

An essential stage in the correct operation of the magnetometer is the precise calibration of the measurement position, in both vertical and horizontal senses. This is because the SQUID system will not yield a correct measurement unless the sample being measured is exactly located in the centre of the sensing pick up coils, and has the correct azimuthal orientation relative to the reference direction in these coils. A computer programme is available to allow the first stage of this calibration.

In this procedure, the sample transport system sends the sample holder, containing a standard calibration sample (comprising a magnetic needle with a stable permanent magnetisation of 15-20 mA/m in its intensity), to a position just above the pickup coils, with the magnetic moment pointing approximately towards the reference azimuth of these coils. The sample is then moved progressively downwards, at

steps of 0.5 mm, readings of its magnetisation being measured after each step, until it passes through the lower boundary of the pick-up coils. Fig.2.2.2 shows a typical calibration curve, in which a minimum value between the two maximum values represents the optimum position at which the measured sample should be located. This optimum position value is then stored in the memory of the computer controlling the sample insertion system. This calibration can be checked approximately by measuring the distance from the centre point of the sample to the top of the magnetometer, when the sample is in the measurement position. This distance should be the same as that from the top of magnetometer to the centre of pick-up coils, shown in Fig.2.2.1.

To calibrate the azimuthal orientation, the same calibration sample is first measured on a Molspin spinner magnetometer to specify the precise direction of the magnetic moment. This sample is then measured on the cryogenic magnetometer, and the azimuthal position of the holder is progressively changed until the magnetic moment of the calibration sample lies along the reference axis of the SQUID. This axis can then be identified and marked on the top plate of the magnetometer.

Although, theoretically, the cryogenic magnetometer yields a precision of about 0.01-0.05 mA/m as mentioned above, it was found in the present study that in the optimum condition, in which the magnetometer was cooled and shielded properly, the "noise level" of the magnetometer (ie the measured intensity with no sample or holder present in the pick up coils) was typically <0.003 mA/m. To fully utilise this low noise level, it is very important to reduce the magnetic moment of the sample holder to the minimum possible value. The standard holder is made from Mylar and consists of three thin layers of this material wound into a tube. This produces a typical magnetisation of about 0.05 mA/m or more. However, when the two outer layers were removed from the part of the holder containing the sample under measurement, so that only one thin layer was left, the magnetisation of the holder could be reduced to less than 0.01mA/m without unduly weakening the holder strength. A similar low holder-intensity value could be obtained by cutting away most of the cylindrical sides of a triple Mylar tube, leaving only three very

narrow vertical strips supporting the sample together with the non-magnetic base plate. For either type of holder it was found possible to measure the magnetisation of samples with intensities down to about 0.04 mA/m, with a 95% confidence angle (α_{95}) less than 10° for a typical triple measurement.

2.2.2) Demagnetiser.

An important part of palaeomagnetic laboratory work is to check the magnetic stability of the samples investigated and to remove unwanted low stability components of magnetisation such as viscous components acquired in the present field, in order to reveal the stable components of magnetisation of interest. Two conventional types of demagnetisers have been used in the present study in order to achieve this. One is the alternating field (a.f.) demagnetiser and the other the thermal demagnetiser.

The a.f. demagnetiser assemblage consists of two pairs of Helmholtz coils, which are mounted on the top of the cryogenic magnetometer and shielded together with the magnetometer to protect the sample from being remagnetised in the laboratory field during the demagnetisation process (see Plate 2.2.1). One of the pairs of coils has its field axis vertical and the other has its axis horizontal; the former is responsible for demagnetising the sample along its z-axis and the latter along the x and y axes. An alternating current of 800Hz flows in each pair of coils in turn during demagnetisation. This is first increased to the appropriate value to produce the desired magnetic field. After being held at this value for 3-5 seconds the field is then reduced smoothly and continuously down to zero during a period of 10-30 seconds, depending on the peak field value used. After demagnetisation along the first (x) axis, the sample is then turned through 90° about the vertical axis and demagnetised along its y-axis. It is then moved to the vertical coil, where it is then demagnetised along the z-axis. Its magnetisation is then measured. The demagnetiser is powered by a high-fidelity power amplifier, the signal amplitude being controlled by computer (see Plate 2.2.2).

There is also a computer programme for calibrating the magnetic

field value used for demagnetisation. A pair of small pick-up coils with their axes perpendicular to each other are wound onto a sample-size (25 mm) plastic cylinder and placed in the sample holder. The pick up coils are lowered to the centre of the upper demagnetising coils. Power is applied to this coil and the position of the holder is adjusted (both in height and in azimuth) until the optimum output is obtained. The process is then repeated for the lower demagnetising coil. By comparing the outputs from the pickup coils in the two positions and changing appropriate control parameters in the computer, the fields from the vertical and horizontal demagnetisation coils are adjusted to be the same, to within ±0.1mT.

Plate 2.2.3 shows the thermal demagnetiser (Schonstedt instrument company, Model TSD1) and its controller. This type of demagnetiser consists of three parts; one is a heating compartment, the other a cooling chamber, and the third is the controller. A cylindrical shield, which is made of three layers of μ-metal surrounds the heating compartment. A further two layers (giving a total of five) shields the cooling chamber, so that residual magnetic fields are reduced to less than 5 nT in the cooling chamber. Heating is achieved by a non-inductively wound furnace. The heating temperature is contralled by means of a thermocouple and proportional temperature controller. A temperature range from room temperature to over 700^{o}C is available on the controller panel.

Once a demagnetisation temperature is set, the thermocouple and controller allow the temperature to rise in a relatively short time (~10 min) to a value close to the required temperature, after which heating is slower to allow the temperature to progressively reach the required value. For each group of samples demagnetised, the heating time varies from 30 to 45 min, depending on the set value of temperature. It is important to allow sufficient time for the magnetic moments of grains within the samples to be homogeneously demagnetised. Consequently it is necessary to use longer heating times for higher temperature. When the samples have reached the desired temperature, they are pushed into the cooling chamber (contained in a supporting quartz "boat") and cooled to room temperature by an electric fan, usually within about 20-30 min.

The maximum value of the residual magnetic field along the cooling chamber was typically less than 5 nT in the centre of the chamber, but increased dramatically to more than 100 nT at the outer end of the chamber (~100 mm to the open end). No significant increase of the residual field is found at the join between the heating and cooling chamber. Fig.2.2.3 shows the distribution of temperature in the heating oven. A ~25 cm interval near to the middle of the oven shows a fairly homogeneous (~±5 to 10°C) temperature distribution, particularly below 400°C. Samples were demagnetised while located within this part of the oven and each sample was placed in the same position during successive demagnetisation steps. The distance between adjacent samples in the oven depended on their magnetic moments. For example, if the magnetic intensity is about 0.5 mA/m, the magnetic field at 1 cm from a sample (assuming the sample represents a magnetic dipole) would be less than 5 nT. therefore, the distance between samples could be set from half to 1 cm without any risk of interaction between magnetic fields of adjacent samples.

2.2.3) The pulse magnetiser.

The characteristics of acquisition of isothermal remanent magnetisation (IRM) is an important method by which the magnetic mineralogical constituents of a sample may be investigated. As mentioned in Chapter I, magnetite and hematite in sediments will produce very different IRM acquisition curves, by means of which the magnetic constituents could be revealed in a semi-quantitative way. The Molspin pulse magnetiser used to magnetise the samples (see Plate 2.2.4) applies a strong pulse of direct magnetic field to the sample, by discharging a powerful capacitor. The procedure is simple. The sample is inserted in the central hole of the magnetising coil with its z-axis parallel to the coil axis. On pushing the start button the voltage of the capacitor bank is charged slowly, and can be read by means of a meter on the control panel. Once the charging is finished, discharge occurs and the value of the applied field can be read from a digital meter. The available field range of this instrument is up to 860 mT. The magnetised sample is then measured on a Molspin fluxgate magnetometer. The set value of the pulse magnetic field was found to

be systematically lower than the actual field applied during discharge, which is read from the digital meter. The final output value must be read directly from the digital meter very quickly at the start of discharge, which makes precise reading if the field value different.

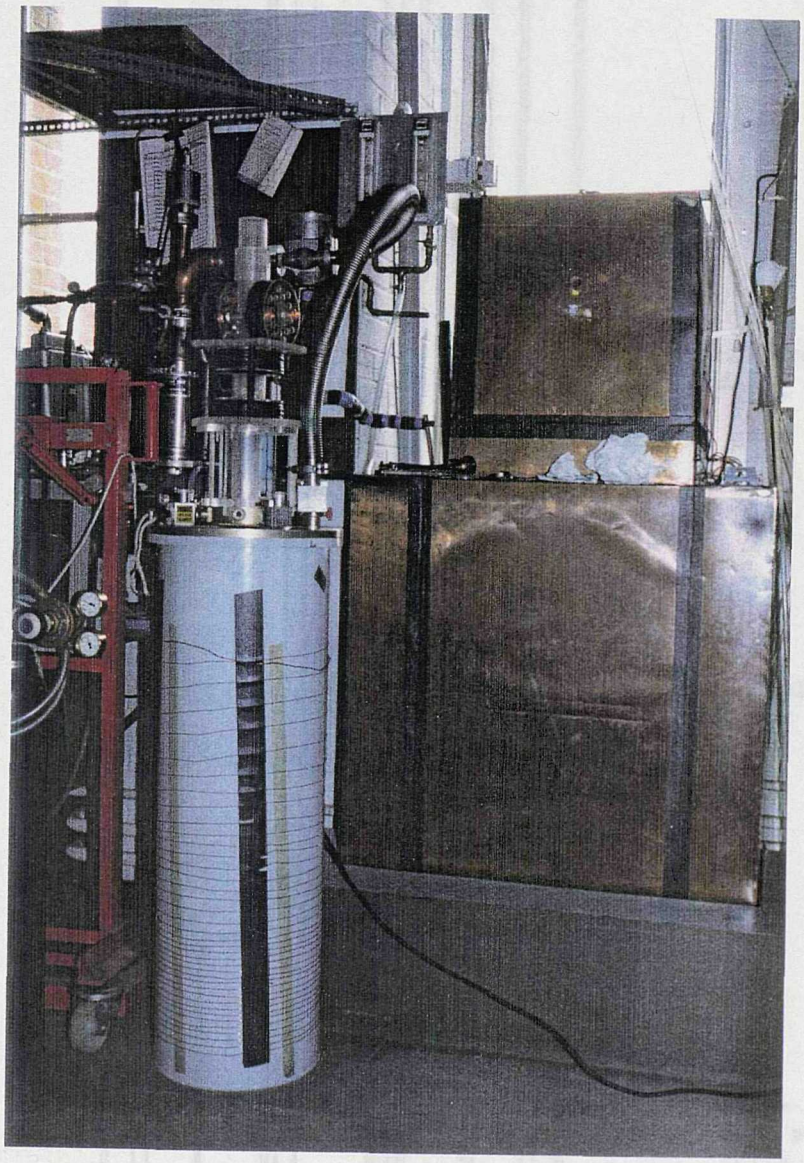

Plate 2.2.1 Assemblage of cryogenic magnetometer and 2-axis af demagnetiser. The copper-clad box in the the background contains the magnetic shielding chamber, in which the cryogenic magnetometer assemblage is mounted, when in use.

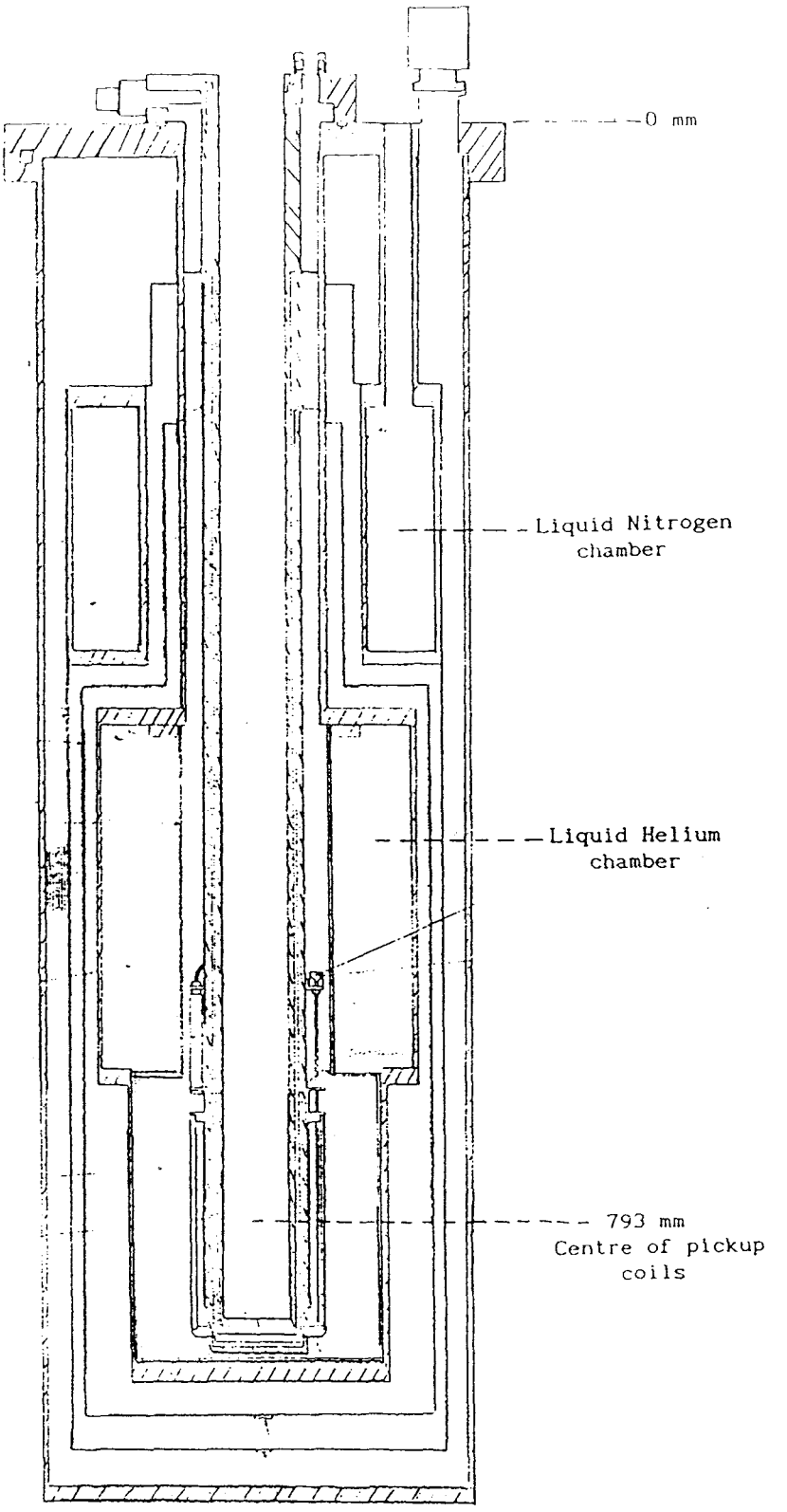

Fig.2.2.1 Basic configuration of the cryogenic magnetometer, the distance from the top plate to the centre of the pickup coils is 793 mm.

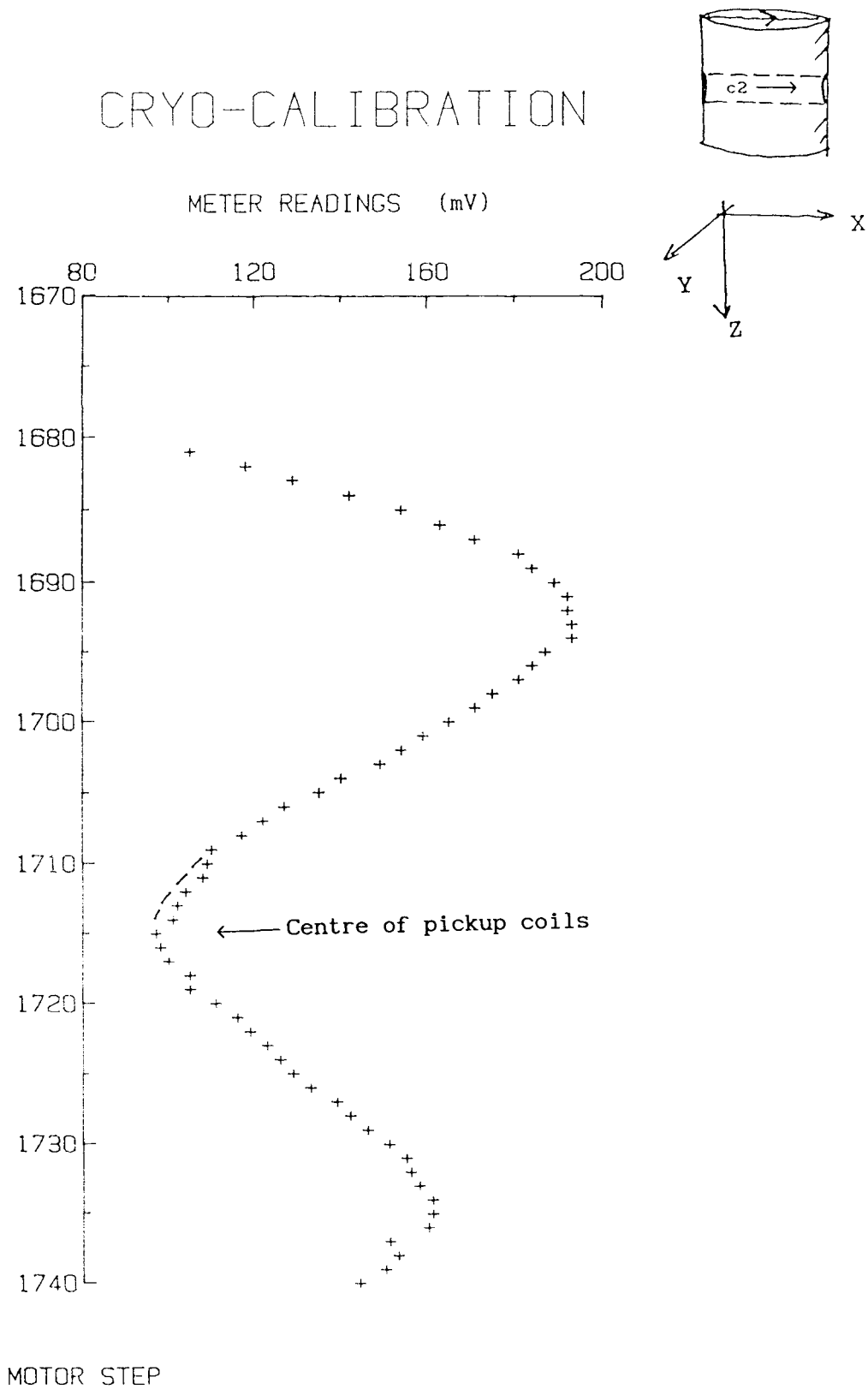

Fig.2.2.2 A downstepping calibration curve for the cryogenic magnetometer. The minimum value of the meter readings corresponds with the centre of the pickup coils. The insert diagram shows the orientation of the calibration sample, with its magnetic moment in the horizontal direction.

Plate 2.2.2 Control panel for cryogenic magnetometer. The three instrument boxes at the right hand side are the power amplifier and controllers for the af demagnetiser.

Plate 2.2.3 Thermal demagnetiser and its controller.

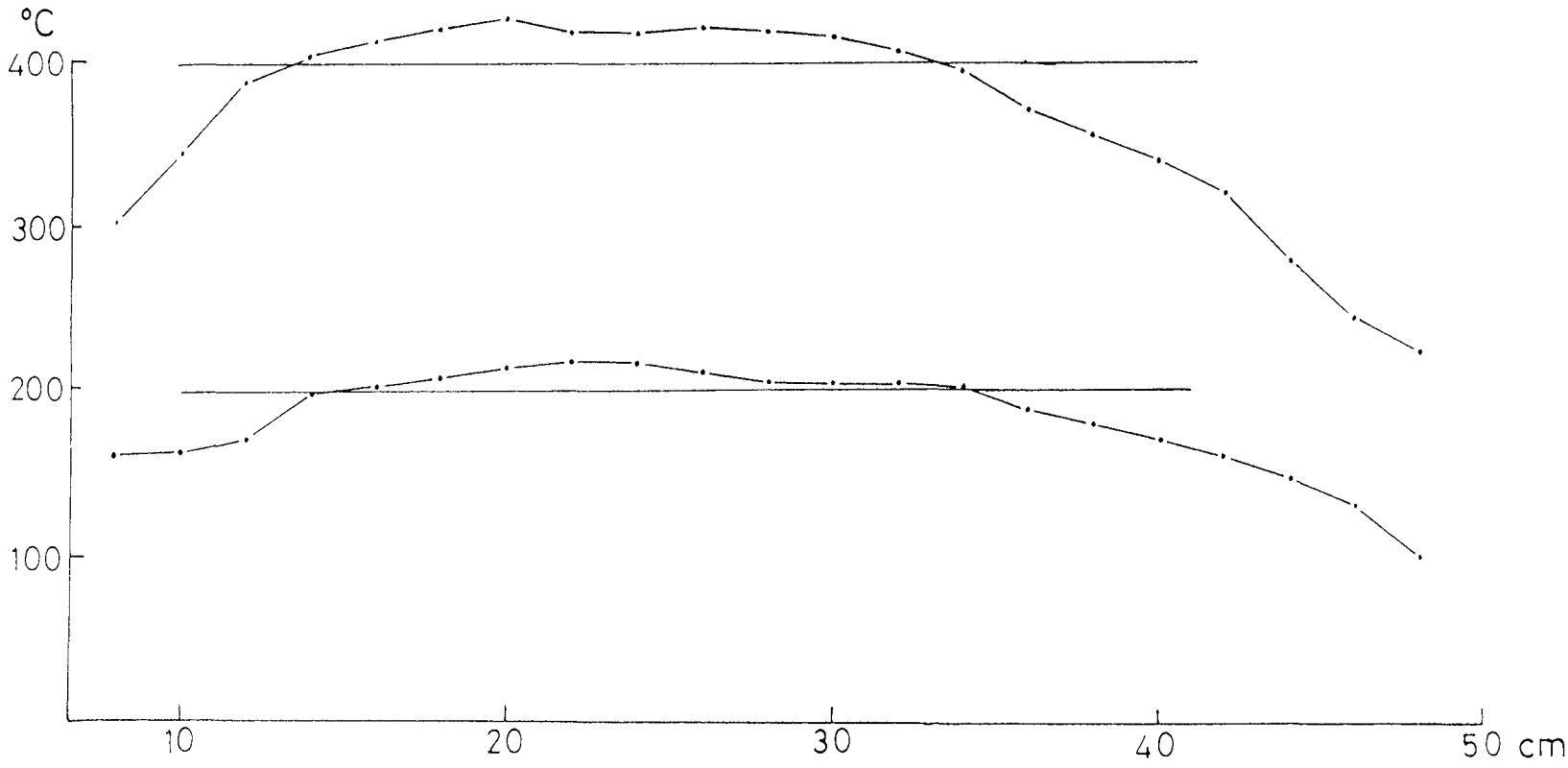

Fig. 2. 2. 3 Distribution of temperature in heating chamber of the thermal demagnetiser. The two curves refer to set temperatures of 200°C and 400°C respectively. Distance measured from the door of the heating chamber.

Plate 2.2.4 Pulse magnetiser (in the front place).

§2.3 Mathematics of palaeomagnetic data processing and data expression

2.3.1) Field and bedding correction of magnetic vectors.

Palaeomagnetic analyses commonly involve the spatial transformation of the coordinate systems in which the palaeomagnetic vectors are specified. The main coordinate transformations used are those involved in the field and bedding corrections. During field work (§2.1 of this chapter), an orientation mark was drawn permanently on each of the samples. The position of this mark is related to the direction of geographic north in sample coordinates. Vectors measured in sample coordinates are required to be transformed into coordinates in which they can be geologically or geomagnetically explained. The principle of these transformations is given in the following discussion.

For any two sets of coordinates in space with the same origin, there exist a relationship between them:

	x	y	z
X	ℓ_1	m_1	n_1
Y	ℓ_2	m_2	n_2
Z	ℓ_3	m_3	n_3

.....(2.3.1)

where (x, y, z) and (X, Y, Z) represent the two coordinate sets and (ℓ_i, m_i, n_i) (i=1, 2, 3) the direction cosines between the pairs of axes in the two coordinate systems. The matrix

$$\begin{pmatrix} \ell_1 & m_1 & n_1 \\ \ell_2 & m_2 & n_2 \\ \ell_3 & m_3 & n_3 \end{pmatrix} \qquad \text{.....(2.3.2)}$$

is called the transformation matrix. In the special case of a two dimensional coordinate system, this matrix becomes

$$\begin{pmatrix} \ell_1 & m_1 \\ \ell_2 & m_2 \end{pmatrix} \qquad \text{.....(2.3.3)}$$

A two-dimensional transformation can be applied to those cases in which a given coordinate plane (defined by two of the coordinates) is rotated around the third coordinate axis.

In palaeomagnetic field work, two different orientation systems have been commonly used, one for cores (drilled or hammered) and the other for hand samples. Fig.2.3.1 shows the orientation system used for drilled (or hammered) cores, in which the z axis is parallel to the sampling tube, or cylindrical sample axis. The azimuth of the x-z plane defines a direction with respect to geographic north. The angle between this plane and north is called "Z azimuth" (or ZAZ) according to the Southampton University palaeomagnetic laboratory convention. The x and y axes define a plane which is perpendicular to the core axis. The angle between the z axis and the vertical is called "Z plunge" (or ZPL). Because the sampling tubes are randomly inserted into the sedimentary beds, it is necessary to transfer the coordinates system from the "samples" to the "geographic" system, in which the X-axis is directed towards north, the Z-axis is downwards and the Y-axis is towards the east (note: X, Y and Z are the new coordinates for geographic system).

This transformation is commonly called the "Field Correction". It offers a view of the relationship between remanent vectors in existing beds and geographic north, without restoring the bedding plane to the horizontal. This transformation is achieved by first rotating the sample coordinates around the y axis, so that the z axis is directed downwards (related to Z-axis) and x axis horizontal (related to X1-axis, an intermediate coordinate), without changing the component of the remanent vector along the y axis. Then, the revised coordinates are rotated around the Z axis, so that the X1-axis points to the north and y axis to the east without changing the component of the remanent vector along the new Z axis. Now the remanent vector is specified in the geographic coordinate system. Fig.2.3.1(b) indicates this transformation.

According to equation (3.3.3) and Fig.3.3.1(b), the transformation matrix for the first step as described above should be

$$\begin{pmatrix} X1 \\ Z \end{pmatrix} = \begin{pmatrix} \cos(ZPL) & \cos(90^\circ - ZPL) \\ \cos(90^\circ + ZPL) & \cos(ZPL) \end{pmatrix} \begin{pmatrix} x \\ z \end{pmatrix}$$

that is,

$$\begin{cases} X1 = x\cos(ZPL) + z\sin(ZPL) \\ Z = -x\sin(ZPL) + z\cos(ZPL) \end{cases} \quad \ldots\ldots (2.3.4)$$

where x, z, X1 and Z are components of the remanent vector specified in the old and new coordinate systems respectively. The second rotation can then be carried out, in which the Z axis is kept stable and the X1-y plane is rotated, until the X1-axis points towards the geographic north and the Y-axis towards the east.

$$\begin{pmatrix} X \\ Y \end{pmatrix} = \begin{pmatrix} \cos(ZAZ) & \cos(90^\circ + ZAZ) \\ \cos(90^\circ - ZAZ) & \cos(ZAZ) \end{pmatrix} \begin{pmatrix} X1 \\ y \end{pmatrix}$$

that is,

$$\begin{cases} X = X1\cos(ZAZ) - y\sin(ZAZ) \\ Y = X1\sin(ZAZ) + y\cos(ZAZ) \end{cases} \quad \ldots\ldots (2.3.5)$$

where y and X1 are components of the vector specified in the second coordinate system, and X, Y are components in the final coordinate system, which is the same as the geographic one. Now, the three values of coordinate components of the remanent vector in the geographic system, which are related to the original system, can be combined together:

$$\begin{cases} X = (x\cos(ZPL) + z\sin(ZPL))\cos(ZAZ) - y\sin(ZAZ) \\ Y = (x\cos(ZPL) + z\sin(ZPL))\sin(ZAZ) + y\cos(ZPL) \\ Z = -x\sin(ZPL) + z\cos(ZPL) \end{cases}$$

or

$$\begin{cases} X = x\cos(ZPL)\cos(ZAZ) - y\sin(ZAZ) + z\cos(ZAZ)\sin(ZPL) \\ Y = x\cos(ZPL)\sin(ZAZ) + y\cos(ZAZ) + z\sin(ZAZ)\sin(ZPL) \\ Z = -x\sin(ZPL) + z\cos(ZPL) \end{cases} \quad \ldots\ldots (2.3.6)$$

The hand sample orientation system is shown in Fig.2.3.2. In this case, the x axis is conventionally parallel to the strike direction of the surface of the sample, which is measured with respect to geographic north. The y axis is in the dip direction, 90° degrees clockwise from the strike direction (under the right hand rule) and parallel to the

surface of the sample. Therefore, the z axis is perpendicular to the surface of the sample and regarded as positive when downwards. In the laboratory, the hand samples are usually cut with their oriented surfaces on the top. The coordinate transformation is carried out in a similar way to that described above. First, keeping the x-axis stationary and rotating the y-z plane so that the z-axis becomes vertical and the y-axis horizontal. Then, keeping the z axis stationary, the x-y plane is turned around the z axis, while the x axis points towards geographic north and the y-axis towards the east. The first step can be represented by:

$$\begin{pmatrix} Y1 \\ Z \end{pmatrix} = \begin{pmatrix} \cos(DIP) & \cos(90^\circ+DIP) \\ \cos(90^\circ-DIP) & \cos((DIP) \end{pmatrix} \begin{pmatrix} y \\ z \end{pmatrix}$$

or

$$\begin{cases} Y1 = y\cos(DIP) - z\sin(DIP) \\ Z = y\sin(DIP) + z\cos(DIP) \end{cases} \quad \ldots\ldots\ldots (2.3.7)$$

where DIP is the angle between the z axis and the vertical. Then the procedure is followed by the rotation of the x-Y1 plane:

$$\begin{pmatrix} X \\ Y \end{pmatrix} = \begin{pmatrix} \cos(STR) & \cos(90^\circ+STR) \\ \cos(90^\circ-STR) & \cos(STR) \end{pmatrix} \begin{pmatrix} x \\ Y1 \end{pmatrix}$$

or

$$\begin{cases} X = x\cos(STR) - Y1\sin(STR) \\ Y = x\sin(STR) + Y1\cos(STR) \end{cases} \quad \ldots\ldots (2.3.8)$$

where STR is the strike direction of the hand sample. Finally, combining these equations, we have

$$\begin{cases} X = x\cos(STR) - y\sin(STR)\cos(DIP) + z\sin(STR)\sin(DIP) \\ Y = x\sin(STR) + y\cos(STR)\cos(DIP) - z\cos(STR)\sin(DIP) \\ Z = y\sin(DIP) + z\cos(DIP) \end{cases} \quad \ldots (2.3.9)$$

After application of this field correction, the remanent vector is specified in the geographic coordinate system.

A similar transformation principle can be applied also to the bedding correction, by which the remanent vector will be specified in a coordinate system that represents a horizontal state of the bedding (assuming the original depositional surface was horizontal). After

field correction for either core or hand samples the coordinates are geographic, x being to the north, y to the east and z downwards. The coordinate transformation for the bedding correction is effectively the reverse of the field correction for a hand sample. The x-axis is rotated into the strike direction of the bedding around the z-axis. The y-z plane is then rotated so that the y axis is parallel to the dip of the beds. The new x-y plane is then rotated back to the geographic system, so that the final x-axis is towards the north and the z-axis still downwards. This process involves two steps of rotation and its rotation formula can be easily deduced following the principles outlined above. The orientation of a remanent vector in the coordinates after bedding correction offers a view of its assumed original direction, if the magnetism predates folding.

2.3.2) Expression of palaeomagnetic data

Directions of magnetisation can be represented as lines radiating from the centre of a unit sphere. These lines intercept the surface of the sphere. If the sphere is projected onto a horizontal or vertical plane through its centre, the direction of magnetisation can be expressed as a point on either plane. The two projections commonly used are the equatorial equal-area projection and polar equal-area projection (Fig.2.3.3). The polar equal-area projection which is used more than the other preserves the relative areas of the division on the sphere, and is useful for providing a correct impression of the distribution of points over the surface of the sphere; on this projection, a circle is projected as an ellipse with its minor axis along a radius and equal to the diameter of the circle. In polar projections it is normal practice to project the lower hemisphere only. Points on the upper hemisphere (negative inclinations) are plotted as open symbols on the projection, and on the lower hemisphere (positive inclinations) as closed symbols.

Spherical projections allow presentation of the direction, but not the magnitude of the magnetisation vector; to illustrate the change in magnitude during demagnetisation, it is necessary to employ a separate J/J_o versus demagnetising field or temperature graph. However, the magnitude and direction of the vector can, be represented by components

along three orthogonal coordinate axes, x, y and z, where x is conventionally referred to the north, y to the east and z to the vertically downward direction. A vector of magnetisation J is then the resultant of its three orthogonal components (Fig.2.3.4(a)).

$$x = J \cdot \cos D \cos I, \quad y = J \cdot \sin D \cdot \cos I \text{ and } z = J \cdot \sin I \quad \ldots (2.3.10)$$

In the projection method described originally by As (1960), Wilson (1961) and Zijderveld (1967), the end of the NRM vector is projected onto two orthogonal planes, one horizontal and one vertical (Fig.2.3.4b). By convention, solid symbols express projection onto the horizontal plane and open symbols projection onto the vertical plane. The axes are scaled in units of magnetisation. As the sample is progressively demagnetised, these projections will trace out paths defined by collective changes in declination D, inclination I and intensity J. It is advantageous to take the intersection of the two planes (either E-W or N-S) as the abscissa.

If the NRM is a vector comprising only a single component, its magnitude will be progressively reduced by demagnetisation, but its direction will remain unchanged and the projections on the horizontal and vertical planes will move along two straight lines towards the origin of the coordinates (see Fig.2.3.4b). If the magnetisation is multi-component, then the demagnetisation path will trace out a straight line, provided that only one component is being subtracted at a time, but this straight line segment will not pass through the origin. The advantage of orthogonal plots is that they give an immediate impression of the number of components constituting an NRM, and the degree to which their blocking-temperature or coercivity spectra overlap. They are capable of showing both single-component and multi-component behaviour, which may not be evident plotting the data on a spherical projection, where only the magnetisation direction can be illustrated (Piper 1987).

2.3.3) Fisher and Bingham statistics.

Fisher (1953) developed a method for the statistical analysis of a population of directions, which is routinely employed in

palaeomagnetism. It is based on a circularly-symmetrical density function, in which the directions are regarded in terms of their projections as points onto a sphere. In a manner analogous to the two-dimensional Gaussian distribution, it is proposed that they have a probability density, $p(\psi)$:

$$p(\psi) = \frac{\kappa}{4\pi \sinh\kappa} \exp(\kappa \cos\psi) \qquad .....(2.3.11)$$

where ψ is the angular distance between any point on the sphere and the mean of the population; when $\psi = 0$, the density is a maximum. The precision parameter, κ, varies from infinity when all the directions are identical, down to zero when the the directions are uniformly distributed over the surface of the sphere. The value of κ may be estimated from an approximation k (with N>7 and κ>3)

$$k = \frac{N-1}{N-R} \qquad .....(2.3.12)$$

where N is the population of the directions and R the resultant magnitude of the N directions. In practice, the directions of a population can be represented on a stereographic projection and their intensities are given unit weight in the calculation. Therefore, the resultant of N directions of magnetisation has a length R:

$$R^2 = (\sum_{i=1}^{N} x_i)^2 + (\sum_{i=1}^{N} y_i)^2 + (\sum_{i=1}^{N} z_i)^2 \qquad .....(2.3.13)$$

where x_i, y_i and z_i are the projections on three axes of these directional vectors with unit length. Provided that the N directions are non-identical, R is less than N. There is a certain probability that the vectors come from a random population if R is less than a critical value Ro. Watson (1956) summarized the 95% significance level, Ro, for a population of N vectors. If the calculated value of R is less than Ro, the population of directions can be considered to be random at this probability level.

The mean direction derived from the resultant vector as above is then calculated as

$$x = \frac{1}{R}\sum_{i=1}^{N} x_i, \quad y = \frac{1}{R}\sum_{i=1}^{N} y_i, \quad z = \frac{1}{R}\sum_{i=1}^{N} z_i$$

$$\bar{D} = \tan^{-1}\left(\frac{y}{x}\right) \quad \text{and} \quad \bar{I} = \sin^{-1}\left(\frac{z}{R}\right) \qquad \ldots(2.3.14)$$

where x, y and z are the direction cosine of the resultant vector. $\bar{D}$ and $\bar{I}$ are the mean direction of the population.

Although the precision parameter k related to the degree of grouping of the original vectors, it is not obvious when the population N increases to a large one and $k \rightarrow \infty$. Therefore, it is more useful to consider the angular distance between the true mean direction and the calculated mean for a particular probability. Fisher (1953) showed that the angular radius of the circular cone of confidence, $\alpha_{(1-p)}$, about the resultant vector is:

$$\cos\alpha_{(1-p)} = \frac{N-R}{R}\left[\left(\frac{1}{P}\right)^{\frac{1}{N}} - 1\right] \qquad \ldots(2.3.15)$$

At the 95% confidence level for N≥5 (McFadden 1980)

$$\alpha_{95} \approx \frac{140}{\sqrt{kN}}$$

For most palaeomagnetic studies, it is commonly assumed that the sets of palaeomagnetic directions satisfy a Fisher distribution and the the above analysis is used. However, many tests have shown (eg Onstott, 1980) that directions and poles are seldom distributed precisely according to the Fisher formula. In this case, a circular distribution of directions converts into an oval-shaped distribution and the distribution of geomagnetic virtual poles on application of the axial dipole formula is also shaped into an elongate distribution. In particular, when an application of intersections of great circles (eg yielded by insufficient demagnetisation or extra-overlapping of secondary components) is carried out, the distribution of intersection points will typically show an elongate or oval-distribution (eg Townsend and Hailwood 1979). Onstott (1980) has advocated the use of the Bingham (1964) density function to palaeomagnetic analysis, because it can generate distributions which are circular, elliptical or

distributed along a great circle, according to the parameters selected.

To compare with the Fisher distribution function, the Bingham distribution has a more complicated form:

$$f(L,U,K) = \frac{1}{4\pi\, d(k)} \exp[k_1(L,u_1)^2 + k_2(L,u_2)^2 + k_3(L,u_3)^2] \quad ..(2.3.16)$$

where L is a population of points on a sphere represented by direction cosines, U = (u1, u2, u3) is the matrix of three orthogonal, normalized vectors, and K= diag(k_1, k_2, k_3) is the matrix of concentration parameters. The constant of integration, d(k), is given by a spherical integration on the unit sphere. For an application of the two dimensional case, setting k_3= 0. Then the Bingham density function reduces to

$$f(L,U,K) = \frac{1}{4\pi\, d(k_1,k_2)} \exp[k_1(L,u_1)^2 + k_2(L,u_2)^2] \quad ...(2.3.17)$$

The characteristic direction in Fisher statistics is represented by **R**, which is calculated from vector summation, whereas a set of eigenvectors represents the characteristic direction in Bingham statistics. Given N points on a unit sphere, each with a direction (l_i, m_i, n_i) and mass p_i, the shape or configuration of these N points is most effectively described by considering their moment of inertia about a fixed direction, $u = (u,v,w)^T$, given by

$$\sum p_i(l_i^2 + m_i^2 + n_i^2) - \sum p_i(l_i u + m_i v + n_i w)^2 \quad ...(2.3.18)$$

(Mardia 1972). This equation can be written into matrix form:

$$T = \begin{pmatrix} \sum l_i^2 & \sum l_i m_i & \sum l_i n_i \\ \sum l_i m_i & \sum m_i^2 & \sum m_i n_i \\ \sum l_i n_i & \sum m_i n_i & \sum n_i^2 \end{pmatrix} \frac{p_i}{\sum p_i} \quad ...(2.3.19)$$

The eigenvectors ($t_{min}, t_{int}, t_{max}$) and eigenvalues ($\tau_{min}, \tau_{int}, \tau_{max}$) of the matrix T are analogous to the vector summation resultant, **R**. The eigenvectors, t_{min}, t_{int} and t_{max} are the best estimates of the true eigenvectors, u_1, u_2 and u_3, and the eigenvalues, τ_{min}, τ_{int} and τ_{max}

are the basis for statistical inference. If the distribution of directions is unipolar, like that in the Fisherian case, and p_i = 1, then the mean vector, **R**, will tend to coincide with the eigenvector, τ_{max}. As shown in Table 2.3.1, adapted from Mardia (1972), the distribution of these N points can be qualitatively described by the relative magnitudes of the eigenvectors (τ_{min}, τ_{int}, τ_{max}).

Table 3.3.1 Relation between Bingham statistical parameters and vector distributiions (from Mardia 1972).

nature of the eigenvalues	Bingham concentration parameters k_1, k_2	type of distribution
1) $\tau_{min} \approx \tau_{int} \approx \tau_{max}$	$k_1 \approx k_2 \approx 0$	uniform
2) $\tau_{min} < \tau_{int} \ll \tau_{max}$	$k_1 < k_2 \ll 0$	unimodel, if R is large, bimodel otherwise, and elliptically shaped.
3) $\tau_{min} \approx \tau_{int} \ll \tau_{max}$	$k_1 = k_2 \ll 0$	unipolar if R is large, bipolar otherwise.
4) $\tau_{min} \ll \tau_{int} < \tau_{max}$	$k_1 \ll k_2 < 0$	asymmetric girdle, elliptically shaped.
5) $\tau_{min} \ll \tau_{int} \approx \tau_{max}$	$k_1 \ll k_2 \approx 0$	symmetric girdle.

Although in Fisher statistics the dispersion of the distribution is described by the concentration parameter (or precision parameter) κ, called the "unbiased estimate", Bingham statistics has no such analogous unbiased estimate, as simple as that equivalent to k. In both of these statistical methods, the estimates **R** or ($t_{min}, t_{int}, t_{max}$) are surrounded by a region in which it probable that the true direction u or (u_1, u_2, u_3) is located. For the Fisherian case, **R** is enclosed within a cone of confidence of radius, α_{95}, which is integrated from the distribution of the concentration parameter, κ, conditional on **R**. The analogues in Bingham statistics would be based on a distribution function for $k=(k_1, k_2, 0)$ conditional on the eigenvalues ($\tau_{min}, \tau_{int}, \tau_{max}$).

[Note: A computer programme is available in the palaeomagnetism laboratory, which calculates the essential parameters of Bingham statistics for a set of directional values. They are the eigenvalues, ($\tau_{min}, \tau_{int}, \tau_{max}$), the eigenvectors ($t_{min}, t_{int}, t_{max}$) which are represented by declinations and inclinations of each vector, precision

parameters (k_1, k_2) and the 95% confidence value. It should be noted that the calculated eigenvectors ($t_{min}, t_{int}, t_{max}$) are labeled x-, y-, z-axis respectively in the output from this programme.]

2.3.4) Analysis of multi-components and great circle fitting.

The magnetic vector can be described by a line in three-dimensional space. The tip of the vector is a point which traces out a path with progressive demagnetisation (see §2.3.2 of this chapter). Depending on the composition of the vector, this path may trace out a straight line or a curved line. A straight line usually results from the progressive removal of a single magnetic component; if this is the only component present, the point migrates towards the origin. A curved path lying in a plane occurs when two discrete magnetic components (not co-linear) are being simultaneously removed at different rates. A path which does not lie in a plane is produced by the simultaneous removal of three or more components (Halls 1976, Dunlop 1979).

The single magnetisation in the linear example is simply demonstrated by the clustering of directions on a spherical projection and the linear convergent paths (for both horizontal and vertical planes) on an orthogonal vector plot, which is conventionally called a demagnetisation "stable end point" (SEP, see Fig.2.3.5a). For the case of two remanences which have different blocking temperature or coercivity spectra, a great circle trajectory of the directional vectors may be recognised, followed by a clustering of points on the stereographic projection (or a linear trace towards the origin on the vector plots), if the softer spectrum of blocking temperature (or coercivity) does not overlap the harder one (which in some cases represents the primary component, see Fig.2.3.5b).

However, in many cases, the directional trajectory shows a continuous trend towards a certain area on the projection (representing either a normal or reverse polarity) without actually reaching a stable end point. This may be because of either strong-overlap of the two blocking temperature or coercivity spectra (Dunlop, 1979) or an insufficient level of demagnetisation (eg see Fig.2.3.6).

A numerical method for analysing great circle convergence has been developed in the present study to define the characteristic stable direction represented by the higher blocking temperature (or coercivity) part of the spectrum. It is similar to the method described by Halls (1978), but does not involve complicated least squares computation.

The equation for a great circle on a unit sphere, which has the same origin as the sphere, can be represented by a set of equations as follows:

$$\begin{cases} X^2 + Y^2 + Z^2 = 1 & \text{(unit sphere)} \\ A + B + C = 0 & \text{(the plane through the origin)} \end{cases} \qquad \ldots(2.3.20)$$

where the first equation represents the unit sphere and the second is a plane which passes though the same origin as the sphere. A, B, and C are the direction cosines of the vector pole to this plane. The intersection curve of these two equations represents a great circle on the unit sphere. According to geometry, the direction of the pole to this plane (i.e. the "pole vector") can be derived from the vector product of any two vectors within this plane, as follows:

$$\text{e.g.} \quad \begin{cases} \vec{a} = (a_1, a_2, a_3) \\ \vec{b} = (b_1, b_2, b_3) \end{cases}$$

$$\vec{a} \times \vec{b} = \begin{vmatrix} \vec{i} & \vec{j} & \vec{k} \\ a_1 & a_2 & a_3 \\ b_1 & b_2 & b_3 \end{vmatrix} = \left\{ (a_2b_3 - a_3b_2),\ (a_3b_1 - a_1b_3),\ (a_1b_2 - a_2b_1) \right\} \qquad \ldots(2.3.21)$$

where the a_i and b_j (i, j = 1,2 and 3) are the vector components of $\vec{a}$ and $\vec{b}$ on the x, y and z axes respectively. Those components within the large bracket ,{ }, are the components of the pole to the required plane (ie the pole vector).

A portion of a great circle trend, defined by at least three

vector points and having a clear trend towards an end point as the demagnetisation level increases, will be able to define a set of more than three pole vectors, each derived from the product of successive pairs of magnetisation vectors. Thus, the three products are formed by multiplying the first and second vectors, the second and third vectors and the first and third vectors respectively. Therefore, for any given directional trajectory the total number of pole vectors for a single fitting plane is $(N \times N-N)/2$, where N is the number of vector points defining the trend. The mean value of these pole vectors will then define a mean pole direction representing the best estimate of the pole to the great circle trend. Fisher statistics can be used for calculation of the mean of the pole vectors, assuming that the distribution of this pole vector set follows a Fisher statistical distribution. Alternatively, Bingham statistics can be used.

Fig.2.3.7 shows an example, in which the directional trend is defined by a set of seven vector points distributed randomly around part of a great circle (the equator of the projection). The number of calculated pole vectors is $(7 \times 7-7)/2 = 21$. These are distributed symmetrically around the vertical (centre of the projection) with an elongated shape. Fisherian statistics yielded a mean direction for the set of poles as Dec = 28.5° and Inc = 89.2°, Whereas the Bingham statistics gave a maximum eigenvector, τ_{max}, of Dec = $4.4^{\circ}$and Inc = 89.5°. Therefore, there is not a significant difference between results from the two statistical methods in this case and for convenience Fisherian statistics could be reasonably applied to this calculation.

A set of different directional trends will yield a set of great circles, each represented by Equation 2.3.20. There will be two antiparallel intersection points on the unit sphere formed by any given pair of converging great circles. These points can be defined from the product of the mean pole vectors for the individual great circles. Using the same method as described above (Equation 2.3.21), the direction cosines of the intersection points are

$$\alpha = \begin{vmatrix} B_1 & C_1 \\ B_2 & C_2 \end{vmatrix} = B_1C_2 - B_2C_1$$

$$\beta = \begin{vmatrix} C_1 & A_1 \\ C_2 & A_2 \end{vmatrix} = C_1A_2 - C_2A_1 \qquad \ldots(2.3.22)$$

$$\gamma = \begin{vmatrix} A_1 & B_1 \\ A_2 & B_2 \end{vmatrix} = A_1B_2 - A_2B_1$$

where A, B and C have the same meaning as in (2.3.20) and $i(i=1,2)$ represents the given pair of planes.

Fig.2.3.8 shows an example of the calculation for an intersection point, in which two directional trajectories were chosen from a stereographic projection. A graphic method using the equal area projection was first applied and produced a "predicted" intersection point for these two trajectories at Dec = 295° and Inc = -39° (the minimum reading on the equal area projection is 1°). Then the great circle fitting calculation was followed. This gave a result Dec = 297° and Inc = -37°, which is only 2° different from the result using the graphic method.

However, because each pair of directional trends can produce two antipodal intersections, unless the results from equation (2.3.22) are constrained in some way, the resulting sets of intersection points will be randomly distributed on the unit sphere. In order to constrain the results, it is necessary to specify whether the directional trend defined by each great circle is towards a "normal" or "reverse" polarity. The programme then determines the intersection points for either the normal or the reverse polarity group of vectors.

This is carried out by the following procedure. First, an expected mean direction is defined. For example, for a reverse polarity this might have a declination of 180° and an inclination of -60°. Then a coordinate transformation (analogous to §2.1) is carried out to rotate this reverse polarity vector to the centre of the projection (ie to change the inclination to -90°. This rotation is applied to each of the intersection points in turn. Those intersections on the new upper hemisphere will then be accepted, while

those on the lower hemisphere will be inverted before incorporation into the mean vector calculation. If the directional trajectories used for the calculations are all well defined (ie. with long and smooth trajectories and low Fisher 95% confidence values (α_{95}) for the group of pole vectors), the calculated intersections will be mostly concentrated around the pole of the projection with, perhaps, just a few scattered points closer to the corresponding equator. Consequently, the pre-chosen mean direction for the coordinate transformation would not cause significant error in the intersection judgement or the final mean pole for this set of intersections. Of course, if the final mean pole for the intersections departs significantly from the predicted mean, then the whole procedure can be repeated by inputting an alternative "predicted" mean direction value. The group of intersection points is then subjected to Bingham statistical analysis to determine the mean direction and α_{95} confidence ellipse.

A major advantage of this new method over the original method of Hall (1976,1978) is that the present programme uses the final set of intersection points to work out the statistical parameters. Thus the eigenvector t_{max} and eigenvalue τ_{max} is utilized, and this is more insensitive and robust with respect to change in the sample population or outlying spurious data points than the t_{min} value. In contrast, Hall's (1978) method uses the pole direction to do this, ie. the eigenvector t_{min} and eigenvalue τ_{min} are used. Therefore, caution must be exercised when applying Hall's method (Onstott 1980). A computer program has been written to accomplish this analysis, named "G./Inters." within the large program "RMSTERO4" (see Appendix 13).

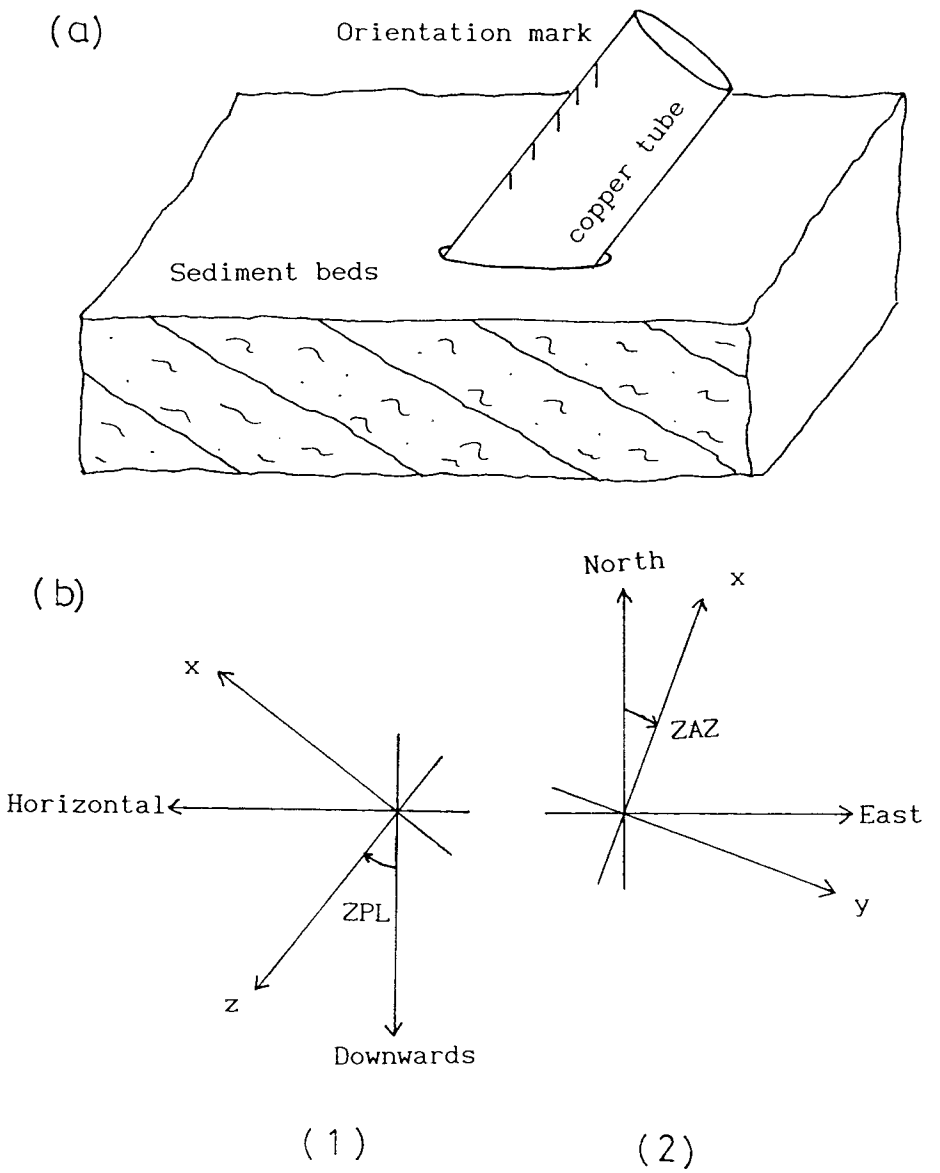

Fig. 2.3.1 Orientation system for cored sample. (a) A copper tube is inserted into the sediment beds with the orientation arrow upwards (-z axis). (b) separate two-dimensional coordinates for a sample, in which the z-axis in (b-1) is along the tube-axis; after transferred x-axis to horizontal and z-axis to vertical, (b-2) indicates the intermediate coordinates with resect to the geographic one.

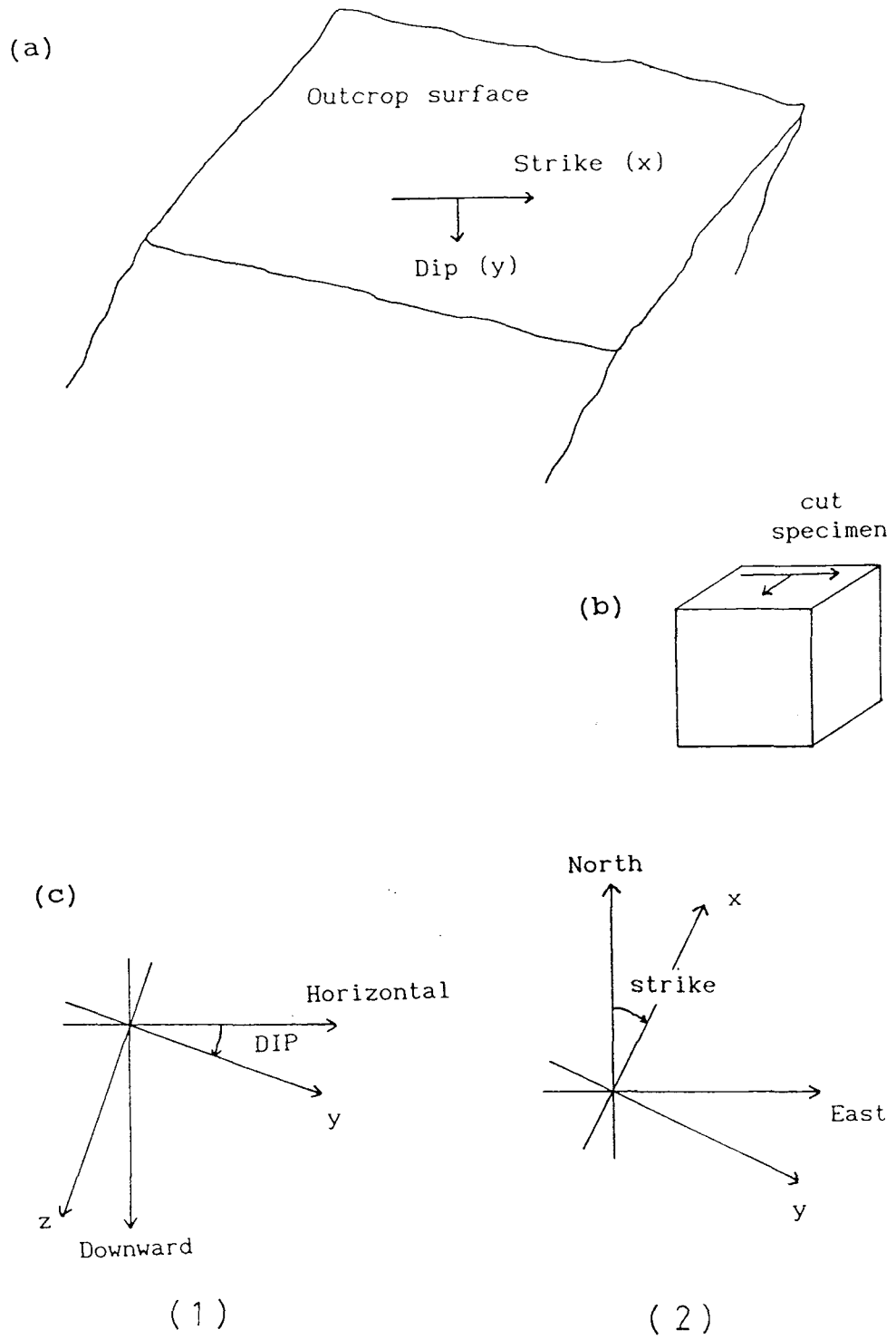

Fig. 2.3.2 Orientation system used for hand samples. (a) Orientation mark on the surface of hand sample. (b) Cut specimen with orientation mark on its top. (c) Separate two-dimensional coordinates for hand sample, in which the y-axis in (c-1) is along the dip and z-axis perpendicular to sample surface; after transferred y-axis to horizontal and z to vertical, (c-2) indicates the intermediate coordinates with respect to the geographic one.

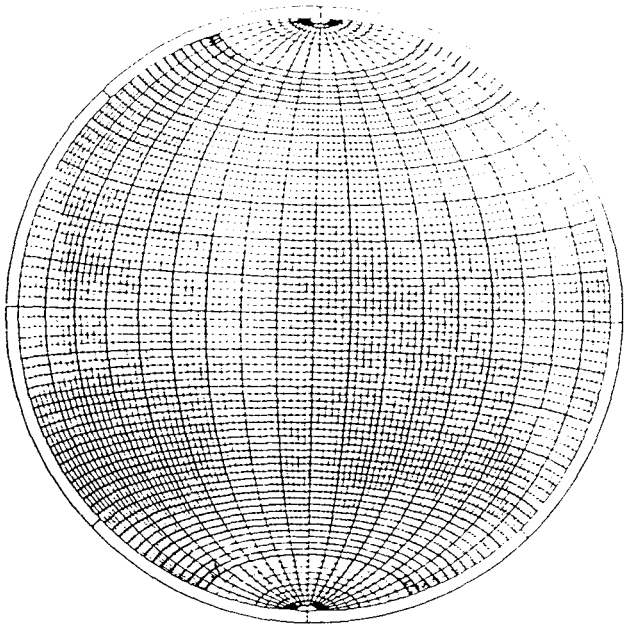

(a) Equatorial equal-area (Lambert or Schmidt) projection

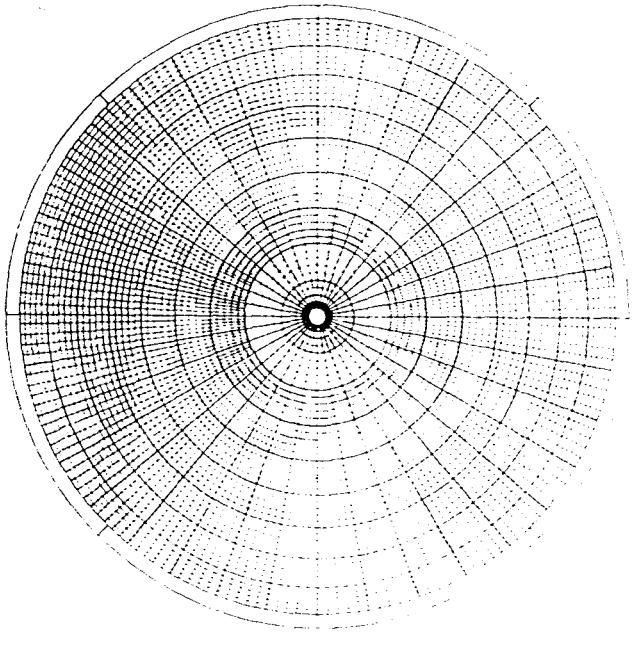

(b) Polar equal-area (Lambert) projection

Fig. 2.3.3 Equal area projections conventionally used in palaeomagnetic studies.

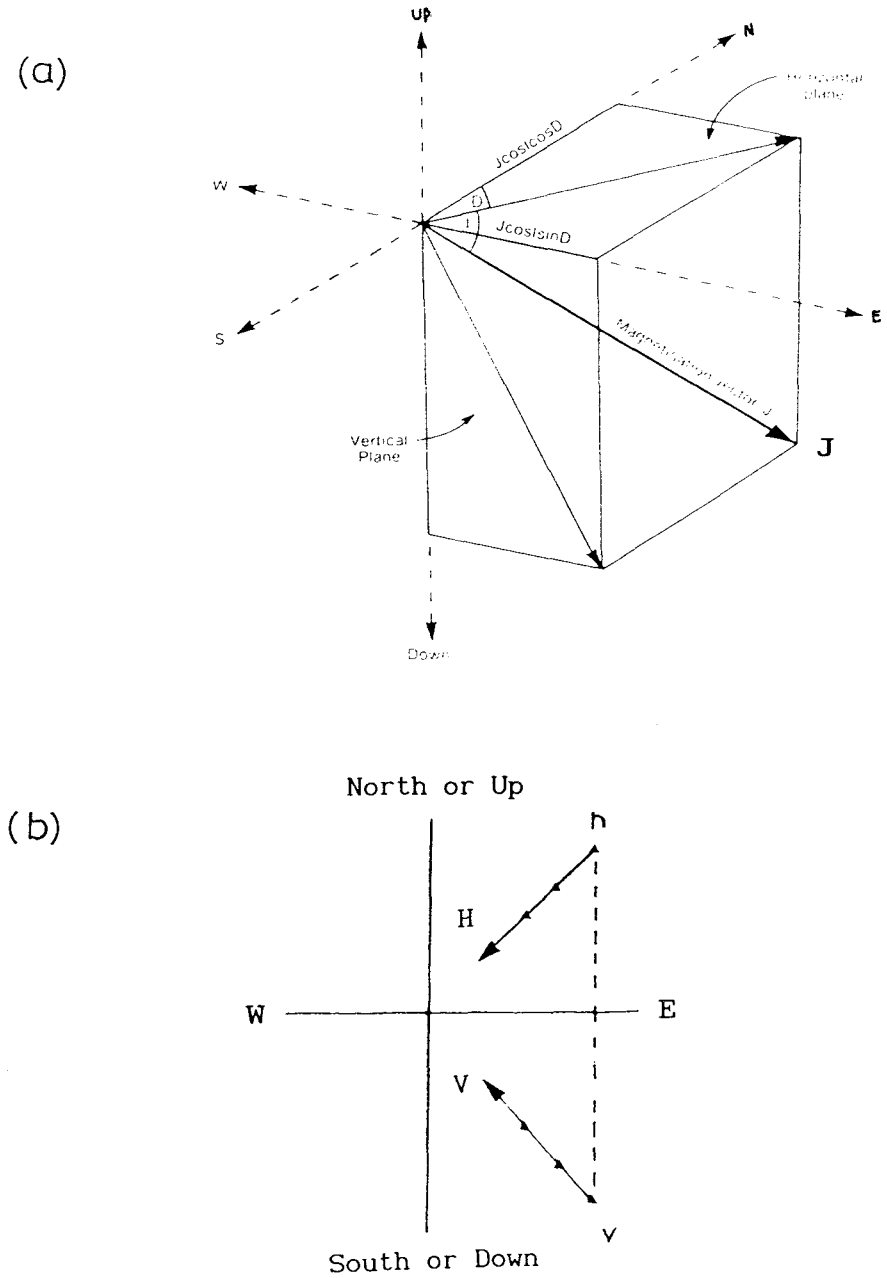

Fig. 2.3.4 (a) Projections of magnetisation J onto three axes of geographic coordinates, (b) demagnetised magnetic vector in a coordinate plot with combined horizontal and vertical planes, in which h represents the component projected onto the horizontal plane and V the component on the vertical plane (from Piper 1987).

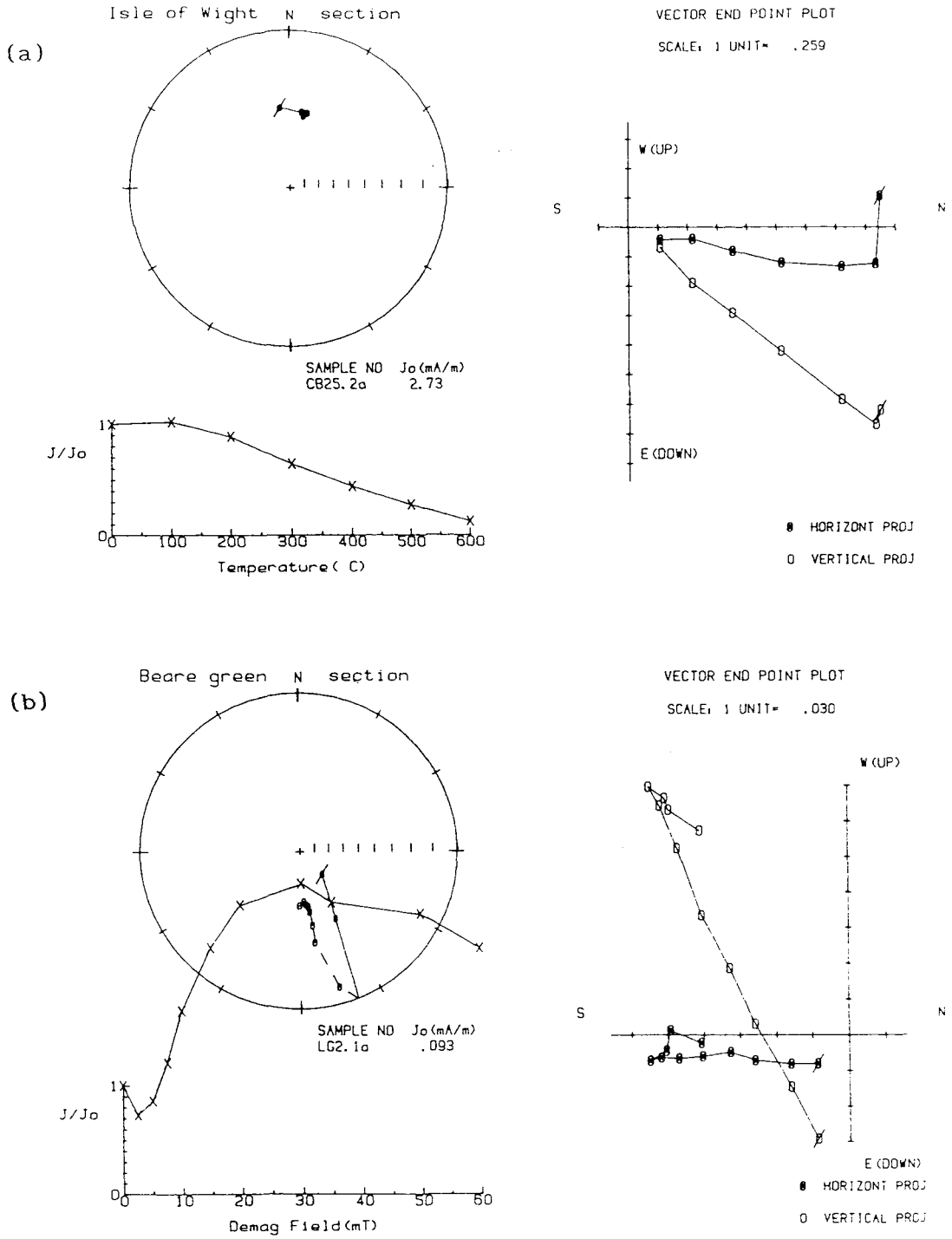

Fig. 2.3.5 Single and multi-component magnetisation in sedimentary samples revealed by thermal and a.f. demagnetisations. (a) Single component and (b) two components, one of which is removed by demagnetisation at 30 mT and the other revealed at 30-60 mT.

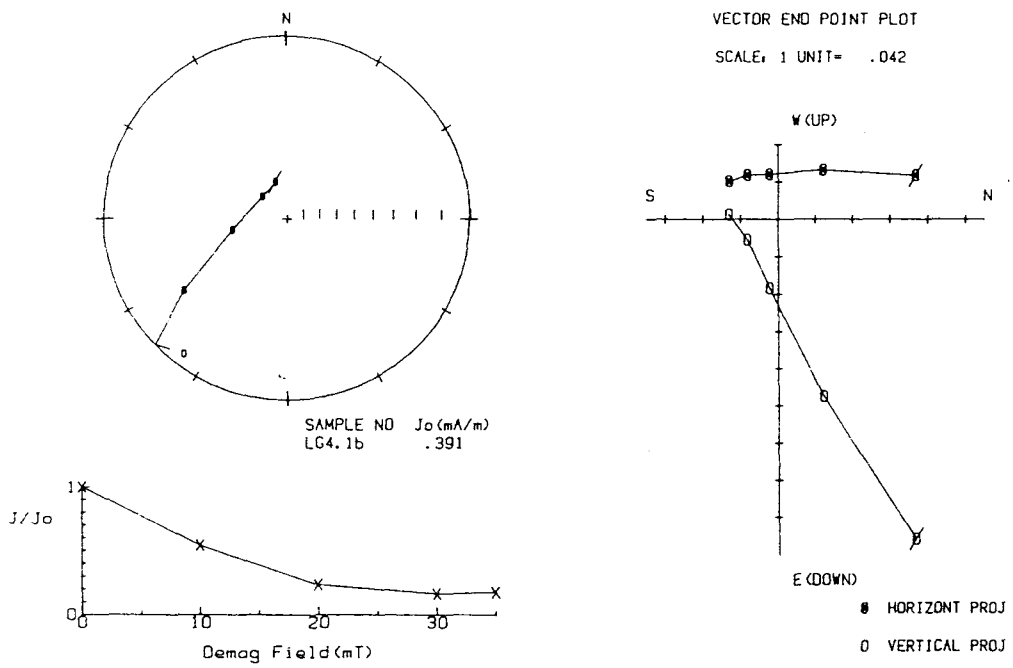

Fig.2.3.6 An example of a sample showing a directional trajectory towards a reverse polarity by 35 mT a.f. demagnetisation.

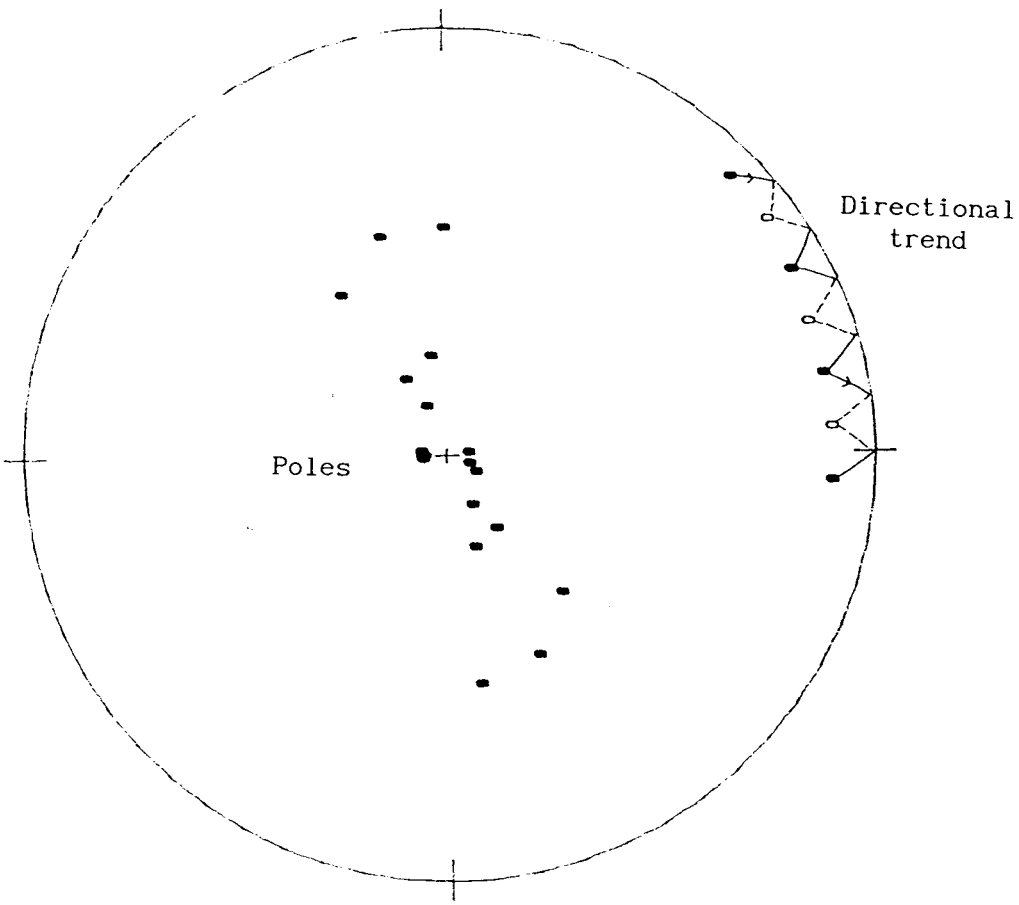

Fig. 2.3.7 An example of a set of points distributed about part of a great circle (with each point about 6-10° away from the great circle, which is represented by the equator of the projection). The calculated poles (from Equation 2.3.21) to the great circle are shown. The distribution shows an elongate incomplete symmetrical pattern, probably caused by the shortness of the tested directional trend. The mean pole direction is Dec = 28.5°, Inc = 89.2° for Fisherian statistics and Dec = 4.4°, Inc = 89.5° for Bingham statistics.

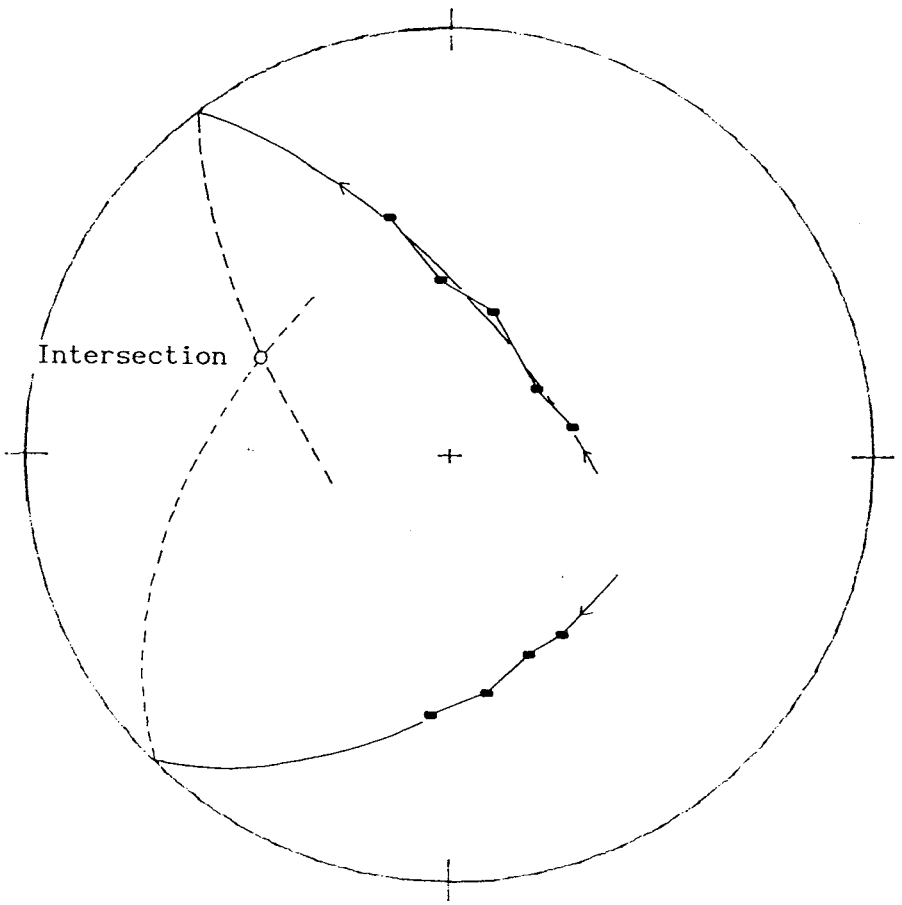

Fig.2.3.8 An intersection produced by two directional trends towards a reverse polarity end point. The direction of the intersection point is Dec = 295°, Inc = -39° for the graphical method and Dec= 297°, Inc = -37° for the great circle fitting calculation.

CHAPTER III GEOLOGY OF THE LOWER CRETACEOUS IN SOUTHERN AND SOUTHEAST ENGLAND

§3.1 The Lower Cretaceous and its distribution in the UK.

d'Omalius d'Halloy (1822) originally introduced the term "*terrain cretaces*" to describe the conspicuous chalk formations of NW Europe. The term takes its name from "*creta*", the Latin for chalk. This is the most conspicuous rock-type in Europe, and Cretaceous chalk formation are also well know from other parts of the world, including North America and Western Australia. The Cretaceous strata have been subdivided principally on the basis of ammonite zonations.

In total, 12 Stages have been defined in the Cretaceous period. The Late Cretaceous (or Upper Cretaceous) and Early Cretaceous (or Lower Cretaceous) are generally accepted as the major subdivisions of the whole period. The Cretaceous period lasted about 69 m.y. (Hallam *et al* 1985), the Upper Cretaceous having a duration of ~29.5 m.y. and the Lower Cretaceous ~39.5 m.y.. Table 3.1.1 summarizes the durations of the Cretaceous stages (from Hallam *et al* 1985). The earlier Cretaceous ages (Berriasian to Barremian) are considered by Hallam *et al* (1985) to have a reliability of only ±5 m.y. in this time scale. The reliability of the Aptian ages is little better, but those of the Albian are probably about ±3 m.y. The Late Cretaceous dates are now considered reliable to about ±1 m.y., in terms of the radiometric time scale (Hallam *et al* 1985).

In the Late Jurassic, a wide-spread phase of earth movements (the Late Cimmerian movement) transformed most of northwest Europe into a land area. The lower Cretaceous sediments then accumulated in several discrete basins around the British Isles and northwest Europe. Fig.3.1.1 shows some of the principal depositional basins. On mainland Britain, there were three Lower Cretaceous depositional areas: 1) North of the Anglo-Brabant Massif, from Norfolk to east Yorkshire, where shallow water sediments accumulated on a stable platform. This area is limited to the east and north by the Dowsing Fault line and its continuation, the Market Weighton Hinge (MWH), 2) The Yorkshire Basin, which is the northward continuation of the former area, north of the

MWH, in which the Speeton Clay accumulated. 3) The Wessex-Weald Basin, which was part of the Anglo-Paris Basin until the Aptian stage. This basin maintained an intermittent connection with the East Midland Shelf through a narrow seaway fringing the western margins of the Anglo-Brabant Massif (Rawson *et al* 1978).

The Lower Cretaceous deposits of Britain may be divided into the following stages: 1) Valanginian, 2) Hauterivian, 3) Barremian, 4)Aptian and 5) Albian. The series yields evidence of deposition under very different conditions in the northern and southern areas of England. The northern group of deposits (eg the Spilsby Sandstone, Claxby and Tealby Beds, Speeton Clay, etc.), which occur in Lincolnshire and Yorkshire, is marine throughout, whilst the southern or Wealden group, found in the Weald area, the Isle of Wight, the southern coastal area of Dorset and Oxfordshire etc., shows evidence of lacustrine conditions which became marine in the Aptian and Albian stages.

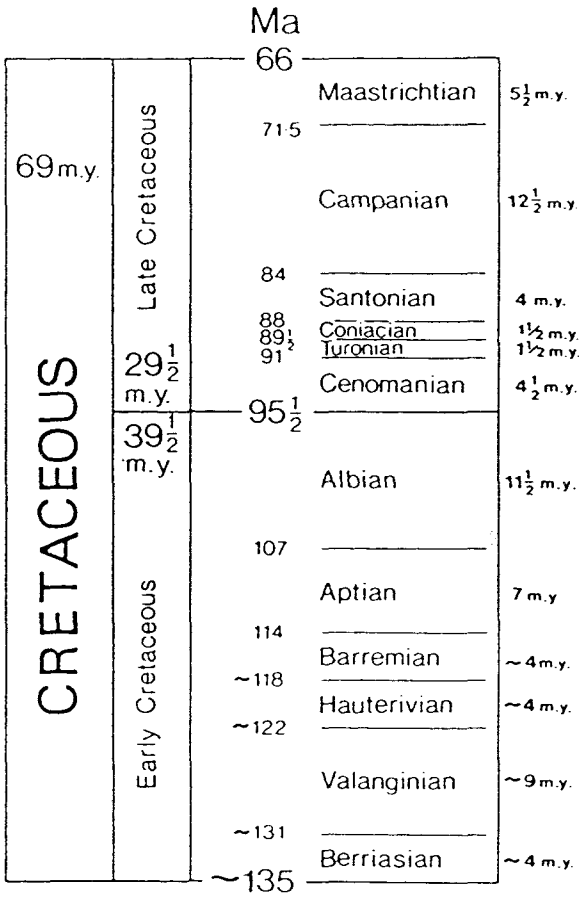

Table 3.1.1 Chronological subdivisions of the Creatceous, based on Hallam (1985).

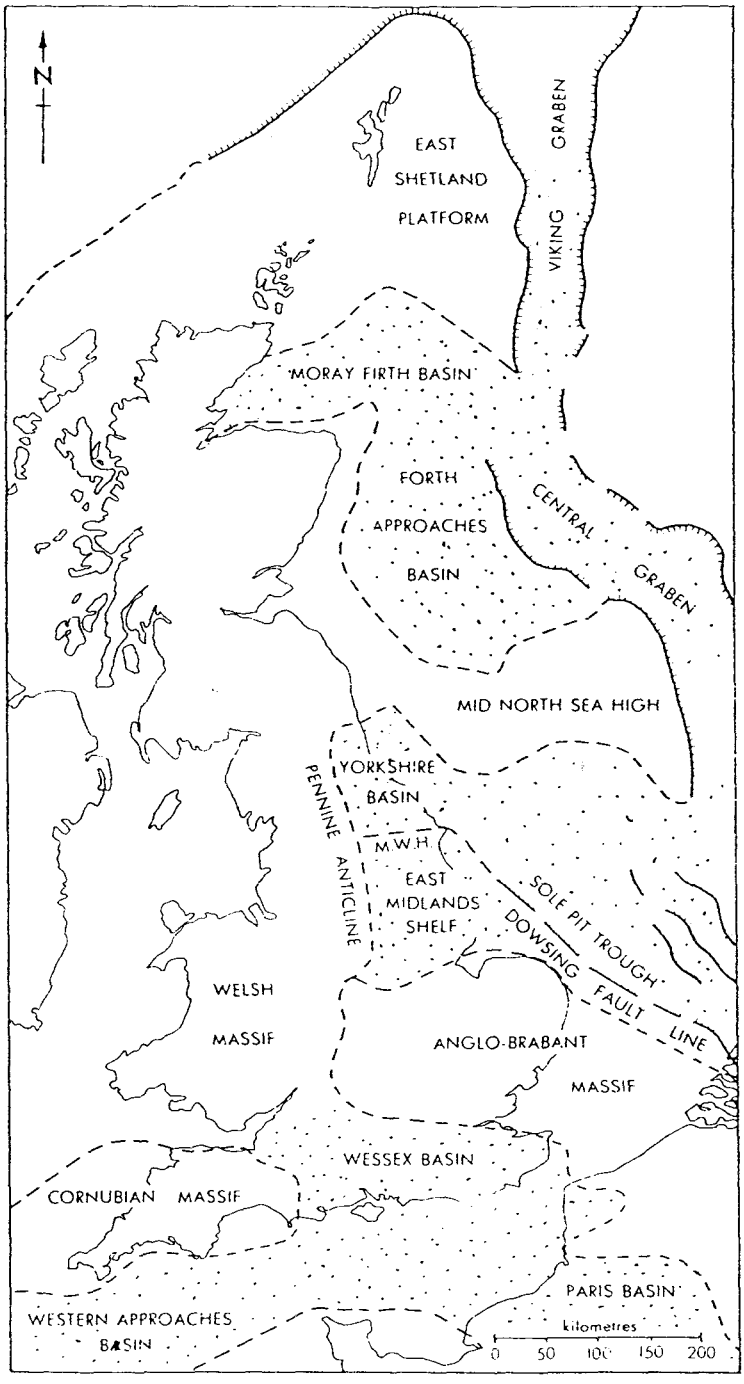

Fig. 3.1.1 The main depositional areas in Britain during the Cretaceous stippled). Note the Sole Pit Trough was inverted during the Cretaceous, M.W.H. ——Market Weighton Hinge (after Rawson *et al* 1978).

§3.2 Geology of the Wessex-Weald Basin.

3.2.1) Depositional environment.

For magnetostratigraphic studies, the Wessex-Weald area of south-southeast England presents more suitable exposures than its counterpart in northeast England, where, although biostratigraphic zones are well-defined from ammonite and other species, the weathered outcrops make it difficult to sample systematic profiles for the purpose of palaeomagnetic study.

Near to the Jurassic-Cretaceous boundary, important tectonic movements took place over much of NW Europe. An invasion of the sea spread over a large part of southern England. The Wessex-Weald Basin was formed during that time. Casey (1963) and Howitt (1964) identified the principal palaeogeographic features at the very early stage of the Cretaceous in southern England by contouring the base of the Purbeck Beds defined from borehole data throughout the region. Fig.3.2.1 shows the contour chart. It can be seen that, although the whole basin belongs to the same depositional regime, a structural high to the northwest of the Isle of Wight separates the Weald Basin to the east from the Wessex Basin to the west (along the southern coastal area of England). Fig.3.2.2 shows the relation between the Wessex-Weald Basin and the northern deposition regions in the Cretaceous. The Weald Basin was connected intermittently to the northern area by a seaway through north Oxfordshire. At the same time the Wessex Basin was mainly drained from the northwest to the southeast into the Paris Basin (Stewart 1978).

Stewart (1978, 1981, 1983) and Allen (1955, 1959, 1975) have investigated the two depositional sub-basins for many years. Available evidence suggests that both basins had non-marine depositional environments and that rivers draining from the flood-plain brought high suspended-load stream sediments into the basins. Strong currents occurred periodically and alternated with channel-dry periods due to seasonal change. The climate was typically a tropical one. Allen (1955, 1959, 1965, 1967) has long considered that the main sedimentary body, the Weald Clay of the Weald Basin, probably spans the Hauterivian

stage and the entire Barremian stage. This is supported by spore (Hughes and Moody-Stuart 1967) and ostracod (Anderson 1973) evidence. However, the lack of ammonite and ostracod data for the Wessex Basin makes age estimates for the Lower Cretaceous deposits of this area difficult. Recently Hughes and McDougall (1989) have found some evidence of small pollen palynomorphs using scanning electron microscopy (SEM). The results suggest that the main sedimentary body, the Wessex Formation, which extends from the Isle of Wight westerly to Swanage and Worbarrow Bay is mostly of Barremian age with its lower part of Hauterivian age.

3.2.2) Lithostratigraphy of the Wealden Beds.

Fig.3.2.3 summarizes the main features of the Lower Cretaceous sediments of the Wessex and Weald Basins. The sedimentology of these basins is relatively simple. In the Isle of Wight, two formations can be recognized below the Aptian Stage, in the interval which is the main concern of the present study. These are the Wessex Formation in the lower part (Stewart 1978) (previously termed the Wealden Marls as listed in Fig.3.2.3) and the Vectis Formation in the upper part (previously Wealden Shales). In Dorset the majority of the sedimentary succession representing this interval comprises variegated marls and sandstones. These are also overlain by the Lower Greensand Formation. In the Weald District the Wealden Beds are separated into the Hastings Beds below and the Weald Clay Formation above. These are overlain by the equivalent of the Lower Greensand Formation, which is subdivided into several clearly identifiable lithological units. The relative ages of the formations discussed above and their correlations to the geological stages are based on limited biostratigraphic information, and some controversies still exist (eg Kerth and Hailwood 1988, Hughes and McDougall 1989).

Although the two sub-basin areas of southern England represent separate depositional basins with different depositional histories, the depositional environment was similar in both, represented by continental type sediments. The Isle of Wight area lay in the Wessex Basin, and only the upper part of the sequences (about 200 m), extending through the Vectis and Wessex Formations, is exposed. The

Wealden Group reaches a maximum thickness of 700 m at Swanage Bay, west of the Isle of Wight (Arkell 1947). The sequence becomes thinner rapidly to the west of Swanage and, 45 km away at Durdle Door, it is only 70 m thick (see Fig.3.2.4). The thinning is largely associated with a facies change within the fluvial Wessex Formation from braided stream and possible alluvial fan facies at the basin edge to meandering stream and overbank facies at the basin centre (Stewart 1978, 1981). The Wessex Formation is dominated by vari-coloured mudstones and siltstones interpreted mainly as flood-plain deposits, with subordinate sandstones representing the deposits of mixed-load, meandering streams.

The Wessex Formation is overlain by the geographically more restricted Vectis Formation (see Fig.3.2.3), which has a maximum thickness of 60 m at Atherfield in the southwest Isle of Wight. This formation then diminishes in thickness rapidly westwards to less than 30 m at Compton Bay, northwest of Atherfield, and is only about 10 m thick at Punfield Cove, Swanage. The westerly attenuation continuous through Purbeck, reducing then to 4 m at Corfe Castle and to zero at Worbarrow Bay. This formation consists of evenly stratified dark shales with occasional thin bands of shelly limestone in the Isle of Wight, where its lower part conformably overlies the Wessex Formation. Anderson (1967) proposed that the sediments of the Vectis Formation belong to the *Cypridea valdensis* ostracod zone of presumed upper Barremian age. However, Arkell (1947) thought that it is possible there is an important break between the Wessex Formation and the Vectis Formation, and that the latter belongs to a later period.

The maximum thickness of the Wealden sediments in the centre of the Weald Basin is approximate 850m. Two major divisions, the Hastings Beds and the Weald Clay, can be recognized. Allen (1975) has proposed the idea that the sequences represent the deposits of braided rivers (arenaceous) and muddy braided plains (argillaceous) deposited under the influence of tectonic movement. Fig.3.2.5 shows the general distribution of the Wealden Beds in the Weald Basin. During the period of deposition of the Hastings beds, the depositional environment remained shallow, channeled and vegetated. Some dinosaur footprints occur, together with abundant megaspores. Intense bioturbation reflects slow deposition rates and perhaps nearshore positions. The

transition to the Weald Clay period was gradational with a low level of stream activity. The work of Casey and Gallois (1973) suggested that the ensueing transgression was from the north but spasmodic connection between the North Sea and the Tethys Sea is believed to have existed through this region.

3.2.3) Structures in the Basin.

The geological structure of the Wessex-Weald Basin is controlled by a series of synclines and anticlines. In the Weald Basin the structure is dominated by an anticlinal structure, initiated by Alpine earth movements (Gallois 1965) and with its main axis west-easterly. In the Wessex Basin the southern flank of a syncline can be recognized with its axis directed nearly west-east. The age of the structural movement is believed to be later than the Palaeogene (Rawson *et al* 1978). The main features of the structure in the Weald Basin are shown in Fig.3.2.5. The lowest beds present are the Purbeck Beds, which lie near to the centre of the anticline. These are followed by the Hastings Beds and the Weald Clay, overlain in turn by the Chalk Formation. Faults are well-developed in the central area of the anticline, mainly being caused by the tectonic movement (Reeves 1968). The dip in the Weald beds, due to the anticlinal structure is relatively small, generally around 5-10°. Fig.3.2.6 shows a schematic section of the Wealden Beds in this district.

In contrast to the Weald District, the principal structure of the Wessex Basin is part of a syncline, with its far south flank eroded by the English Channel. This feature gives the investigated area a particular advantage, allowing a look into the core of the syncline. The dip varies from about 20° in the Isle of Wight and Swanage Bay, to 30-48° in Worbarrow Bay, 80-85° in Mupe Bay and Lulworth Cove and to a reversed bedding dip, about 95-110°, in Durdle Door (Arkell 1947). Faults are poorly developed although some can occasionally be seen.

A notable feature of the Wealden Beds of southern Dorset is the presence of certain distinctive Coarse Quartz Grit layers (CQG) deposited intermittently within the variegated clays of the Wessex Formation. These run, in a discontinuouss way, from Swanage Bay to

Worbarrow Bay and then from Mupe Bay to Lulworth Cove across land, and finally end up at Durdle Door. This feature provides a useful datum plane for stratigraphic measurement and correlation. The CQG develops more layers to the east of Worbarrow towards Swanage, in places separating into three or four sporadic segments (see Fig.3.2.4). These totally disappear in the Isle of Wight, where only some fine sandstone layers exist in the Wealden Beds. The principal layer of the CQG running through Worbarrow to Durdle Door has been regarded by some as a chronostratigraphic marker although some detailed features could not be correlated across the region (Arkell 1947).

3.2.4) Biostratigraphic and magnetostratigraphic dating in the Wessex Formation.

Biostratigraphic dating of the Wealden Beds in the Weald Basin and Wessex Basin has had only very limited success. The main problem in the Weald Basin is the very limited exposures of fossiliferous sediments available, most of which occur in a calcareous or ferruginous band where the main bio-species, ostracods, have usually been leached out from the weathered clay (Anderson 1967). Data are only available from sporadic exposures and a single borehole in Warlingham, Surrey (Geological Survey 1956). The borehole is situated near the margin of the basin so that the sequence is highly condensed and may not be complete (Anderson 1967). Hughes and his colleagues (1958, 1973, 1989) investigated the Wealden Beds of the Wessex Basin for many years by means of palynological records of *Cicatricosisporites*. However, a clear correlation, either between sections within the depositional basin or with those from the rest of the world (particularly in France) is not possible.

Anderson's (1967, 1973) evidence from ostracods supports Allen's (1955, 1959, 1965, 1967) contention that the Weald Clay, the main body of the Wealden Beds in the Weald Basin, spans part of the Hauterivian and the entire Barremian stage. Only one ostracod species, *Paranotacythere diglypta*, is known in both the Wealden Beds and the marine boreal Lower Cretaceous. This is recorded from the Lower Hauterivian of Yorkshire, West and East Germany (Neale 1973), Poland and the Paris Basin. Hughes and Croxton (1973) have correlated the

Worbarrow Bay section of southern Dorset with the Warlingham borehole and proposed that the CQG layer should be correlated to a depth level of about 1700 ft in the Warlingham Borehole, for which a late Valanginian-Hauterivian age has been proposed. This model was questioned by Allen for many years (Hughes and McDougall 1989) and a new correlation of Hughes and McDougall (1989) suggests that the CQG and the base of the Wessex formation on the Isle of Wight correspond to a depth of 1420 ft in the Warlingham borehole. This gives an age estimate of around the Barremian-Hauterivian boundary (Fig.3.2.7). This result was significantly improved by using the scanning electron microscope (SEM) for the micropalaeontological studies.

A pioneering palaeomagnetic study was carried out on the Vectis Formation of the upper part of the Wealden Beds on the Isle of Wight by Kerth and Hailwood (1988). A distinctive reverse polarity zone was found in the formation and this was thought to represent the uppermost reversed event before the start of the long normal polarity "quiet zone" of the middle Cretaceous. On this basis it was correlated with Chron CM0 of the standard marine magnetic polarity sequence (Fig.1.3.7). This proposal raises significantly the age of the upper Wealden Beds from the previously proposed position (within the upper Barremian stage) to the Lower Aptian Stage. In the present study the magnetostratigraphy of this interval has been investigated further.

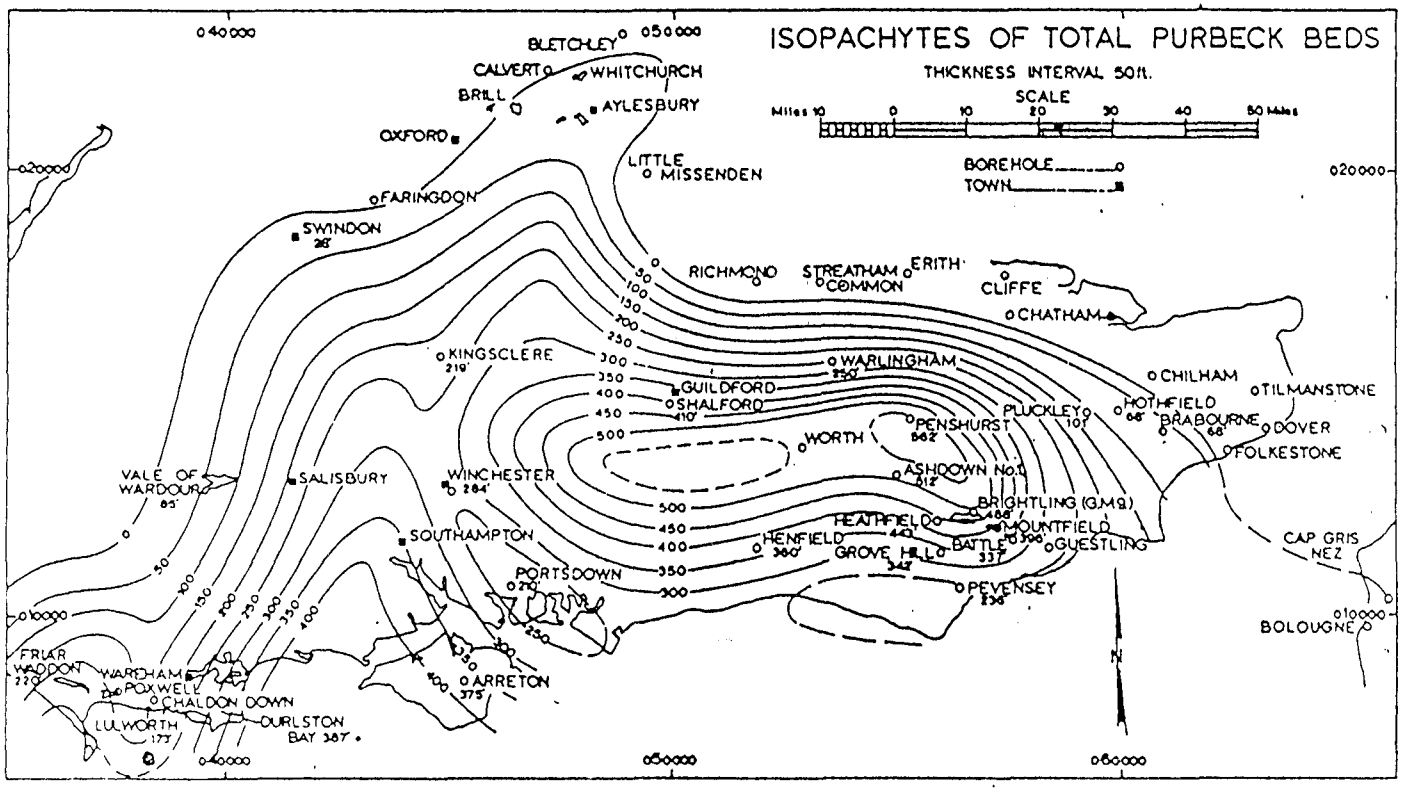

Fig. 3.2.1 Contour chart of isopachytes of Purbeck Beds (pre-Cretaceous) in southern and southeast England. This gives a view of the depositional basement for Cretaceous sediments and was controlled by structural subsidence (from Howitt 1964).

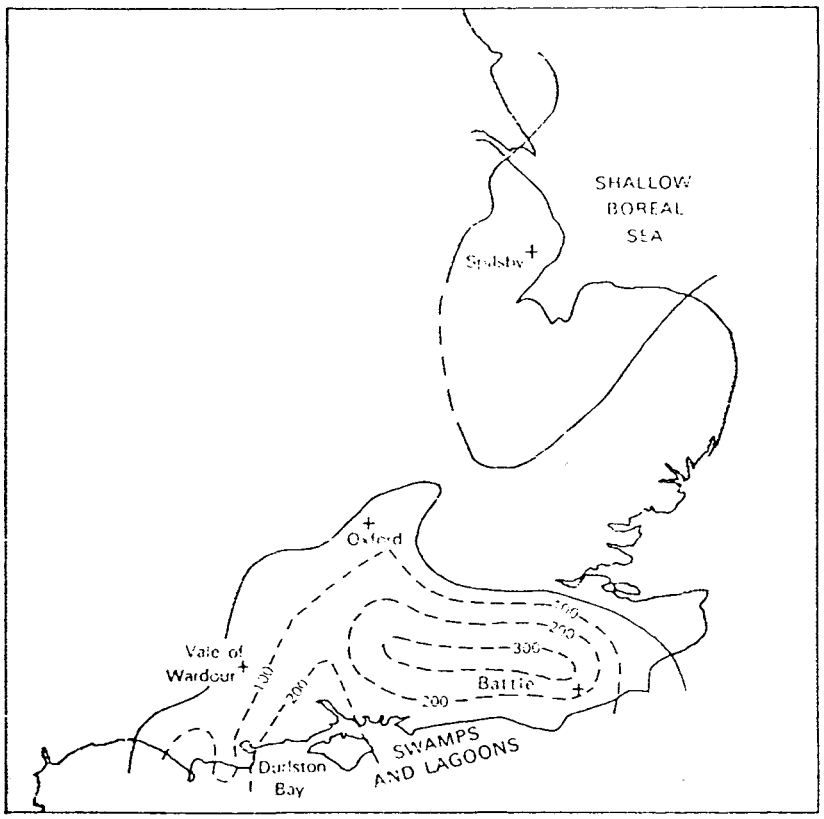

Fig. 3.2.2 Relation between the Weald-Wessex Basin and the northern depositional region of the Cretaceous. A possible intermittent connection existed north of Oxford to the North Sea (after Casey 1963). Contours are the same as Fig. 3.2.1.

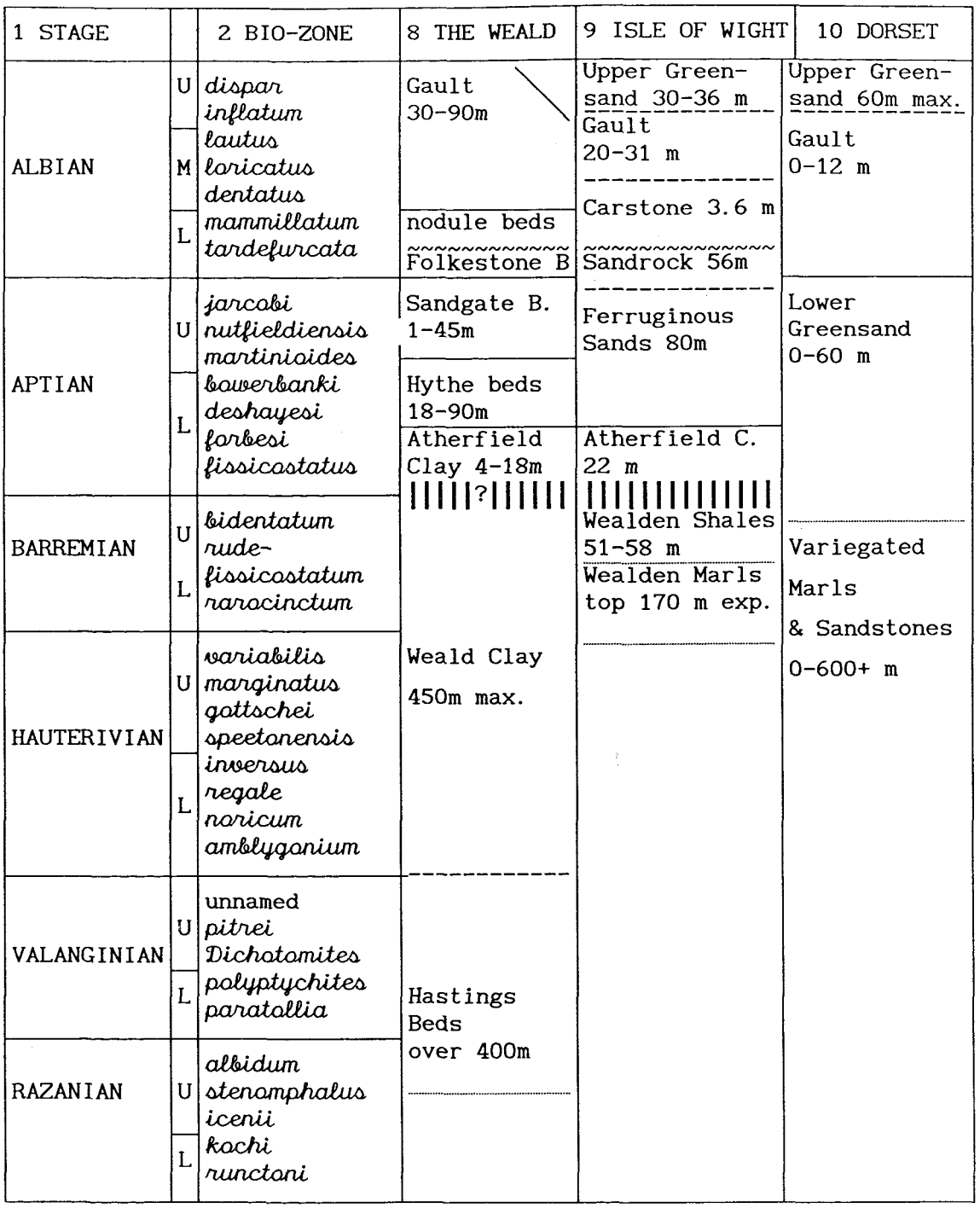

Fig. 3.2.3 Cretaceous stratigraphy of southern England. Column numbers and nomenclature follow Rawson *et al* (1978). The Wealden Shales and Wealden Marls formations were renamed later as Vectis and Wessex Formations respectively (see Stewart 1981).

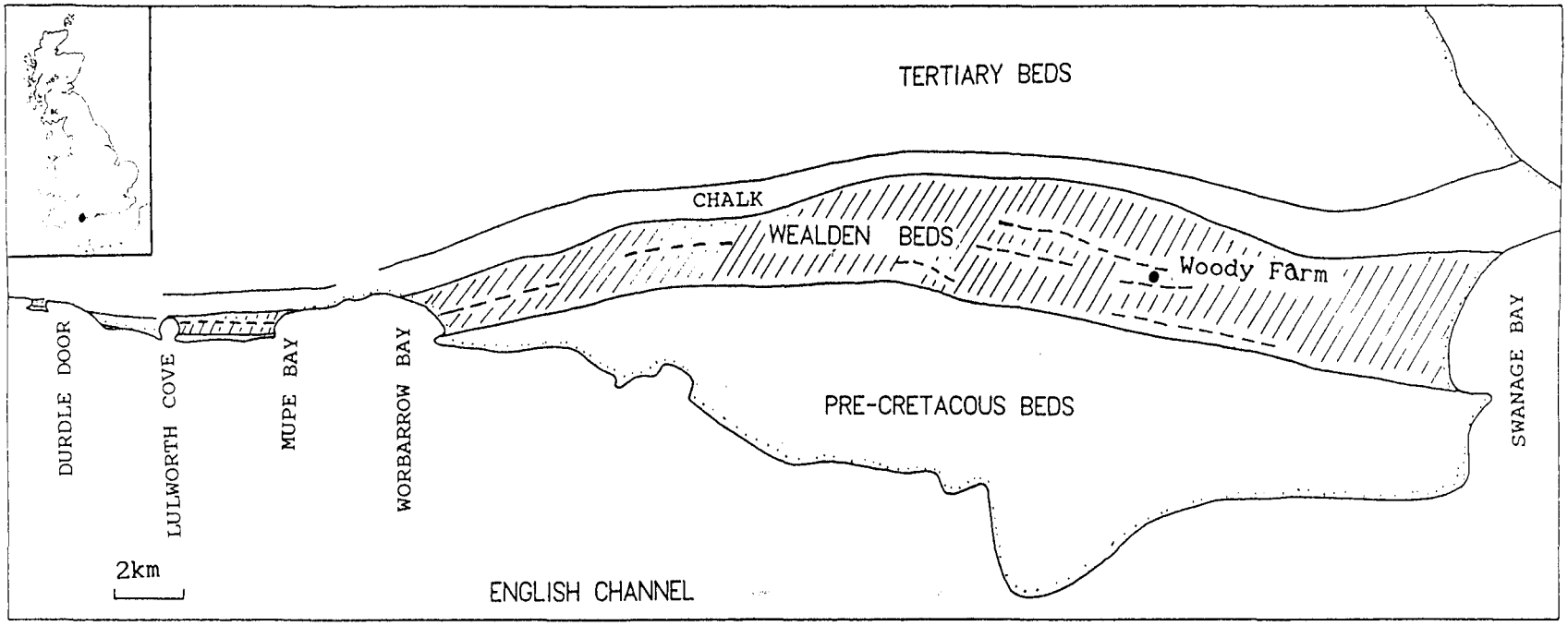

Fig. 3.2.4 Schematic geological map of the southern coastal area of Dorset. The shaded parts represent the Wessex Formation and dashed lines are the Coarse Quartz Grit (CQG).

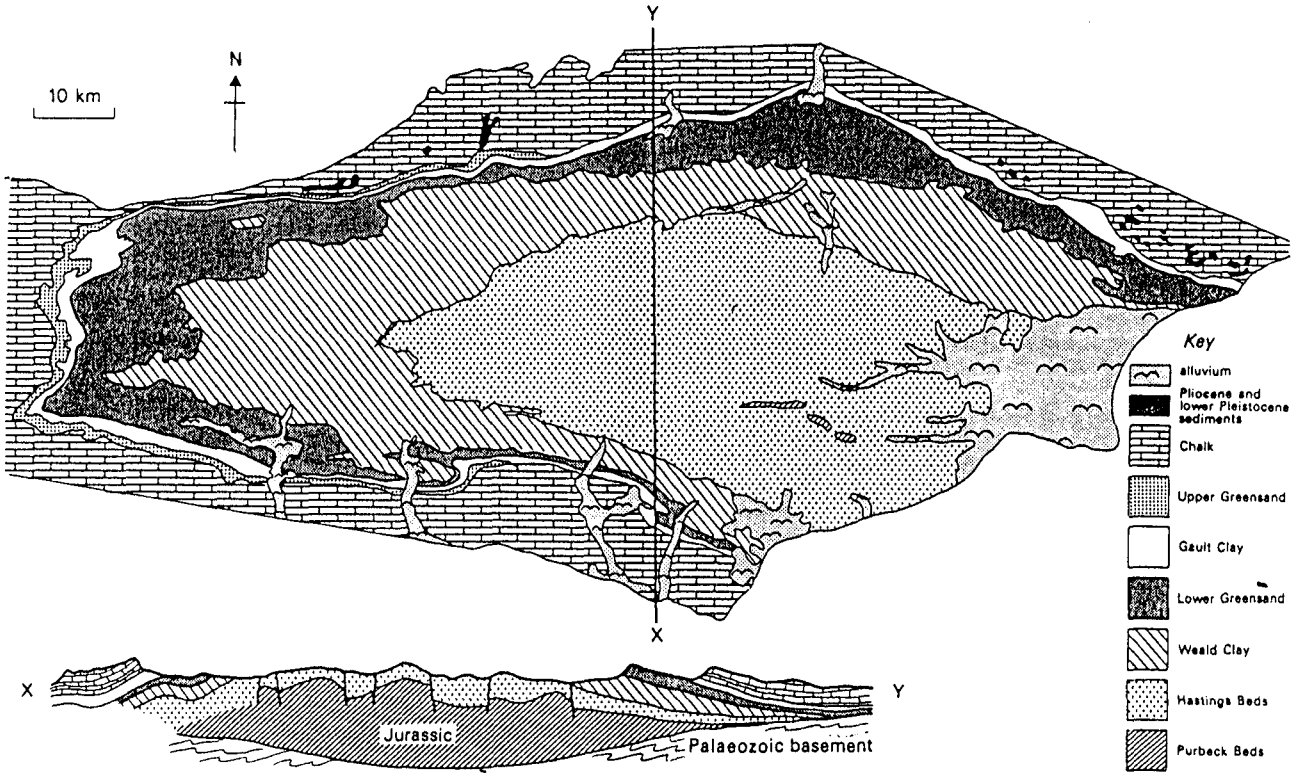

Fig. 3.2.5 Geological sketch map and cross-section of the Wealden Beds in the Weald District, southeast England (after Gibbons 1981).

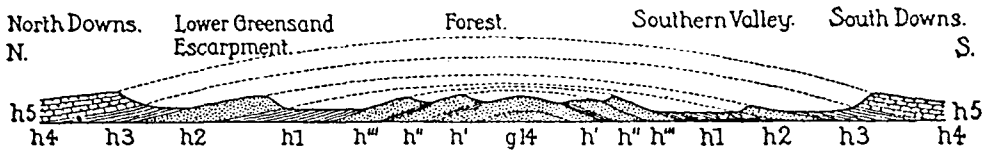

Fig. 3.2.6 A schematic cross-section of the Weald anticline (Boswell 1929). h_5= Chalk, h_4= Upper Greensand, h_3= Gault, h_2= Lower Greensand, h_1= Weald Clay, h'''=Tunbridge Wells Sand, h''= Wadhurst Clay, h'= Ashdown Sands and g_{14}= Purbeck Beds.

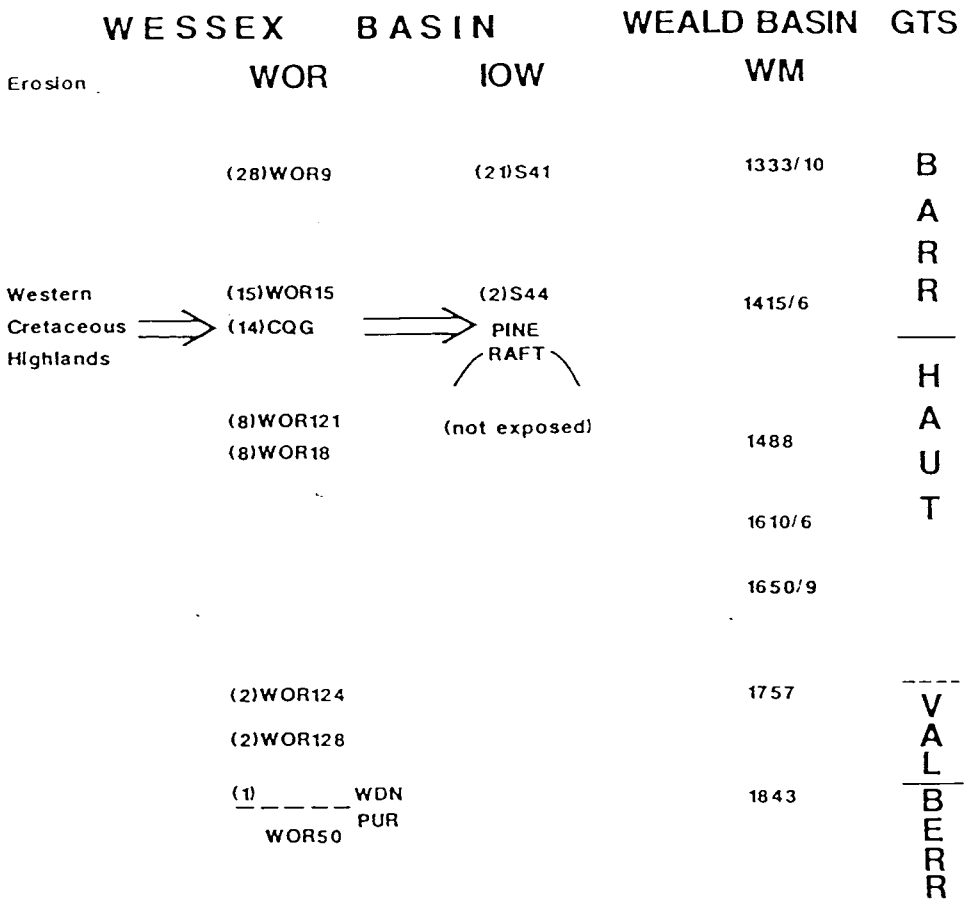

Fig. 3.2.7 Palynological correlation of the Wealden Beds in different Basins (from Hughes & McDougall 1989). The columns are not to scale but samples at the same horizon are believed to give an approximate time correlation. WOR: Worbarrow Bay, IOW: the Isle of Wight, WM: Warlingham Borehole, GTS: Geological Time Scale. Numbers in brackets on the WOR column are Arkell's (1947) classification of lithological units, numbers on the WM column are borehole depth in feet. WOR9, S41, etc. are sample numbers. The Pine Raft is at Hanover Point.

§3.3 Geology of sampling localities.

Sections through the Wealden Group sediments of the Wessex-Weald Basin were sampled at seven different localities, of which five were along the southern coast area of the Wessex Basin and two were inland in the Weald District. The sampling localities were tied in to geological and ordnance survey maps, and to profiles previously measured by other workers (eg. Arkell 1947, Worssam 1978). Careful measurements of the positions of the sampling sites within the local stratigraphy were carried out with corrections being made for apparent dip. The readings of stratigraphic height in each section are regarded as having an accuracy to within a few centimeters for each neighbouring sampling site and a few decimeters up to a meter for estimating the gaps between some sub-sections (ie lateral extension of the working section to a nearby fresh exposure above or below it).

3.3.1) The Isle of Wight section (GR 376845).

Among several available sections of the Lower Cretaceous Wealden Beds on the Isle of Wight, which are distributed along the southeast and southwest coasts, the best one for magnetostratigraphic purposes is probably the one extending from Compton Bay to Hanover Point, located stratigraphically just below the Vectis Formation (see Figs.3.3.1a and b). Stewart (1978, 1981) has carried out detailed investigations into the lithostratigraphy and published a detailed stratigraphic log for the locality at which samples were taken for the present study. Fig.3.3.2 shows the complete stratigraphic sequence measured by Stewart (1978).

The total thickness of the Wessex Formation has previously been recorded as 170 m (eg. see Rawson 1978), but measurements from both Stewart (1978) and the present study give a total thickness of about 137 m between Hanover Point and the base of the Vectis Formation. The major lithology of the section is red and grey-mottled clays and silt-clay. A total of nine principal sandstone units occur within this sequence, these sandstones providing important reference levels to the lithological description of Daley and Insole (1984). The coastal cliff topography leads to rapid erosion, thus maintaining the section in a

fresh state. Slumping occurs only locally, so that there are no significant sampling gaps in the magnetostratigraphic section.

The section is located near the northwest flank of the anticline whose core lies at Hanover Point (Fig.3.3.1b). However, the southeast flank of this anticlinal structure is not well-exposed and the section on this flank extends approximately along the strike direction. The beds on the sampled section dip towards the NNW with a mean strike direction of 260° and a shallow dip angle in the range 15-20°. In total, 60 separate sites were sampled from the whole section during the first field trip. This gives a mean stratigraphic interval between sites of about 2 m or more. A second visit to the section was made to carry out some complementary work and to resample an interval of about 20 m close to the Compton Grange Sandstone at a total of 13 sampling sites (due to some sites being unsampleable during the first trip as a result of the high tide).

The section sampled by Hughes and McDougall (1989) for their palynological investigation is located on the southeast flank of Hanover Point. Therefore, the biostratigraphic events defined by Hughes and McDougall (1989) were not located directly in the section sampled for the present palaeomagnetic study.

3.3.2) Swanage Bay section (GR 033805).

One reconnaissance field trip was arranged to visit this most easterly outcrop of the Wealden Beds on the mainland part of the Wessex Basin. Fig.3.3.3 shows the schematic section for this locality given by Arkell (1947). Because the southernmost part of the section is on the beach, there is little sign of outcrop. From the beach restaurant and a series of beach huts along the northern part of the beach, a discontinuous outcrop can be seen under a cover of plants and man-made objects. Apparent dip of the bedding along the section is rather shallow, ranging from 7° to 20°. This leads to difficulties in tracing the beds. Arkell (1947) complained that it is not easy to obtain direct measurements of thickness, owing to the great thickness of irregularly-bedded and rapidly varying marls which form a large proportion of the Wealden Beds of Swanage Bay and cannot be

satisfactorily sub-divided. The total thickness of the formation can only be estimated by measuring the dip at a number of points and drawing a scale section. The calculated thickness is about 900 m in total. Because of the weathering and poor exposure, the Swanage Bay section was not sampled for the present study.

3.3.3) Worbarrow Bay section (GR 869801).

About 18.8 miles west of Swanage Bay is Worbarrow Bay (see Fig.3.3.4). The coast line exposing this section extends from the northwest to the southeast and the Wealden Beds can be clearly traced along the beach-cliff, with the Jurassic Purbeck Beds underlying to the southeast and the Greensand and Chalk Formations overlying to the northwest. The total thickness of the Wealden Beds at this locality is considerably less than that at Swanage Bay, being reduced to 457 m. The variegated Wealden Marls and sandstones give this beautiful bay its brilliant red, orange, yellow and purple cliffs, particularly in its middle part. The southeastern part of the section is much closer to the beach than the northwestern part and the upper part, particularly the upper 100 m of the Wealden Group, is located at the back of the cliffs. Almost the whole of the formation is well-exposed, with a dip to the north, steep enough for direct measurement of stratigraphic height. A notable lithological feature is that near to the middle of the section, about 200 m below the top of the formation, there is a Coarse Quartz Grit (CQG) layer about 7 m thick, which can be traced continuously eastwards on land for about 11 km before it disappears. Three or four other coarse quartz grits occur further to the east, in the vicinity of Woody Farm to Godlington Farm; however, near Swanage Bay only one CQG layer can be recognized and this is poorly developed. The CQG layer at Worbarrow consists of various grain pebbles, with diameters ranging from 2 cm to 2-3 mm, and conglomeratic iron-stone, sand and interbedded clay seams.

Arkell (1947) summarized the stratigraphic sequence at Worbarrow Bay and listed 35 discrete lithological units. Stewart (1978) found that some parts of the section could not be measured directly due to seasonal slumping. In his measurements, the part of the section below

the CQG is nearly complete but that above has two major unmeasurable gaps due to slumping. Measurements of the thickness for the lower part of the section, from the CQG down to the lowest exposed beds near to a small stream (whose southeast side leads down to Worbarrow Tout), in the present study gave values closely similar to those of Stewart (1973), with an estimated error less than 5 m. In the upper part of the section, from the CQG to the base of the Lower Greensand, there are three significant gaps whose thicknesses could be estimated (the lowest one appears to roughly match one of the slumping gaps described by Stewart (1973)). The boundary between the Wessex Formation and the Lower Greensand Formation is badly weathered. A sampling gap with an estimated thickness of several meters occurs at the boundary.

The total thickness of the Wealden Beds available for palaeomagnetic study in the Worbarrow Bay section is about 350-360 m, from the lowest available beds to the base of the Lower Greensand, with an estimated total error of about ±20 m. A total of 119 sites were sampled in this long section, giving an average stratigraphic interval of 2.9 m. A rough estimation of the timespan of this sampling interval, based on the later magnetostratigraphic data obtained, is $\sim 5 \times 10^4$ years. This should ensure that polarity intervals of subchron or longer duration should be identified (see Table 2.1.1).

Hughes and McDougall (1989) carried out a detailed examination of small pollen palynomorphs from this section including very small angiospermid and other pollen species. Fig.3.3.5 shows their sampling scheme, in which the Arkell (1947) bed numbers were identified. The main sources of palynological information are bed 8 (~80 m below the CQG), bed 15 (a little above the CQG) and bed 28 (~100 m above the CQG). The interval between them is about 90 m. Their conclusion is that the sedimentary sequence between beds 2 and 28 should include the boundary between the Barremian and Hauterivian Stages.

3.3.4) Mupe Bay section (GR 844799).

About 1.5 mile west of Worbarrow Bay is Mupe Bay. (see Fig.3.3.4). The total thickness of the Wealden Beds in this section is

reduced to about 220-230 m and the dip of the bedding is dramatically increased to a value of about 80° to the north. A CQG layer about 7-10 m thick, occurs in the upper part of the section, ~80 m below the top. Arkell (1947) did not give detailed description of the section, due to its short distance from Worbarrow Bay. Near the top of the Wessex Formation some slumping and plant-covering caused sampling difficulties and a sampling gap of about 20 m exists at the top part of the section. The stratigraphic interval between the top of the Wessex Formation and the base of the Lower Greensand Formation is about 8 m. Arkell (1947) proposed that, because the position of the CQG is higher at Mupe Bay relative to that at Worbarrow Bay, a significant thickness of the upper part of the Wessex Formation might have been removed by erosion before commencement of deposition of the Lower Greensand Formation, on the basis of a correlation of the CQG layers in the two sections.

The lower part of the section is relatively complete, down to its base, which is submerged beneath sea level during high tides. A conspicuous oil sand band lies about 27 m above the base (Arkell 1947); one palaeomagnetic sampling site lies close to this band (site MP89) and the lowest two sites are below it. Therefore, only about 9 m of the section below the oil sand band was sampled due to a shortage of sampling tubes and poor exposures at the time of the field work. Sediments in this section are similar to those in Worbarrow Bay, consisting of red, grey and grey-mottled clays or silty clays with some fine sandstone bands. The CQG appearing in the upper part of the section has a rather different appearance from that at Worbarrow, which has a finer overall grain size and smaller size pebble bands within it.

91 sampling sites were occupied in the Mupe Bay section with an average separation of 2.5 m. Few detailed lithologic or biostratigraphic studies of this section have been reported, probably because of its close proximity to the more-accessible Worbarrow Bay section. Therefore, it is difficult to make direct comparison with the other sections based on published stratigraphic information. However, a recent study by Hesselbo and Allen (1991) describes the sedimentology of the lowest part of the Wealden sediments at Mupe Bay and Bacon Hole, focusing on a 7 m interval in the vicinity of the oil sand band. These

authors report that there is a significant erosion surface just below the oil sand band at Mupe Bay, which can be compared with a short section in the Bacon Hole section (Fig.3.3.4). The eroded beds were probably 8-9 m in thickness.

3.3.5) Lulworth Cove section (GR 828798).

The Wealden Beds can be clearly traced westwards along the coast from Mupe Bay to Lulworth Cove (Fig.3.3.4). Although the Wealden beds are exposed in both the east and west flanks of the Cove, the western exposure is practically inaccessible because of serious weathering. The eastern part of the cove provides a good section for palaeomagnetic research through part of the Wealden beds. However, at the time of the present field work, the part below the CQG was so slumped that it could not be sampled reliably. Therefore, only the upper part of this section, starting just below the CQG layer,was sampled. The sampling was continued into the overlying Lower Greensand (which is very thin, not more than a few inches this locality) and the Gault Formations, ending up at the lower boundary of the Chalk Formation.

The base of the Chalk was used as a reference for palaeomagnetic sampling. Arkell (1947) described the sedimentary beds below the Chalk as the Gault Formation (or Upper Greensand), which has a thickness of about 40 m (?) with a basal pebble bed resting on the Wealden Beds below. The Gault beds are divided into a lower part containing a black bed and an upper part which is dominantly green. In the present study, a measurement of the thickness of the Gault Formation indicated a thickness of about 100 m for the beach section. The difference between the two measurements is probably due to measurements being made at a different locality to that of Arkell (1947). The boundary between the Gault Formation and the Wealden Beds was not clearly identifiable due to landslips in its vicinity. However, the sediment color for the Wealden beds is distinctive, so that there was little doubt over the approximate position of the boundary.

A CQG layer occurs in the middle to upper part of the Wealden section at Lulworth. The stratigraphic height from the CQG to the Wealden-Gault boundary is about 62 m which agrees well with the

measurement of Arkell (1947). The CQG can be traced clearly from Mupe Bay to Lulworth Cove on land. Therefore, the two CQG layers provide a correlatable reference between the two areas, in spite of some ambiguousty over the position of the Wealden-Gault boundary at Lulworth Cove. Because the Gault has a Albian age (Rawson *et al* 1978), there is definitely an erosion gap between the Wealden and the Gault in the Lulworth Cove section, which makes it impossible to use the top of the Wealden Beds as a reference point.

The sediments above the CQG are more sandy than those below it. The upper beds consist mainly of variegated marls and sands, and red colour beds represent a relatively low percentage of the section in this part. Below the CQG, only 11.5 m of beds were sampled; this means that the rest of the lower sequence corresponding to about 100 m of section at Mupe Bay was not available for sampling. The bedding dips nearly to the north with an angle of about 75-80° in the vicinity of the CQG. In total, 50 sites were sampled with a relatively large interval, 2-8 m, between sites in the Gault Formation and a smaller intervals, 0.7-2.0 m, in the Wealden Beds. There is little evidence from biostratigraphy and only very poorly preserved fossils appear in the lower part of Gault Formation at this locality (Arkell 1947).

3.3.6) Durdle Door section (GR 807803).

The most westerly exposure of the Wessex Formation along the southern coast of Dorset is at Durdle Door. The section is fully exposed on both sides of the promontory of Durdle, where it can be followed along the strike from beach level on one side to the crest of the col and down to the beach on the other side. The strata are all inverted and show steep dips to the south. The lower beds dip about 110°N and curve upwards to 95°N near the top. From about the CQG layer upwards in the section, the dip is only 95°N at beach level. The section is almost complete on the east side of the promontory (Man-O'-War Cove) where a thickness of 70 m was measured along the foot of the cliff. However, the western part of the section cannot be properly measured because of more serious slumping and weathering conditions at the time of the present study. In the eastern section, both the upper and lower parts of the section are affected by slumping

problem. In the lower part, about 7 m of beds, which are covered by the footpath, cannot be sampled and the upper boundary (between the Wealden and the Gault formation) could not be seen clearly. The measured stratigraphic interval between the top of the Wealden and the Chalk (which is not clearly exposed at its base) is about 21 m (?). Therefore, how much of the sediments have been eroded from the top of the Wealden beds is unknown.

The grain size of the sediments in the Durdle Door section is coarser than that in the other sections to the east. Sandy clays and sand bands appear in most of the section and their colour is dominantly grey and mottled-grey-yellow, with little red colour to be seen. Some thin lignite layers occur in the upper part of the section. The CQG layer appears in the upper part, where it has a thickness of about 10 m. However, the CQG cannot be traced from Lulworth Cove through Oswald's Bay to Durdle on land, so that it is uncertain whether the CQG at Durdle Door can be directly matched with that at Lulworth Cove. Arkell (1947) also described a minor occurrence of lignitic CQG mixed with some variegated marls at the very bottom of the section. This might have some significance in comparison with the other sections.

No biostratigraphic information is available for the Durdle Door section, but geologically this section represents the very westerly margin of the Wessex Basin. 44 sites were sampled in the nearly 60 m of Wealden beds exposed, with an average interval of 1.2-1.5 m between sites.

3.3.7) The Weald District.

Besides the major palaeomagnetic study of Wealden sediments along the southern coastal area of England, a reconnaissance study of the Weald Clay of southeast England was carried out during the first year of this study. However, because of the considerable difficulty in locating suitable sampling localities and correlating among those available, which have scattered distributions, mostly in brickwork pits, only limited progress was made.

The general features of the geology of the Wealden district are

illustrated in Fig.3.2.5. The principal structure is an anticlinal formation with its core located near to Hastings, on the south coast, and its axis running approximately in a west-east direction. The exposed Weald anticline is surrounded by Chalk. The Wealden beds are overlain by the Lower and Upper Greensand Formations. The Weald Clay occupies a wide area in this district, particularly in the western part. The core area of the anticline mostly exposes the lower part of the Wealden formation (ie the Hastings Beds) with the underlying Purbeck beds showing only localised exposure (due to their shallower dips).

The Weald Clay Formation has been investigated and exploited for brick making since the last century because of its commercial value. Worssam (1978) summarized the results of previous studies, together with data from boreholes drilled in this area. Borehole and outcrop evidence suggest that the Weald Clay attains a thickness of some 450 m in the western Weald and gradually thins to the east. The predominant type of sediment in the Weald Clay formation is laminated silty clay, with the lamination more-or-less disrupted by bioturbation (Worssam and Ivimey-Cook 1971).

The clays are greenish grey or medium grey in colour. In general, they can be described as comprising a mixture of illite and disordered kaolinite (Highley 1976). They weather to a pale grey and mottled yellowish brown near the ground surface. Because deposition of the Weald Clay is believed to have taken place in shallow fresh to slightly brackish water, with intermittent brackish-marine incursions, the interaction of deposition and tectonic subsidence of the Weald Basin is expressed in a cyclic nature of the Weald Clay sediments. On a large scale, the Weald Clay as a whole comprises two major cyclic units, the lower characterized by *cyrena* and *small-paludina* limestone, and the upper by *large paludina* limestones.

However, mapping of these formations, particularly on the northern side of the Weald (based mostly on boreholes data), is not complete enough for the boundary between these two lithological divisions to be well-established (Worssam 1978). Subdivision of the Weald Clay in the western part has been proposed by Thurrell *et al* (1968), who divide the

Weald Clay into 11 units. These extend from Bed 1 (the Horsham stone at Warnham brickwork pit) to Bed 11 at the very edge of the Weald Clay Formation near to Newdigate brickwork pits. Figs.3.3.6a and b show the lateral and vertical distribution of the subdivisions respectively in the western part of the Weald. These data are mainly from boreholes. There are only 4 large brickwork pits distributed between Southwater and Newdigate (see Fig.3.3.6a) and from the vertical profile (Fig.3.3.6b) it is clear that a single borehole could not penetrate the complete stratigraphic sequence.

Two sampling localities were visited, one at Langhurst (Warnham brickwork pit) and the other at Beare Green, near to the Newdigate brickworks. The horizontal distance between the two localities is about 5 miles and a general bedding dip of about 3-5° towards the north can be scarcely measured. Plates 3.3.1a and b show part of the Langhurst sampling sections, in which the two sections are separated oppositely for about 80-100 m by the pit. Although some general stratigraphic features of the beds could be recognized, the weathering state looks more advanced than that of the Wessex Formation in southern England. At each sampling locality, two independent sections were sampled for repeatability test (see Chapter II). At Langhurst, these sections comprised 19 and 16 sampling sites respectively. At Beare Green they comprised 11 and 9 sampling sites respectively with a separation of profiles for a few meters along a pit bank.

For the Langhurst brickwork pits, many sedimentological and biostratigraphical investigations have been reported (eg. Worssam 1978, Allen 1975, Prentice 1962 etc), and detailed descriptions of the section are available. Two separated sections were sampled in a working pit near to the middle of the area currently being worked for brick clay. One of these was in a northwest bank (Plate 3.3.1a) and the other in a southeast bank (Plate 3.3.1b). Correlation between the two sections is difficult because of the complicated sedimentary environment (eg see Prentice 1962) and well-developed faults (this area is on the west-east axis line of the Wealden anticline).

A sand/limestone layer could be clearly recognized in each section. By comparison with the sediment features, colours and

surrounding sedimentary units described by Worssam (1978), the layer in the northwest bank section is considered to represent Bed No.11 (note that this is a sub-division of the beds and different from the general division given by Thurrell *et al* 1968) with a very thin siltstone layer (Bed No.13) at its top, about 1.5 m higher. That in the southeast bank is probably Bed No.5, with dark grey shales around it. Both of these units should belong to Bed 2 of Thurrell *et al* (1968). However, neither of these sand/limestone layers appears on the other section but at the position where they should have appeared only a general colour change can be identified. An overall colour change from dark grey at the base to yellow-brown in the upper part can be recognized in both sections. Below the possible Bed No.11 the colour is dominated by dark grey, and surrounding and above it, it is dominated by yellow-brown. Because the depositional environment is very complicated, even the possible Bed No.5 sandstone layer cannot be traced for the few meters to the south east bank section. However, correlation between the two banks is complicated by the presence of minor faults, such as that cutting into the possible Bed No.11 (Plate 3.3.1a).

Stratigraphically, the Langhurst sections should be lower than those at Beare Green, with the former in Bed 2 and the latter in Bed 9 or 10 of Thurrell *et al* (1968) (see Fig.3.3.6a). However, the exact stratigraphic gap between the sections sampled at the two localities is unknown. Biostratigraphic evidence for dating the beds comes mainly from boreholes, for example, the Warlingham Borehole (1956) in the northwest margin of the anticline. Hughes (see Worssam 1978) proposed, on the basis of palynological evidence, that the Weald Clay should have a late Valanginian or early Hauterivian age, but Allen (1955, 1967, 1975) held the view that the Weald Clay Formation probably spans the Hauterivian and the entire Barremian stage, and that Weald Clay deposition probably continued into the Aptian stage, although there is no faunal evidence for this (Casey 1961, Rawson *et al* 1978). Later studies (eg Anderson 1973, Hughes 1973) have thrown little further light on this problem.

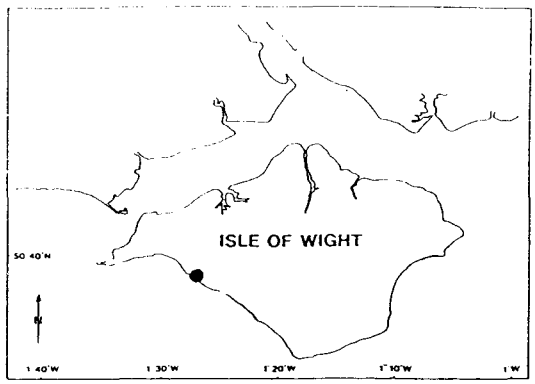

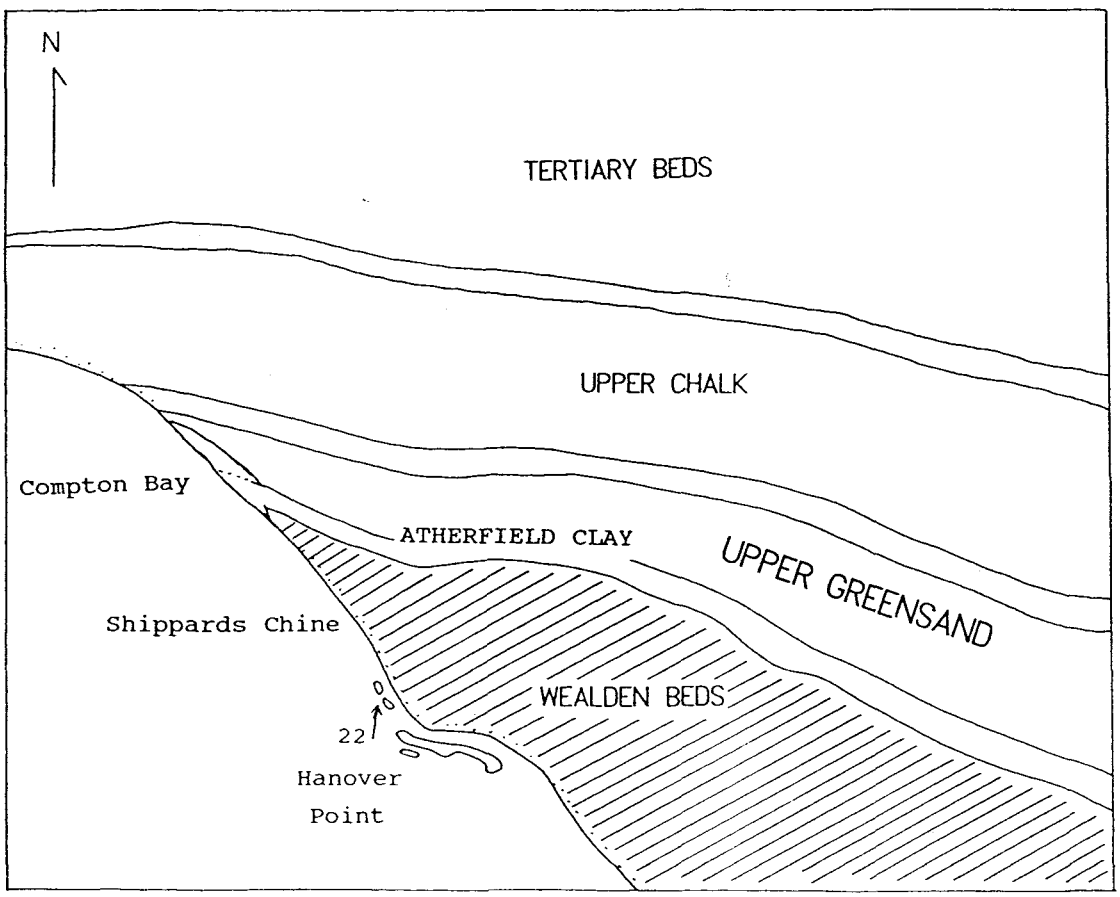

Fig. 3.3.1a Schematic geological map of the southwest coast of the Isle of Wight. The shaded part represents the Wessex and Vectis Formations and arrow with number are dip direction and angle.

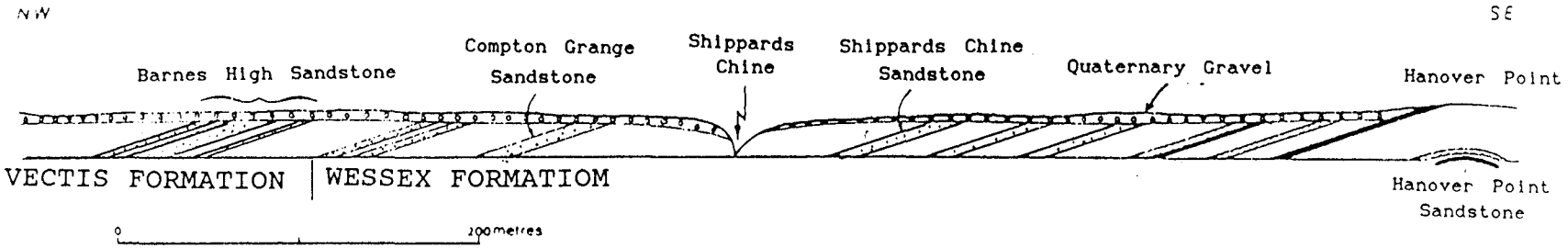

Fig. 3.3.1b Sampling profile along the coast from the boundary of the Wessex and Vectis Formations to Hanover Point. (from Daley & Insole 1984)

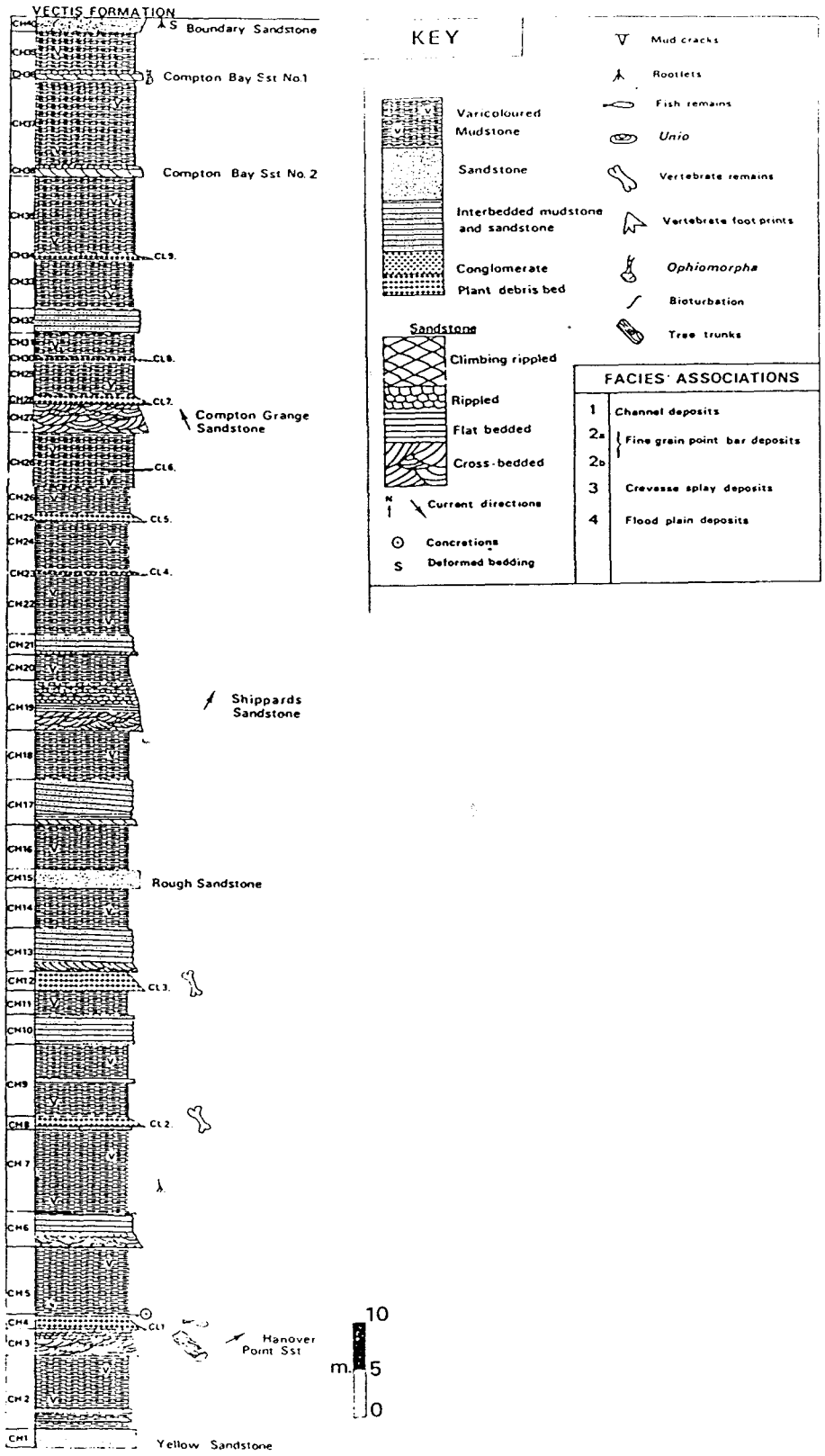

Fig. 3.3.2 Lithological log of the Wessex Formation on the Isle of Wight at the locality sampled for this palaeomagnetic study (from Stewart 1978).

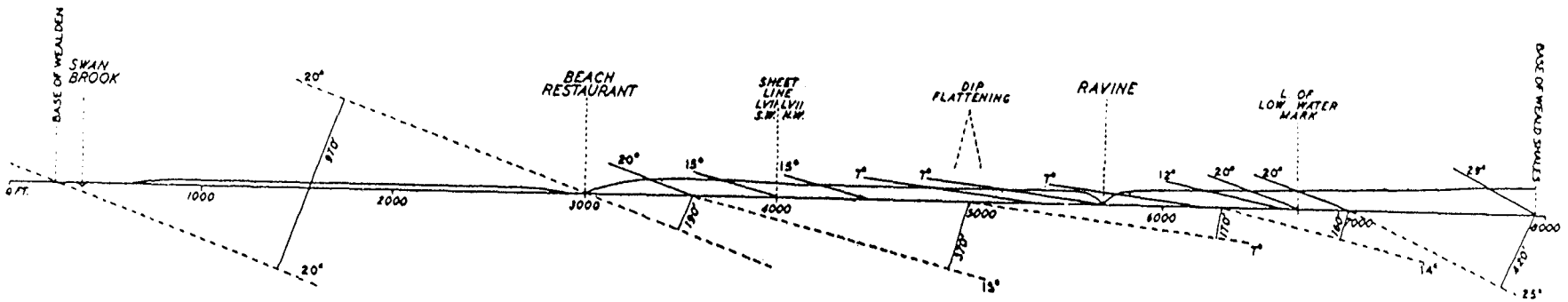

Fig. 3.3.3 Schematic profile through the Cretaceous beds in Swanage Bay. Solid lines are measured apparent dip, dashed lines are average dips used for calculating thicknesses (from Arkell 1947).

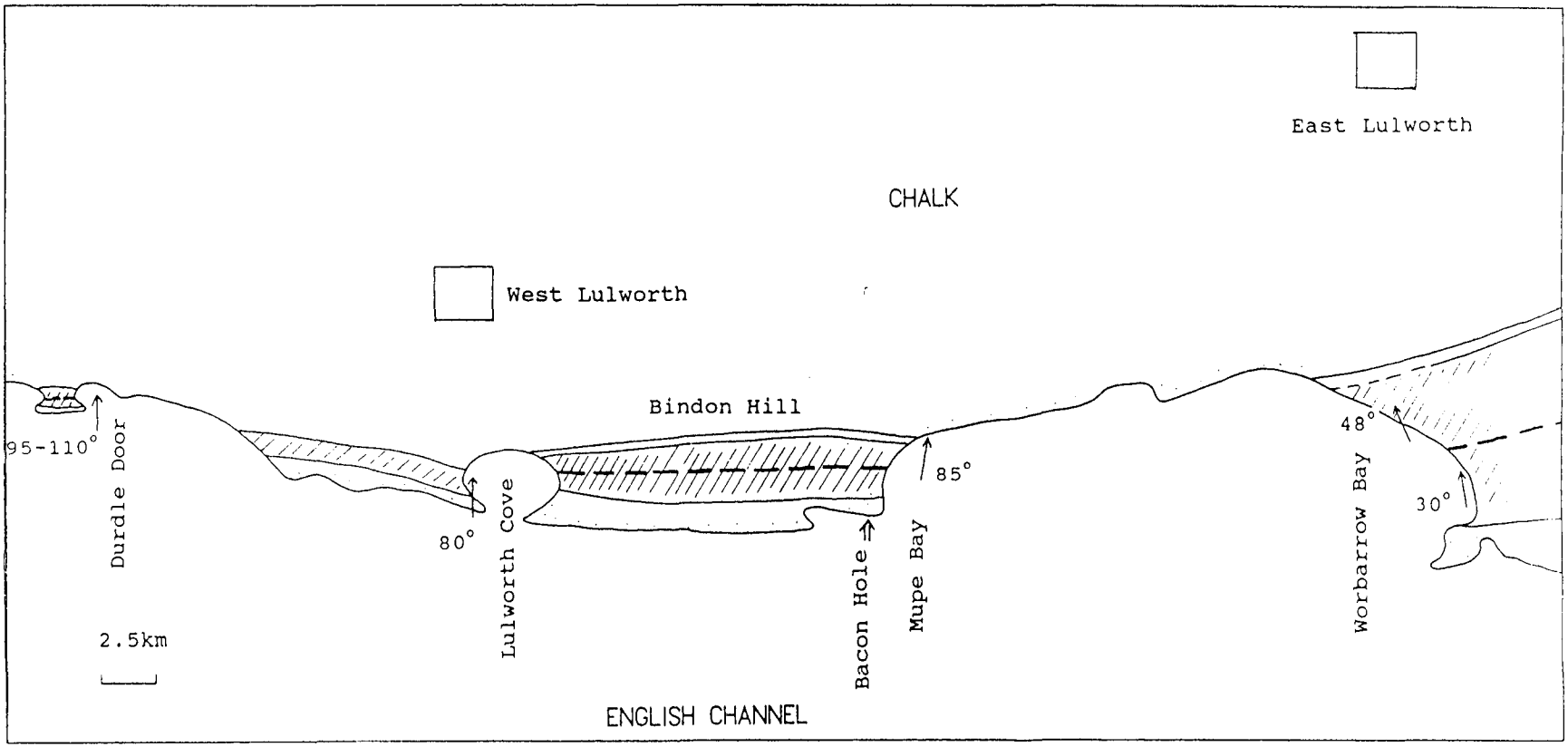

Fig. 3.3.4 Enlarged schematic geological map for the coastal area of southern Dorset from Worbarrow Bay to Durdle Door. The shaded area represents the Wessex Formation, and thick dashed lines represent the Coarse Quartz Grit (CQG). Arrows are the dip direction (with dip angle also shown) of the beds.

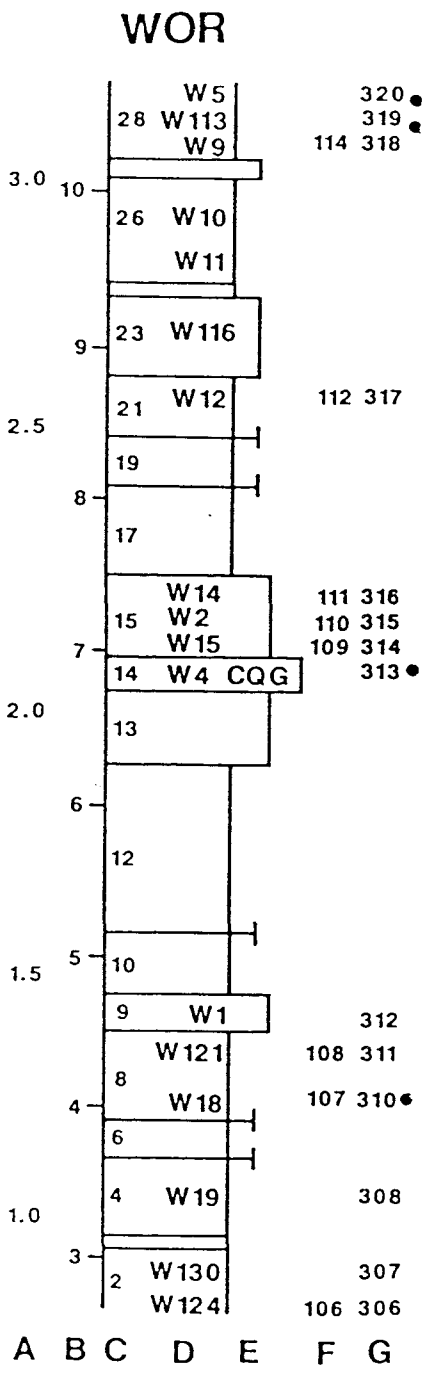

Fig. 3.3.5 Sampling scheme for biostratigraphic investigation of the Worbarrow Bay section (from Hughes & McDougall 1989). A: stratigraphic height in hundred meters, B: height in hundred feet, C: bed number (Arkell 1947), D: biostratigraphic -sample numbers, E: lithological indications, F: biostratigraphic event numbers for, "*cicatricosi*" (Hughes & Croxton 1973) and G: bio-event numbers for pollen (Hughes & McDougall 1989).

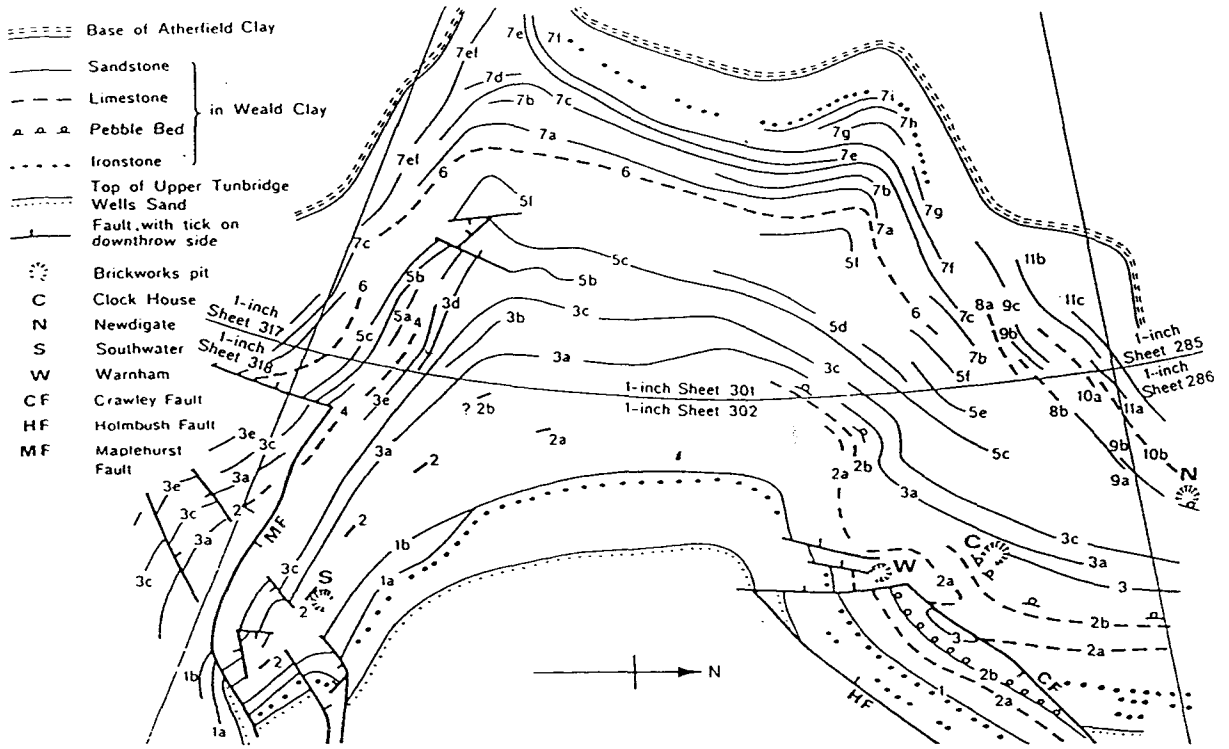

Fig. 3.3.6a Classification of the Weald Clay Formation around the western flank of the Weald District. The map is not scaled (from Worssam 1978). Numbers suffixed by letters represent the Bed Number classification of Thurrell *et al* (1968) from 1 to 11.

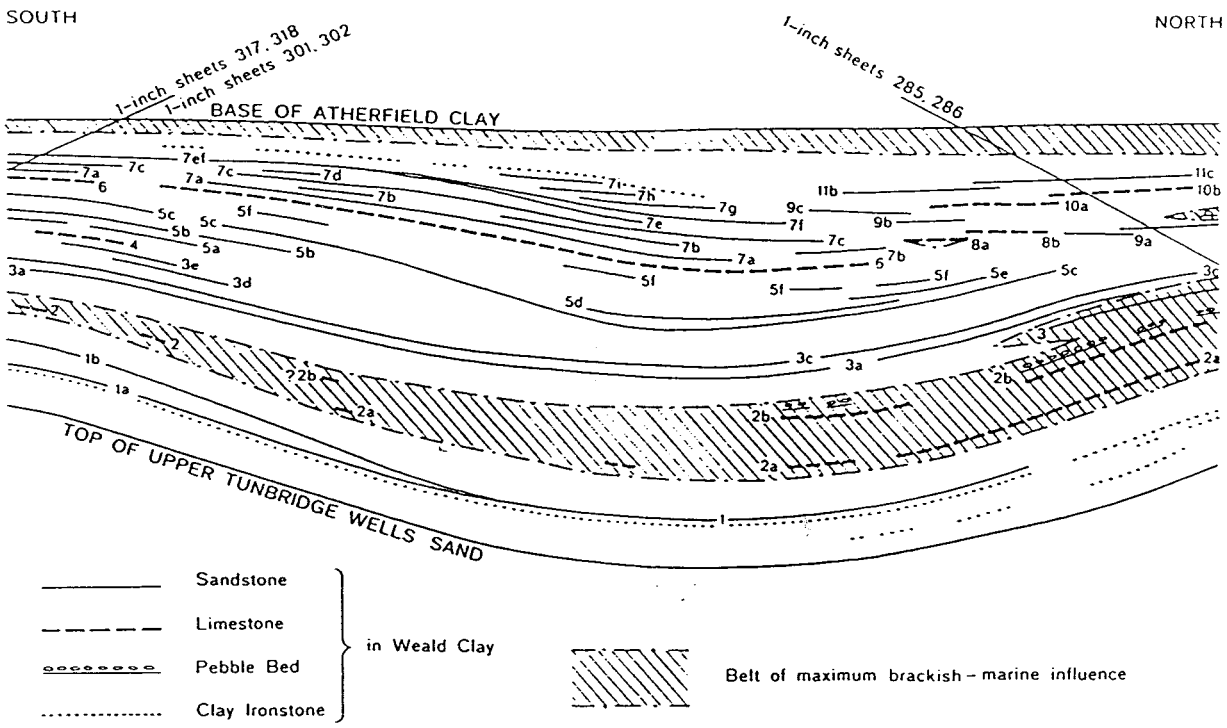

Fig. 3.3.6b A generalized cross section of the Weald Clay of the western part of the Weald, based on Fig. 3.3.6a and not to scale (from Worssam 1978).

Plate 3.3.1a The northwest sampling section in Langhurst (Warnham) brickwork pits. Sampling work started from the bottom to the top. The sand/limestone bed in the middle is the possible Bed no. 11.

Plate 3.3.1b The southeast sampling section in the same pit. Sampling work was from the bottom to the top. The arrow points the sand/limestone layer near to the bottom, which is the possible Bed no.5.

CHAPTER IV PALAEOMAGNETIC RESULTS FROM THE LOWER CRETACEOUS SEDIMENTS AND THEIR CORRELATIONS

§4.1 Palaeomagnetic Results.

4.1.1) Procedures.

Three principal laboratory methods have been used for the purpose of this magnetostratigraphic study, namely a.f. (alternating field) demagnetisation, thermal demagnetisation and IRM acquisition (isothermal remanent magnetisation), in which the former two were used to test the stability of magnetisation in the samples and to remove low stability components and the third was used to investigate the nature of the magnetic minerals present.

The reliability of the palaeomagnetic data produced by laboratory analyses is dependent on a number of factors, of which the working condition of the instruments is very important. Therefore, regular checks of the residual magnetic field in the thermal demagnetiser as well as the calibration of the a.f. demagnetiser and the measuring position of the sample in the cryogenic magnetometer were made. For some pilot samples, both double and triple measurements were carried out on the cryogenic magnetometer and small demagnetisation steps (for example, 2.5, 5, 7.5, 10 and 15 etc. up to 35 mT) were used to be sure that their characteristic magnetic properties were fully established before processing other samples from the same group using single measurements and less-detailed demagnetisation analyses. The demagnetisation method (a.f. or thermal) was generally selected according to the magnetic constituents of the samples in question, as determined from IRM acquisition; thus, thermal treatment would be preferentially employed for those containing hematite as their main magnetisation bearer and a.f. demagnetisation for those with magnetite or titanomagnetite.

4.1.2) Palaeomagnetic results from the Isle of Wight section.

The Wessex Formation on the Isle of Wight comprises the Wealden Marls, of which the dominant lithologies are red and yellow-mottled

clays. Some light grey to grey clays are also present. For the red, yellow-mottled or grey-red clays, the IRM analyses indicate that hematite or a similar magnetic mineral is the dominant magnetic constituent. Fig.4.1.1 shows a set of IRM acquisition curves for some typical samples chosen from the section, according to their colour. For samples with grey and light grey colour (Figs.4.1.1a and d) the IRM curves show the typical characteristics of magnetite or titanomagnetite as the dominant mineral, with magnetic saturation being reached in applied field of only 0.2-0.3 T. In contrast, the the IRM acquisition curves for the red and grey-red marls do not reach the saturation state in applied fields up to 0.85 T, indicating that hematite (or some other high coercivity mineral) dominates in them.

Fig.4.1.2 displays the statistical distribution of NRM intensity values for all samples in this section. The logarithmic mean value is 6.597 mA/m, with some samples having values higher than 70 mA/m. Thus, the typical NRM intensity values are several orders of magnitude greater than the "background noise" values for the cryogenic magnetometer (≤0.03 mA/m). Fig.4.1.3a shows the variation of NRM intensity with stratigraphic height for the Compton Bay - Hanover Point sequence. It can be seen that most samples have NRM intensities less than 10 mA/m in the upper part but below 90m a higher proportion of samples have intensities greater than this value

At a stratigraphic height of about 98-102 m (Fig.4.1.3b) is the Compton Grange Sandstone (CGS) which lies within a part of the section with a generally weak NRM intensity. However, other thinner sandstone layers in the lower part of the section are not always associated with weaker NRM intensities.

A set of pilot a.f. demagnetisation analyses for 15 samples indicates that most samples, (with the exception of those showing grey or light-grey colours), have strong resistance to a.f. demagnetisation, the NRM intensities showing little reduction during treatment in fields up to 35 mT on the cryogenic system demagnetiser and further treatment up to 50 mT on the Molspin demagnetiser (Fig.4.1.4a). Therefore, the remaining 95 samples were subjected to progressive thermal demagnetisation. Because these clay samples are relatively soft and

moist, the first step was to let them dry out at room temperature in the laboratory environment (on the basis that if the water content is not significantly high, the process of drying would not produce a significant secondary magnetic components in the laboratory field). After stripping the cling film wrapping from the dried sediment and transferring the orientation marks to the hardened sediment surface the samples were then ready for thermal demagnetisation using the conventional method. A pilot thermal demagnetisation test showed a progressive decreases in intensity during treatment up to ~600°C or above (Fig. 4.1.4b).

For most samples a demagnetisation Stable End Point (SEP) was quite well-defined. After field and bedding correction, most of the characteristic magnetisation vector directions concentrate in the northern part of the lower hemisphere on a stereographic projection (for details see Appendix 1). Fig. 4.1.5 shows these SEP directions before and after bedding correction. The mean directions are

Dec =359°, Inc =65° (before bedding correction)
and Dec =357°, Inc =45° (after bedding correction)
with α_{95}=2° (N=78).

(The value of α_{95} is not affected by the bedding correction, since the dip is quite uniform throughout the section). Although the mean direction before the shallow bedding correction is closer the present geomagnetic field direction (Dec=0° , Inc=68° for Southern England), it does not include the field direction within its 95% confidence limit.

The mean direction after bedding correction is shallower than the predicted direction for the Lower Cretaceous in this area. [The predicted geomagnetic field direction of the Lower Cretaceous for Southern England is mainly derived from two sources, one of them interpolated from the palaeogeographic maps of Smith *et al* (1981), in which the expected inclination should be around 60° and declination about 10°. The other is from the magnetostratigraphic investigation by Galbrun (1985) of the Berrias Limestone Formation, France, which gives an estimated field direction for Southern England of about Dec =0.4° and Inc =55° with α_{95}=3°. No other palaeomagnetic directional data

have been identified for the Lower Cretaceous of stable NW Europe, although some data are available for allochthonous parts of southern Europe (eg Lowrie & Alvarez 1984). Therefore, in present study the predicted geomagnetic field direction for the Lower Cretaceous is adopted as an average value of Dec=5° and Inc=57° with 95% confidence limits α_{95}=3°].

Kerth and Hailwood (1988) also noticed this shallower inclination phenomenon in the overlying Vectis Formation and they explained this as reflecting possible palaeomagnetic depositional "inclination errors" (King 1955) or post-depositional compaction effects in this rapidly-deposited terrigenous shale formation. The same considerations may also apply to the rapidly deposited (Hughes & McDougall 1989) marls of the Wessex Formation.

It is interesting to note that nearly all of the samples which were subjected to thermal demagnetisation, show only a single significant magnetisation component, which, in most cases, is identified in the temperature range 100° to 500° or 600°C. With the exception of only 8 isolated samples, the polarity of this characteristic magnetisation is normal. Two possible explanations may be considered for these results. Firstly, these sediments may have been remagnetised (eg by the acquisition of a CRM) during a normal polarity interval (such as the recent Brunhes normal polarity chron). This consideration might be supported by the fact that the SEPs concentrate closer to the present geomagnetic field direction before applying the shallower bedding correction (Fig.4.1.5) . However, this might be a coincidence. Secondly, this characteristic normal polarity magnetic component may reflect a "primary" magnetisation which was acquired during or very soon after the sediments were deposited (Payne and Verosub 1982). Since the Wessex Formation was probably deposited during the long Cretaceous normal polarity chron (which terminated at Chron CM0 in the Vectis Formation, see Kerth and Hailwood 1988), it is quite possible that the latter explanation is correct.

Although the majority of the samples show a normal polarity characteristic magnetisation, some individual samples exhibit clear reverse polarities after demagnetisation at high temperatures (most are

from one of the pair of samples at the sampling site, the other showing the opposite polarity, possibly due to their coming from different sampling levels, see Chapter II). Fig.4.1.6 shows examples of two such samples. These isolated reverse polarity intervals may represent short-period magnetic events or "excursions" within the Early Cretaceous normal chron (C34N).

4.1.3) The Worbarrow Bay section (The Dorset Coast).

Four separate one-day field trips were required to sample this longest section of the Lower Cretaceous in southern England. The general condition on the section was good, as a series of storms had washed off the weathered surface near beach level. The dominant lithologies are red, mottled, grey and yellow clays and silty clays, particularly in the middle of the section, with the upper and lower parts being increasingly dominated by grey or light grey colours. Fig.4.1.7 shows some typical examples of IRM acquisition curves, in which the red clay (d), red-grey-mottled clay (c), and yellow clays (f) produce IRM acquisition curves that suggest hematite as the dominant magnetic mineral. Grey (e) and white grey clays (a) display characteristics that suggest magnetite as the dominant magnetisation carrier.

The NRM intensity values for all samples from the Worbarrow Bay section are summarized in Fig.4.1.8. The log mean NRM intensity value for the section is 1.089mA/m, which is much lower than that for the Isle of Wight section. The majority of values are lower than 2.0 mA/m, although the whole distribution spectrum has a wide range, up to 12 mA/m.

Fig.4.1.9a shows the variation of NRM intensity with stratigraphical height in this section. In comparison with the Isle of Wight section (Fig.4.1.3a) the NRM intensity variation with height at Worbarrow Bay shows more systematic change. Since NRM intensity changes may represent changing properties of the magnetic minerals present, which might link to changes in depositional environment, the NRM intensity logs might prove useful for correlating different sections throughout the area and for investigating depositional

environments. In Fig.4.1.9b, four principal magnetic intensity "events" have been identified, in each of which the intensity values are significantly greater than the typical "background" value for the rest of the section. These lie in the approximate height ranges 280-315 m, 180-240 m, 145-165 m and 80-125 m, and they are labeled as 1, 2, 3 and 4 respectively. Although the intensity values for each of these events are distinguishably higher than the background value, the actual values differ from one "event" to another. The position of the coarse quartz grit (CQG) (see Chapter III) is also plotted, since this provides a useful lithostratigraphic marker. The CQG lies near the top of NRM intensity "event" 3 (Fig.4.1.9c).

In total, 279 samples from this section were subjected to either a.f. or thermal demagnetisation. The details are summarized in Appendix 2. A relatively small proportion (36 out of 279) of the samples were subjected to thermal treatment, on the grounds that (i) the results from pairs of pilot samples treated by the two methods (both from the Worbarrow Bay and the Isle of Wight sections) showed the same characteristic magnetisation polarities, (ii) there is evidence that heating of some samples above about 350°C leads to chemical alteration (eg Fig.4.1.10f) and (iii) in general the samples from Worbarrow Bay showed a greater response (in terms of decrease in intensity) to a.f. demagnetisation than did the samples from the Isle of Wight section. Those samples from the Worbarrow Bay section subjected to thermal treatment are mainly located in the middle part of the section and carry either normal or reverse polarity characteristic magnetisations. In this part the sequence contains more red and red-mottled clays than in the remainder of the section.

Fig.4.1.10 shows typical examples of both a.f. and thermal demagnetisation, in which the thermal treatment mainly reveals a single significant magnetic component in each sample. Fig.4.1.11 summarizes all characteristic magnetisation directions with normal and reverse polarities determined from either a.f. or thermal demagnetisation, Figs.4.1.11a and c show the data before application of the bedding correction and Fig.4.1.11b and d after this correction. The overall mean directions are

Dec =29°, Inc =84° (before bedding correction)
and Dec =3°, Inc =38° with α_{95} =4° (N=129)

(after inverting the reverse polarity vectors).

It is significant that the characteristic directions before the relatively steep bedding correction (30-48°) differ significantly from the predicted Lower Cretaceous geomagnetic field direction and the present field direction (see §4.1.2). After bedding correction it becomes closer to the predicted geomagnetic field direction for the Lower Cretaceous than the present field direction. That means this characteristic direction may be pre-folding and may represent the primary component. As with the Isle of Wight section, the overall mean direction for the Worbarrow Bay section has a shallower inclination than expected (see §4.1.2).

A proportion of the reverse polarity samples (approximately ~20%) did not show well-defined SEPs, but instead, during demagnetisation, their magnetic vectors showed directional trajectories towards the supposed reverse polarity end point. In this case, the great circle fitting method (see Chapter II) was applied to the bedding corrected data. The corresponding intersection points are displayed in Fig.4.1.12. After applying Bingham statistics to the intersection points, the overall mean direction is Dec =170°, Inc =-36°, with 95% confidence limits =28° in the elongate direction and 11° perpendicular to this direction (11 directional trends involved).

Although most samples from this section produced reliable polarity determinations for magnetostratigraphic purposes, a few samples (about 15% of the whole set), exhibited very "noisy" behaviour during demagnetisation, particularly for those with relatively weak magnetic intensity, so that a reliable polarity assessment could not be made for them. Typical examples are shown in Fig.4.1.13.

4.1.4) The Mupe Bay section (The Dorset Coast).

Mupe Bay lies some 1.5 mile west of Worbarrow Bay (see Fig.3.3.4). A remarkable characteristic of this section is that the dip of the

bedding is near vertical (85°), so that the whole sequence can be sampled in a relatively short distance along the foreshore. Only one significant sampling gap (~20 m in thickness) exists at the very top of the section. A second notable feature is that the red clays, which are dominant in the Isle of Wight and the middle part of the Worbarrow Bay sections, represent a small part of the section at Mupe Bay, much of the sequence being represented instead by grey, mottled and mottled-yellow clays.

Fig.4.1.14 shows some examples of IRM acquisition curves for samples from Mupe Bay. The grey and white grey clays (a and d) show characteristics of magnetite as the dominant magnetic carrier, whereas the mottled-yellow and red-mottled clays (b and c) show characteristic of hematite, but with a small proportion of magnetite in same samples.

Fig.4.1.15 shows the statistical distribution of NRM intensity values for this section. The logarithmic mean intensity value is 0.482 mA/m which is lower than that for the Worbarrow Bay section and considerably lower than that for the Isle of Wight section, possibly reflecting the changes of depositional environment and sedimentation along the southern coast of Dorset at the time of deposition.

As with the Worbarrow Bay section the variation of intensity with stratigraphic height at Mupe Bay (Fig.4.1.16a) shows several relatively high intensity "events". Three such events can be recognized, namely at 160-200 m, 90-130 m and possibly also at 40-60 m. These are termed "event 1, 2 and 3" respectively (Fig.4.1.16b). The CQG appears in the Mupe Bay section at 130-137 m above datum (Fig.4.1.16c), just above the NRM "event 2".

All samples, 182 in total, were subjected to a.f. demagnetisation treatment, on similar grounds to those for the Worbarrow Bay section (see §4.1.2). Fig.4.1.17 shows some examples of the a.f. demagnetisation response for both normal and reverse polarity samples. In the majority of cases the directions of magnetisation remain close to the expected normal or reverse polarity direction during demagnetisation above about 10 mT, but because the corresponding intensity changes are small or irregular, linear segments through the

origins of the vector end point plots (ie true SEPs) could only be defined for a small proportion of the samples. Thus for the majority of samples the characteristic magnetisation direction (CMD) was defined by Fisher statistical analysis rather than linear regression. These directions are summarized in Fig.4.1.18. The overall mean direction is

Dec =166°, Inc =57° (before bedding correction)
and Dec =5°, Inc =37° (after bedding correction)
with α_{95}= 5° (N=85)

Although a few samples show crude directional trends during demagnetisation, these are generally too poorly defined to justify application of the great circle fitting method to them. An important feature demonstrating the reliability of the remanent magnetisation preserved in this sedimentary formation and used for the purpose of the magnetostratigraphic investigation is the "positive" fold test. Thus, before application of the bedding correction the normal and reverse polarity vectors depart significantly from the expected direction for the late Mesozoic and the present geomagnetic field (see §4.1.2) (Figs.4.1.18a and c). However, after bedding correction they are more close to the expected direction (Fig.4.1.18b and d).

However, as with the Worbarrow and Compton Bay section, the mean inclination for the Mupe Bay section is shallower than expected. Although the magnetisation of the majority of samples clearly pre-dates the folding, approximately 10 % of the samples carry strong normal polarity overprints in the present field direction which cannot be removed by a.f. demagnetisation (Fig.4.1.19). Unfortunately, because of the friable nature of these samples it was not possible to subject them to thermal demagnetisation, in an attempt to remove the overprints. Such samples could not be used in the magnetostratigraphy.

4.1.5) The Lulworth Cove section (The Dorset Coast).

The Lower Cretaceous beds can be traced westwards from Mupe Bay to Lulworth Cove (Fig.3.3.4). Because the lower part of the section at Lulworth Cove was not being available due to slumping (see Chapter III), only the sequence extending from just below the CQG up to the

Gault Formation was investigated, with a total stratigraphic thickness of about 200 m. Apart from the dominant dark green colour of the Gault Formation, the upper part of the Wealden Beds are mainly grey, yellow-mottled silty clays with minor amounts of red clay. The clays are more silty than those in the Mupe Bay section. The IRM acquisition experiments (see Fig.4.1.20) show that the grey clay (a) has magnetite as the dominant magnetisation carrier. The mottled-yellow sandy clays (b) contain much more magnetite than their equivalents at Worbarrow and Mupe Bay (see Fig.4.1.14b). The samples from the Gault Formation (c) indicate that magnetite is the dominant constituent.

The log mean NRM intensity for this section (Fig.4.1.21) is 0.479 mA/m, which is similar to that for the Mupe Bay section (0.482 mA/m). Fig.4.1.22a shows the variation of NRM intensity with stratigraphic height in this section. As with the sections discussed earlier, zones of localized high NRM intensity can be identified. These define two principal intensity "events" in the upper part of the Wessex Formation, one of which is at 60-85 m and the other below 20 m. No such NRM intensity "events" were identified in the Gault Formation which is characterized by a constant low value throughout. This may reflect the significant difference in depositional environment between the Wessex and Gault Formations.

The CQG at Lulworth Cove lies just above an NRM intensity event ("event 2"), in a similar position to that observed at Mupe Bay (Fig.4.1.22c). Thus, these lithologically related features appear to provide a suitable basis for correlation between the two sections. Unfortunately, because of the missing lower part of the Wessex Formation in the Lulworth Cove section, it is not possible to establish whether NRM events correlatable to events 3 and 4 at Mupe Bay are present at Lulworth Cove.

About 100 samples from the Lulworth Cove section were subjected to progressive a.f. demagnetisation treatment in applied fields up to 35 mT. Fig.4.1.23 displays an example of the demagnetisation behaviour of one sample from the Wessex Formation and one from the Gault Formation. The general quality of the demagnetisation data for samples from the Gault Formation is poorer than that for the Wessex Formation (see

Appendix 4), due to their lower remanence intensity and generally less stable demagnetisation behaviour.

Fig.4.1.24 and Fig.4.1.25 summarize the CMDs (characteristic magnetisation direction) for the two formations respectively. The mean direction for the the Gault Formation, is

Dec =183°, Inc =60° (before bedding correction)
and Dec =23°, Inc =34° (after bedding correction)
with α_{95} =11° (N =11);

and that for the Wessex Formation is

Dec =175°, Inc = 52° (before bedding correction)
and Dec =15°, Inc =38°)after bedding correction)
with α_{95} =9° (N =22).

For both formations the mean direction before bedding correction differs substantially from the predicted geomagnetic field direction for the Lower Cretaceous and present field direction, while that after bedding correction agrees much more closely with the predicted vector, though having a shallower inclination. Few samples showed clear directional trends, so that application of the great circle fitting method was not appropriate for these results.

As with the Mupe Bay section, a small proportion (~15%) of the samples from the Lulworth Cove section carry a characteristic magnetisation whose direction before bedding correction is close to the present geomagnetic field direction, whilst the direction after bedding correction differs from any reasonable predicted direction for the Mesozoic (Fig.4.1.26). This is clear evidence for a post-folding magnetisation in such samples, so that the palaeomagnetic data from them could not be used for magnetostratigraphic purposes.

Although there is no overall difference between the a.f. demagnetisation behaviour of samples from the Gault Formation and that of samples from the Wealden Beds, more samples from the Gault Formation showed magnetic overprints or instability than from the Wealden

Formation (~25% and 14% respectively, see Appendix 4).

4.1.6) The Durdle Door section (The Dorset Coast).

The western-most section of the Wessex Formation sampled along the southern coast of Dorset is the Durdle Door section, where, because of a significant reduction in thickness of the sediments, only 44 sampling sites were occupied. There is no way to trace on land the CQG layer from Lulworth Cove, through St.Oswald's Bay to the Durdle section (Fig.3.3.4), although a CQG layer is apparent in the Durdle Door section.

The sediments are much coarser than those to the east and the lithology is dominated by white grey and grey silty and sandy clays with little mottled to yellow colours. All three IRM acquisition curves illustrated (see Fig.4.1.27), which are chosen from sediments with different colours, show magnetite as the dominant magnetic constituent, in marked contrast to the section on the Isle of Wight.

The log mean NRM intensity value for this section (0.234 mA/m) is the lowest of all sections studied (see Fig.4.1.28). The variation of NRM intensity with stratigraphical height is shown in Fig.4.1.29a. Two rather poorly-defined NRM intensity "events" can be recognized. The top one extends from 35 to about 50 m, possibly to the top of the section at 60 m above datum. The lower one lies beneath the 10 m level, but its base is not defined. These events are labelled "1" and "2" respectively (Fig.4.1.29b).

The CQG layer appears within event "1" and shows an increase in thickness to about 10 m compared with its equivalents in the other sections. The author found no obvious sign of another CQG immediately above the supposed event "2" in a similar position to that identified at Lulworth Cove (Fig.4.1.22) and Mupe Bay (Fig.4.1.16). However, Arkell (1947) noticed an "indefinite lignitic quartz grit" within the lowest variegated marls during his earlier studies of the section. It is possible that this represents the lateral equivalent of the CQG defined at Lulworth Cove and Mupe Bay. In this case, the upper CQG represents a new layer which appears above the lower one, as the latter

becomes indistinct to the west. This observation agrees with the pattern of CQG layers in other areas, particularly, around Woody Farm (see Fig.3.2.4), where the layers appear at different stratigraphic levels and each extends only for a few miles or less.

Eighty five samples from the Wessex Formation of Durdle Door have been subjected to incremental a.f. demagnetisation up to 35 mT. Fig.4.1.30 shows examples of two samples with normal characteristic magnetisations. Demagnetisation characteristic directions were defined for only 41% of the samples from the Durdle Door section, 26% showing directional trends towards a clear polarity end-point (in this section mainly a normal polarity) and the remaining 33% providing no meaningful results (either because of magnetic instability, or the presence of clear post-folding magnetisation components, which could not be removed by a.f. demagnetisation). An example of a sample showing a probable post-folding magnetisation is illustrated in Fig.4.1.32. This may reflect the greater tectonic disturbance that the Durdle Door section has suffered.

Fig.4.1.31 shows the "reliable" CMDs isolated (after elimination of those showing post-folding or erratic characteristics). The overall mean direction is

Dec =173°, Inc =39° (before bedding correction)
and Dec =6°, Inc =38° (after bedding correction)
with α_{95} =11° (N=21).

As with the other Dorset coast sections, the bedding-corrected vectors show a much closer conformity to the predicted Early Cretaceous vector than the values before bedding correction. This indicates that magnetisation pre-dated folding.

4.1.7) Conclusions for palaeomagnetic results from Southern England.

Table 4.1.1 summarizes the whole set of mean values of characteristic magnetisation directions (CMD) before and after bedding correction for the investigated sections through the Wessex Formation

in Southern England. Fig.4.1.33 displays the mean CMDs for each section in this area, together with the predicted geomagnetic field direction for the Early Cretaceous (see §4.1.2) before and after the bedding correction. Apply the fold test criterion proposed by McElhinny (1964), (although this method was criticized by McFadden & Jones (1981) and McFadden (1990), the simplicity of the test is still appreciated), the value of $k_2/k_1=26$ (k is the Fisher precision parameter and k_1, k_2 represent the parameters before and after bedding corrections respectively) which is much higher than the reject value of 3.44 for this mean direction, indicating 95% significance of the positive test. The trend of the distribution of the CMDs in (a) is particular to the general strike of bedding.

It is clear that the characteristic magnetisations after thermal and a.f. demagnetisation are reliable for magnetostratigraphic purpose. The fold test in this area plays an important role in confirming that the characteristic remanent magnetisation of the Wessex Formation was undoubtedly acquired before the major tectonic movements (Middle Tertiary, Chapter I). Furthermore, the regular appearance of normal and reverse polarity intervals in the Worbarrow and Mupe Bay sections indicates that the characteristic magnetisation may have been acquired very soon after the sediments were deposited.

Although it was considered that the problem of shallower inclination from the Wessex Formation, to compare the predicted geomagnetic field direction of the Lower Cretaceous (§4.1.2), might be caused by post-depositional compaction effects (Kerth & Hailwood 1988), it may question about the precision of the predicted field direction. Therefore, further investigation should be carried out to provide more evidence of the predicted direction for the stable NW Europe plate.

Table 4.1.1 The overall mean directions of characteristic magnetisation for each of the sections through the Wessex Formation of Soutern England

SECTION	MEAN DIR. (normal p.)	MEAN DIR. (reverse p.)	OVERALL MEAN (before B.C.)	OVERALL MEAN (after B.C.)
IOW	DEC INC 359° 65° α_{95}=2°N=78		DEC INC 359° 65°	DEC INC 357° 45°
WORBARROW BAY	DEC INC 190° 84° α_{95}=4°N=115	DEC INC 203°-72° α_{95}=13°N=14	DEC INC 29° 84°	DEC INC 3° 38°
MUPE BAY	DEC INC 192° 54° α_{95}=5°N=85	DEC INC 322°-55° α_{95}=25°N=13	DEC INC 166° 57°	DEC INC 5° 37°
LULWORTH COVE	DEC INC 175° 52° α_{95}=9°N=22		DEC INC 175° 52°	DEC INC 15° 38°
DURDLE DOOR	DEC INC 173° 39° α_{95}=11°N=21		DEC INC 173° 39°	DEC INC 6° 38°
			OVERALL MEAN(for all sections) (before B.C.)	(after B.C.)
			DEC INC 167° 80° α_{95}=32°N=5 k=6.6	DEC INC 5° 39° α_{95}=5°N=5 k=185.9

Note: p.=polarity. B.C.= bedding correction. N: sample number. DEC: declination and INC: inclination.

4.1.8) Beare Green clay pit sections (Newdigate, SE England).

The Beare Green clay pit was sampled for magnetostratigraphic work in the first year of this study, as part of a pilot investigation of the Weald Clay Formation of SE England. Two short profiles were sampled, covering a stratigraphic height of only 3.5 m. These two sections are in a slope in the brickwork pit, which was worked a long time ago. Each section is only about 2 m in length. The sediments are dark grey silty clays.

IRM acquisition experiments indicate that magnetite is the main magnetic bearer (Fig. 4.1.34) and NRM intensity is fairly strong, with a log mean value of 16 mA/m (Fig. 4.1.35). Thus palaeomagnetic determination for these sections were intrinsically more precise than for the Dorset coast and Isle of Wight sections. Fig.4.1.36 gives two examples of response to a.f. demagnetisation. All samples yielded comparatively well-defined demagnetisation SEPs, of normal polarity. However, because of the very restricted length of the sections studied the results have limited magnetostratigraphic value, apart from indicating the presence of a 3.5 m normal polarity interval near the top of the Weald Clay Formation (possibly in Beds 9-10 of Thurrell *et al* (1968), see Fig.3.3.6a).

4.1.9) Langhurst quarry sections (Warnham, the Weald Clay, SE England).

About 5 miles to the south of Newdigate brickworks is the Warnham brickwork pits. These consist of a series of working pits extending southwards from near Langhurst. Unfortunately many of the older pits are now overgrown with vegetation or have suffered surface deterioration, so that they are less-suitable for magnetostratigraphic investigations.

Palaeomagnetic samples were taken from 19 sites in one section on a northwest bank and 16 sites in a second section on a southeast banks. The total stratigraphic interval represented is about 14-15 m (compared with the total thickness of the Weald Clay in the Warnham area of ~50 m (Worssam 1978)). The IRM acquisition curves (Fig.4.1.37) indicate that

the dark grey silty clays (a and b) in the lower part of the sections (see Plate 3.3.1) are dominated by magnetite but those from the upper part with mottled or yellow-brown colour (c and d) contain significant amounts of hematite. In some cases (eg sample LG35.1c, Fig.4.1.37d) both minerals can be identified. On the basis of these results, a.f. demagnetisation treatment should be suitable for most samples, except those in the upper part of the sections.

Fig.4.1.38 shows the statistical distribution of NRM intensity values for both sections. The overall log-mean value is 0.466 mA/m. This is much lower than that for the Beare Green sections, indicating a possible depositional environment change from the lower part to the upper part of the Weald Clay period. Figs.4.1.39a and 4.1.40a show the variation of NRM intensity with stratigraphic height in the two sections. Generally, the variations of NRM values do not show as many marked changes as those observed in the Dorset Coast and Isle of Wight sections. However a conspicuous high NRM intensity "event" is identified in the "northwest" bank section. A sand/limestone layer lies just beneath this event and provides a useful lithological marker (Figs.4.1.39a and b). Following the terminology used for the Dorset Coast sections, this NRM event is termed "event 1". In contrast, the section on the southeast bank shows smaller fluctuation of intensity but two possible poorly-defined intensity "events" are identified in Fig.4.1.40b. The lower of these lies just below a sand/limestone marker bed which is probably not the correlative of the sand/limestone bed observed in the "northwest" bank section).

In total, 77 samples were subjected to progressive a.f. demagnetisation up to 35 mT. A small proportion of these was then subjected to further treatment, up to 60 mT on the Molspin demagnetiser. Fig.4.1.41 presents some examples of samples which show well defined characteristic magnetisations. As with the Wealden Beds of southern Dorset, some samples from the Langhurst sections do not yield stable end points, but instead clear directional trends are apparent during demagnetisation. Fig.4.1.42 shows the SEPs for both normal and reverse polarities and Fig.4.1.43 the intersections defined from converging great circles. The overall mean direction for the SEPs is

Dec = 359°, Inc = 45° with α_{95} =5° (N =42)

(after application of a very shallow bedding correction of about 5° to the north and inverting the reverse polarity SEPs). The inclination is somewhat shallower than that for the predicted field direction at this locality. The mean direction defined from the great circle intersections for the reverse polarity samples has a Dec =182°, Inc =-41° and 95% confidence limit =18° in the elongate direction and 5° perpendicular to this direction (6 directional trends involved). Thus, there is a good agreement between the mean directions defined from the SEP analysis and that defined from the great circle intersections.

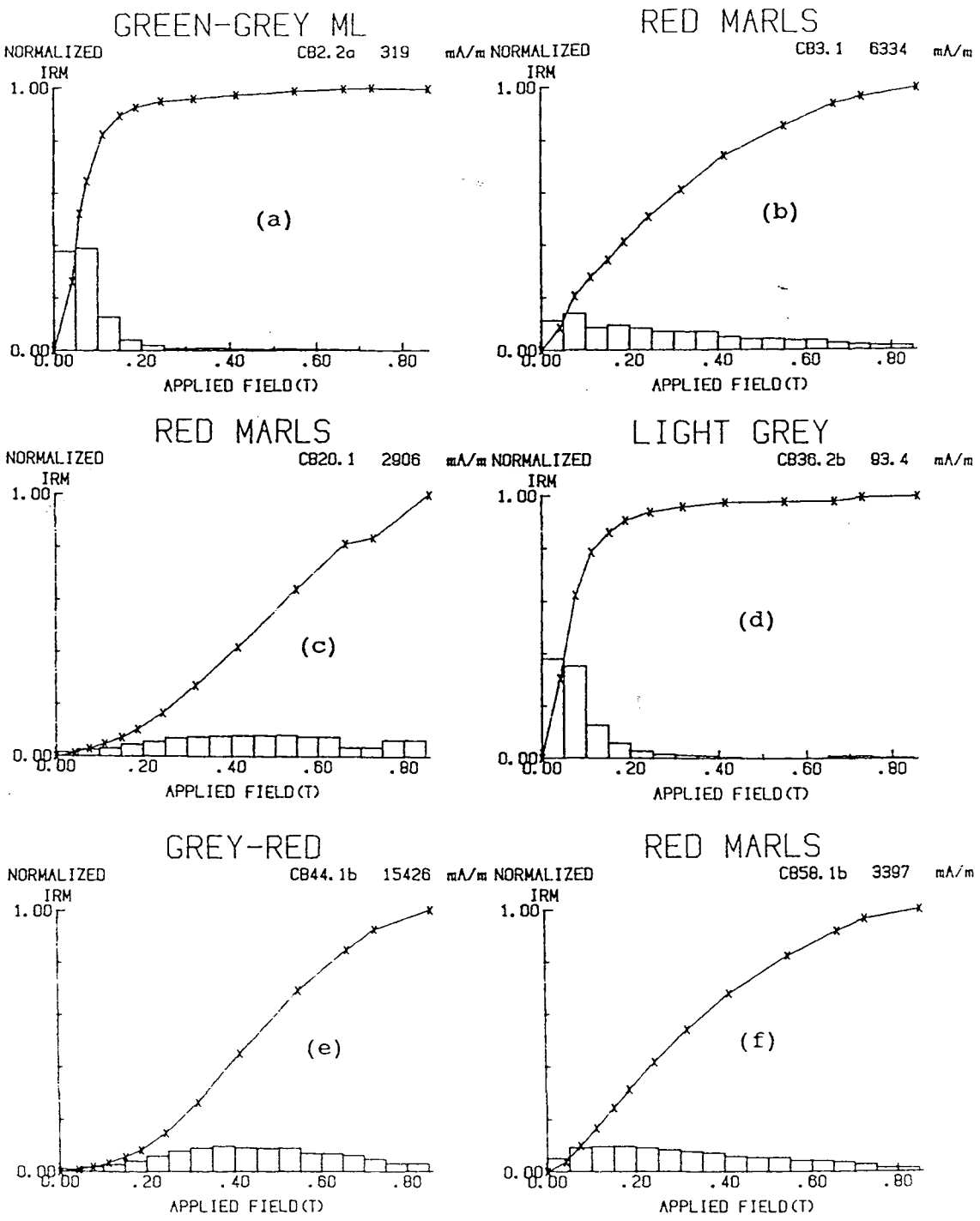

Fig. 4.1.1 Some examples of IRM acquisition curves for samples of the Wessex Formation from the Isle of Wight (Compton-Hanover Point) section.

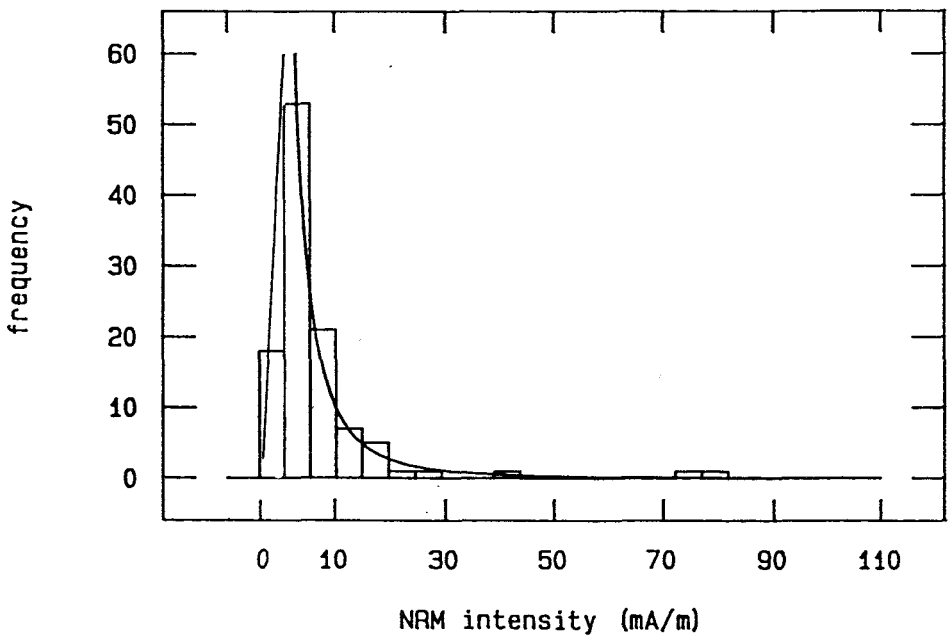

Fig. 4.1.2 NRM intensity histogram for samples from the Wessex Formation of the Compton-Hanover Point (Isle of Wight) section. It follows a logarithmic distribution (the smooth curve plotted).

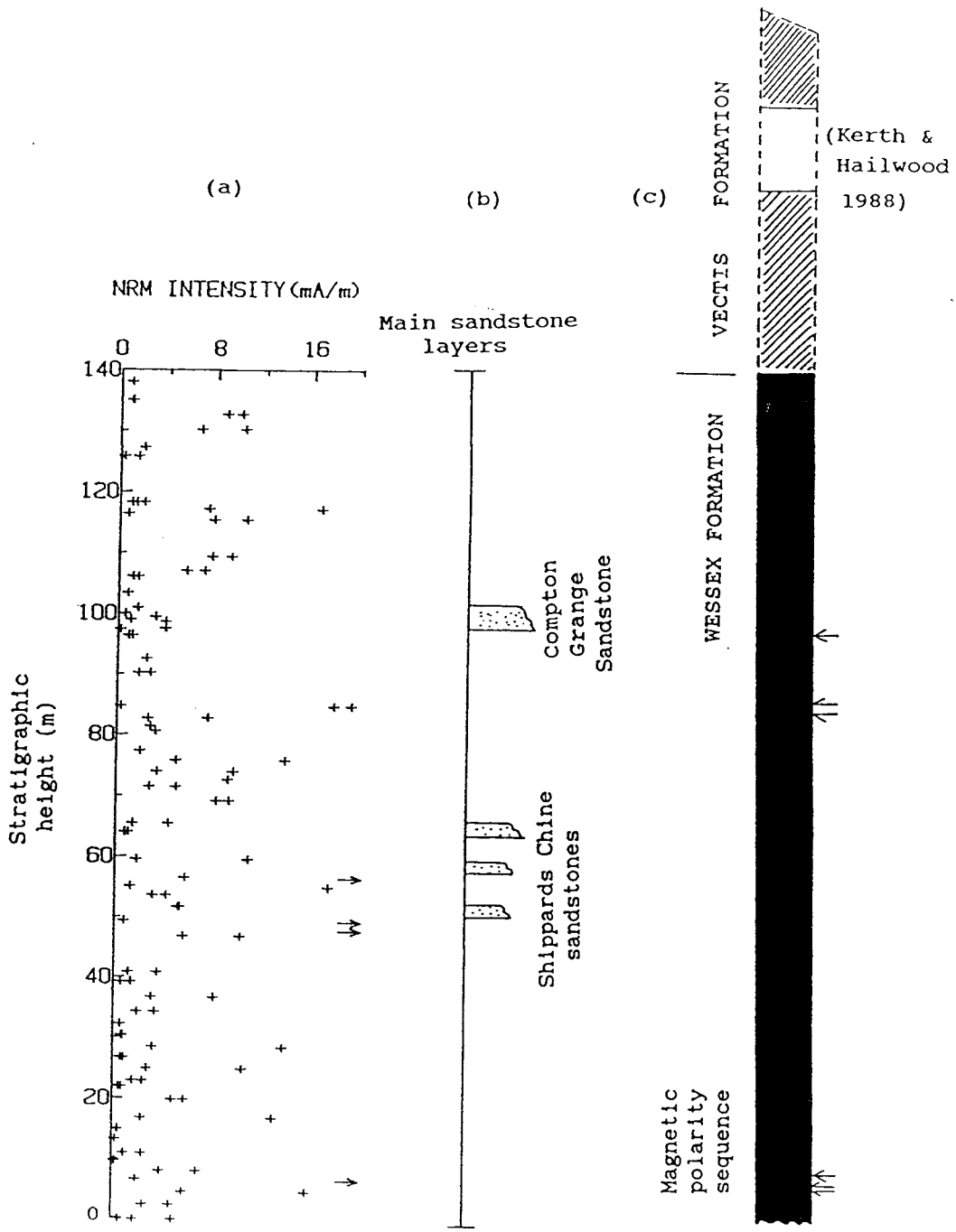

Fig. 4.1.3 (a) Variation of NRM intensity with stratigraphic height for the Compton-Hanover Point sequence. The stratigraphic height is measured from the Hanover Point and the sequence extends up to the boundary between the Wessex and Vectis Formations. Arrows represent NRM values >20 mA/m. (b) Distribution of main sandstone layers. (c) Magnetic polarity sequence with the previous results for the Vectis Formation (Kerth & Hailwood 1988) shown at the top. Black and hachure represents normal polarity, white represents reverse polarity. Arrows indicate individual isolated reverse polarity samples.

Fig. 4.1.4 Example of demagnetisation results (using (a) a.f. and (b) thermal methods) for samples of the Wessex Formation from the Compton-Hanover Point section, Isle of Wight. Solid symbols on the stereographic projection represent vector directions with positive inclination and open symbols negative inclination. On the Vector End Point Diagrams shown at the right, solid circle symbols represents points on the horizontal plane and open symbols on the vertical plane.

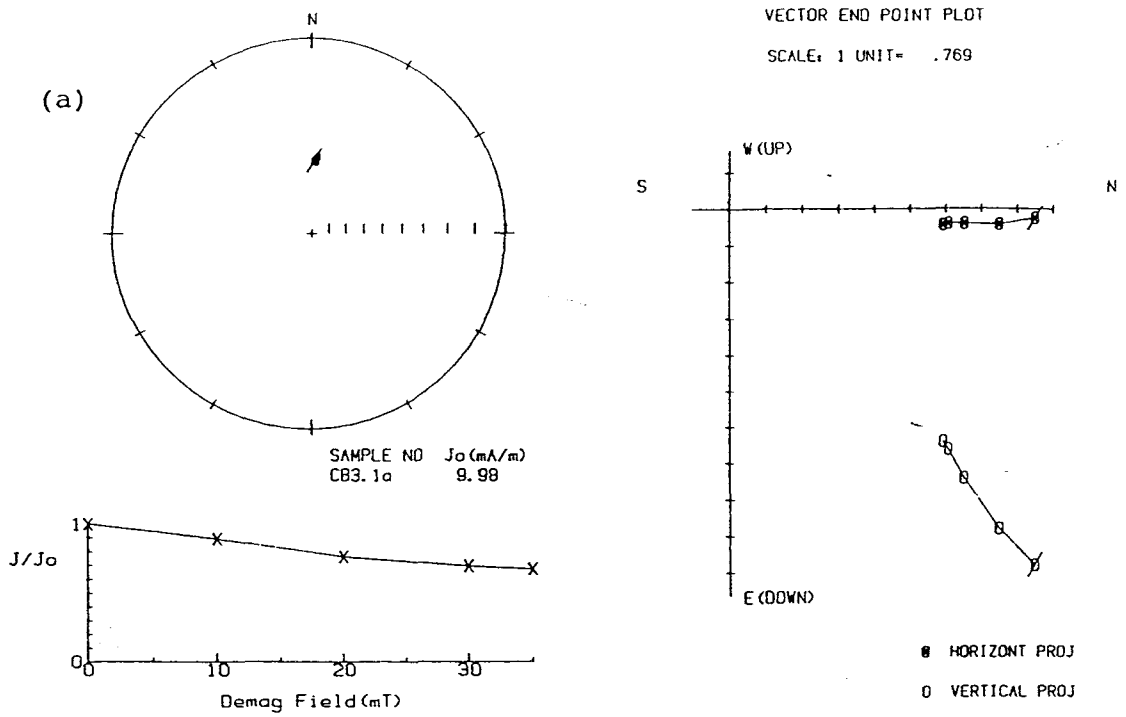
(a)
N
SAMPLE NO Jo(mA/m)
CB3.1a 9.98
J/Jo
1
0
0
10
20
30
Demag Field(mT)
VECTOR END POINT PLOT
SCALE: 1 UNIT= .769
W(UP)
S
N
E(DOWN)
HORIZONT PROJ
VERTICAL PROJ

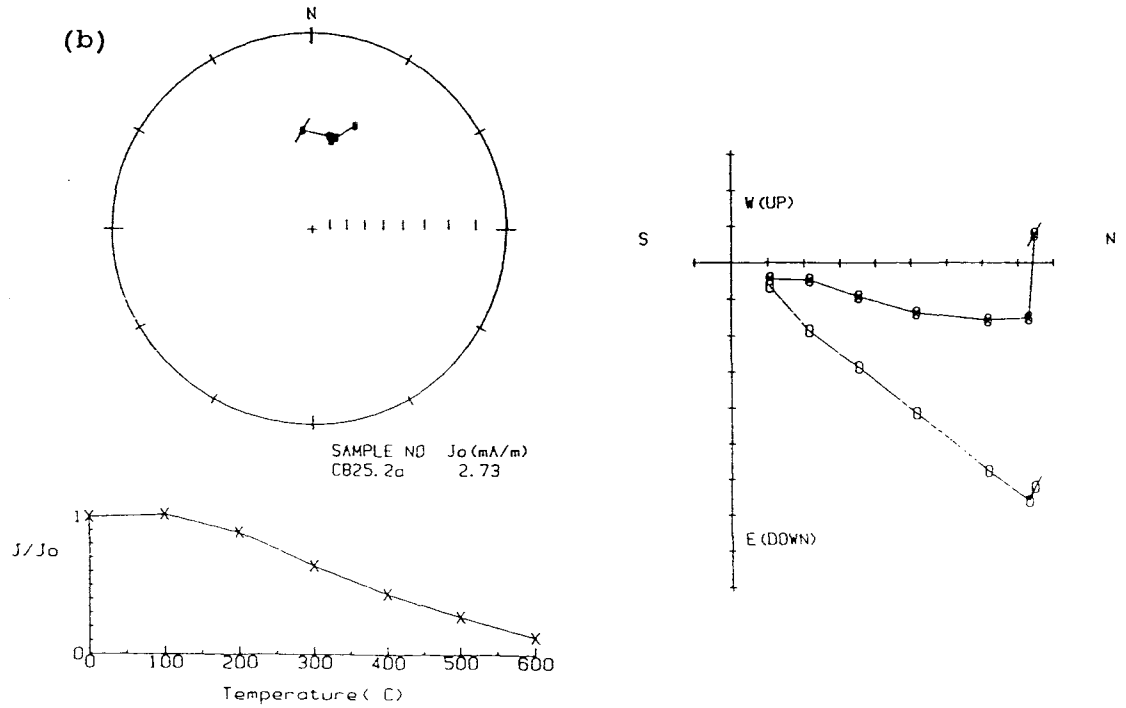
(b)
N
SAMPLE NO Jo(mA/m)
CB25.2a 2.73
J/Jo
1
0
0
100
200
300
400
500
600
Temperature(C)
W(UP)
S
N
E(DOWN)

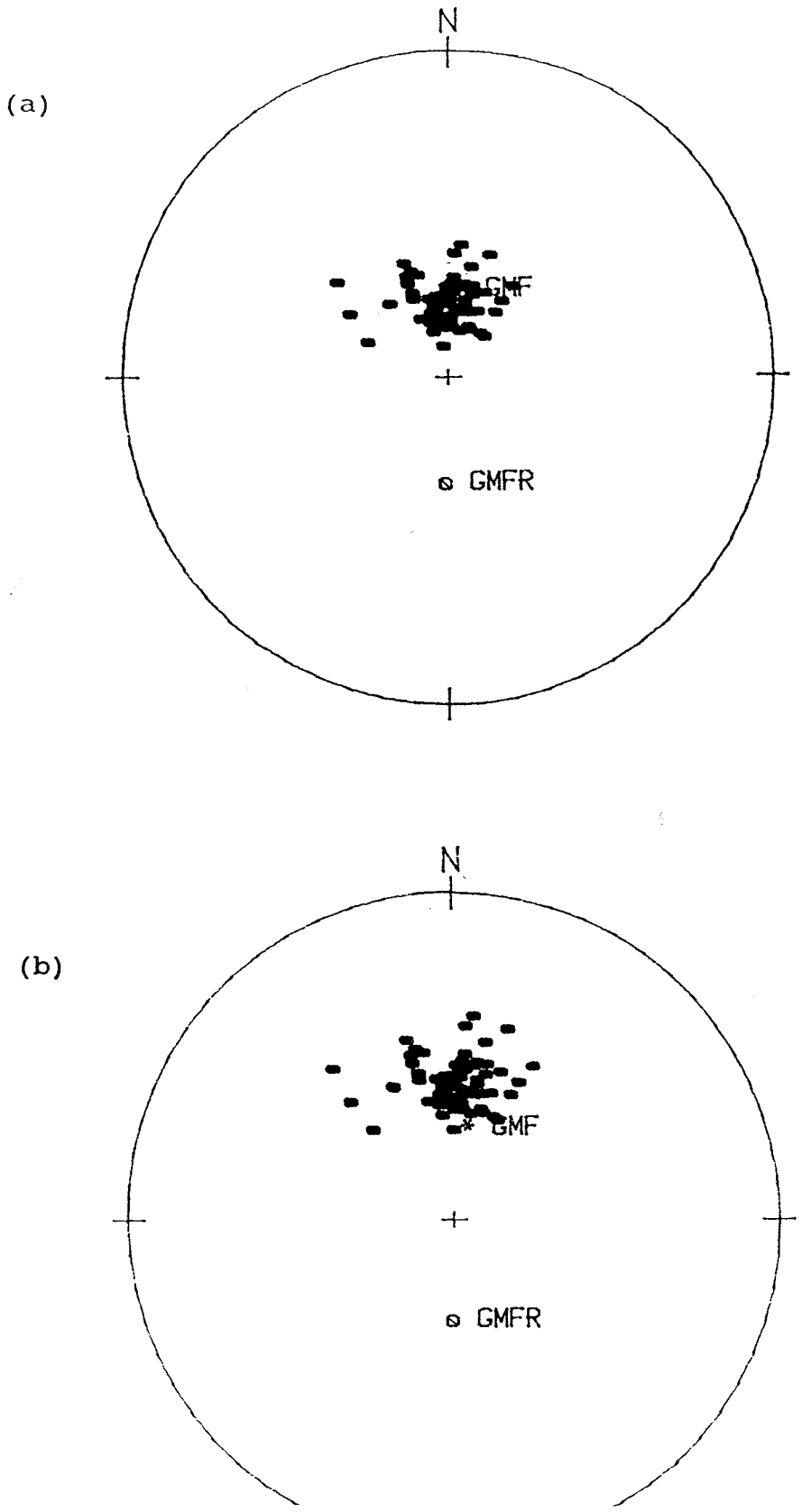

Fig. 4.1.5 Plot of SEP (vector Stable End Point) directions on equal area projection for samples from the Compton-Hanover Point (Isle of Wight) section. (a) before bedding correction, (b) after bedding correction. *GMF and oGMFR are defined as Fig. 4.1.11. Solid symbols, lower hemisphere.

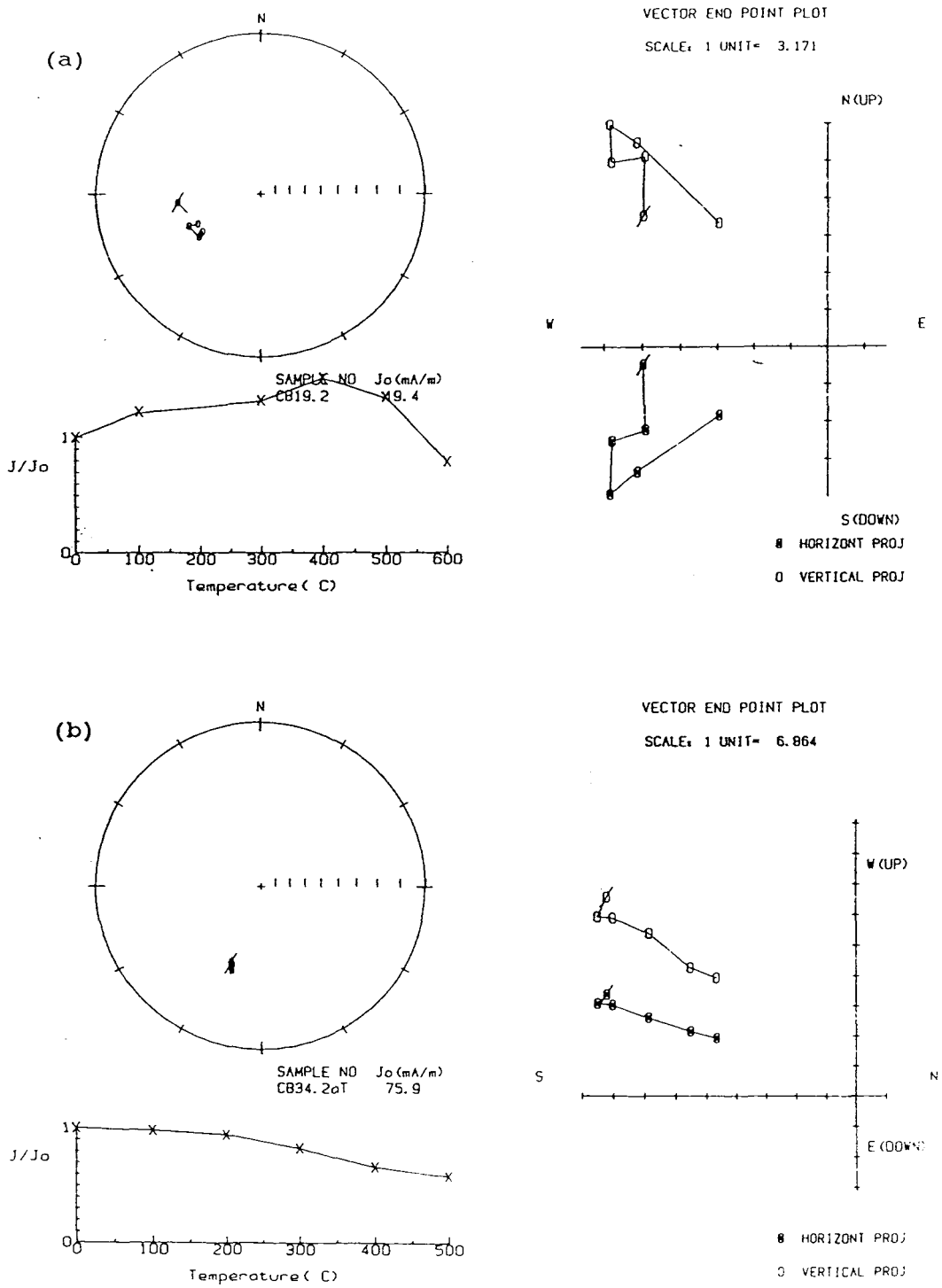

Fig. 4.1.6 Examples of reverse polarity magnetisations identified in isolated samples within the long normal polarity sequence of the Isle of Wight Wessex Formation section. Symbols and conventions as in Fig. 4.1.4.

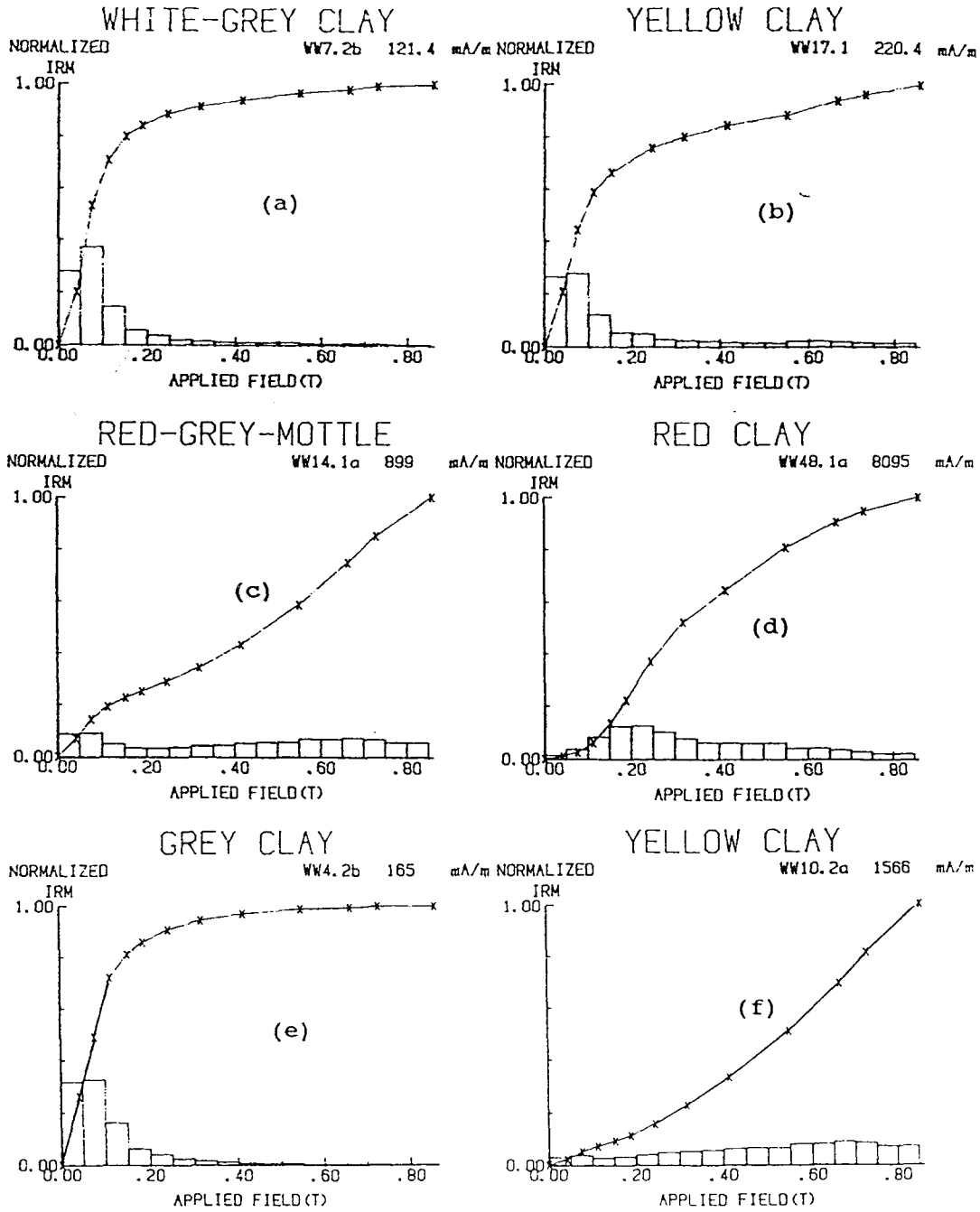

Fig. 4.1.7 Examples of IRM acquisition curves observed for samples of the Wessex Formation from the Worbarrow Bay section, classified according to the sediment colour.

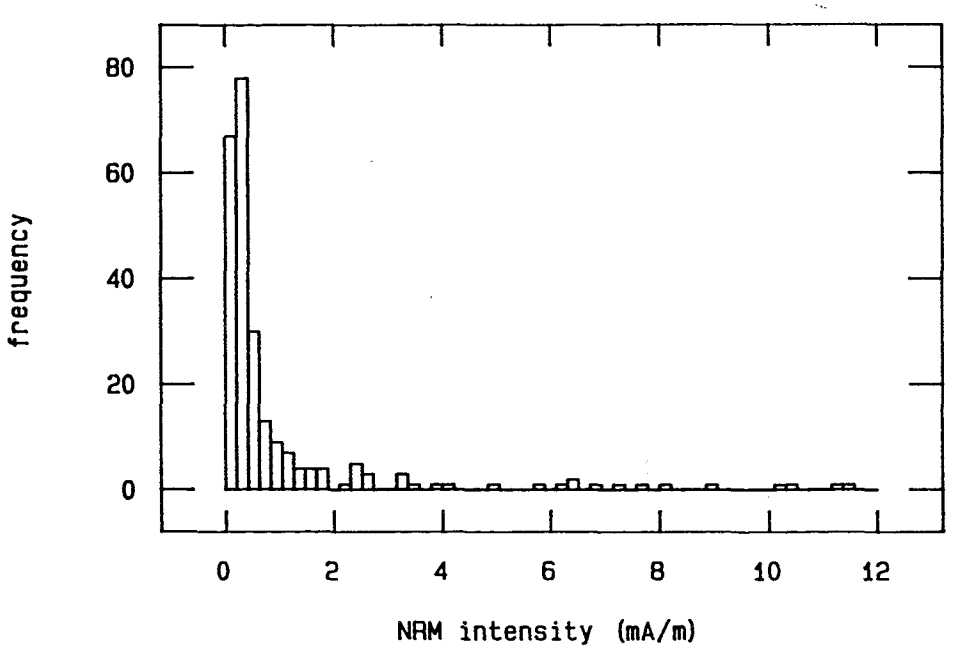

Fig. 4.1.8 Statistical distribution of NRM intensity values for the Wessex Formation of the Worbarrow Bay section.

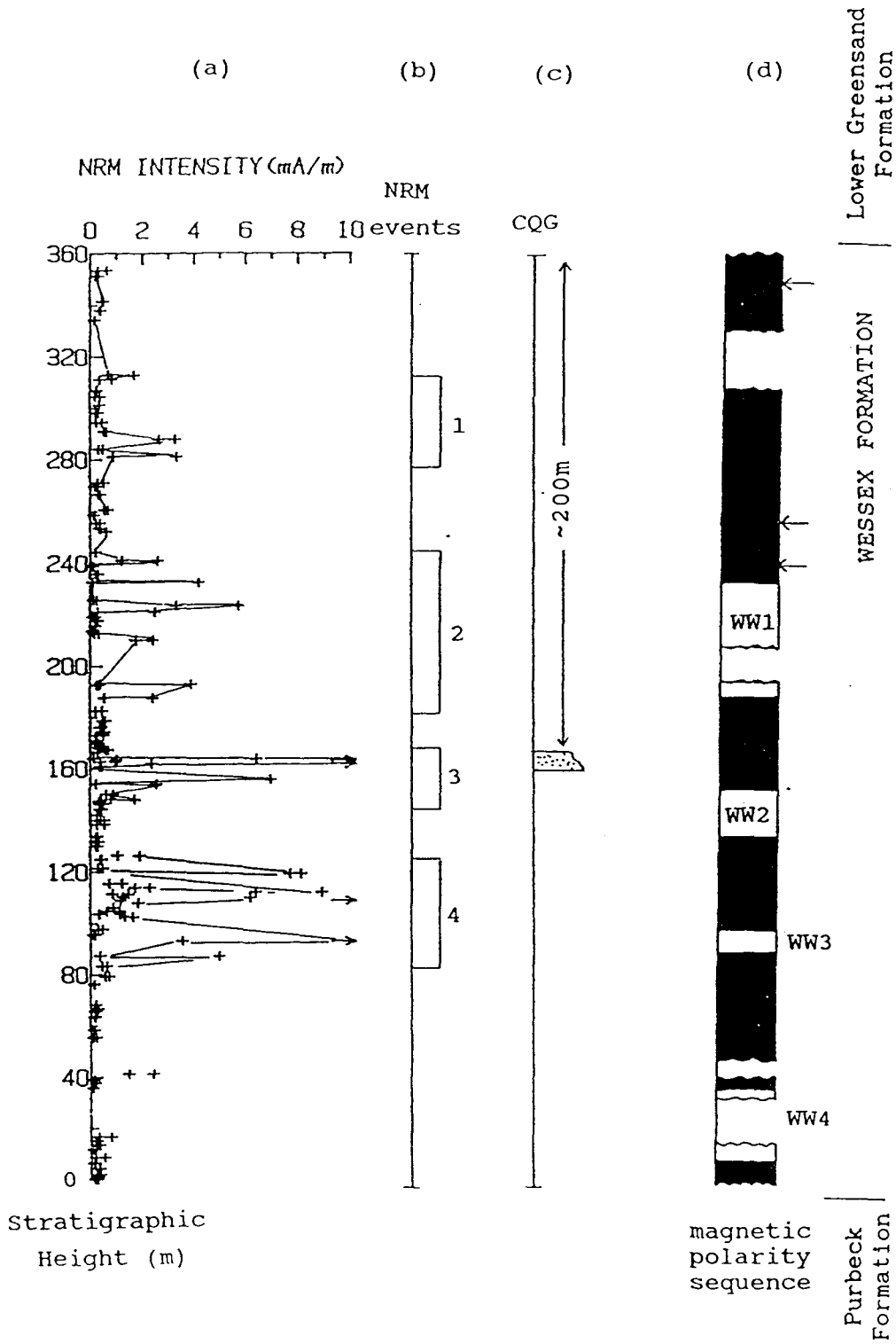

Fig. 4.1.9 (a) Variation of NRM intensity with stratigraphic height for the Worbarrow Bay section. The section top is ~10 m below the base of the Lower Greensand Formation and the bottom lies within Bed No. 2 of Arkell (1947). (b) recognizable NRM intensity "events", (c) position of the Coarse Quartz Grit in this section and (d) magnetic polarity sequence identified. WW1-4 represent reverse polarity intervals. Other symbols as in Fig. 4.1.3.

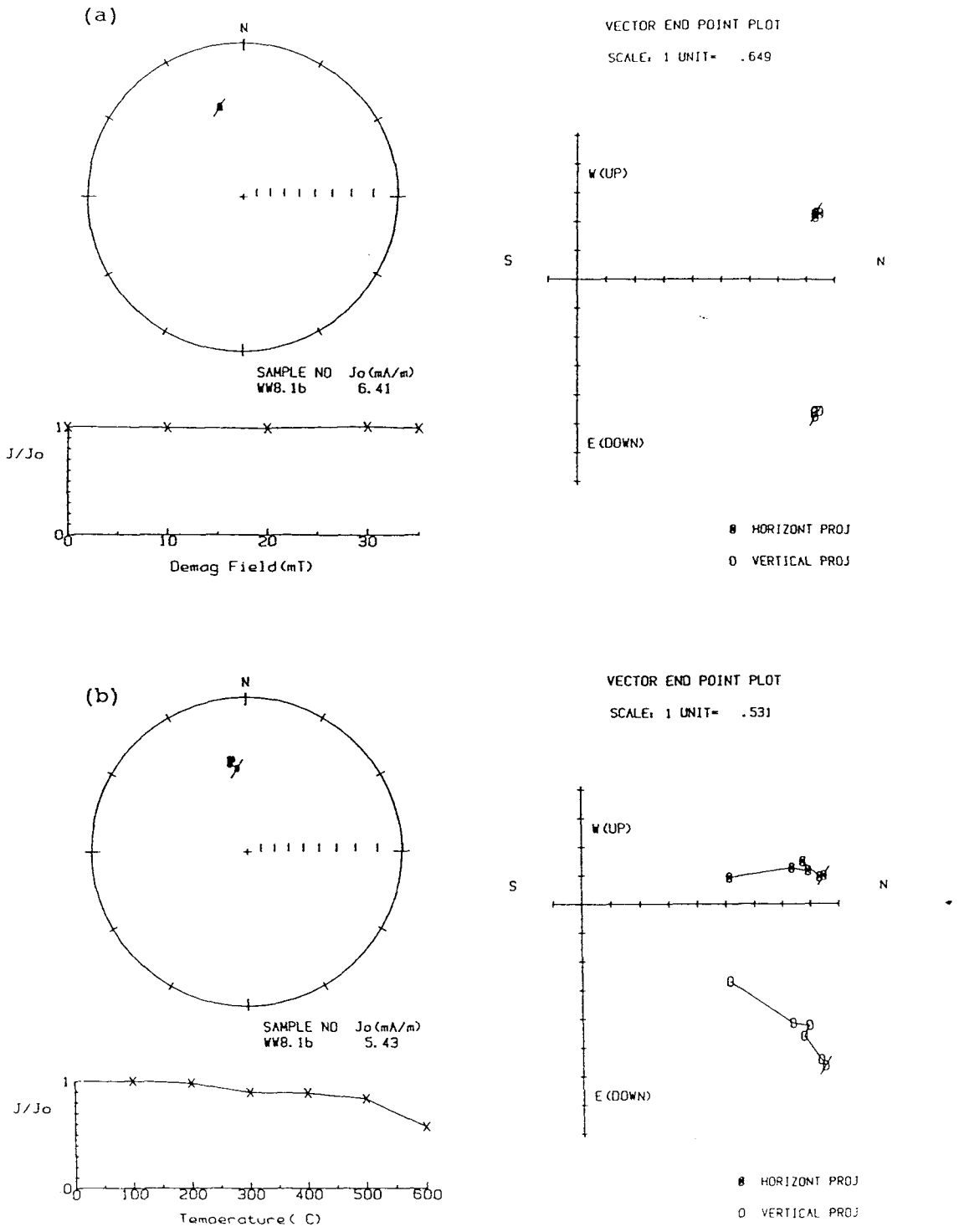

Fig. 4.1.10 Examples of comparative demagnetisation results (using a.f. and thermal methods) for pairs of samples of the Wessex Formation from the Worbarrow Bay section. Symbols and conventions as in Fig. 4.1.4.

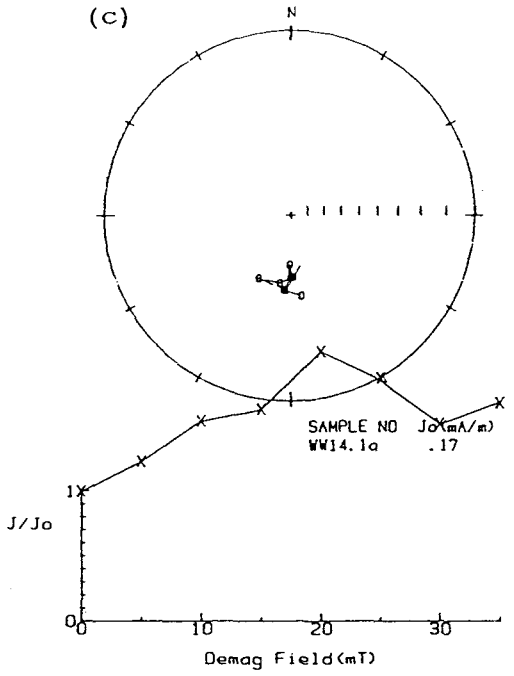
(c)
N
SAMPLE NO Jo(mA/m)
WW14.1a .17
J/Jo
1
0
0
10
20
30
Demag Field(mT)

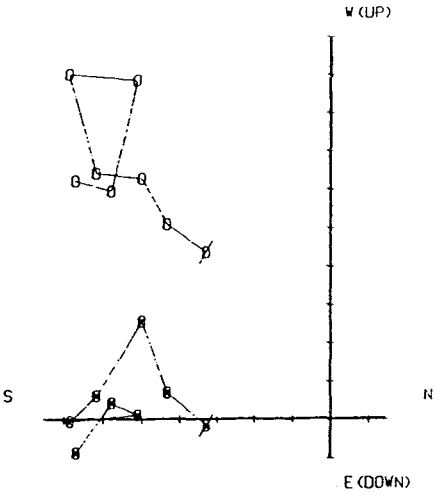
W(UP)
S
N
E(DOWN)

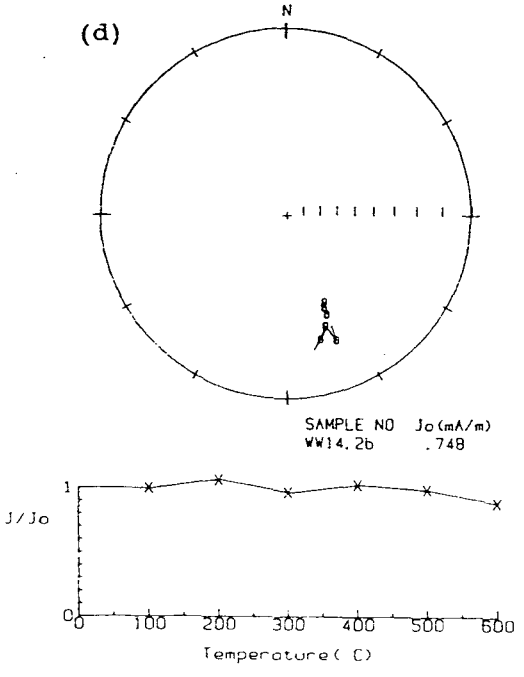
(d)
N
SAMPLE NO Jo(mA/m)
WW14.2b .748
J/Jo
1
0
0
100
200
300
400
500
600
Temperature(C)

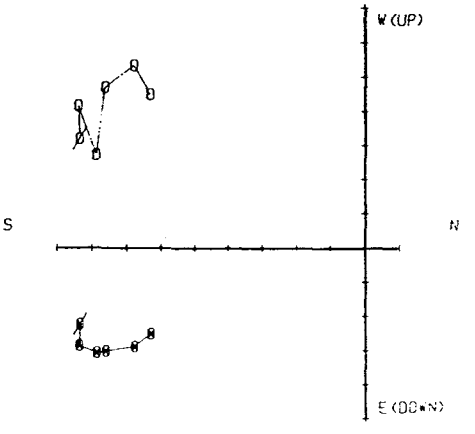
W(UP)
S
N
E(DOWN)

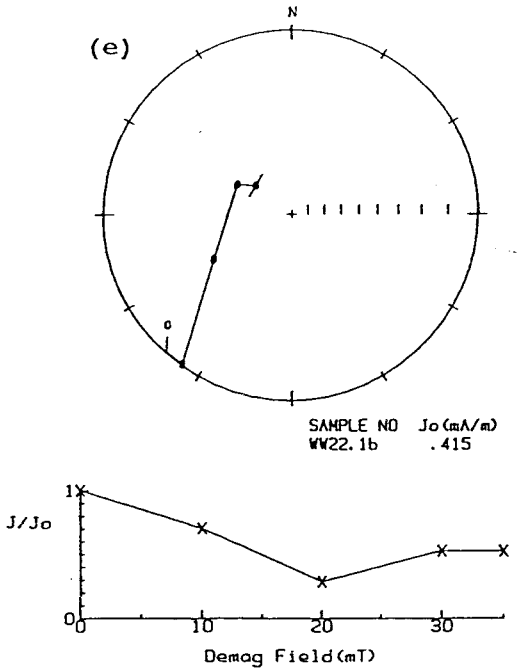
(e)
N
SAMPLE NO Jo(mA/m)
WW22.1b .415
J/Jo
1
0
0
10
20
30
Demag Field(mT)

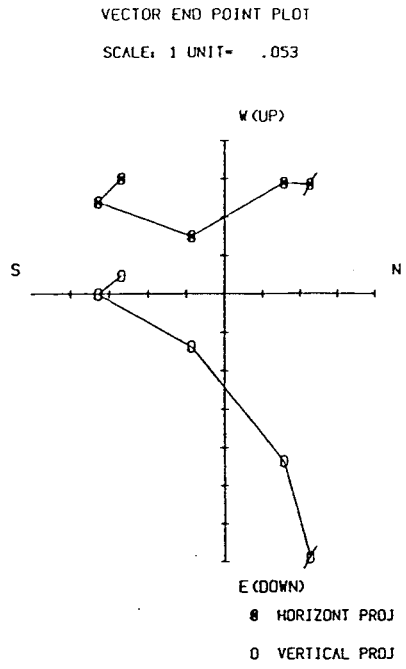
VECTOR END POINT PLOT
SCALE: 1 UNIT= .053
W(UP)
S
N
E(DOWN)
HORIZONT PROJ
VERTICAL PROJ

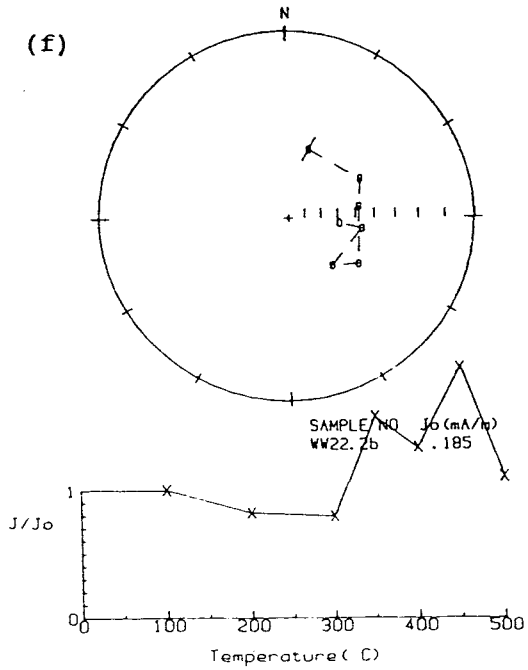
(f)
N
SAMPLE NO Jo(mA/m)
WW22.2b .185
J/Jo
1
0
0
100
200
300
400
500
Temperature(C)

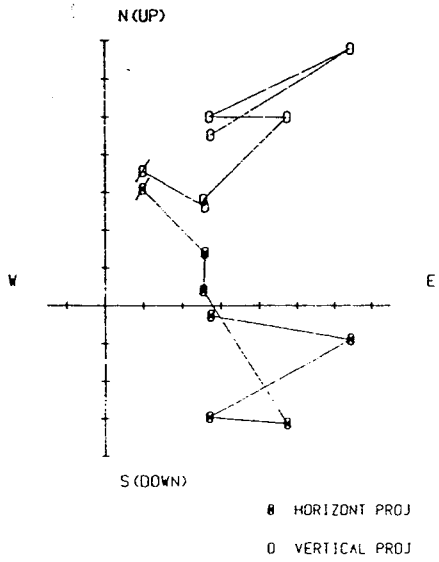
VECTOR END POINT PLOT
SCALE: 1 UNIT= .038
N(UP)
W
E
S(DOWN)
HORIZONT PROJ
VERTICAL PROJ

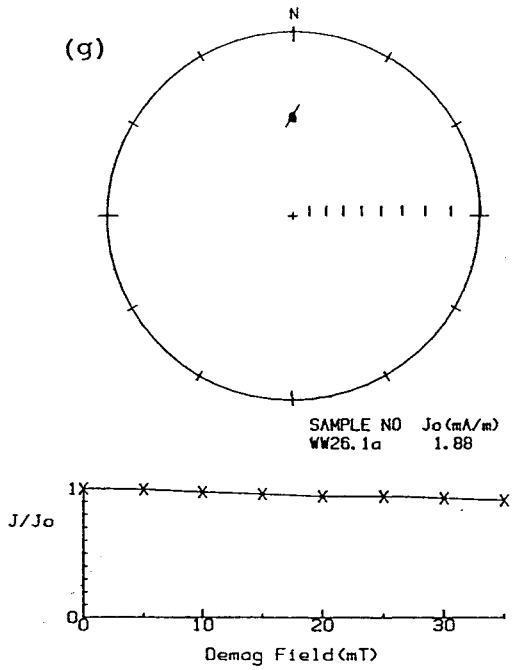
(g)
N
SAMPLE NO Jo(mA/m)
WW26.1a 1.88
J/Jo
1
0
0
10
20
30
Demag Field(mT)

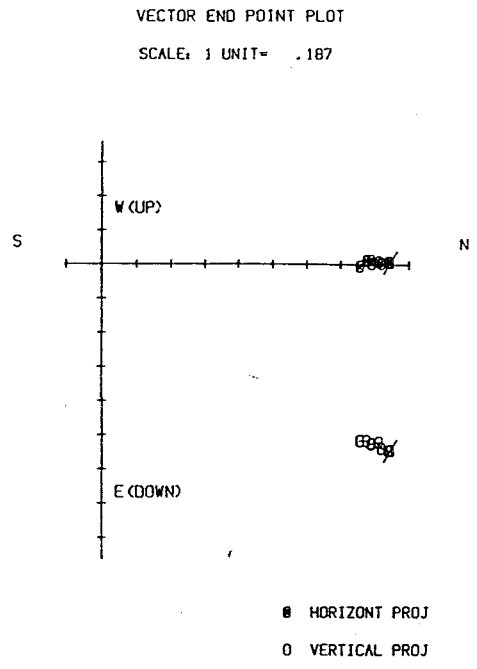
VECTOR END POINT PLOT
SCALE: 1 UNIT= .187
W(UP)
S
N
E(DOWN)
HORIZONT PROJ
VERTICAL PROJ

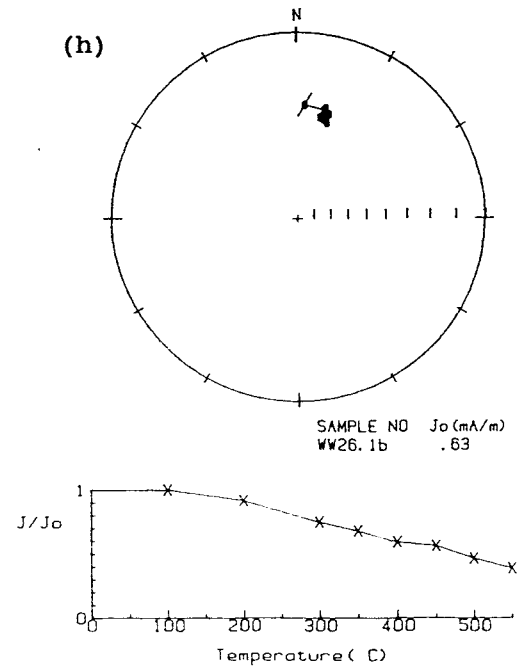
(h)
N
SAMPLE NO Jo(mA/m)
WW26.1b .63
J/Jo
1
0
0
100
200
300
400
500
Temperature(C)

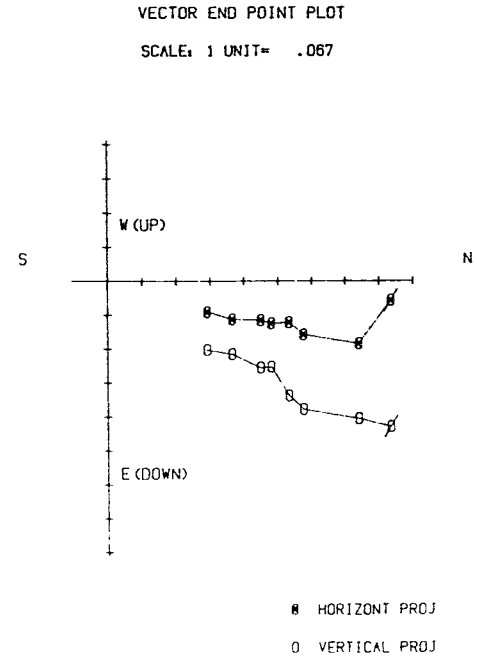
VECTOR END POINT PLOT
SCALE: 1 UNIT= .067
W(UP)
S
N
E(DOWN)
HORIZONT PROJ
VERTICAL PROJ

Fig. 4.1.11 Plots of characteristic magnetisation directions for samples of the Wessex Formation from the Worbarrow Bay section. (a) and (b) are for normal polarity SEPs and (c) and (d) for reverse polarity SEPs. (a) and (c) are before bedding correction and (b) and (d) after bedding correction. *GMF and oGMFR are predicted geomagnetic field directions for the Lower Cretaceous, for normal and reverse polarities respectively; solid symbols - lower hemisphere and open symbols - upper hemisphere.

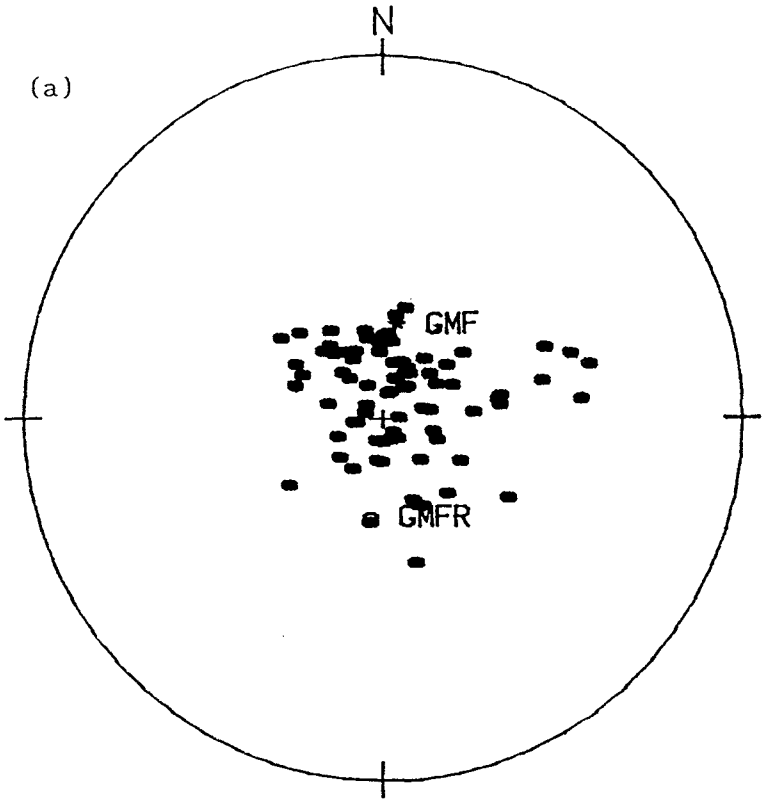
(a)
N
GMF
GMFR

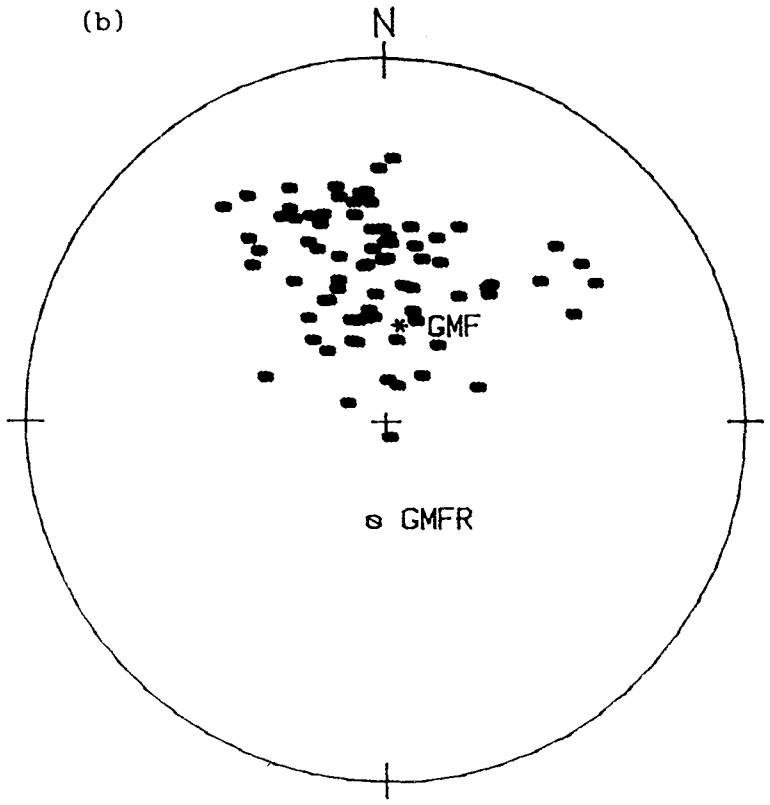
(b)
N
GMF
GMFR

(c)

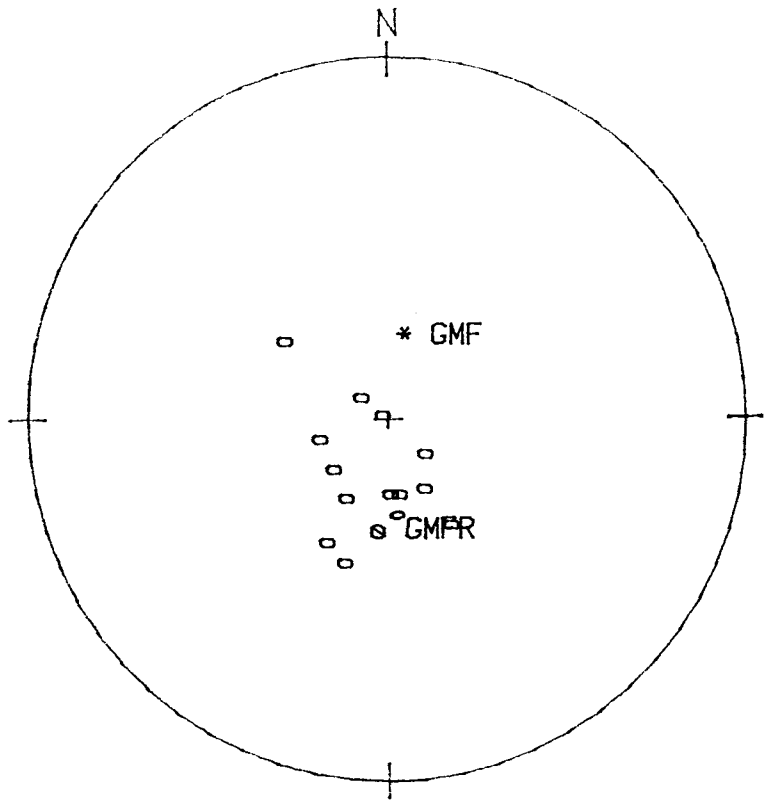

(d)

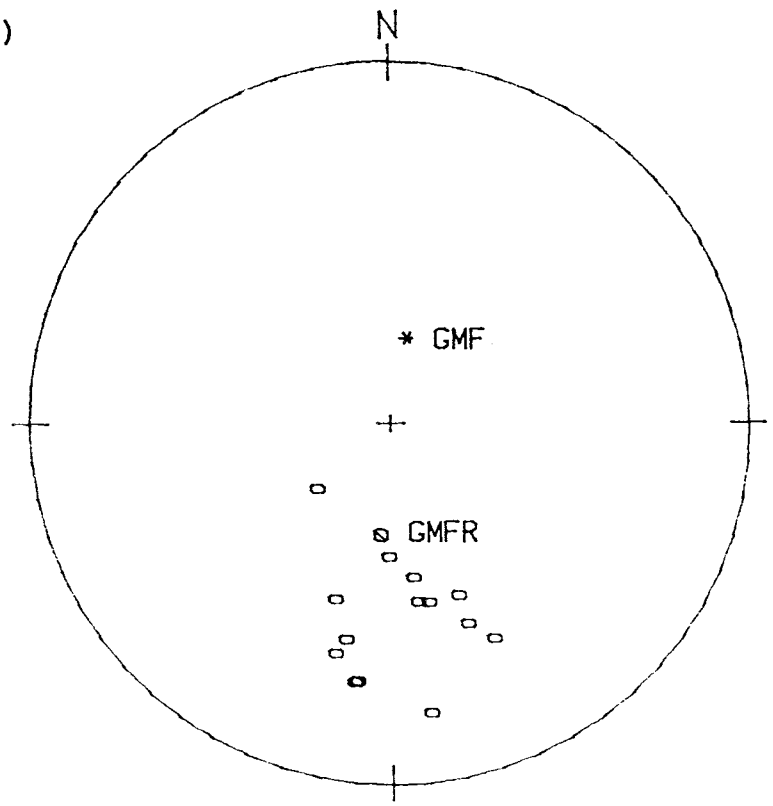

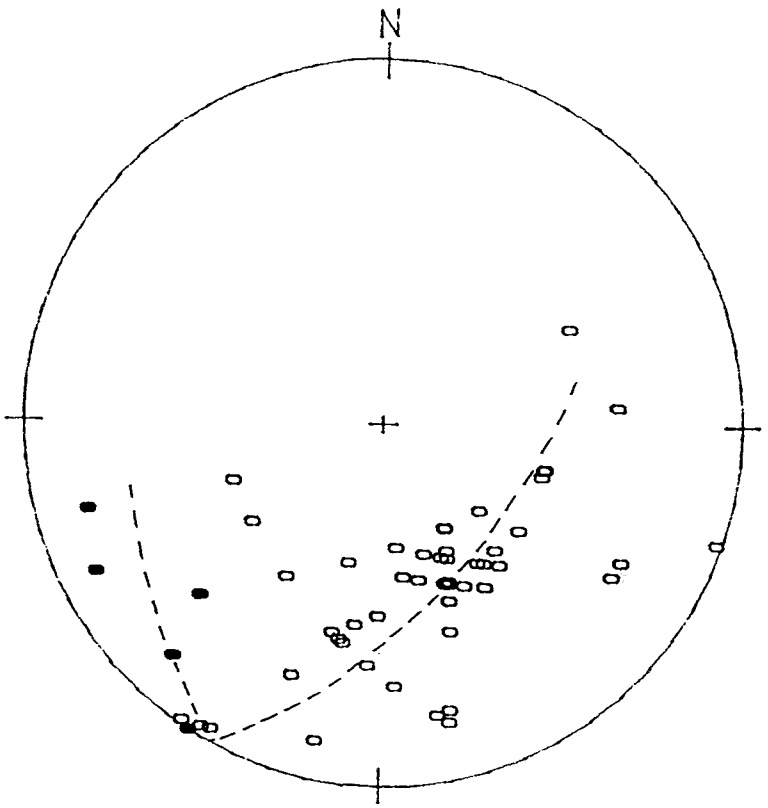

Fig. 4.1.12 Intersections produced by the great circle fitting method for those samples showing directional trends towards reverse polarity end points. The distribution of points is elongated along the trend indicated (for explanation see Chapter II), (Wessex Formation, Worbarrow Bay).

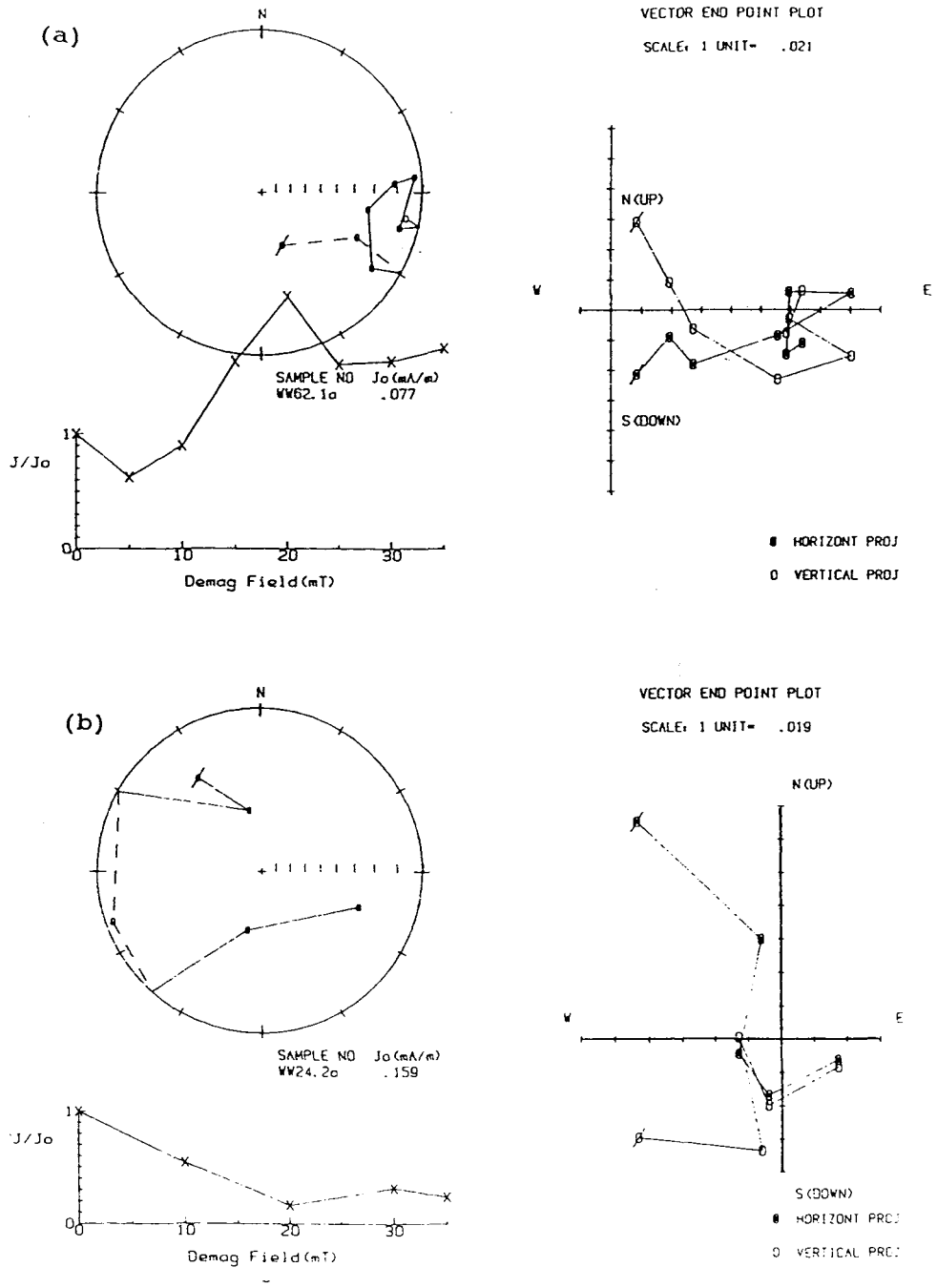

Fig. 4.1.13 Examples of samples from the Wessex Formation of Worbarrow Bay showing complex or erratic behaviour during demagnetisation, so that reliable polarity assessments are not possible. Symbols and conventions as in Fig. 4.1.4.

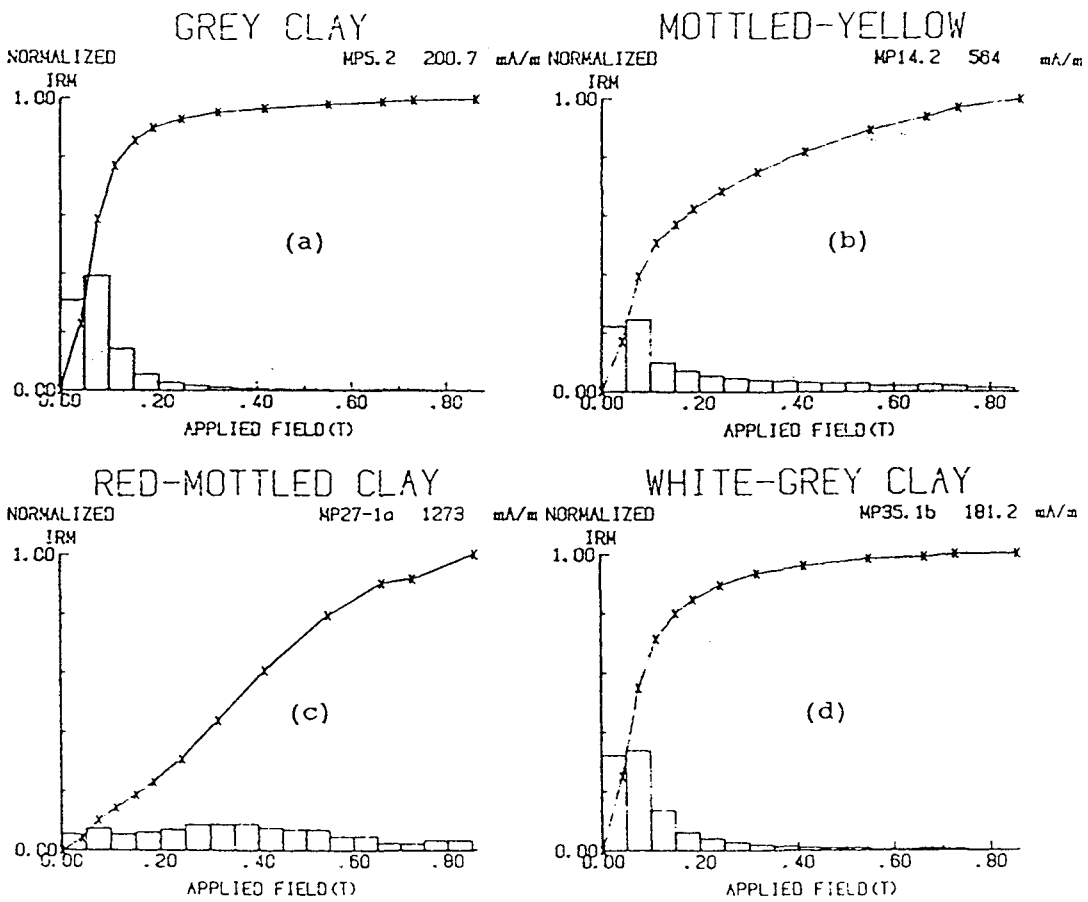

Fig. 4.1.14 Examples of IRM acquisition curves for samples of the Wessex Formation from the Mupe Bay section. The dominant colour of each sample is indicated.

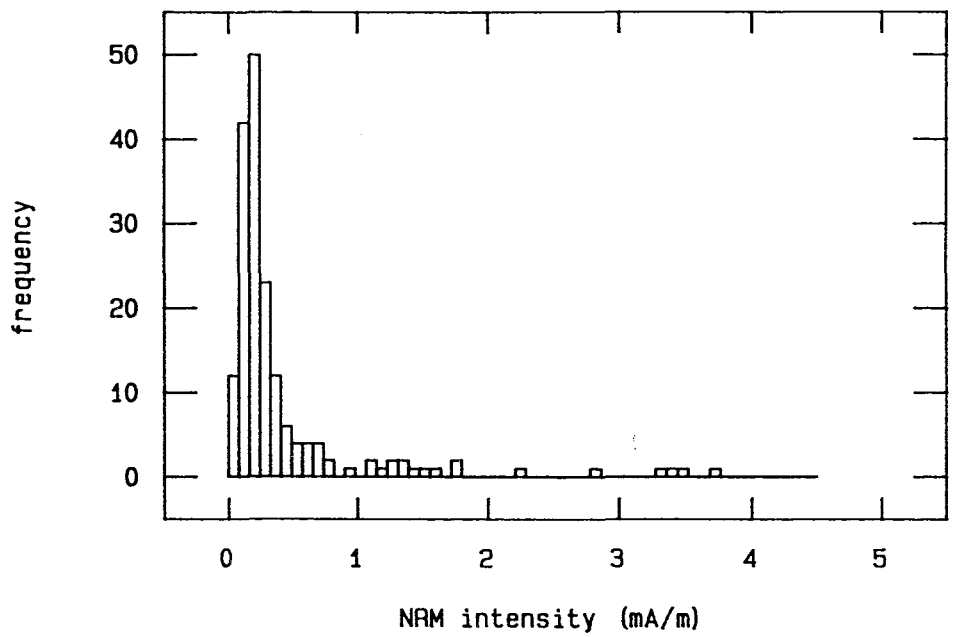

Fig. 4.1.15 Statistical distribution of NRM intensity values for samples of the Wessex Formation from the Mupe Bay section.

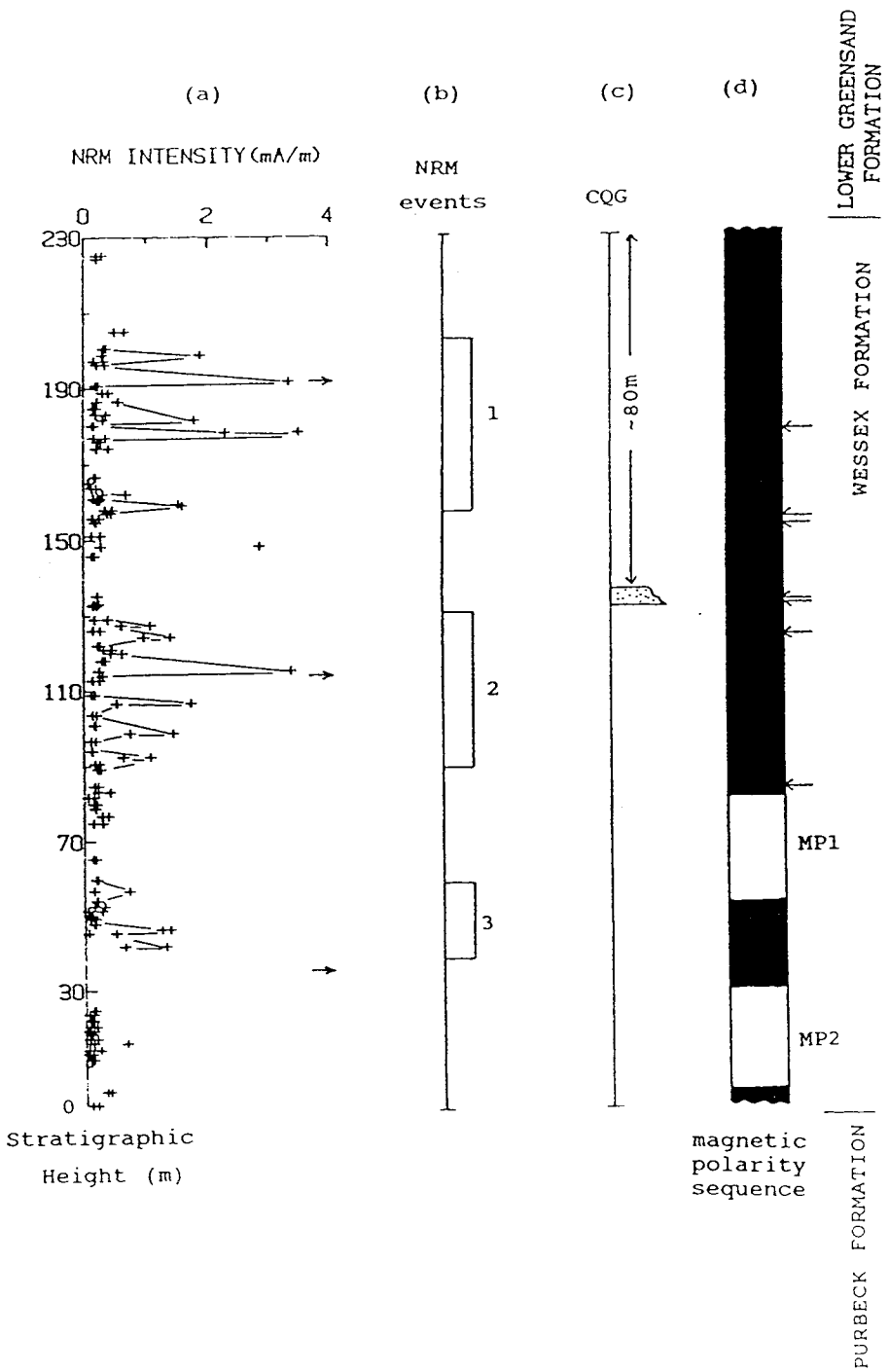

Fig. 4.1.16 (a) NRM intensity variation with stratigraphic height for the Wessex Formation, Mupe Bay. The section top is ~8 m below the base of the Lower Greensand Formation and the bottom is ~20m above the Purbeck Beds. (b) recognizable NRM intensity events. (c) The position of the CQG layer in the Mupe Bay section. (d) magnetic polarity sequence for the Mupe Bay section. Other symbols as Fig. 4.1.3.

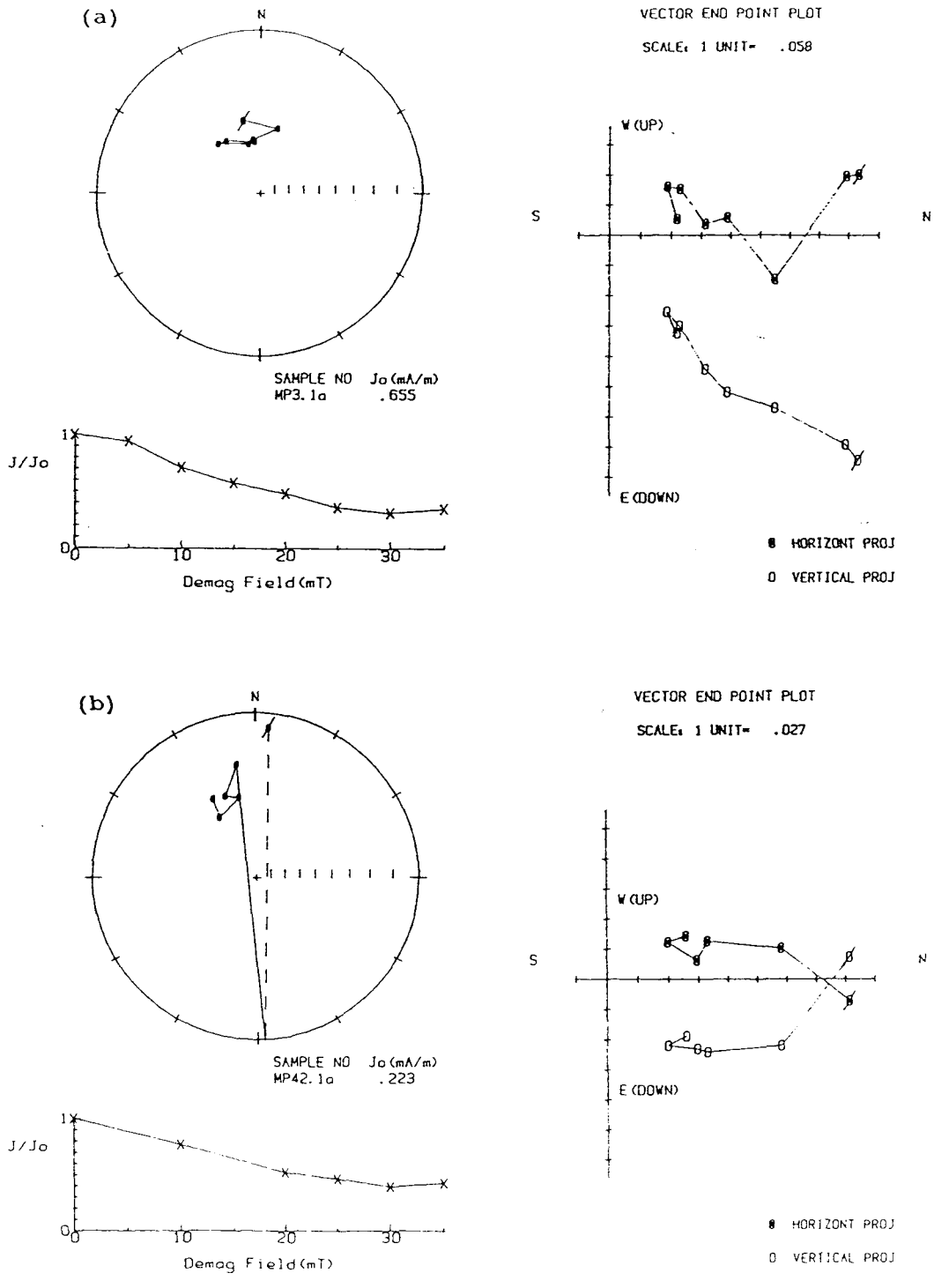

Fig. 4.1.17 Some examples of a.f. demagnetisation results for samples from the Wessex Formation of the Mupe Bay section. (a) and (b) for normal polarity and (c) and (d) for reverse polarity. Symbols and conventions as in Fig. 4.1.4.

(c)

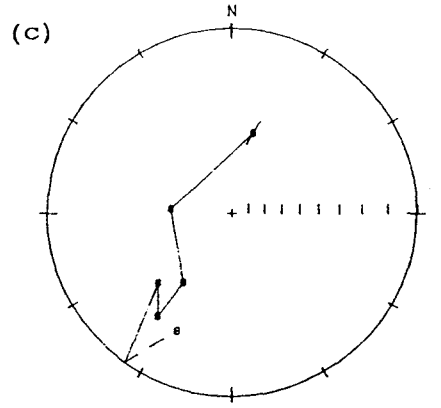

SAMPLE NO Jo(mA/m)
MP62.1a .146

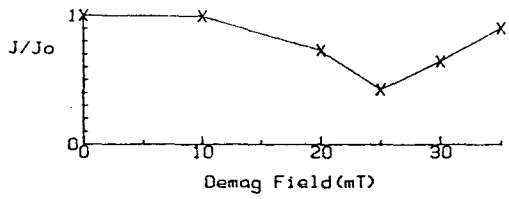

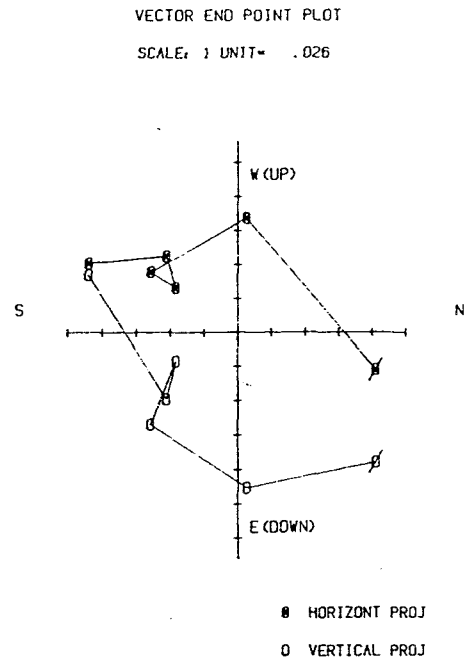

(d)

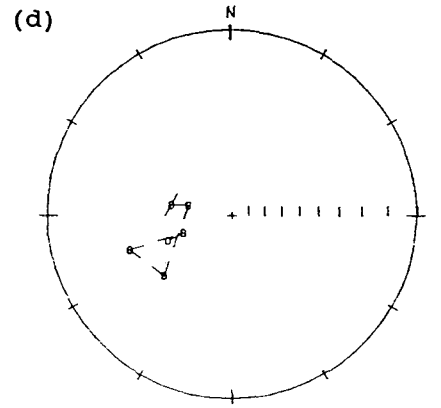

SAMPLE NO Jo(mA/m)
MP85.2 .192

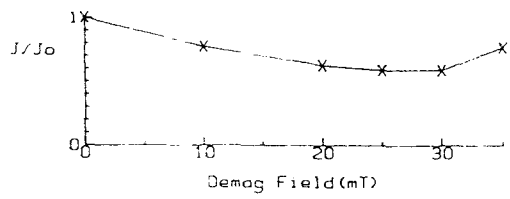

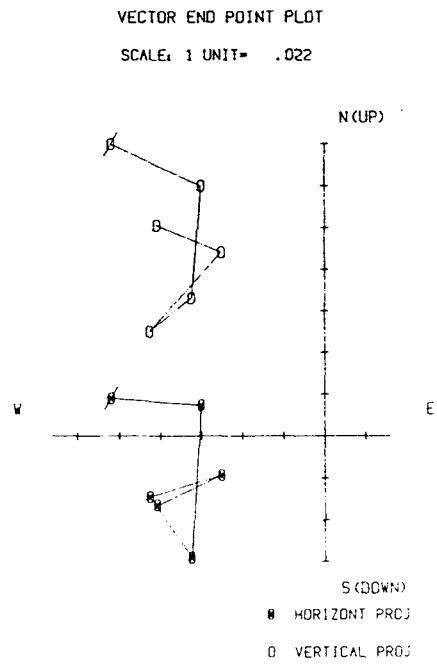

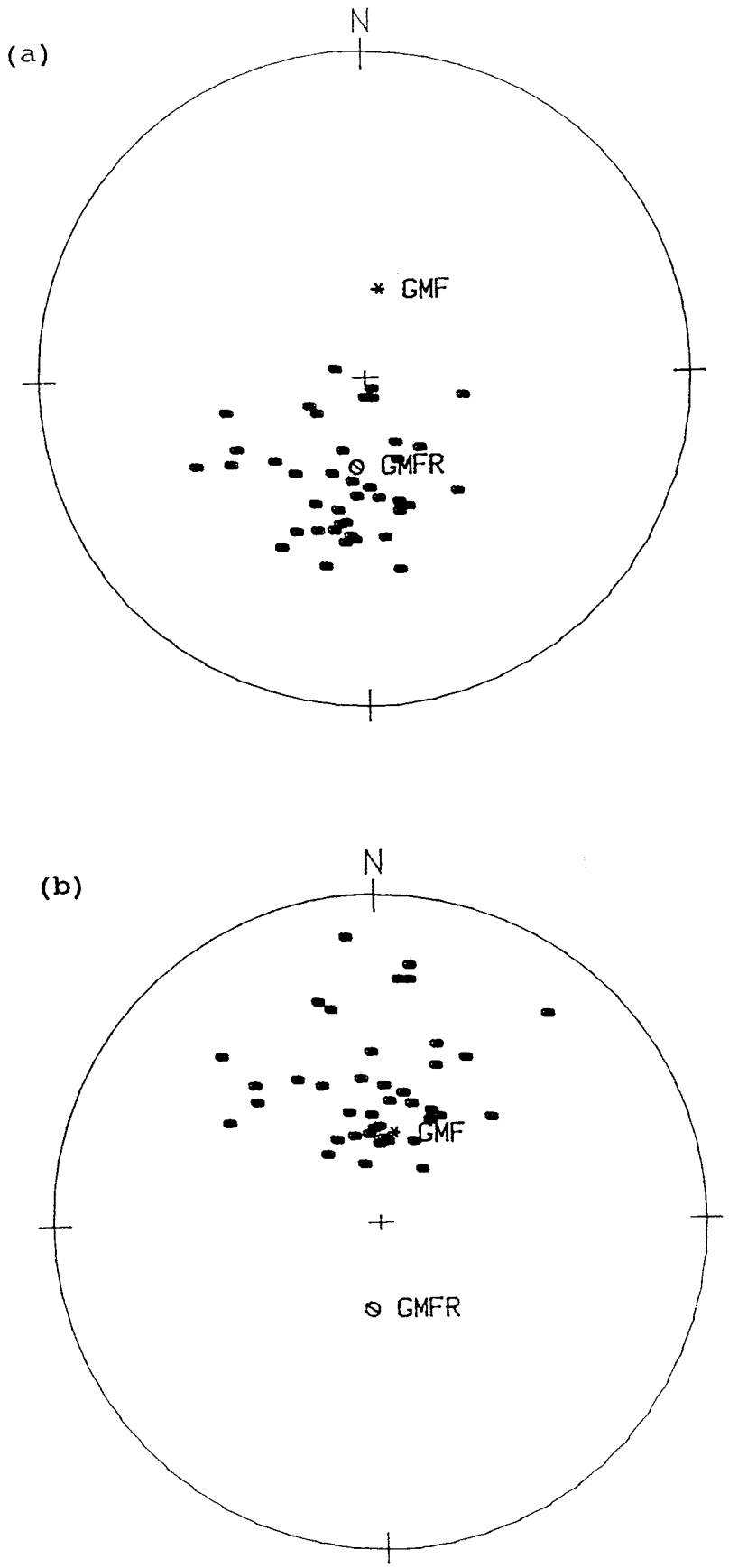

Fig. 4.1.18 Characteristic magnetisation directions for samples of the Wessex Formation from the Mupe Bay section. (a) and (c) are before bedding correction and (b) and (d) after the steep bedding correction. Symbols as Fig. 4.1.5 and 4.1.11.

(c)

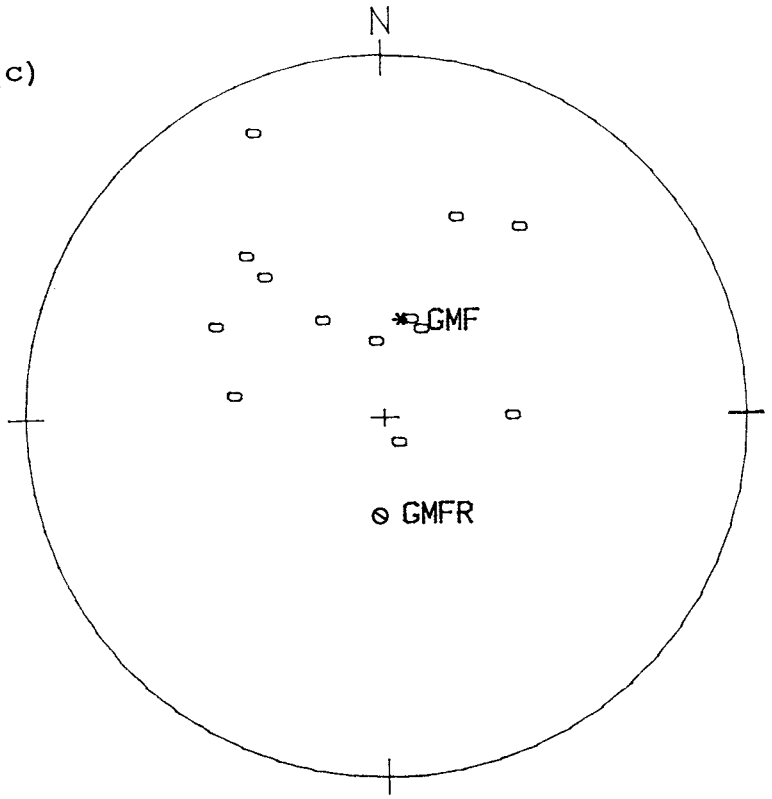

(d)

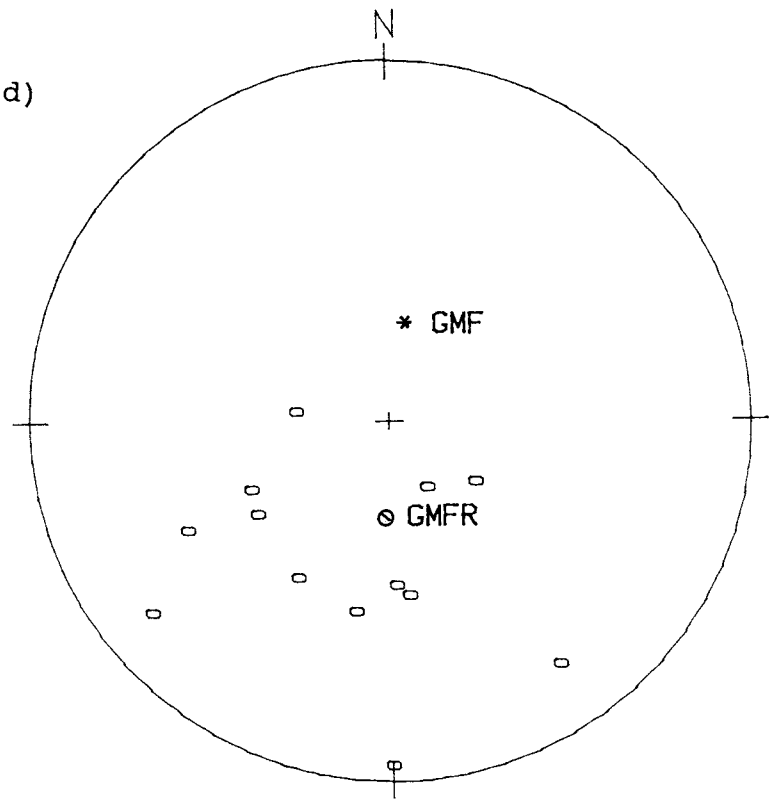

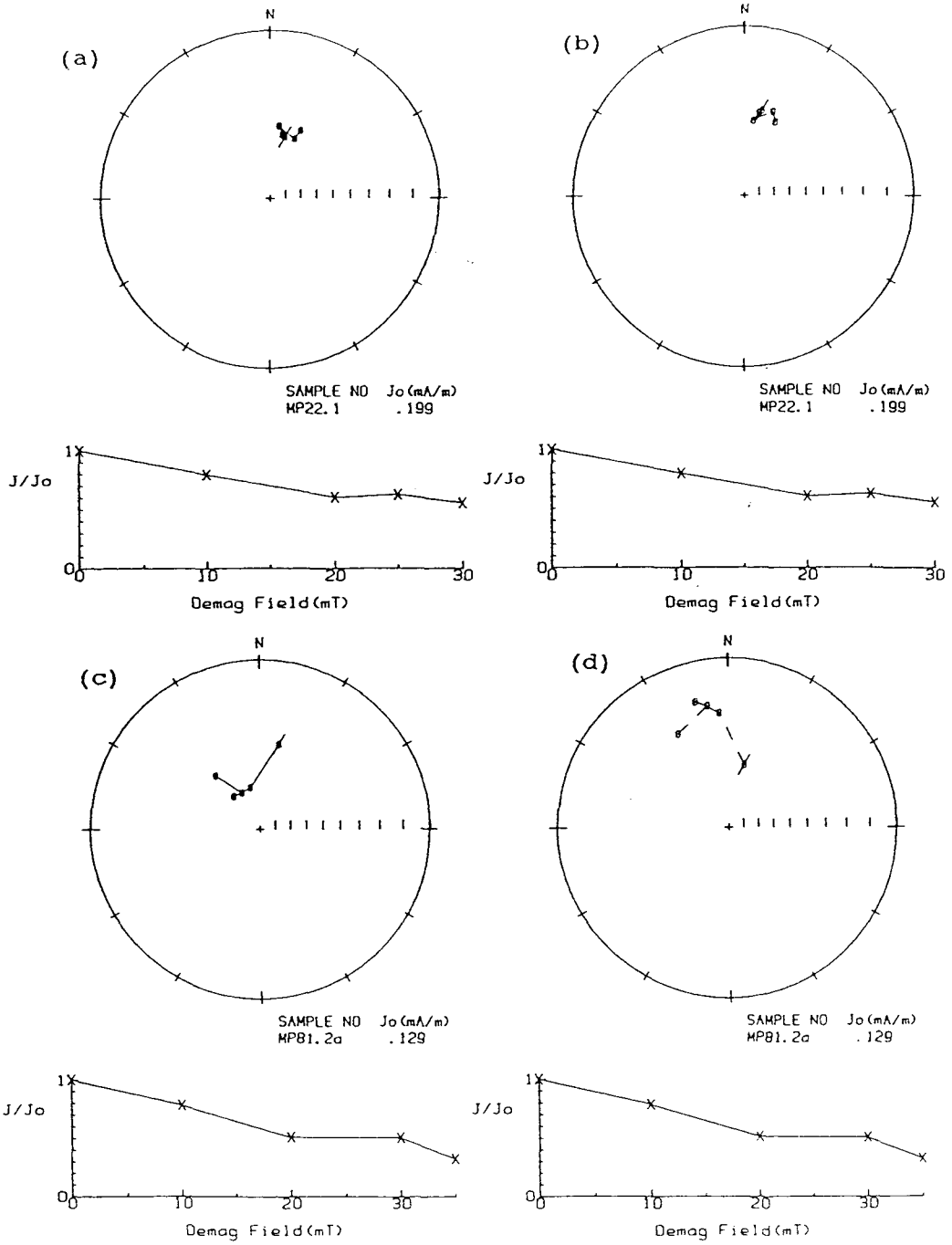

Fig. 4.1.19 Some examples of samples exhibiting clear post-folding magnetisations, which could not be removed by a.f. demagnetisation. Thus the magnetic vector before bedding correction (a) & (c) lies near to the present geomagnetic field direction but after the bedding correction the vectors move to a geomagnetically unrealitic direction (Wessex Formation, Mupe Bay). Symbols and conventions as in Fig. 4.1.4.

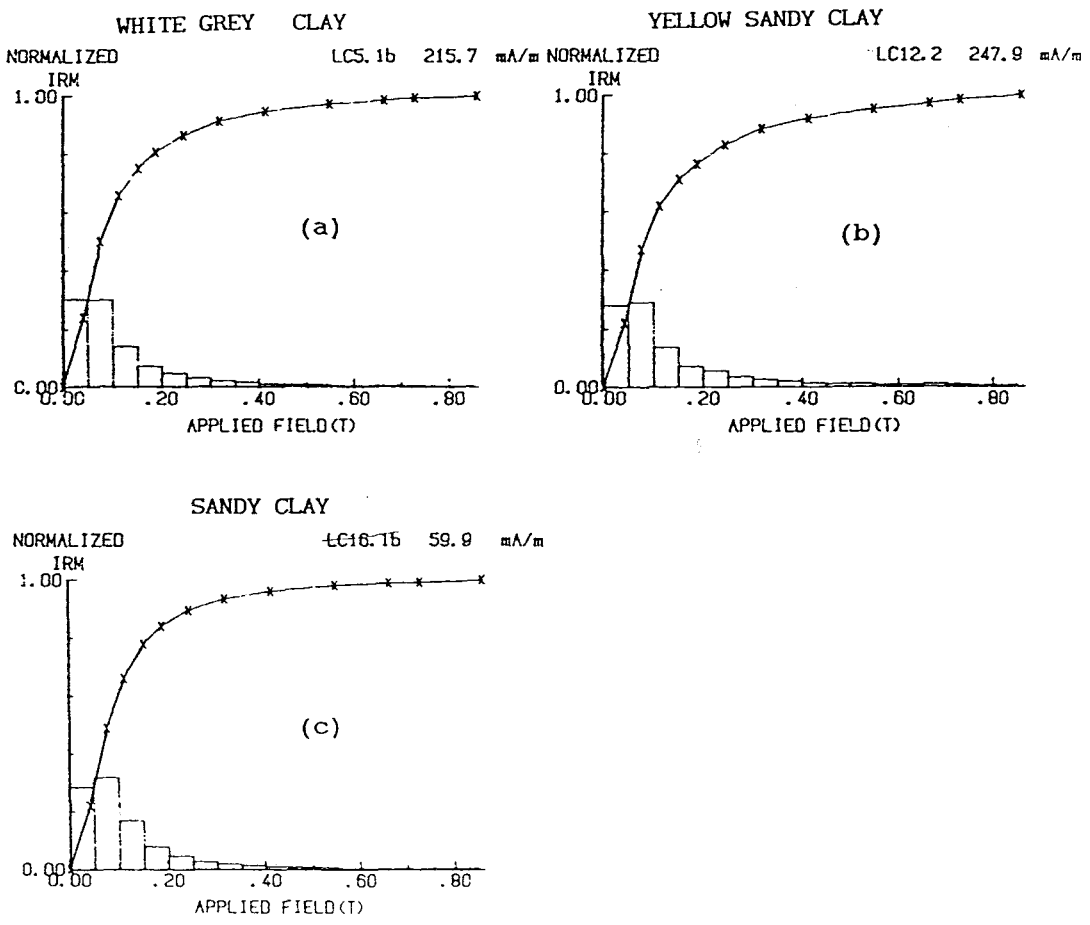

Fig. 4.1.20 IRM acquisition curves for samples from the of Lulworth Cove section. (a) and (b) from the Wessex Formation and (c) is from the Gault Formation.

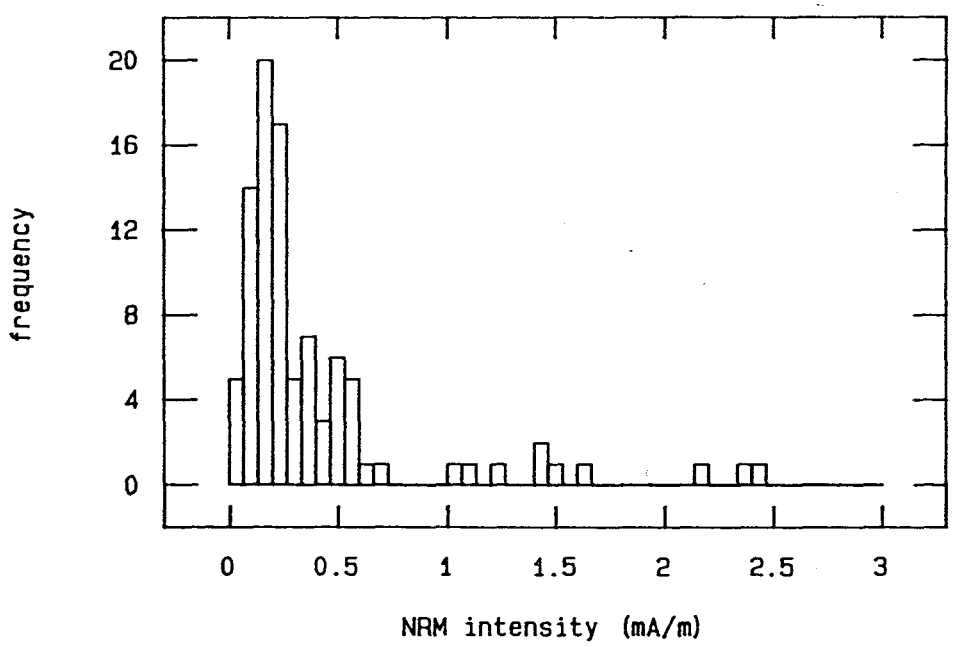

Fig. 4.1.21 Statistical distribution of NRM intensity values for samples of the Wessex and Gault Formations from the Lulworth Cove section.

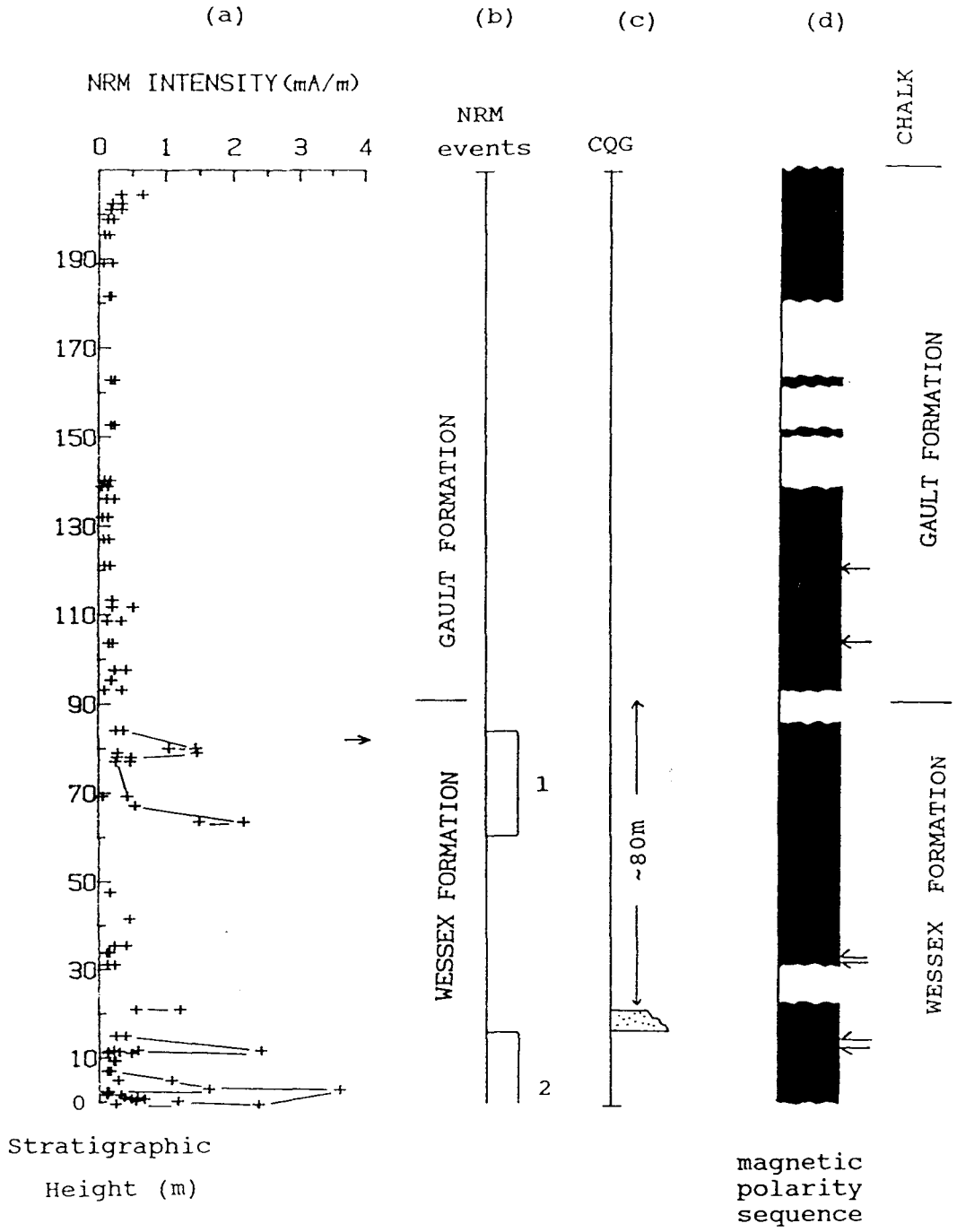

Fig. 4.1.22 (a) NRM intensity variation with stratigraphic height for the Lulworth Cove section. The section top is just below the base of the Chalk Formation and the bottom is ~20 m below the CQG layer. (b) positions of NRM intensity "events". (c) position of the CQG layer. (d) magnetic polarity sequence. Other symbols as in Fig. 4.1.3.

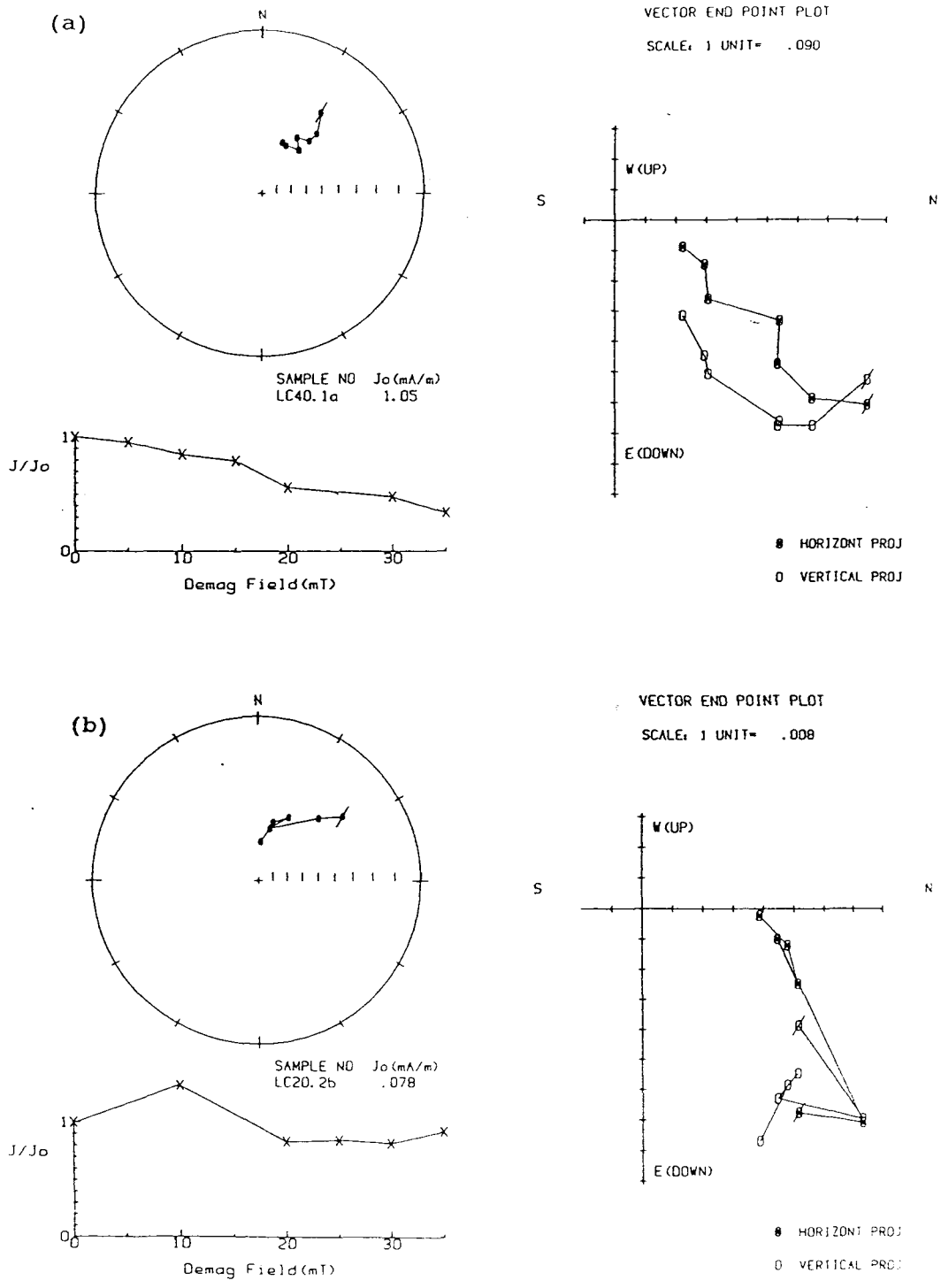

Fig. 4.1.23 Examples of demagnetisation results for samples from the Lulworth Cove section. (a) is from the Wessex Formation and (b) from the Gault Formation.

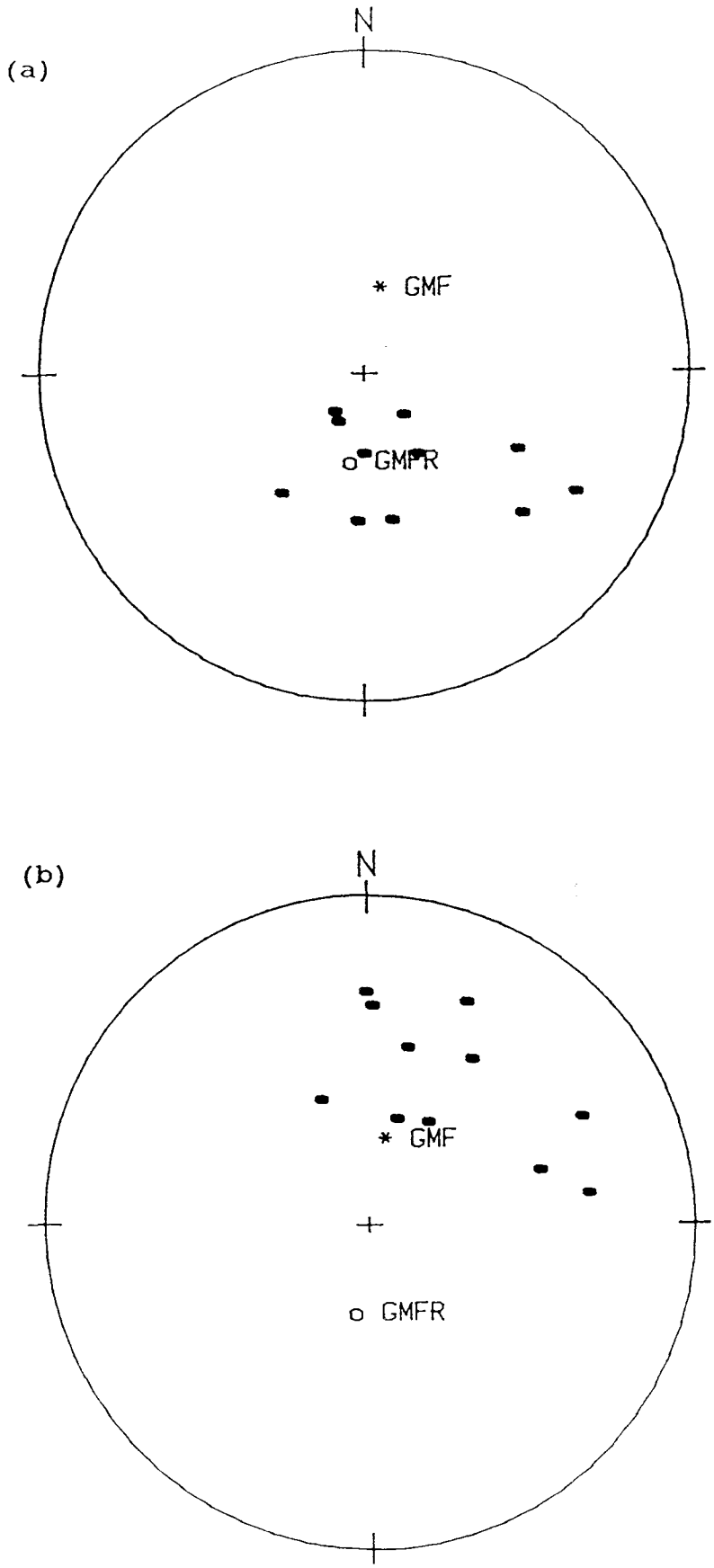

Fig. 4.1.24 Characteristic magnetisation vectors defined for samples of the Gault Formation at Lulworth Cove. (a) before bedding correction and (b) after bedding correction. Symbols as Fig. 4.1.11.

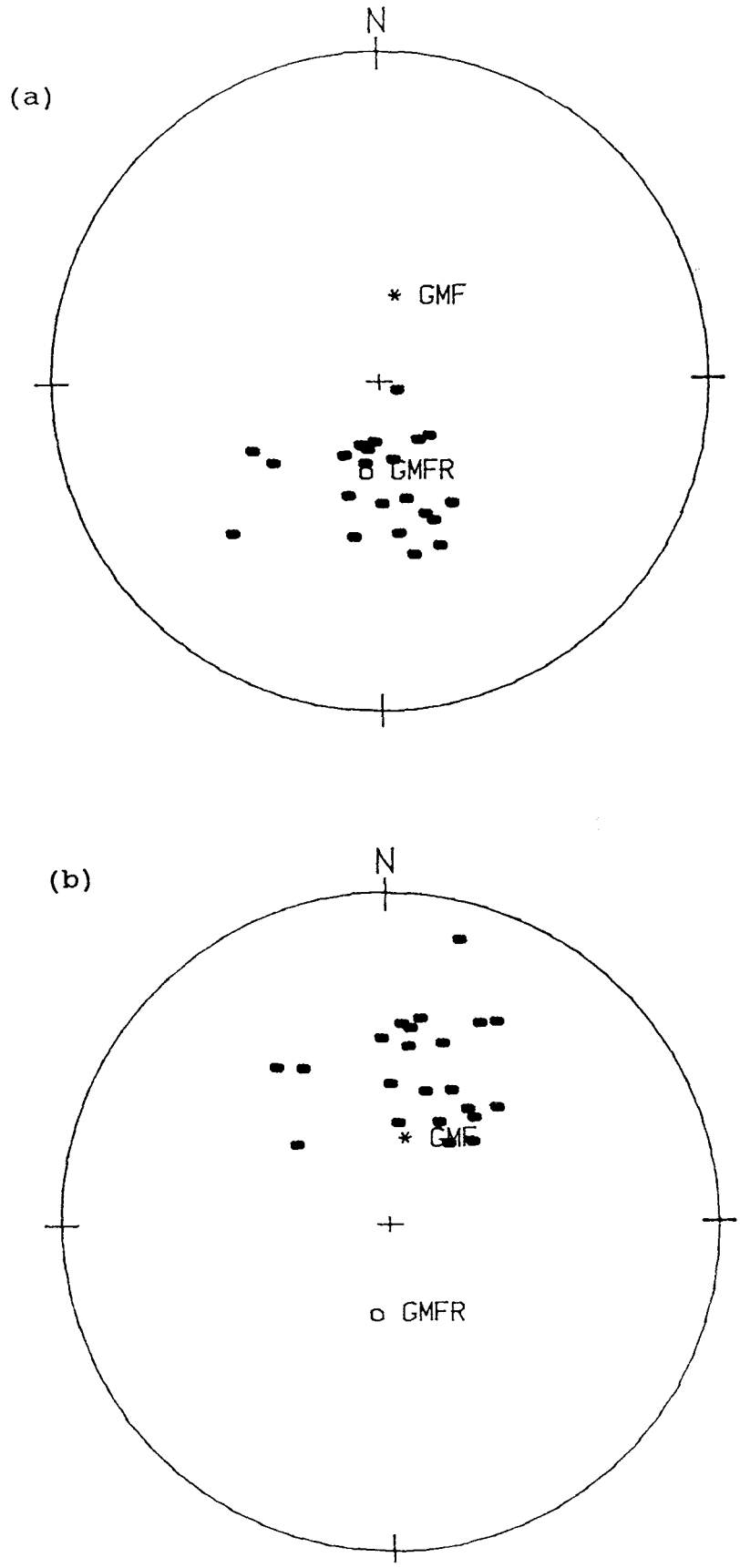

Fig. 4.1.25 Characteristic magnetisation vectors for samples of the Wessex Formation from Lulworth Cove. (a) before bedding correction and (b) after bedding correction. Symbols as in Fig. 4.1.11.

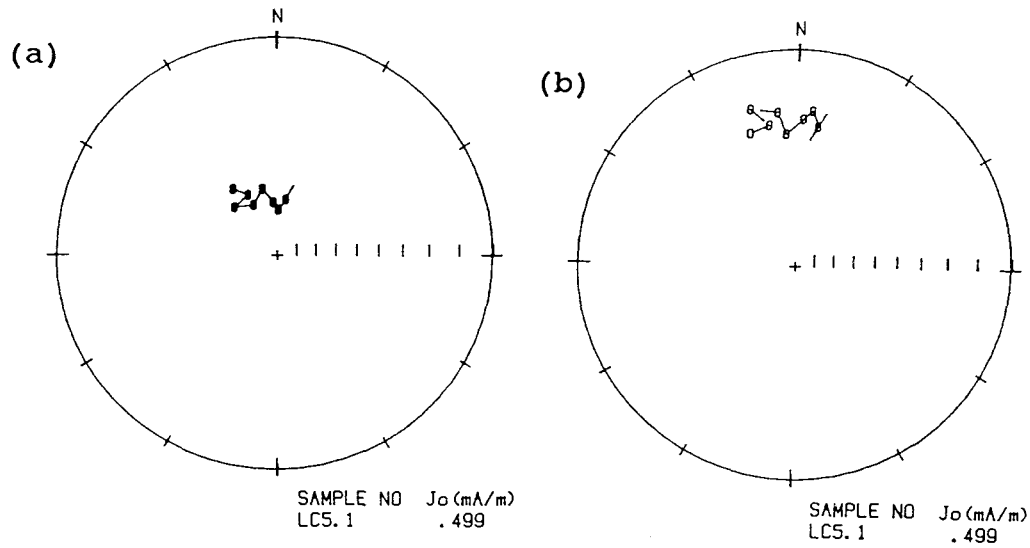

Fig. 4.1.26 Examples of a sample from the Wessex Formation at Lulworth Cove, in which the magnetisation vector before bedding correction (a) is close to the present field vector, while that after bedding correction (b) differs substantially from the latter. This is clear evidence for a post-folding magnetisation in this sample.

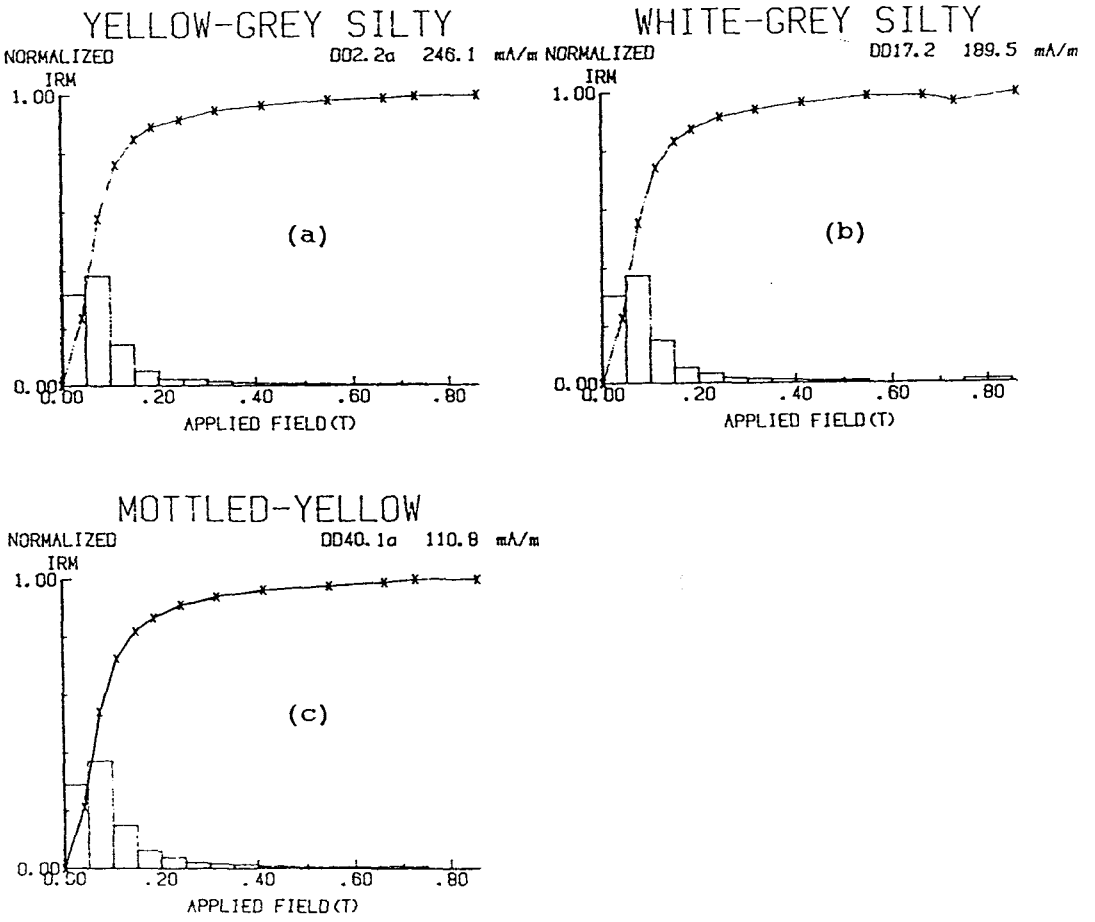

Fig. 4.1.27 IRM acquisition curves for typical samples from the Wessex Formation in the Durdle Door section.

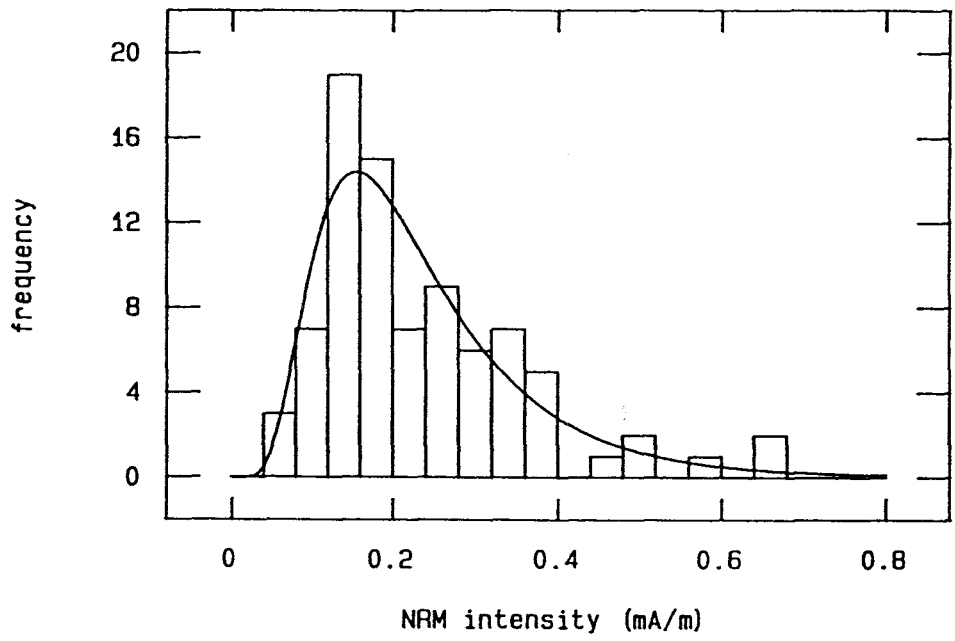

Fig. 4.1.28 Statistical distribution of NRM intensity values for samples of the Wessex Formation from the Durdle Door section.

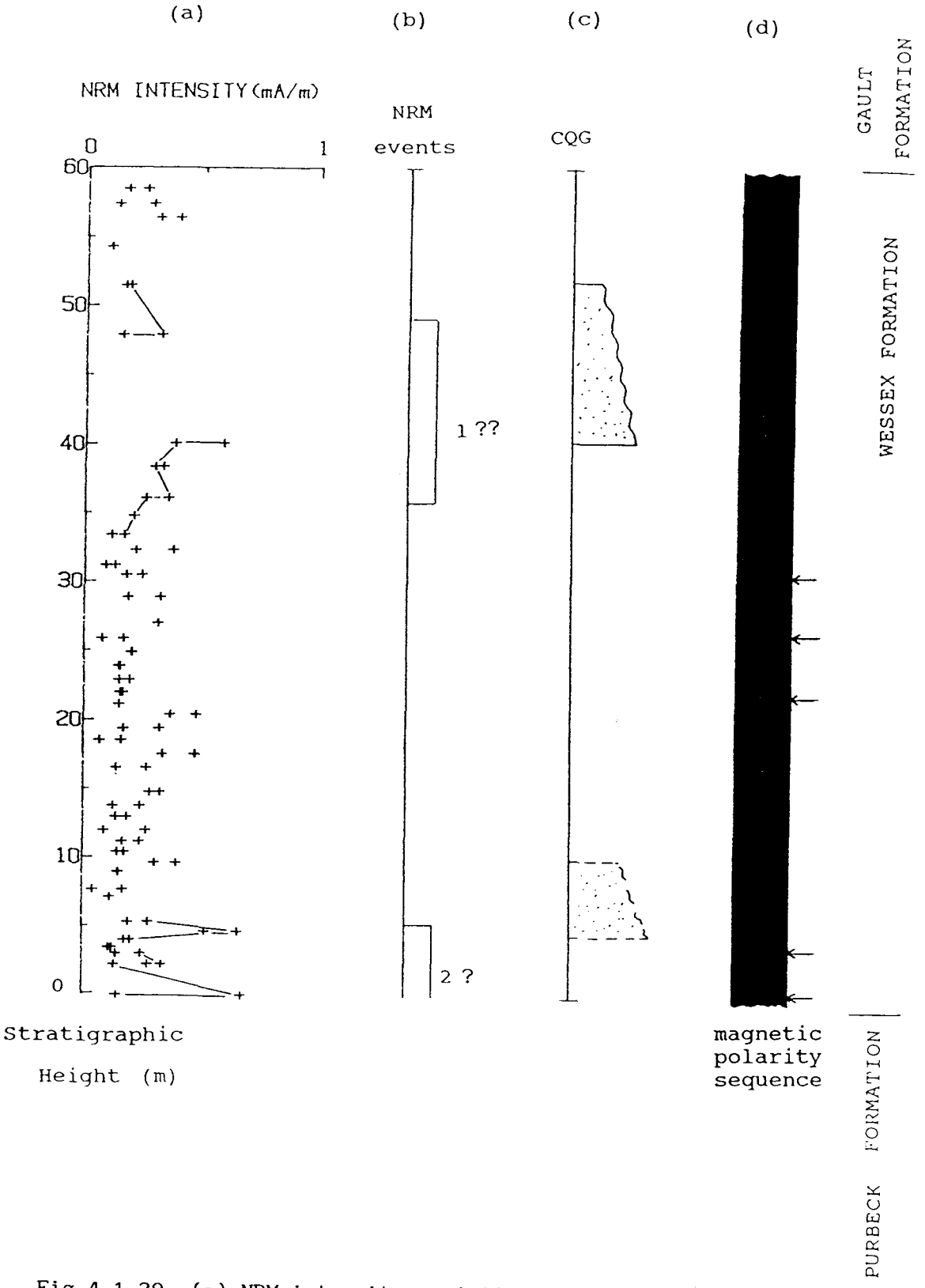

Fig. 4.1.29 (a) NRM intensity variation with stratigraphic height in the Durdle Door section. The top of the section is ~21 m below the Chalk Formation and the bottom is ~7 m above the Purbeck Beds. (b) recognizable NRM events. (c) CQG layers; the lower of these is the Lignitic Quartz Grit recognized by Arkell (1947). (d) magnetic polarity sequence. Other symbols as in Fig. 4.1.3.

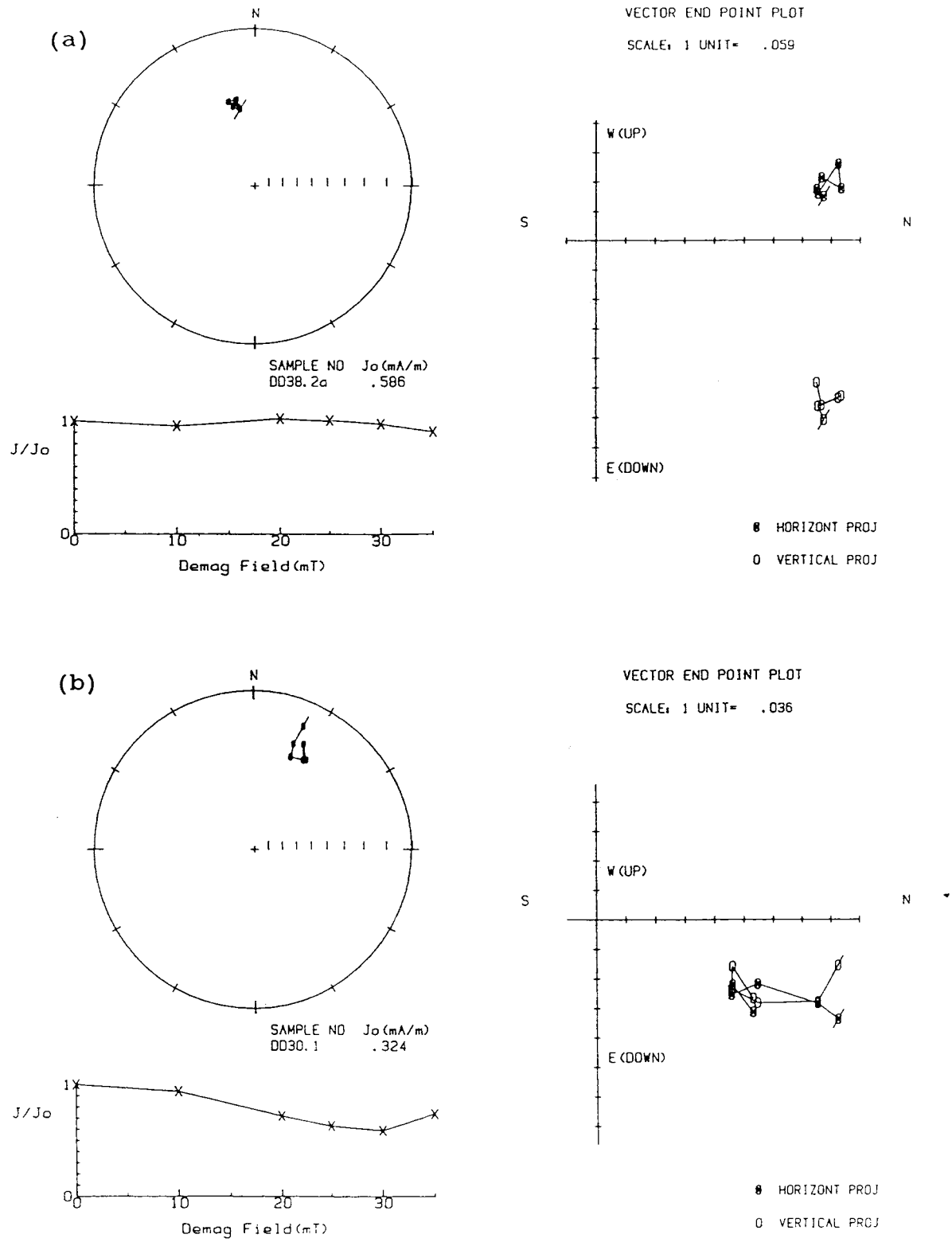

Fig. 4.1.30 Examples of a.f. demagnetisation results for samples of the Wessex Formation from the Durdle Door section (after bedding correction). Symbols and conventions as Fig. 4.1.4.

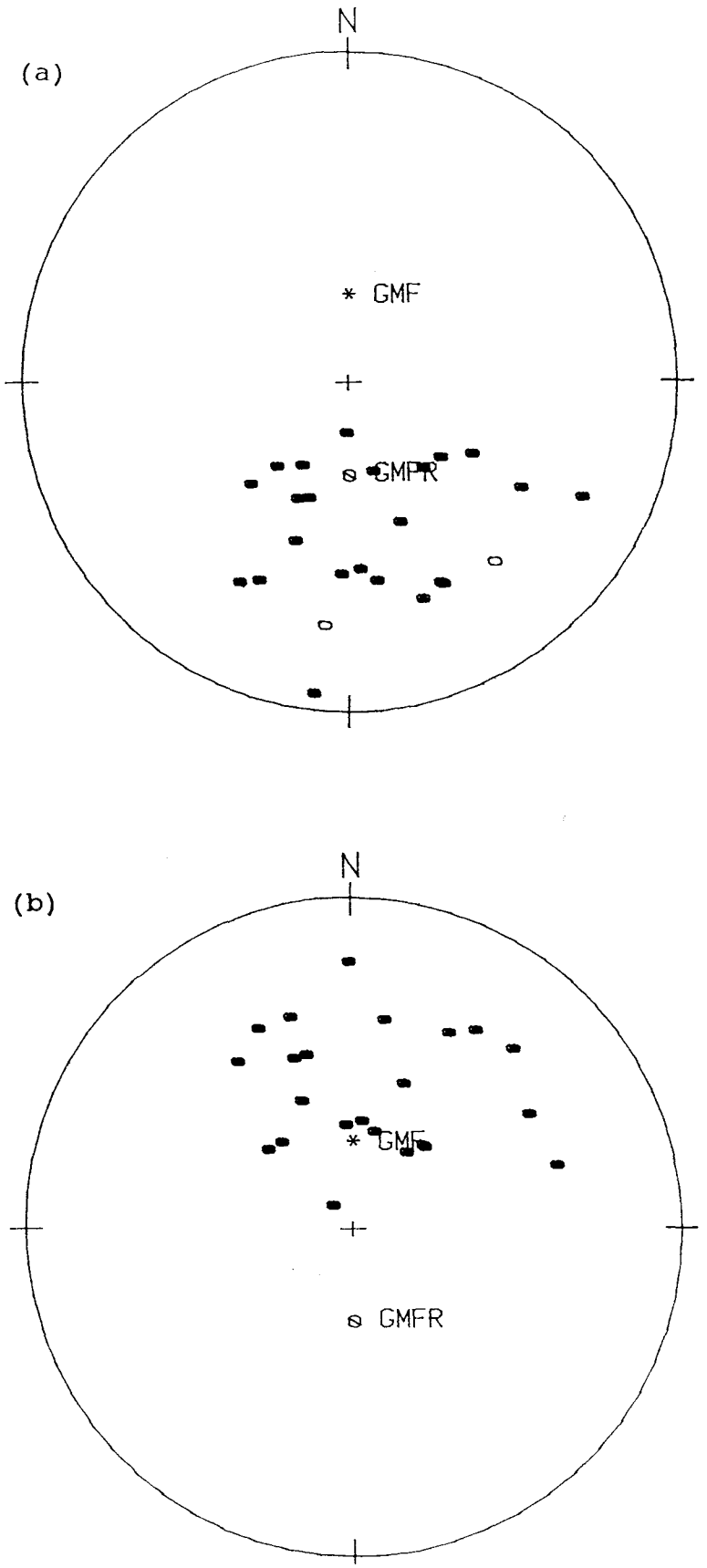

Fig. 4.1.31 Characteristic magnetisation direction for samples of the Wessex Formation from the Durdle Door section. (a) Before bedding correction and (b) after the correction. Other symbols as Fig. 4.1.11.

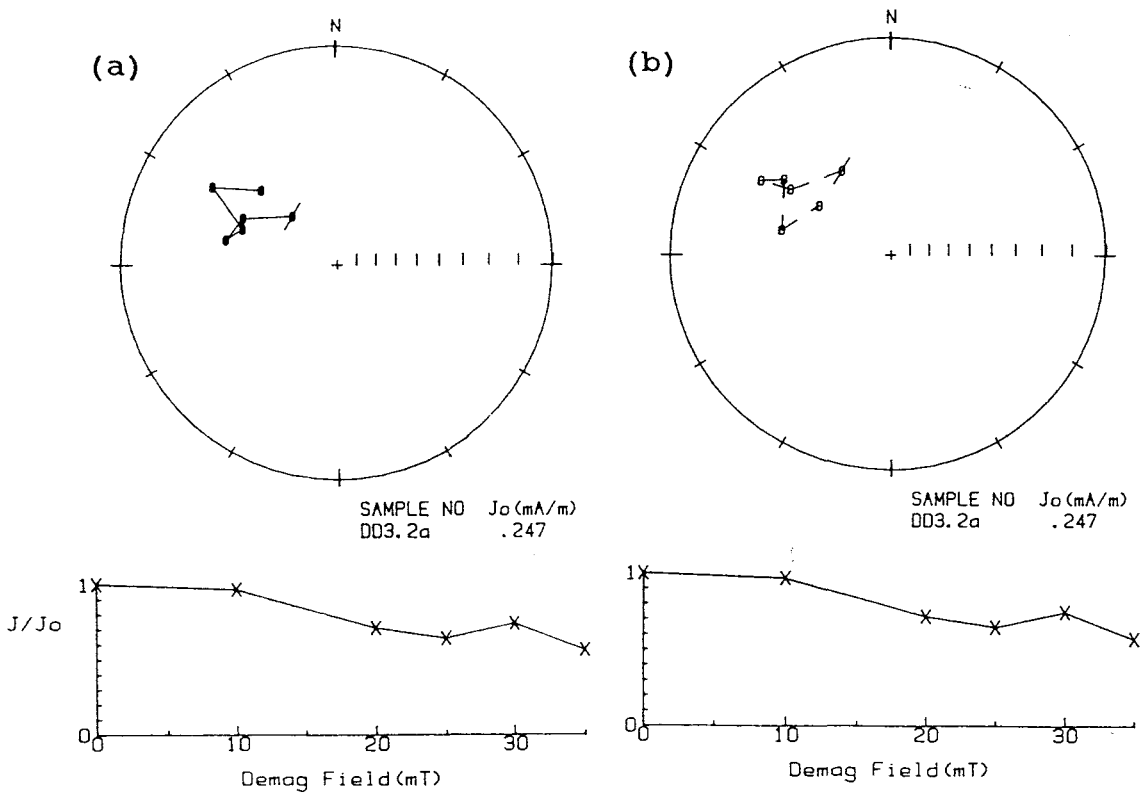

Fig. 4.1.32 Example of a sample from the Wessex Formation of Durdle Door with a probable post-folding characteristic magnetisation (a) is before bedding correction and (b) after bedding correction. Symbols and conventions as Fig. 4.1.4.

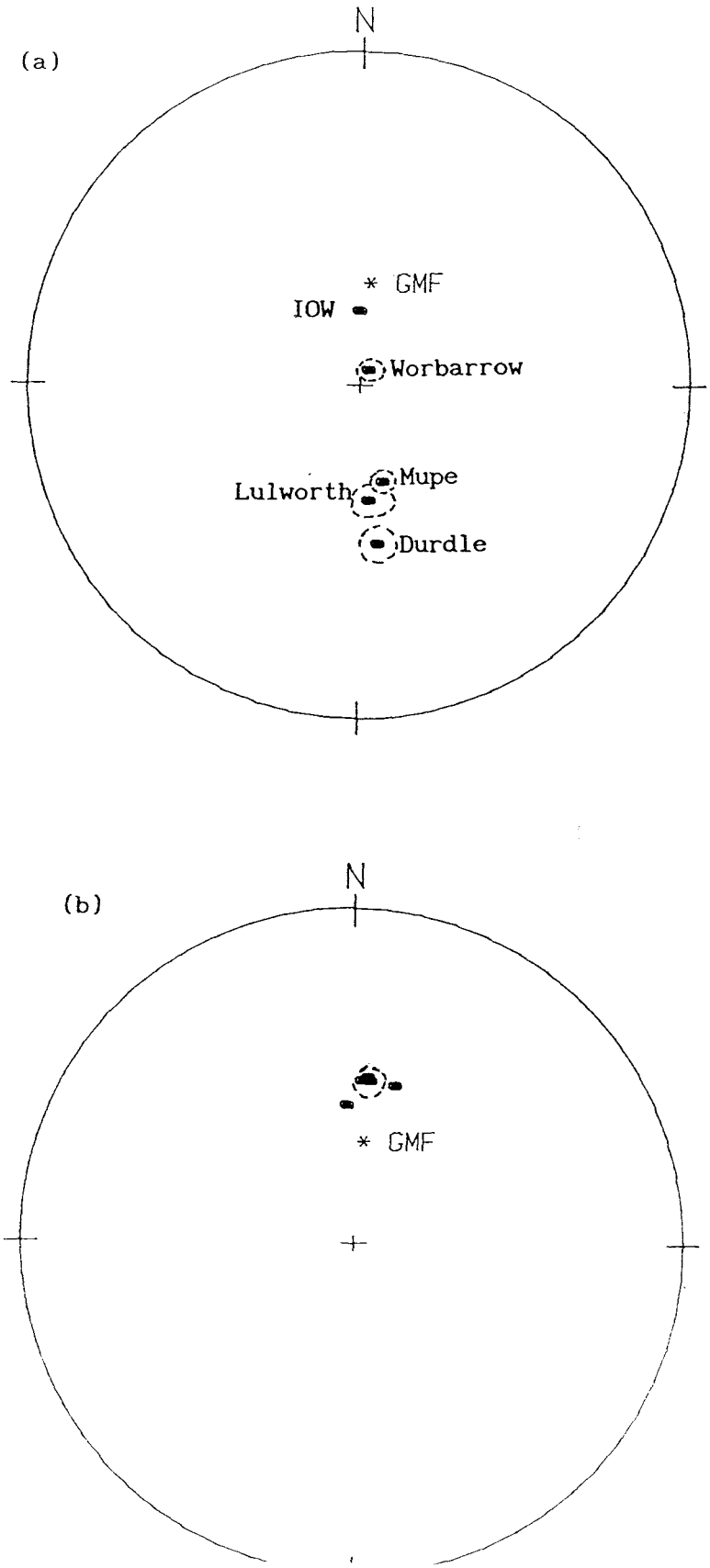

Fig. 4.1.33 Mean characteristic magnetisation directions with Fisher 95% confidence limits (dash line circles) for all sections through the Wessex Formation studied in Southern England. (a) before bedding correction and (b) after bedding correction. Symbols as Fig. 4.1.11.

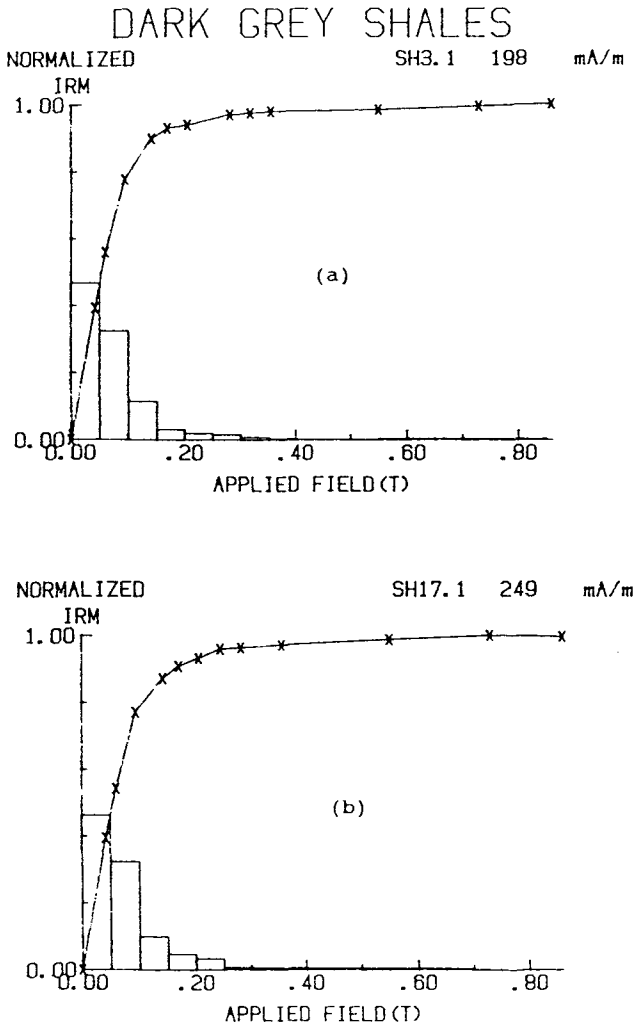

Fig. 4.1.34 Examples of IRM acquisition curves for samples of the Weald Clay Formation from the Beare Green sections.

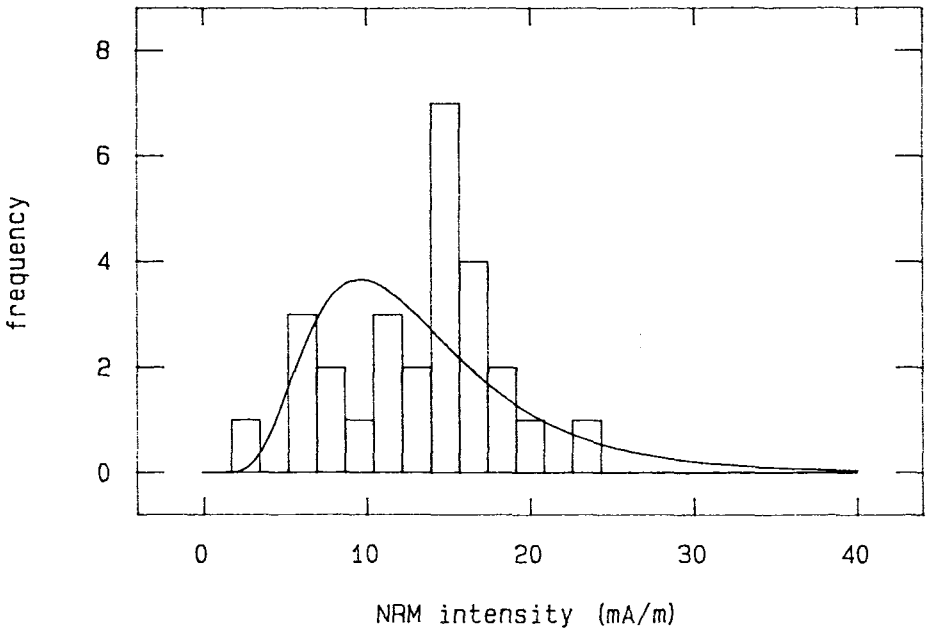

Fig. 4.1.35 Statistical distribution of NRM intensity values for the Weald Clay of the Beare Green clay pit sections.

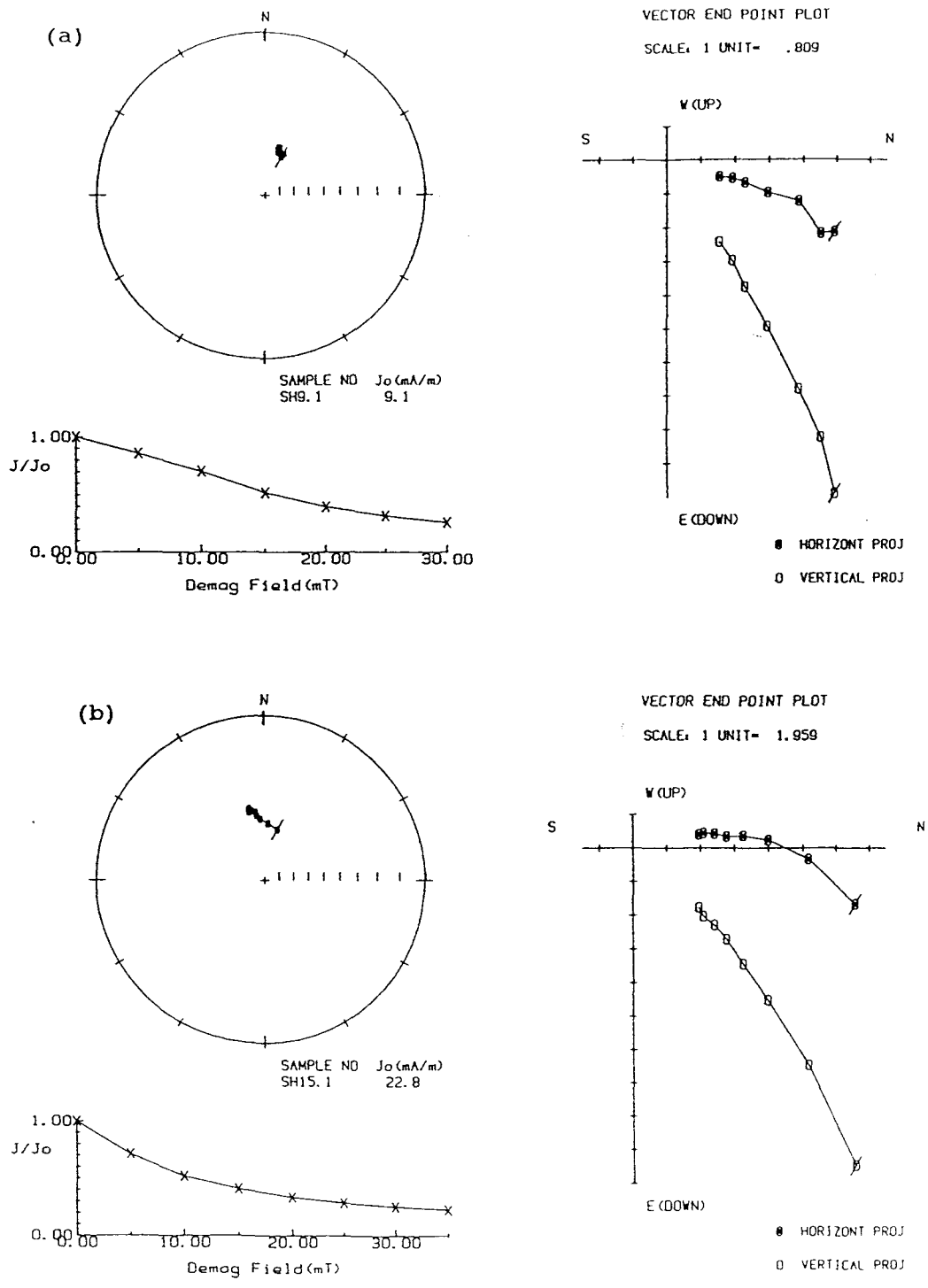

Fig. 4.1.36 Examples of typical a.f. demagnetisation results for samples of the Weald Clay from the Beare Green sections. Symbols and conventions as Fig. 4.1.4.

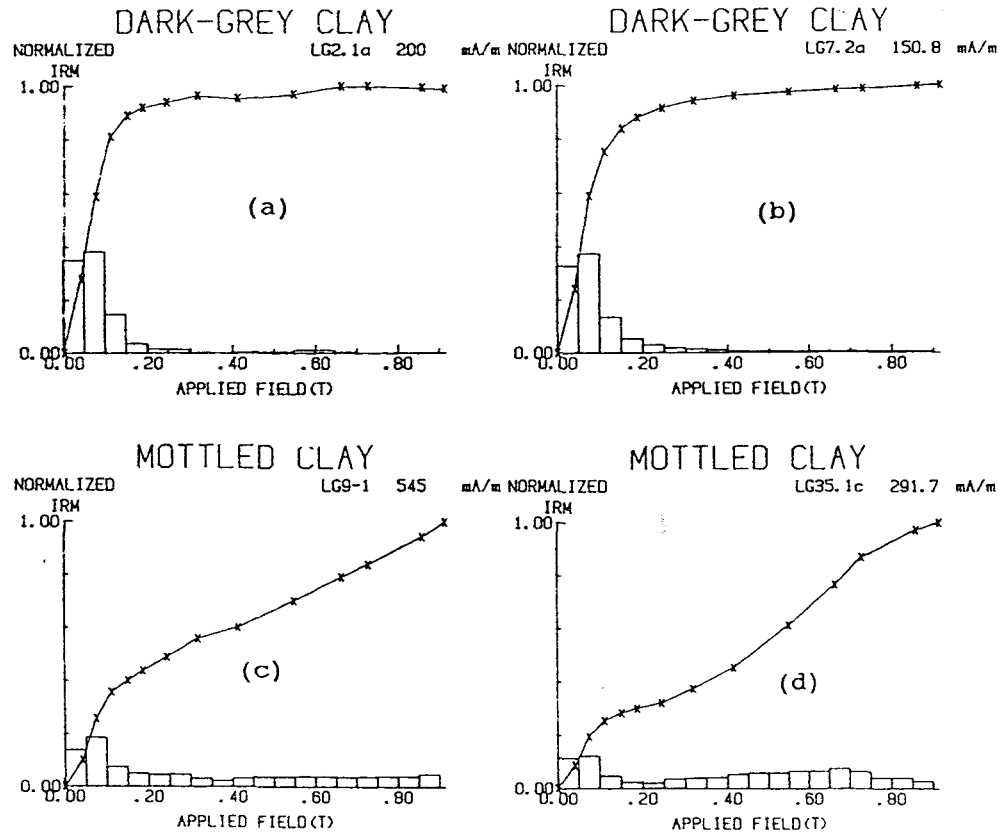

Fig. 4.1.37 IRM acquisition curves for samples from the Langhurst sections.

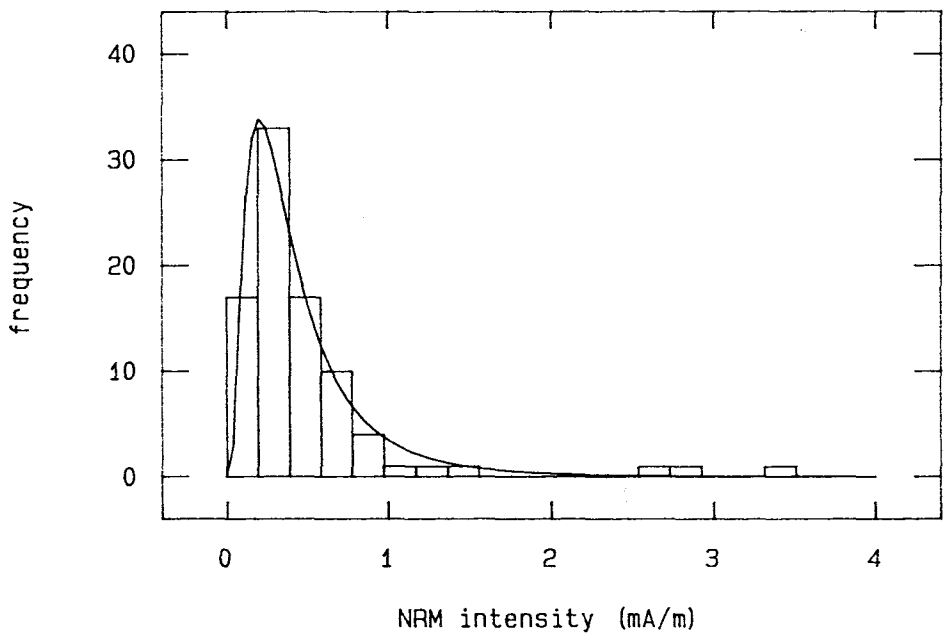

Fig. 4.1.38 Statistical distribution of NRM intensity values for the Weald Clay in the Langhurst sections.

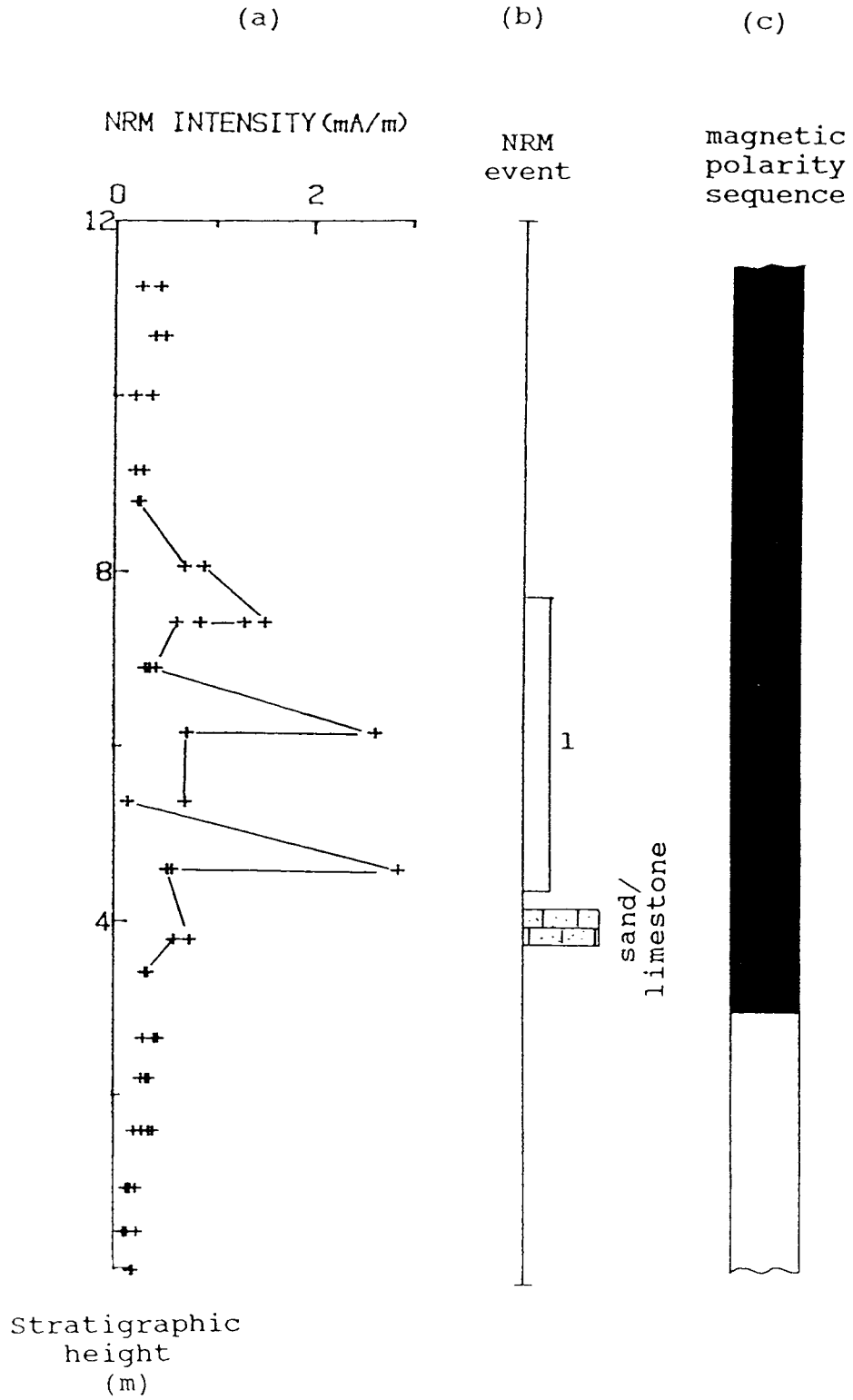

Fig. 4.1.39 Summarized magnetic result logs for the "northwest" section in Langhurst quarry (Warnham). (a) variation of NRM intensity values with stratigraphic height. (b) recognized NRM intensity "event" and the position of the sand/limestone layer in this section. (c) magnetic polarity sequence. Symbols as Fig. 4.1.3.

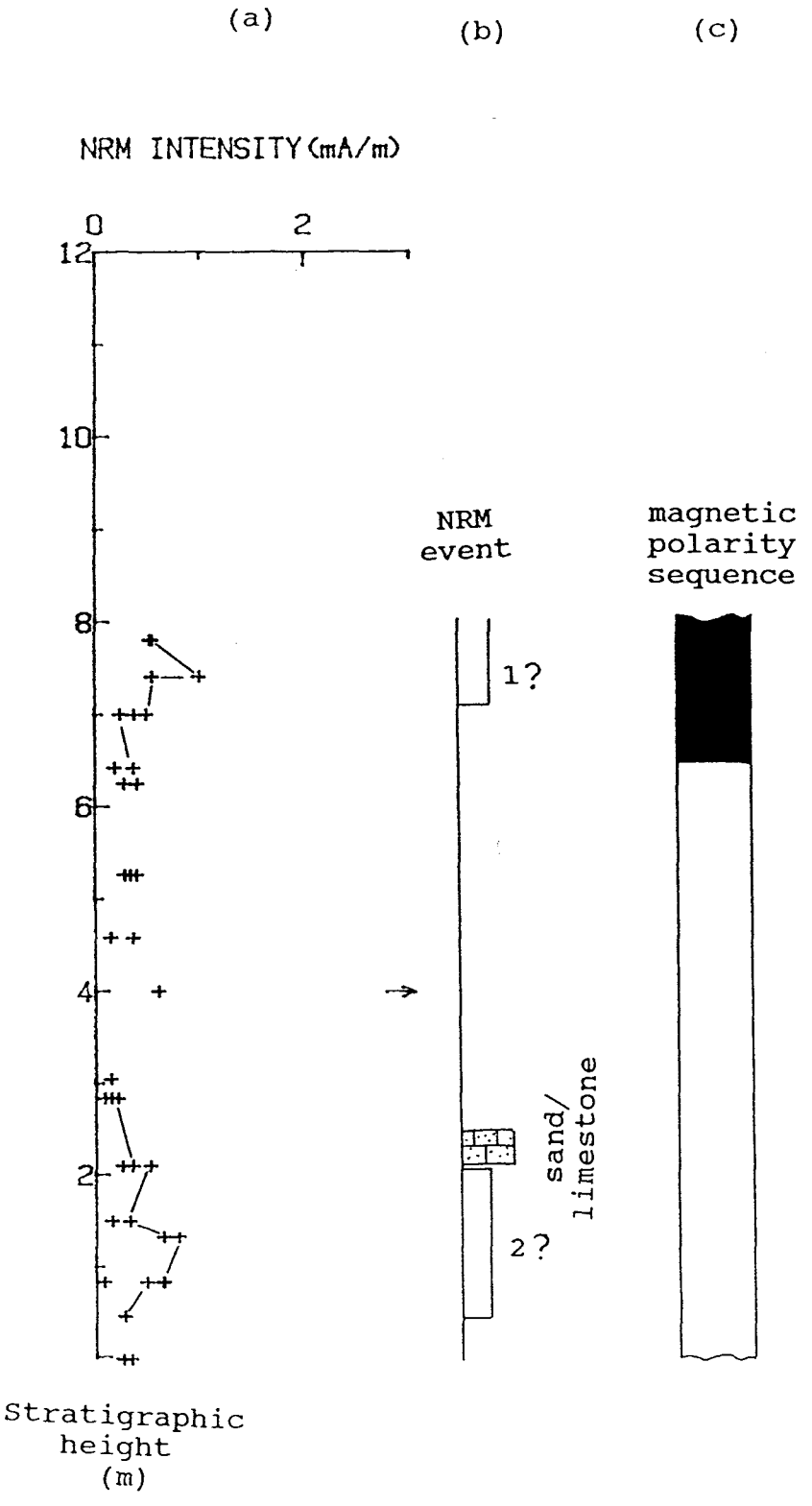

Fig. 4.1.40 Summarized magnetic result logs for the "southeast" section in Langhurst quarry. Convention as for Fig. 4.1.39.

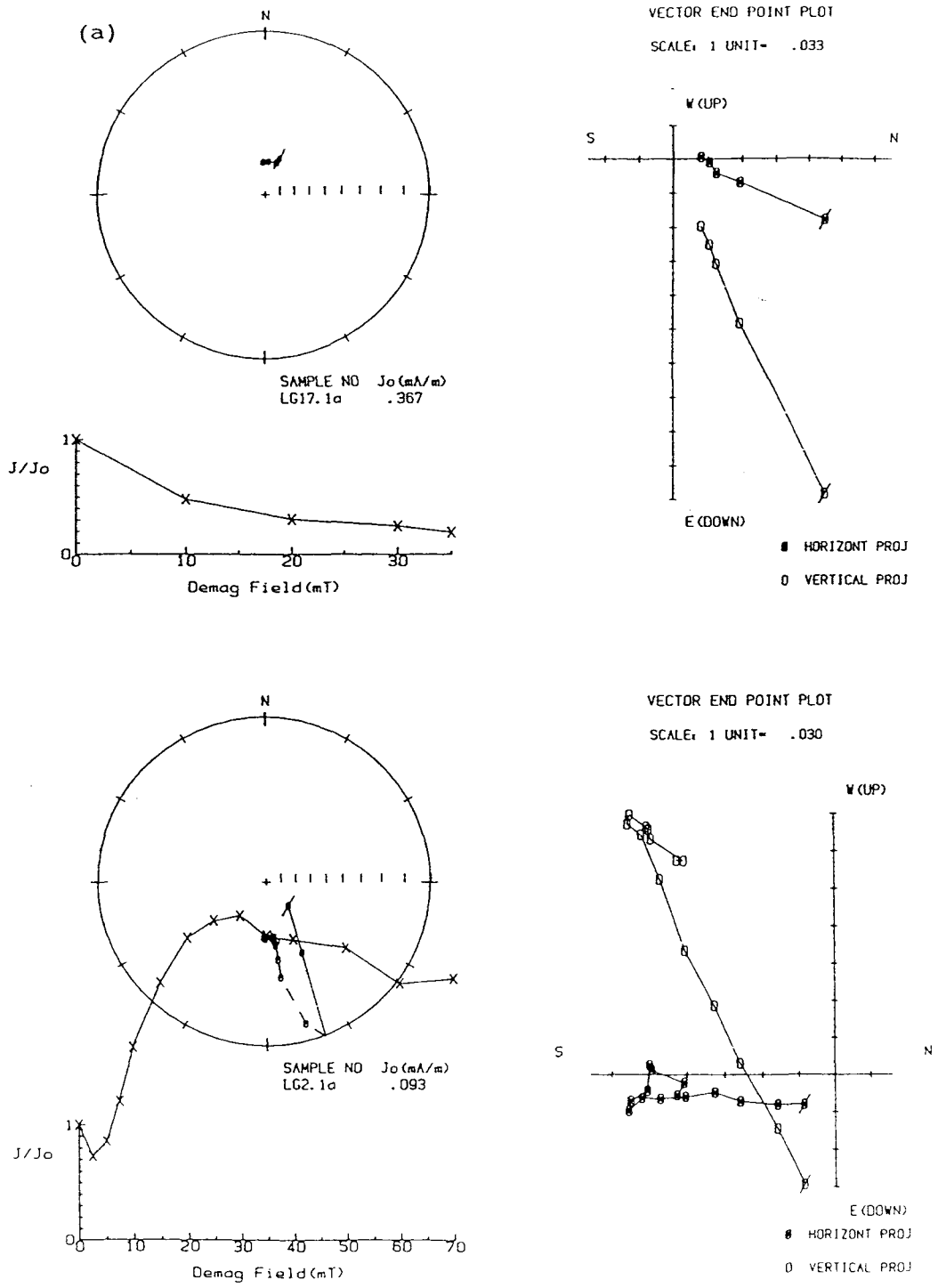

Fig. 4.1.41 Examples of a.f. demagnetisation results for samples of the Weald Clay from the Langhurst sections. Symbols and conventions as in Fig. 4.1.4.

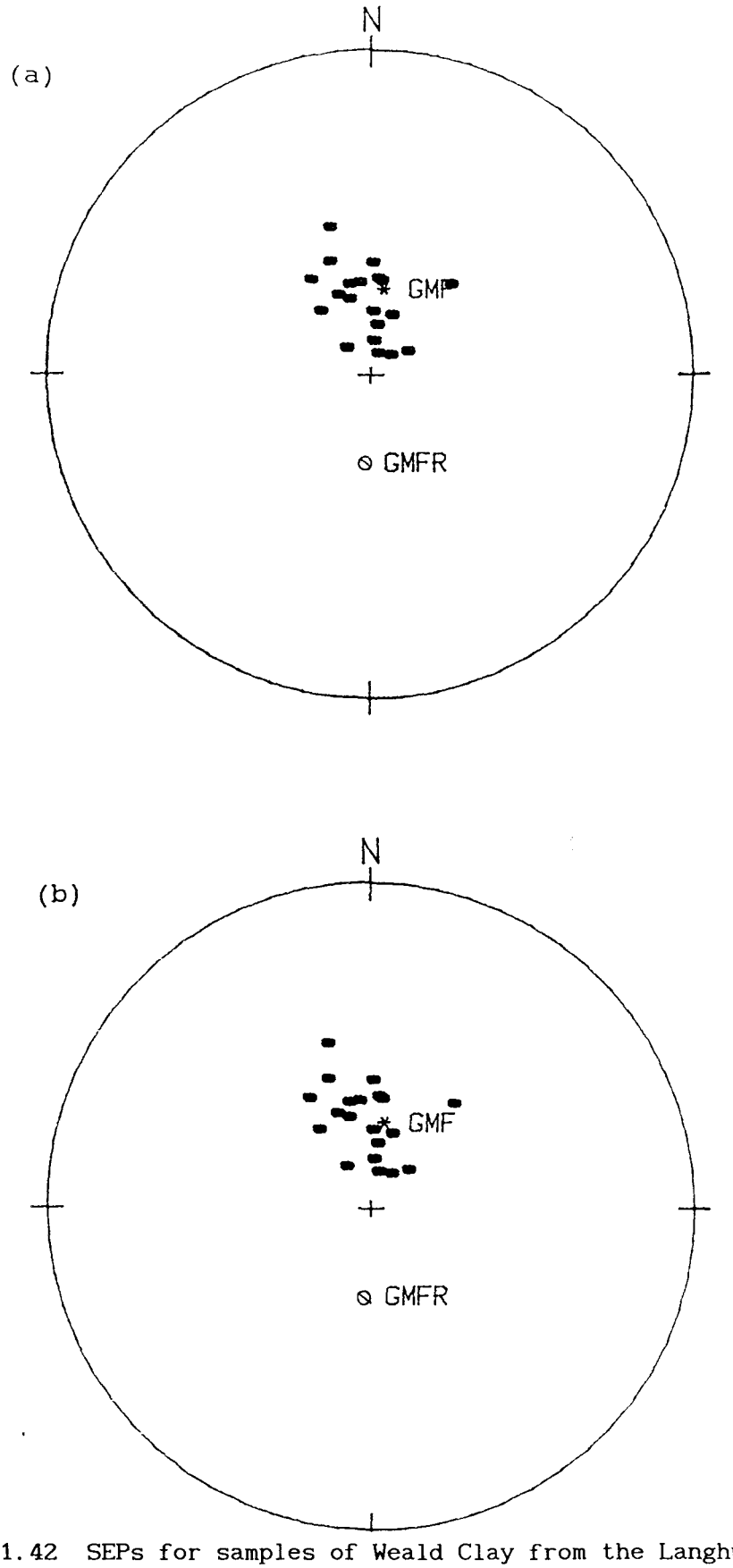

Fig. 4.1.42 SEPs for samples of Weald Clay from the Langhurst sections. (a) Before bedding correction and (b) after correction. (c) and (d) for the reverse polarity SEPs in these sections. Symbols as Fig. 4.1.11.

(c)

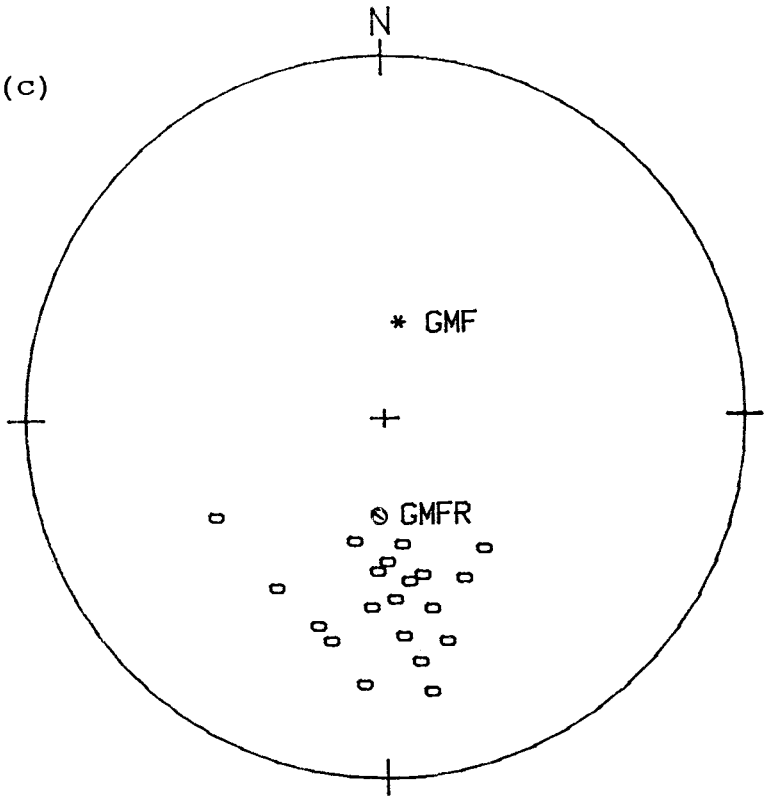

(d)

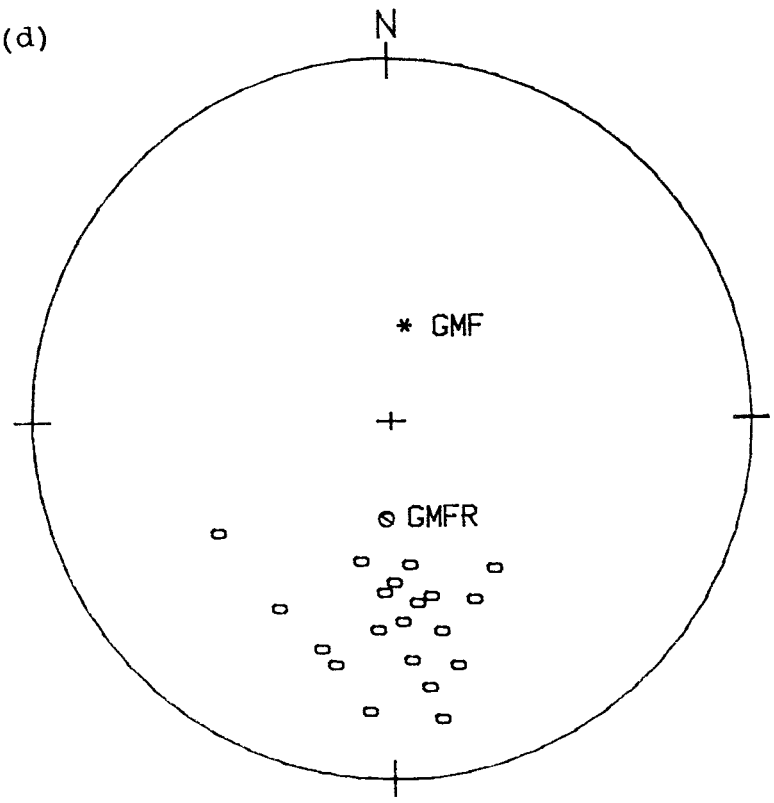

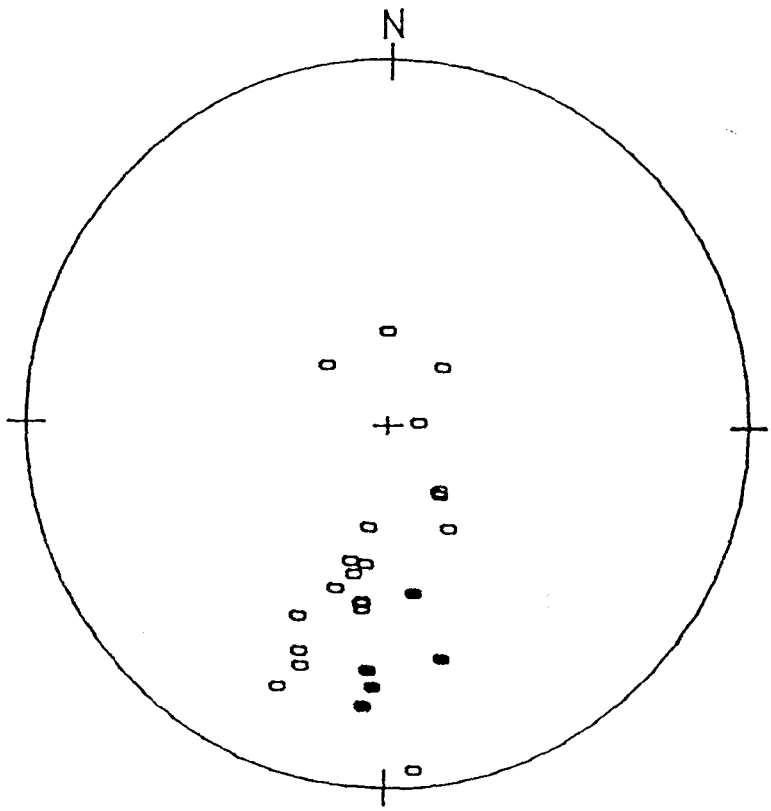

Fig. 4.1.43 Great circle intersections produced for samples showing directional trends towards reverse polarity during a.f. demagnetisation (Weald Clay, Langhurst sections). Symbols as Fig. 4.1.11.

§4.2 Magnetostratigraphic sequences in the Wessex Formation of Southern England and their correlations

4.2.1) Production of magnetic polarity sequences.

The basic principle of magnetostratigraphy is to use the magnetic polarities of samples collected systematically from a geological unit to define a magnetic polarity sequence and then to correlate this with other magnetic sequences produced from other geological formations of a similar age. Ideally, this is done by plotting stratigraphic logs of declination and inclination yielded by SEPs for all samples (eg. see Kerth and Hailwood 1988). However, when the remanent magnetisation preserved in the sediment is very weak (<1.0 mA/m), the SEPs become more scattered around the supposed mean magnetic field direction because of the increasing difficulties in determination of the weak magnetic moment, even by the sensitive cryogenic magnetometer. If a significant proportion of the samples do not display SEPs or CMDs from progressive demagnetisation (either by a.f. or thermal method), then reliable stratigraphic plots of magnetic declination and inclination values cannot be produced.

In the present study, the polarity of the stable characteristic magnetisation of each sample, where well-defined, is indicated by the letter "N" (for normal) or "R" (for reverse polarity). Such polarity assignments may be based either on the definition of an SEP (or CMD) or the identifications of a clear demagnetisation trend. For samples showing less reliable results (eg "noisy" demagnetisation trends, in which the successive points may be scattered quite widely around the overall great circle trend, or where more than one trend may be present) a question mark is attached to the polarity assignment. The polarity assignment for each sample are summarized in Appendix 1-12.

4.2.2) Magnetic polarity sequences from southern England.

1) The Isle of Wight section.

The Wessex Formation on the Isle of Wight has yielded a polarity sequence which is almost entirely normal, with just a few isolated

samples exhibiting a reverse polarity. The mono-polarity sequence is shown in Fig.4.1.3c, accompanied by the NRM intensity log and an indication of the main features of the lithological sequence. The magnetostratigraphic results of Kerth and Hailwood (1988) for the overlying Vectis Formation are also shown. Two groups of isolated reverse polarity samples (indicated by arrows) occur, one around a stratigraphic height of about 90 m and the other near the bottom of the section.

The approximate position of this long normal polarity sequence, relative to the standard geomagnetic polarity time scale (GPTS) may be estimated from the position of Chron CM0 which was defined by Kerth and Hailwood (1988) within the overlying Vectis Formation (about 30 m above its base). Therefore, it is probable that the Wessex Formation was deposited during the long normal polarity interval between Chron CM0 and CM1. However, because of lack of further information concerning the sequence below Hanover Point, the position relative to Chron CM1 cannot be estimated from the existing data for the Isle of Wight section.

2) Worbarrow Bay section.

The greatest thickness of the Wessex Formation in southern Dorset is exposed at Worbarrow Bay, where the section spans some 360 m. Sampling gaps (maximum of ~20-30m) exist in certain parts of the sequence, normally because of slumping or difficult access, so that the overall polarity sequence comprises five separate "sub sequences" (right hand column of Fig.4.1.9). The polarity of the sediments in these gaps can be estimated from interpolation of the adjacent data, but clearly this leads to some uncertainties. The details of the polarity zonations are as follows.

At the top of the section is a long normal polarity interval, ~120m thick, with only a few isolated reverse polarity samples. This passes down into a reverse polarity magnetozone, termed "WW1", some 40m in thickness. Below this, a second normal polarity magnetozone encompasses the CQG and the underlying reverse polarity interval, termed "WW2", has a thickness of about 25 m. The minor reverse

polarity magnetozone, named "WW3", less than 5 m thick while at the very bottom of the section a reverse interval "WW4", with a possible maximum thickness of 36m, is split by a sampling gap.

The palaeomagnetic determinations for the uppermost normal polarity interval are generally good and almost all samples involved exhibited normal polarity SEPs. The boundary between the uppermost normal polarity interval and magnetozone WW1 is clear, located at 70 m above the CQG layer, (within Arkell's Bed 23). WW1 is defined by 13 sampling sites, but with a slumping gap about 13m in its lower part. 54% of the samples defining this magnetozone showed well-defined reverse polarity, but 30% of the samples exhibit erratic normal polarity behaviour and 15% yielded no meaningful polarity information. The poorer definition of reverse magnetozone WW1 in comparison with the overlying normal polarity magnetozone may relate to a partial normal polarity overprint in the present geomagnetic field, which would be more apparent in the reverse polarity interval. The existence of this reverse magnetozone is supported also by the clear distinction in magnetic properties, in comparison with the overlying and underlying normal polarity intervals.

The normal polarity interval between WW1 and WW2 is well-defined by some 70% of the samples from the 17 sampling sites in this interval exhibiting clear normal polarity information. The polarities of 18% of the set were checked by thermal demagnetisation following the progressive a.f. demagnetisation. Only 9% of the samples showed possible reverse polarities, which may be due to local magnetic overprint effects.

Magnetozone WW2 exhibits similar magnetic behaviour to WW1. Its upper boundary lies just beneath the CQG layer, at a level corresponding to Arkell's Bed 13. This reverse interval is defined by 12 sampling sites. 63% of the samples in it have relatively well defined reverse polarities. Five independent samples (which had not been a.f. demagnetised) were thermally demagnetised. They exhibited reverse polarity behaviour. 10% of the samples exhibited erratic magnetic behaviour and yielded no reliable polarity data. Finally, 25% of the samples in this interval did not show well-defined polarity

after 35 mT a.f. demagnetisation. This indicates the process of a widespread magnetic overprint. In spite of this uncertainty, this reverse interval is clearly distinguished from the overlying and underlying normal polarity sequences.

Magnetozone WW3 is a short reverse interval about 25 m below WW2. The normal interval between is also well-defined, on the basis of thermal demagnetisation data from 9 samples. Its upper boundary lies within Arkell's Bed 10, in which red clay is dominant. WW3 has a thickness of less than 10m and most samples in this interval exhibit reliable reverse polarity.

Magnetozone WW4 is the lowest reverse polarity in this section. Its upper boundary lies within Arkell's Bed 2, close to the gully and stream which a big gap in the section and separate Bed 1 from the lowest beds. Although 8 sampling sites define this interval, there is a 19 m gap in its middle. The overall maximum thickness (including the gap) is 36 m. 70% of the samples within it show reverse polarity behaviour but a significant proportion of these are not well defined (see Appendix 2). At the base of the section is a well-defined normal polarity interval.

In conclusion, a series of at least four reverse polarity magnetozones have been defined in the dominantly normal polarity Wessex Formation section at Worbarrow Bay.

3) Mupe Bay section.

The magnetostratigraphy of this section is closely similar to that of the upper part of the Worbarrow Bay section (above the base of WW2). The upper top reverse polarity interval at Mupe Bay is named MP1. It is a little shorter than its counterpart WW1 (Fig.4.2.1). Fig.4.1.16d summarizes the magnetic polarity sequence at Mupe Bay. The normal polarity interval at the top of the section has a thickness of about 130 m. The CQG, in contrast to that at Worbarrow Bay, appears about 50 m above the upper reverse polarity magnetozone (MP1).

Most samples within the upper long normal polarity interval have

well-defined SEPs, but with some erratic samples, about 11% yielding no meaningful information. 13% of the samples exhibited poorly defined magnetic behaviour, possibly of reverse polarity. There is no significant sampling gap within this interval except for a 19 m gap near the very top. Some isolated samples around both the upper and lower boundary of the CQG exhibited reverse polarities with well-defined SEPs or directional trends. These intervals lasted only 1-2 m.

The uppermost reverse polarity interval, MP1, lies about 130 m below the top of the formation and has a thickness of about 35 m, defined by 10-11 sampling sites. The overall characteristics are similar to that of magnetozone WW1 at Worbarrow Bay, namely a number of samples exhibiting demagnetisation trends towards a reverse polarity, but there are few well-defined SEPs. The lower boundary of this magnetozone is unambiguous but the upper one is not well-defined, because of a mixed polarity pattern (both normal and reverse polarity existing in the same part). Therefore, the estimate length of MP1 varies from ~30 to 35 m.

A clear normal polarity interval which is mainly defined by SEPs separates MP1 from the underlying reverse magnetozone, MP2, which appears ~30 m above the base of the section. 12 sampling sites define this 25 m reverse polarity interval. Because of a sampling gap at its top, the exact length is uncertain, but may be greater than 25 m. Although most samples in it show either SEPs or directional trends towards reverse polarity, they all are relatively poor-defined (see Appendix 3), probably indicating the effects of a serious magnetic overprint. Samples from the lowest two sampling sites show possible normal polarities.

Stephen *et al* (1991) thought the sedimentary sequence below the oil sand band, in which the two lowest sampling sites were located, has an eroded gap of about 8 m. This gap is not so obvious, but the two sampling sites may lie below it. Although 3 of the samples from these two sites show a normal polarity, the fourth is reversed.

4) Lulworth Cove section.

A mono-normal polarity sequence was defined in this 202 m section. Fig.4.1.22d displays the whole log, with the CQG in its lower part. There are two major sampling gaps in it, one about 45 m long in the upper part of the Gault Formation and the other, 20m long, in the Wessex Formation just above the CQG layer. The boundary between the Gault Formation and the Wealden is estimated from the colour change.

The Gault Formation has a relatively poorly-defined long normal polarity interval throughout, in which 27% of the samples did not yield meaningful polarity information due to the problems discussed in §4.1.4. The polarities of the majority of samples were defined from demagnetisation vector trends, only 25% of the samples exhibiting CMDs. The data for the Wessex Formation below is better than that for the Gault, particularly in the part of the section above the CQG, which was defined mostly by CMDs. Around the CQG, near both its upper and lower boundary, some isolated samples showed reverse polarity, similar to that observed in the Mupe Bay section. The lowermost part of this section is also dominated by a well-defined normal polarity interval. If the CQG, which is traced from Mupe Bay to Lulworth Cove, is used as a reference to compare the two sections, then in the 22 m gap above the CQG a normal polarity would be expected. The lowest part of the Lulworth Cove section is estimated to lie some 30m above the reverse polarity interval represented at Mupe Bay by MP1.

5) Durdle Door section.

A mono-normal polarity sequence was also defined in this short, westmost section. There is no significant sampling gap within the section but its upper boundary with the Gault Formation is not so clear and the gap between the Wessex and Chalk Formations (the Gault Formation was covered by slump during the field work) was estimated at more than 20 m. The lower boundary with the Purbeck Beds is a fault-controlled contact. In spite of the overturned bedding (dip 95-110°N) and much coarser grain size, most samples yielded reliable polarity results. However, 25% of the samples did not give any meaningful polarity information and only 37% exhibited SEPs and CMDs.

Some isolated samples exhibit reverse polarity behaviour after progressive a.f. demagnetisation, these are located mainly in the middle of the section and in its lowest part.

Fig.4.1.29d shows the polarity sequence defined at Durdle Door, with the relatively thick CQG in its uppermost part, and the possible further lignitic "grit" layer (Arkell 1947) near the bottom of the section. Some single samples showing reverse polarities appear near to the latter layer. This situation is similar to that at Lulworth Cove and Mupe Bay, which is possible evidence indicating that the CQG layer at Lulworth Cove might be traced to Durdle Door to match the lower lignitic grit, rather than the upper CQG.

4.2.3) Magnetostratigraphic correlations for the Wealden Beds in southern England.

The correlation of the magnetic polarity sequences from southern England are based not only on the observed sequence of normal and reverse polarity magnetozones, but also on other geological and palaeomagnetic evidence. Thus, the CQG layers play an important part in correlating the sections from Worbarrow to Durdle Door, although not being present in the Isle of Wight section (which is more than 50 km distant from Worbarrow Bay).

A common reference level adopted in the Wealden Beds of the Wessex Basin for correlations might be the upper boundary of the formation. During that time a marine transgression extended over the whole area and the Wealden facies changed into a totally different depositional and sedimentary facies (Allen 1965, 1975, Stewart 1978, 1983, Simpson 1988). However, the erosion at the top of the Wessex Formation (Arkell 1947) must also be considered in such correlations. In comparison with the upper reference level, all lower boundaries of the Wealden with the Purbeck Beds in this area are poorly exposed. Therefore, the correlation process must start from the top and work downwards towards the lowest available bases.

Fig.4.2.1 summarizes the magnetostratigraphy of the five sections defined in southern England, in the order of their relative localities

from east to west. The Wealden Beds on the Isle of Wight show a conformable contact with the overlying marine facies. Therefore, the reference level here is very clear. The upper boundary of the Wessex Formation in both the Worbarrow and Mupe Bay sections are not as clear as that in the Isle of Wight section. Some erosion is possible at this level, but the corresponding stratigraphic interval is uncertain. Therefore, the top of the two sections are provisionally plotted slightly lower that the top of the Isle of Wight section (Fig.4.1.1).

On the basis of biostratigraphic data, Hughes and McDougall (1989) tried to correlate the interval around and below the CQG at Worbarrow Bay with the lowest part of the Isle of Wight section, which lies just above the beds at Hanover Point. However, the magnetostratigraphic evidence do not support such a correlation. These data indicate that the part of the section on the Isle Wight, above the Hanover Point beds, is still within the long normal polarity quiet zone between Chron CM0 (Kerth and Hailwood 1988) and CM1, which is identified in the Worbarrow Bay section as WW1 in the present study. The part of the section can also be correlated to the upper part of the Mupe Bay section which also exhibits a long normal polarity zone.

The isolated reverse polarity events within the long normal polarity intervals might be helpful in correlating these long sections more accurately. Thus the isolated reversals around the stratigraphic heights of 80-100 m in the Isle of Wight section (Fig.4.1.3) and 170-190 m in Mupe Bay section (Fig.4.1.16) might be correlated. Some of those at the very bottom of the Isle of Wight section might correlate with those at just above the WW1 and MP1 magnetozones. It is a potential possibility that the Isle of Wight section might reveal a reverse polarity event if the section could be extended downwards below the anticlinal core at Hanover Point.

The correlation between the Worbarrow and Mupe Bay sections seems quite clear because both sections exhibit well-defined reverse polarity intervals at almost the same stratigraphic level (referred to their tops). However, the CQG layer in the Mupe Bay section is about 60 m higher than MP1 whereas the one in the Worbarrow Bay section lies within the normal polarity interval between WW1 and WW2. The lengths

of MP1 and WW1 are slightly different, probably reflecting variations in the local depositional rate. Unfortunately, the Mupe Bay section cannot be traced further downwards, below magnetozone MP2. Therefore, the counterparts of reverse magnetozones WW3 and WW4 at Worbarrow Bay were not observed at Mupe Bay.

It has previously been suggested (Arkell 1947) that the CQG layer at both Worbarrow and Mupe Bays are correlatable. In this case, the top of the Mupe Bay section would have been removed significantly by erosion before the marine facies sedimentation took over. However, from both geological and magnetostratigraphic evidence this seems improbable. Although Stephen *et al* (1991) discovered an erosion surface in the lower part of the Mupe Bay section, no significant erosion surface has been found at the top. Biostratigraphic evidence is lacking. Magnetostratigraphic evidence shows some isolated reversals around the CQG in the Mupe Bay section, but it is unreasonable to attempt to correlate these with the much thicker magnetozones WW1 and WW2 at Worbarrow Bay. Furthermore, the majority of the samples around the CQG at Mupe Bay showed a well-defined normal polarity after demagnetisation and application of bedding correction, which indicated that the sediments are unlikely to be magnetically overprinted.

The pattern of NRM intensity events around the CQG layers are different in both sections (Figs.4.1.9 and 4.1.16). Thus the CQG at Worbarrow Bay lies within the NRM "event 3" which has a thickness of only about 20m, whereas the CQG at Mupe Bay lies above the NRM "event 2" which has a thickness of some 40 m.

The section at Lulworth Cove can be correlated unambiguously with that at Mupe Bay through direct tracing of the CQG between the sections. It may be significant that some isolated reverse polarity samples lie above and below the CQG, at both Lulworth and Mupe Bay. However, it is uncertain how much of the top of the Wessex Formation in these two sections has been eroded. The palaeomagnetic correlation suggests a possible thickness of 30-40 m of Wessex Formation sediments may have been removed from the eastern sections before the start of Gault Formation deposition. If the CQGs are correlated between the

Lulworth Cove and Mupe Bay section (Fig.4.2.1), the NRM "event 2" at Lulworth Cove (Fig.4.1.22) can be compared with "event 2" at Mupe Bay, which appears just below the CQG layers in both cases.

The mono-normal polarity sequence in the Durdle Door section did not provide as useful magnetostratigraphic information as was available for the other sections. However, the CQG can be correlated between Durdle Door, Lulworth Cove and Mupe Bay. The combination of the CQG layers and NRM intensity events also constrains the possible thickness of sediment eroded from the top of the Wessex Formation as about 30m.

4.2.4) Correlations with GPTS.

Fig.4.2.1 summarizes the magnetic polarity sequences from the five investigated sections of the Wessex Formation and also shows the composite polarity sequence. Combining the result from Kerth and Hailwood (1988), the composite sequence has a reversed interval, named VF1, at its top. The sequence is followed downwards by four reverse intervals in the Wessex Formation, named WS1, WS2, WS3 and WS4, in which WS1 and WS2 are defined at both Worbarrow Bay and Mupe Bay, but WS3 and WS4 are defined only at Worbarrow Bay.

Comparison of this composite sequence with the Geomagnetic Polarity Time Scale (GPTS) (Kent & Gradstein 1985) is possible by means of the limited biostratigraphic evidence from the Isle of Wight and Worbarrow Bay sections provided by Hughes and McDougall (1989). According to the latter authors Arkell's Bed 28 corresponds to a middle Barremian age (Fig.4.2.2a). The reverse magnetozone WS1 lies within Bed 23, 50 m below Bed 28 (Fig.4.2.2b). Therefore, it is reasonable to correlate WS1 with the Chron CM1, which is allocated to the middle to lower part of Barremian stage around 122-123 Ma. The biostratigraphic evidence of Hughes & McDougall (1989) correlates the CQG layer to just beneath the Barremian/Hauterivian stage boundary. However, the magnetostratigraphic evidence puts the CQG layer between magnetozones WS1 and WS2, and if WS2 is correlated to Chron CM3, then the CQG layer at Worbarrow Bay will correlate with the lower part of the Barremian stage, with an age of ~123 Ma. The biostratigraphic evidence from Bed 8 provides an estimated age of middle to upper Hauterivian

(unfortunately, Hughes and McDougall (1989) did not give scaled ages for their dating), and the reversal WS3's upper boundary is within Bed 10, 20-30 m above Bed 8. It would be possible to correlate WS3 with Chron CM5 which is also in the upper Hauterivian. The reversal WS4's upper boundary is in Bed 2, 40-50 m below Bed 8. Therefore, it is reasonable to correlate it to the middle Hauterivian, and the underlying beds to the lower part of Hauterivian stage with an age around 128.5 Ma to 131 Ma.

The correlation between the Isle of Wight section and the GPTS is not so well constrained because Hughes and McDougalls' biostratigraphic evidence for the Isle of Wight section is from the southeast flank of the anticline rather than the same section as the present study. The correlations discussed above provide some further information on the age of the Isle of Wight Wessex Formation studied, placing this in the upper half of the Barremian stage.

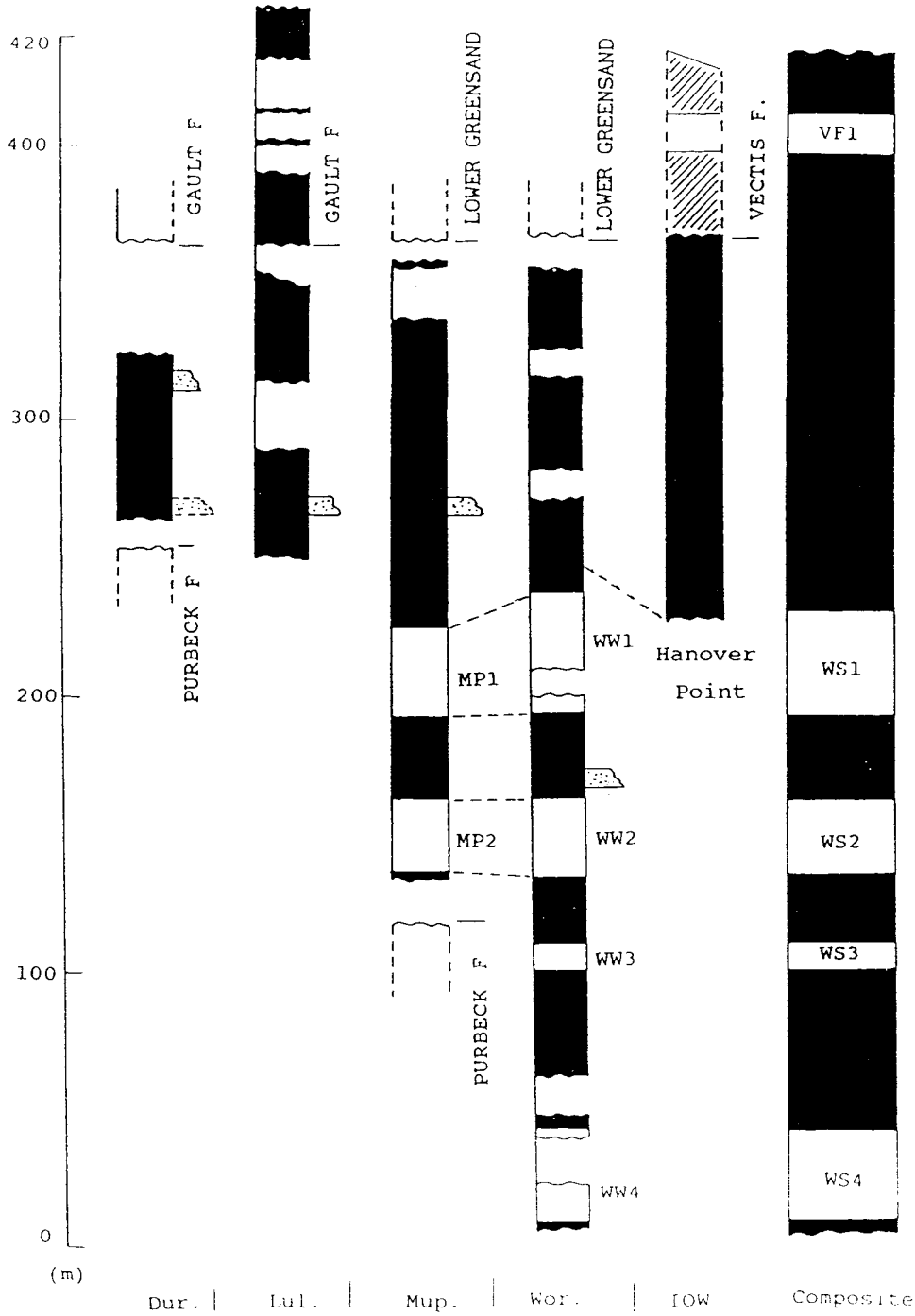

Fig. 4.2.1 Summarized magnetic polarity sequences for the Wessex Formation at different localities in Southern England. The right hand column represents the composite sequence. The codes WS (Wessex Formation) and VF (Vectis Formation) are used for the reverse polarity magnetozones in the composite section.

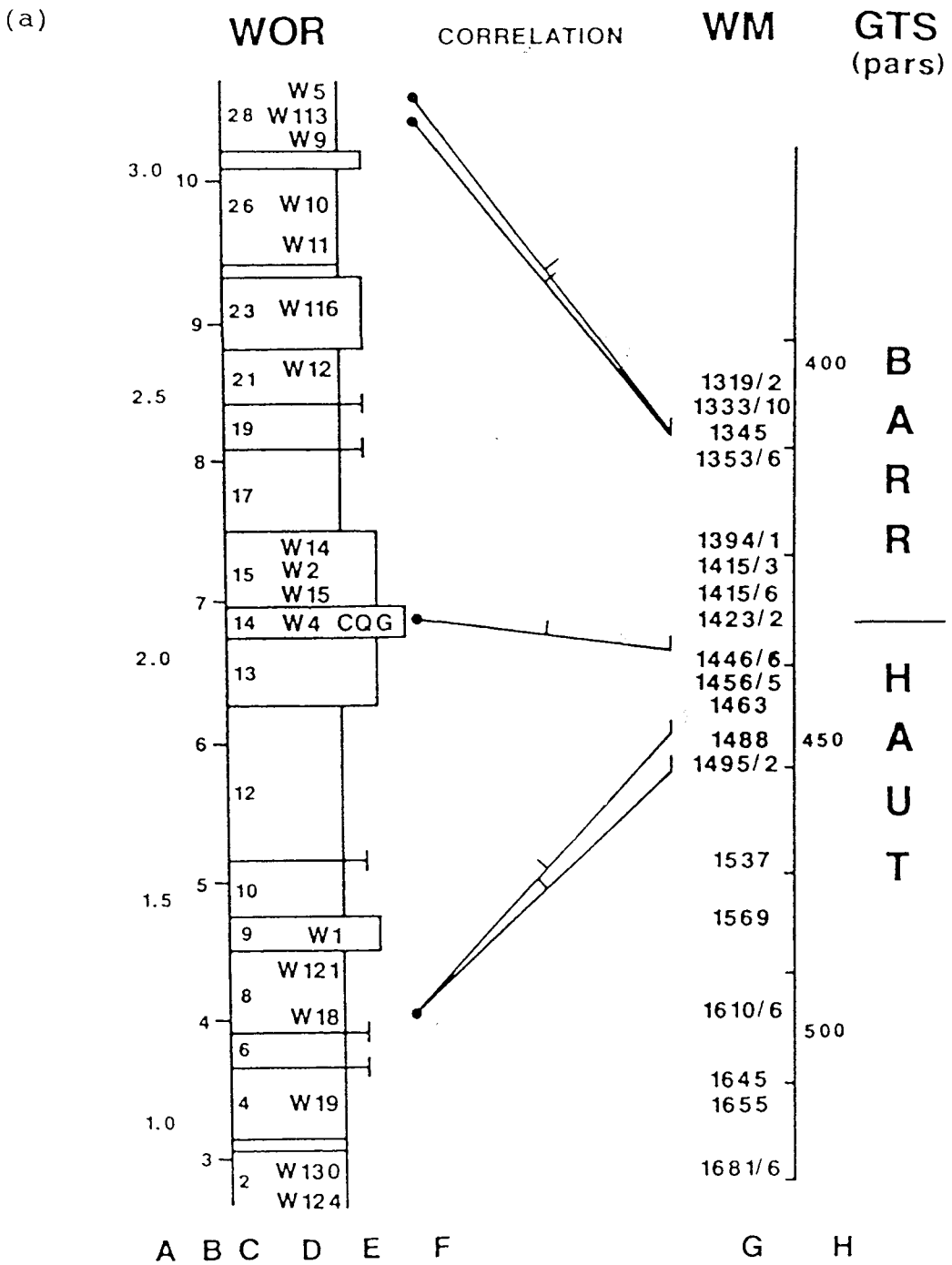

Fig. 4.2.2 (a) Biostratigraphic correlations for Worbarrow Bay (WOR), Warlingham Borehole (WM) and the Geological Time Scale (GTS). The main biostratigraphic evidence in the Worbarrow Bay section is from Bed 8, Bed 14 (CQG) and Bed 28 (Hughes & McDougall 1989). Conventions and symbols for A to F as in Fig. 3.3.5. G: borehole depth in feet and H: depth in metres.

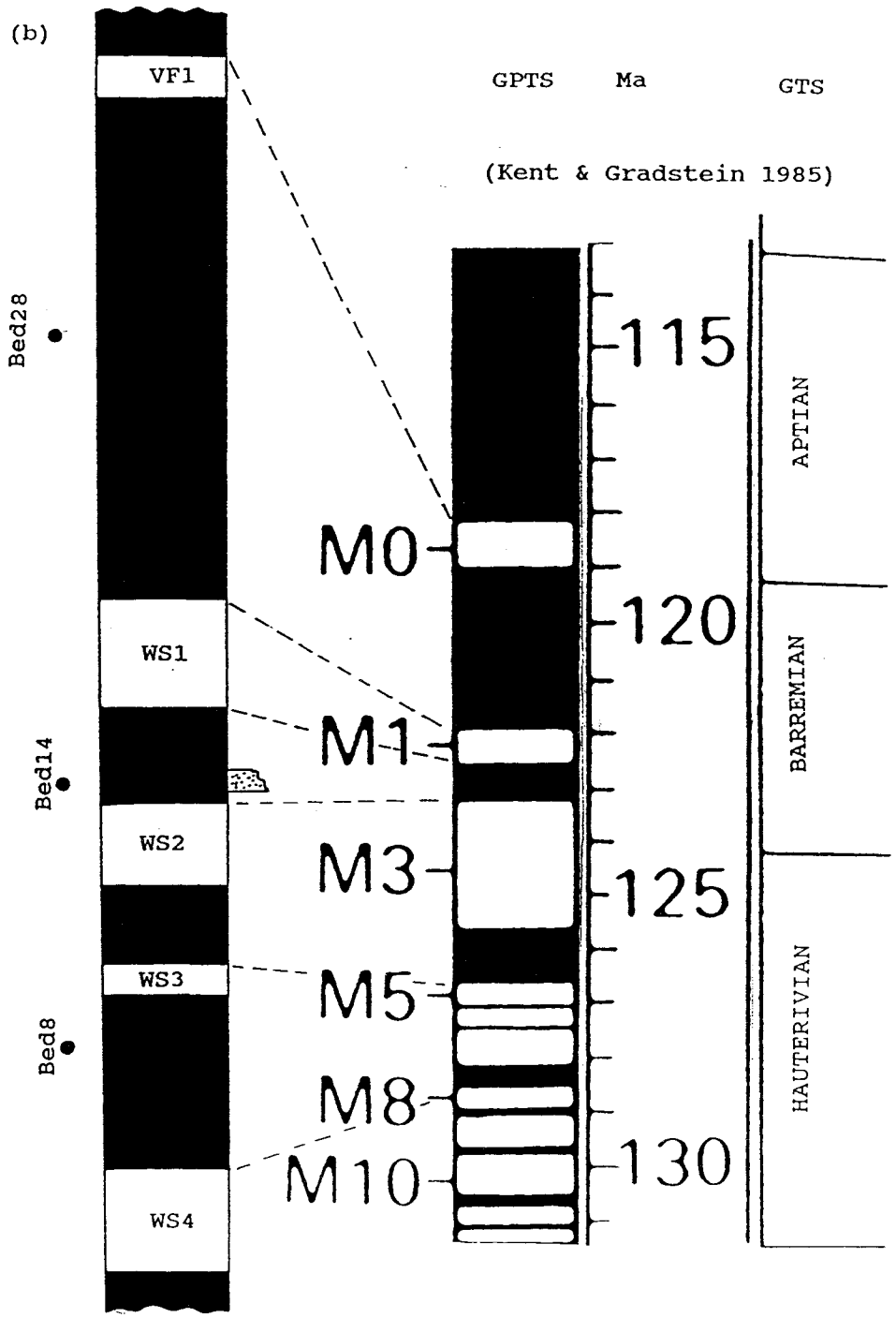

Fig. 4.2.2 (b) Magnetostratigraphic correlation for the Wessex Formation of southern England with the GPTS and GTS. The solid points on the left hand side are the datum levels for biostratigraphic evidence from Fig. 4.2.2a.

§4.3 Magnetostratigraphic sequences in the Weald Clay Formation from southeast England and their correlation

The two mono-normal polarity sequences defined in the Beare Green sections made it impossible to identify these sections in the GPTS for the Lower Cretaceous.

The two sections at Langhurst (Warnham brickwork pit) are more useful, since both exhibit distinguishable normal and reverse polarity intervals. Fig.4.1.39c and Fig.4.1.40c show the magnetic polarity and lithological sequences. A possible lithological correlation between them has been previously discussed in §3.1. Magnetostratigraphic sequences also yielded good evidence for correlation (see Fig.4.3.1). For the section in the northwest bank of the pit, the upper part exhibits a long normal polarity interval about 8.2 m thick, but encompassing 3 single well-defined reverse polarity events (see Appendix 6), possibly either reflecting a magnetic overprint or representing minor reverse polarity events such as those observed in the Wessex Formation of southern England. The lower 2.5m of the section is dominated by a well-defined reverse polarity interval with only one sample exhibiting a normal polarity behaviour. The southeastern section exhibits a shorter normal polarity interval in its upper part, about 1.5 m thick, and with only one sample showing a reverse polarity. The underlying 6.5 m of beds is dominated by a reverse polarity interval.

The two sand/limestone layers are apparently located at different levels relative to the magnetic polarity sequences. The upper one (in the northwest bank) lies near at the bottom of the normal polarity interval and the lower one (in the southeast bank) near the middle of the reverse interval. Although the correlation of these section seems simple, the lack of a general (eg biostratigraphic) reference for the these reversals makes it impossible to link them to the GPTS. The only constraint which the magnetostratigraphic data provide is that Bed No.2 in the Weald Clay Formation (in which these sections are located) probably lies in the Lower Barremian or Hauterivian Stages, where more frequent changes in magnetic polarity occurred, rather than the Upper Barremian, which was dominated by normal polarity.

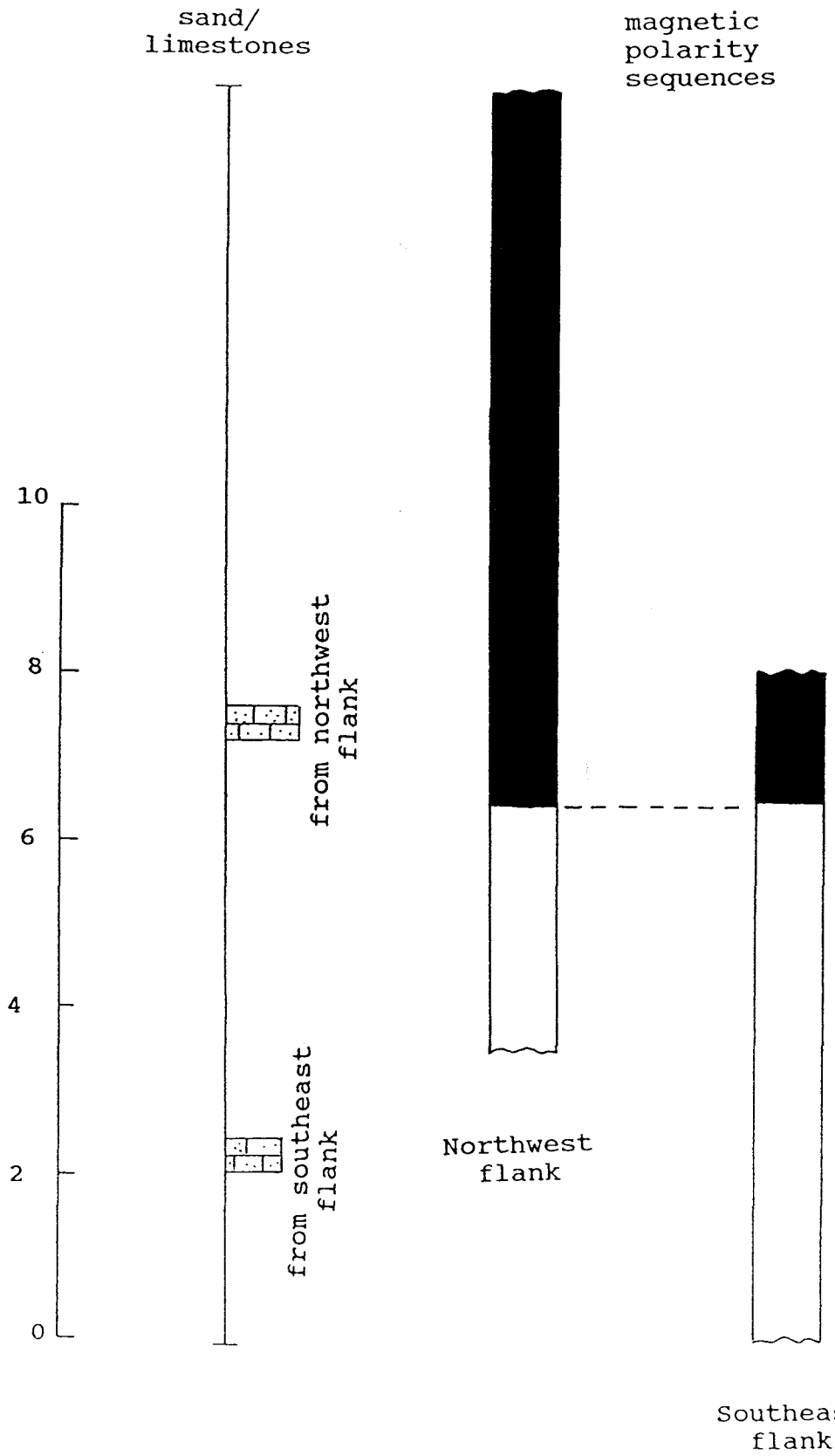

Fig. 4.3.1 Correlation of Magnetic polarity sequences in the Langhurst brickwork pit sections.

CHAPTER V OLIGOCENE GEOLOGY OF SOUTHWEST ENGLAND AND NORTHWEST BELGIUM

§5.1 General geological situation of Oligocene in Northwest Europe.

5.1.1) General geological situation.

At the end of Cretaceous, the Atlantic Ocean was already well over a thousand kilometers wide, the central area of the North sea was continuing to subside as it had done since at least Early Jurassic times, and the two areas were connected via a strait on the site of the western half of the English Channel. This strait widened out eastwards into a large part of southeast England, the rest of the English Channel and the Paris Basin, and extended thence over the low countries to Denmark and North Germany. This period resulted in the deposition of the Reading and London Clay Formations in southern England during the Palaeogene (Curry *et al* 1978). Only some higher parts of Ireland, Devon, Brittany and Cotentin remained emergent. In the Eocene Stage, southern England and northwest Europe were still experiencing this period of marine transgression.

The Oligocene epoch is around the middle of the Tertiary. The term "Oligocene" was introduced by Beyrich (1854), who defined its lowest fossil-bearing unit, the sands of Magdeburg and Egln in Germany, which mark an important marine transgression. A sharp drop in the world temperature has been postulated for early Oligocene time and polar glaciation may have caused a general fall in sea-level (Cavelier 1986). However, in the low countries the sequences still remain almost entirely marine (Vandenberghe 1981). Meanwhile, in the Paris Basin, the eastern and western Channel areas and parts of south-east England, folding, faulting and other structural movements were initiated, in mid- or late-Oligocene times (Curry *et al* 1978). It was at about this time that fault-controlled basins developed in pre-Mesozoic rocks in association with NW-SE structural lines, both in south-west England (Bovey, Lundy, etc.) and in Brittany (Rennes). The Neogene rocks of East Anglia are the southwesterly fringe of the deposits of the North Sea Basin, and Neogene sequences in the central part of the western

approaches English Channel testify to the local subsidence at that time

Fig.5.1.1 shows the general distribution of Tertiary sediments around England and part of northwest Europe. It can be seen that marine sedimentation (dated as around Palaeogene age) mainly concentrated in the Hampshire Basin, part of the English Channel, the Paris Basin and Belgium. In southwest England non-marine deposits were laid down in scattered places.

5.1.2) Dating and correlation of Tertiary sediments.

Workers on Tertiary biostratigraphy in the past have relied mostly on the comparison of fossil assemblages rather than on the presence or absence of individual species until about 30 years ago, when some intensive studies of microfossils led to the recognition that several different groups have considerable value in stratigraphical correlation (Curry *et al* 1978). From the 1950's to 1960's Bolli (1957) and Banner and Blow (1965) defined a series of zones, based on planktonic foraminifera, to subdivide the Tertiary Beds into more than 20 zones. They introduced the now widely used P (Palaeogene) and N (Neogene) zonal notation, designating their newly-defined zones as P1-19 and N1-23 (N1 = P20) with a time span from early Oligocene to Recent (see Fig.1.3.4). Blow (1969), Bolli (1966) and Berggren (1969, 1985) subsequently refined these zonations. Within the circum-equatorial belt the foraminiferal zonal sequences have almost world-wide validity. Another useful microfossil group, the discoasterids are found, related to the coccolithophorids and have considerable potential value in dating and correlation (Bramlette and Riedel 1954). Martini (1970) and Martini and Worsley (1970) designed a total of 46 zones (numbered NP1 to NP25 and NN1 to NN21, with the former relating to the Palaeogene and the latter to the Neogene). A number of correlations have been made with the foraminiferal zones (P ~ N system) of Banner and Blow (1965) (also see Fig.1.3.4).

Besides the biostratigraphic methods of correlation, which provide an indication of relative age, radiometric methods can provide numerical dates, but these are not yet sufficiently precise to be of value in Pre-Pleistocene stratigraphy, except in cases where

biostratigraphical control is very good. On the other hand, the radiometric methods are mainly based on igneous rock which are difficult to relate to the biostratigraphical records in sedimentary sequences. Most recently, palaeomagnetism has been involved in Tertiary dating and correlating investigations. Combining detailed biostratigraphic information, palaeomagnetic results provides an independent absolute dating and correlating method for Tertiary Beds. For example, Townsend and Hailwood (1985) had been successful in correlating the Palaeogene sedimentary beds from Hampshire and the London Basin, and more recent work has been carried out by Ali and Hailwood (unpublished) for the Early Tertiary sediments in Northwest Europe.

The present study was stimulated by the enormous interest in dating and correlating the Tertiary beds around parts of Northwest Europe. Two regions have been studied; one is in Southwest England where sedimentation was dominated by a fault-controlled subsiding in a continental environment and the other is a shallow marine depositional environment in Belgium, one of the low countries. The former sedimentary sequence has rather poor biostratigraphic control.

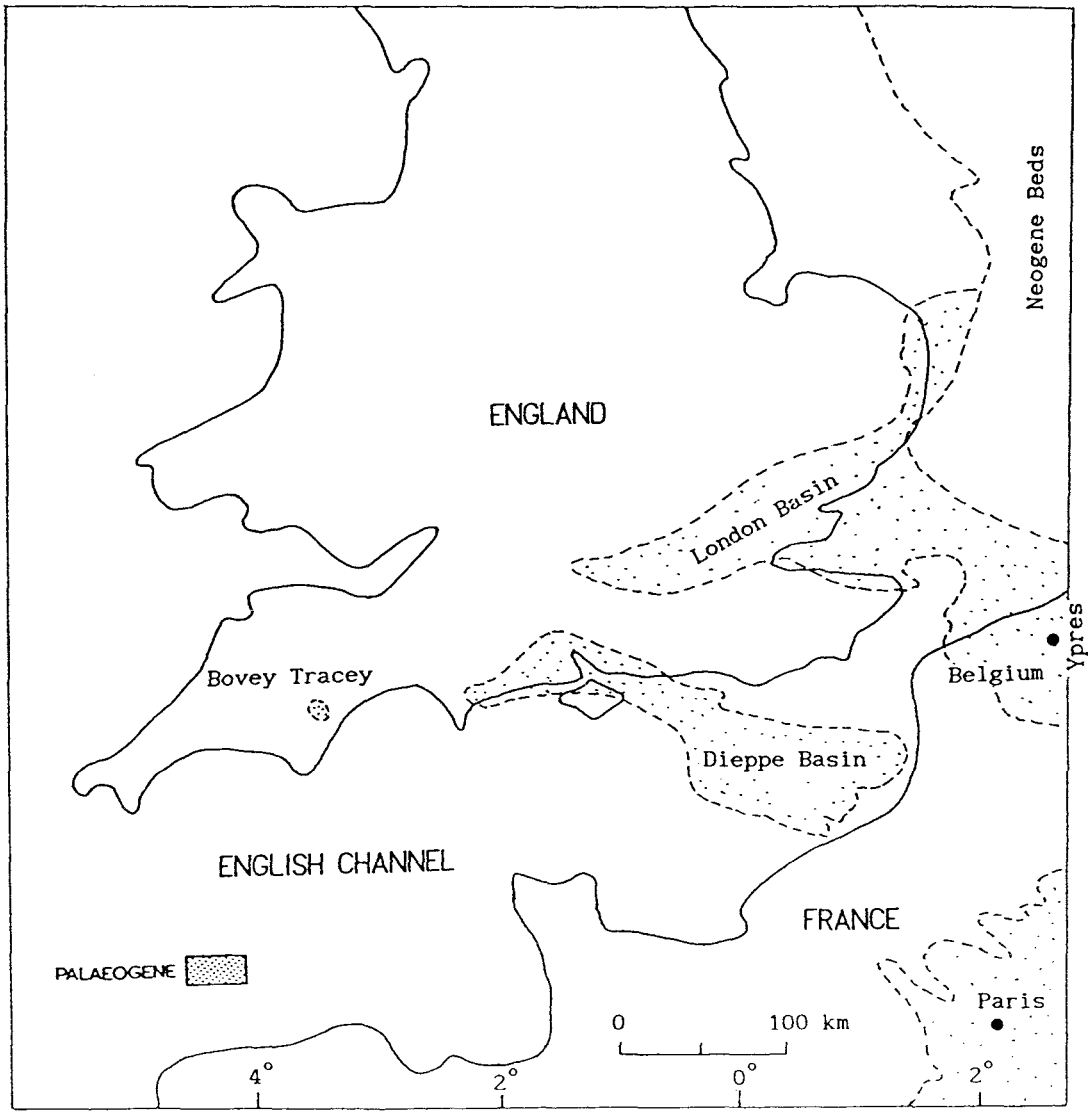

Fig. 5.1.1 Distribution of Tertiary (mainly Palaeogene) sedimentary beds in England and northwest Europe (after Curry *et al* 1978).

§5.2 Geology of Bovey Basin, Southwest England.

5.2.1) Bovey Formation.

The Bovey Basin was an area of continental deposition during the Oligocene. Geologists have concerned themselves with the Bovey Basin for many years and there is a considerable literature but little of it is modern. More recently, Edwards (1976) described this formation systematically, based on a synthesis of information from industrial "ball clay" work pits and boreholes. The formation of the Bovey Basin was initiated by Alpine movements, which possibly reactivated Hercynian structures to give wide spread dextral wrench faulting of the Armorican peninsula on northwest-southeast and NNW-SSE lines (Dearman 1963). After the movement, along the wrench fault, the Green Cliff - Sticklepath - Lustleigh - Torquay line (see Fig.5.2.1), Tertiary sediments accumulated in fault-defined depressions, particularly at Bovey and Petrockstow.

Edwards (1976) thought that the Bovey Basin has a broadly simple structure, with a deep central trough containing up to 1245 m of sediment (also see Fasham 1971), flanked on its eastern side by a thinner "shelf" depositional sequence, and with a major fault along the western margin. Fig.5.2.2 shows the suggested model of evolution of the Bovey Basin, in which A represents the original situation in the very early Tertiary, B (Phase 1) indicates the early sedimentation in the faulting basin, and C (phase 2) shows the present structure of the Bovey Basin with its eastern shelf sequences being worked by industrial interest but its base still poorly defined. The Bovey sediments are typical of plastic deposits in an enclosed partially fault-controlled subsiding fresh-water basin. The sedimentation is considered to represent a complex interplay of flood-plain, lacustrine and possibly alluvial environments; it is unlikely that the Bovey Basin was ever the site of a large deep "permanent" lake (Edwards 1976).

Although the Bovey Basin consists of a great thickness of about 1245 m of sediments from its base, only about the uppermost 350 m are exposed at the surface or revealed by boreholes. The major ball-clay producing area in the Bovey Basin lies along the eastern side of the

main basin, and as a result the stratigraphy of this area is relatively well-known, while other parts of the basin are only poorly known.

The Bovey Formation revealed so far consists of two major sediment units, the Abbrook Clay and Sand (abbriated to "ACS") and the Southacre Clay and Lignite ("SCL"). Some other sedimentary units, such as the Rinslade Clay (25 m?) and the Chudleigh Knighton Clay (45 m?),can be recognized around the north and south margins of the basin. These are considered as intermediate in age between the two major units. However, in the main part of the clay-producing area these two units display a conformable contact in many boreholes. Fig. 5.2.3 shows a set of boreholes arranged from southwest to northeast in the main clay producing area, in which the two sediment units show a conformable contact with a south westerly dip.

The Abbrook Clay and Sand (ACS) comprises a thickness of around 145m of non-carbonaceous high-silica clays and sands, generally grey in colour and with subordinate brown clays, but lignites are rare. A typical borehole (GR 860474722, drilled by IGS 1969) near to the investigation area shows that its upper part is red and pink-mottled clay, generally quite silty, passing downwards by gradual increase of coarse material into red-mottled brown very fine sands. The basal part of the unit is characterized by some siliceous clay, sands and mottled silty clay, the mottling being caused by ferric oxide (Edwards 1976). Two subdivisions can be recognized in this unit by their silica contents. The lower of these is exposed in John Acres Lane quarry and was sampled for the present study. The upper part was not well-exposed during the field work, so that its thickness and relation with the underlying units are unknown.

The junction between the ACS and SCL units is a horizon at which grey clays and sands give way to a generally silt-free and sand free sequence of brown clays and lignites. This passage is not always sharp, and in some places, the division has to be selected arbitrarily. The thickness of the SCL unit varies from 30m to at least 67m but having an average value about 38m. These clays range from light brown to dark chocolate brown or black in colour and contain fragments of lignitic materials. The most striking feature of the SCL sequence is

the presence of lignite beds, generally alternating with brown clays.

The fossil wood and other macrofossils, leaves, fruits and seeds, are poorly preserved, and were described by Chandler (1957), who showed them to be restricted to an Oligocene age. The pollen and spore assemblages were investigated by Boulter and Wilkinson (1977). All evidences supported Chandler's conclusion by comparison with material from the Hampshire Basin and elsewhere. The age of the upper part of the Bovey Formation is shown to range from Early to Middle Oligocene, probably with Eocene sediments at the lower part (Curry *et al* 1978).

5.2.2) Geology of sampling localities.

Three localities in the east flank of the Bovey Basin were sampled for the present study. These are John Acres Lane quarry, Longmarsh quarry and a drilled borehole SD485 which is supposed to penetrate the two stratigraphic units. Fig.5.2.4 shows the geographic localities of the three sections. Geologically, in the northeast flank of the Bovey Basin, a general NW-SE strike of about 150° with a shallow southwesterly dip can be recognized. Fig.5.2.5 shows the geological distribution of the Bovey Formation in its northeast flank, in which the John Acres Lane quarry is within the ACS unit range and Longmarsh quarry is in the narrow strip of SCL exposure. The borehole SD485 is located about 550 m southwest of the John Acres Lane quarry (Fig.5.2.4).

1) Longmarsh quarry section (GR 852758).

Longmarsh quarry has been opened for many years and some excavation is still carried out in its different parts. The palaeomagnetic sampling work was carried out along a freshly dug bench, probably not more than half a year old. The section is about 10 m below the ground surface and has a total length about 217 m along the digging bench which is nearly west-east oriented and faces north. The apparent dip of the beds exposed on the bench varies from 8-13° and the true dip angle coincides with the general dip in this area about 11-15° towards the southwest. The true stratigraphic thickness of the beds sampled is about 25-33 m.

Fig.5.2.6 is a schematic diagram to indicate the sediment bedding and sampling site arrangement. From the lower to the middle part of the section there are a number of lignite layers, but the upper part is dominated by white clay and some orange sand bands. It is possible that the sampled section extends up into the top of the SCL unit but it is not clear if the lower part is complete. The industrial company working in this area suggests that the lowest part of the SCL unit appear in some underground mines around this area (Edwards 1976). The orange sand band at the top of the section seems an important reference level, which also appears in many borehole logs. 27 sampling sites were occupied in the 217 m long section. Therefore, the average stratigraphic sampling interval was less than 1.3 m.

2) John Acres Lane quarry section (GR 861751).

From the Longmarsh quarry to John Acres Lane is about 1.2 km southeasterly. Like Longmarsh, John Acres Lane was also excavated by digging engineering and there is a very fresh section (digging-bench) available. Fig.5.2.7 shows a schematic diagram which was surveyed in April 1988 and Plate 5.2.1 shows the lower part of the section. The section was about 10 m below the ground surface with its strike direction at 150° SE nearly perpendicular to the true bedding. This quarry mainly exposes the Abbrook Clay and Sand (ACS), with a very different character from the section at Longmarsh quarry (in the SCL unit). It mainly consists of grey clays in the upper part and mottled clay and sand at the base. There are number of fine sand bands within the thick clay and, particularly, there is "sand waste" band in the lower part of the section. It is believed that this was buried some 200 years ago by mining work. This band is about 4 m thick. The bedding angle along the bench is about 10-15° towards the southwest. The total stratigraphic thickness of this section is about 40-45 m.

The correlation between the section of this quarry and that at Longmarsh quarry was unknown during the field work. According to Edwards (1976), the section at John Acres Lane represents the main part of the ACS unit, but possibly with its very upper part not complete. On the other hand, the John Acres Lane quarry section possibly just

reveals one third of the ACS unit, its lower part not having been seen in the present study. There is no biostratigraphic information reported from this section. In total 34 sampling sites were occupied in this section, which gives an average sampling interval of about 1.3m.

3) Borehole SD485 (GR 860746).

This borehole was drilled in July 1988. It lies to the southwest of John Acres Lane quarry, about 550-600 m away, beside the B3193 road. Fig.5.2.8 indicates the geographic situation of John Acres Lane quarry and the borehole SD485. The borehole penetrated a depth of 57.9m from the ground surface. Generally the drill machine had a sufficiently high recovery ratio and there is no significant gap, except for some lignite bands which were washed out in its upper part. Fig.5.2.9 displays the borehole log, in which the upper part shows a number of minor gaps, in which lignite bands were washed out by the drilling, and the lower part is almost complete. The boundary between the SCL and ACS units was identified at ~40 m. These two units seem to have a conformable contact. The SCL unit extends to about 33.5 m below the ground surface, if the surface cover is ignoredand the sand band at the very top of it. This thickness is similar to that of the exposure in the Longmarsh section. The sampling work for the palaeomagnetic study was started from a borehole depth of 11.2 m. This depth is just below an orange sand band which could compare with the very top part of the Longmarsh quarry section.

Because the general bedding dip in this area is about 10-15° towards the southwest (240°) and the distance between the borehole and John Acres Lane quarry along the dip direction is about 400 m, the penetration of 57.9 m by the borehole would be expected to reach a stratigraphic level around the middle part of the John Acres Lane section. This consideration could be proved by comparison of sediments at the base of the borehole with the middle part of the John Acres Lane section, where the former exposes some brown to dark-brown mottled silty and very silty clays and the latter also shows a brown to dark-brown silty clay band (see Plate 6.2.1). Therefore, within the ACS unit, the borehole and the John Acres Lane section both have a

common reference level for stratigraphic correlation. However, there is still no biostratigraphic information available from the borehole SD485. 54 levels were sampled in the borehole cores with an average sampling interval of about 1 m.

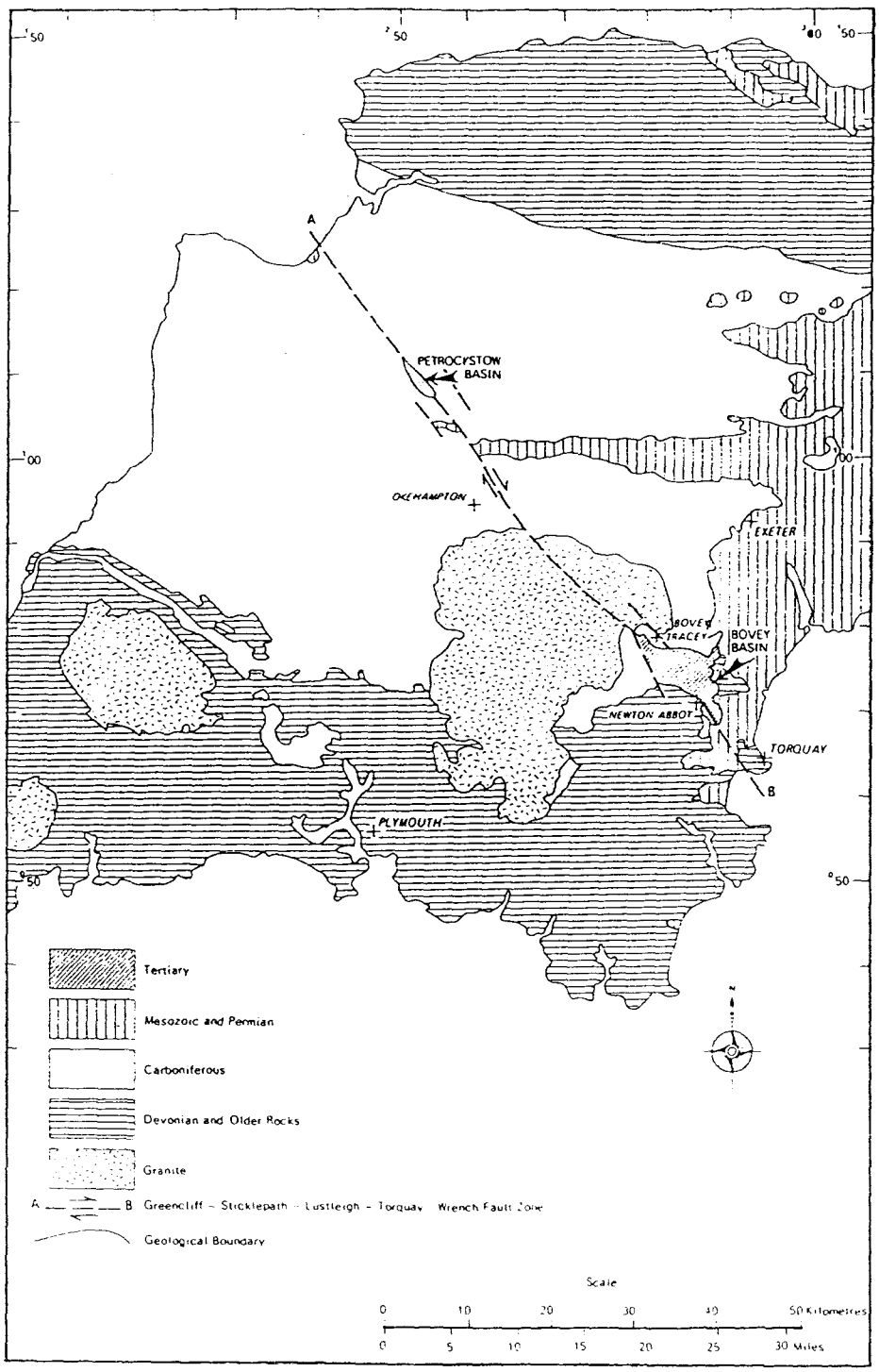

Fig. 5.2.1 General geological map of part of south-west England. The Bovey and Petrockstow Basins are shown along the wrench fault A-B (from Edwards 1978).

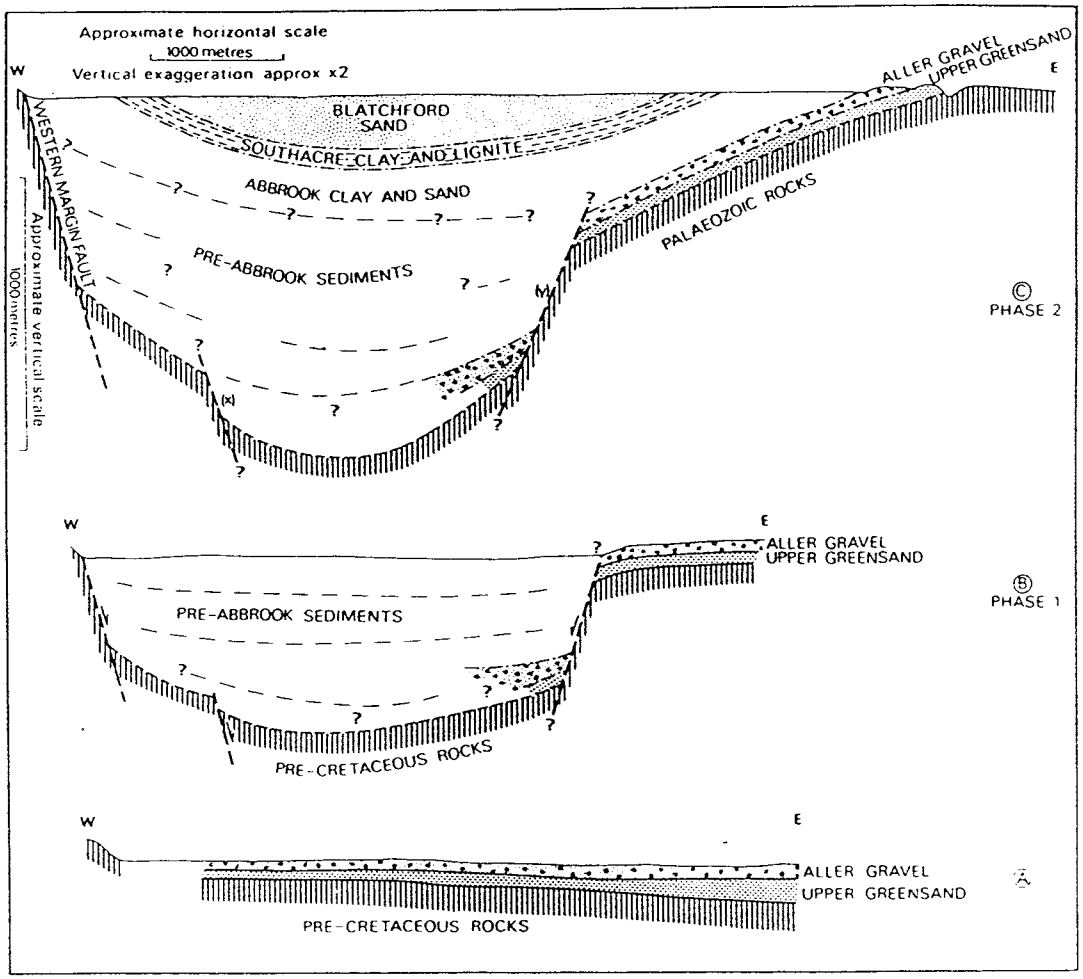

Fig. 5.2.2 Reconstruction of the evolution of the Bovey Basin since the Cretaceous (from Edwards 1978). The present study was concentrated at the east flank of the basin (c, phase2).

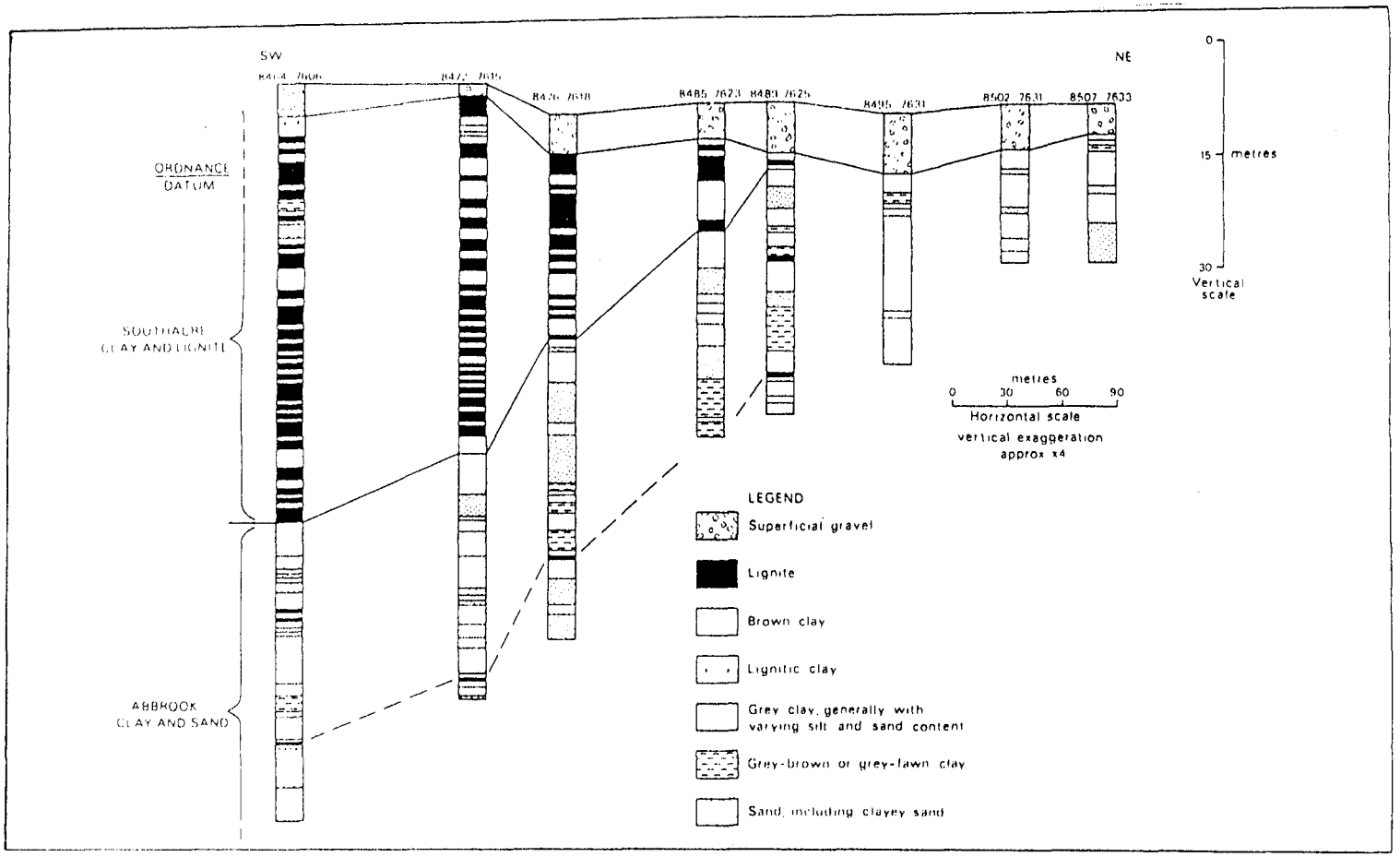

Fig. 5.2.3 A cross-section based on a series of borehole logs which show the vertical distribution of the Abbrook Clay and Sand and Southacre Clay and Lignite sequences, from the centre to the northeast flank of the basin (from Edwards 1978).

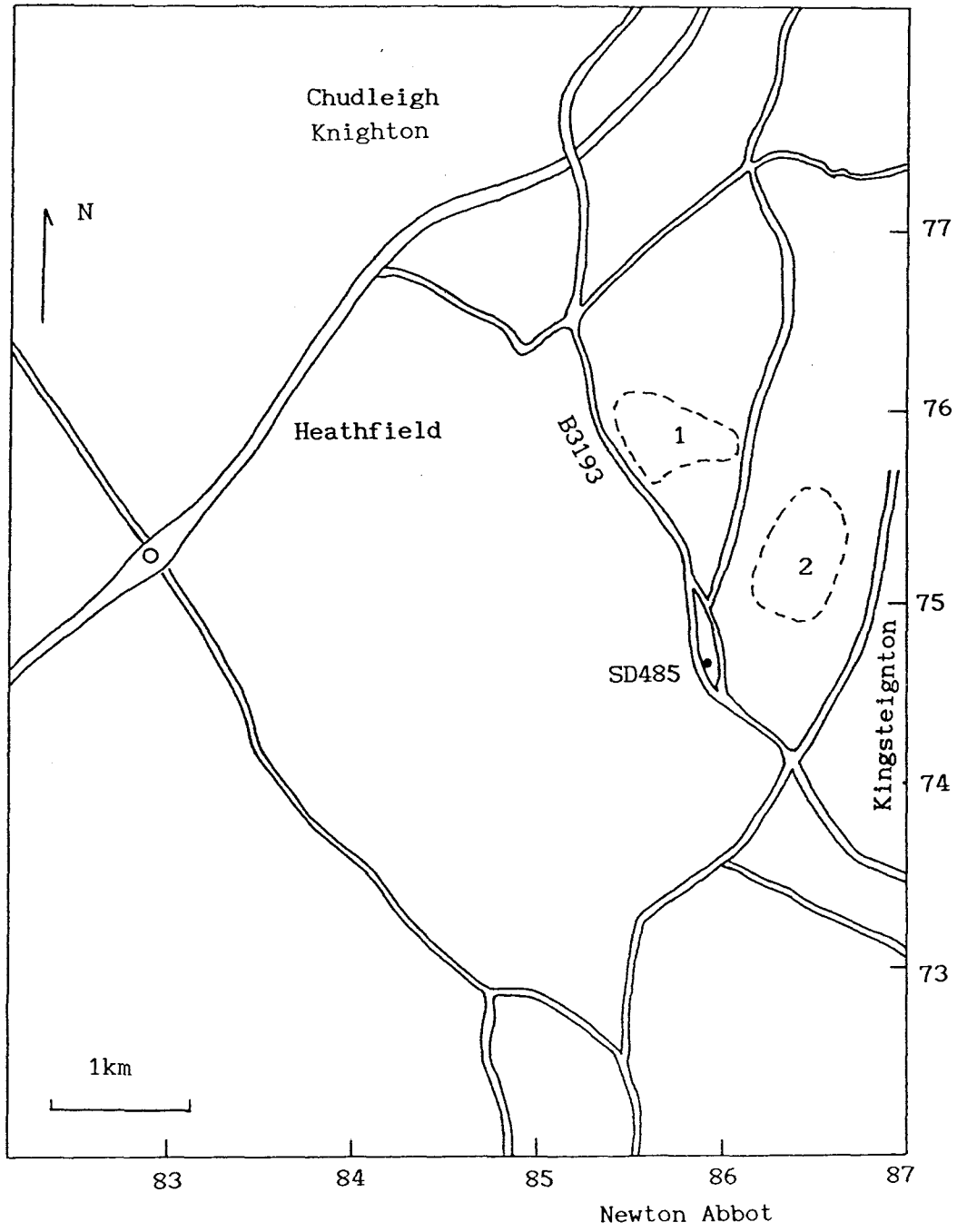

Fig.5.2.4 Geographic localities of the field work in the present study. 1: Longmarsh quarry and 2: John Acres Lane quarry, the borehole is shown as a solid point. The map is marked by Ordnance survey coordinates.

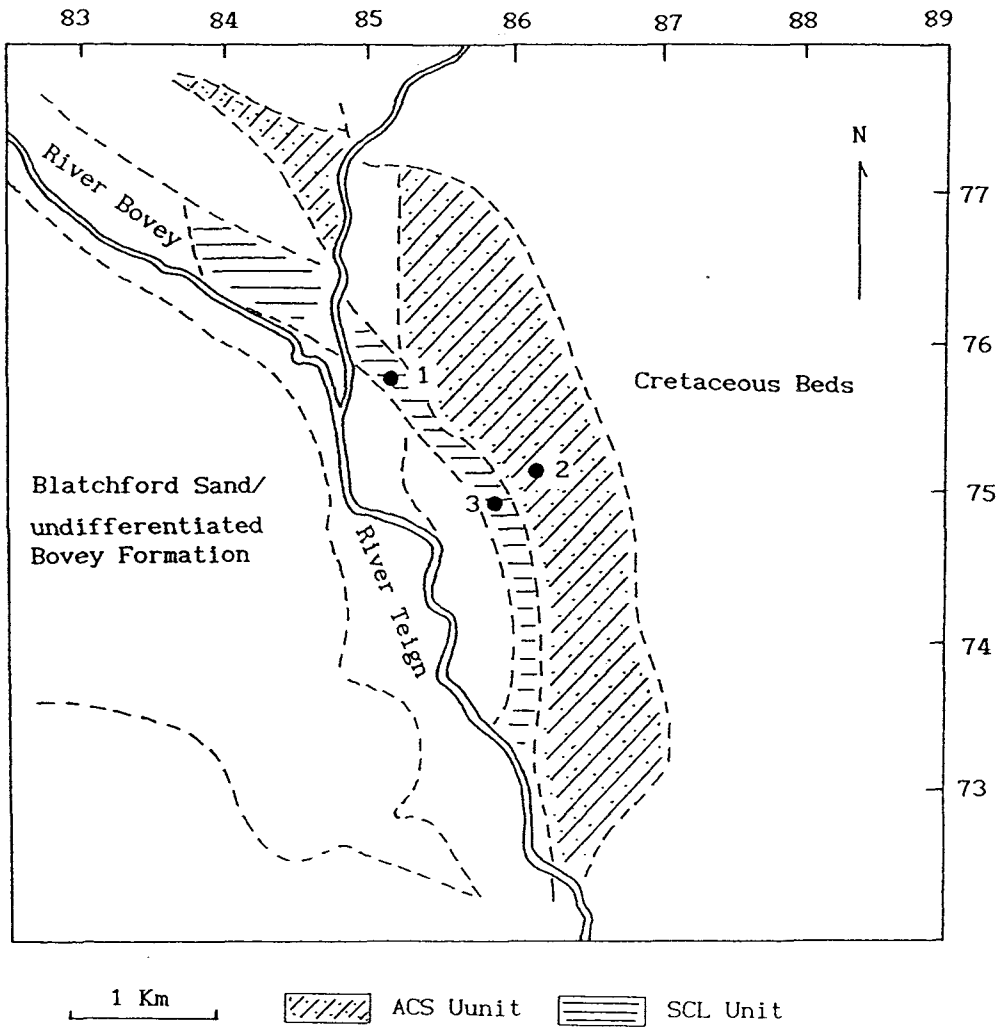

Fig.5.2.5 General geological map shown the distribution of the Abbrook and Southacre sequences in the northeast flank of the Bovey Basin. Sampling localities are shown. 1: Longmarsh, 2: Johnacres Lane and 3: Borehole SD485. The map is marked by ordnance coordinates.

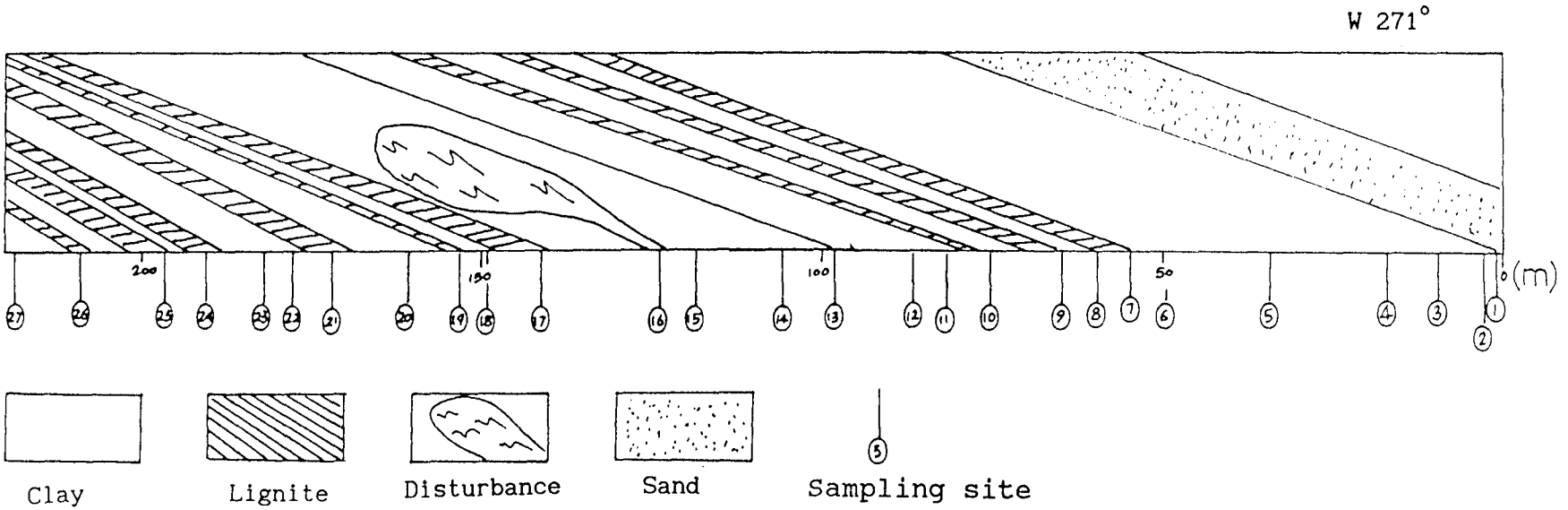

Fig. 5.2.6 Schematic diagram of the Longmarsh quarry section. The vertical is not to scale.

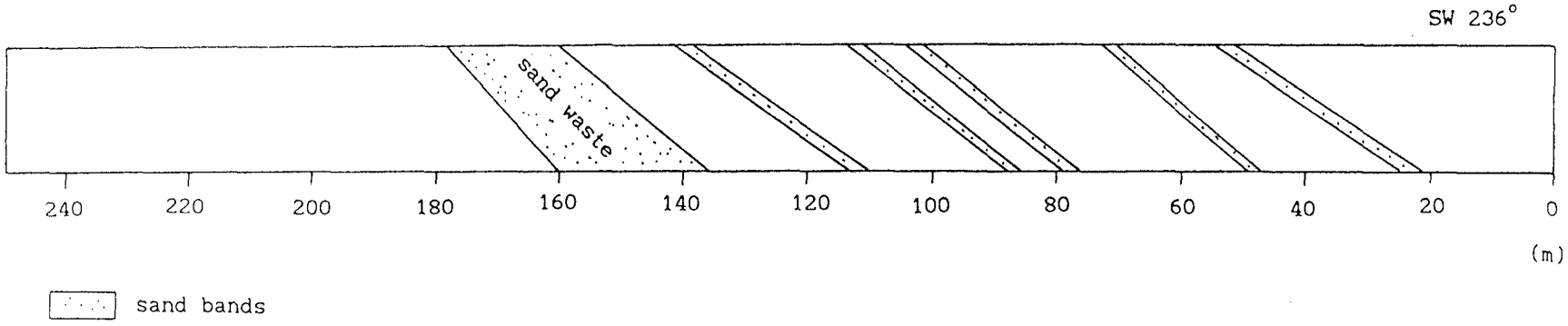

Fig. 5.2.7 Schematic diagram of the Johnacres Lane quarry section. The white part represent clays. The vertical is not to scale.

Plate 5.2.1 The lower part of Johnacres Lane quarry section. The right hand brown band can be compared with the base of the Borehole SD485.

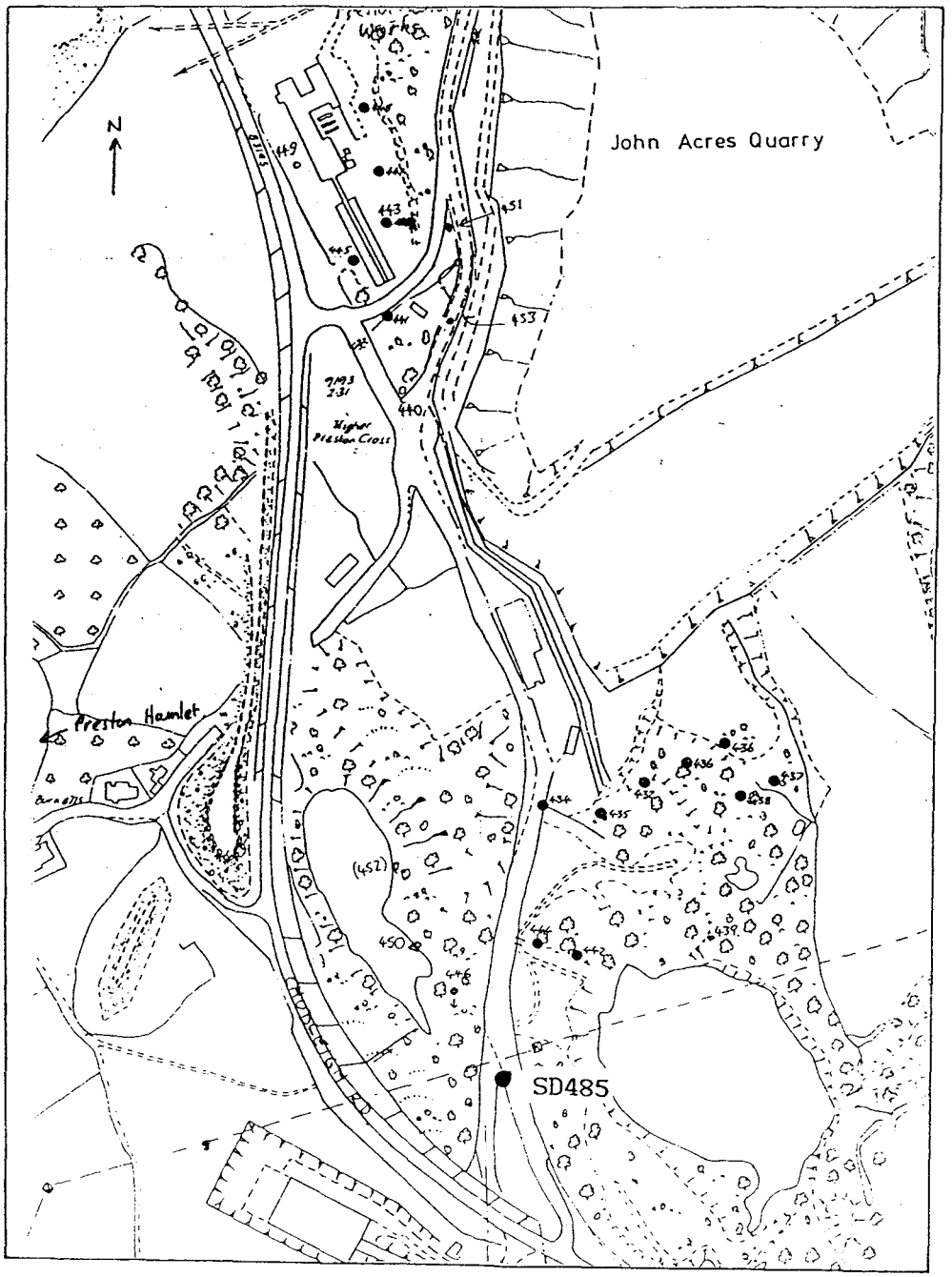

Fig. 5.2.8 Geographic map shown the localities of John Acres Lane and the Borehole SD485. In the area there are many other previously drilled boreholes shown as solid points.

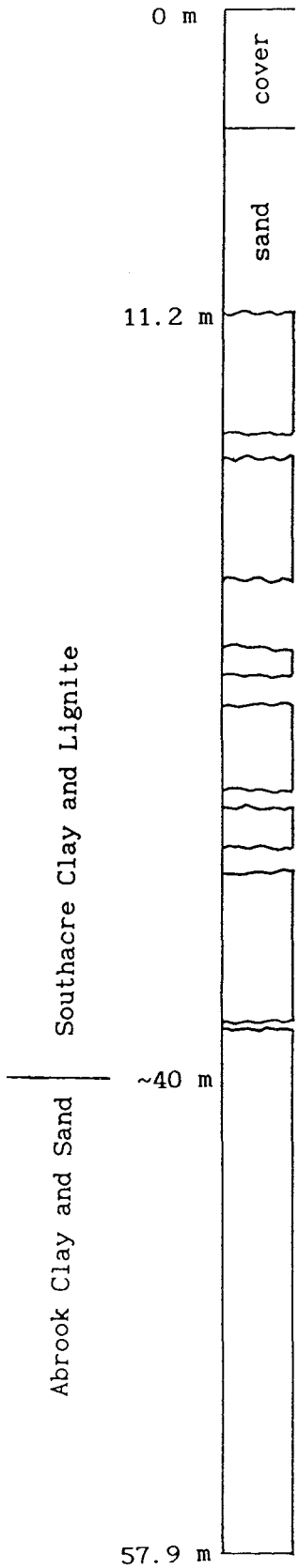

Fig.5.2.9 The borehole SD485. Gaps are caused by washed lignite segments and remaining parts are mainly the "ball clay". Sampling started from depth 11.2 m.

§5.3 Geology of the Boom Clay Formation, Northwest Belgium.

5.3.1) Oligocene geology of Northwest Europe.

During the Tertiary, sea-level fluctuations across shelf areas resulted in a complex cyclic sedimentation pattern, developing across continental northwest Europe and southern England. At that time Belgium lay near to the southwestern margin of an extensive depositional basin centred in the North Sea region. Starting from the beginning of the Palaeogene, the sea transgressed into the Paris Basin and this transgression brought thick clastic deposits not only into France, but also into northwest Belgium, particularly during Eocene and Oligocene times. These sedimentary beds can be divided into several principal categories: carbonate deposits from the Paleocene, sand and clay deposits from the Eocene and Oligocene, and uniquely sand deposits from the Miocene and Pliocene. Although there are certain stratigraphic hiatuses, the stratigraphical column of the Belgium Tertiary deposits represents an almost complete sedimentary sequence (Vandenberghe 1978, Curry *et al* 1978).

A general study of Belgian Palaeogene stratigraphy started from the second part of the 19th century. More recently, Gulinck (1965), Marechal and De Breuck (1979) and Vandenberghe (1978) have summarized and discussed this classic sequence. In the 1970s, a study of the Kallo Well, which was located 10 km west of Antwerp and drilled by the Foraky Company in 1965 led to a major advance in the knowledge of the Belgium Tertiary beds. Because of its position, the Kallo Well revealed one of the most complete sequences of post-Palaeozoic strata in Belgium and penetrated 444 m of Cenozoic beds (Steurbaut 1986). In the following lithological and biostratigraphical investigations the whole log was classified particularly the Boom Clay Formation, which was assigned to nannofossil zone NP23 (Martini 1971) (see Fig.1.3.4). Both boreholes and ground outcrops in the Antwerp area show a continuous marine sequence extending from the Eocene to the Oligocene stage.

The main sediment beds of the Oligocene in northern Belgium consists of two lithological units, the lower one, Berg Sand Formation,

containing *Nucula* is overlain by the Boom Clay Formation. These beds are called the Rupelian, from the Rupel, a tributary of the river Scheldt (Dumont 1849). Above these beds, there is a recognizable top Oligocene bed, defined as the Chattian Stage. In the eastern Campine it is the Voort Sands Formation and near Antwerp the Edegem Sands Formation. Above this formation the Oligocene-Miocene boundary is marked by a marine regression, following which the Houthalen Sands were deposited. Fig.5.3.1 shows the general depositional distribution during the middle Tertiary around the Antwerp area of northwest Belgium. The general strike of these sedimentary beds is about 300°. A series of sequences from Palaeocene to Miocene in age from the south-southwest to the north-northeast of the Antwerp area. The general bedding dip in this area is about 1° to the northeast; therefore, on a local scale the bedding is almost horizontal.

5.3.2) The Boom Clay Formation.

Because of its high commercial value, the Boom Clay has been investigated extensively and many brickwork pits have been opened. The Boom Clay Formation consists of about 50 m of carbonate rich clay deposited in a coastal shallow sea environment, not deeper than 50 m and with a subtropical climate (Vandenberghe 1978). It is exposed south of Antwerp and can be traced as far as the Netherlands for several hundred kilometers, where it dips steeply to about 250 m below the ground surface. Vandenberghe (1978) described the Boom Clay as a detrital deposit whose marine character is marked by the fauna and the chemical properties and mineralogy. Vandenberghe (1978) established a detailed lithostratigraphic subdivision of the Rupelian deposits, based on various criteria. Septaria layers, colours and certain grain size anomalies were found to have particular importance. These same criteria can be applied wherever Rupelian deposits are appropriately exposed and accessible (Bosch & Hager 1984).

Fig.5.3.2 shows the summarized whole log of the Boom Clay formation exposed around the Antwerp area. The alternation of the beds of some tens of centimeters is striking and indicates a rhythmical sedimentation. There is notably a distinct sedimentary boundary between the lower grey clay (argile grise) and the upper black clays

(argile noire) at a depth of 28.5m. Towards the top of the lower grey clay there is a pink layer (couche rose at Meter 23) underneath which the clay is lightly carbonated and above which the clay is decalcified. Above the grey-black clay boundary there are two very silty horizons (couches trés silteus, around Meter 25) which are situated very close together in the upper black clay. The sedimentary structures suggest that the cycle takes its origin from the periodic influence of wave activity on the bottom of a shallow sea. The black layers (couches noire) of the clay are a result of the enrichment of organic matter. With the exception of two such layers in the lower grey clay, all the others are grouped in the upper black clay.

Septaria layers are a very important reference in the classification of the formation, which was deposited in a very rich carbonate depositional environment. Vandenberghe (1978) incorporated all septaria layers into a sequence of eight different horizons (S1-S8) (see Fig.5.3.2). Later more layers were identified and defined from S9 to S12 (Vandenberghe unpublished) near Antwerp and the S1 to S9 were compared with the sediment beds in Winterswijk area of West Germany (Bosch & Hager 1984). In the Boom Clay Formation, these septaria layers are mainly distributed in the upper part of the formation and only two occur below the pink (couches rose) layer.

Another very important feature of the formation, which affects the palaeomagnetic study is the common occurrence of the mineral pyrite (FeS_2). There are two major layers in the formation which have apparent crystal grains (couche de pyrite), the lower one is just below the pink layer around a height of 23 m and the other is in the upper part of the formation, at around 30m. At septaria layer S5, the cracks of the silty carbonate deposits are covered with octahedral crystals of pyrite. Besides these, throughout the upper part of the Boom Clay Formation scattered mineral pyrite is frequently present. Vandenberghe *et al* (1986) explain the occurrence of pyrite during the transition from Rupelian to Chattian, as due to a major part of the Boom Clay Formation being eroded, followed by regressive diagenesis of the upper part of the remaining formation. This regressive diagenesis caused a general carbonate dissolution which resulted into ferroan calcite and octahedral iridescent pyrite coating of the septae and other deposits.

During the time span from Late Middle Eocene to the Middle Oligocene, the nannofossil assemblages of the Belgian Basin show a progressive imprisonment in species and generally also in individuals. Species appear and disappear gradually. These events are evenly spread over a considerable period. In the classic Kallo Well borehole the biostratigraphic evidence shows that in the late Middle Eocene very rich nannoflora were present, with a high diversity (c.40 species), but by the late Eocene these had dramatically reduced to about 10-16 species, representing a progressive decrease in temperature of surface water. The maximum reduction in diversity occurs some 5 m above the base of the Boom Clay Formation. It may represent the maximum cooling event in the Belgian Palaeogene. Afterwards, higher up in the Boom Clay it shows a progressive enrichment to a maximum of about 25 species (Müller 1970).

The Boom Clay Formation has been examined for its nanno-fossils mainly in the brickwork pit called "De Roeck and Ver strepen" (Boom) by many authors, including Bramlette and Wilcoxon (1967), Müller (1970), Roth (1970) and Martini (1971). According to these authors, it belongs to nannozone NP23, which contains *Reticulofenestra bisecta, Isthmolithus recurvus* etc. This determination has put the Boom Clay Formation in a period between 34.5 and 30 Ma, which corresponds with foram zones P21a and P19-20.

Although a successful correlation between the Boom Clay Formation and the Rupel Formation at the Winterswijk area of the Netherlands and the Hoerstgen area of the Lower Rhine District of W.Germany are made by Bosch and Hager (1984), little information about the correlation with English Oligocene sediments is available. The Bovey Formation is determined as having a probable age of around 33 Ma (Curry *et al* 1978); however, there is no significant biostratigraphic evidence (Chandler 1957, Edwards 1976) to allow a correlation between it and the Boom Clay Formation.

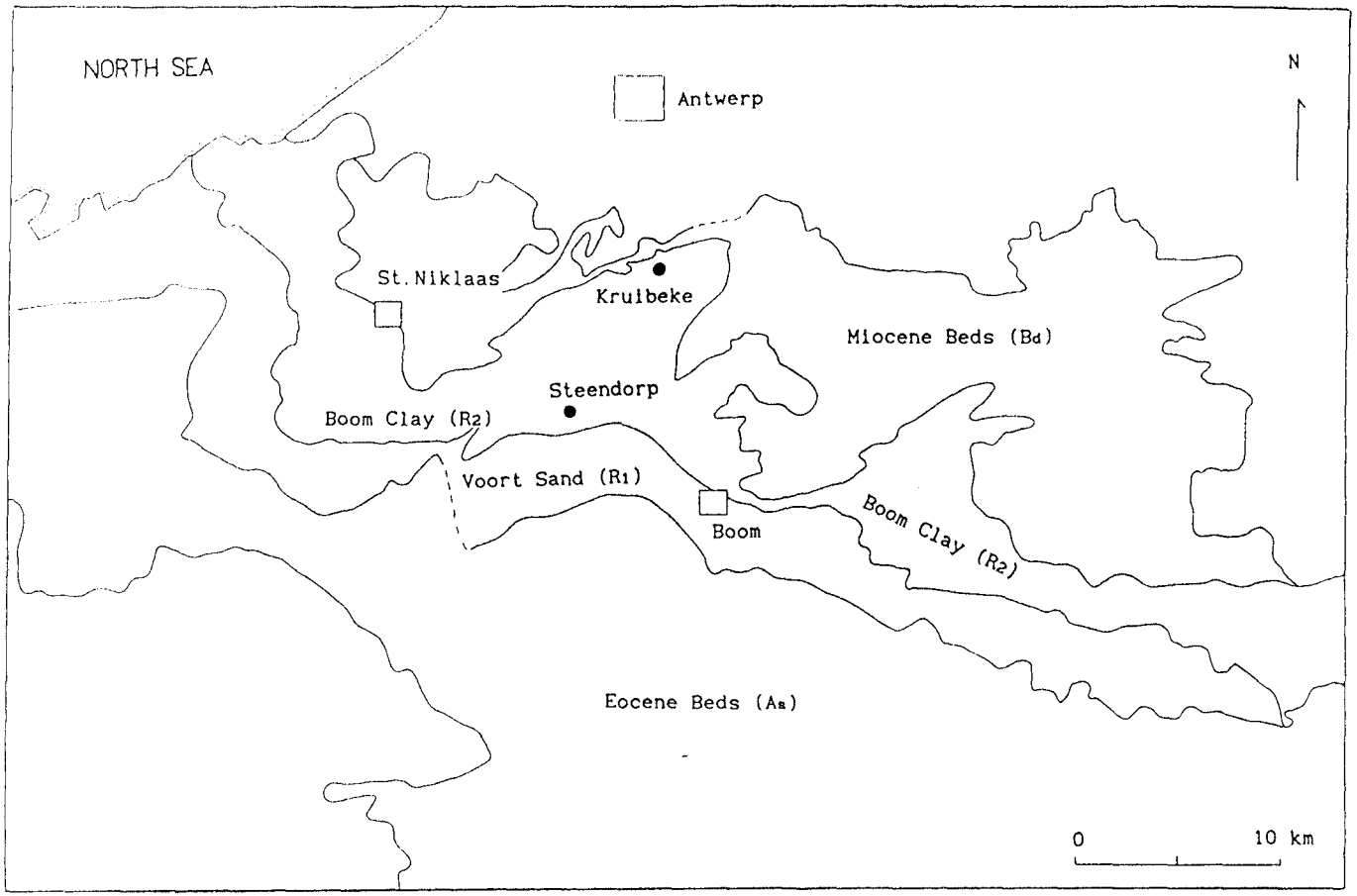

Fig. 5.3.1 Schematic geological map of Antwerp-Boom area, northwest Belgium, showing distribution of the Palaeogene beds in the area. (after the geology map of Institute Cartographie Militare 1945).

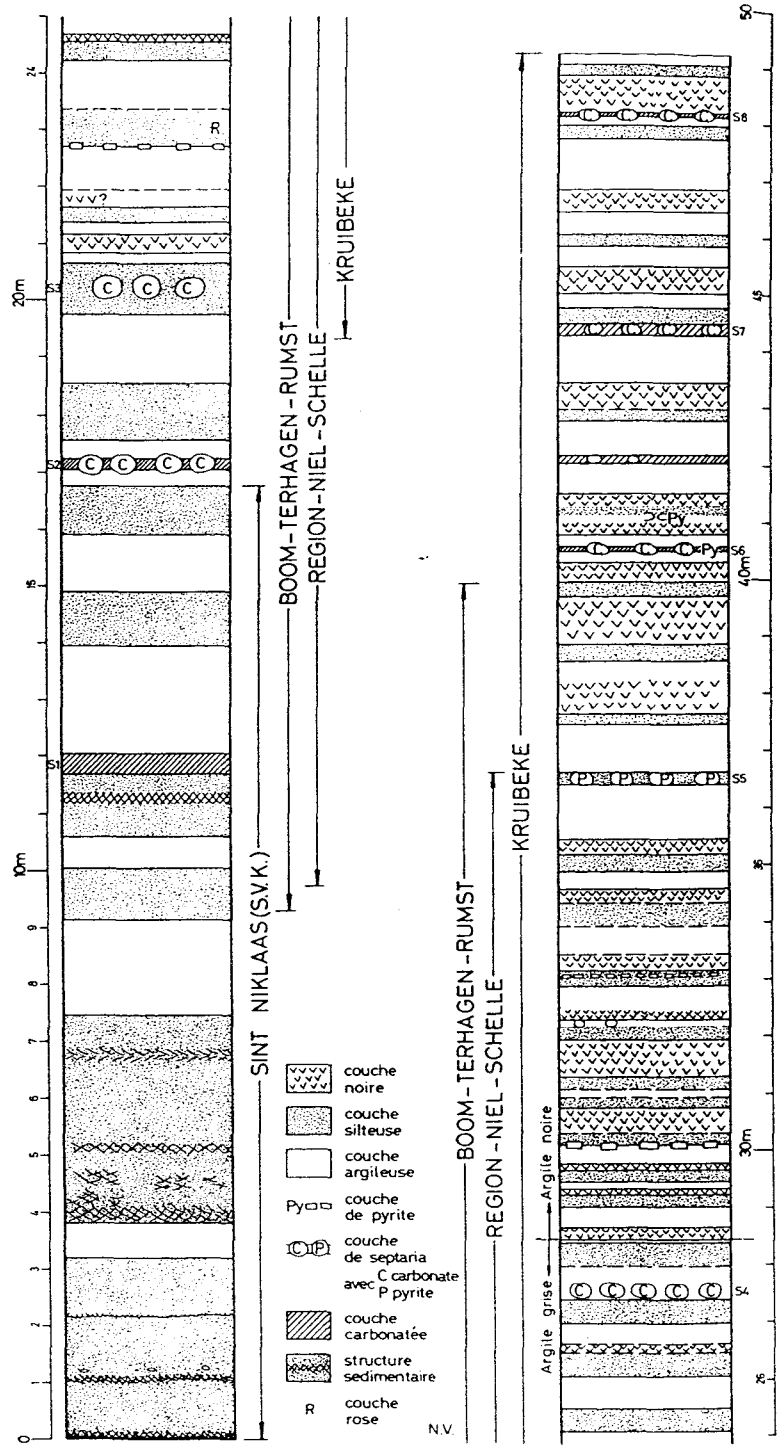

Fig. 5.3.2 Summarized lithological sequence of the Boom Clay Formation, also with main distribution areas for the clay formation. S1-8 represent the Septaria layers (from Robaszynsk & Dupuis 1983).

§5.4 Geology of sampling localities.

A systematic sampling of the main part of the Boom Clay Formation was done by McGrail (1987) supervised by Hailwood and Vandenberghe etc in October 1986 around the Antwerp-Boom area. A detailed record of the sampling was given by McGrail (1987) and full preparation of the specimens was carried out also by McGrail, in which the same method and procedure of sampling and sample preparation were adopted as those described in Chapter II of this thesis.

Fig.5.4.1 shows the geographic localities sampled around Antwerp. The work is concentrated in three localities, the Sint Niklaas, Steendorp and Kruibeke quarries, respectively. The St.Niklaas and Steendorp quarries expose the lower part of the formation (R_2) (Fig.5.3.1), overlying the Berg Sand Formation, R_1. The Kruibeke quarry lies near the northeast boundary of the Boom Clay and Miocene beds. Fig.5.3.2 gives part of the correlation among different localities, in which the St.Niklaas quarry exposes the lower part of the formation upwards to just below the Septaria layer S2 and the Kruibeke quarry exposes the upper part of the formation between Septaria layers S3 and S8.

However, the condition of these exposures during the field work meant that continuous sampling of the entire formation was not possible. Only 10m of sediments were available in the St.Niklaas quarry, extending from Meter 7 to just beneath the Septaria layer S2 (Fig.5.3.2). The Kruibeke quarry gave an almost complete exposure from Septaria layer S3 to S8, in two separate sections, a lower one and an upper one, with a quarry bench step between (around S5). The whole section of Kruibeke gives nearly 30 m stratigraphic thickness of the beds, the lower part being 16 m thick and the upper more than 13 m thick. However, Vandenberghe (1978) did not give any information about the correlation of the Steendorp quarry section, prior to McGrail's (1987) field work. Vandenberghe positioned the Steendorp quarry section stratigraphically parallel to the St.Niklaas quarry section, in which only 6 m sediment beds were available. Vandenberghe identified the Steendorp section starting at meter 12.5 (Fig.5.3.2) to

meter 18.5 above the Septaria layer S2 and ~2m below the Septaria layer S3.

At these localities, sampling work was carried out on rather fresh exposures. McGrail (1987) made a detailed record of the sampling at each quarry and carefully transferred the apparent distance between each pair of sampling sites to the stratigraphic height. There are 30 sampling sites for the St.Niklaas section, 12 sites for the Steendorp section and 81 sites for the Kruibeke quarry, respectively. This gives an average stratigraphic interval of 0.35m between successive sampling sites. If we assume the sampled stratigraphic interval lasts about 2.75 m.y. (based on the present study, using the magnetostratigraphic pattern, as discussed in Chapter VI), the average sampling interval would cover a time span about 2.5×10^{4} yr, which is sufficient enough to reveal the minimum polarity sub-chron (Table 1.1.1, Chapter I).

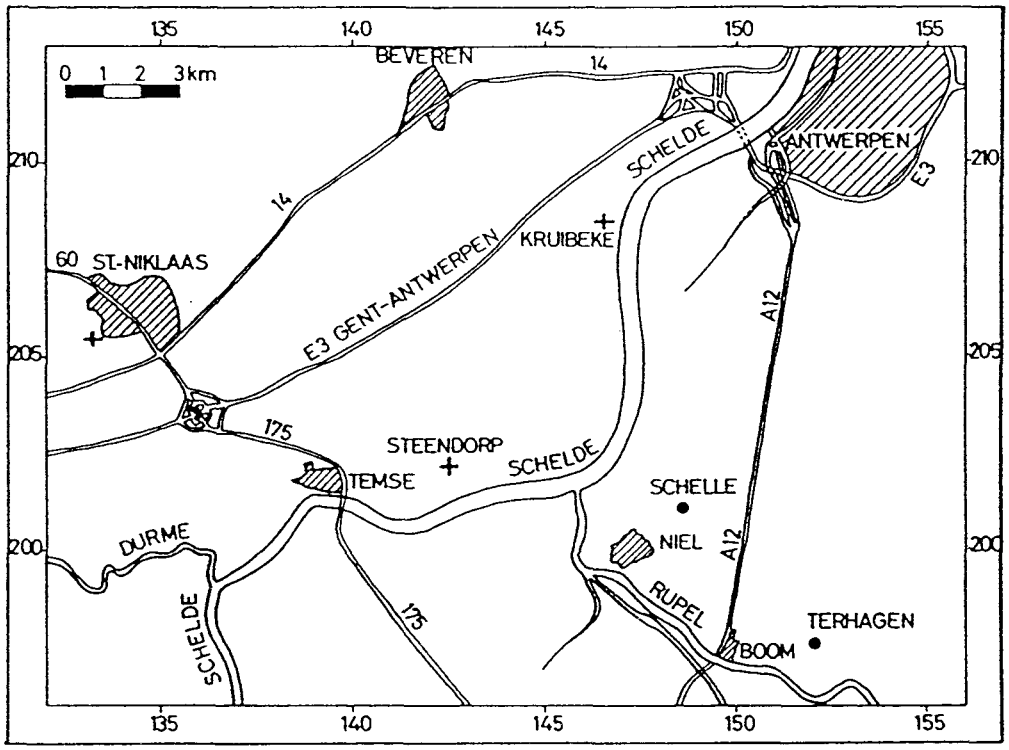

Fig. 5.4.1 Geographic map shown sampling localities in Antwerp-Boom area. Crosses represent the three brickwork pits (after Steurbaut & Herman 1978).

CHAPTER VI PALAEOMAGNETIC RESULTS FROM THE OLIGOCENE BEDS OF SOUTHWEST ENGLAND AND NORTHWEST BELGIUM

§6.1 Palaeomagnetic results from the Bovey Formation and their reliability

6.1.1) Longmarsh quarry section (Southacre Clay and Lignite).

The dominant sediments in this unit are white to grey clays with many bands of lignite. The IRM acquisition curves shown in Fig.6.1.1 indicate that the major magnetic constituent is magnetite which gives the IRM curves relatively sharp turns to saturation at magnetic field lower than 0.1 T. However, the maximum values of the magnetisation acquired in the maximum applied magnetic field of 0.86 T are rather lower than those observed for the Wealden Beds (eg see Figs.4.1.7 and 4.1.37), indicating a lower contents of magnetic minerals. A probable source for the magnetic minerals in the Bovey Formation is erosion of the nearby Dartmoor granite.

The NRM intensity of samples from this section is very weak with a log mean value of 0.099 mA/m. Most values are below 0.3 mA/m (see Fig.6.1.2). These weak intensities made determination of the direction of magnetisation and the magnetic polarity of the stable component relatively difficult. The plot of NRM intensity against stratigraphic height (Fig.6.1.3a) displays a generally uniform distribution from the top to the bottom of the section but with a relatively high value at the very top. Using a similar terminology to that determined for the Wealden deposits, this has been termed NRM intensity "event 1" (Fig.6.1.3b).

70 samples have been subjected to incremental a.f. demagnetisation, during which triple or double measurements on the cryogenic magnetometer were carried out frequently to be sure that the results and the working condition of the magnetometer were as reliable as possible. In many cases two separate specimens were taken from each core sample, for palaeomagnetic analyses. (These were labelled "a" and "b" respectively, see Chapter II) . Fig.6.1.4 gives some examples of responses of the samples to a.f. demagnetisations, in which the samples

yielded relatively a good polarity determinations but their relatively weak magnetic intensity remains scarcely reduced by the demagnetisation process.

Some samples show "noisy" behaviour at higher demagnetisation level (see Fig.6.1.5), usually >25 mT. In such cases, polarity assignments were based on the "undisturbed" part of the response (which may include a directional trend or a "SEP". For those samples with extremely weak intensities, (lower than 0.05 mA/m), the a.f. demagnetisation process was still carried on using closely spaced steps from 2.5 mT to 35 mT, but double or triple measurements were adopted, to better define the remanence after each step. If the magnetic vector showed "regular" behaviour during demagnetisation and if, after field and bedding correction, the direction of the magnetic vector lay in a reasonable region related to a certain polarity, then this would be accepted as a reliable result. Fig.6.1.6 illustrates two examples, for which the residual magnetic moment of the sample holder was around 0.004-0.007 mA/m.

Fig.6.1.7 summarizes the characteristic magnetisation directions (CMDs, see Chapter IV) yielded by a.f. demagnetisation. The overall mean direction after bedding correction is

$$\text{Dec} = 359^{\circ},\ \text{Inc} = 51^{\circ} \text{ with } \alpha_{95} = 10^{\circ}\ (N=32)$$

(see Table 6.1.1). The predicted magnetic field direction in Southern England for the mid-Tertiary, determined mainly from igneous rock sequences, is Dec $=2^{\circ}$ and Inc $=59^{\circ}$ (Piper, 1988). Thus the characteristic magnetisation direction (CMD) inclination for the Longmarsh section is shallower than expected. Unfortunately, few samples within the reverse polarity intervals exhibited high quality directional trends during a.f. demagnetisation; therefore, the great circle fitting method could not be applied in this case.

6.1.2) John Acres Lane quarry section (Abbrook Clay and Sand).

John Acres Lane quarry is situated some 1.5km to the southeast of Longmarsh quarry (Fig.5.2.4). The sediments in this 37m thick section

have a very different facies from the Longmarsh section (see §5.2.7). The IRM acquisition curves shown in Fig.6.1.8 for some samples of white and light brown silty or sandy clays indicate that magnetite is still dominant in this formation but probably with small amounts of hematite in some samples.

The NRM intensity has a lower mean value of 0.096 mA/m compared with that for the Longmarsh section. The variation of NRM intensity with stratigraphic height (Figs.6.1.10a and b) indicates some recognizable "events" of increased intensity. NRM "event 2", appears around 35 m, "event 3" around 20-23 m, and "event 4" near the bottom of the section, at around 5 m. (Note: the numbering of NRM intensity "events" precedes from the top of the sedimentary sequence to the bottom. Since the John Acres Lane section represents the lowest part of the sequence, "event 1" is not defined in this section).

112 samples from this section were subjected to progressive a.f. demagnetisation treatment and most of them produced reliable polarity determinations. Fig.6.1.11 presents some examples. The polarity of >55% of the samples was defined from directional trends. The interval is dominated by reverse polarity. About 10% of the samples did not yield meaningful polarity determinations, due to the weakness of their magnetic intensity. Fig.6.1.12 illustrates two examples. Fig.6.1.13 summarizes the CMDs for samples from this section. The overall mean vector after bedding correction has a direction:

$$\text{Dec} = 359^{\circ},\ \text{Inc} = 58^{\circ} \text{ with } \alpha_{95} = 11^{\circ}\ (N=17)$$

(see Table 6.1.1).

6.1.3) Borehole SD485 (SCL and ACS unit).

Borehole SD485 is located 500 m southwest of John Acres Lane quarry (Fig.5.2.4). This borehole plays an important role in correlating the two major stratigraphic units. The IRM acquisition curves (Fig.6.1.14) show evidence of magnetite as the major magnetisation bearer, but possibly with some small amount of hematite.

The NRM intensity has an even lower mean value (0.087 mA/m) than that for John Acres Lane section (Fig.6.1.15), may relate to a systematic magnetic property change from the northwest to the southeast in this area.

Three main NRM intensity "events" are defined for this borehole (Figs.6.1.16a and b). At the top, in the depth interval 11-12 m, the NRM "event 1" may be compared with the NRM "event 1" at the very top of Longmarsh section, however, the intensity value for this "event" is not particularly high.

Below this event there seems no apparent increase in NRM intensity values for both borehole log and Longmarsh section, until a depth lower than 30 m in the borehole. At a depth of around 32-35 m, NRM "event 2", was identified. However, in the Longmarsh section (Fig.6.1.3), there was no significant evidence for an NRM intensity increase at a comparable level. In the lower part of the borehole log, a relatively long event was identified, termed NRM "event 3". The NRM "event 2" in the John Acres Lane section and "event 3" in the borehole may be compared. In both sequences, the stratigraphic interval between the two NRM events is about 20 m. Although an NRM intensity event in the lowest part of the John Acres Lane section could be recognized, there is no counterpart in the borehole log due to a lack of penetration to this level.

Because of the importance of the borehole log, which links the two major sediment units in the upper part of the basin, thermal demagnetisation was carried out as a complement to the a.f. demagnetisation, in order to confirm the polarity determinations, particularly for the upper part of the borehole. The thermal treatment was carried out at a temperature interval of 50°C starting from 100°C and for most samples the magnetisation became too weak for further measurement above about 250°-300°C. Figs.6.1.17 and 6.1.18 give some examples of the results of both thermal and a.f. treatment for samples from the same levels, in which, because of their relatively weak remanent magnetisation, these samples showed noisier signals during thermal demagnetisation than those defined during a.f. demagnetisation.

However, the results agreed each other. Fig.6.1.19 summarizes the CMDs from Borehole SD485. The mean inclination value is Inc =45°, but the declination is not defined, due to the reference line on each drilled core pieces being arbitrary.

6.1.4) Conclusion.

Table 6.1.1 summarizes the demagnetisation results from the three sections of the Bovey Formation. Because of the shallow bedding angle in this area, the fold test was less applicable than for the Cretaceous beds in Southern England. Fig.6.1.20 illustrates the distribution of overall mean CMDs for the two quarry sections before and after bedding correction, in which the overall mean directions after bedding correction are closer to the predicted geomagnetic field direction for the Tertiary (see 6.1.1). Demonstration of the reliability of the remanent magnetisation of these samples is mainly based on the a.f. and thermal demagnetisation tests and the regular appearance of normal and reverse polarities in these sequences.

Table 6.1.1 Summary of characteristic magnetisation directions for the Bovey Formation.

SECTION	CMD before B.C. (normal p.)	CMD before B.C. (reverse p.)	OVERALL MEAN before B.C.	OVERALL MEAN after B.C.
Longmarsh	DEC INC 12° 43° α_{95}=13°,N=17	DEC INC 190°-45° α_{95}=15°,N=15	DEC INC 11° 44° α_{95}=10°,=32	DEC INC 359° 51°
John Acres Lane	DEC INC 14° 51° α_{95}=7°,N=10	DEC INC 194°-50° α_{95}=19°,N=7	DEC INC 14° 50° α_{95}=11°,N=17	DEC INC 359° 58°
	Overall mean for The Bovey Formation DEC INC (before B.C.) 12° 47° α_{95}=6° N=49		Overall mean for The Bovey Formation DEC INC (after B.C.) 359° 54°	

p.= polarity, B.C.=bedding correction.

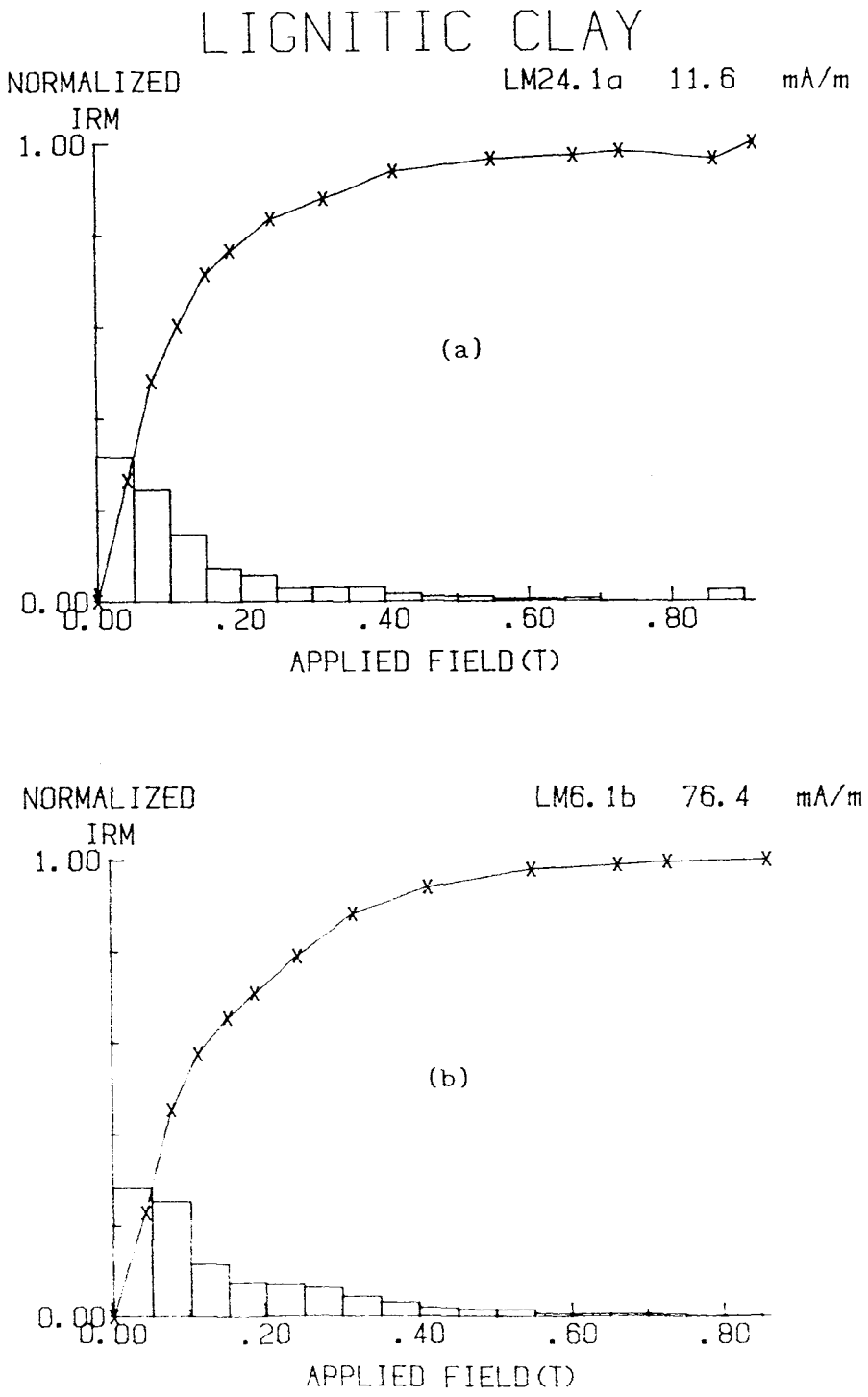

Fig.6.1.1 Examples of IRM acquisition curves for samples from Longmarsh quarry section, Bovey Formation.

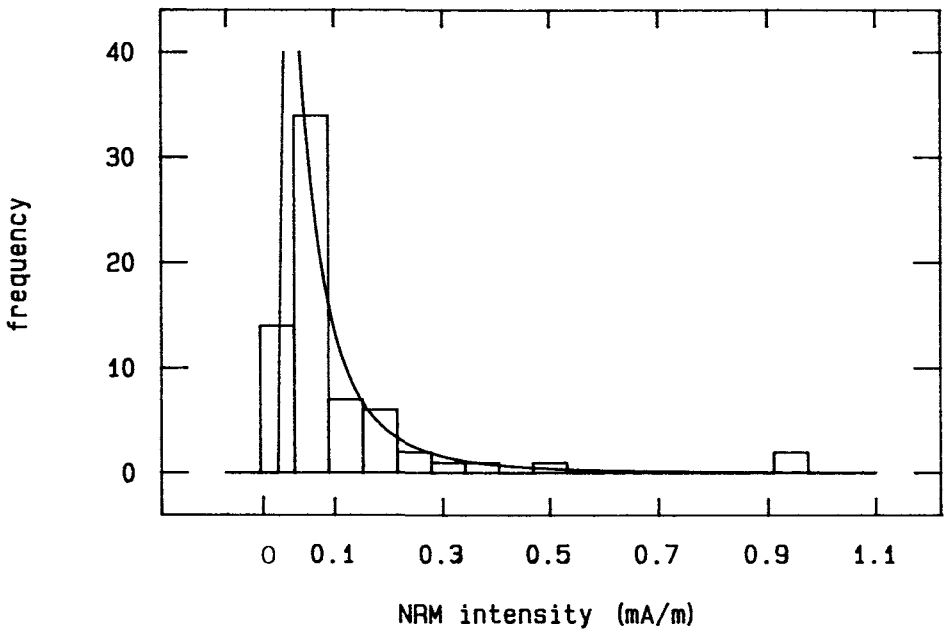

Fig.6.1.2 Statistical distribution of NRM intensity of samples from Longmarsh quarry section, Bovey Formation.

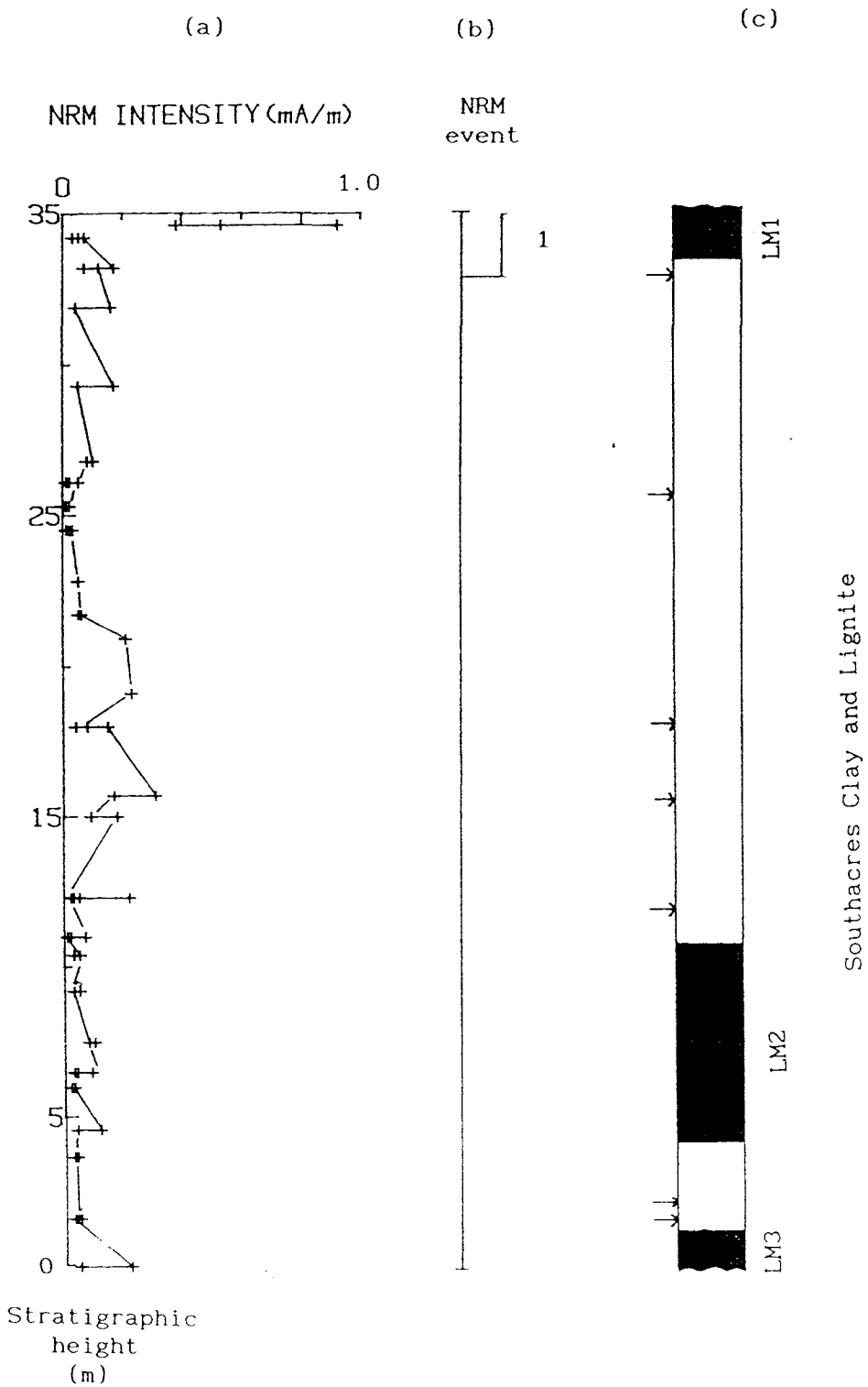

Fig. 6.1.3 (a) Variation of NRM intensity values with stratigraphic height for samples from the Longmarsh section. (b) Recognizable NRM intensity increase event with stratigraphic height. (c) Magnetic polarity sequence. Symbols and conventions as in Fig. 4.1.3.

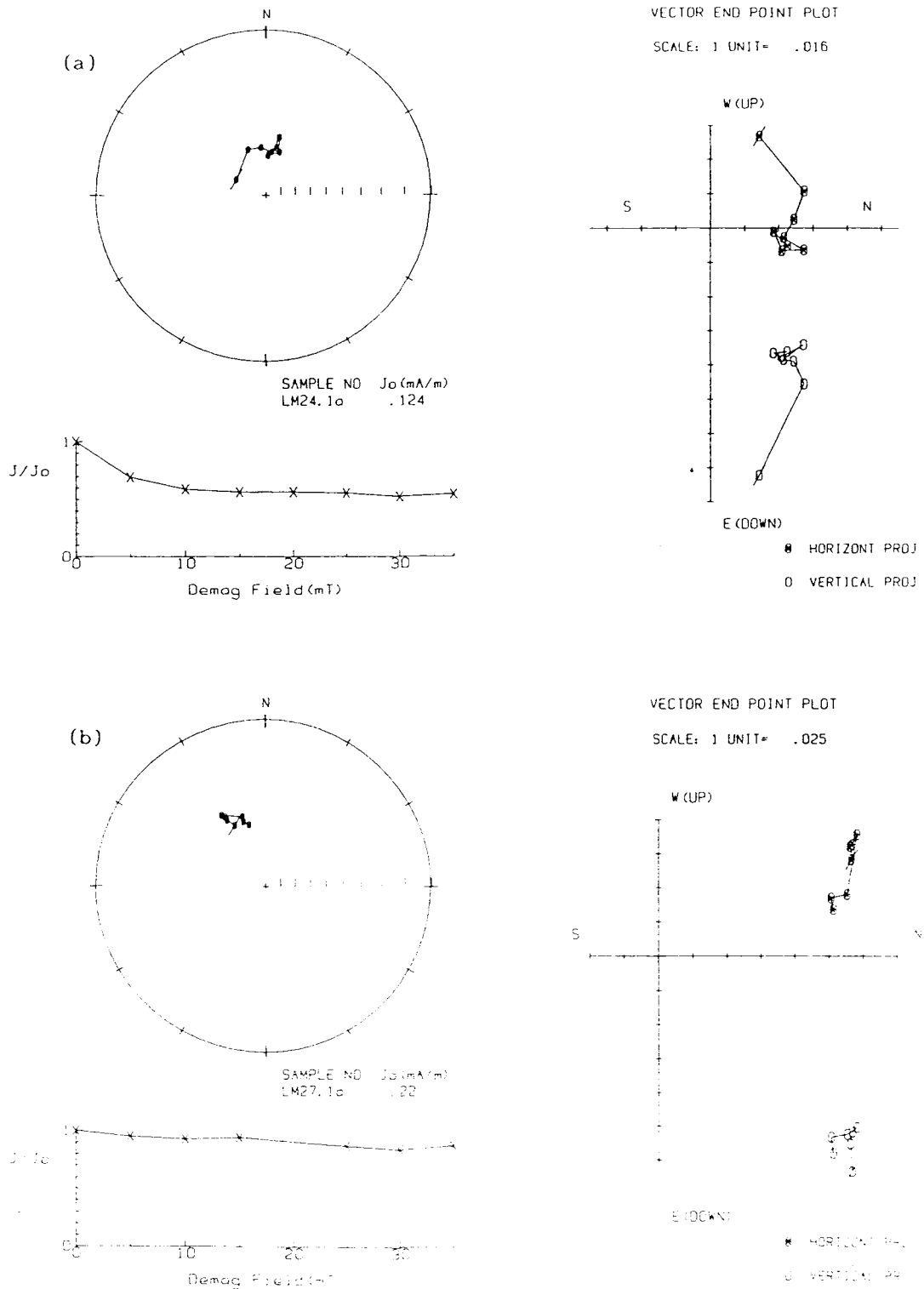

Fig.6.1.4 Examples of a.f. demagnetisation results for samples from the Longmarsh section, Bovey Formation. Symbols and conventions as in Fig.4.4.4.

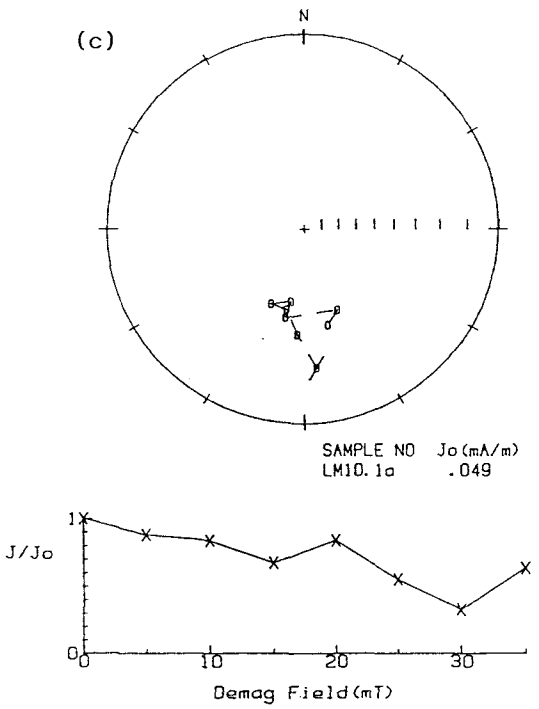
(c)
N
SAMPLE NO Jo(mA/m)
LM10.1a .049
J/Jo
1
0
0
10
20
30
Demag Field(mT)

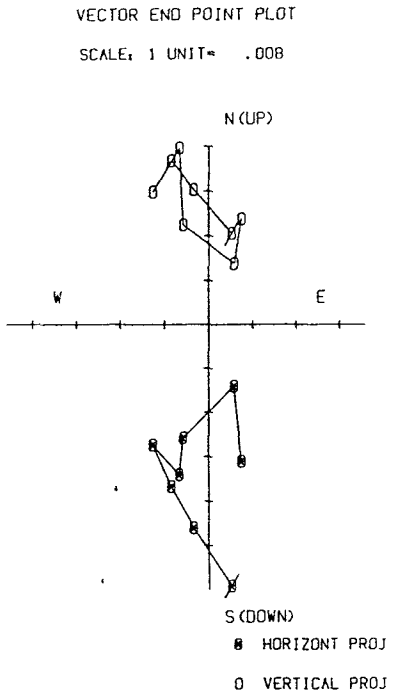
VECTOR END POINT PLOT
SCALE: 1 UNIT= .008
N(UP)
W
E
S(DOWN)
HORIZONT PROJ
VERTICAL PROJ

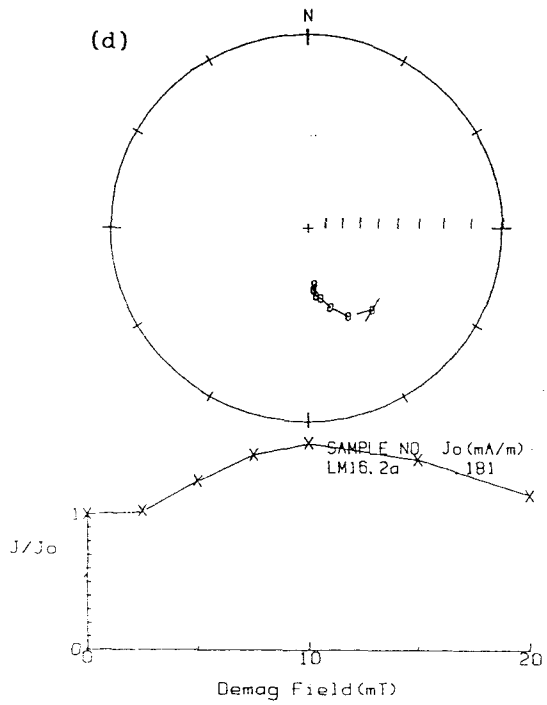
(d)
N
SAMPLE NO Jo(mA/m)
LM16.2a .181
J/Jo
1
0
0
10
20
Demag Field(mT)

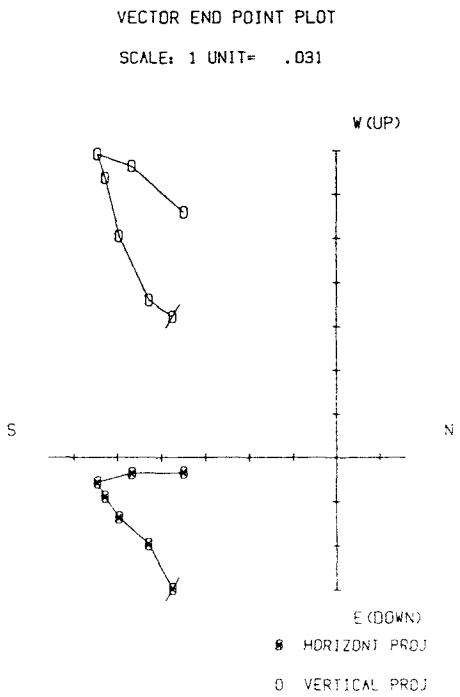
VECTOR END POINT PLOT
SCALE: 1 UNIT= .031
W(UP)
S
N
E(DOWN)
HORIZONT PROJ
VERTICAL PROJ

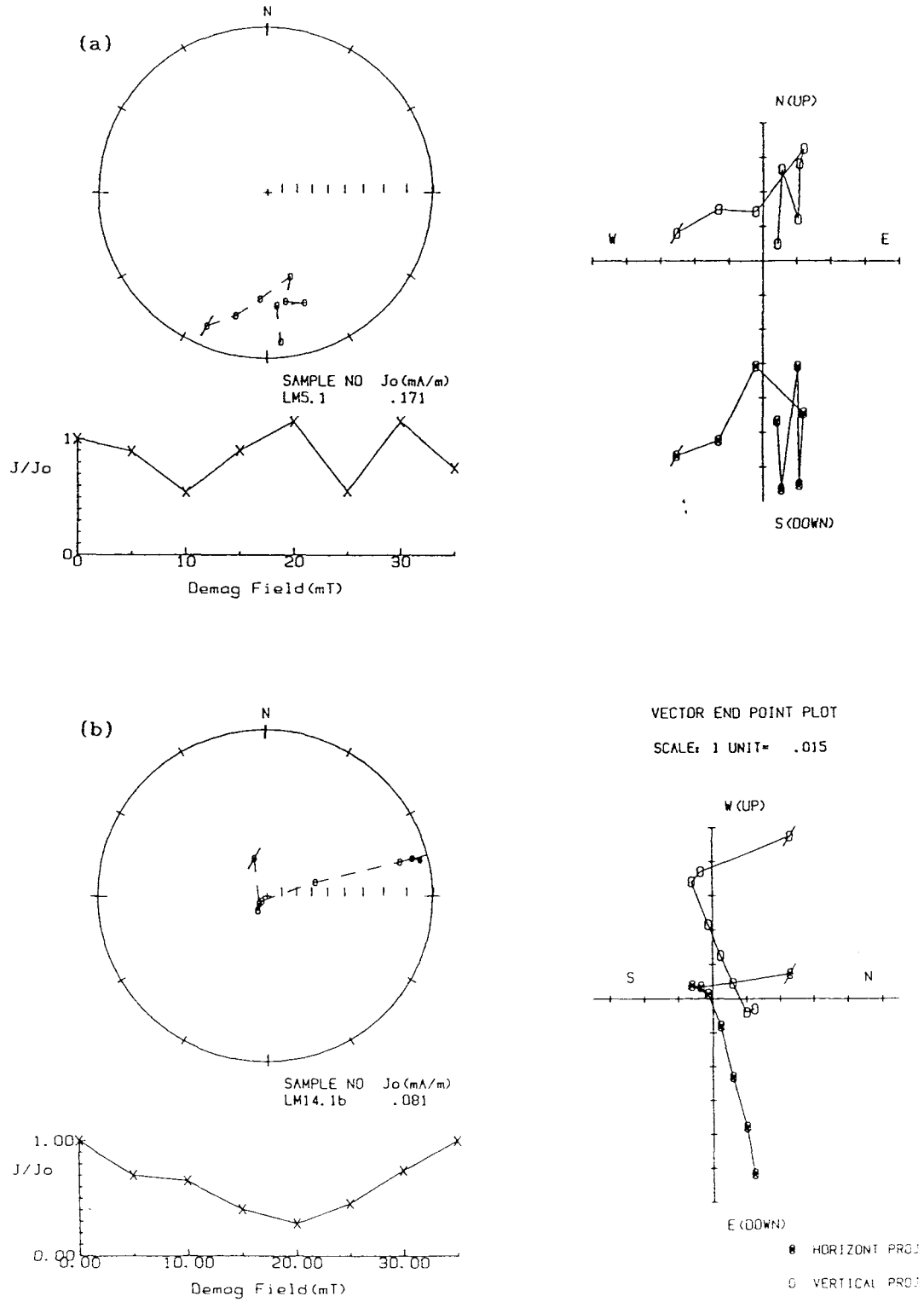

Fig.6.1.5 Examples of samples from the Longmarsh section with changeable magnetic vectors at higher demagnetisation levels. Both of them are regarded as having reverse polarity character. Symbols and conventions as in Fig.4.1.4.

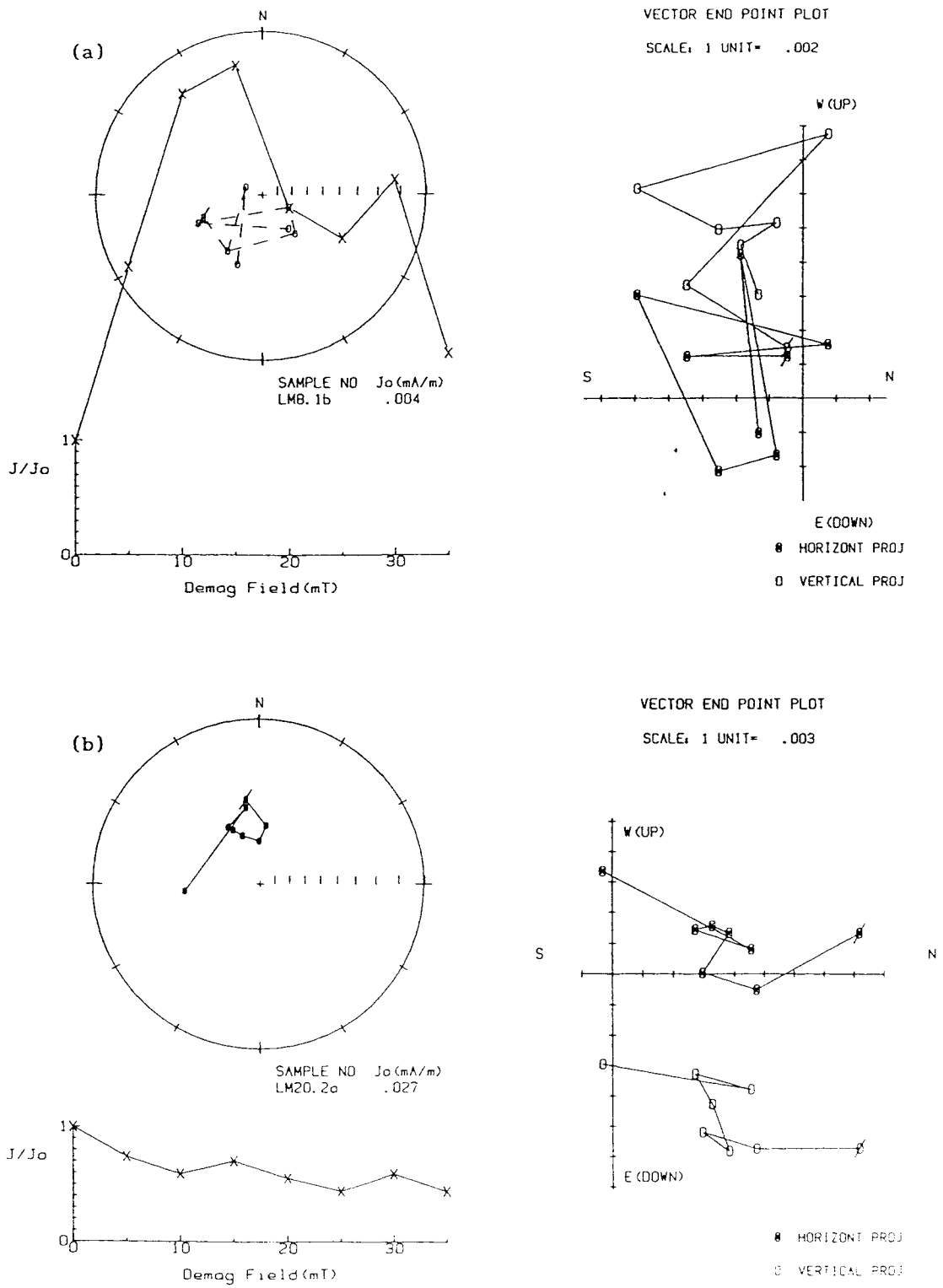

Fig.6.1.6 Examples of samples from the Longmarsh section with extremely low magnetic intensity values but which still yield relatively well-defined polarity determinations for reverse and normal polarities respectively. Symbols and conventions as in Fig.4.1.4.

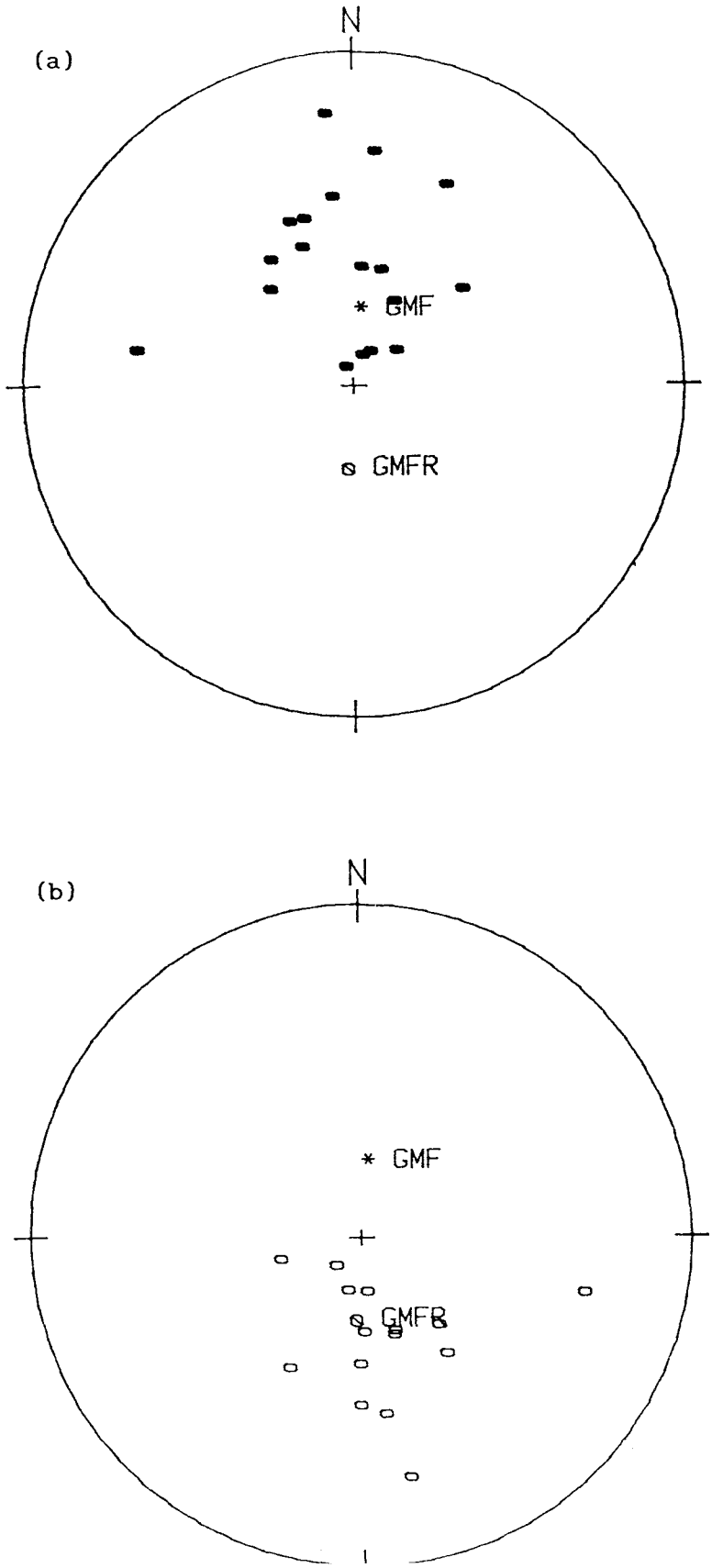

Fig. 6.1.7 Summarized CMDs of samples from the Longmarsh section for both (a) normal and (b) reverse polarity. Symbols and conventions as in Fig. 4.1.11.

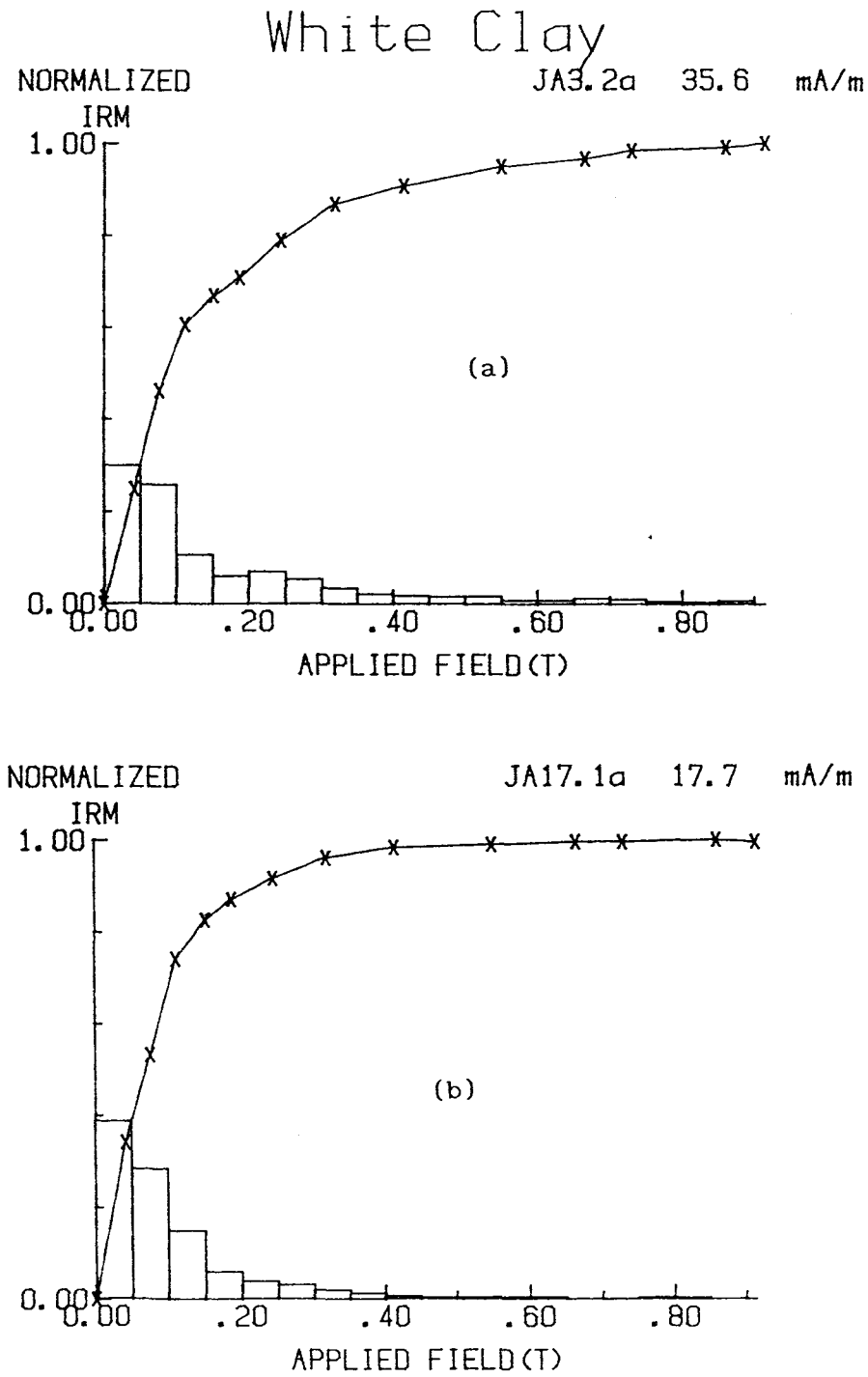

Fig.6.1.8 Examples of IRM acquisition curves for samples from the John Acres Lane section, Bovey Formation.

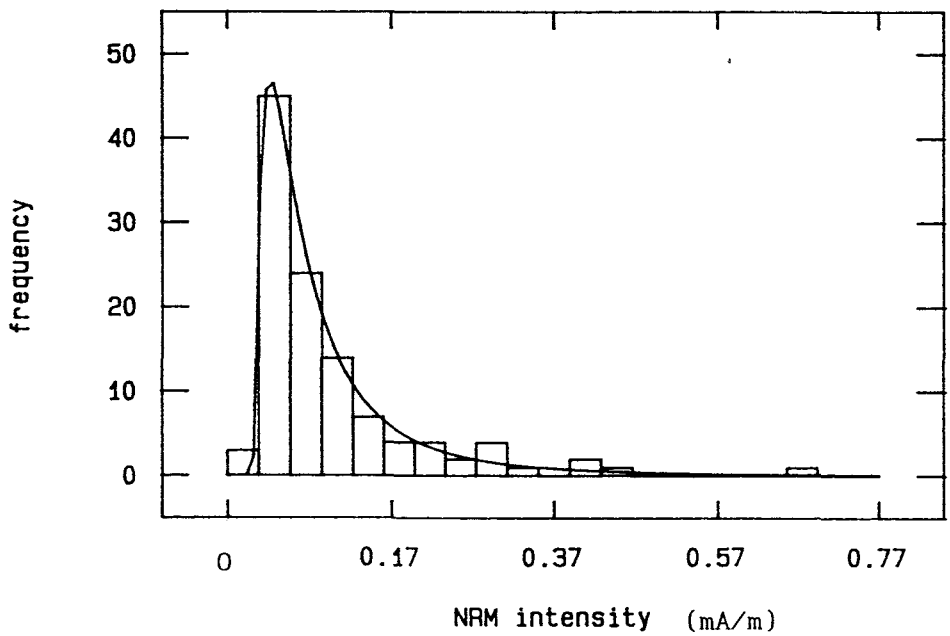

Fig.6.1.9 Statistical distribution of NRM intensity values of samples from the John Acres Lane section, Bovey Formation.

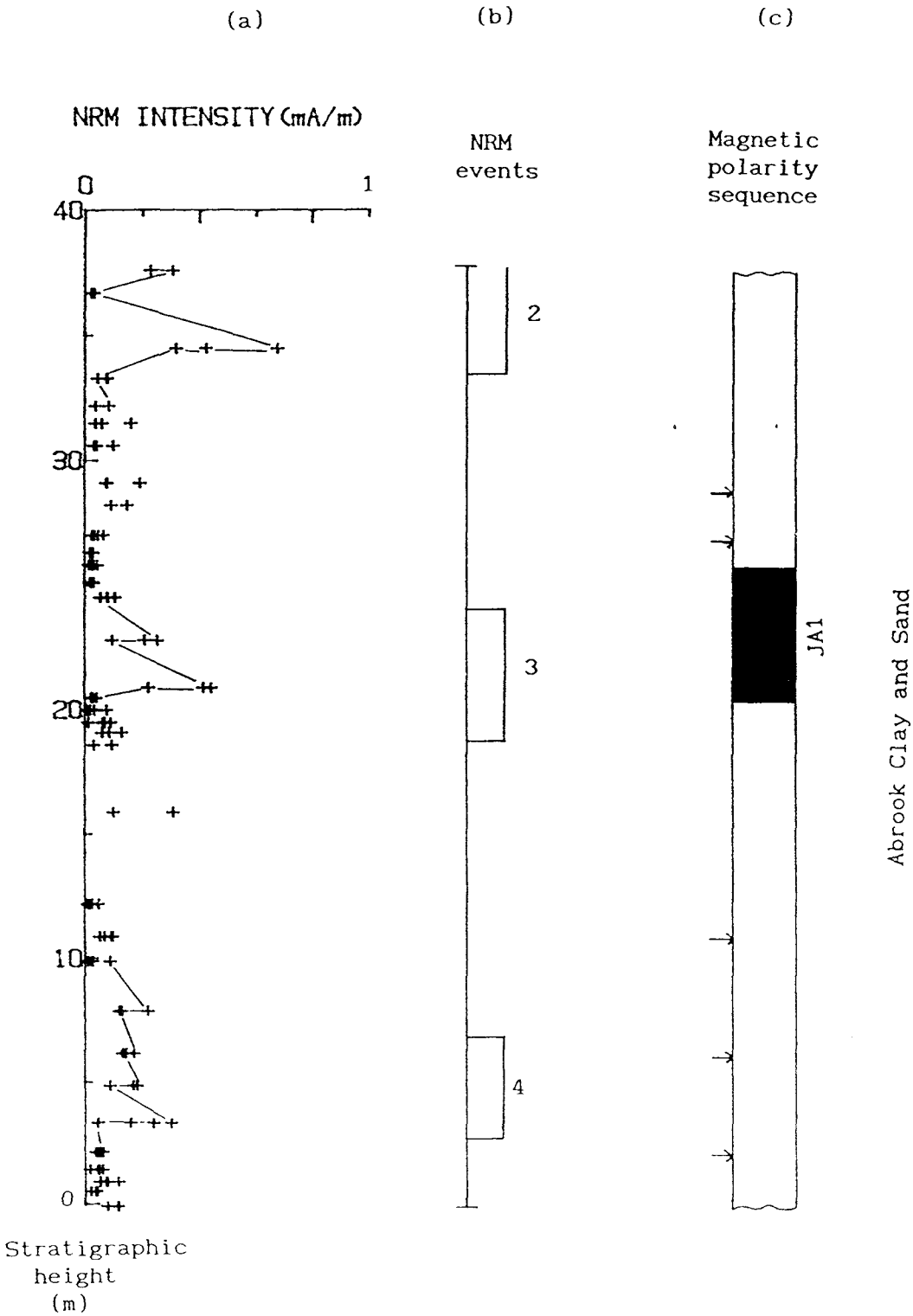

Fig. 6.1.10 (a) Variation of NRM intensity values with stratigraphic height for John Acres Lane section, (b) recognizable NRM intensity "events", (c) magnetic polarity sequence. Symbols and conventions as in Fig. 4.1.3.

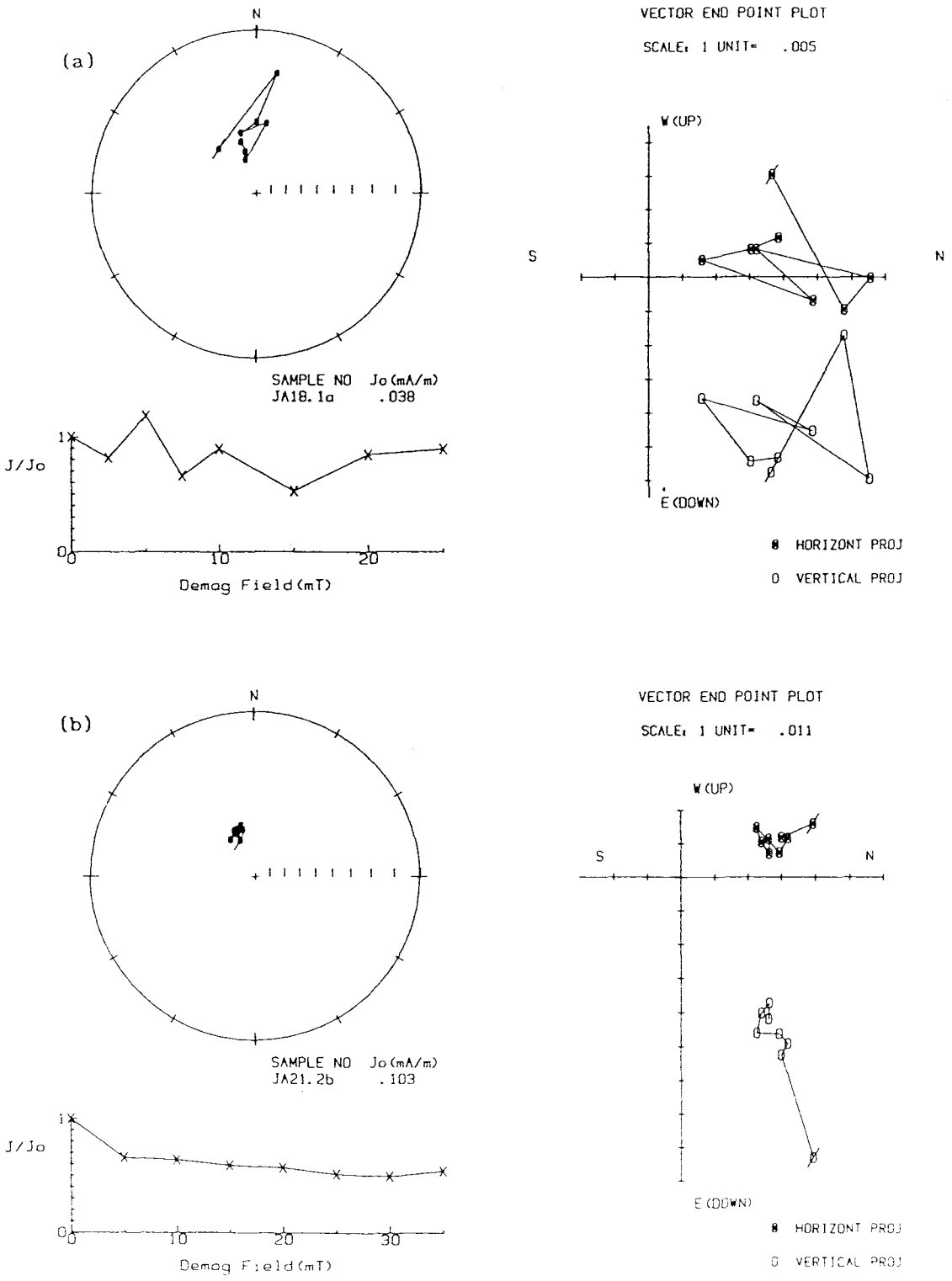

Fig.6.1.11 Examples of a.f. demagnetisation of samples from John Acres Lane section, Bovey Formation. Symbols and conventions as in Fig.4.1.4.

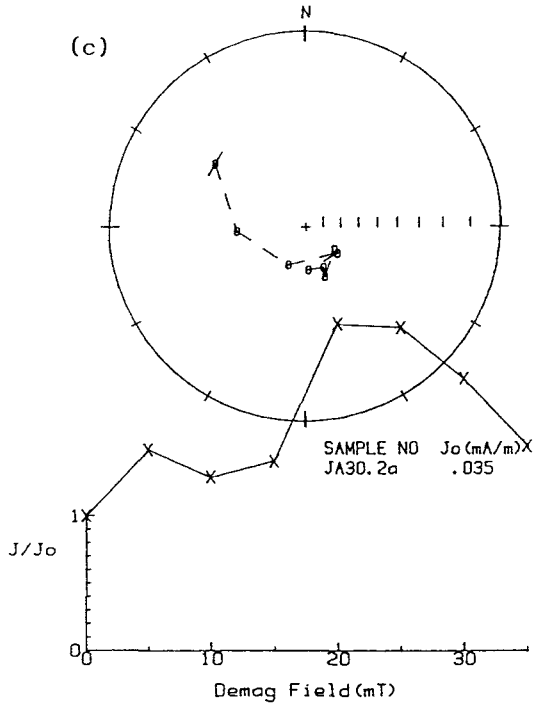
(c)
N
SAMPLE NO Jo(mA/m)
JA30.2a .035
J/Jo
1
0
0
10
20
30
Demag Field(mT)

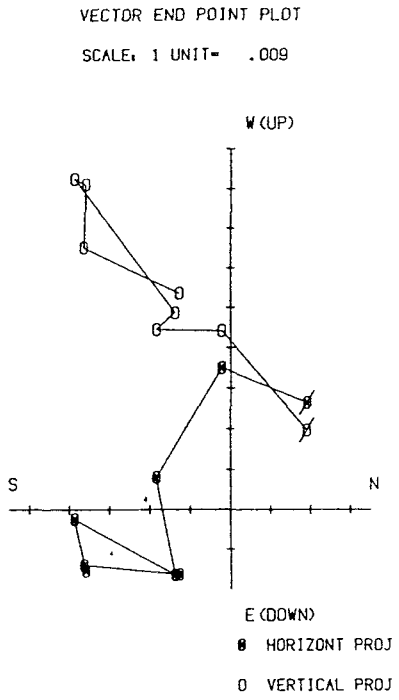
VECTOR END POINT PLOT
SCALE: 1 UNIT= .009
W(UP)
S
N
E(DOWN)
HORIZONT PROJ
VERTICAL PROJ

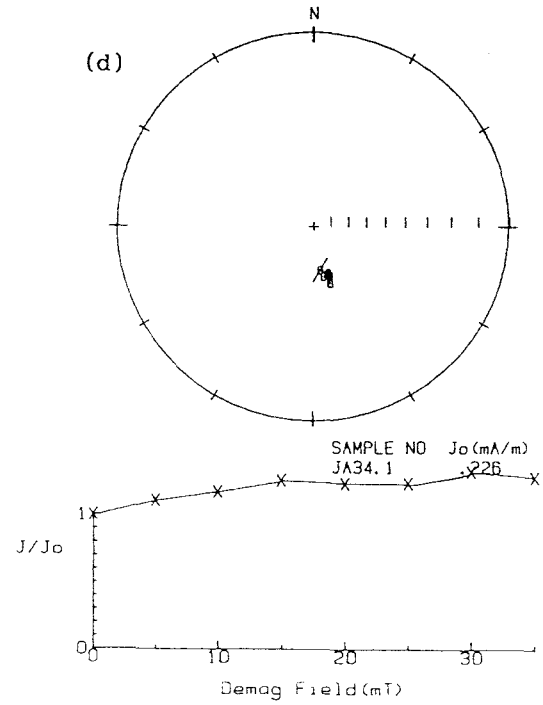
(d)
N
SAMPLE NO Jo(mA/m)
JA34.1 .226
J/Jo
1
0
0
10
20
30
Demag Field(mT)

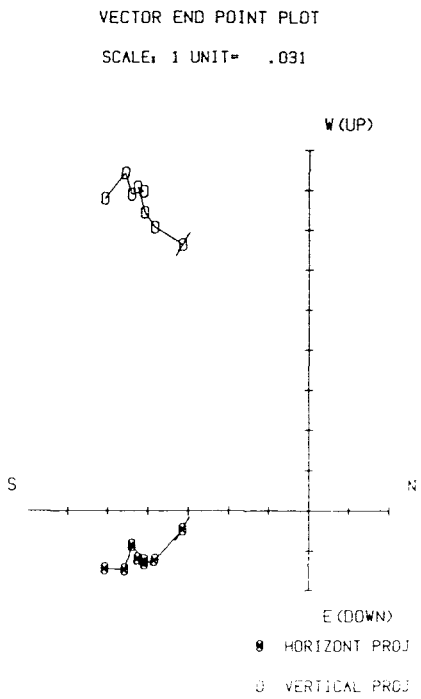
VECTOR END POINT PLOT
SCALE: 1 UNIT= .031
W(UP)
S
N
E(DOWN)
HORIZONT PROJ
VERTICAL PROJ

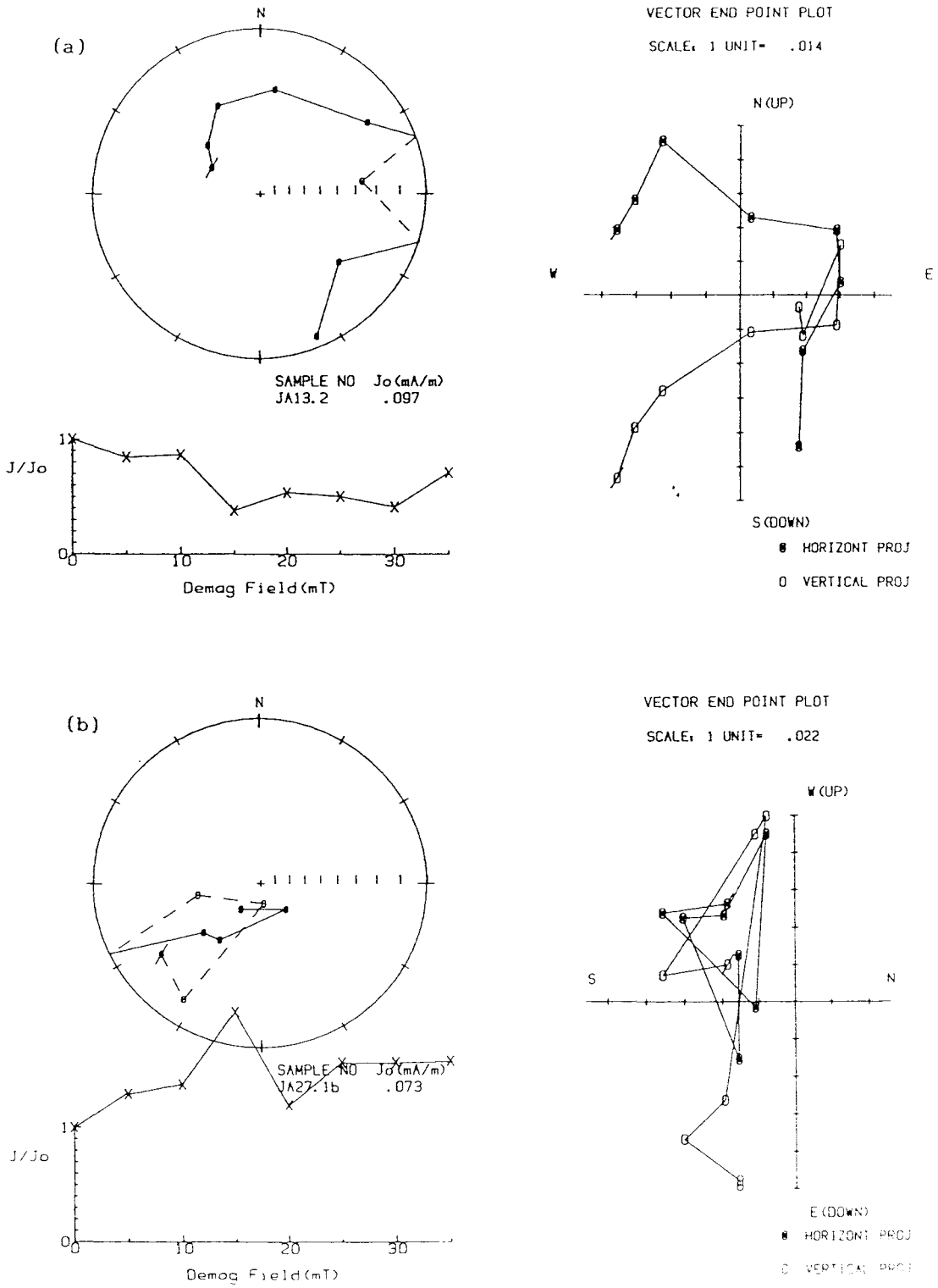

Fig. 6.1.12 Examples of samples from John Acres Lane section exhibiting "noisy" demagnetisation behaviour, and no clearly defined magnetic polarity. Symbols and conventions as in Fig. 4.1.4.

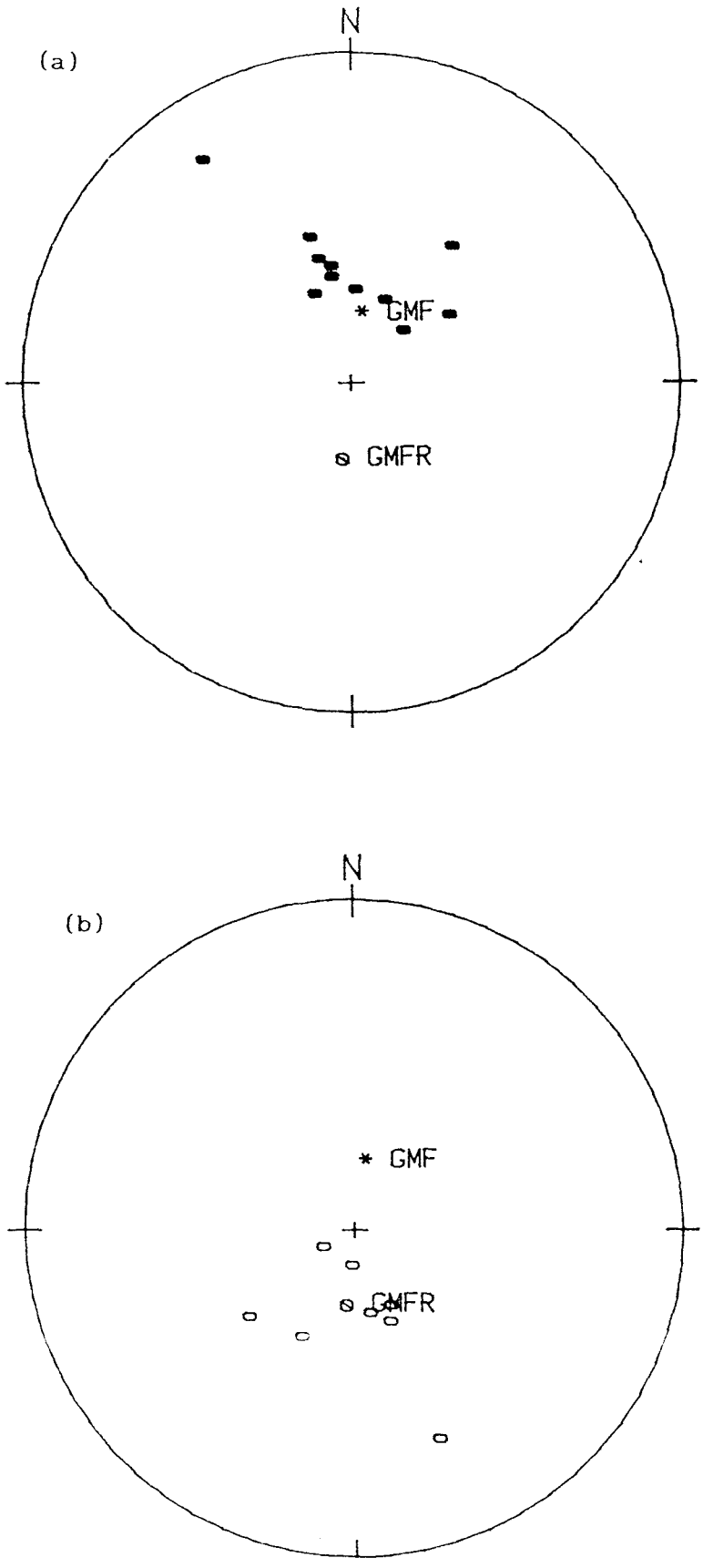

Fig.6.1.13 Summarized CMDs for samples from John Acres Lane quarry section, (a) normal polarity (b) reverse polarity. Symbols and conventions as in Fig.4.1.11.

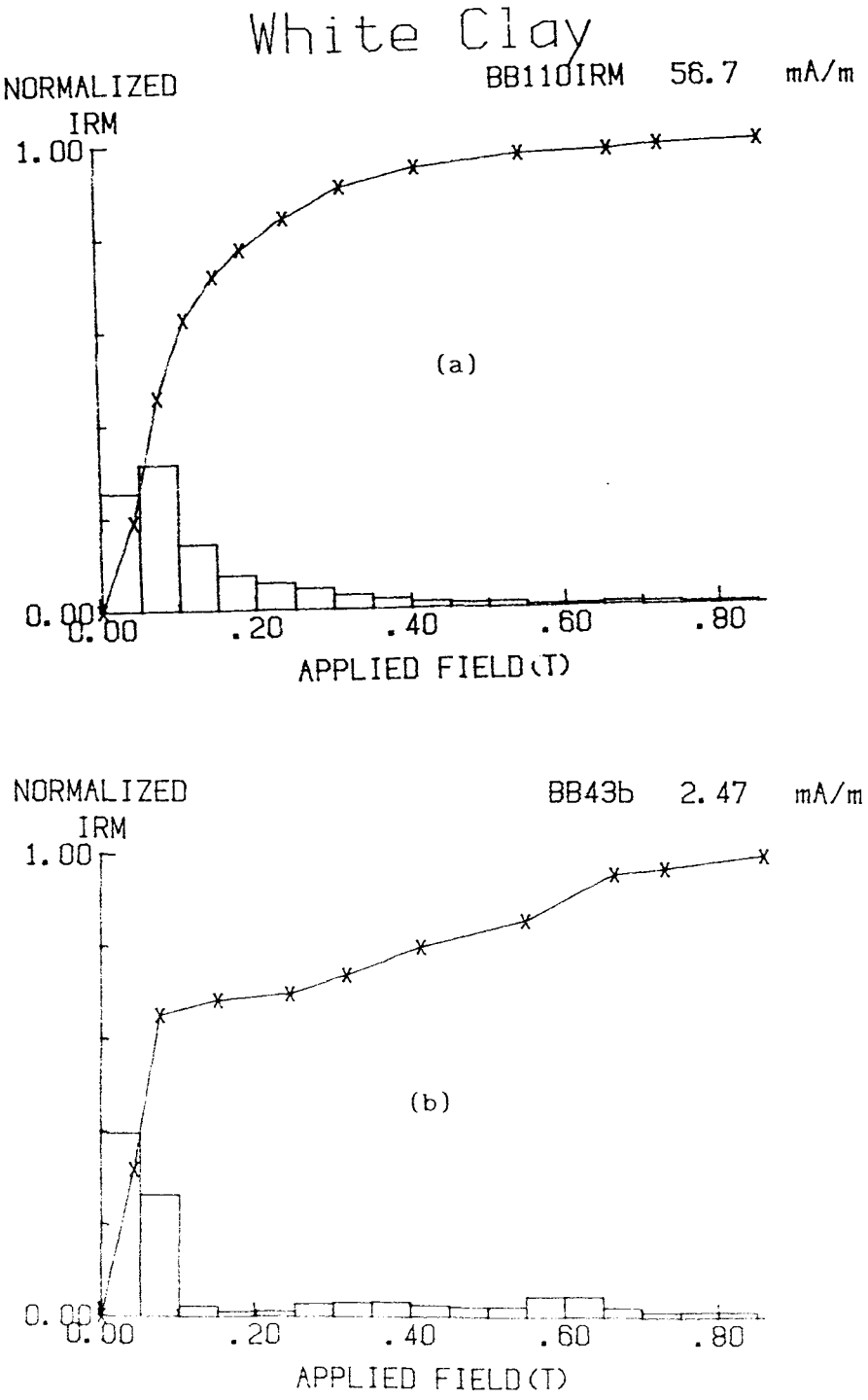

Fig.6.1.14 Examples of IRM acquisition curves for samples from Borehole SD485, Bovey Formation.

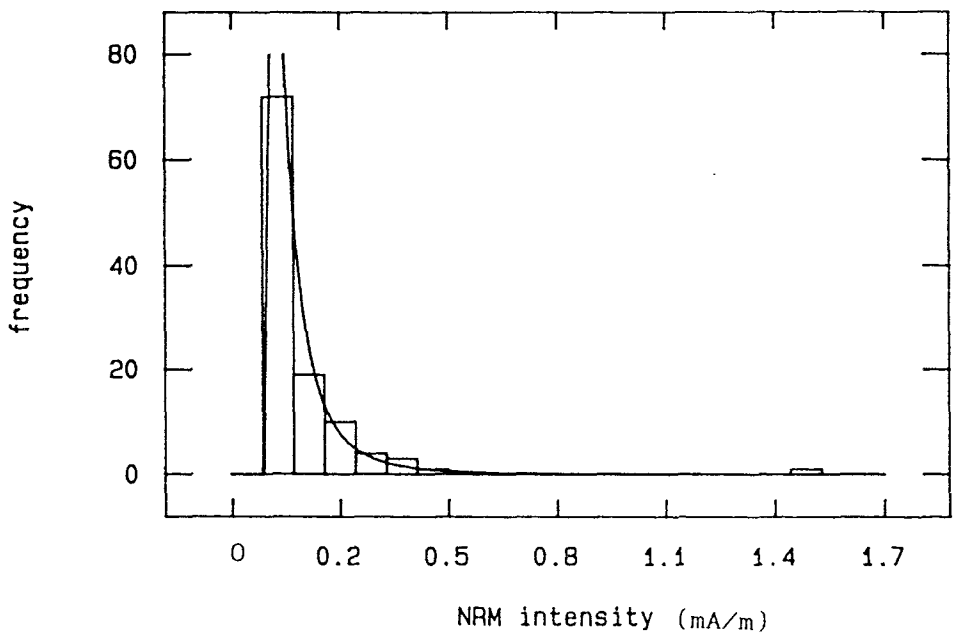

Fig. 6.1.15 Statistical distribution of NRM intensity values for samples from Borehole SD485, Bovey Formation.

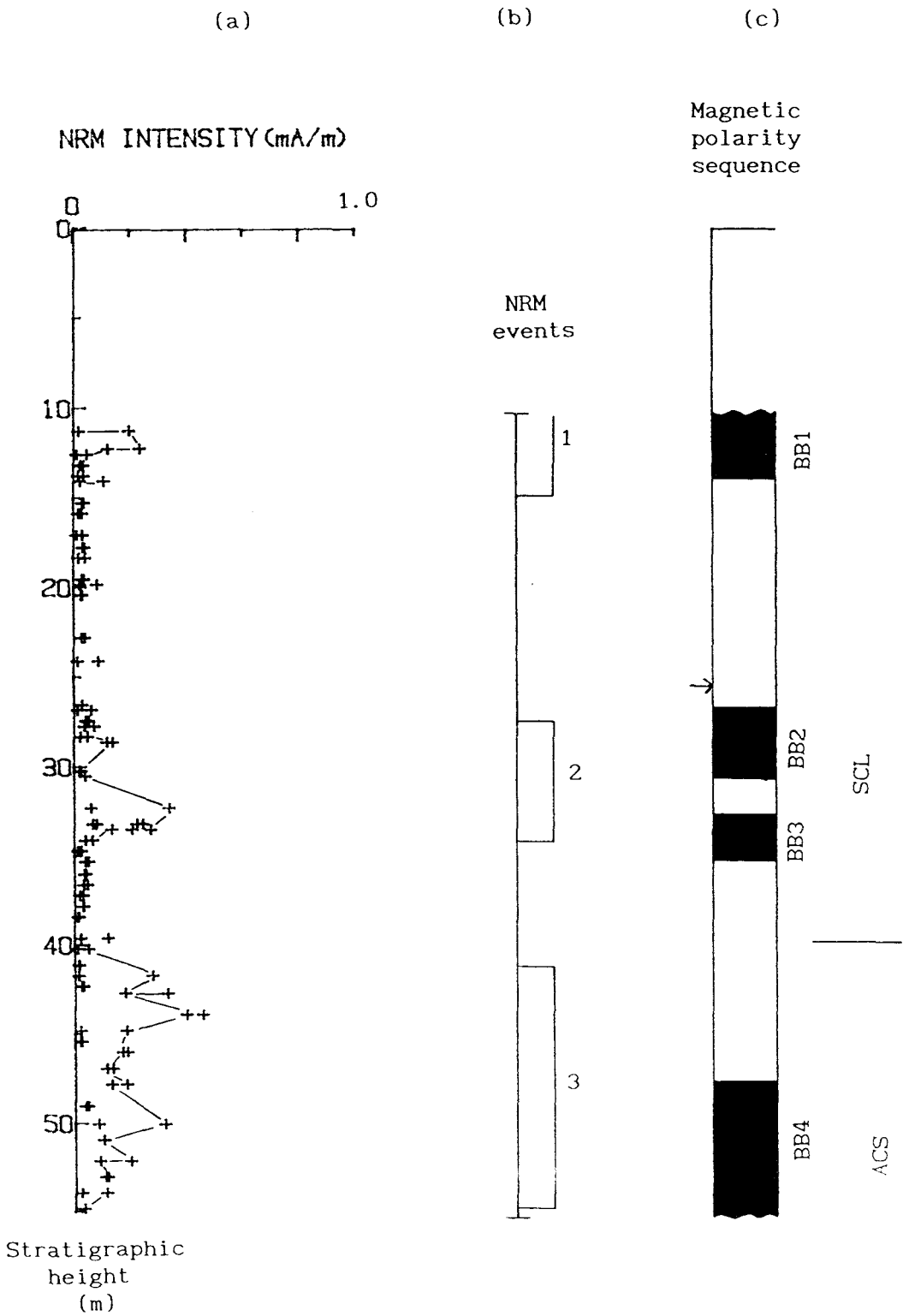

Fig.6.1.16 (a) Variation of NRM intensity values with depth for samples from Borehole SD485, Bovey Formation. (b) recognizable NRM intensity "events" in the borehole section. (c) magnetic polarity sequence. Symbols and conventions as in Fig.4.1.4.

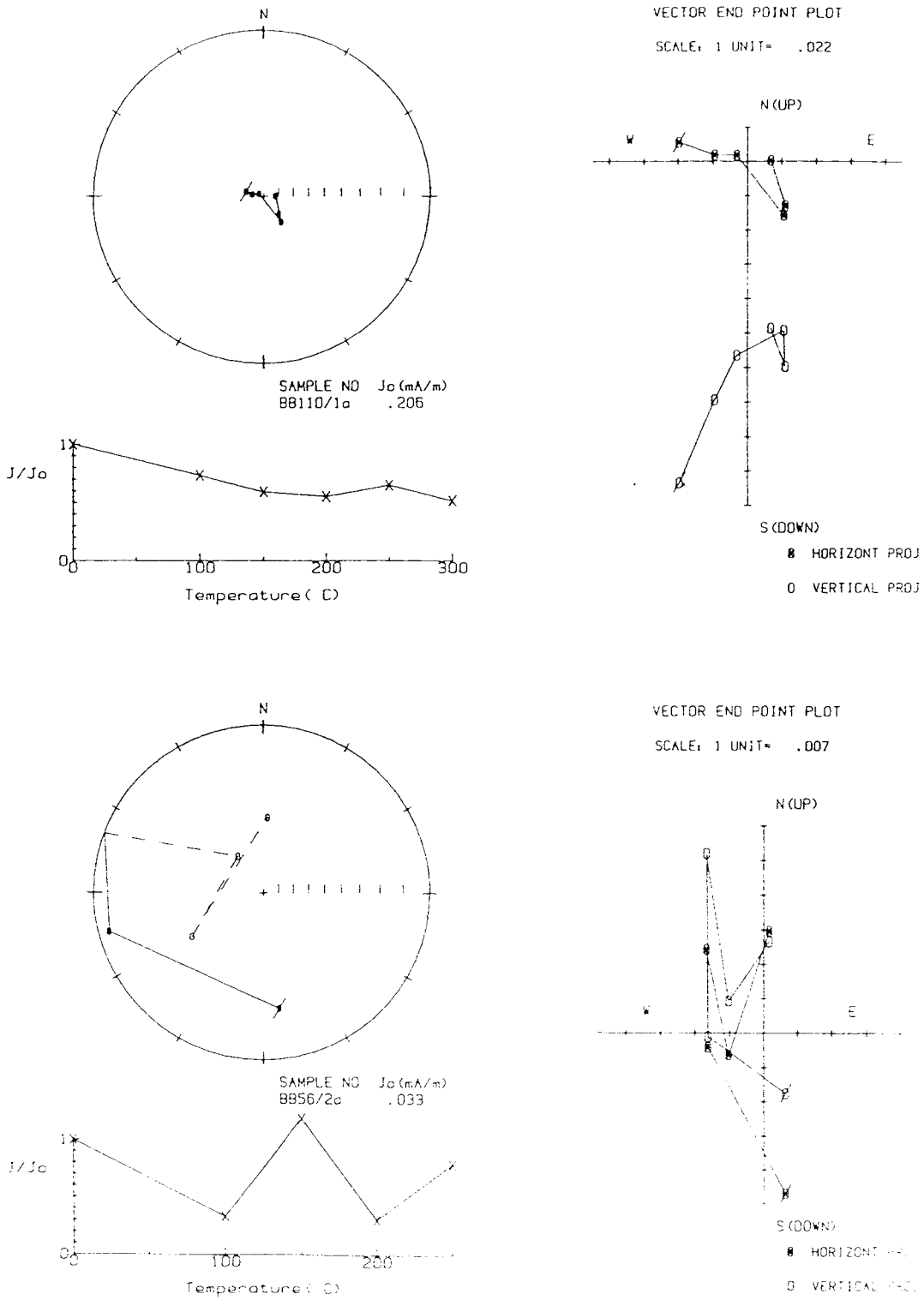

Fig. 6.1.17 Examples of thermal demagnetisation for samples from Borehole SD485, Bovey Formation. (a) a sample with normal polarity and (b) probable reverse polarity. Symbols and conventions as in Fig. 4.1.4.

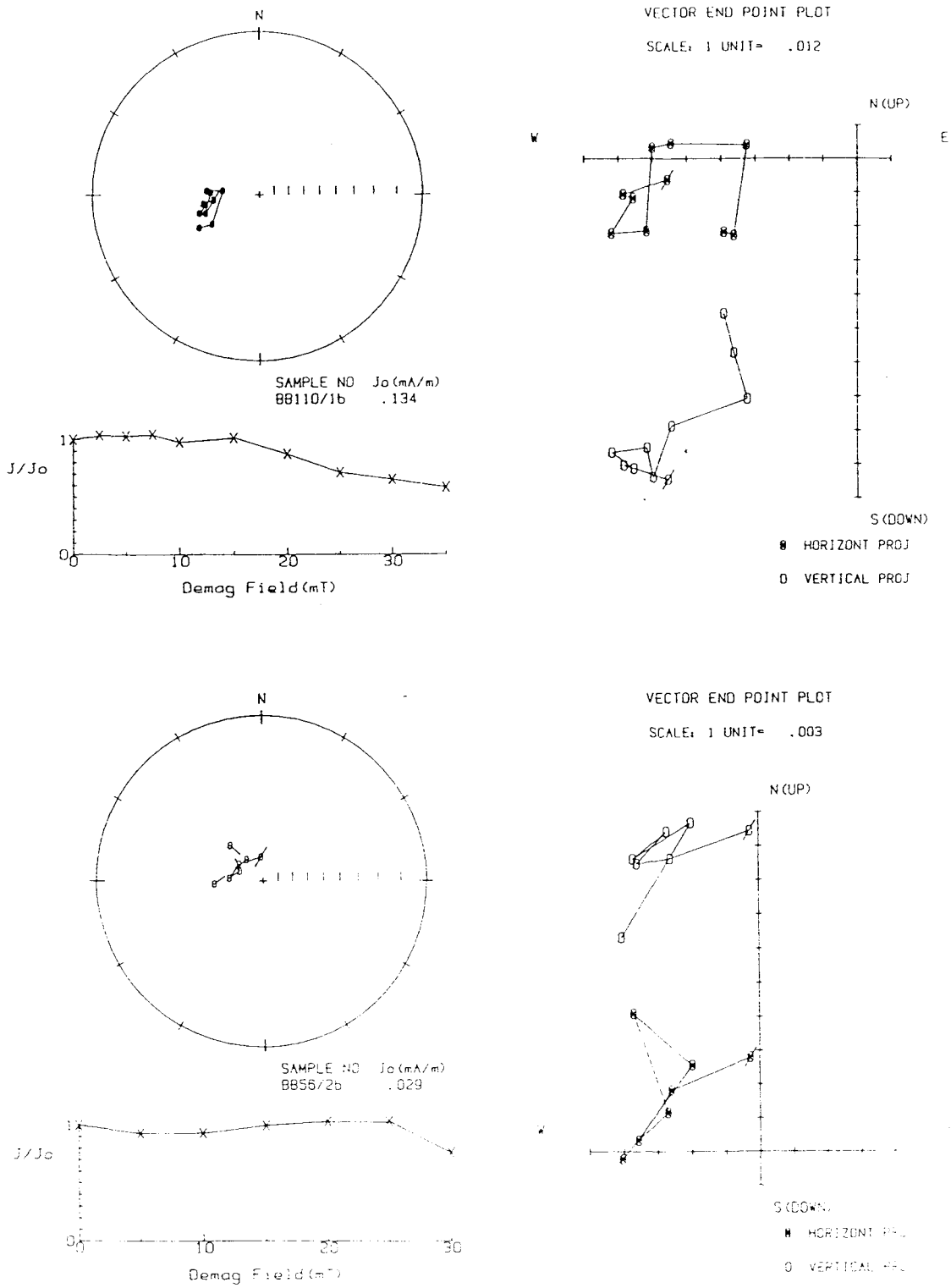

Fig.6.1.18 Examples of a.f. demagnetisation results for samples from the same sites as Fig.6.1.17, Borehole SD485, Bovey Formation. (a) normal and (b) reverse polarity. Symbols and conventions as in Fig.4.1.4.

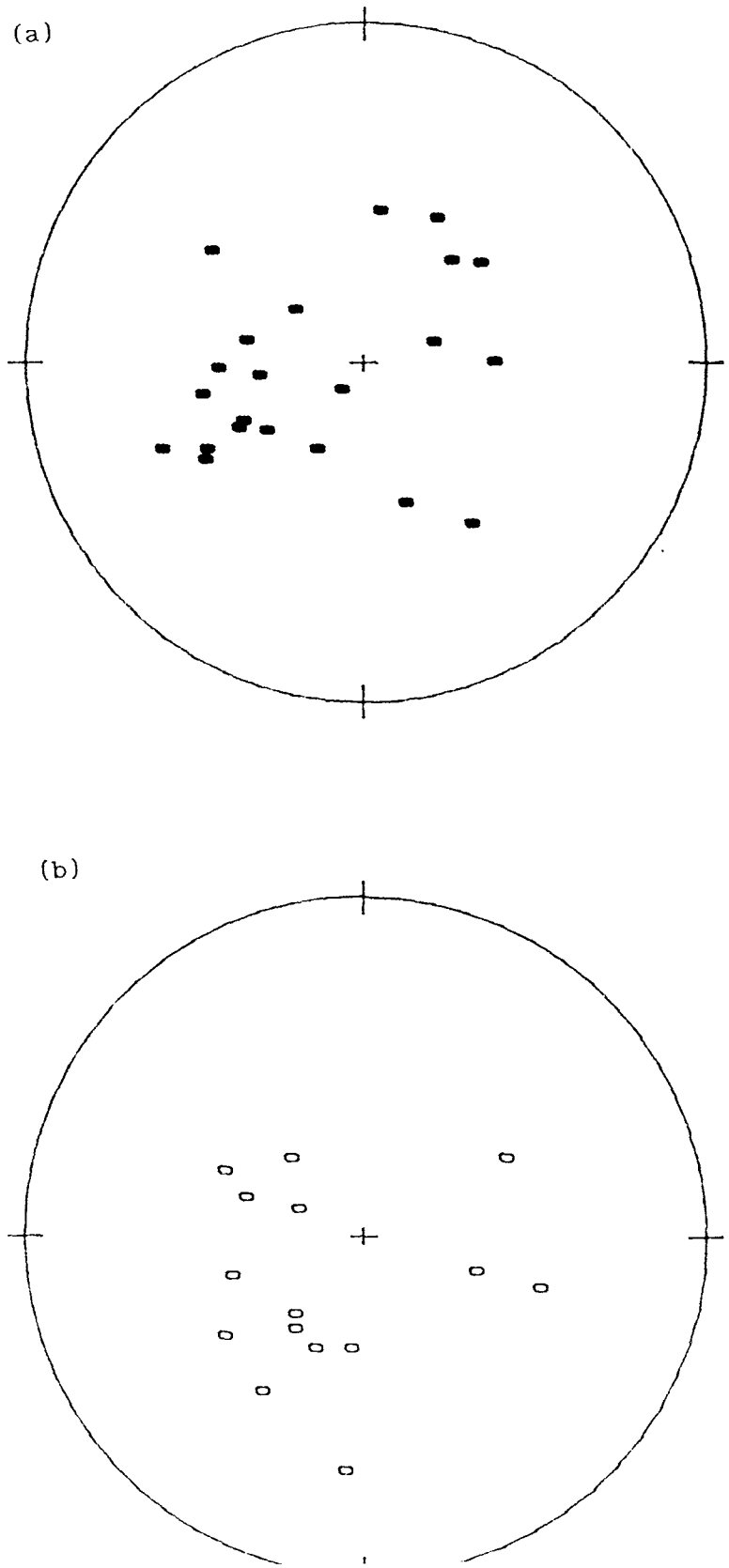

Fig.6.1.19 Summarized CMDs for samples from Borehole SD485, Bovey Formation, in which their declinations are not specified. (a) normal polarity vectors and (b) reverse polarity. Symbols and conventions as in Fig.4.1.11.

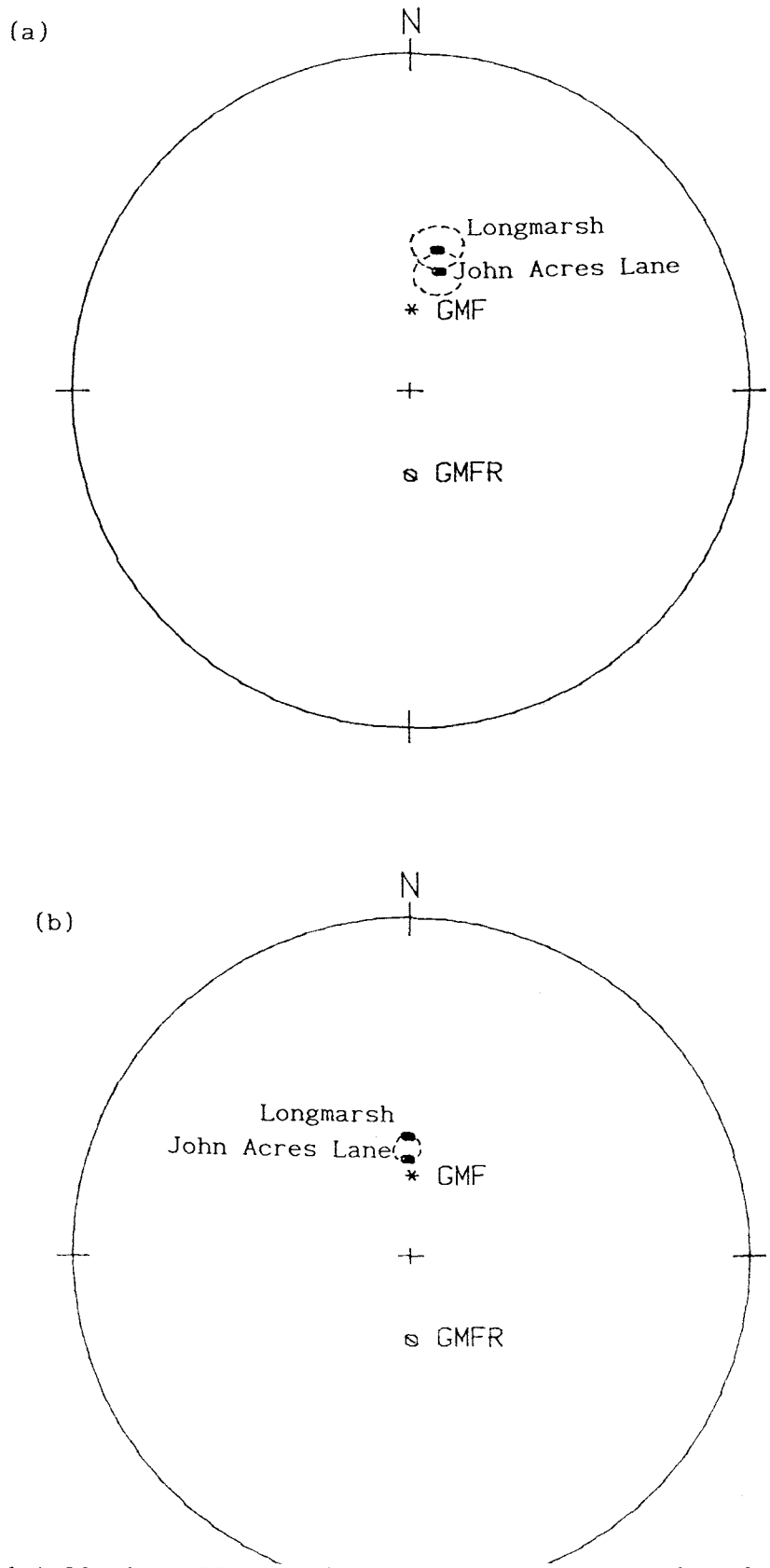

Fig. 6.1.20 Overall mean directions from Longmarsh and John Acres Lane quarry sections, Bovey Formation. (a) Before bedding correction and (b) after bedding correction. Symbols and conventions as in Fig. 4.1.11.

§6.2 Magnetostratigraphy of the Bovey Formation section and their correlations

6.2.1) Longmarsh quarry section.

Fig.6.1.3c shows the magnetic polarity sequence yielded from the Longmarsh section. From its top, just below the orange sand, is a short interval of normal polarity about half a meter thick, which is well-defined by the CMDs from 4 samples. This normal polarity zone is termed LM1. (Note: the Early Oligocene period is dominated by reverse polarity intervals, so the nomenclature refers to the shorter normal polarity intervals). This section is then followed downwards by a long reverse polarity interval about 23 m in stratigraphic height, defined by 17 sampling sites. Although most samples show well-defined reverse polarity magnetisation, based either on CMDs or directional trends, about 16% of the samples in this interval exhibit normal polarity behaviour during a.f. demagnetisations, which is thought to be the affect of a magnetic overprint (Appendix 7).

Below this reverse interval is a normal polarity zone, at least 8m thick, and extending to the bottom of the section. It contains a possible short 2m reverse interval in its lower part. The upper part of this normal interval (termed magnetozone LM2) is defined by 6 sampling sites and two thirds of the samples within it exhibit CMDs with normal polarity characters. The underlying 2 m reverse polarity interval is defined from two sampling sites. Although 6 specimens in this interval were subjected to a.f. demagnetisation, only two of these exhibited reliable polarity determinations. The lowest sampling site exhibited a well-defined normal polarity CMD (defining magnetozone LM3). Therefore, the short reversed event between LM2 and LM3 is questionable and its existence can only be proved by magnetostratigraphic correlation with other section.

6.2.2) Borehole SD485.

This borehole is believed to extend through the Southacre Clay and Lignite (SCL) into the upper part of the Abbrook Clay and Sand (ACS) unit (see Fig.5.2.9). Fig.6.1.16c presents the magnetic polarity

sequence defined for this borehole. The sequence is marked, from a depth of 11.2 m beneath the ground surface, by a relatively well-defined normal polarity interval at its top, with a thickness of about 2 m, defined by 5 sampling levels. This interval is termed magnetozone BB1 (see Appendix 9). Downwards it is followed by a long reverse polarity interval with a thickness about 13 m, defined by 12 sampling levels. Polarity determination for most samples in this interval are based on directional trends, only one quarter of the samples having well defined CMDs. This reflects the effects of the partial magnetic overprints.

The underlying 9 m interval is dominated by normal polarity but with a 2 m reverse polarity interval in its middle, defined by three sampling sites, in which most samples had well defined reverse polarity and distinguishable from the surrounding normal polarity intervals. The normal polarity intervals are well-defined and less affected by magnetic overprints, particularly the lower one. These two normal polarity intervals are termed BB2 and BB3, respectively.

Beneath magnetozone BB3 the Abbrook Clay and Lignite unit is reached, at a depth of about 40 m. This lies within a long reverse interval, some 13 m in stratigraphic thickness. The downwards transition from lignitical clays to white-grey clays, corresponds with an improvement in the quality of the palaeomagnetic data, some 50% of the samples from the Abbrook Clay and Sand unit showing clear CMDs and the other half quite well defined directional trends.

The lowest normal polarity interval, BB4, has a thickness of about 6m and extends to the bottom of the borehole. It is defined by 6 sampling sites. It seems to carry a more extensive magnetic overprint than magnetozones, BB2 and BB3, one third of the samples showing erratic trends of possible reverse polarity character. However, the overall patterns of these interval are indication of a dominant normal polarity (see Appendix 9).

6.2.3) John Acres Lane quarry.

This section is about 500 m northeast of the locality of borehole

SD485. It is dominated by a long reversed polarity interval, but with a well-defined normal polarity interval in its middle part. The upper reverse interval has a thickness 12 m (Fig.6.1.10c). A set of samples at the top of the section show well-defined CMDs, but due to the weak magnetisation, the remaining 63% of this reversed interval is defined mainly from directional trends towards reverse polarity. About 20% of the samples in it did not yield any meaningful polarity information.

The normal polarity interval, termed JA1, has a thickness of 5.5m. 55% of the samples in this interval show clear CMDs, only 2 samples yielding meaningless information. The boundaries of this normal polarity interval are quite clearly defined.

Below magnetozone JA1 is a long reverse sequence, which extends for about 20 m to the base of the section. 17 sampling sites define this interval; however, only 10% of the samples show clear reverse polarity CMDs. Most samples show demagnetisation directional trends towards reverse polarity. At the suspect "sand waste" layer only one sampling site was occupied and the demagnetisation results show that 2 independently oriented samples in it have well-defined directional trends to reverse polarity, indicating that the supposed "waste" might in fact be an *in-site* sand layer. In spite of the dominant reversed polarity in this part of section, about 19% of the samples mainly in the middle of this interval, appear to carry a normal polarity magnetisation, some of them having well-defined CMDs, believed to represent strong magnetic overprints.

6.2.4 Magnetostratigraphic correlations for the Bovey Formation.

A combination of geological and magnetic information makes it relatively easy to correlate the three sections studied. However, because of lack of biostratigraphic information and significant lithological markers (such as the Coarse Quartz Grit (CQG) layers within the Wessex Formation), the comparison here is based mainly on general geological and geometrical information, together with the magnetic stratigraphy.

Fig.6.2.1 summarizes the correlation, in which the Borehole SD485

is the linking section between the Longmarsh and John Acres Lane quarries. Both the Longmarsh quarry section and the borehole section start from just below the orange sand layer. On this basis the upper normal polarity intervals, LM1 and BB1, in the two sequences can be correlated. The length of the underlying reverse polarity interval differs between the two sections, with the Longmarsh reversed interval being some 10m longer than that in the borehole sequence. This may possibly reflect variation of depositional rate in this area.

An interesting comparison can be made between the lower part of the Longmarsh quarry section and the middle part of the borehole section, where both sequences include normal polarity intervals (LM2, LM3 and BB2, BB3) with short reversed intervals in their middles. However, the normal interval LM2 is about 2m longer than interval BB2. Because of the incomplete normal zone at the base of the Longmarsh section, the length of this zone cannot be compared with its counterpart BB3 which is about 2 m long. In general, the sedimentation rate in the Longmarsh seems to have been significantly greater than that in the borehole section.

The lower part of the borehole, which is believed to represent the Abbrook Clay and Sand (ACS) unit, can be compared with the John Acres Lane section. The absence of signs of normal polarity at the very top of the John Acres Lane section indicates that it lies some distance below the top of the ACS, which is defined in a reverse polarity interval in the borehole. The very bottom of the borehole is believed to lie in the middle part of the John Acres Lane section (Chapter V). Therefore, the magnetic polarity pattern can be compared in these two sections. The lowest normal polarity interval BB4, which probably is not complete, can be correlated with the normal polarity event JA1.

The comparison between magnetozone BB4 and JA1 indicates that both of them have an approximate length of nearly 6 m, but BB4 seems not complete even with one sample having a possible reverse polarity behaviour at its base (see Appendix 9). Fig.6.2.1d constructs the composite magnetostratigraphic sequence according to the evidence from each indicated sediment sequence, in which the normal polarity zones are named BF1-4 (from Bovey Formation).

The investigated three sections, as a pioneer study, do provide a generally clear picture of the magnetostratigraphy in this area for the upper part of Bovey Formation. Available (very limited) biostratigraphic data indicate that the probable age of the Bovey Formation is middle Early Oligocene. On this basis the composite sequence defined in Fig.6.2.1 can be compared with the appropriate part of the GPTS, shown in Fig.1.3.4. It is tentatively proposed that the set of normal polarity magnetozones BF1 to BF4 correlate with Chron C10 to C12 respectively, as shown in Fig.6.2.2.

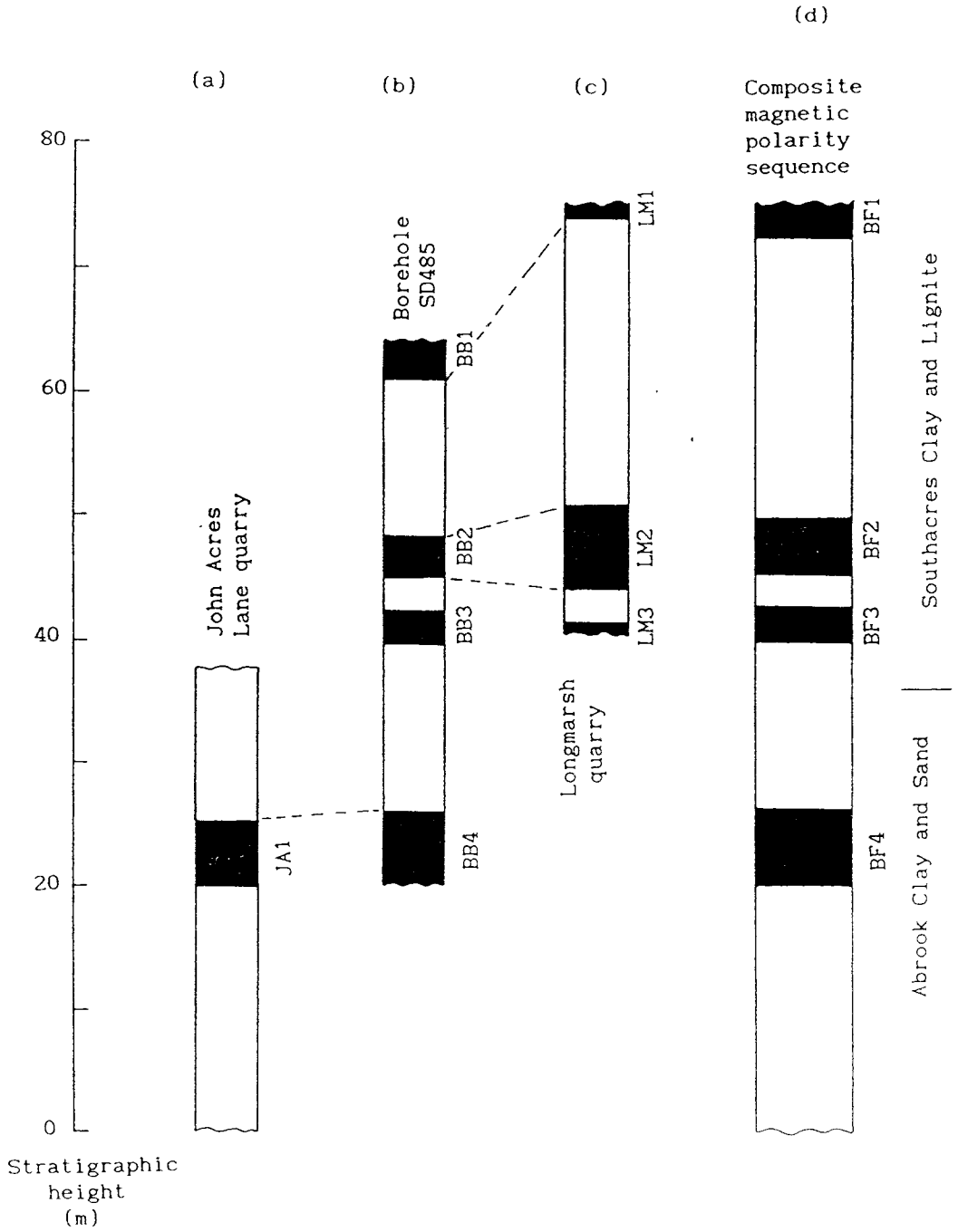

Fig.6.2.1 Summarized magnetic polarity sequences from the Bovey Formation. The the normal polarity events in the composite magnetic polarity sequence (d) are coded BF1-4. Other symbols and conventions as in Fig.4.1.3.

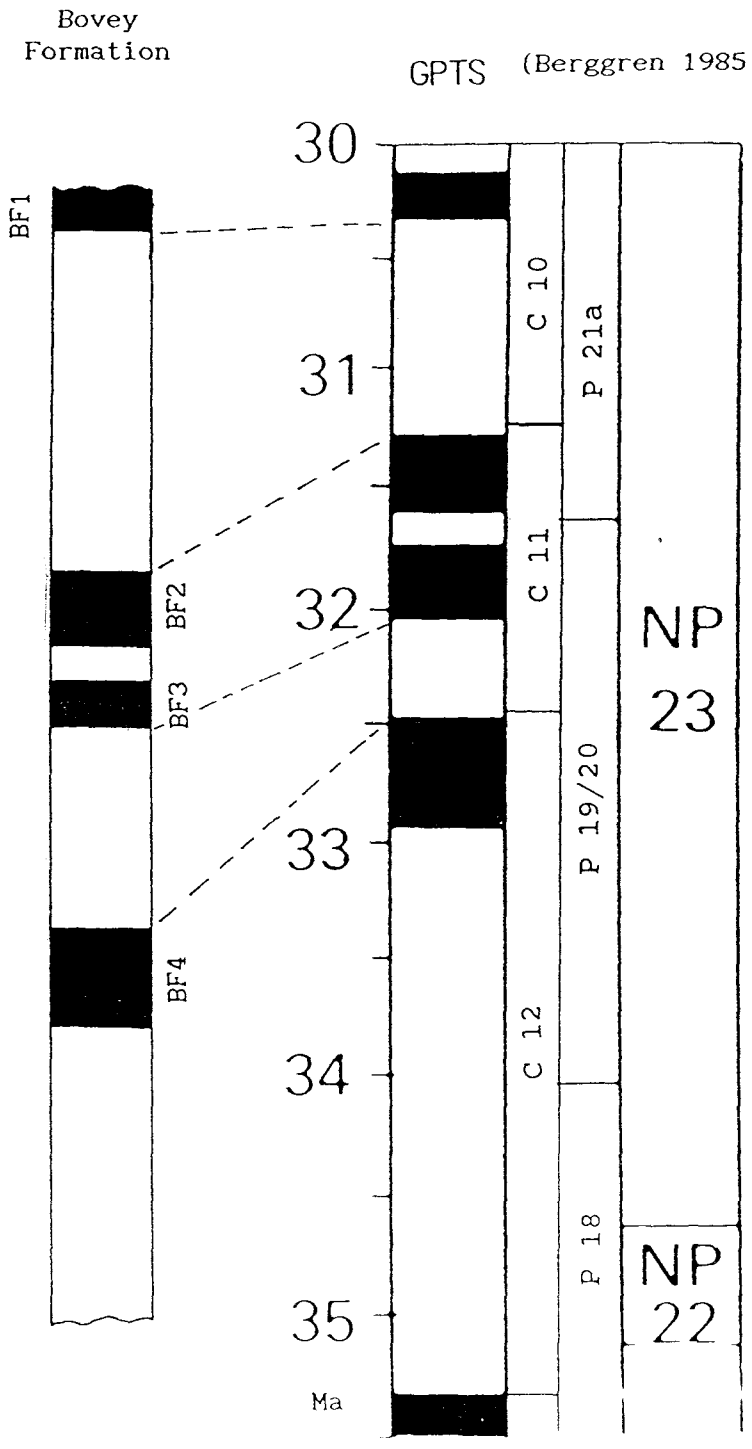

Fig.6.2.2 Correlation of the magnetostratigraphic sequence from the Bovey Formation with the GPTS of Berggren (1985). Symbols and conventions as in Fig.4.1.3.

§6.3 Palaeomagnetic results from the Boom Clay Formation

A preliminary study of the remanent magnetisation of Boom Clay samples was carried out by McGrail (1987), mainly by means of the Molspin fluxgate magnetometer, with a few samples being measured on the cryogenic magnetometer. This work concentrated on NRM measurements, with a small amount of a.f. demagnetisation work being carried out up to 20 mT. McGrail reported that the viscous components (VRM) in these samples are rather changeable with time and their weak magnetic intensity made the magnetisation undeterminable on the Molspin magnetometer.

6.3.1) St.Niklaas quarry section.

This lies in the lower part of the Boom Clay sequence where it is dominated by clays and silty clays with a few carbonate layers. The IRM acquisition curves (Fig.6.3.1), indicate that magnetite is the major magnetisation carrier in these samples but with some small amount of hematite, since the IRM acquisition curves do not quite reach their saturation state in applied field up to 0.6 T.

Fig.6.3.2 displays the NRM intensity distribution, which has a log mean value of 0.173 mA/m. This is fairly low for determination of these samples on the Molspin magnetometer. Fig.6.3.3 shows the variation of NRM intensity with stratigraphic height, in which the values remain fairly uniform.

All 47 samples were subjected to a.f. demagnetisation up to 35 mT. Fig.6.3.4 gives some typical examples of the a.f. demagnetisation behaviour of samples yielding normal and reverse polarities respectively. However, 45% of the samples from this section exhibited directional trends (Fig.6.3.5) rather than SEPs, during demagnetisation (see Appendix 10). This indicates the presence of a significant magnetic overprint in these sediments, which is only partly removed by a.f. demagnetisation.

The low coercivity component defined from the first few a.f. demagnetisation steps was determined for each samples, to try to

establish whether it represents the present geomagnetic field, a component arising from sample storage in the laboratory environment, or the sampling procedure. Fig.6.3.6 shows the distribution of these low coercivity components in (a) sample coordinates and (b) geographic coordinates (in the former, the present geomagnetic field direction was transferred into the average sample coordinate system), since most cores had a similar azimuth (259°) and similar dip (58°) (with $\alpha_{95}=2°$). This indicates that most low coercivity components are concentrated the present geomagnetic field direction (Fig.6.3.6b) but with some departing from it, was possibly reflecting sample storage in the laboratory environment.

Fig.6.3.7 shows a summary of the SEPs and CMDs defining both normal and reverse magnetic polarities. The overall mean direction of remanent magnetisation is

$$\text{Dec}=359°,\ \text{Inc}=53°\ \text{with}\ \alpha_{95}=12°\ (N=14)$$

(see Table 6.3.1).

6.3.2) Steendorp quarry section.

This is the shortest section in this area and it is also regarded as representing the lower part of the Boom Clay Formation, mainly within the Septaria layers S1 and S2, but with its upper boundary a little higher (~1.5 m) than the St.Niklaas quarry section. The IRM acquisition curves (Fig.6.3.8) indicate that magnetite is the main magnetic constituent and that its content is probably higher than that in the St.Niklaas quarry. The log mean NRM intensity value (0.234 mA/m, Fig.6.3.9) is somewhat higher than that for the St.Niklaas section.

Fig.6.3.10a illustrates the NRM intensity variation with stratigraphic height. Despite the shortness of the section and small number of samples available, some minor changes in NRM intensity variation can be recognized, at around 4 m height but without classification.

15 samples in this section were subjected to a.f. demagnetisation. Nearly half of them define directional trends towards a characteristic polarity. Fig.6.3.11 shows two examples, in which (a) is classified as normal polarity and (b) as a directional trend to reverse polarity. These examples illustrate a common problem with the magnetisation of samples from this section, which appear to carry erratic overprints which could not be removed by a.f. magnetisation and cause the magnetic vectors commonly to remain at some peculiar direction, or show a directional trend towards some poorly defined positions on the equal area projection. This caused difficulty in defining their polarity characters.

Fig.6.3.12 illustrates the distribution of low coercivity components for this section. It is apparent that these components are concentrated along the minus z-axis in sample coordinate frame (see Fig.6.3.12a), instead of surrounding the present geomagnetic field direction. After the field correction for each sample, these components concentrate within the north-upper hemisphere on the projection. It is concluded that the samples from the Steendorp section have been affected more seriously by the sampling procedure. A few reliable CMDs were defined for this short section (see Appendix 11).

6.3.3) Kruibeke quarry section.

This section covers a major part of the Boom Clay Formation, nearly 30 m in stratigraphic height, and extends up to the top of the formation. The section starts from the base of septaria layer S3, which is about 2 m higher than the top of the Steendorp section. 15 samples from the whole section were tested for their IRM acquisition properties. All samples displayed IRM acquisition curves indicative of magnetite (Fig.6.3.13), and some of the curves reached magnetic saturation at fields even lower than 0.2 T (see Fig.6.3.13g). This could possibly be related to the presence of pyrite, since at the level of this sample there is an apparent pyrite layer.

The log mean NRM intensity (0.343 mA/m, Fig.6.3.14) is higher than that for the St.Niklaas and Steendorp sections. The distribution of NRM intensity with stratigraphic height is shown in Fig.6.3.15a, in which an apparent high NRM intensity event can be recognized in the interval between the base of the section and a height of ~14m. The peak of the event is at around 10 m.

Progressive a.f. demagnetisation was carried out on 112 samples from this section. Fig.6.3.16 presents some examples. Most samples show a good response to a.f. demagnetisation. Fig.6.3.17 summarizes the SEPs and CMDs defined for both normal and reverse polarity samples. The vectors are relatively scattered. The overall mean direction of stable magnetisation is

$$\text{Dec} = 5^{\circ},\ \text{Inc} = 44^{\circ} \text{ with } \alpha_{95} = 14^{\circ}\ (N=23)$$

(see Table 6.3.1). Fig.6.3.18 shows the intersections produced from those samples with well-defined directional trends towards reverse polarity. The overall mean direction defined from these intersections is Dec =157°, Inc =-59° (12 directional trends involved).

The magnetic polarities of more than 40% of the samples were based on directional trends. Similar problems to those encountered in the Steendorp section (see §6.3.2) were identified in the Kruibeke section, many of the CMDs showing wildly dispersed directions which differ significantly from the expected axial dipole field direction (see Fig.6.3.19). Fig.6.3.20 shows the distribution of low coercivity components for this section. An apparent departure from the present geomagnetic field direction could be recognized for the lower coercivity components in both sample and geographic coordinates. Particularly, in sample coordinates they simply concentrate around the lower left hand corner, which might have been caused by sample storage in the laboratory environment.

It is possible that this secondary component is related to the presence of pyrite in this sequence. Unfortunately, due to the shortage of samples from this section (almost all samples were

subjected to a.f. treatment), thermal demagnetisation could not be applied.

6.3.4) Conclusion.

The preliminary magnetostratigraphic results for the Boom Clay Formation is encouraging, in spite of the complication discussed above. Although the fold test cannot be applied to this formation, because of the generally low dips, the the regular occurrence of a normal and reverse polarity pattern within the beds is indicative of a possible primary magnetisation, which is variably masked by secondary components. Table 6.3.1 summarizes the CMDs for the St.Niklaas and Kruibeke sections.

Table 6.3.1 Summary of mean characteristic magnetisation directions for Boom Clay Formation.

SECTION	CMD (normal p.)	CMD (reverse p.)	OVERALL MEAN
St.Niklaas	DEC INC 16° 55° α_{95}=20°,N=6	DEC INC 164°-50° α_{95}=15°,N=8	DEC INC 359° 53° α_{95}=12°,N=14
Kruibeke	DEC INC 340° 50° α_{95}=15,N=15	DEC INC 205°-34° α_{95}=22,N=8	DEC INC 5° 44° α_{95}=14,N=23
		Overall mean for Boom Clay Formation DEC INC 2° 48° α_{95}=9,N=37	

p.= polarity.

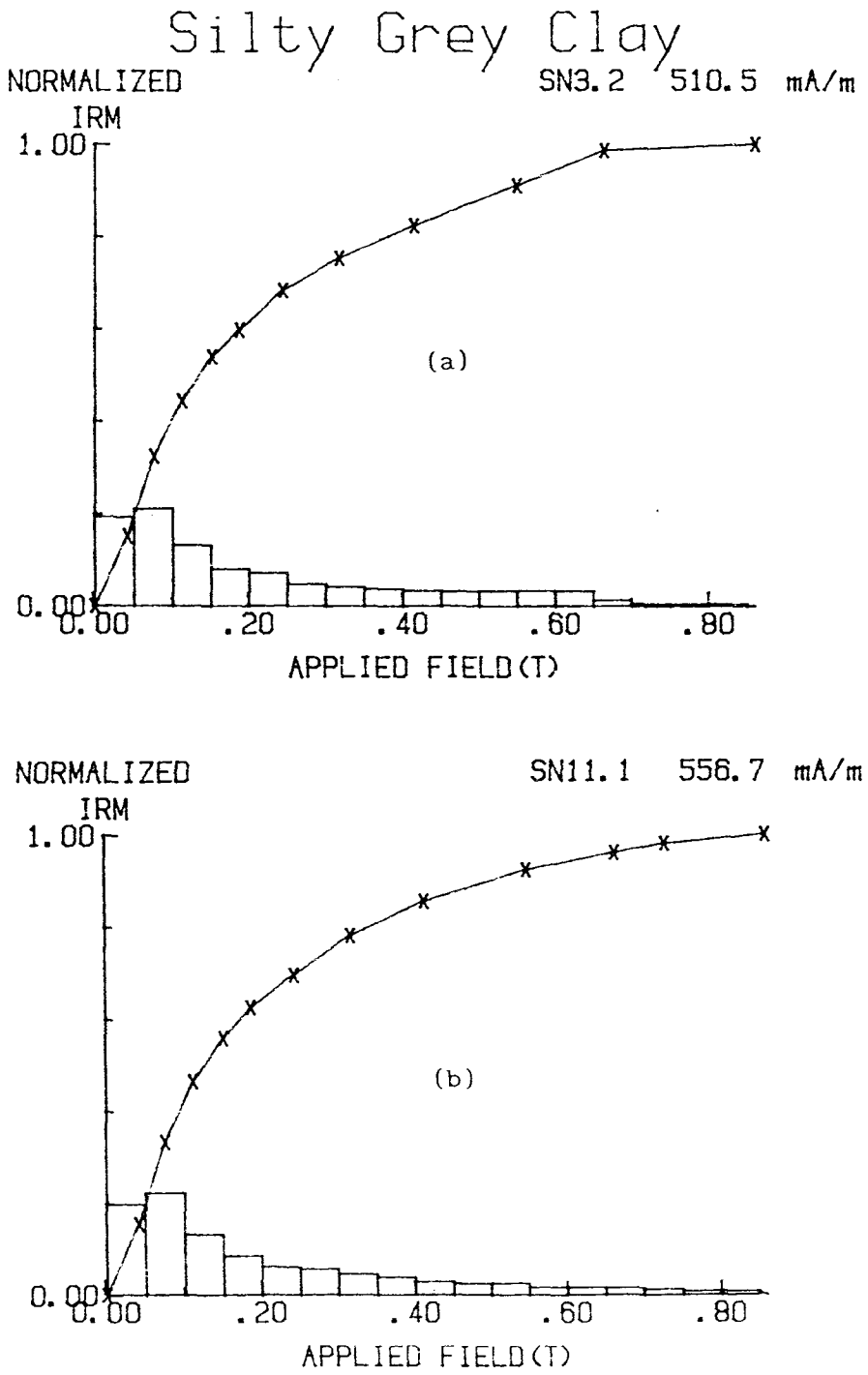

Fig.6.3.1 Examples of IRM acquisition curves of samples from St.Niklaas quarry section, Boom Clay Formation.

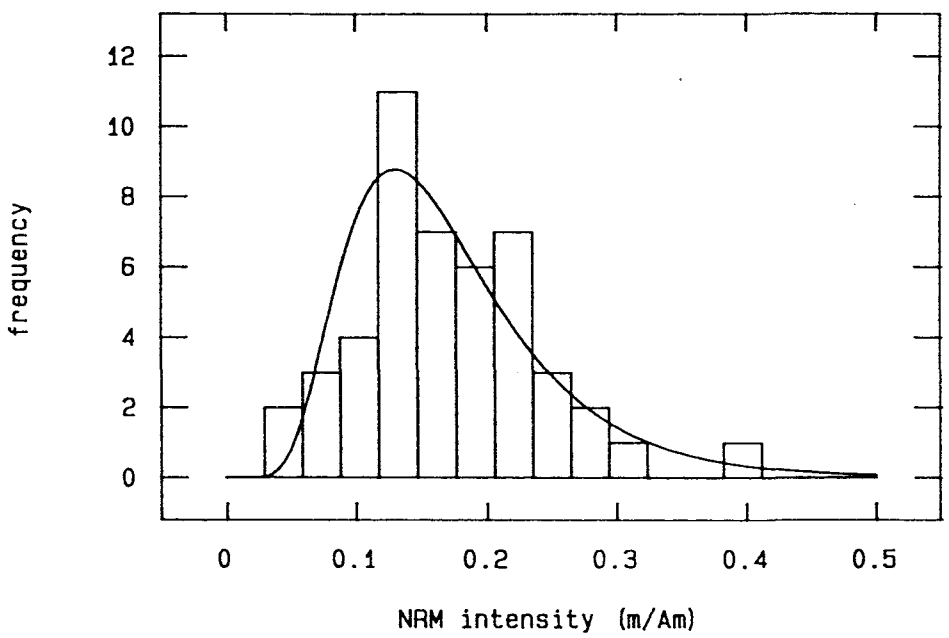

Fig.6.3.2 Statistical distribution of NRM intensity values of samples from St.Niklaas section, Boom Clay Formation.

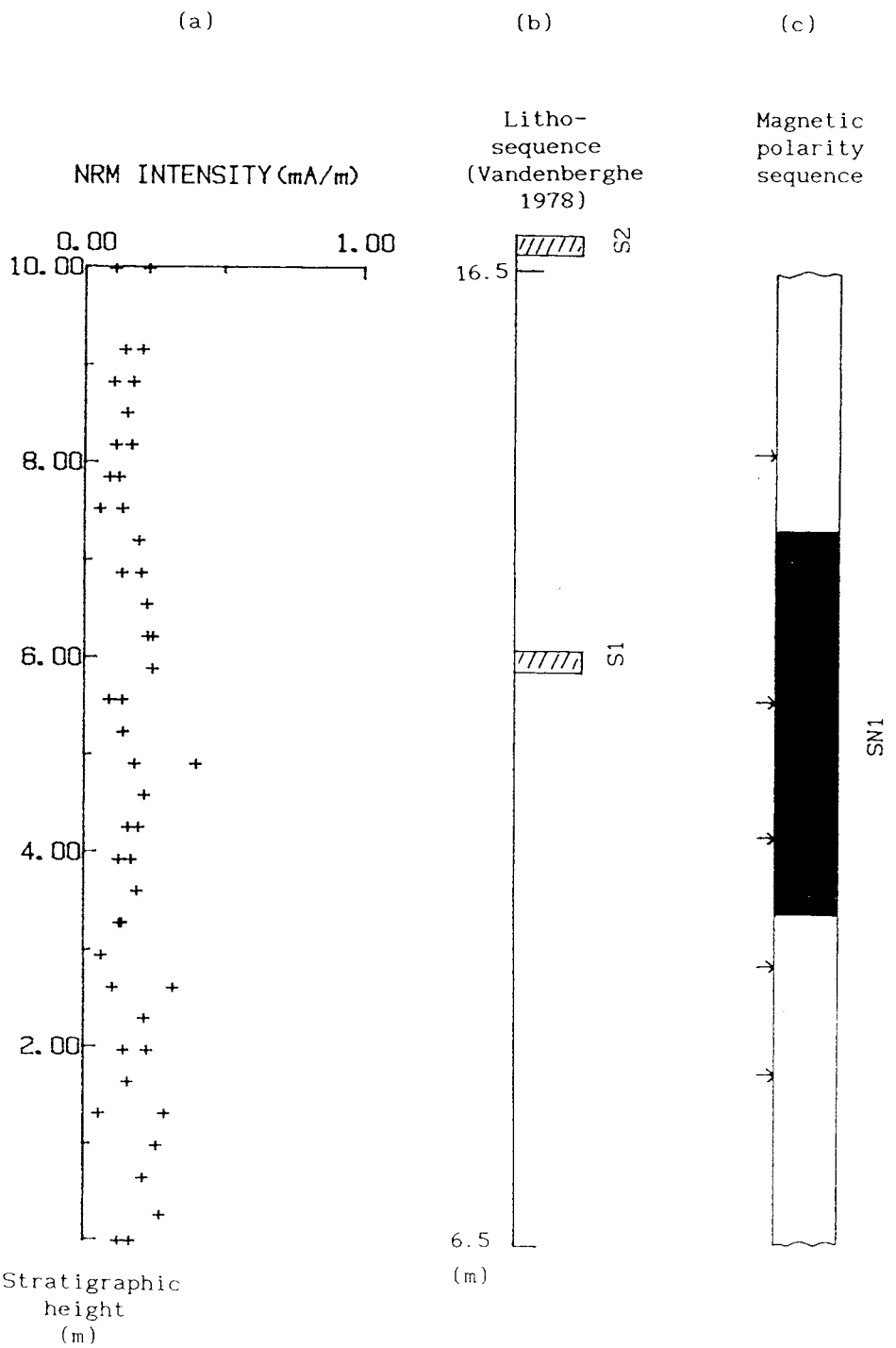

Fig.6.3.3 (a) Variation of NRM intensity values with stratigraphic height for St.Niklaas section, Boom Clay Formation. (b) Septaria layers identified in this section and the height values are referred to the sedimentary sequence in Fig.5.3.2. (c) magnetic polarity sequence. Other symbols and conventions as in Fig.4.1.3.

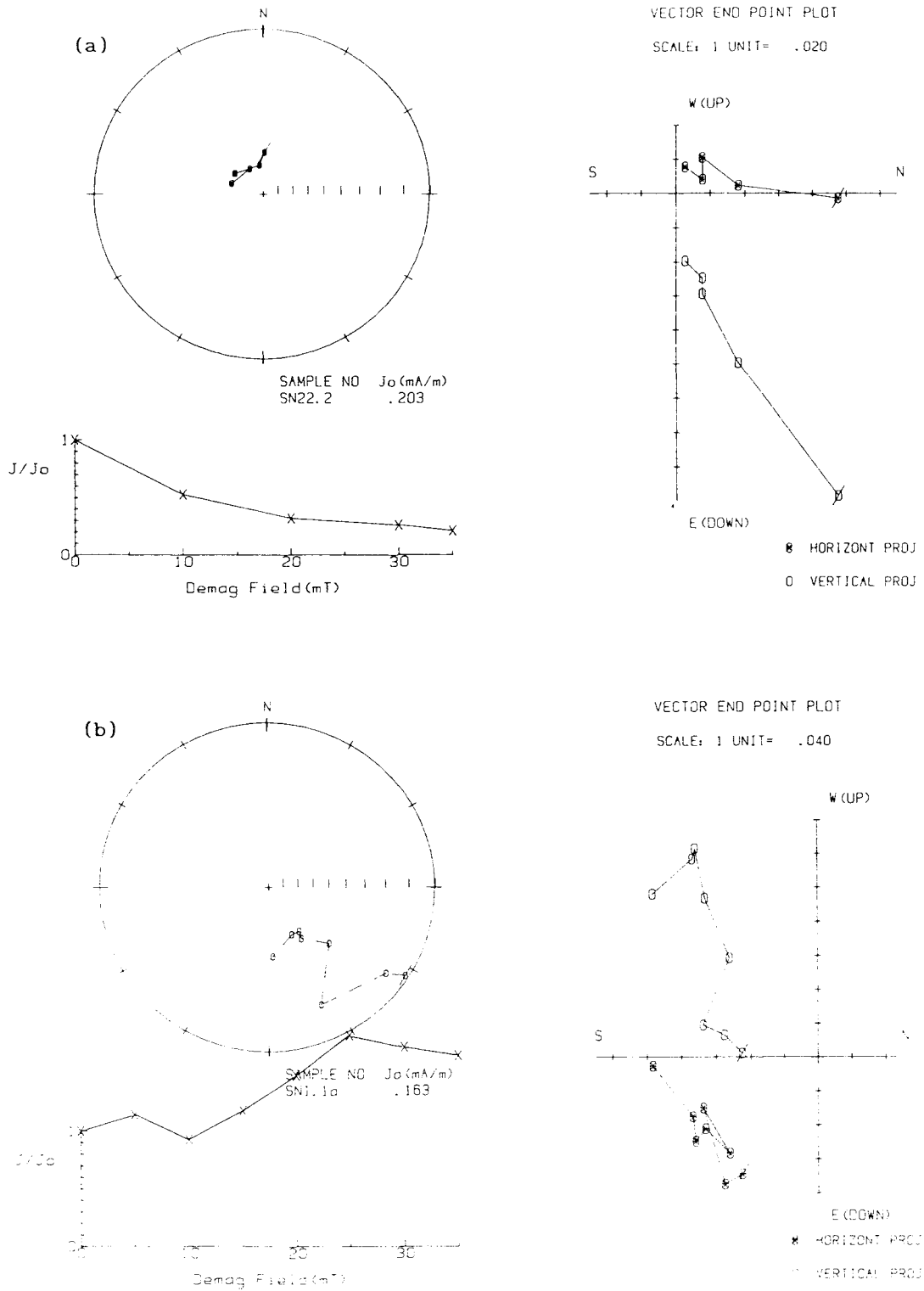

Fig.6.3.4 Examples of a.f. demagnetisation for samples from St.Niklaas section, Boom Clay Formation. Symbols and conventions as in Fig.4.1.4.

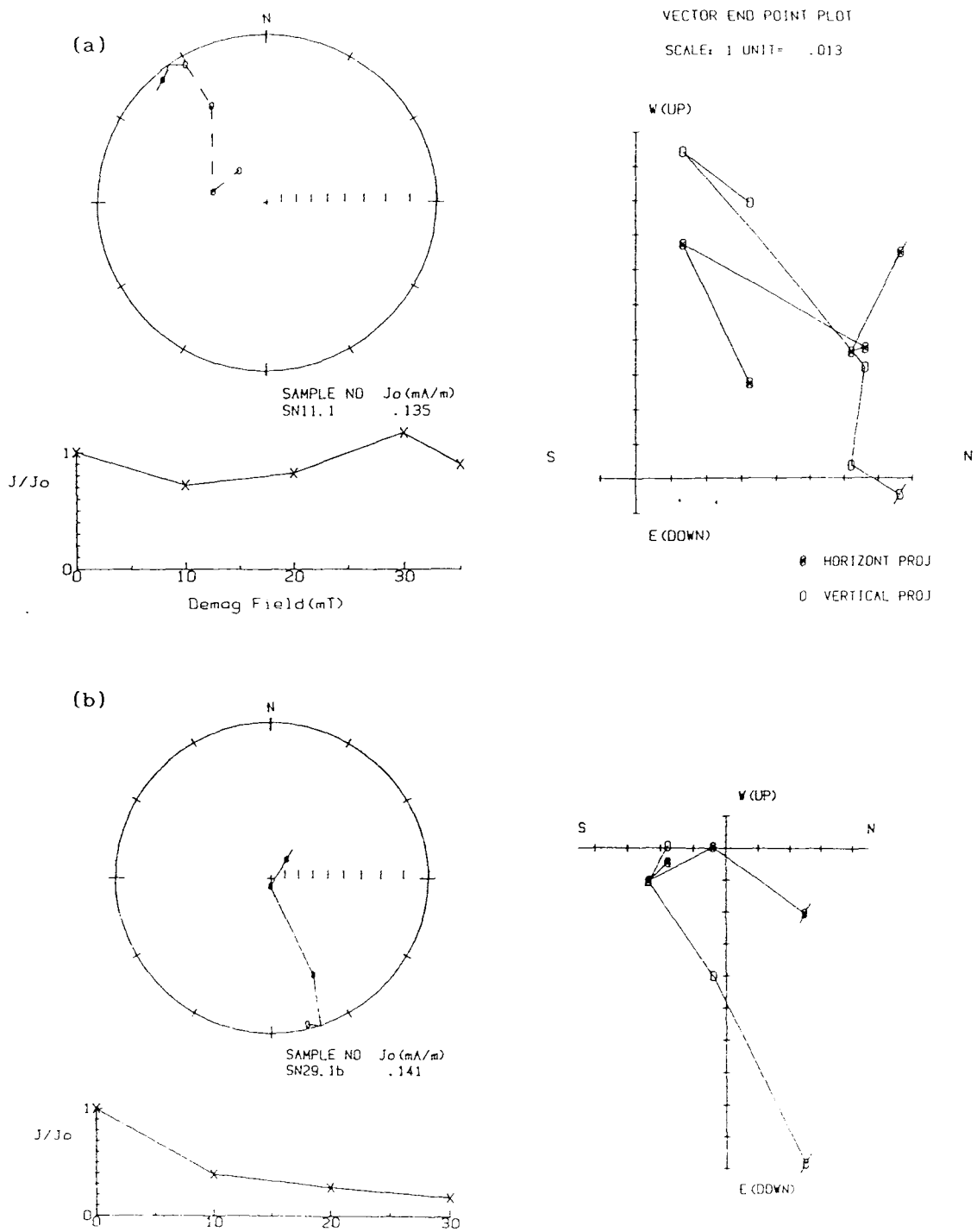

Fig. 6.3.5 Some samples whose magnetic polarities are defined by demagnetisation directional trends. St.Niklaas section, Boom Clay Formation. Symbols and conventions as in Fig. 4.1.4.

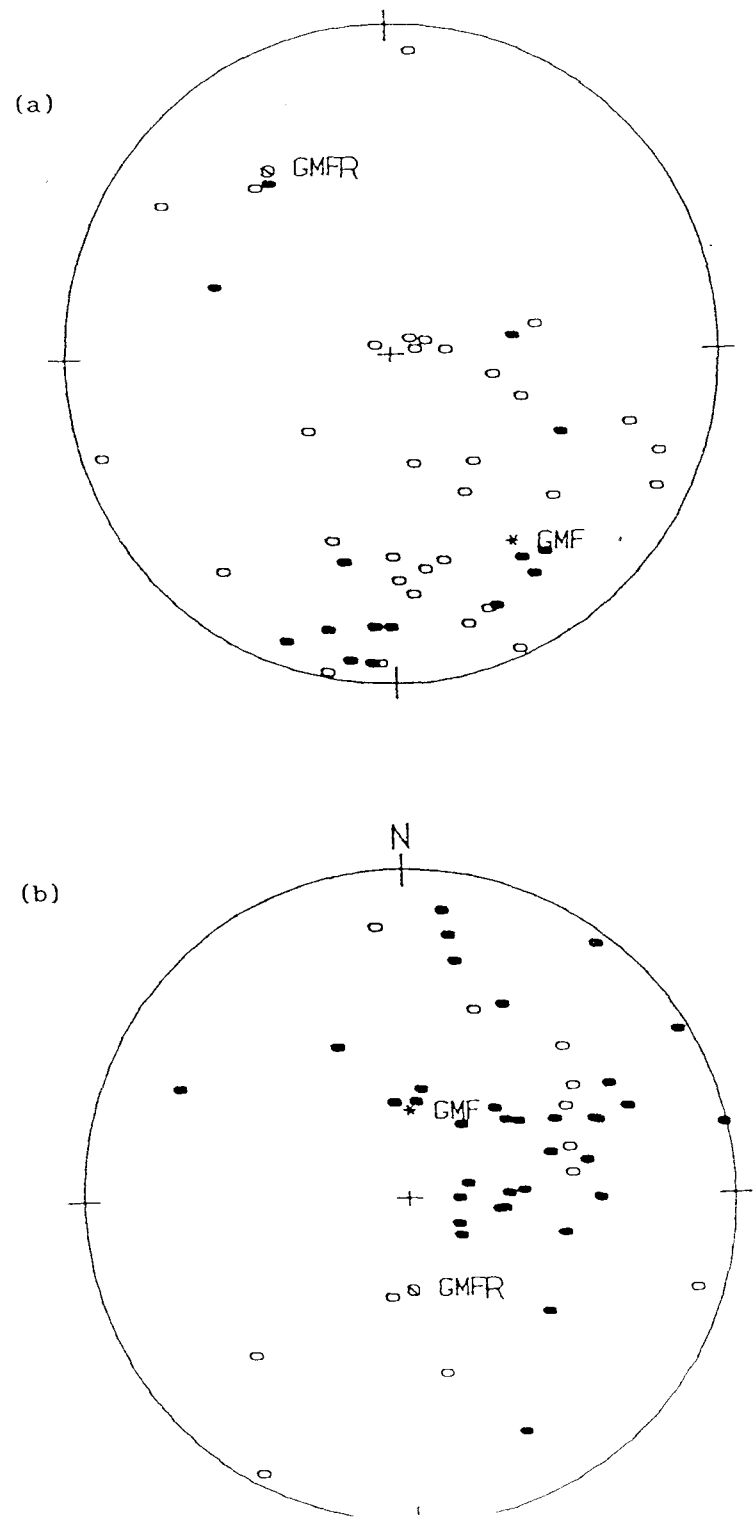

Fig. 6.3.6 Distribution of low coercivity components isolated by a.f. demagnetisation for samples from St.Niklaas quarry section. (a) Components in sample coordinates, in which the geomagnetic field direction for the Tertiary is transferred to this coordinate frame, (b) components in geographic coordinates. Symbols and conventions as in Fig. 4.1.11.

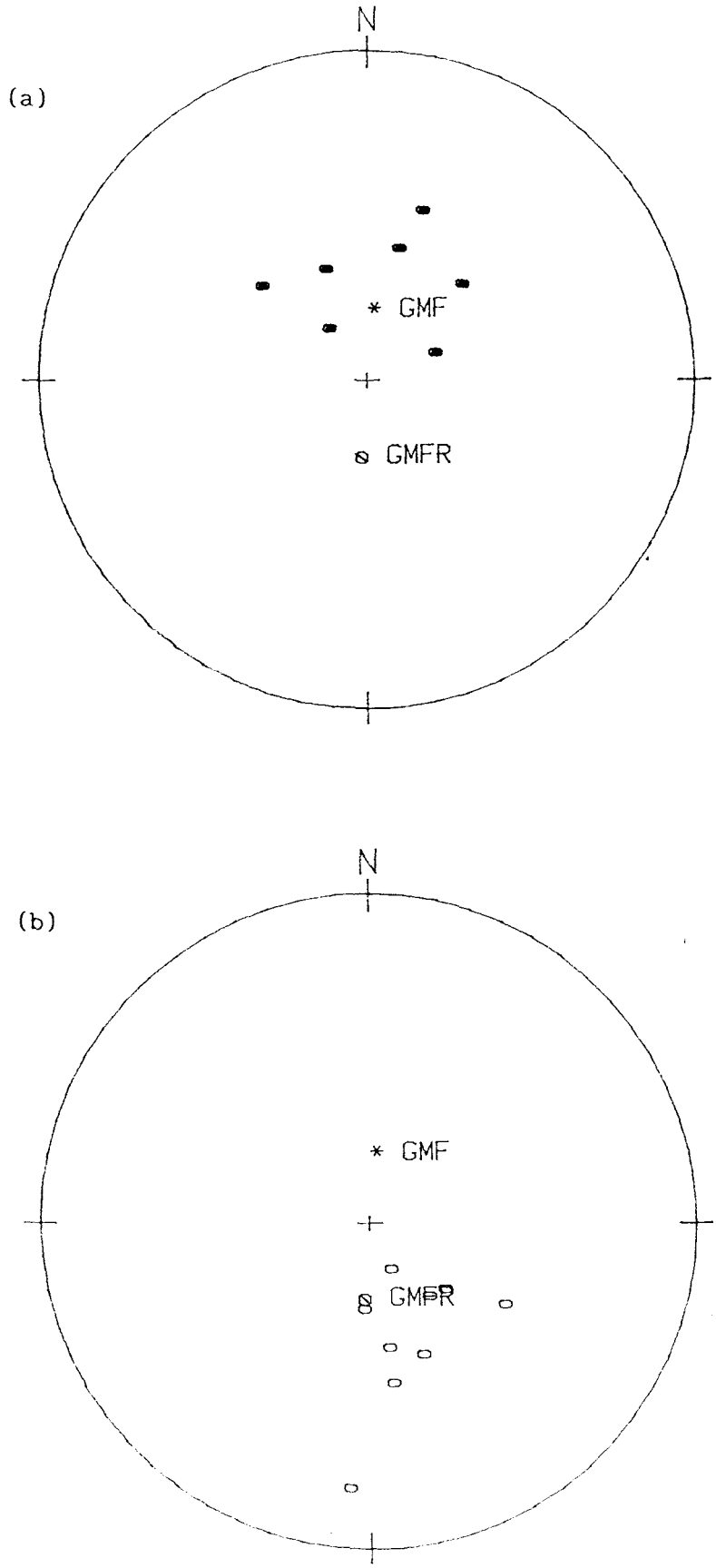

Fig.6.3.7 Summarized CMDs for samples from St.Niklaas quarry section, Boom Clay Formation. (a) normal polarity and (b) reverse polarity. Symbols and conventions as in Fig.4.1.11.

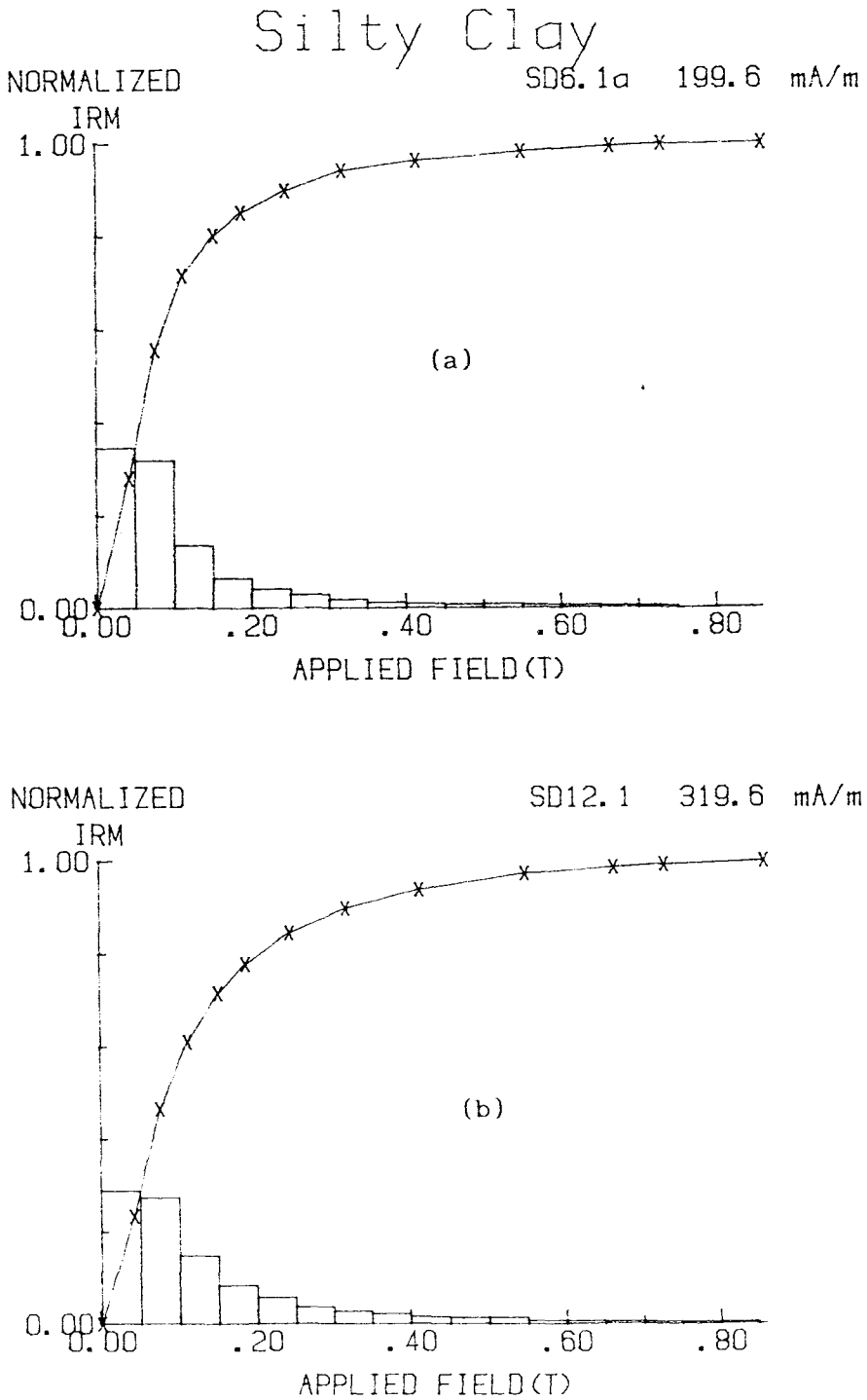

Fig.6.3.8 Examples of IRM acquisition curves for samples from Steendorp section, Boom Clay Formation.

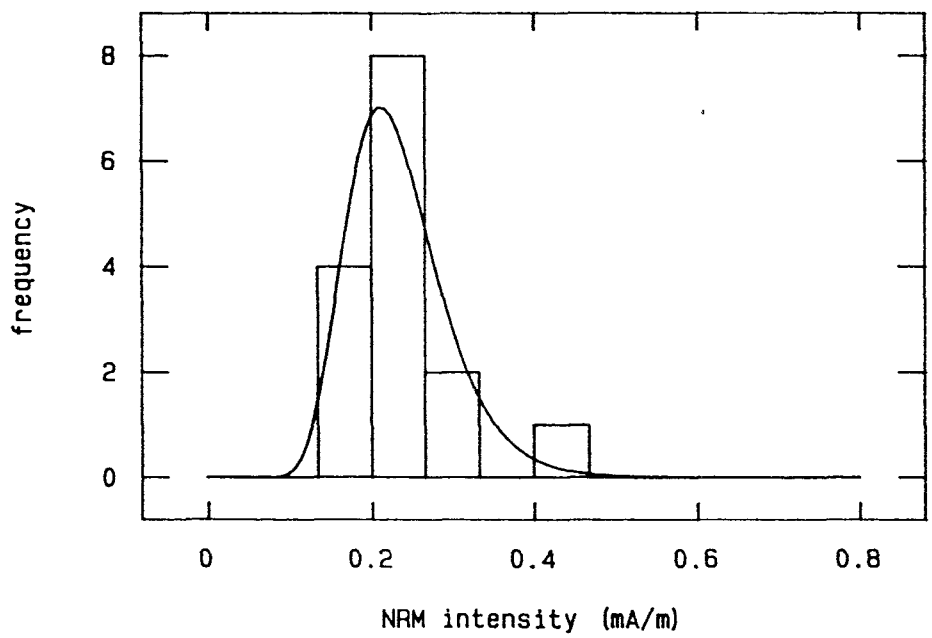

Fig.6.3.9 Statistical distribution of NRM intensity values of samples from Steendorp section, Boom Clay Formation.

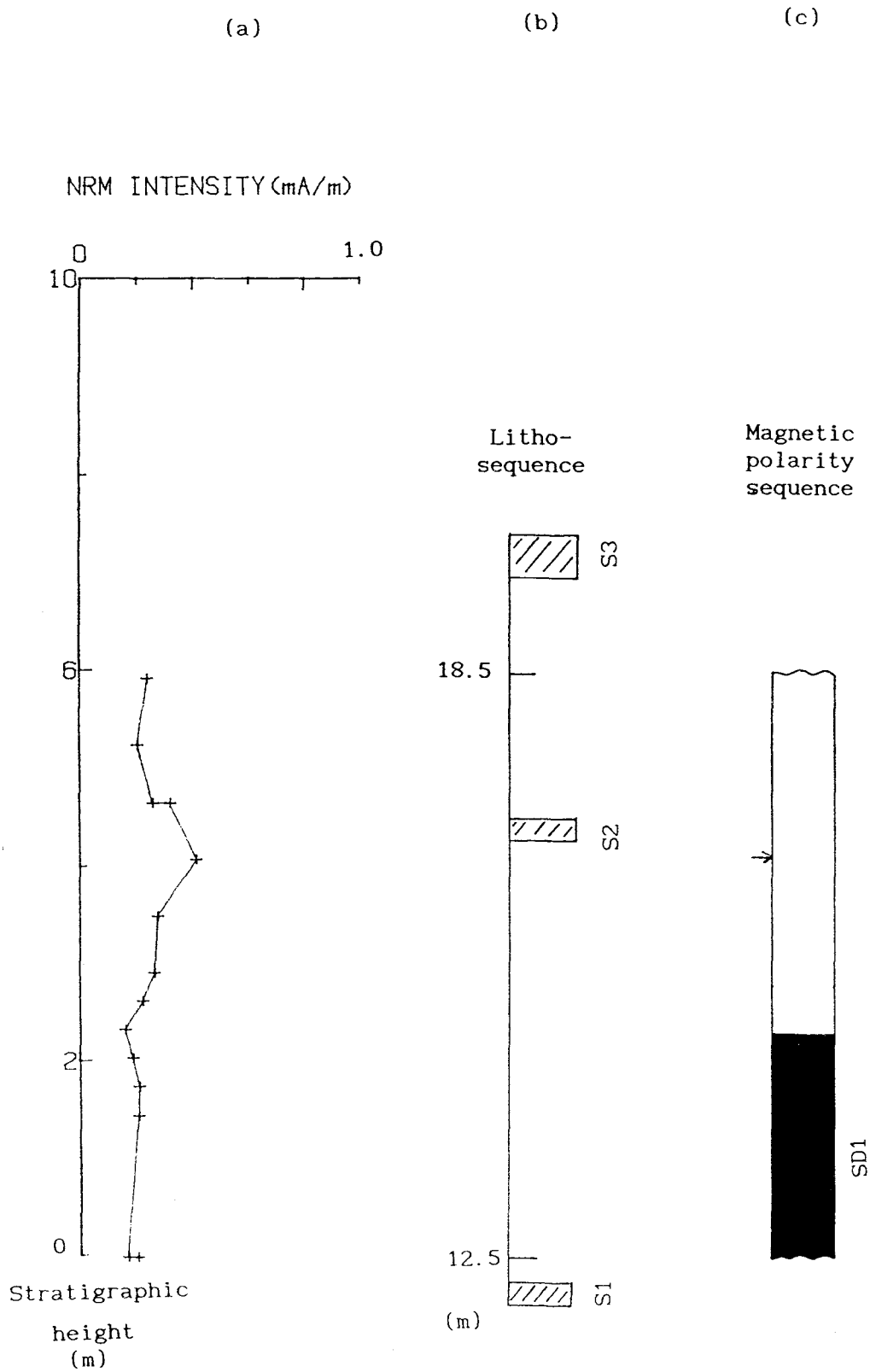

Fig.6.3.10 (a) Variation of NRM intensity values with stratigraphic height for samples from Steendorp section, Boom Clay Formation. (b) Septaria layers (c) magnetic polarity sequence. Other symbols and conventions as in Fig.6.3.3.

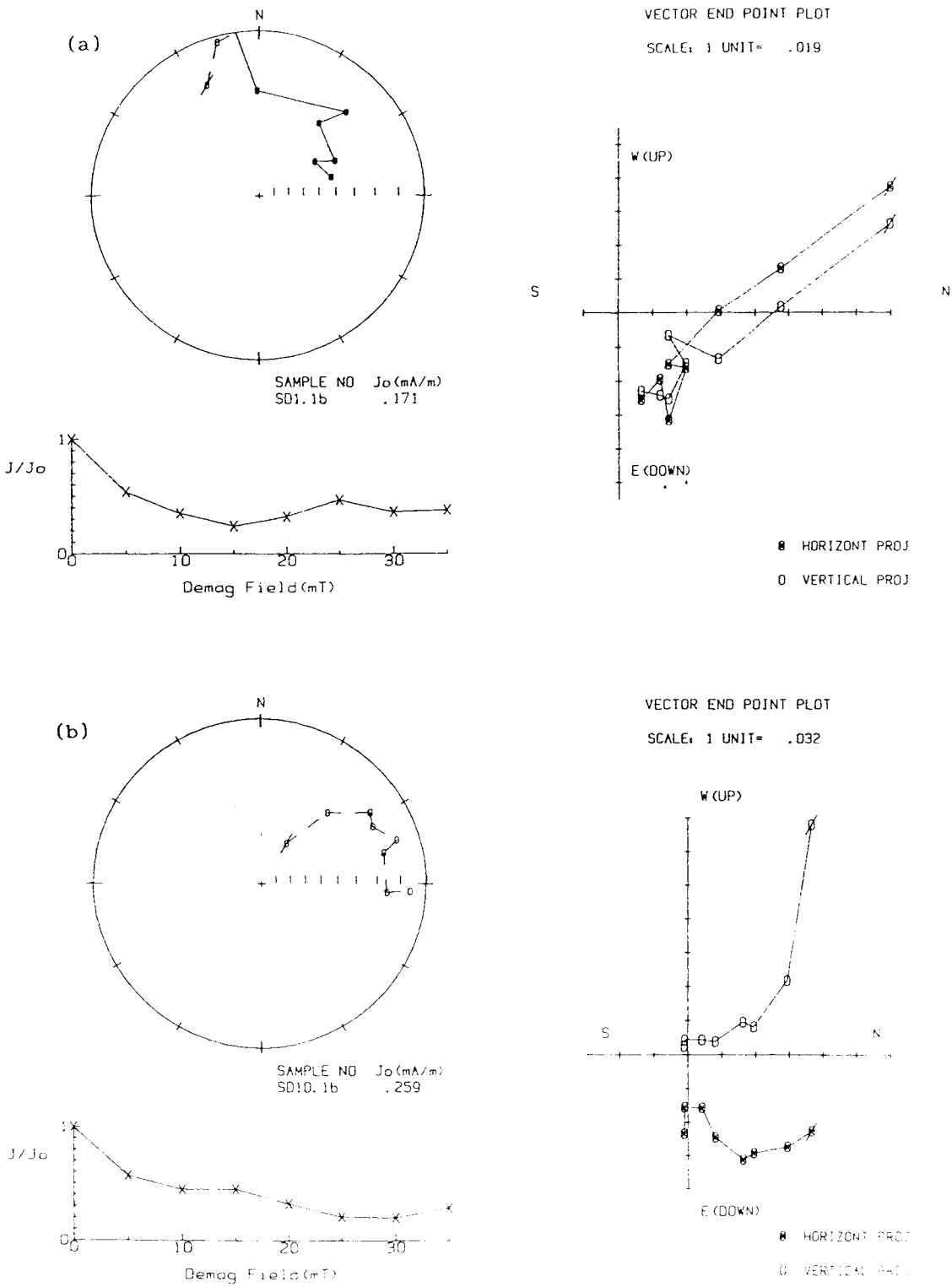

Fig.6.3.11 Examples of a.f. demagnetisation for samples from Steendorp section, Boom Clay Formation. (a) defined as normal polarity and (b) as directional trend towards reverse polarity. Symbols and conventions as in Fig.4.1.4.

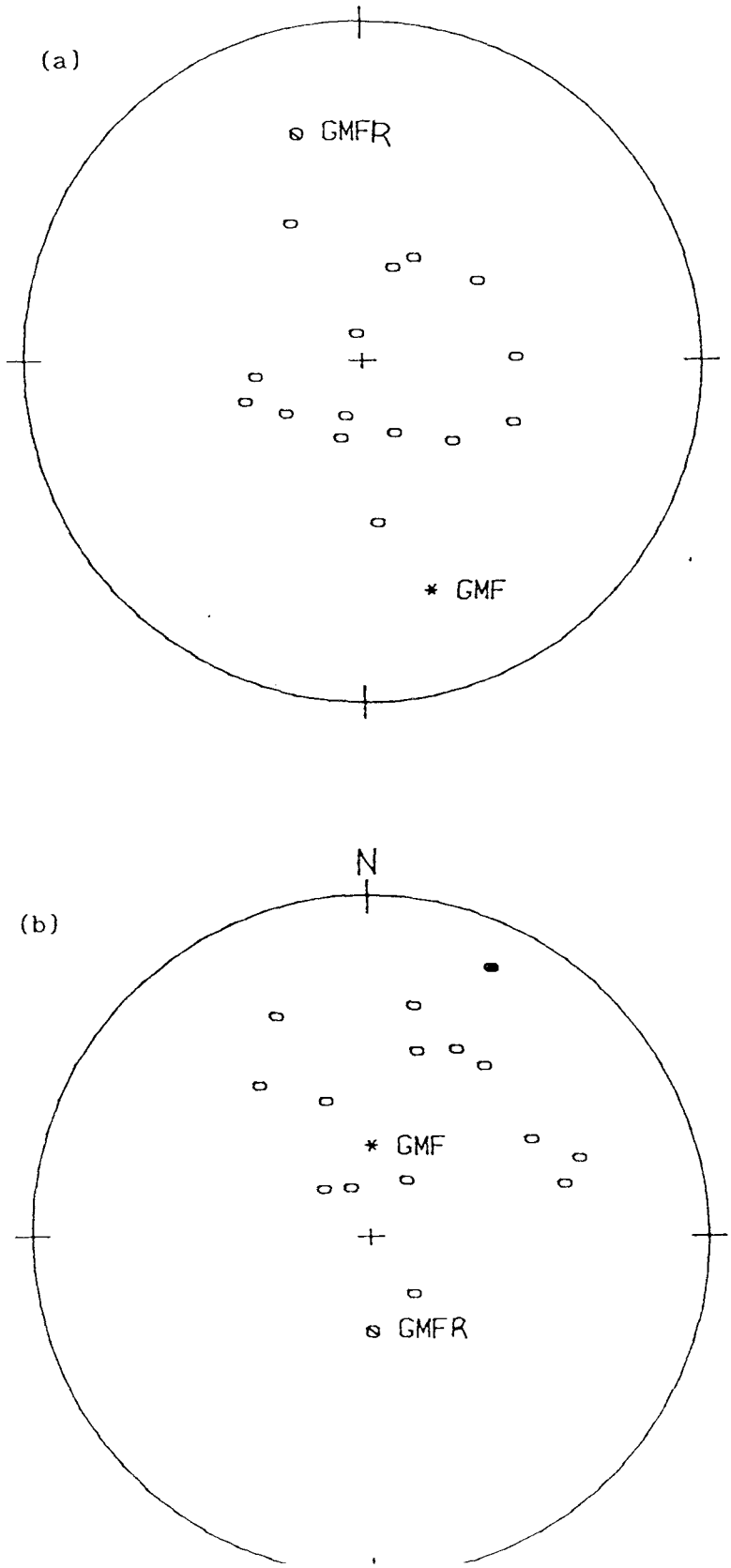

Fig.6.3.12 Isolated low coercivity components by a.f. demagnetisation for samples from Steendorp section. (a) in sample coordinates and (b) in the geographic coordinates. Symbols and conventions as in Fig.6.3.6.

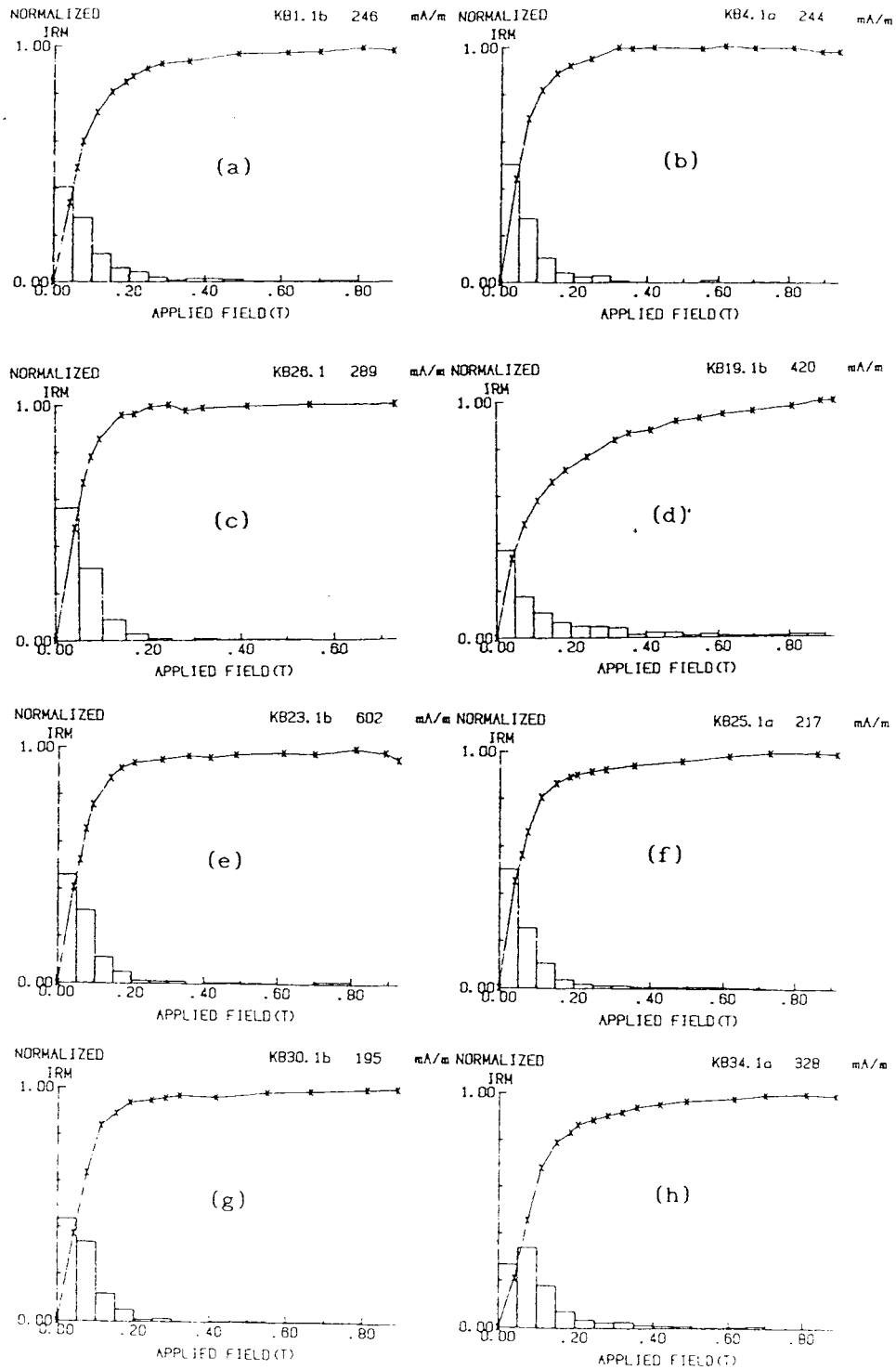

Fig.6.3.13 Examples of IRM acquisition curves for samples from Kruibeke section, Boom Clay Formation.

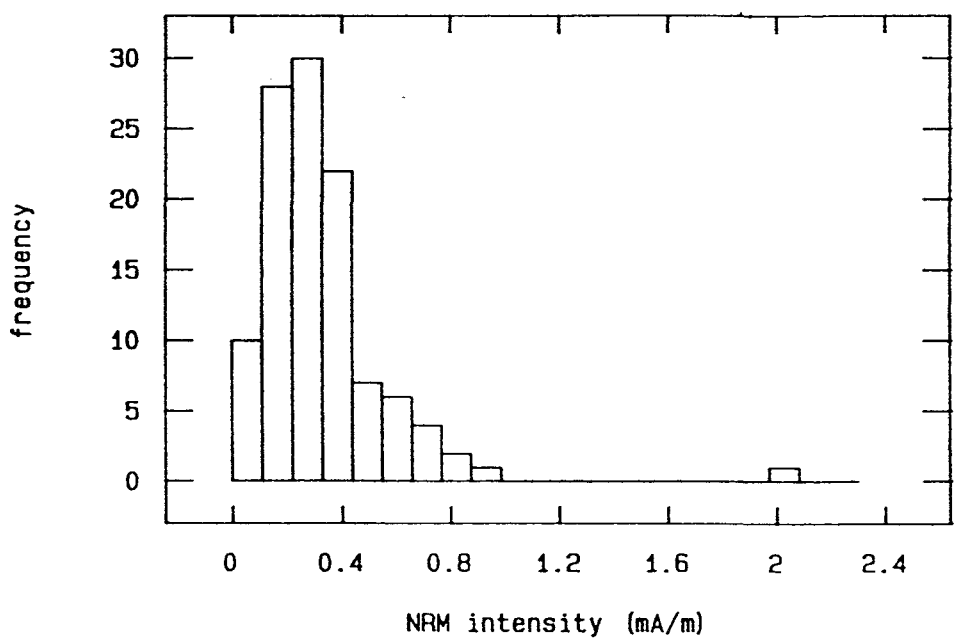

Fig.6.3.14 Statistical distribution of NRM intensity values for samples from Kruibeke section, Boom Clay Formation.

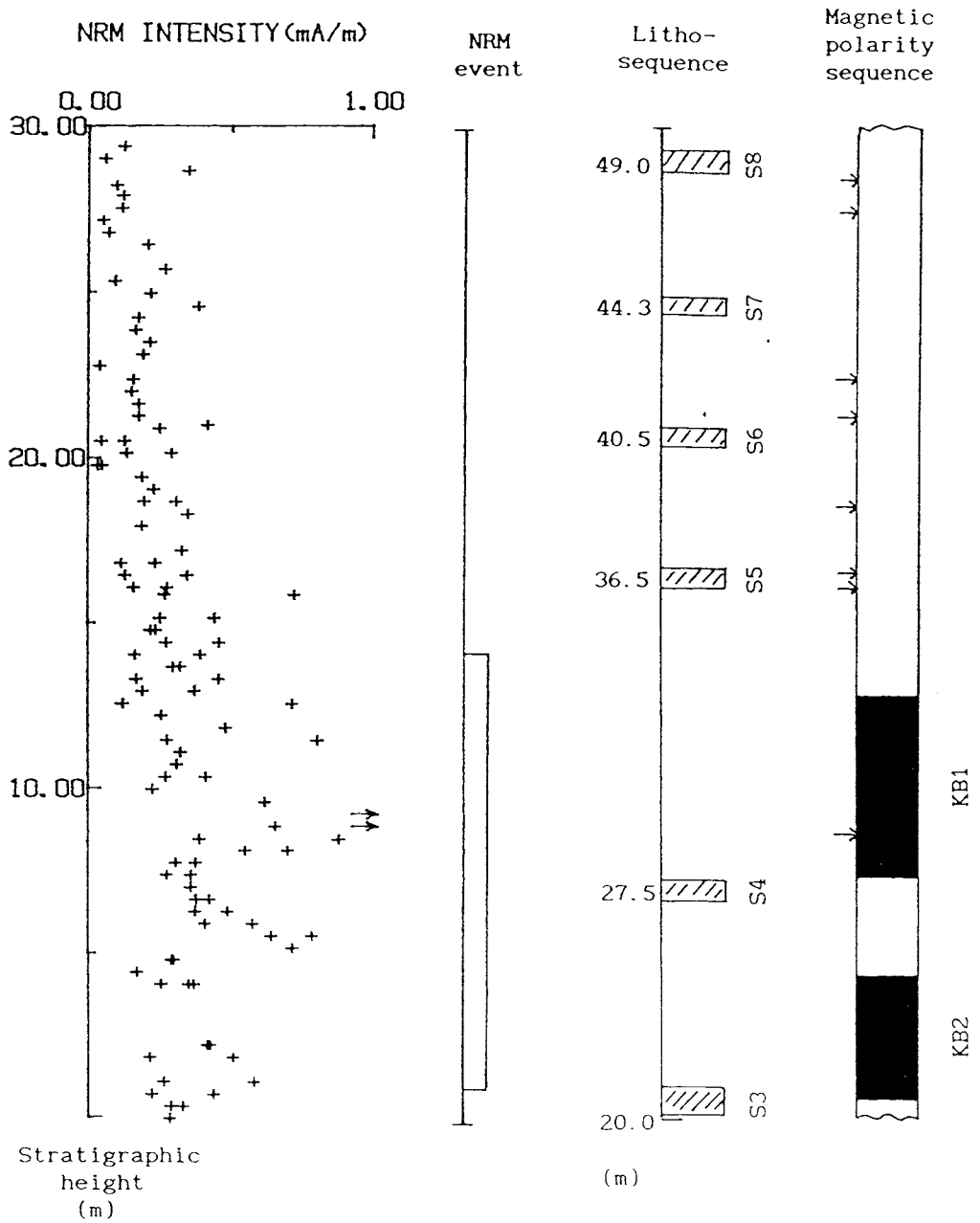

Fig.6.3.15 (a) Variation of NRM intensity values with stratigraphic height for Kruibeke section, (b) recognizable NRM intensity value increase "event", (c) Septaria layers (see Fig.5.3.2) and (d) magnetic polarity sequence. Other symbols and conventions as in Fig.4.1.3.

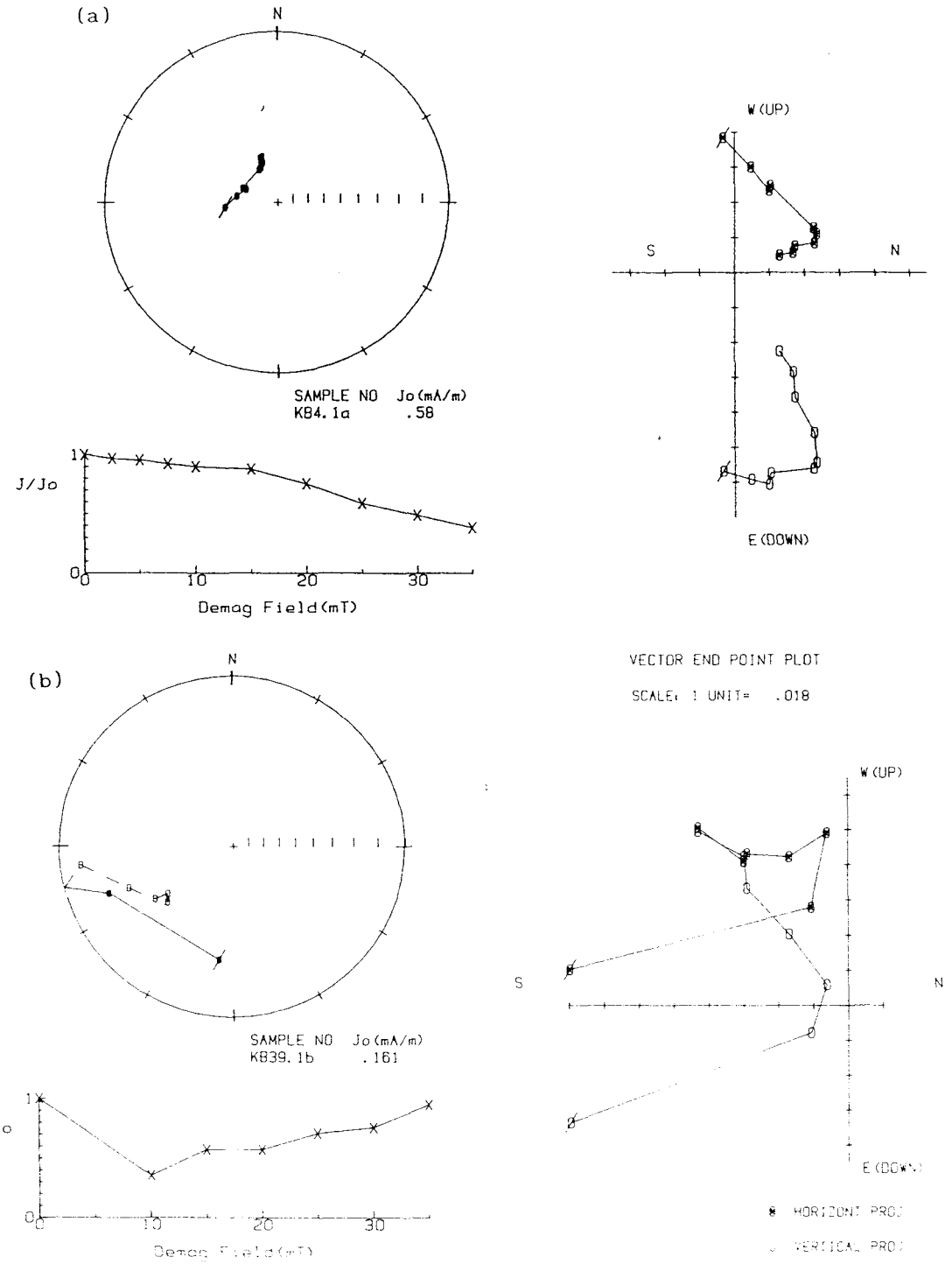

Fig.6.3.16 Examples of a.f. demagnetisation for samples from Kruibeke section. Symbols and conventions as in Fig.4.1.4.

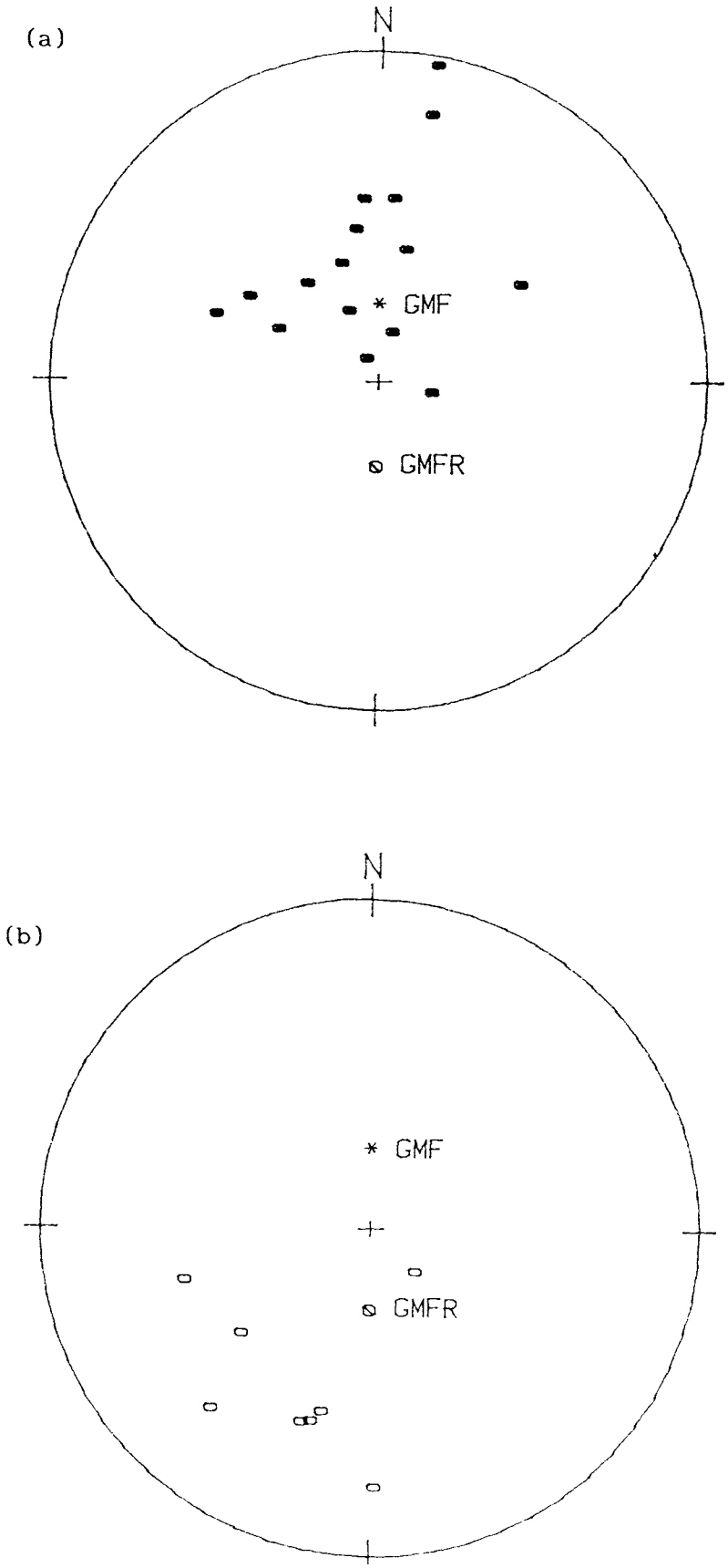

Fig.6.3.17 Summarized CMDs for samples from Kruibeke section, Boom Clay Formation. Symbols and conventions as in Fig.4.1.11.

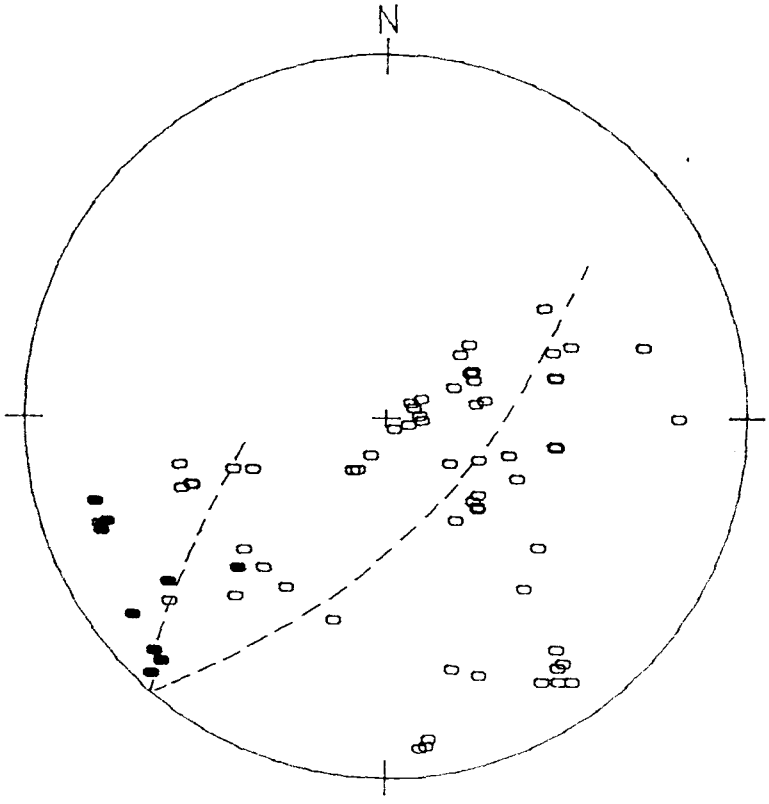

Fig. 6.3.18 Intersections produced by the great circle fitting for samples from Kruibeke section with directional trends towards reverse polarity. The distribution is approximately along the circle as shown. Symbols and conventions as in Fig. 4.1.11.

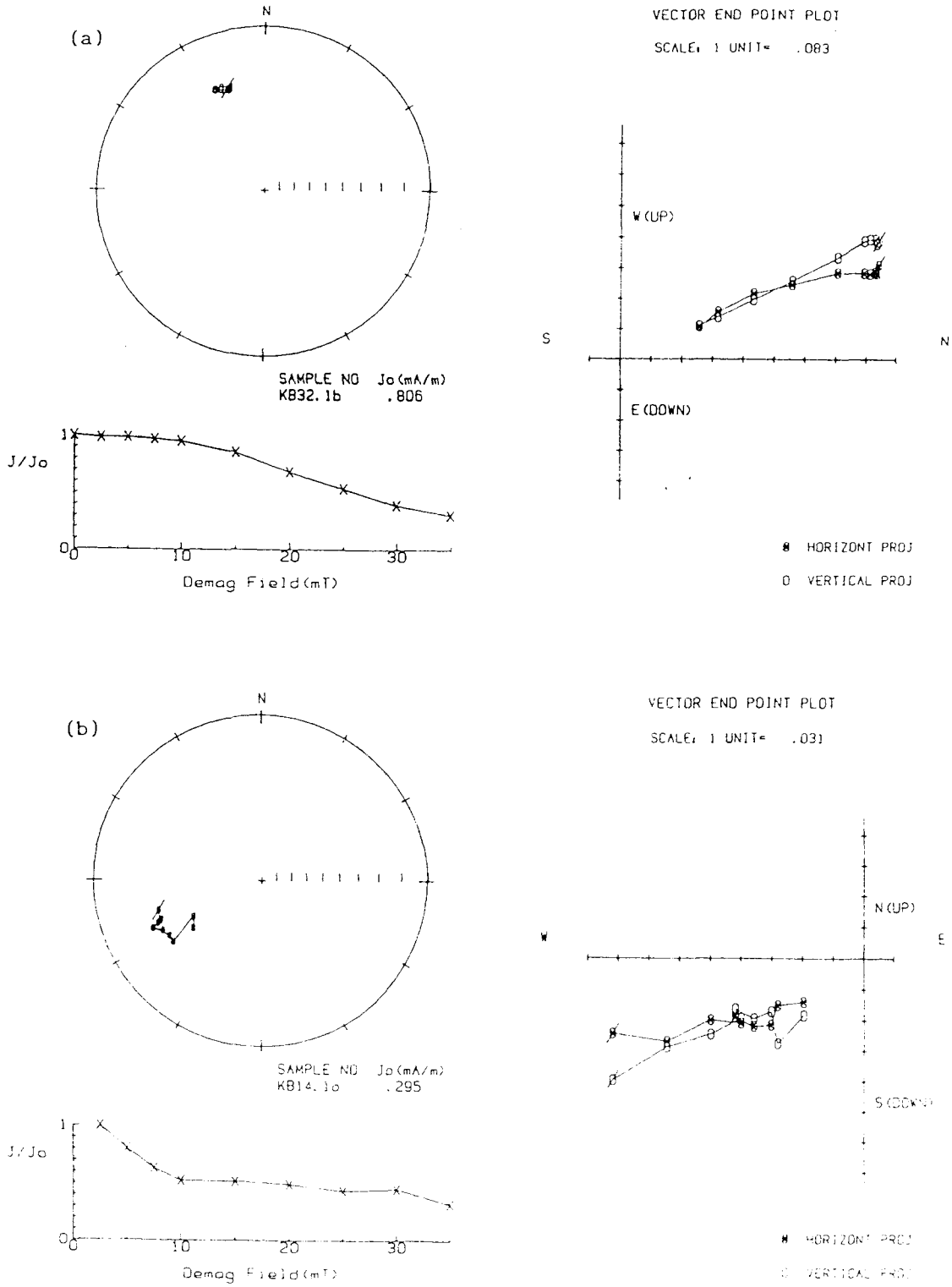

Fig. 6.3.19 Examples of samples from Kruibeke section with scattered CMDs which do not define clear polarities. Symbols and conventions as in Fig. 4.1.4.

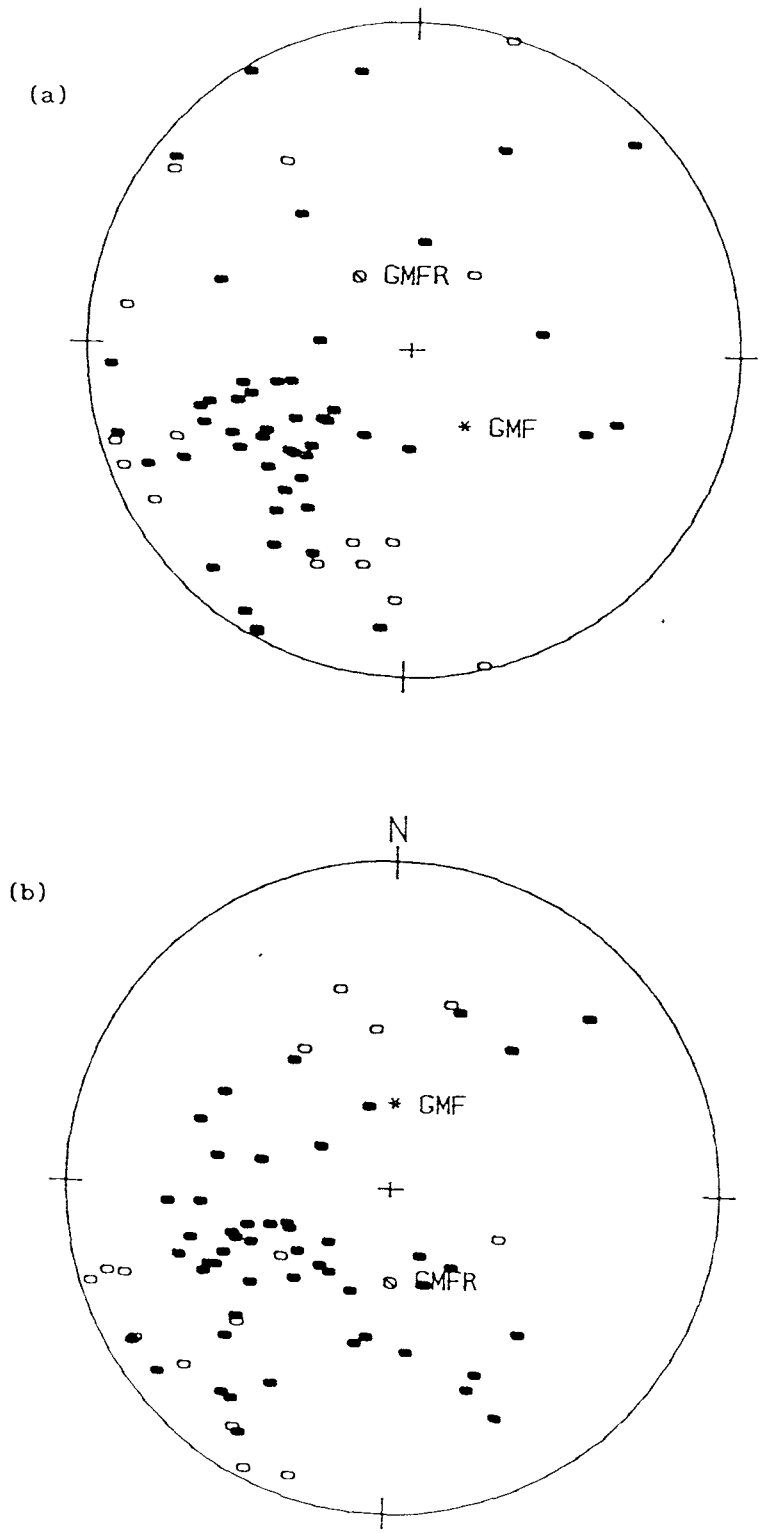

Fig.6.3.20 Isolated low coercivity components, for samples from Kruibeke section. (a) in sample coordinates and (b) in geographic coordinates. Symbols and conventions as in Fig.6.3.6.

§6.4 Magnetic polarity sequences and their correlations for the Boom Clay Formation.

6.4.1) St.Niklaas quarry section.

In spite of the complicated magnetic behaviour of some samples discussed in §6.3, many samples from this section yielded a reliable magnetic polarity.

In the St.Niklaas section a single normal polarity magnetozone, named SN1, is defined in the middle of the 10 m thick section and has a thickness of about 4 m in the vicinity of septarian layer S1. Fig.6.3.3c illustrates the magnetic sequence accompanied by the lithological sequence. 11-12 sampling sites define this normal polarity interval, but only 70% of these samples showed a clear normal polarity defined either by CMDs or directional trends. A further 30% of the samples showed erratic reverse polarities (see Appendix 10). The lower boundary of the magnetozone is much clearer than the upper one. Both the upper and lower parts of the section show a dominant reverse polarity, the upper interval being about 2.8 m and the lower interval about 3.5 m in thickness. 19 sampling sites control these two reversed intervals and 73% of the samples within them show a clear reversed polarity character.

6.4.2) Steendorp section.

In spite of its shortness and the magnetic complications discussed in §6.3.2, the Steendorp section yielded a clear magnetic polarity pattern, in which a reversed polarity interval in the upper part overlies a normal polarity interval. Fig.6.3.10c shows the magnetic polarity sequence with respect to its lithological markers. This sequence spans septarian layer S2. The normal polarity interval, SD1, has a thickness of about 2.5 m is incomplete in its lower part, but having a clear upper boundary. All 6 samples within this interval are characterized by normal polarity, 4 of them showing clear CMDs. The reverse polarity interval above extends for about 3.5 m and is defined by 7 sampling sites, for which most samples showed relatively good polarity determinations (see Appendix 11).

6.4.3) Kruibeke section.

The 30 m section is controlled by 80 sampling sites. The dominant polarity interval within this section is reversed, mainly lying in its upper part and with a thickness of about 17 m. In the lower part of the section there are two separate normal polarity intervals termed KB1 and KB2. Fig.6.3.15c indicates this pattern with its lithological references.

43 sampling sites define the upper long reverse interval, of which 70% of the samples exhibit clear reverse magnetic polarity, defined either by SEPs and CMDs or directional trends. However, 22% of the samples in this interval show normal polarity behaviour during a.f. demagnetisation (see Appendix 12). These samples are nearly uniformly distributed throughout the whole reverse interval, particularly, in the upper 13 m section from septarian layers S5 to S8, where 4 apparent pyrite layers could be recognized. These samples may have acquired their normal polarity during the second diagenesis stage (Vandenberghe 1978) (see Chapter V). This may have occurred not only in the present geomagnetic field, but also during the Late Oligocene period, when the field was dominated by normal polarity events.

The normal polarity interval, KB1, is very distinct from the overlying reverse polarity interval which is defined largely from SEPs and CMDs. 14 sampling sites defined this interval, which has a thickness of about 7.5 m. Its upper boundary is very clear but the lower one is blurred by a mixture of normal and reverse polarities. About 20% of the samples in the lower part of this interval showed erratic behaviour, as shown in Fig.6.3.19.

The KB2 magnetozone is separated from KB1 by a 3.3m reversed polarity interval. However, the latter interval is poorly-defined with nearly half of the samples in it exhibiting erratic behaviour. Its existence could be identified by distinct normal polarity intervals in its upper and lower parts. Magnetozone KB2 is relatively well-defined, particularly in its upper part. Its lower boundary is defined by a short reverse polarity interval, about 0.5 m, from the bottom of the

section.

6.4.4) Correlations of magnetic polarity sequences for the Boom Clay Formation.

Detailed lithological and biostratigraphical investigations of the Boom Clay Formation by Vandenberghe (1978) and other authors provide a good basis for determining a magnetostratigraphic correlation of the Boom Clay Formation sections in the Antwerp area.

Fig.6.4.1 summarizes the three magnetic polarity sequences defined for the Boom Clay. The St.Niklaas and Steendorp quarries are separated by a distance of 10km almost along the strike direction in this area (Fig.5.3.1). Both sections lie in the part below septarian layer S3 (Fig.5.3.2). The magnetostratigraphic sequences can be correlated quite clearly between these two sections by which zone SN1 is linked to zone SD1. However, this comparison is not complete due to the incomplete lower boundary of the SD1.

The Kruibeke section starts from the base of septarian layer S3, which is about 2 m higher than the upper boundary of the Steendorp section. Therefore, its lowest reverse polarity interval can be naturally linked to the continuation of that at the top of the St.Niklaas and Steendorp sections.

Fig.6.4.1e illustrates a composite magnetic polarity sequence from the three separate sections. The normal polarity magnetozones are renamed as BC1, BC2 and BC3 from the top to the bottom. In Fig.6.4.2 this pattern of magnetozones is compared to the Oligocene GPTS of Berggren (1985). The only reasonable magnetic polarity pattern in the GPTS which is broadly compatible with the overall biostratigraphic evidence from the Boom Clay formation, is the sequence from Chron C11 to the upper part of Chron C12 (Fig.1.3.4). Chron C10 does not appear to be correlable with the observed pattern. Therefore, magnetozones BC1 and BC2 are tentatively correlated with the normal polarity intervals within Chron C11. The long reverse interval above BC1 can be compared with the reverse polarity Chron C10R, which is still within

the range of nannofossil zone NP23. Zone BC3 can be correlated with Chron C12N.

In a large scale correlation of the Oligocene beds from both Northwest Belgium and Southwest England, the Rupelian Boom Clay Formation can, to some extent, be compared with the Bovey Formation. Fig.6.4.3 illustrates the correlation. It is possible to match the magnetozones as shown. This correlation suggests that the part of the Bovey Formation studied represents a longer period than the part of the Boom Clay Formation studied, with the former extending upwards to the bottom of Chron C10N and its lower part extending downwards into the long reverse polarity interval of Chron C12. Therefore, the part of the Bovey Formation studied seems to represent a time span of about 30.25 to 34.5-35.0 Ma. The Bovey Formation also has a greater thickness (about 75 m) than the part of the Boom Clay Formation which was sampled for about 43m The reliability of this magnetic correlation depends strongly on the estimated age of the Bovey Formation, for which biostratigraphic data are very scare.

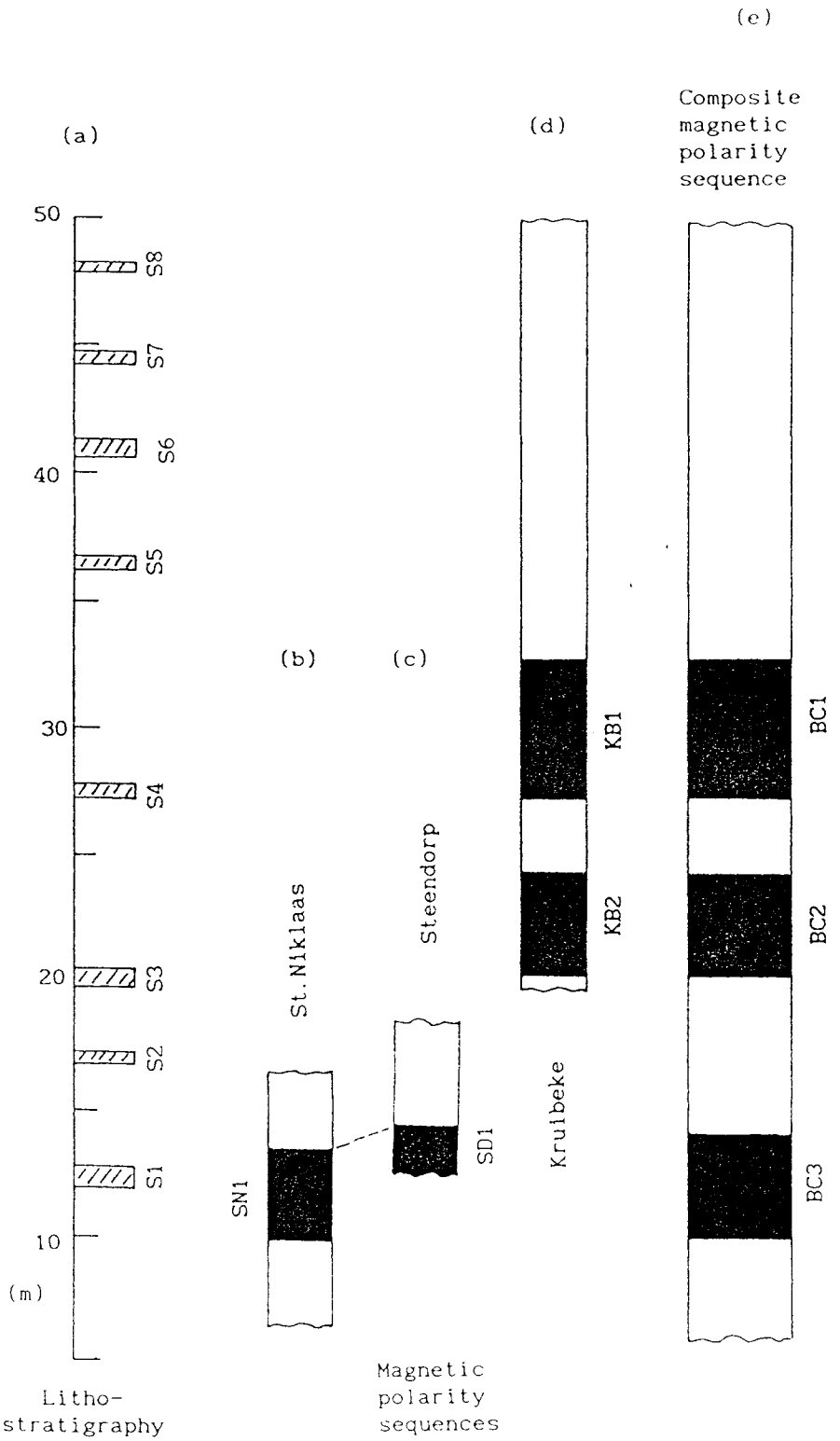

Fig.6.4.1 Summarized magnetic polarity sequences produced from the Boom Clay Formation. (a) Stratigraphic height with sptarian layers shown (see Fig.5.3.2), (b)-(d) magnetic polarity sequences from the three sections and (e) the composite magnetic polarity sequence in which the normal polarity events are termed BC1-3. Symbols and conventions as in Fig.4.1.4.

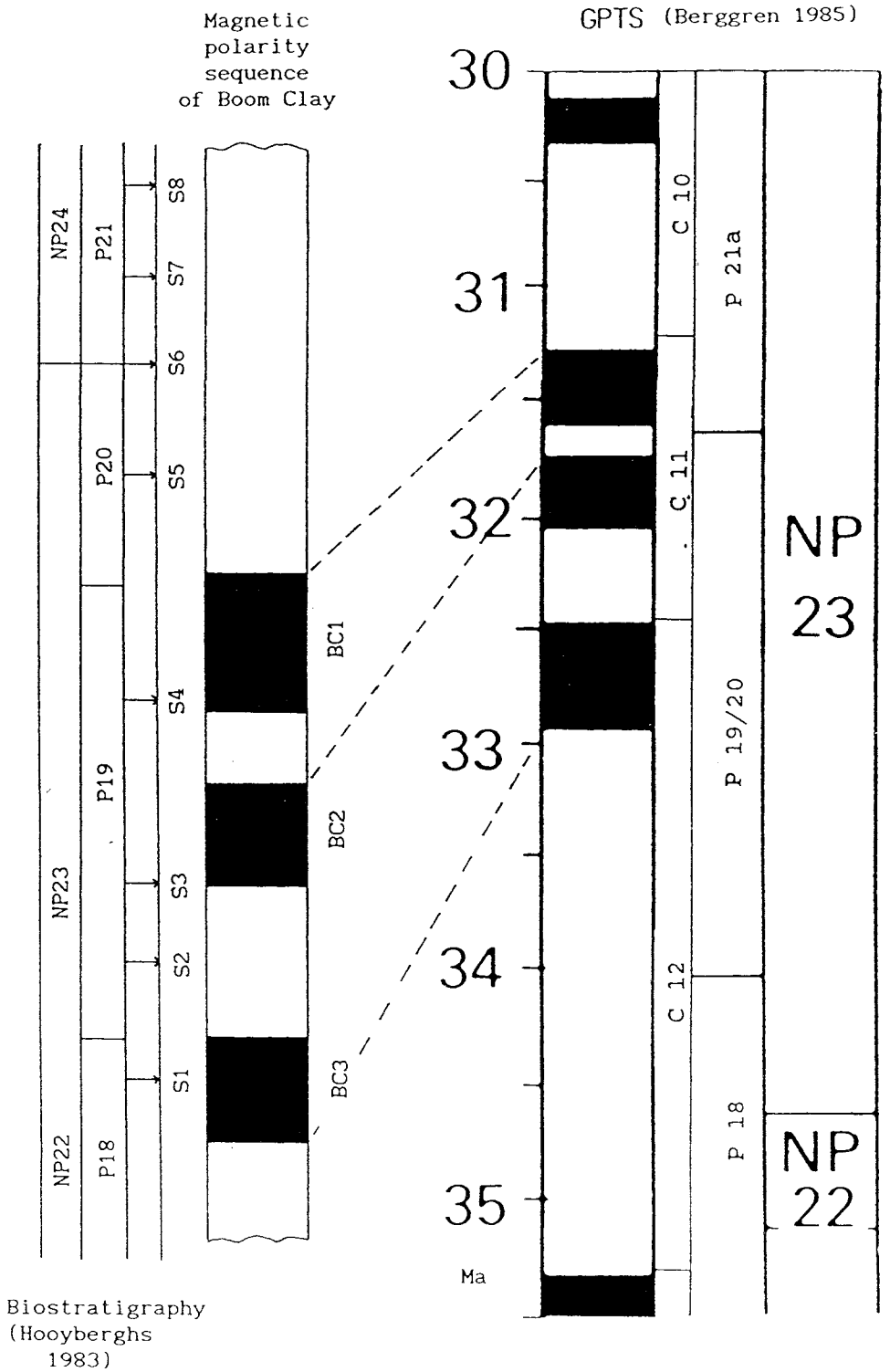

Fig. 6.4.2 Correlation of the magnetostratigraphic sequence from the Boom Clay formation with the GPTS of Berggren (1985). The left column shows biostratigraphic evidence produced from this formation (Hooyberghs 1983). Other symbols and conventions as in Fig. 4.1.3.

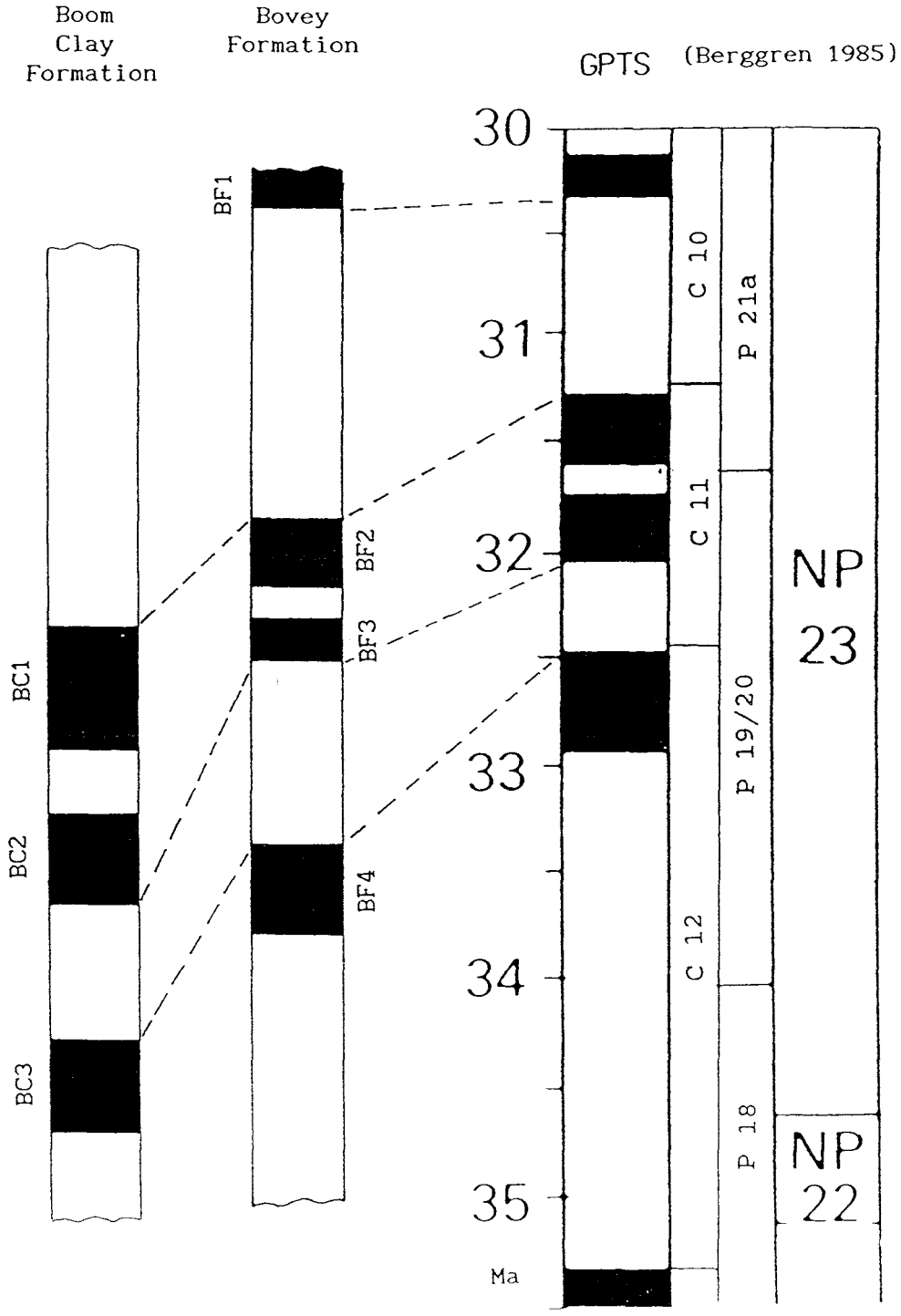

Fig.6.4.3 Provisional magnetostratigraphic correlation between the Boom Clay Formation and the Bovey Formation. Symbols and conventions as in Fig.4.1.3.

CHAPTER VII PRINCIPLES AND METHODS OF MAGNETIC FABRIC ANALYSIS

§7.1. Anisotropy of magnetic susceptibility (AMS)

7.1.1). Magnetic susceptibility and its anisotropy.

Magnetic susceptibility is defined by the relation

$$\left.\begin{aligned} M &= k \cdot H \\ \text{or alternatively } J &= \kappa \cdot H = \frac{\kappa}{\mu_o} B \end{aligned}\right\} \qquad (7.1.1)$$

where a magnetisation per unit volume, M, or per unit mass, J, is induced in a material with volume susceptibility k or mass susceptibility κ by an applied field $B = \mu_o(H + M)$. μ_o is the permeability of freespace. k is dimensionless and the units of κ are m^3/kg. Ferromagnetism (or antiferromagnetism, carried by materials like hematite) is associated with irreversibility and dependence of susceptibility on the magnitude of the applied field, except in sufficiently low applied fields. This "initial susceptibility" defined by equation 7.1.1 is a most important property of materials in palaeomagnetic research.

In general, magnetic susceptibility varies with direction in rocks, ie it is anisotropic. Magnetic susceptibility anisotropy in sediments was first subjected to detailed investigation by Ising (1942). The magnetisation of a rock in a weak magnetic field is related to the intensity of field by

$$\begin{pmatrix} M_1 \\ M_2 \\ M_3 \end{pmatrix} = \begin{pmatrix} k_{11} & k_{12} & k_{13} \\ k_{21} & k_{22} & k_{23} \\ k_{31} & k_{32} & k_{33} \end{pmatrix} \cdot \begin{pmatrix} H_1 \\ H_2 \\ H_3 \end{pmatrix} \qquad \ldots (7.1.2)$$

where M_i (i=1, 2, 3) are the components of the magnetisation vector along three orthogonal axes, H_j (j= 1,2,3) the vector components of the intensity of magnetic field and the set of constants k_{ij} ($k_{ij} = k_{ji}$) represents the components of a symmetric tensor of second rank, called the susceptibility tensor, which relates the magnetic medium to the

applied field in a three dimensional way. The components of the susceptibility tensor are in general non-zero, but there exists an orthogonal coordinate system in which the non-diagonal components of the susceptibility tensor are zero and the above equation becomes

$$\begin{pmatrix} M_1 \\ M_2 \\ M_3 \end{pmatrix} = \begin{pmatrix} k_{11} & & \\ & k_{22} & \\ & & k_{33} \end{pmatrix} \cdot \begin{pmatrix} H_1 \\ H_2 \\ H_3 \end{pmatrix} \qquad \ldots(7.1.3)$$

The components $k_{ii}(i=1,2,3)$ are called the principal susceptibilities and their directions the principal directions. They are usually referred to as the maximum, intermediate and minimum susceptibility axes (k_{max}, k_{int} and k_{min}) (Hrouda 1981).

7.1.2) Magnetic anisotropy in sedimentary rocks.

The possible causes of magnetic anisotropy of rocks are summarized by Banerjee and Stacey (1961) as the following: 1) shape alignment of ferro- and ferrimagnetic grains, 2) lattice alignment of crystals with magnetocrystalline anisotropy, 3) alignment of magnetic domains, 4) stringing together of magnetic grains, 5) stress-induced anisotropy and 6) exchange anisotropy. Further investigation (see Bhatal 1971) has shown that the most important factors controlling the magnetic anisotropy of natural rocks are (1) and (2).

A common purpose of the study of the magnetic anisotropy of sediments is to obtain information on the depositional process of ferromagnetic grains. It has been found (eg Rees 1966,1968,1971; Hamilton 1967; Hamilton *et al* 1968, and Rees & Woodall 1975) that the orientation of ferromagnetic minerals in sediments is affected by several factors. The first and most important factor is the Earth's gravity field, the action of which causes the mineral particles to be deposited with their large surfaces lying flat, parallel to the depositional surface. If the bottom is gently sloped, the grains may roll along the bottom and orientate their long axes approximately parallel to the contour line. On steeper slopes the long axes of grains are oriented much more parallel to the dip direction, according to the laboratory depositional experiments of Rees (1966).

The second important factor is the hydraulic shear exerted by water currents during deposition, which tends to orientate the longer axes of grains parallel to the flow lines. The third important factor is the geomagnetic field, which tends to orientate the longer axes of the ferromagnetic grains parallel to the local magnetic meridian. It has been found that the preferred orientation of ferromagnetic minerals in sedimentary rocks is controlled primarily by the gravitational and hydrodynamic factors, while the geomagnetic field only influences grains smaller than about 0.03-0.05mm (Hrouda 1981). The minimum susceptibility directions have been found to be perpendicular to the bedding under still water sedimentation regimes but these axes may be imbricated by fluid flow or downslope movement. If the ferromagnetic fraction is represented by a magnetically isotropic mineral such as magnetite, the magnetic lineation (defined by the orientation of the maximum susceptibility axis) is usually parallel to the current direction and plunges slightly against the current.

§7.2 Instrumentation and expression of anisotropy of magnetic susceptibility (AMS)

7.2.1) Susceptibility bridge.

An equal impedance bridge system was employed in the present study to determine the bulk susceptibility of samples. This was manufactured by Highmoor Electronics Ltd. Plate 7.2.1 shows the instrument. The bridge has two air-cored coils and two resistances forming an equal impedance bridge (Fig.7.2.1). It is adjusted by mechanically moving a ferrite bar within a set of coils and by setting an adjustable resistance on one of the arms. The instrument is tuned so that the inductance of the pick up coil is set at a suitably low level.

The pick up coil provides an alternating field of 0.01 mT over the sample from an input of a few volts. Sensitivity is controlled by the amplifier with 4 attenuator ranges in which ranges 0 and 1 are for the strongest susceptibility samples and range 3 for the weakest. The measurements are calibrated by different calibration samples, which have various standard values of susceptibility, suitable for different measured samples. Table 7.2.1 lists their constituents and their values.

Table 7.2.1 Constituents and volume susceptibility values for calibration samples.

sample code	type	bulk susceptibility cgs units	bulk susceptibility S.I units	appropriate attenuator position
1	$CuSO_4$	87.3×10^{-6}	1.097×10^{-9}	3
3	$CuSO_4$	84.4×10^{-6}	1.061×10^{-9}	3
2	$(NH_4)SO_4$	292.4×10^{-6}	3.674×10^{-9}	2
4	$(NH_4)SO_4$	439.2×10^{-6}	5.519×10^{-9}	2
6L135-1	rock with	2940×10^{-6}	36945×10^{-9}	1
6L016-2	magnetite	58700×10^{-6}	737.64×10^{-9}	0

N.B: To convert "bulk" susceptibility values in S.I units to "volume" susceptibility divided by volume in m^3.

Three readings on the output meter are taken for each measurement, the first and the third readings being for the fully balanced bridge

without any sample in the pick up coil and the second when the sample is inserted in the coil, thus disturbing the balanced inductance of the circuit. The first and third readings for the balanced bridge should be as close as possible and a wide difference between them reflects instrument drift. Before and after a set of measurements, calibrations of the instruments are carried out carefully to yield a reliable reference for deflections caused by the measured samples.

The relation, $k_s = k_c \cdot d_s/d_c$, was used to work out the bulk susceptibility of the sample measured, where k_c and d_c are the standard volume susceptibility and deflection for the calibration sample, k_s and d_s are the calculated bulk susceptibility and the deflection due to the rock sample. Because the volume of all samples in the present study is almost the same, a rapid comparison of bulk susceptibility among them is facilitated.

7.2.2) Low field torque magnetometer (LFTM).

The method of measuring magnetic anisotropy in terms of the coupling acting on a sample suspended in a magnetic field has been described by Blackett (1952). Ising (1942) designed a form of torque magnetometer in the early days of AMS investigation. King and Rees (1962) gave more details about the torsion balance and evaluated this method of magnetic anisotropy determination (based on a version of Granar's (1958) instrument). An analogous version of the low field torque magnetometer was employed in the present study to determine the AMS properties of the Wealden samples.

Plate 7.2.2 shows the LFTM. The basic principle of the torsion method is measurement of the torque exerted on an anisotropic sample in an applied alternating field, due to the non-parallelism between the field and the induced magnetisation. If magnetic anisotropy is present then the axis of greatest susceptibility, which causes the induced magnetisation, will always tend to turn parallel to the applied field. According to Fig.7.2.2, the components of induced magnetisation along the axes are

$$\begin{cases} M_1 = Hk_1 \cos\theta \\ M_2 = Hk_2 \sin\theta \end{cases} \qquad \ldots(7.2.1)$$

where k_1 and k_2 are the maximum and minimum (principal) susceptibilities in the horizontal plane. The torque exerted on each induced component, along k_1 and k_2, is $BP=\mu_0 HP$, where P is the induced magnetic moment perpendicular to H. Therefore, the effective torque T acting on the sample is

$$\begin{aligned} & T + BP_2 \cos\theta = BP_1 \sin\theta \\ \therefore\ & T = B\,(P_1 \sin\theta - P_2 \cos\theta) \\ & = B\,(\upsilon Hk_1 \sin\theta \cos\theta - \upsilon Hk_2 \cos\theta \sin\theta) \\ & = \frac{1}{2}\,\mu_0 H^2 \upsilon\,(k_1 - k_2) \sin 2\theta \qquad \ldots(7.2.2) \end{aligned}$$

where υ is the volume of the sample. Thus, as the field direction is rotated through 360°, the deflection of the system describes a $\sin 2\theta$ curve, the amplitude of which is proportional to (k_1-k_2) (Collinson *et al* 1967). Granar (1958) developed a method for calculation of the magnetic susceptibility principal axes directions and magnitude from the torque magnetometer measurements. A computer programme is available in the palaeomagnetic laboratory to carried out these computations.

Fig.7.2.3 shows the basic configuration of the LFTM (from King and Rees 1962). The sample holder is suspended from a rigid arm and is located in the centre of a pair of Helmholtz coils, which are separately mounted (to minimize vibrational disturbance). These coils can be manually rotated about the sample holder. Motion of holder is damped by means of disc attached to its base and immersed in an oil bath. The viscosity of the oil is adjusted to provide critical damping. The sample holder is suspended from a fine metal fiber which experiences a torque when the suspended sample is subjected to the applied alternating field. An alternating current is generated and passed through the coils to produce an alternating field of ~5mT upon the sample.

The rotation of the sample is observed by means of a reflected

light beam from a small mirror which is attached to the sample holder. Deflection of the light beam is observed on a translucent ruler, which is graduated in 1 mm divisions. Separate observations for three orthogonal plane, x-y, y-z and z-x, are carried out and five deflections for each plane are measured at 45° intervals, during rotation of the coil through 180°.

Three readings are taken for determining each deflection, the first and last representing "zero" readings, with no current flowing through the coils, and the second that caused by application of the applied field. A simple equation is used to work out the deflection with regard to the "zero" reading, $M_2-(M_1+M_3)/2$ where M_i (i= 1,2,3) are the three readings. The background readings M_1 and M_3 should be as close as possible to give a reliable reference. The 15 readings of torsional deflections for three orthogonal planes were then input into the computer, combined with the bulk susceptibility value for the measured sample, to work out the principal susceptibility directions.

7.2.3) High field torque magnetometer (HFTM).

The basic principle of high field anisotropy measurements is the measurement of the torque exerted on a sample by an applied direct magnetic field due to the anisotropy as the sample is rotated to different azimuths about an axis perpendicular to the field. The torque is given by $T= dE/d\theta$, where E is the energy of magnetisation of sample and θ is the direction of the applied field. T takes the general form

$$T = T_o + T_1 \sin(\theta+\delta) + T_2 \sin 2\theta + T_4 \sin 4\theta + T_6 \sin 6\theta \quad \ldots(7.2.3)$$

where θ is the angle between the field direction and a reference direction fixed in the sample. T_o is due to rotational hysteresis and the $T_1 \sin(\theta+\delta)$ term can arise from inhomogeneous distribution of susceptible material in the sample, non-uniformity of magnetic field or asymmetries in the torque system. The T_2, T_4, T_6, etc terms arise from anisotropy of different types, in which only $\sin 2\theta$ terms arise from shape anisotropy in magnetic particles. Crystalline alignment of cubic minerals (titanomagnetites), textural anisotropy and anisotropy induced

in isotropic material by stress will mainly contribute to other terms (Stacey 1963, Banerjee 1963, Collinson 1967).

Plate 7.3.1 shows the main feature of the HFTM. and Fig.7.2.4 shows a schematic diagram of the system. The sample suspension is mounted on a rigid arm, which is firmly fixed to the wall. The sample holder is attached to a non-magnetic plastic rod, which is suspended from the arm by jeweled bearings. A feedback circuit presents deflection of the sample holder during measurement and the feedback current provides a measure of the torque exerted. The detection device is a split-photocell receiving a light beam reflected from a mirror attached to the suspended system. A strong current flowing in a pair of water-cooled coils produces a strong direct magnetic field, ~0.7 T, between the two poles, which are separated by a gap of 68.9 mm with the measured sample sitting in the middle of the field.

The rotation of the magnetic field produced by the electromagnet is controlled by a motor system which allows the field to turn 360° around the sample and then return to the initial direction. The voltage in the feed back circuit provides the signal input for the Y axis of an X-Y plotter. In order to display the angular position of the magnet with regard to the sample, 8 micro-switches are arranged at 45° intervals around its base; a cam operates these, and via an electrical connection, raises and lowers the recorder pen giving a precise indication of the magnet's position on the drawn curve.

Calibration of the HFTM is carried out by generating a known current and producing a reference deflection; thus, the amplitudes of the torque curves can be measured relative to it. The calibration value is constant for any one gain setting on the x-y recorder and is input to the computer programme, together with the amplitudes of the torque curves, digitised at 45° intervals.

The curves are digitized using the five values from 180° to 360° as the curves were found usually to be unstable from 0° to 180°. As with the low field method, 15 values of deflections are required, five for each of the three orthogonal axes.

It is necessary to avoid anisotropy signals arising from the shape of the samples themselves. Porath *et al* (1966) have studied experimentally the optimum length/diameter ratio for cylindrical samples for high field measurements, ie. the value of ℓ/d for which the difference between the demagnetizing factors parallel and perpendicular to the cylindrical axis is zero. They suggested a small dependence of optimum ℓ/d on field strength, namely ℓ/d=0.88 at B=1.2T, 0.89 at 1.7T and, by extrapolation, 0.90 at infinite field strength. In the present study the ℓ/d ratio adopted was ≈0.88, with the diameter of sample being 2.6cm (which depends on the inner diameter of the sampling copper tube) and the height of the sample being 2.25-2.3cm which, being cut in laboratory.

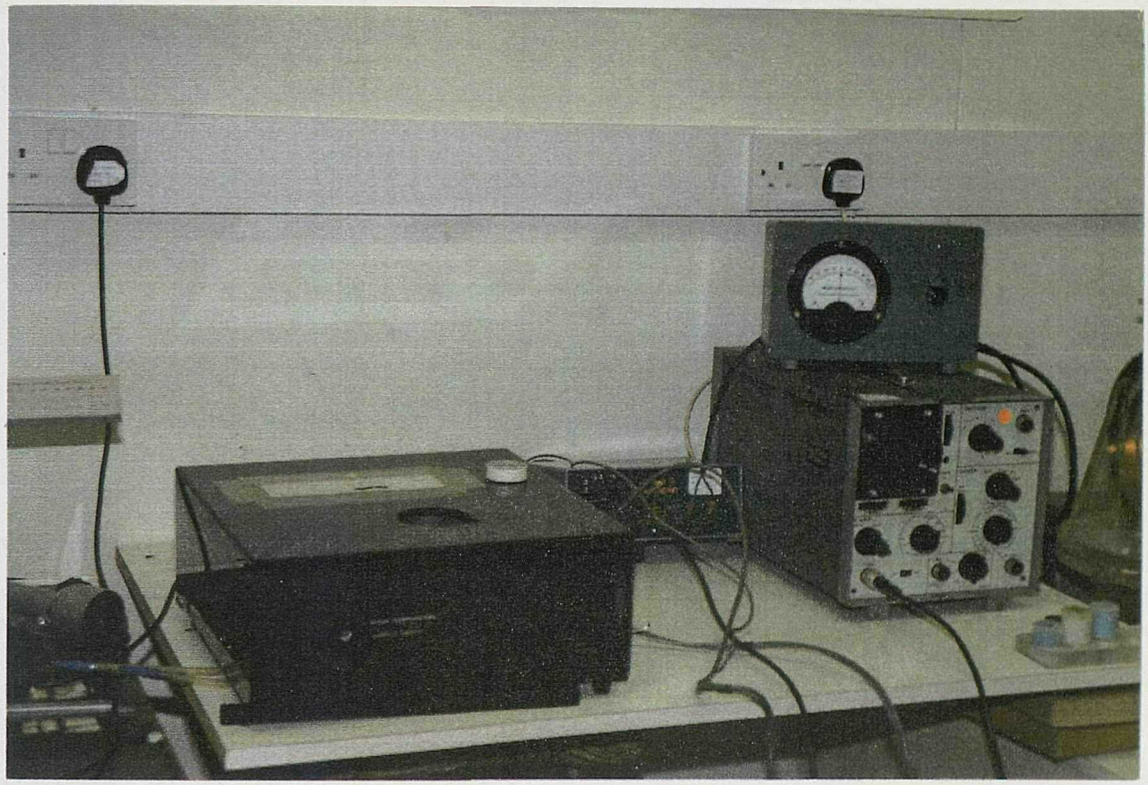

Plate 7.2.1 Highmoor susceptibility bridge.

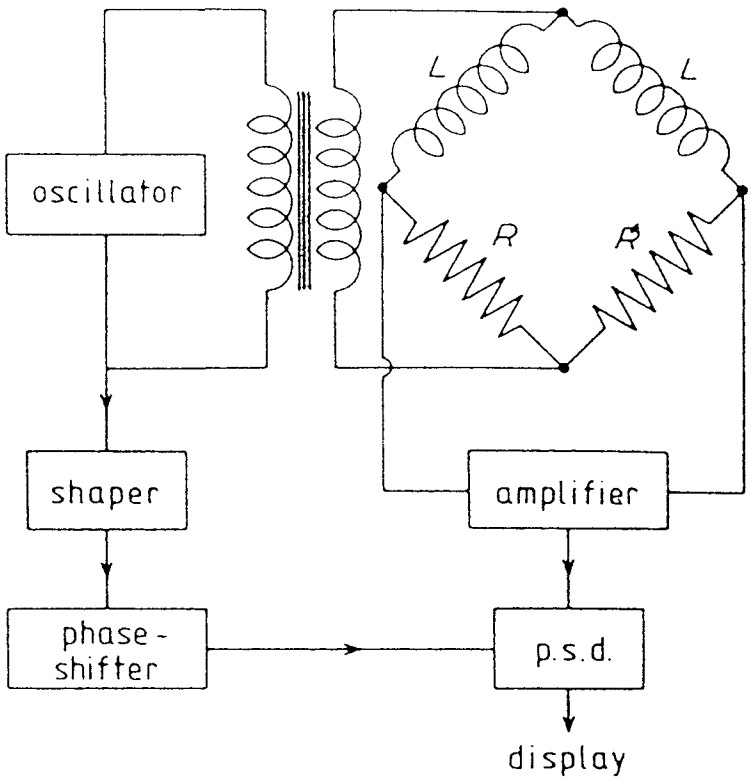

Fig. 7.2.1 Configuration of susceptibility bridge circuit.

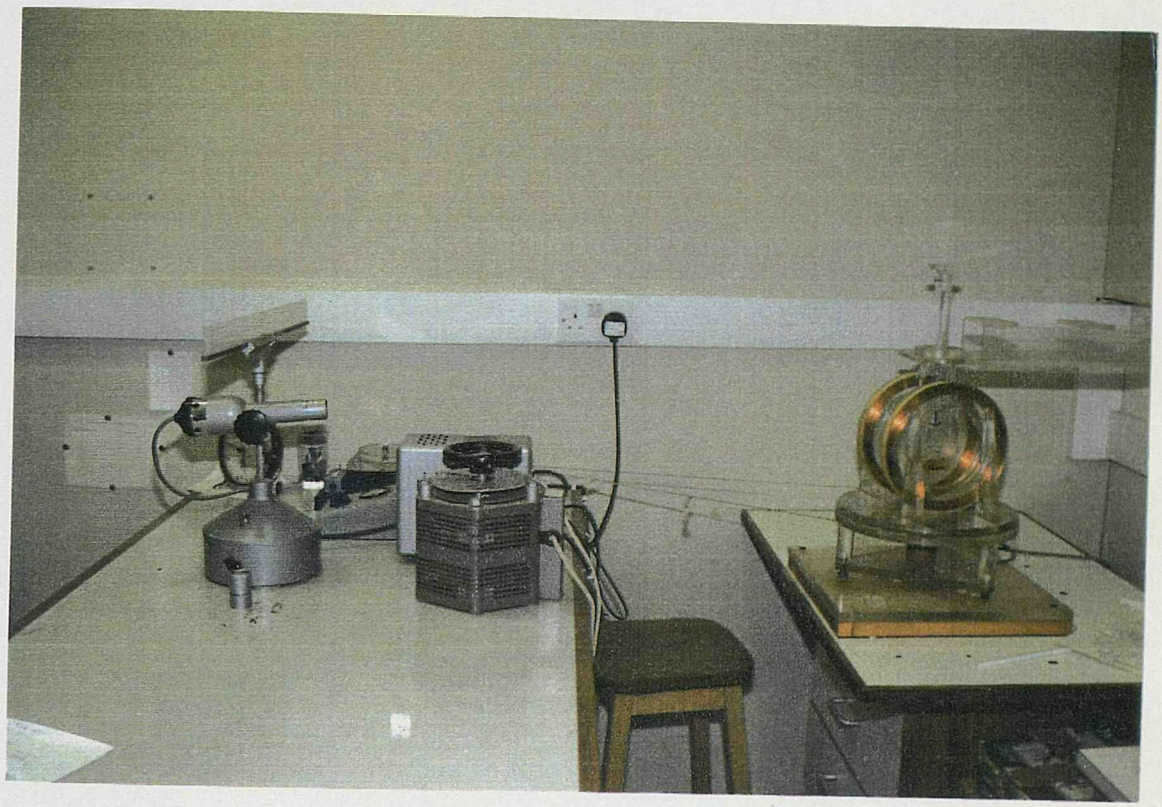

Plate 7.2.2 The low field torque magnetometer (LFTM) in the Oceanography Depatment Laboratory.

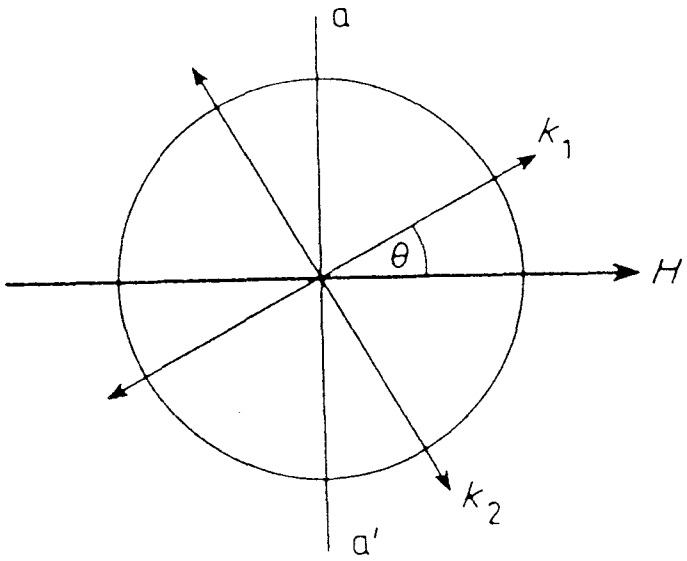

Fig. 7.2.2 Principle of torque magnetometer. H is the applied (direct or alternating) field, $k_1 > k_2$ are the maximum and minimum susceptibility axes within the rotation plane, a-a' is the perpendicular direction to H.

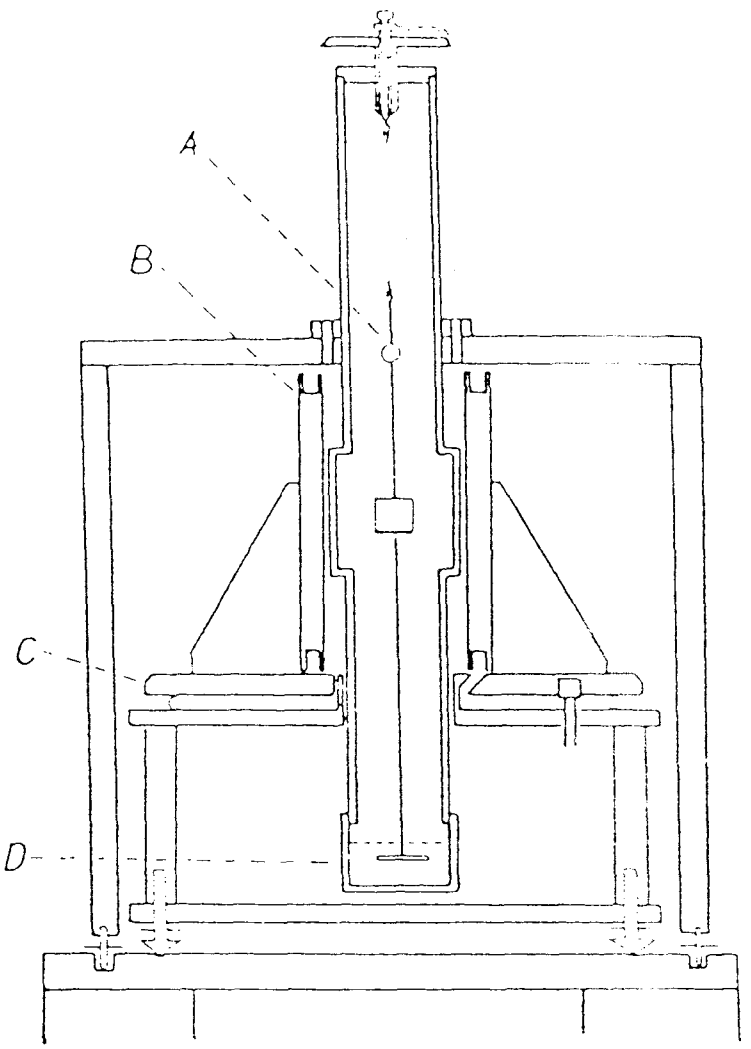

Fig.7.2.3 Basic configuration of the LFTM. (A) suspension system consisting of metal fiber, mirror and sample holder. (B) Helmholtz coils. (C) rotating platform for the Helmholtz coils. (D) damping oil cup.

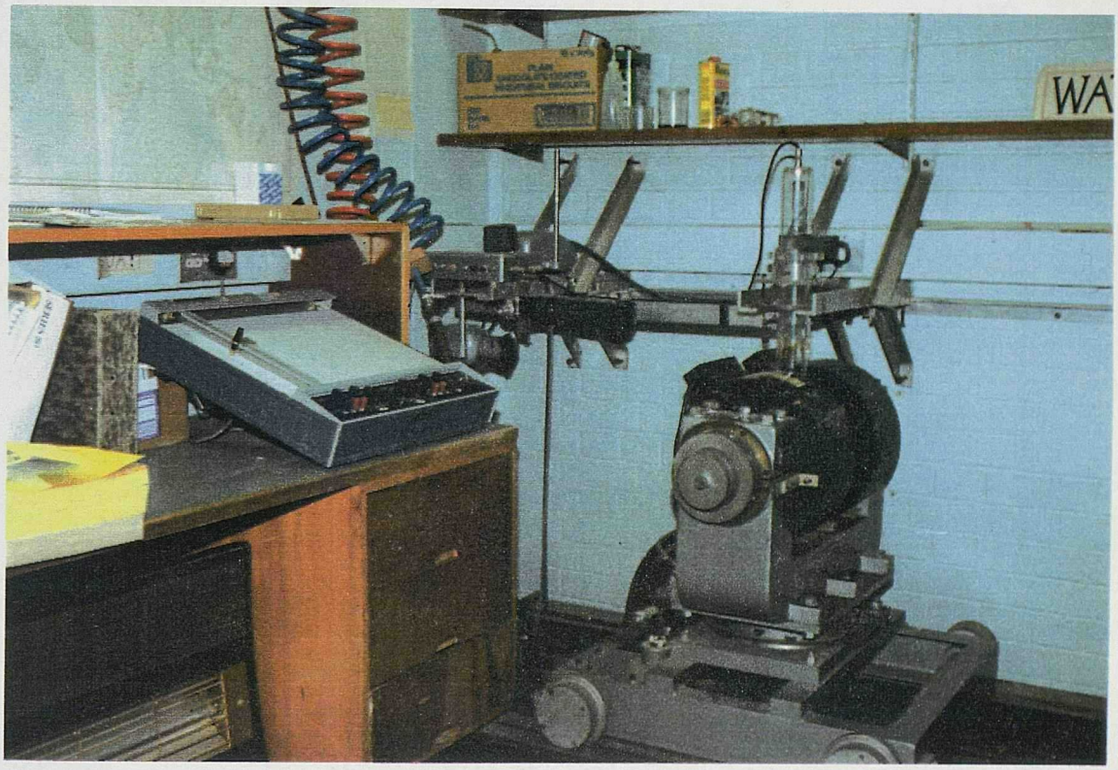

Plate 7.2.3 High field torque magnetometer.

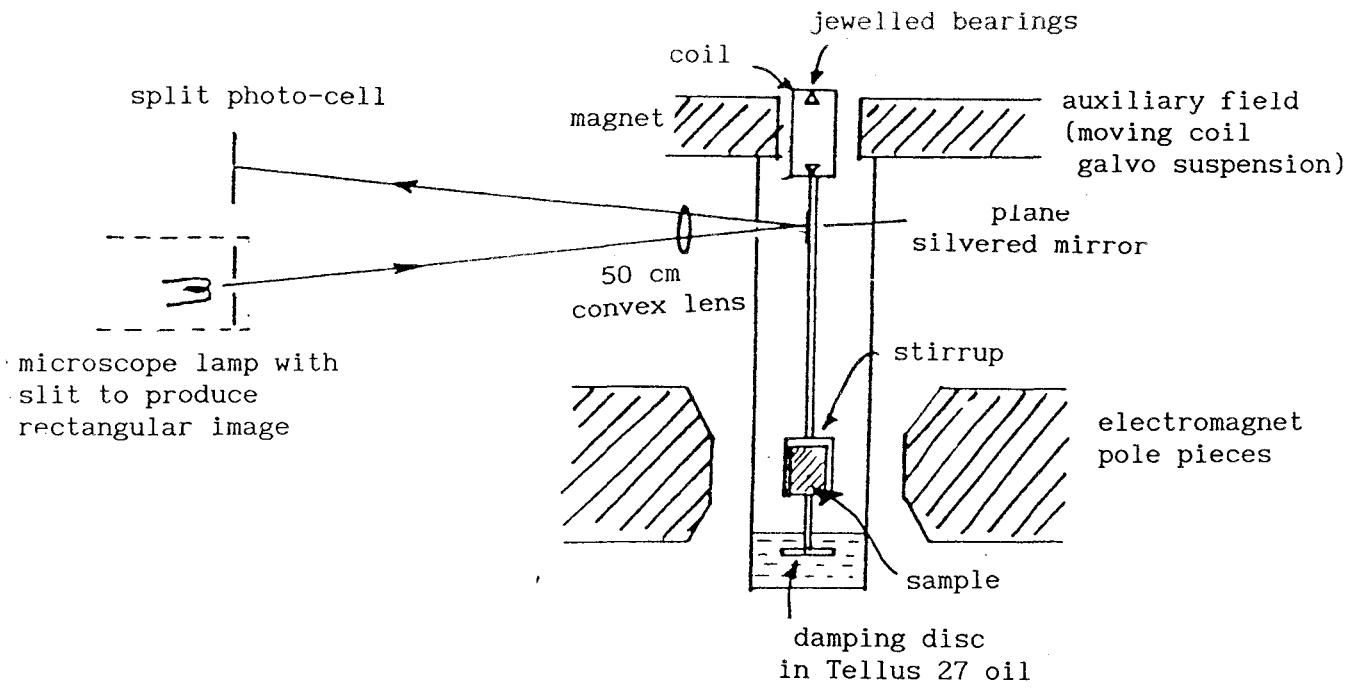

Fig. 7.2.4 Basic configuration of the HFTM.

§7.3 Expression of AMS and error estimates.

The shape and orientation of the susceptibility ellipsoid determined from the measurement of low-field anisotropy and the amplitudes and phases of the torque curves ($\sin 2\theta$) from high-field anisotropy are controlled by the fabric of ferromagnetic minerals in the rock. The degree of anisotropy can be described by means of suitably chosen ratio or differences between the principal susceptibilities. In the present study, the main interest is in attempting to define current flow directions, which might reflect the depositional environment. Therefore, the conventional parameters which were adopted to describe these properties are as follows:

1) Foliation of magnetic anisotropy: $F=(k_{int}-k_{min})/\bar{k}$ (Khan, 1962), where $\bar{k}= (k_{max}+k_{int}+k_{min})/3$. k_{max}, k_{int} and k_{min} are the maximum, intermediate and minimum susceptibility values, respectively. F characterises the intensity of the planar-parallel orientation of ferromagnetic minerals in a rock.

2) Lineation of magnetic anisotropy: $L=(k_{max}-k_{int})/\bar{k}$ (Khan, 1962), where the suffixes have the same meanings as in 1). L describes the intensity of linear-parallel orientation of magnetic minerals.

3) Anisotropy degree, h, is defined as $h=(k_{max}-k_{min})/\bar{k}$ (Owens, 1974). h indicates the intensity of preferred orientation of ferromagnetic minerals in a rock.

The direction of the magnetic lineation is defined as that of the maximum susceptibility and the magnetic foliation is characterized by the planar-parallel orientation of ferromagnetic minerals, which is perpendicular to the minimum susceptibility direction. In addition to the above simple formulae, many other parameters have been introduced. Hrouda (1981) summarized most of them, which have different applications for various purposes. However, none of them has been accepted universally and at present there are no objective criteria for deciding which formulae are the most appropriate (Hrouda 1981). Besides the magnitude parameters, the directions of the maximum and

minimum susceptibility axes can be illustrated on an equal area projection. For a depositional style fabric, the k_{min} direction is normally located close to the pole of projection and the k_{max} axes are located close to the perimeter of the projection.

A further two parameters were used in the present study for representing the quality of the measured data. The first is the "azimuthal anisotropy quotient", q, and the other the instrument error parameter, "G sum percent". The quotient q (Rees 1966) is expressed as

$$q = \frac{k_{max}-k_{int}}{(k_{max}+k_{int})/2 - k_{min}} \qquad \ldots(7.2.4)$$

and is used to provide an estimate of the intensity of the lineation in terms of that of the foliation. Studies of natural sediments, together with laboratory redepositional experiments under carefully controlled conditions, indicate that primary (depositional style) fabrics produced by grain-by-grain deposition commonly correspond with values of q in the range 0.06 to 0.67. Values outside this range frequently represent the effects of secondary processes, such as soft-sediment deformation due to slumping or coring disturbances, or the effect of bioturbation (Hamilton and Rees 1970). In the present study q values lying within the above range, together with k_{min} directions within 15° of the vertical (after bedding correction), are considered as indicative of a "primary style" magnetic fabric.

The second parameter, "G sum percent" or $\sum_{i=1}^{3} G_i\%$, was originally developed by King and Rees (1962) for LFTM measurements. The quantity G is defined in terms of the deflections, $G = \frac{1}{2}(d_2-d_4)$, where d_2 and d_4 are the deflections at 45° and 135° with respect to one of the sample coordinates. Because of the period of 2θ in the resultant curve yielded by rotating the field around the sample, the amplitude of d_2 and d_4 should be the same and G would represent a error estimation of the curve $\sin 2\theta$. $G \longrightarrow 0$, if the curve does not include higher frequency components and instrument errors that would deform the $\sin 2\theta$ curve. Conventionally, the G_i values are also expressed in terms of the mean amplitude of the three $\sin 2\theta$ curves, as $\sum_{i=1}^{3} G_i\%$. This parameter

gives a total estimate of errors introduced in measurements. It was found that, for laboratory depositional experiments the value is typically <30% (King & Rees 1966). However, there is not a fixed criteria for the the upper limit of this value. For example, Hailwood *et al* (1979) adopted a value < 40% for their determination of magnetic anisotropy of marine sediments.

It was found in the present study that most samples giving strong deflections on the LFTM produced G sum percent values generally less than 60%. However, for those with very weak deflections measured on HFTM, the value would increase considerably. Therefore, a maximum value of of 100% for $\sum G\%$ was adopted in the present study for the LFTM determinations and anisotropy data for samples with values outside this range were not accepted.

CHAPTER VIII RESULTS OF MAGNETIC FABRIC DETERMINATIONS AND THEIR SIGNIFICANCE FOR DEPOSITIONAL ENVIRONMENT

§8.1 Initial magnetic susceptibility values and their stratigraphic correlations.

The measurement of initial bulk susceptibility of samples, using the susceptibility bridge, has been described in the previous chapter and all samples were subjected to these measurements. A purpose of the determination of the initial susceptibility was to contribute to an understanding of the depositional environment, because the susceptibility of magnetic grains is mainly linked to the relatively large grains (Hrouda 1981).

8.1.1) Magnetic susceptibility data and correlations for the Wessex Formation of Southern England.

The standard susceptibility bridge measurement was applied to the samples from the southern coastal area of Dorset and the section studied on the Isle of Wight. For most of these sections, one sample, (which usually had been subjected to progressive a.f. demagnetisation), from each sampling site was chosen for the determination of bulk susceptibility. However, for some parts of the sections, eg the middle part of the Worbarrow Bay section, two or more specimens were measured from each site, to give more representative results.

For all samples, Attenuator position 2 of the signal amplifier on the susceptibility bridge was chosen. Calibration sample No.2 (see Table 7.2.1) was used, this having a volume susceptibility value of 3.67×10^{-3}SI units, which caused a deflection on the output meter of about 40-44 scale divisions. Samples from the Isle of Wight section produced deflections in the range from 10 to 40 scale divisions, while samples from other sections produced minimum deflection of 5 scale divisions.

Figs.8.1.1(a) to (e) summarize the statistical distributions of the bulk susceptibility values for each section from the Isle of Wight to Durdle Door. A general variation of the mean bulk susceptibility

values can be recognized along the coast of southern England, from the Isle of Wight section, which produces a log mean value of 2.282×10^{-3} SI unit, followed by Worbarrow Bay 1.144×10^{-3} SI, Mupe Bay 1.786×10^{-3} SI, Lulworth Cove 1.678×10^{-3} SI and Durdle Door section 0.6779×10^{-3} SI. This trend is similar to the NRM intensity variation in this area which also shows a general decrease from east to west. However, for the susceptibility values an exception is the Worbarrow Bay section, which yields a slightly lower mean value of susceptibility than the more westerly sections.

The variations of the bulk susceptibility values with stratigraphic height for all sections are indicated in Figs.8.1.2 to 8.1.6. These diagrams also show the main features of the lithological and magnetic polarity sequences, in order to facilitate comparisons.

In the Isle of Wight section (Fig.8.1.2), which has a dominant normal polarity, the upper part seems to have a distinctly higher susceptibility (depth range from 70 to 137 m). This interval is termed magnetic susceptibility event 1. The lower part of this section shows lower susceptibility values. The boundary is near the upper part of the Shippards Chine Sandstone layers. Around the Compton Grange Sandstone, there seems a possible decrease in the susceptibility values.

In the Worbarrow Bay section, the variation of susceptibility with stratigraphic height (Fig.8.1.3) is significantly different. Above the CQG layer, the susceptibility is generally high (depth range 168-315 m). This interval extends over most of the normal polarity interval in the upper part of the section. However, around the CQG (depth interval 155-165m), the susceptibility values show a very distinct decrease. This effectively separates the section into two parts, each having a relatively high susceptibility. These have been named magnetic susceptibility event 1 and 2, respectively. This variation pattern of the susceptibility values is totally different from that of the NRM intensity values for this section (Fig.4.1.9).

The Mupe Bay section, which can be compared with the upper part of the Worbarrow Bay section according to magnetostratigraphic evidence,

shows a similar pattern of variation of susceptibility values (Fig.8.1.4). The range of low susceptibility values occurs in the depth interval 100 to 150m and indicates the CQG layer (Fig.8.1.4c). This susceptibility variation pattern may be related to the presence of the CQG layer, which might represent a significant change in depositional environment. This pattern shows little similarity to the NRM intensity variation in this section (see Fig.4.1.16).

In the middle of the Lulworth Cove section, an interval of increased magnetic susceptibility values occurs around 65-128 m (Fig.8.1.5). This spans the boundary between the Wessex and Gault Formations. In the lower part of the section, in the depth interval 5 to 15m, there is a recognizable decrease of susceptibility values, which corresponds with the position of the CQG layer (Fig.8.1.5c). Therefore, this decrease range of susceptibility values might be correlated with that around the CQG layer in the Mupe Bay section.

In the Durdle Door section there is only one rise of magnetic susceptibility values, at the very bottom of the section (Fig.8.1.6a). This is termed susceptibility event 1. Above this, the magnetic susceptibility values remain low. The susceptibility variation pattern for this section shows little similarity to that of the other sections, particularly the Lulworth Cove section. However, if consider the potential Lignitic Quartz Grit layer at the bottom of the Durdle Door section (Fig.8.1.6c), the susceptibility "event 1" might compare with the localised increase of susceptibility values immediately below the CQG layer in the Mupe Bay section Fig.8.1.5a).

From the information discussed above, it may be concluded that the magnetic susceptibility values show a general decrease in the vicinity of the Coarse Quartz Grit (CQG) layers. This may represent a change in depositional environment. In general the magnetic susceptibility values show less distinct variations with stratigraphic height than the NRM intensity values discussed in Chapter IV.

8.1.2) Magnetic susceptibility data and correlations for the Weald Clay Formation, southeast England.

All samples from this formation have been subjected to measurements of initial susceptibility. Fig.8.1.7 displays the statistical distribution of susceptibility values, for which the log mean values is 2.664×10^{-3} SI units. This is somewhat higher than the values for the Wessex Formation of the Dorset coast. It might indicate that the two depositional basins had quite different environments and sedimentary sources. However, this value is not very different from that of the Isle of Wight section, although the two sections comprise totally different sedimentary materials (see Chapter III).

Figs.8.1.8a and b illustrate the magnetic susceptibility profiles for the southeast and northwest sections at Langhurst quarry. There is a short range with apparent increase of susceptibility values in the middle of the northwest section (Fig.8.1.8b), in the depth interval 5 to 6m, within the lower part of the normal polarity interval (see Fig.4.1.39c). However, in the southeast section (Fig.8.1.8a), there seems no significant increase in susceptibility values. According to the magnetostratigraphic evidence (Fig.4.3.1) the top of the southeast section may correlate with a stratigraphic height of 4 m in the northwest section, thereby explaining the absence of the susceptibility event in this section. There are no significant signs of increases or decreases of magnetic susceptibility values around the sand/limestone layers in the two sections.

8.1.3) Magnetic susceptibility data from the Bovey Formation, southwest England.

Like their NRM intensities, samples from the Bovey Formation have such a weak magnetic susceptibility character that the Attenuator position 3 on the susceptibility bridge had to be used. The calibration sample had a susceptibility value of 1.097×10^{-3} SI units and produced a deflection on the output meter of about 54 scale divisions. The deflections for most samples were in the range 12 to 25 scale divisions but a few produced stronger deflection, sometimes >60 scale divisions.

Fig.8.1.9 summarizes the statistical distributions of susceptibility values for the Bovey Basin sections. The log mean

values are 0.433×10^{-3} SI units for the Longmarsh section, 0.318×10^{-3} SI units for the John Acres Lane section and 0.2097×10^{-3} SI units for Borehole SD485. Fig.8.1.10 illustrates the variation of magnetic susceptibility with stratigraphic height for these three sections. Generally, the variations are small and so cannot be used for stratigraphic correlations.

8.1.4) Magnetic susceptibility data for the Boom Clay Formation, Northwest Belgium.

Systematic measurements of bulk susceptibility for samples from the Boom Clay formation were carried out using the Attenuator position 2 on the susceptibility bridge. Fig.8.1.11 illustrates the statistical distribution of the susceptibility values, with a log mean of 1.746×10^{-3} SI units. Fig.8.1.12 displays the variation of the magnetic susceptibility values with stratigraphic height for the three sections. There seems no obvious increase range for the susceptibility values and it keeps a constant variation throughout the whole formation.

A general comparison of the susceptibility records for the Boom Clay Formation with those from the Wessex formation of the Lower Cretaceous, shows that the marine sedimentary facies seem to give rather uniform magnetic susceptibility records compared with the continental facies sediments. The marine environment is likely to represent a more quiet and stable depositional environment, in comparison to the continental environment, which might be more variable and sensitive to local environment changes. It is imaginable that, if any major change in depositional condition, produced by climate, sedimentation, etc., occurred, then the marine sediment sequence might give a much clearer and higher resolution record from the magnetic susceptibility variation pattern than the continental facies sequence.

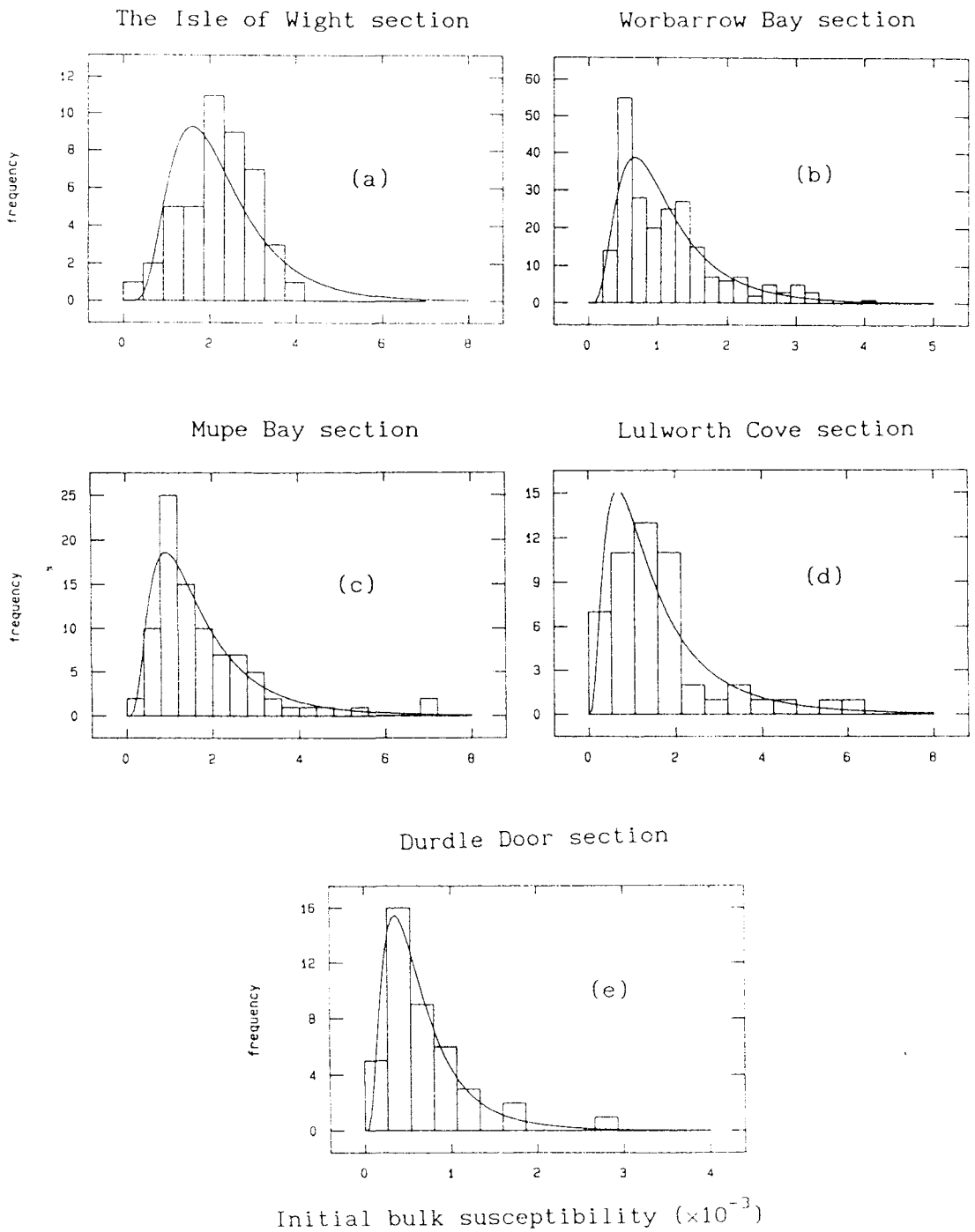

Fig. 8.1.1 Statistical distributions of bulk susceptibility values from the Lower Cretaceous beds of Southern England. The localities are shown on each diagram.

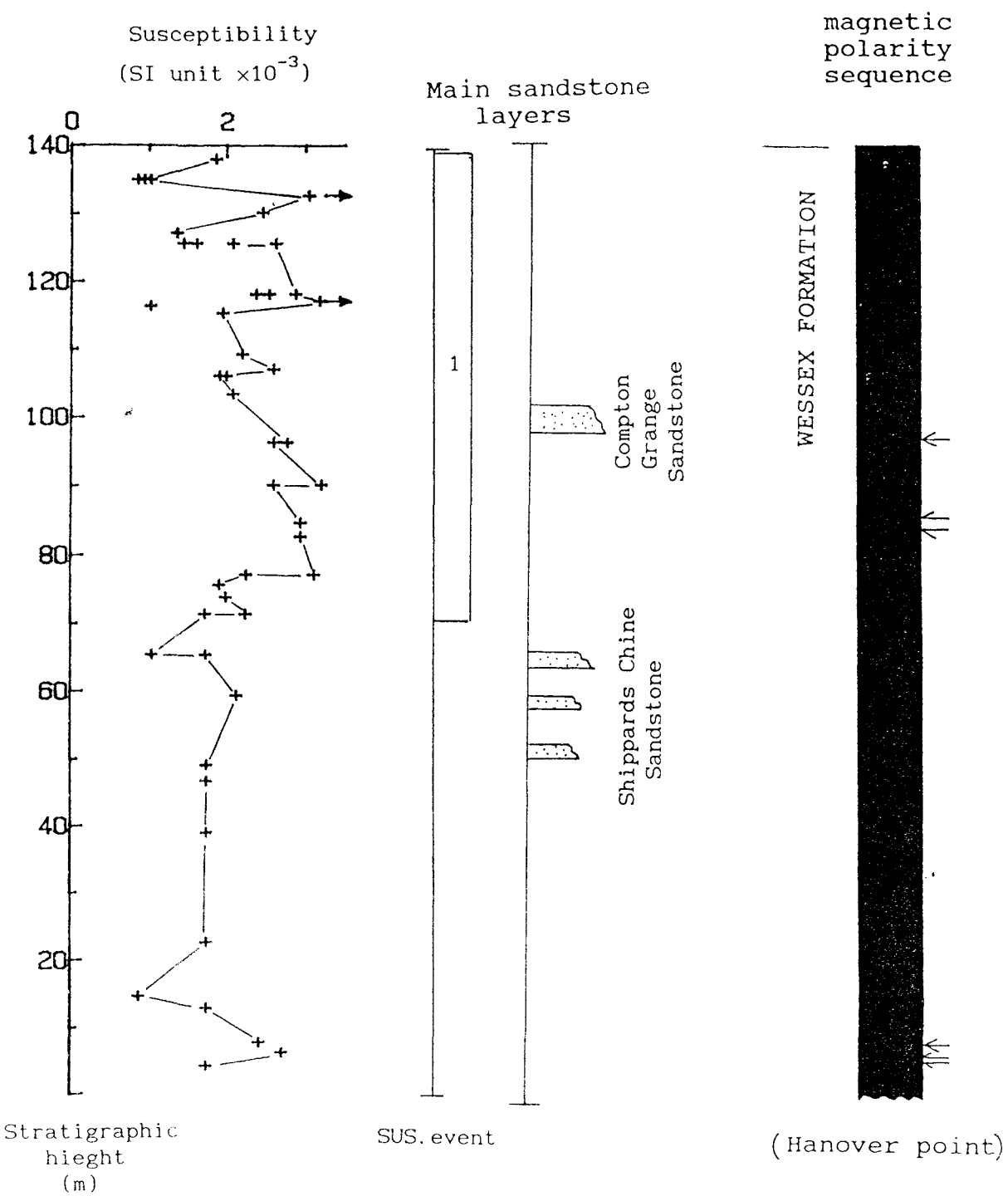

Fig. 8.1.2 Magnetic susceptibility and other relevant properties of the Isle of Wight section. (a) Variation of bulk susceptibility values with stratigraphic height, (b) recognizable susceptibility value "events", (c) main sedimentary features and (d) magnetostratigraphy. Other symbols and conventions as in Fig. 4.1.3.

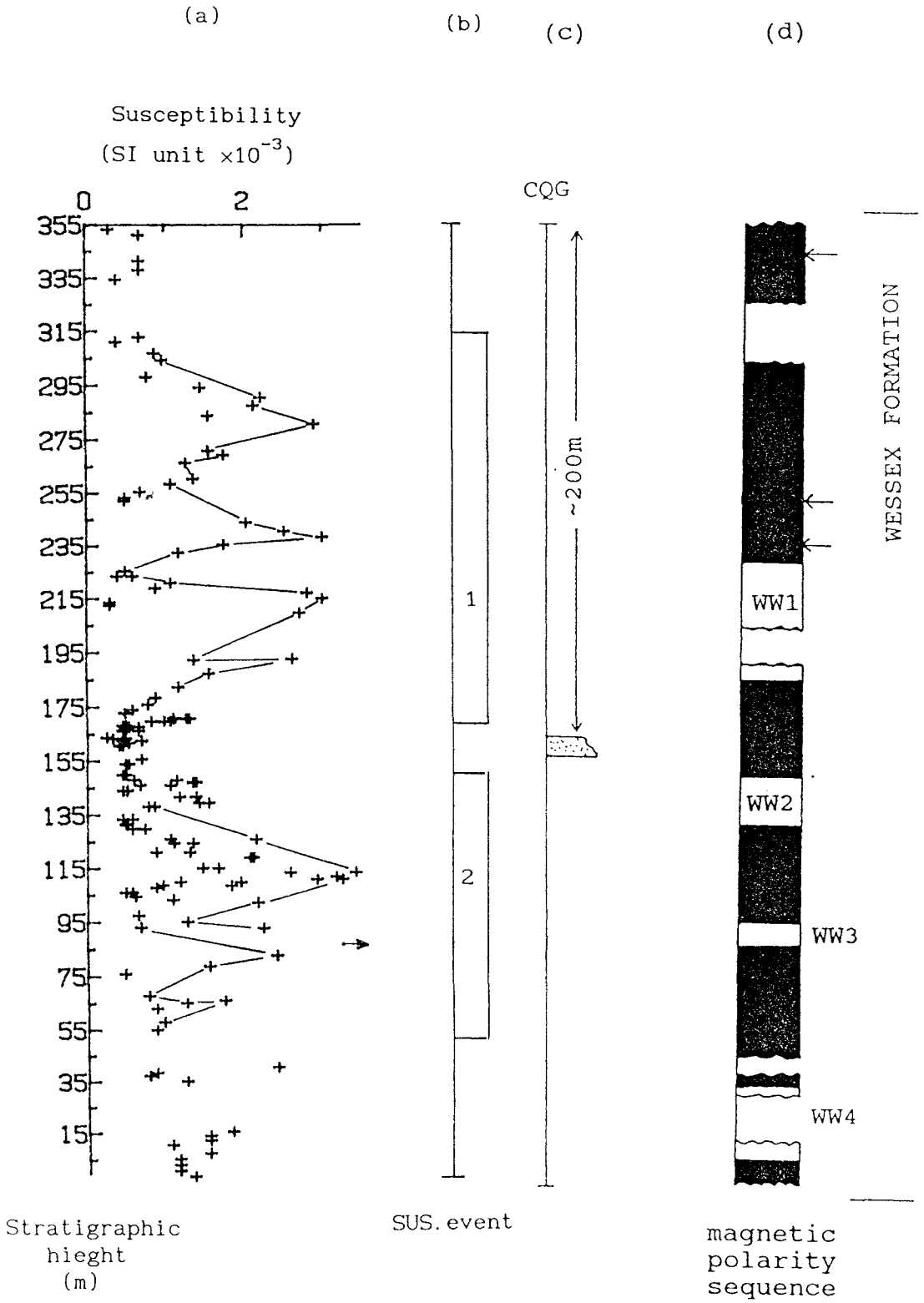

Fig.8.1.3 Magnetic susceptibility values and other relevant properties of the Worbarrow Bay section. Symbols and conventions as in Figs.4.1.3, 4.1.9 and 8.1.2.

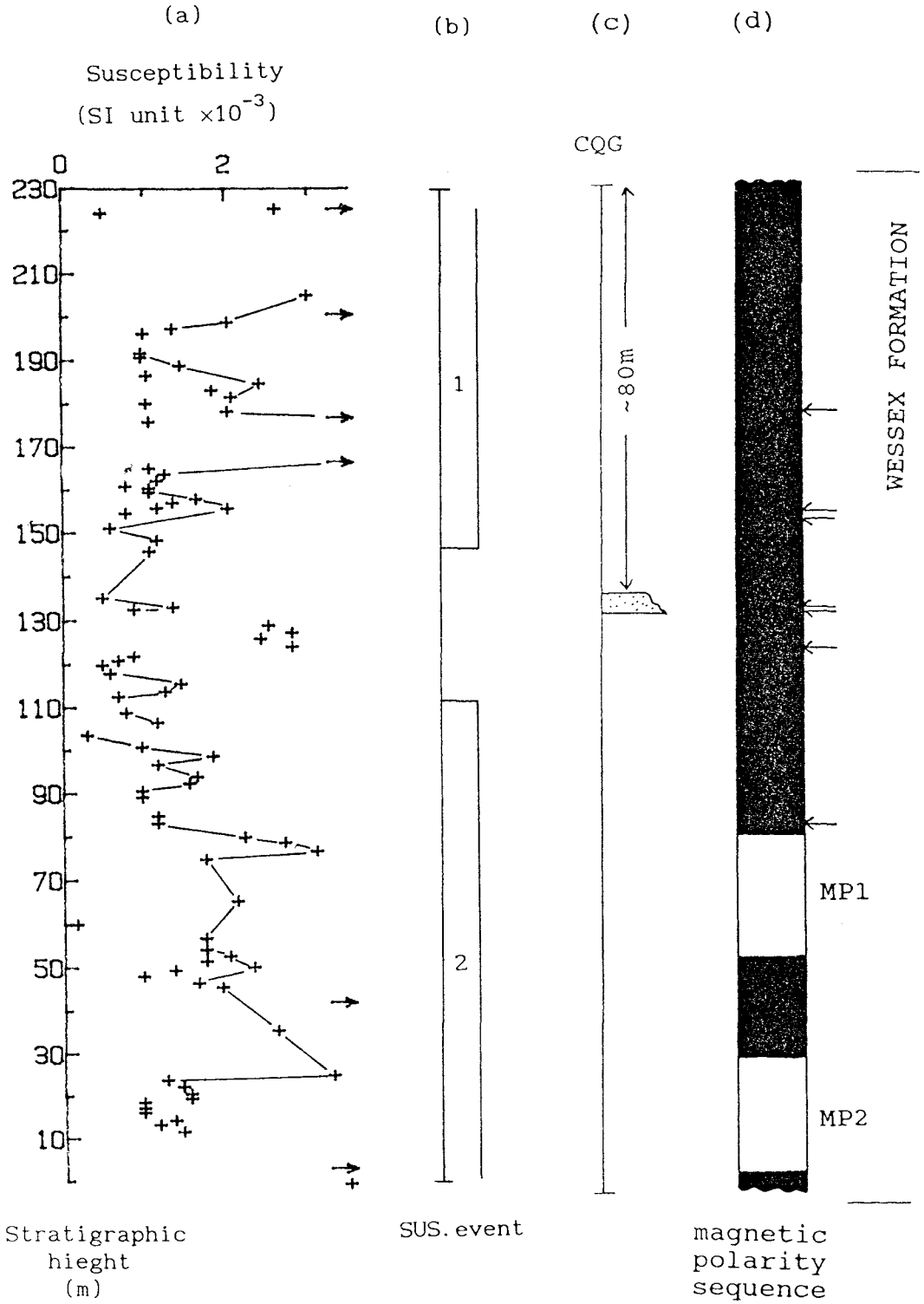

Fig. 8.1.4 Magnetic susceptibility values and other relevant properties of the Mupe Bay section. Symbols and conventions as in Figs. 4.1.3, 4.1.16 and 8.1.2.

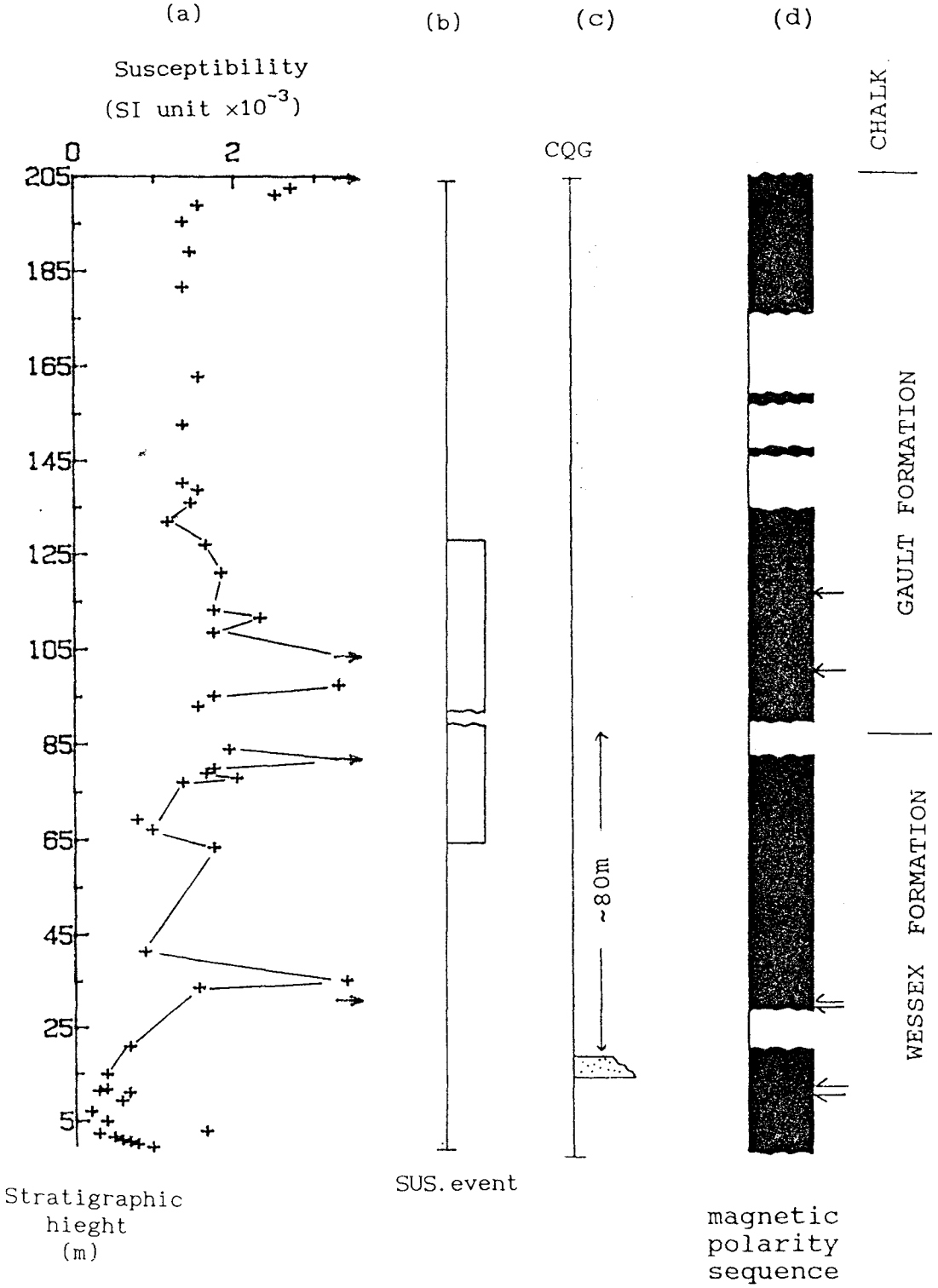

Fig. 8.1.5 Magnetic susceptibility values and other relevant properties of the Lulworth Cove section. Symbols and conventions as in Figs. 4.1.3, 4.1.22 and 8.1.2.

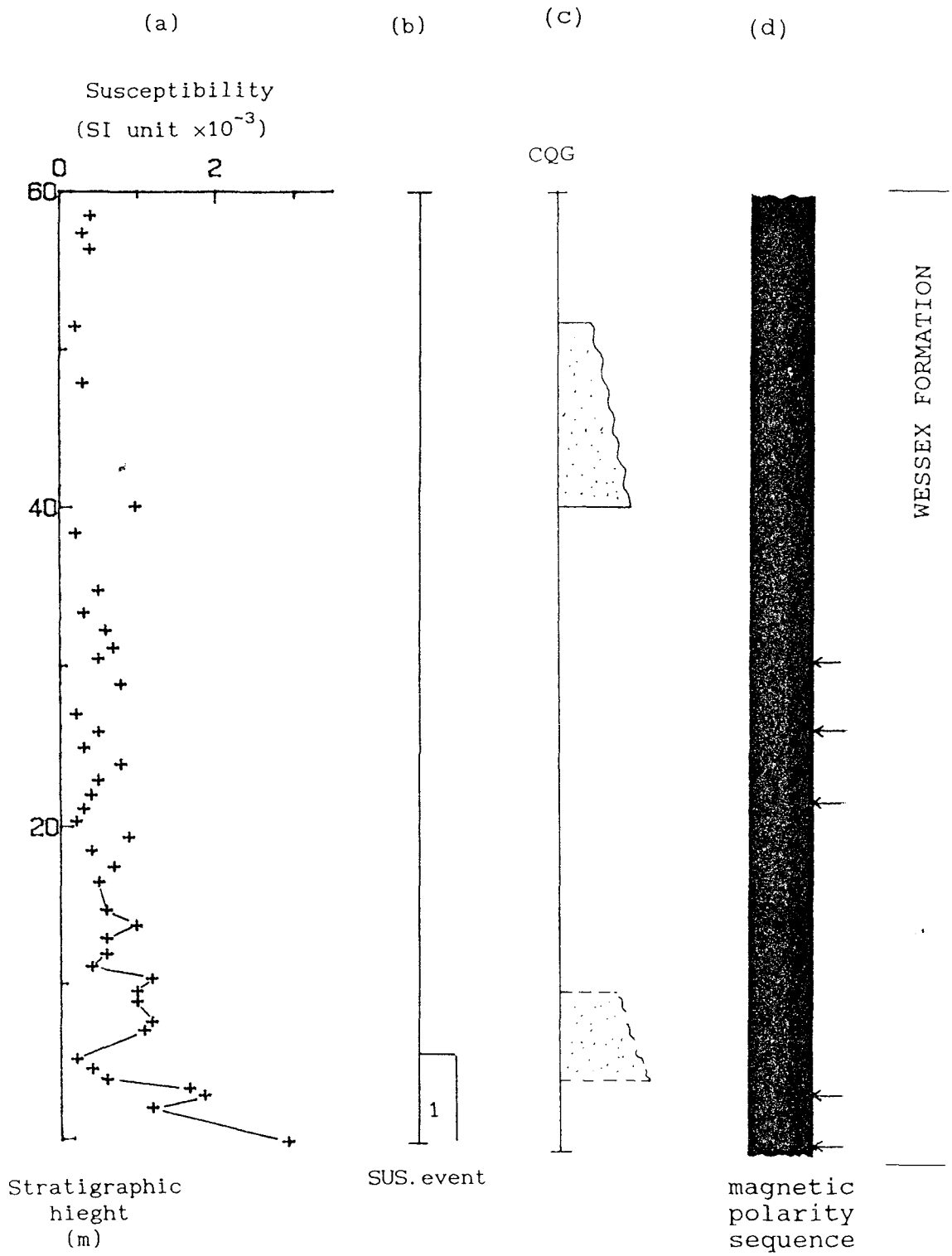

Fig. 8.1.6 Magnetic susceptibility values and other relevant properties of the Durdle Door section. Symbols and conventions as in Figs. 4.1.3, 4.1.29 and 8.1.2.

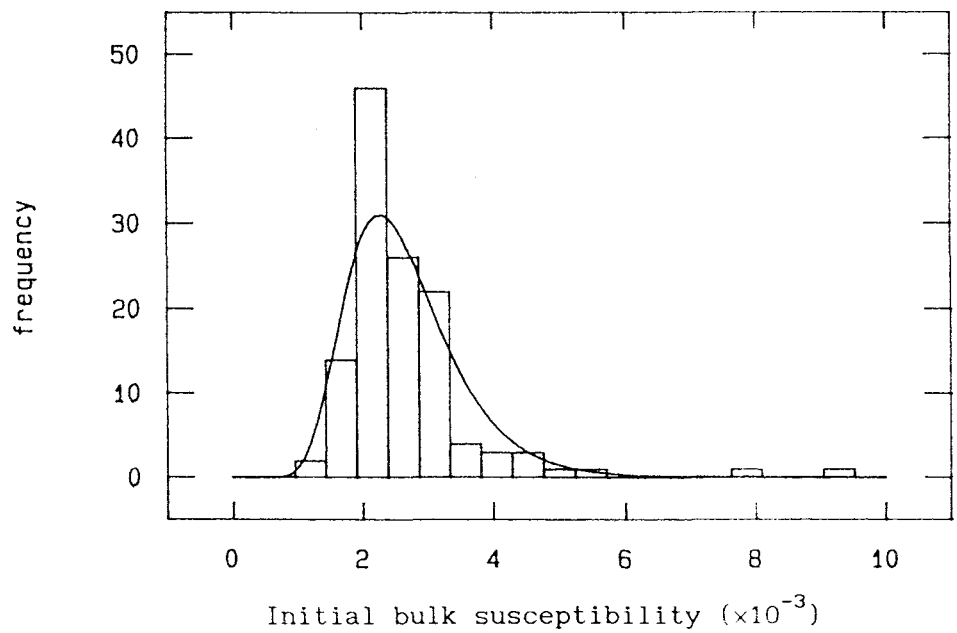

Fig.8.1.7 Statistical distribution of bulk susceptibility values for samples from the Langhurst sections, the Weald Clay Formation.

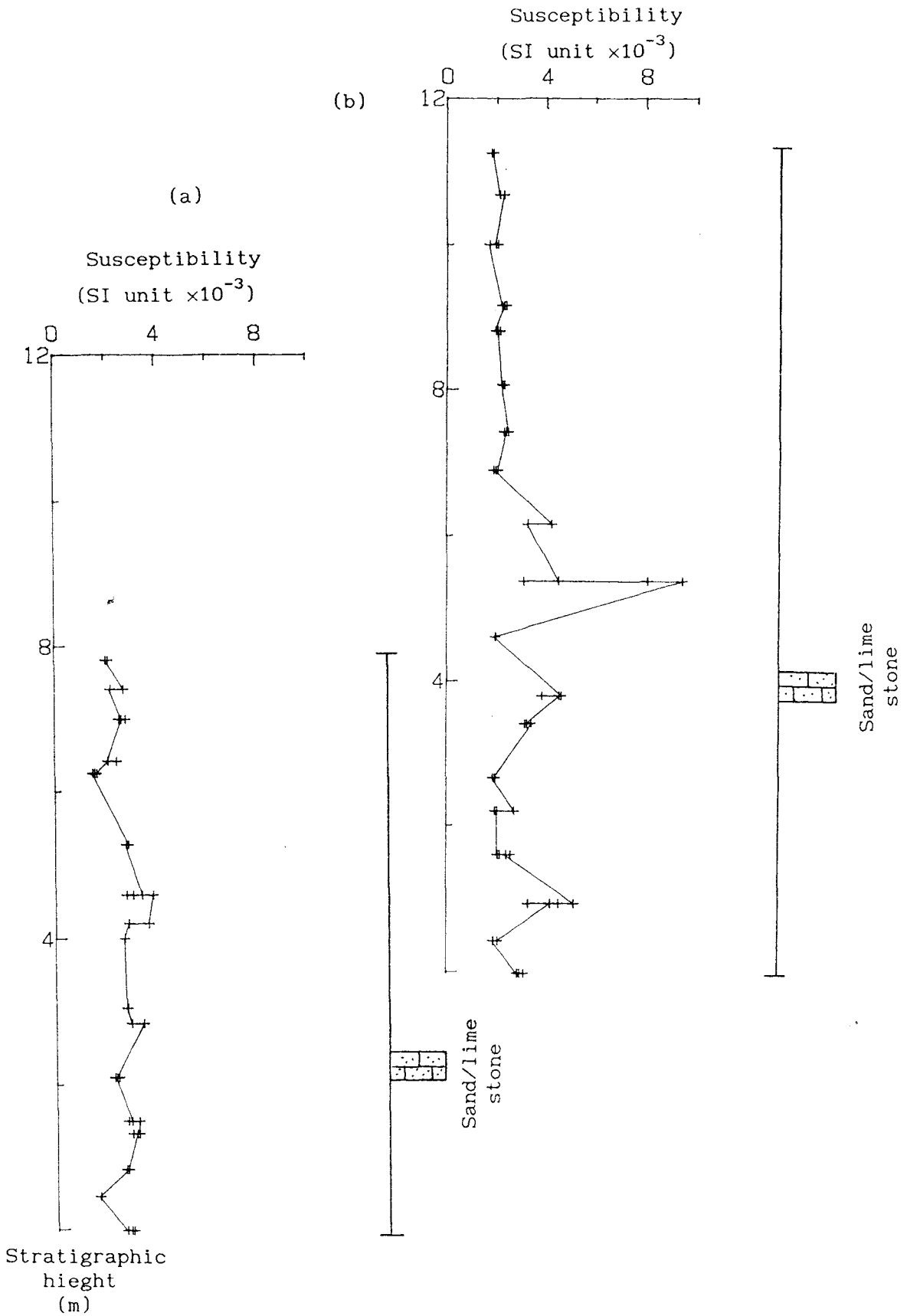

Fig. 8.1.8 Variations of susceptibility values with stratigraphic height. (a) southeast section and (b) northwest section. Symbols and conventions as in Figs. 4.1.39 and 4.1.40.

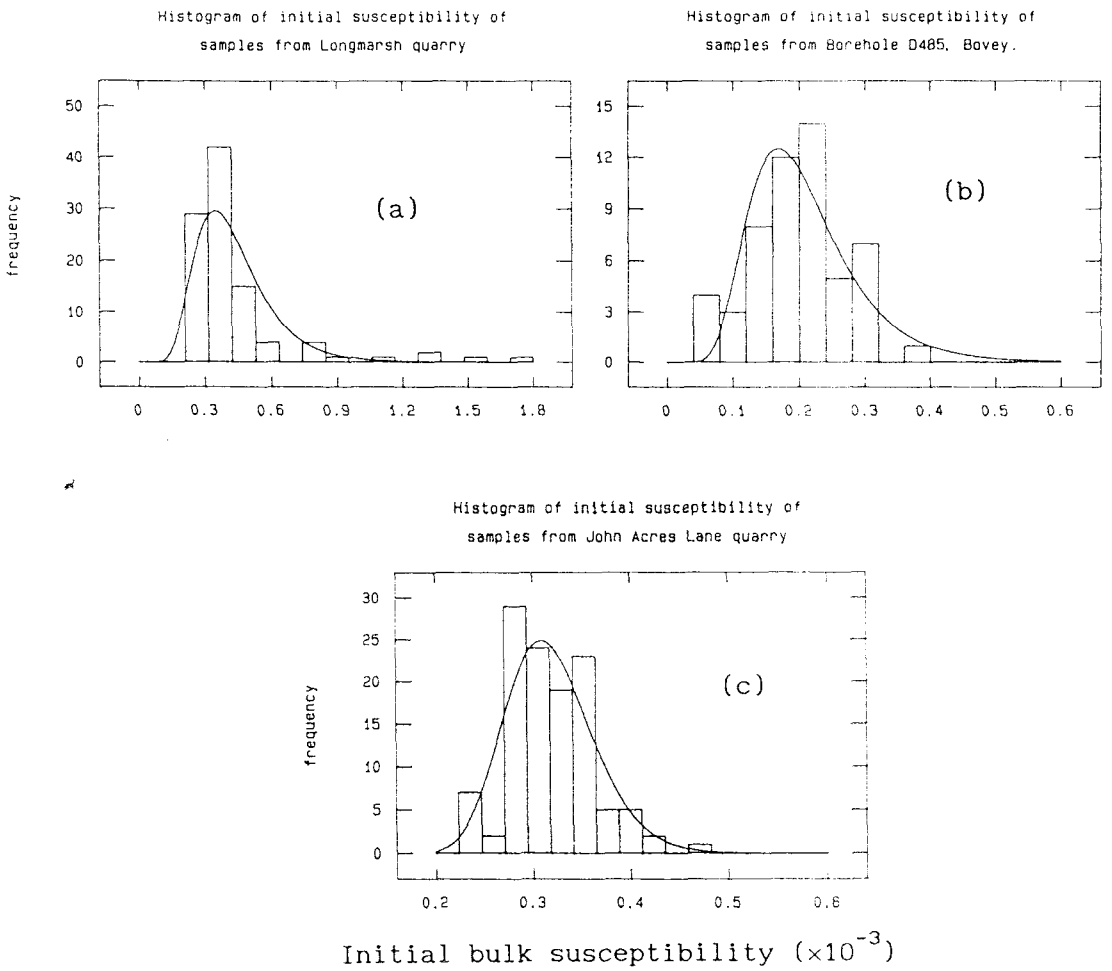

Fig. 8.1.9 Statistical distributions of bulk susceptibility values from the Bovey Formation. The localities are indicated on each diagram.

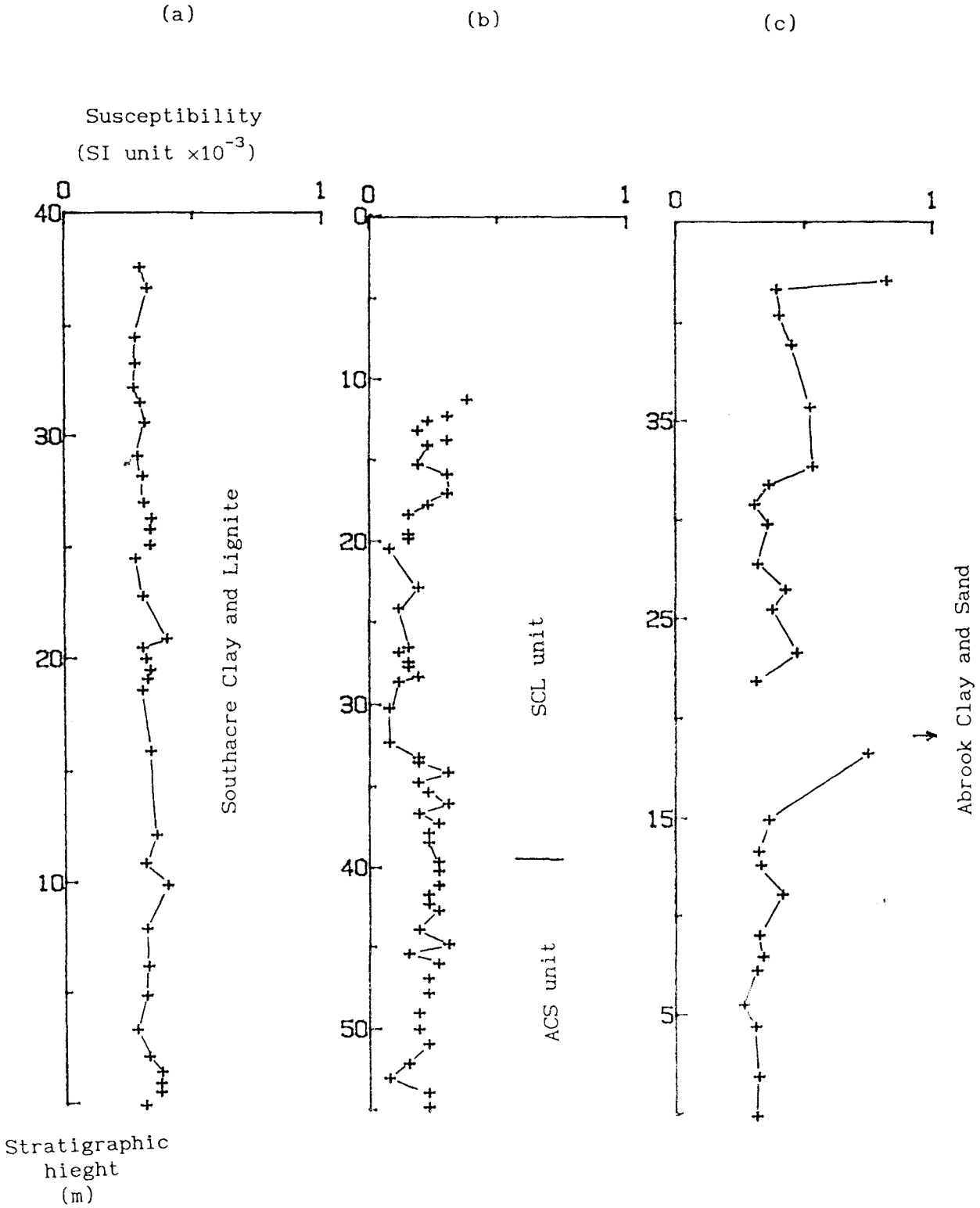

Fig. 8.1.10 Variation of susceptibility values with stratigraphic height for the three sections of the Bovey Formation. (a) Longmarsh section, (b) Borehole SD485 and (c) John Acres Lane section. Sedimentary units are indicated on each diagram. Symbols and conventions as Figs. 6.1.3, 6.1.10 and 6.1.16.

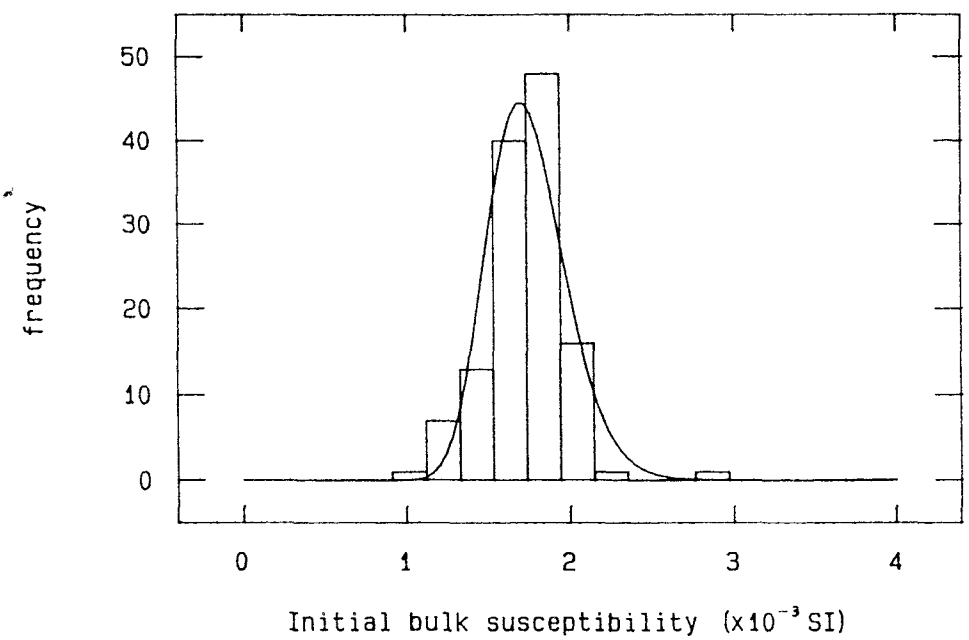

Fig. 8.1.11 Statistical distribution of susceptibility values from the Kruibeke quarry section.

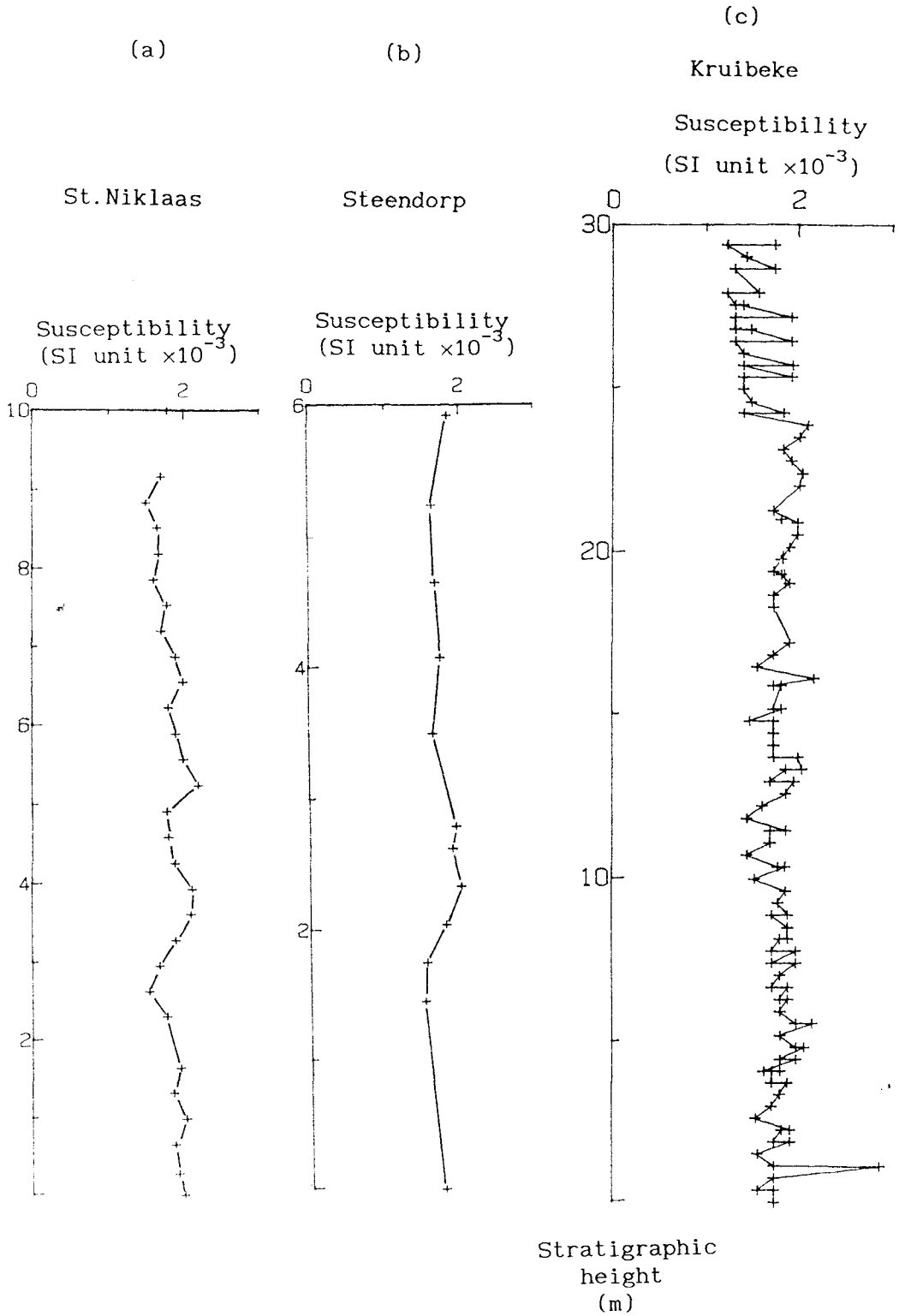

Fig. 8.1.12 Variation of susceptibility values with stratigraphic height for samples from the three sections of the Boom Clay Formation. Symbols and conventions as in Fig. 6.3.15.

§8.2 Results of magnetic fabric measurements.

8.2.1) Magnetic fabric results from the Wessex Formation.

One sample from each sampling site was chosen for the determination of its magnetic fabric, after the sample had been subjected to progressive a.f. demagnetisation. Before the measurement on the LFTM or HFTM, the bulk magnetic susceptibility of the samples was first measured. Attempts were made to measure many samples on the LFTM, but unfortunately very weak deflections were obtained, generally less than 0.3 mm, so that the magnetic signal from the sample would be significantly masked by the instrument "noise" (which produced a typical deflection of 0.1-0.2 mm). This problem was encountered even with the samples having relatively high magnetic susceptibility, from the Isle of Wight and Mupe Bay sections. Therefore, the magnetic fabric of most samples had to be determined on the HFTM, in spite of the fact that the HFTM is prone to produce non-sin2θ components from magnetocrystalline anisotropy and other sources.

The measurements on the HFTM were carried out using the most sensitive range, 40 mV/cm, for the y-axis on the plotter. A direct magnetic field of about 0.7 T (generated by a direct current of 5A) was adopted. Unfortunately, less than 20% of the measured samples from the five sections in southern England produced peak deflections of ≥5 mm, which is regarded as the minimum required to reliably define the sin2θ curve. The maximum deflection for the empty sample holder in the same applied field was found to be about 2-3 mm. Fig.8.2.1 shows some examples of the torque curves produced. These curves were digitized using millimeter graph paper and only the second half cycle of the sin2θ curves were employed for the anisotropy calculations, since the first half-cycle invariably contained significant non-sin2θ components.

Using the acceptability criteria discussed in Chapter VII (the parameter q should lie in the range 0.06 to 0.67, G sum percent should lie ≤100 and K_{min} within 15° of the vertical), only 40% of the total samples measured (that is only 25 samples from the five sections, see Appendix 14) gave reliable magnetic fabric data. Unfortunately not a single sample of the five measured from the Lulworth Cove section

passed these acceptability criteria.

Many samples from the Isle of Wight and Worbarrow Bay section show torque curves with significant non-sin2θ components (see Fig.8.2.2). This may possibly represent the effect of hematite in these samples (see Figs.4.1.1 and 4.1.7, recognizable also from the sample colours).

Fig.8.2.3 summarizes the available results from the HFTM measurements for the Wessex Formation after application of the bedding correction. It can be seen that the minimum susceptibility axes concentrate around the vertical, and the maximum susceptibility directions lie close to the horizontal plane but with a shallow tilt. Fig.8.2.4 show the distribution of K_{max} azimuth plotted on rose diagrams. A general trend can be recognized, in which the K_{max} axes of samples from the Isle of Wight section (Fig.8.2.4a) have a dominant southwesterly grouping, those from the Durdle Door section (d) have a dominantly south-southeasterly grouping, and between them the Mupe Bay (c) and Worbarrow Bay (b) sections show a generally northwest-southeast grouping.

8.2.2) Results from the Weald Clay Formation.

One sample from each sampling site of the four investigated sections, two at Langhurst and two at the Newdigate brickwork pits, was measured on the LFTM. These samples showed relatively strong deflections, probably because of the relative abundance of magnetite (as indicated by the IRM curves, see §4.1). The deflections typically ranged from 2 mm to more than 10 mm. Whereas the empty sample holder produced a typical deflection of about 0.2 mm.

Using the same acceptability criteria as used for the southern England sections (except that the limiting value of G sum percent was reduced from 100 to 60%, because of the stronger deflections), only 40% of the samples acceptable from the Beare Green sections and 38% from the Langhurst sections proved acceptable (see Appendix 15). This low percentage of acceptable samples might be due in part by disturbance of the fabric, caused by the copper tube sampling procedure.

Fig.8.2.5 illustrates the magnetic anisotropy results for the two localities. The samples from Beare Green quarry (Fig.8.2.5a) show a general K_{max} distribution towards the west or southwest, with the k_{min} axes located close to the vertical. Samples from Langhurst quarry show two different k_{max} distributions. Those from the northwest section show a dominant southeast to southwest trend with a possible minor northerly trend. These from the southeast section show a dominant east-west trend.

To investigate the magnetic fabric properties of the Weald Clay Formation in more detail, a block hand sample was collected from the middle part of the Langhurst quarry and was cut into 19 cubic specimens, which were then subjected to magnetic fabric investigation. The LFTM method was applied and good deflections were obtained 52% of the specimens from this block sample satisfied the acceptability criteria which seems to indicate that the knife-cutting method (rather than copper tube) used to take these specimens might be less prone to producing disturbance of the magnetic fabric. The results are shown in Fig.8.2.6 and a very well-defined k_{max} grouping in the southwest quadrant is clearly present. A comparison with the other magnetic data from the Weald Clay Formation indicates a highly variable k_{max} distribution over relatively short distance (<1 mile).

8.2.3) Results from the Oligocene Bovey Formation.

Neither LFTM nor HFTM measurements produced meaningful deflections from the samples from the Bovey Formation. This is probably due to the very low concentration of the magnetic minerals in these sediments.

8.2.4) Results from the Oligocene Boom Clay Formation.

Magnetic fabric work was mainly concentrated on the lower part of the Kruibeke section, which it is thought to be less affected by secondary diagenesis. 51 samples were subjected to measurement using the LFTM. Fairly strong deflections were observed, generally in the range 2.0 to 5 mm. In view of the relatively strong remanent magnetisation and the nature of the IRM acquisition curves (see Fig.6.3.13), this is thought to be due to the presence of a significant

magnetite content.

About 60% of the samples passed the acceptability criteria (see Appendix 16). Fig.8.2.7 summarizes the results, in which a very well-defined foliation plane can be seen with the k_{min} axes concentrated around the vertical and a very good grouping k_{max} axes around the edge of the projection. There is a dominant k_{max} grouping almost north south, but with a subsiding grouping to the north-north-east and south-south-west.

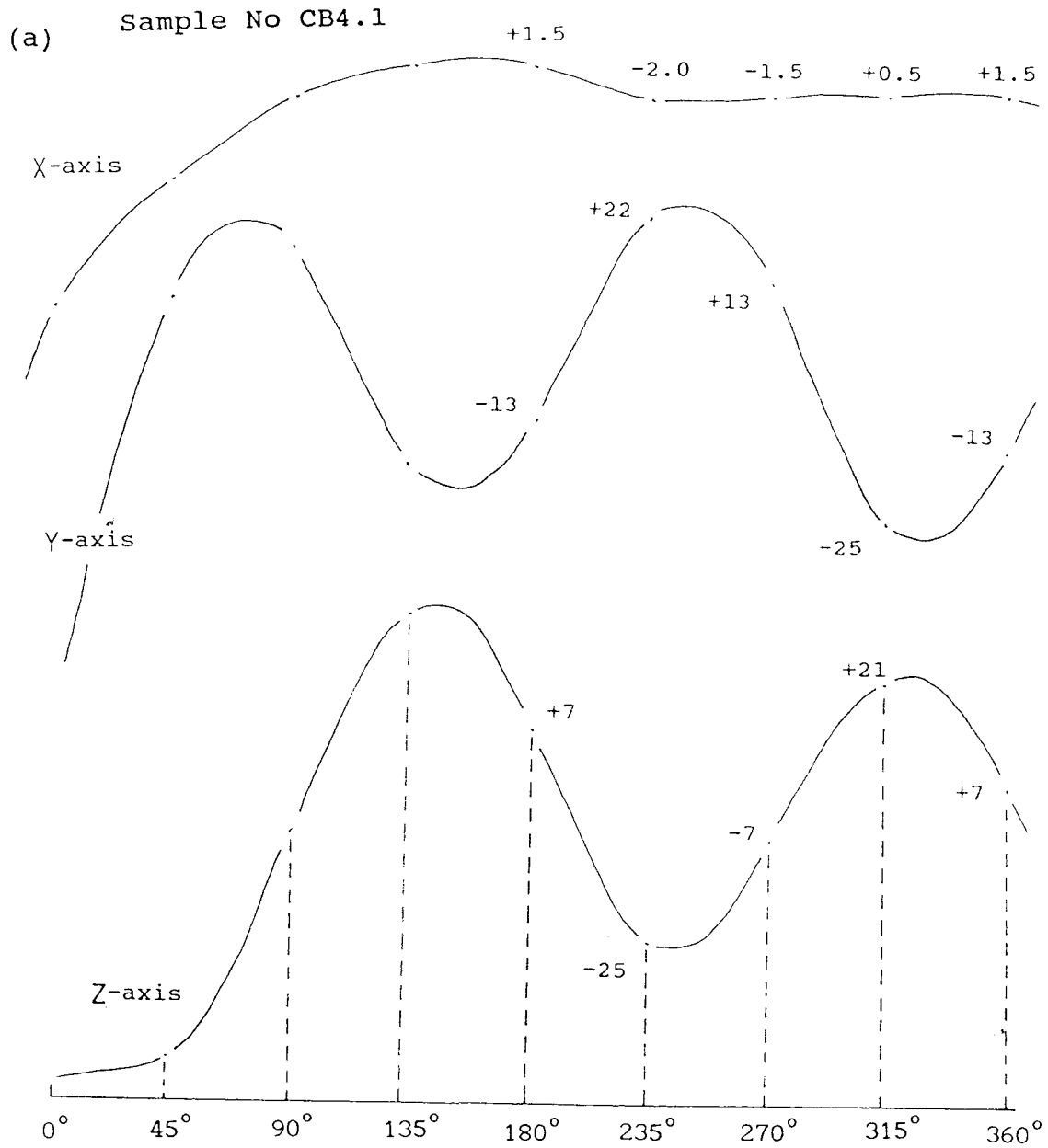

Fig. 8.2.1 Examples of magnetic anisotropy torque curves determined on the HFTM. (a) sample from the Isle of Wight section, (b) sample from the Worbarrow Bay section, (c) sample from the Mupe Bay section and (d) sample from the Durdle Door section. The horizontal axis represents the rotation angle of the applied field with regard to the reference azimuth on the sample. Numbers attached to the curves are the digitized values referred to the (arbitrary) zero line.

(b) Sample No WW2.1a

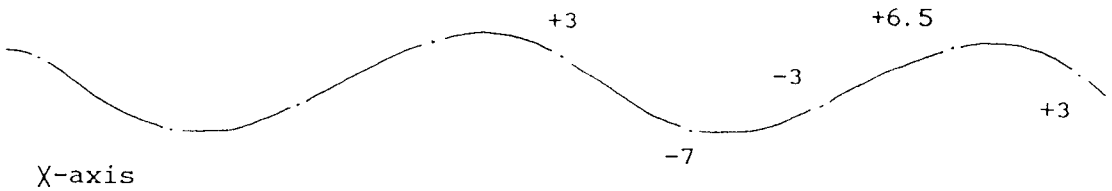

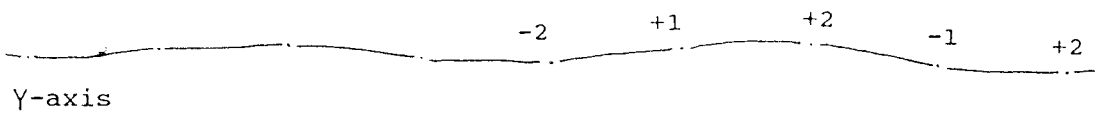

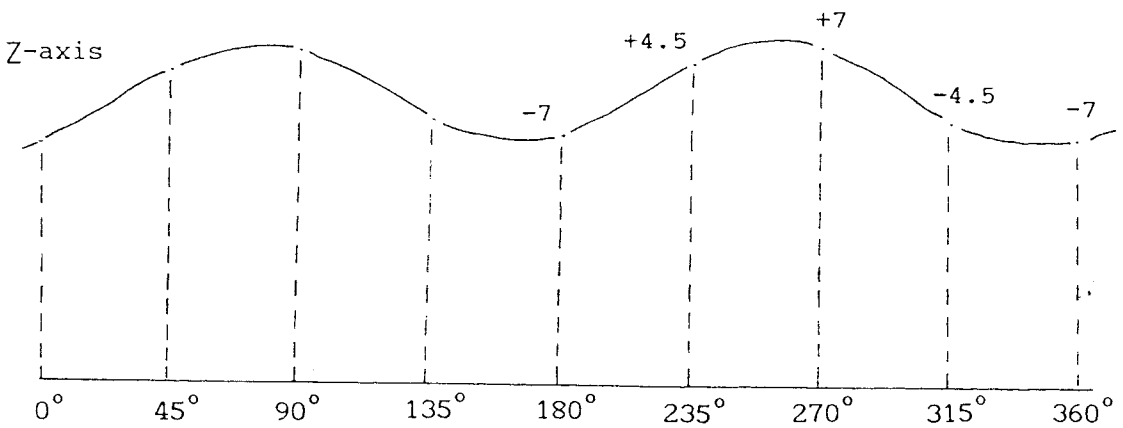

(c) Sample No MP36.1a

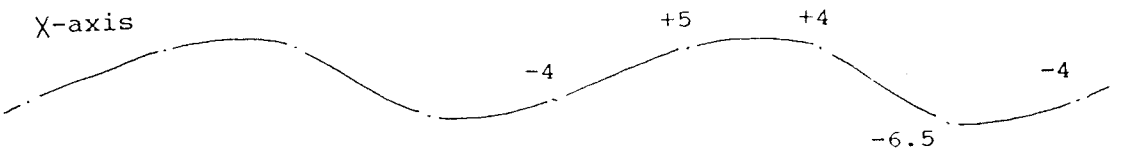

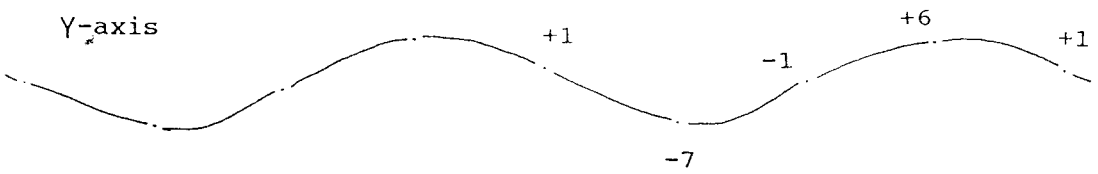

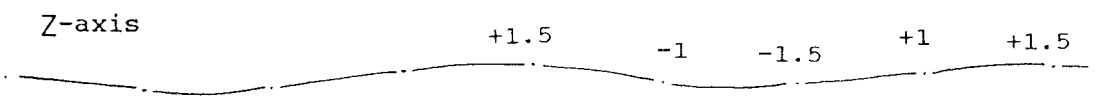

(d) Sample No DD17.1a

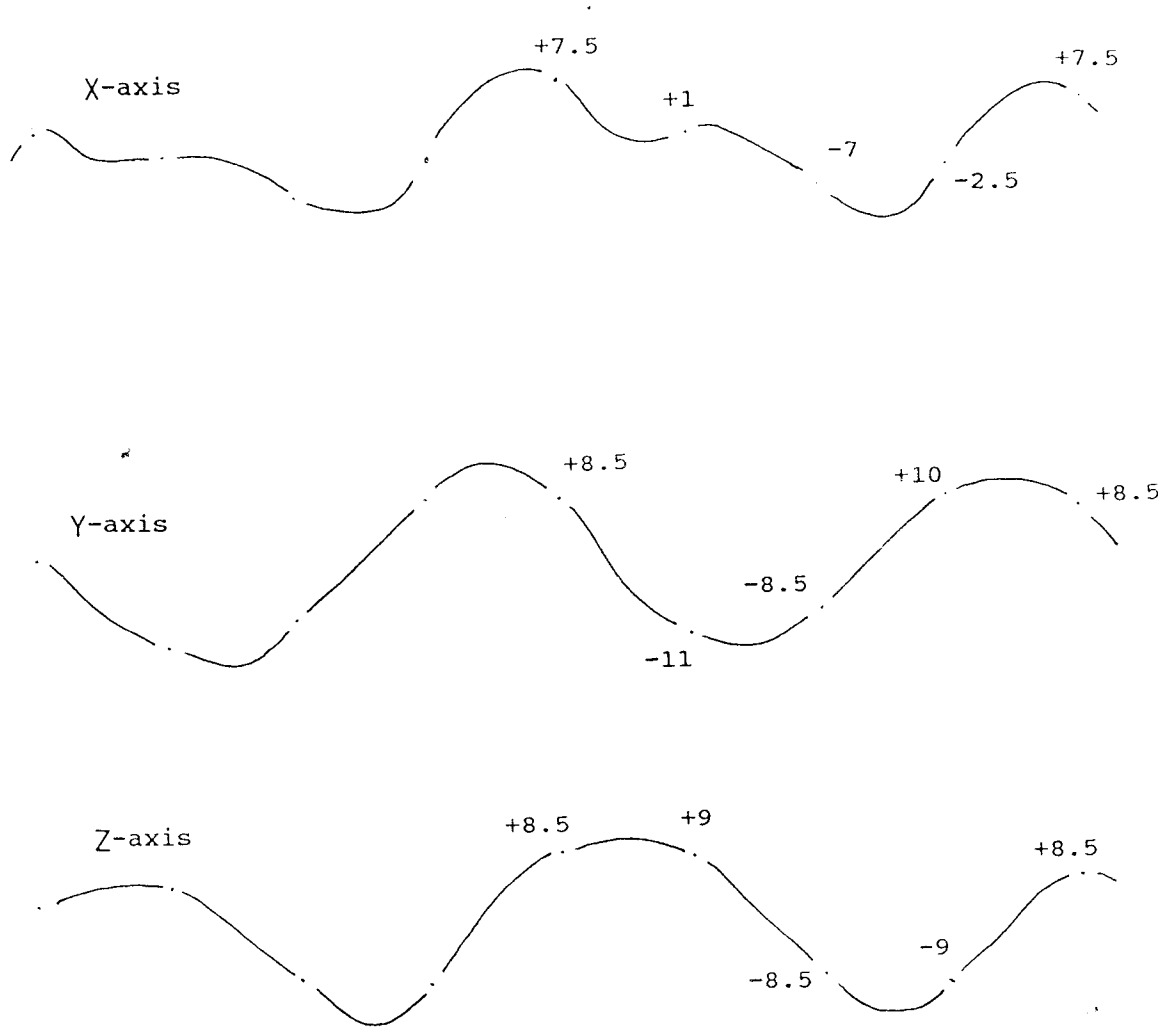

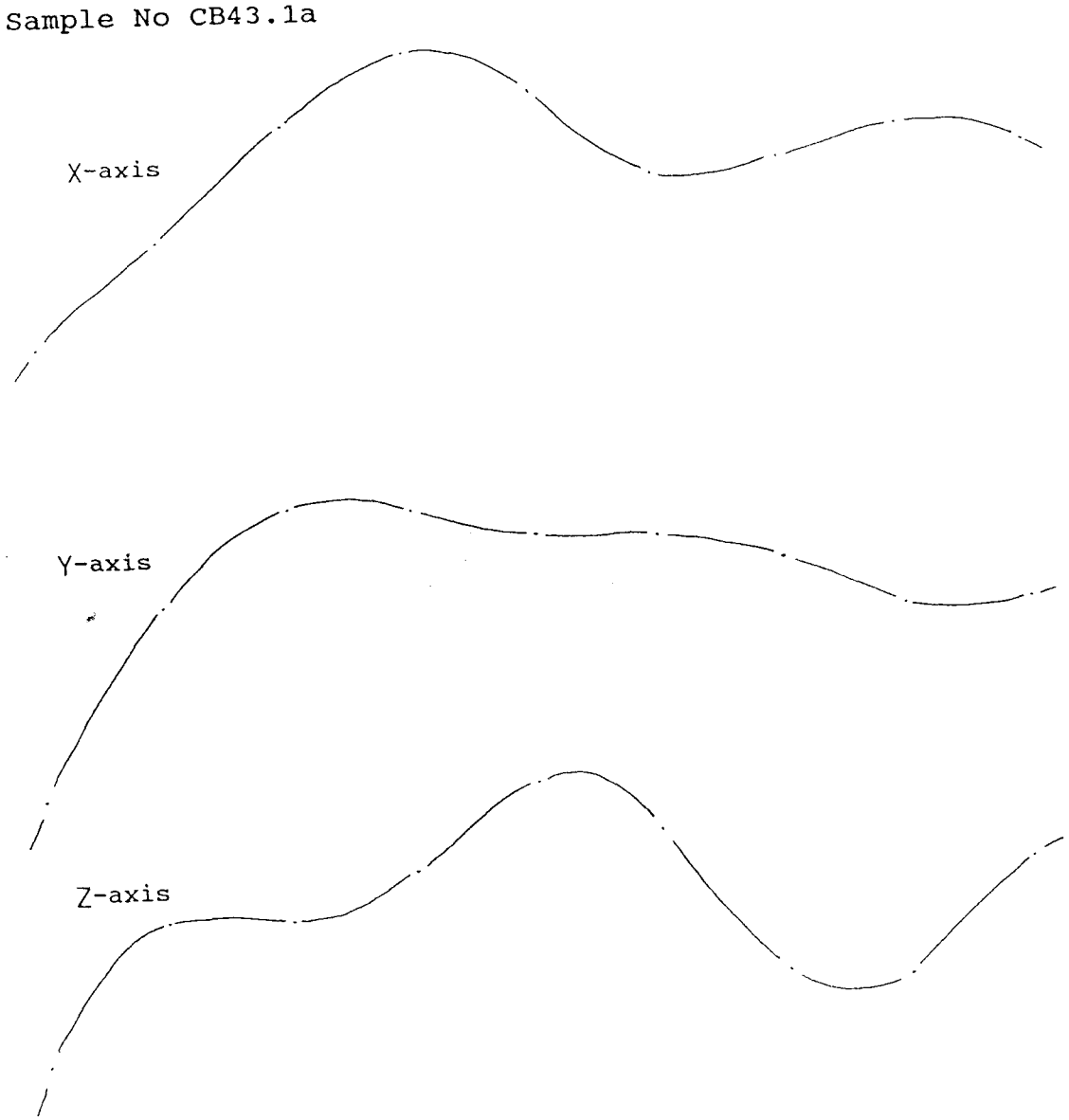

Fig.8.2.2 An example of a torque curve with a significant non-sin2θ component, from sample from the Isle of Wight section, which has hematite as the main magnetisation carrier. Symbols and conventions as in Fig.8.2.1.

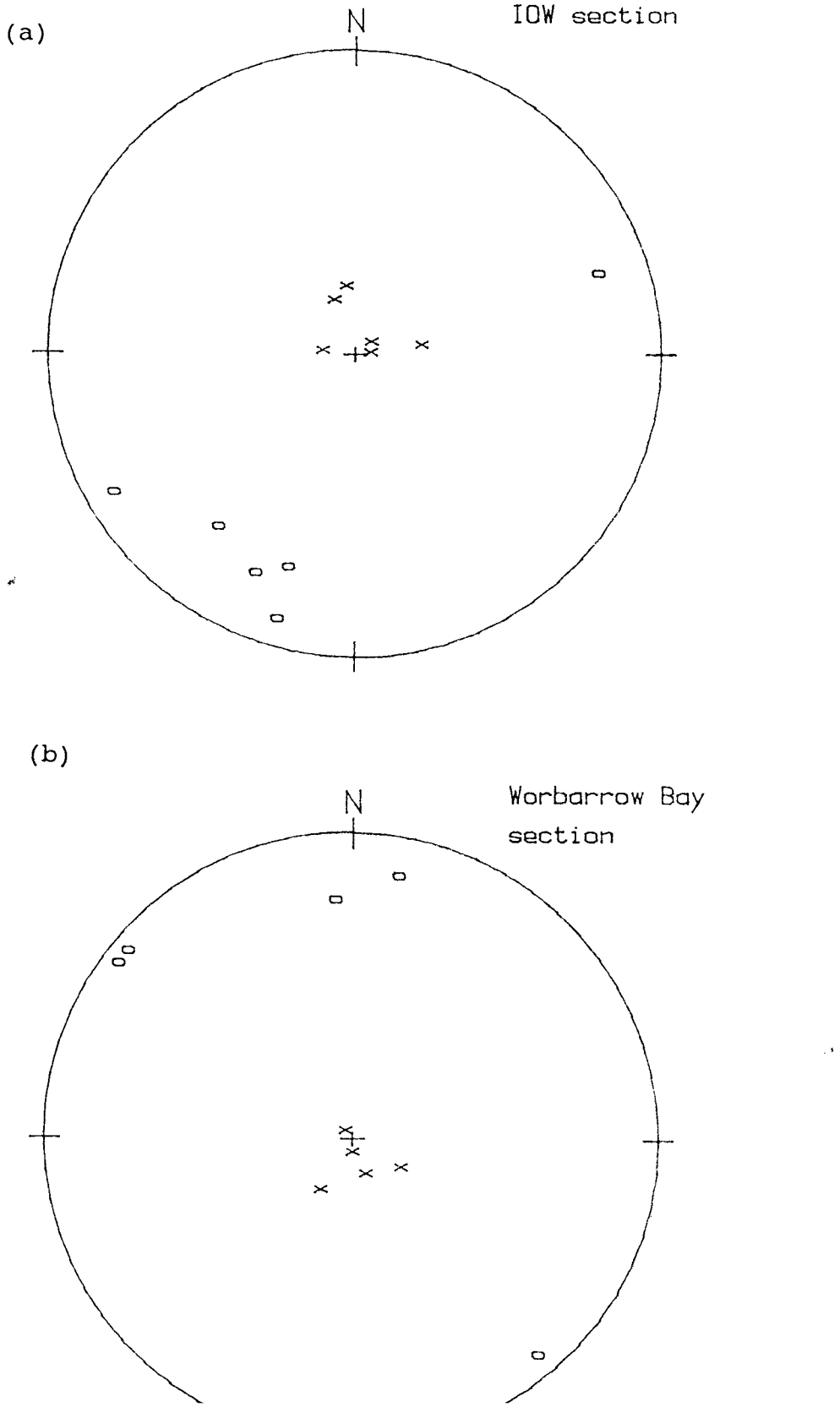

Fig. 8.2.3 The distribution of K_{max} and K_{min} directions from the Lower Cretaceous beds, Southern England. The localities are indicated on each diagram. Open circles represent K_{max} directions and crosses K_{min} directions.

(c)

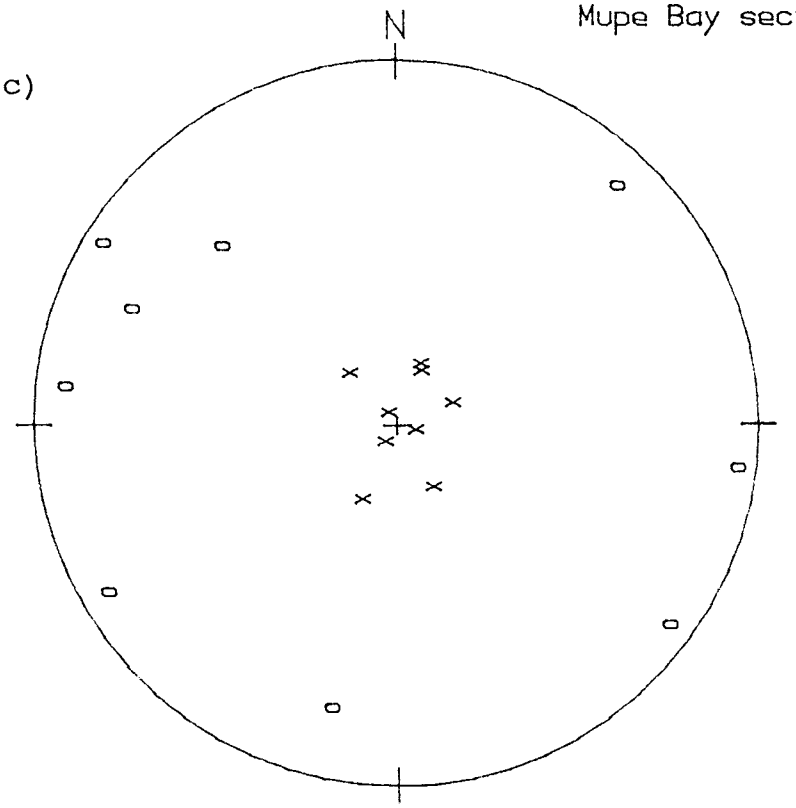

Mupe Bay section

(d)

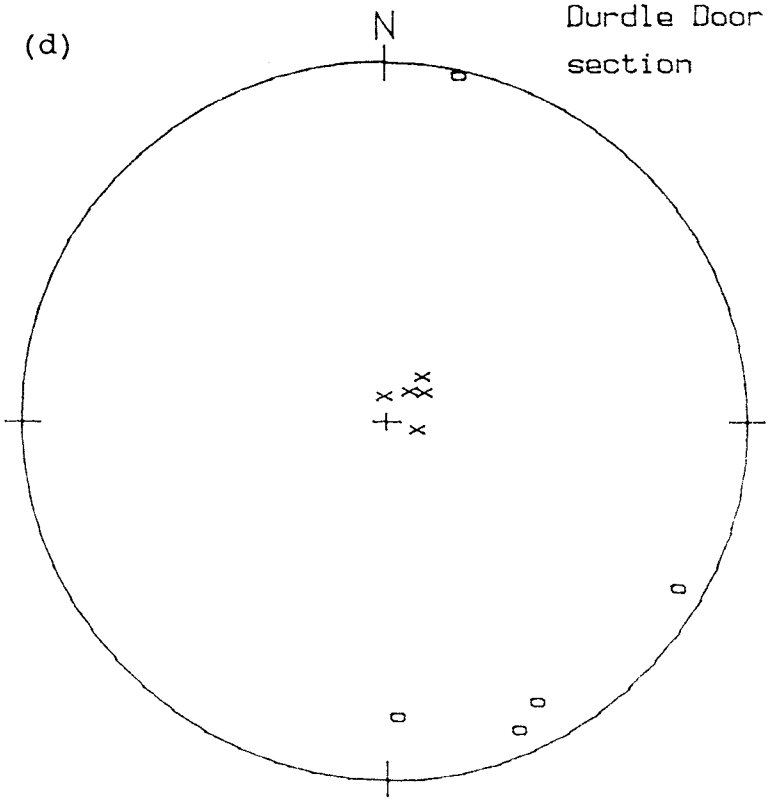

Durdle Door section

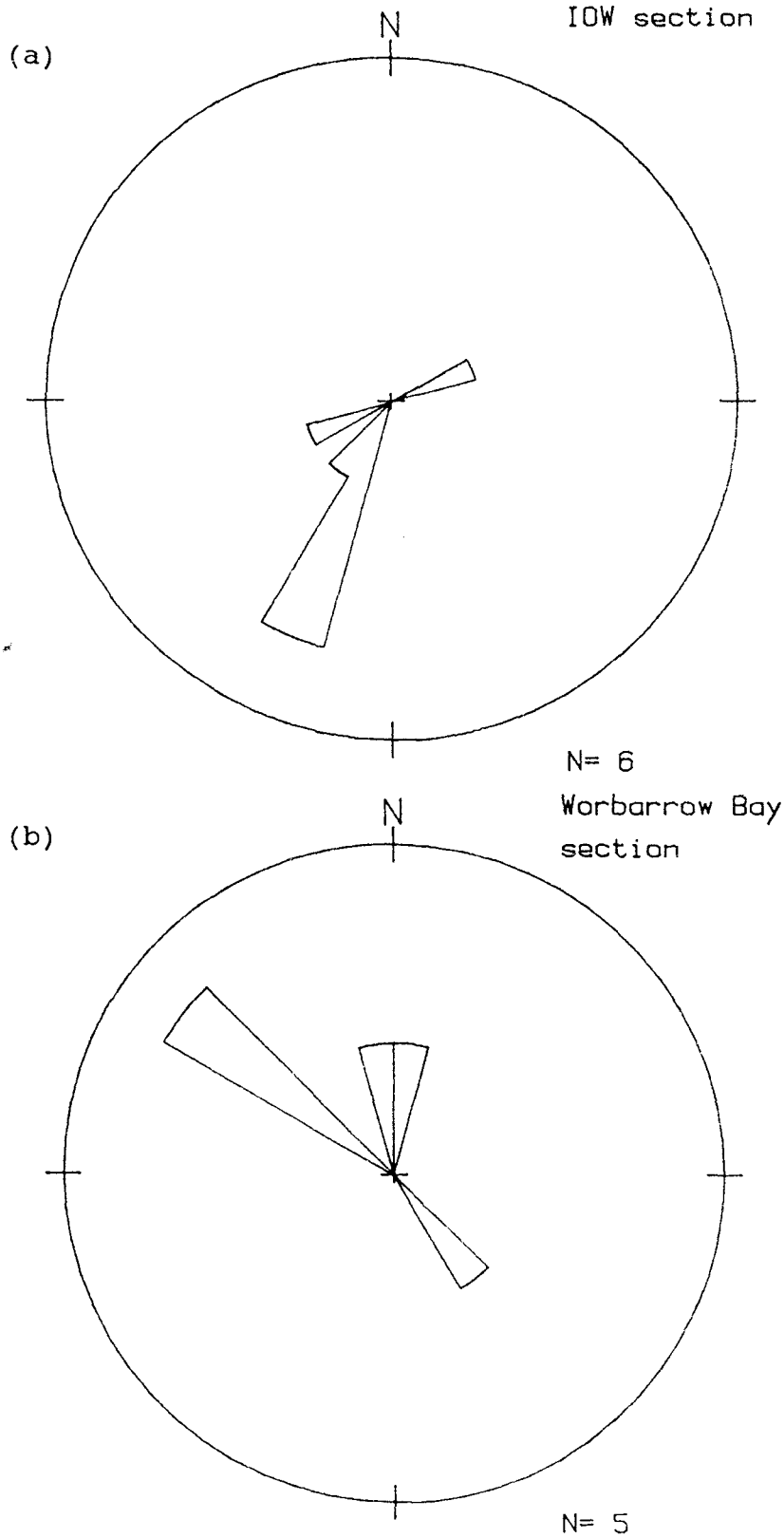

Fig. 8.2.4 Rose Graphs (statistical angular distribution) of the K_{max} axes from Southern England sections. The localities are shown on each diagram. The length of the radius fan represents the number of samples with K_{max} axes within that angular range.

(c)

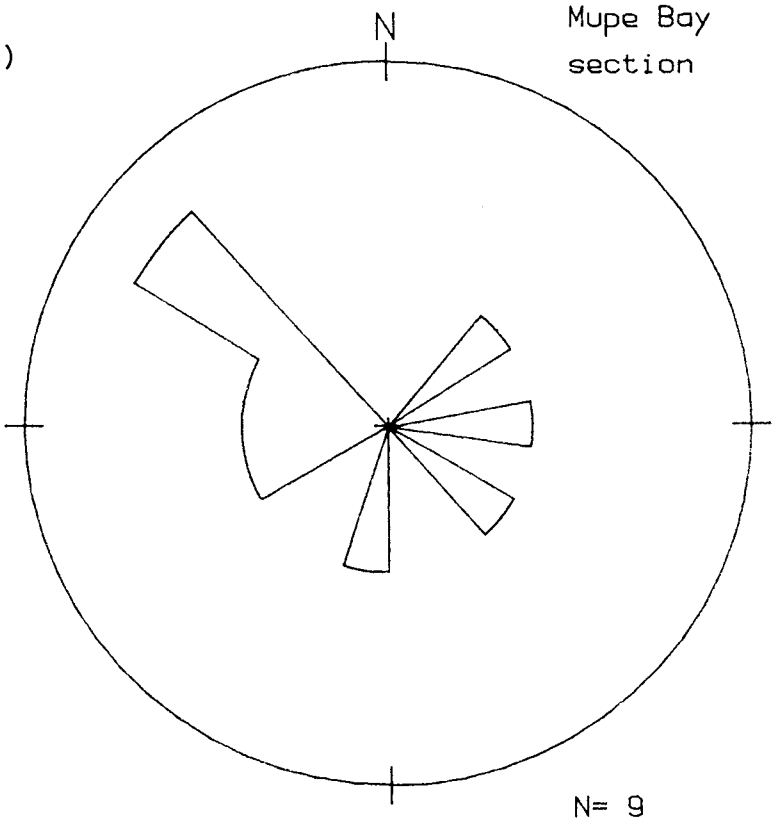

Mupe Bay section

N= 9

(d)

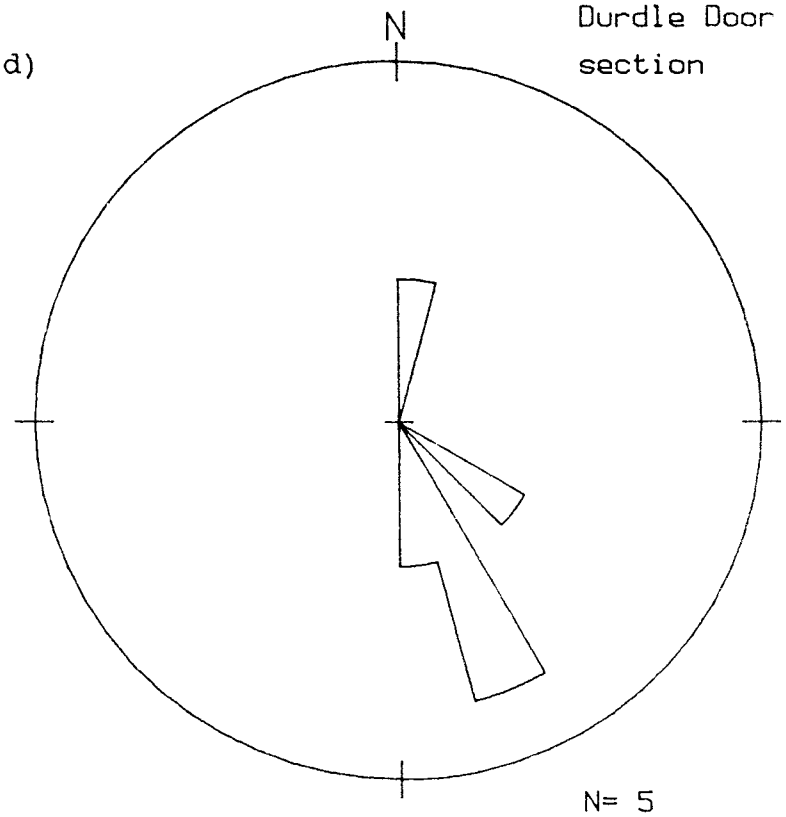

Durdle Door section

N= 5

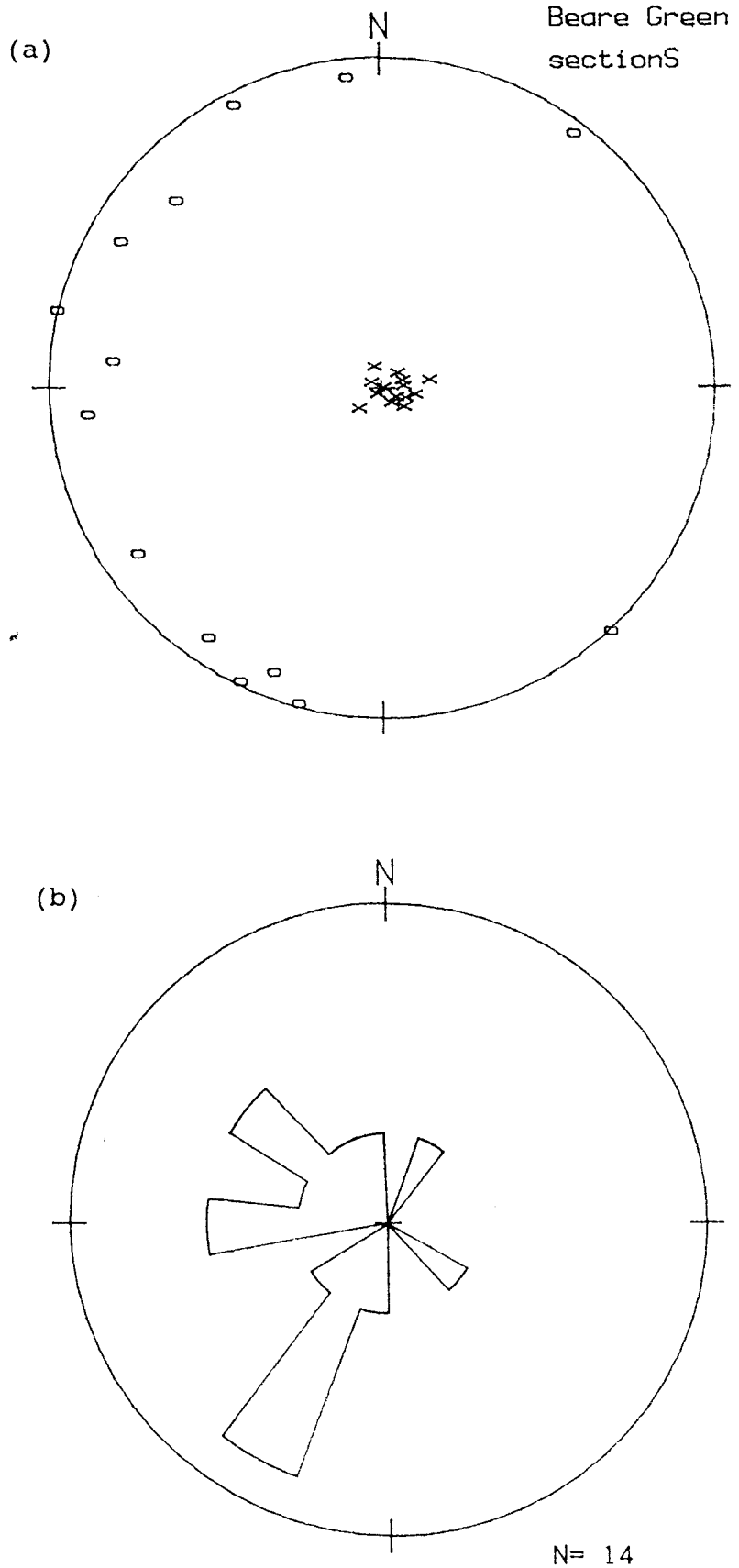

Fig. 8.2.5 (a) and (c) Distribution of k_{max} and k_{min} axes and (b) and (d) corresponding Rose Graphs of K_{max} azimuths for samples from the Weald Clay Formation, Southeast England. Localities are shown on each diagram. Symbols and conventions as in Figs. 8.2.3 and 8.2.4.

(c)

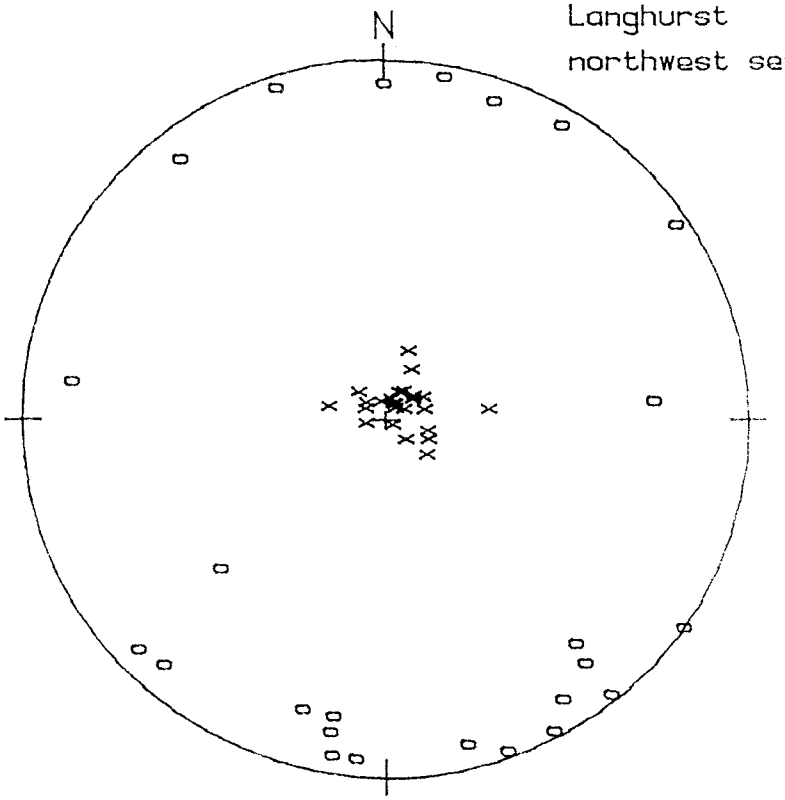

Langhurst
northwest section

(d)

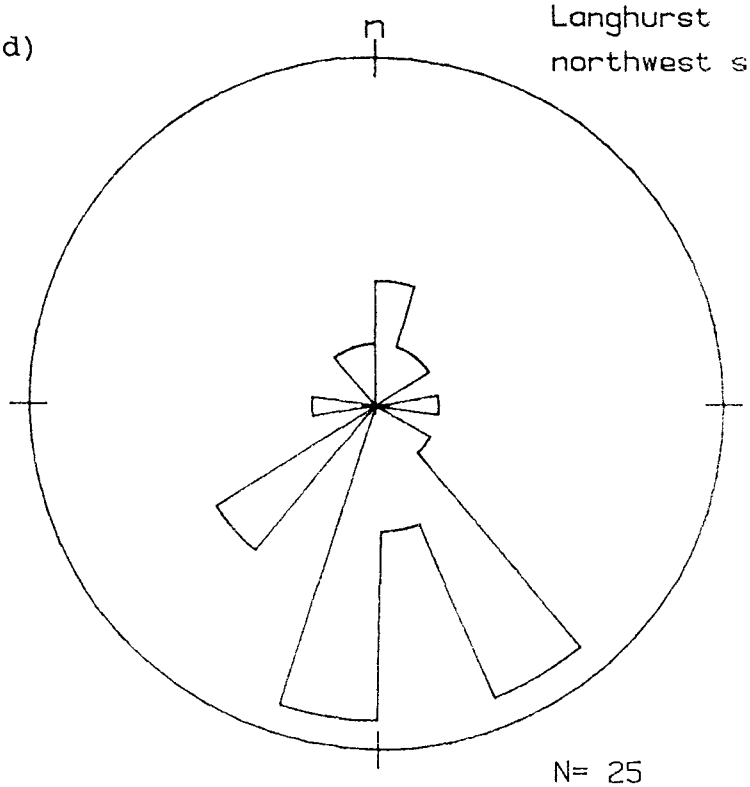

Langhurst
northwest section

N= 25

(e)

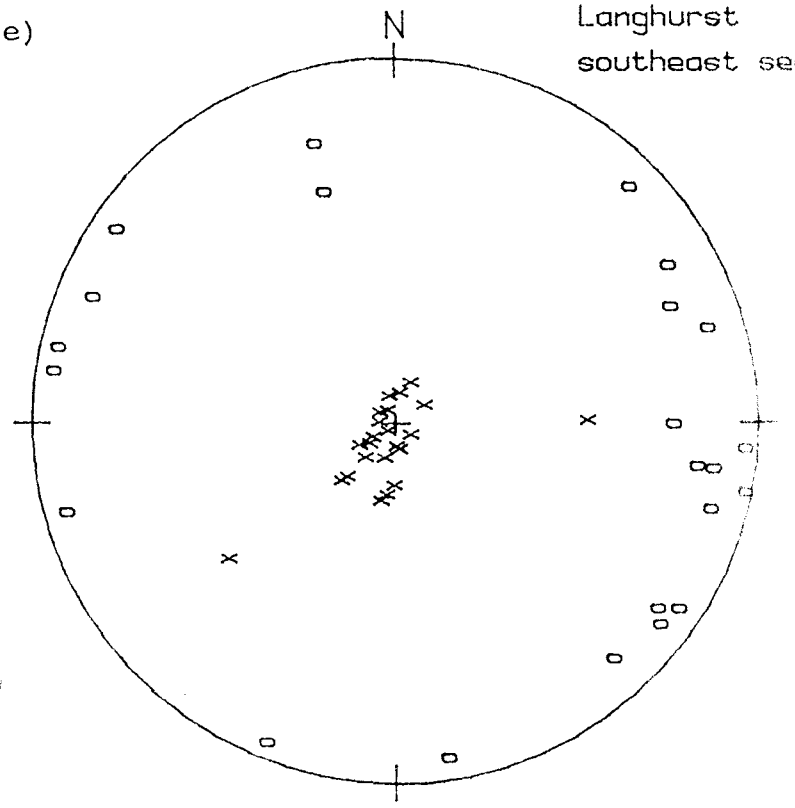

Langhurst
southeast section

(f)

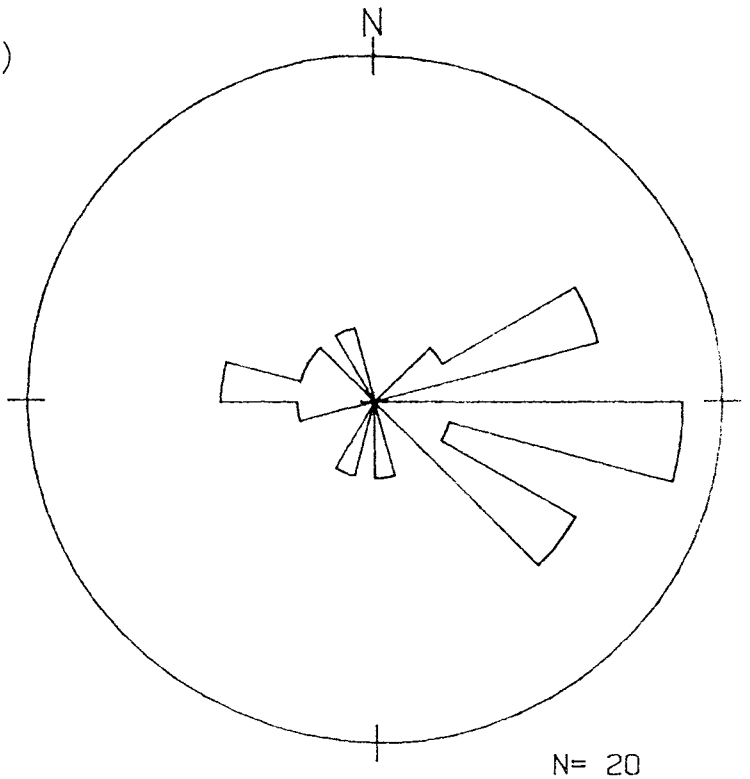

N= 20

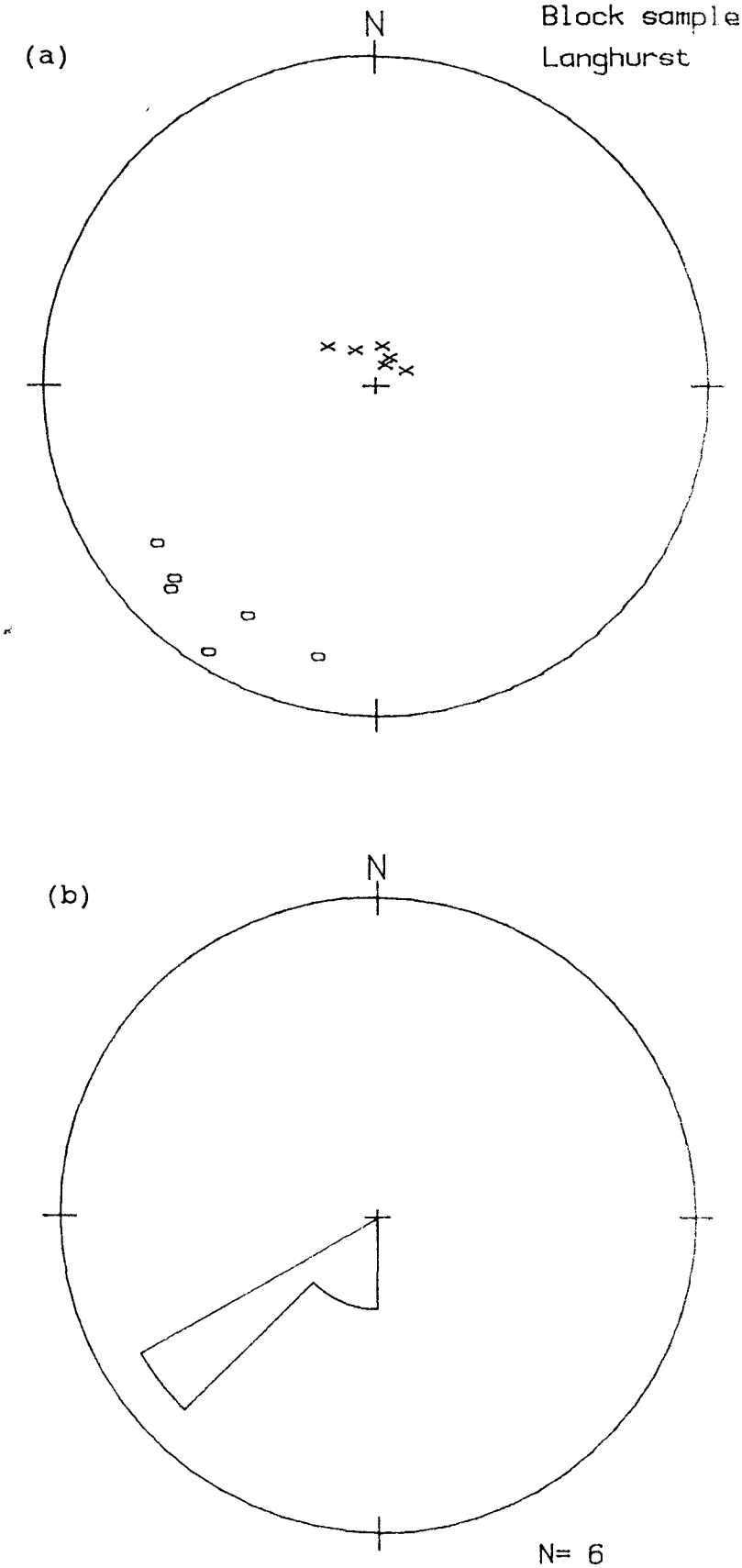

Fig. 8.2.6 Magnetic fabric results from the block sample from the Langhurst quarry. Symbols and conventions as in Figs. 8.2.3 and 8.2.4.

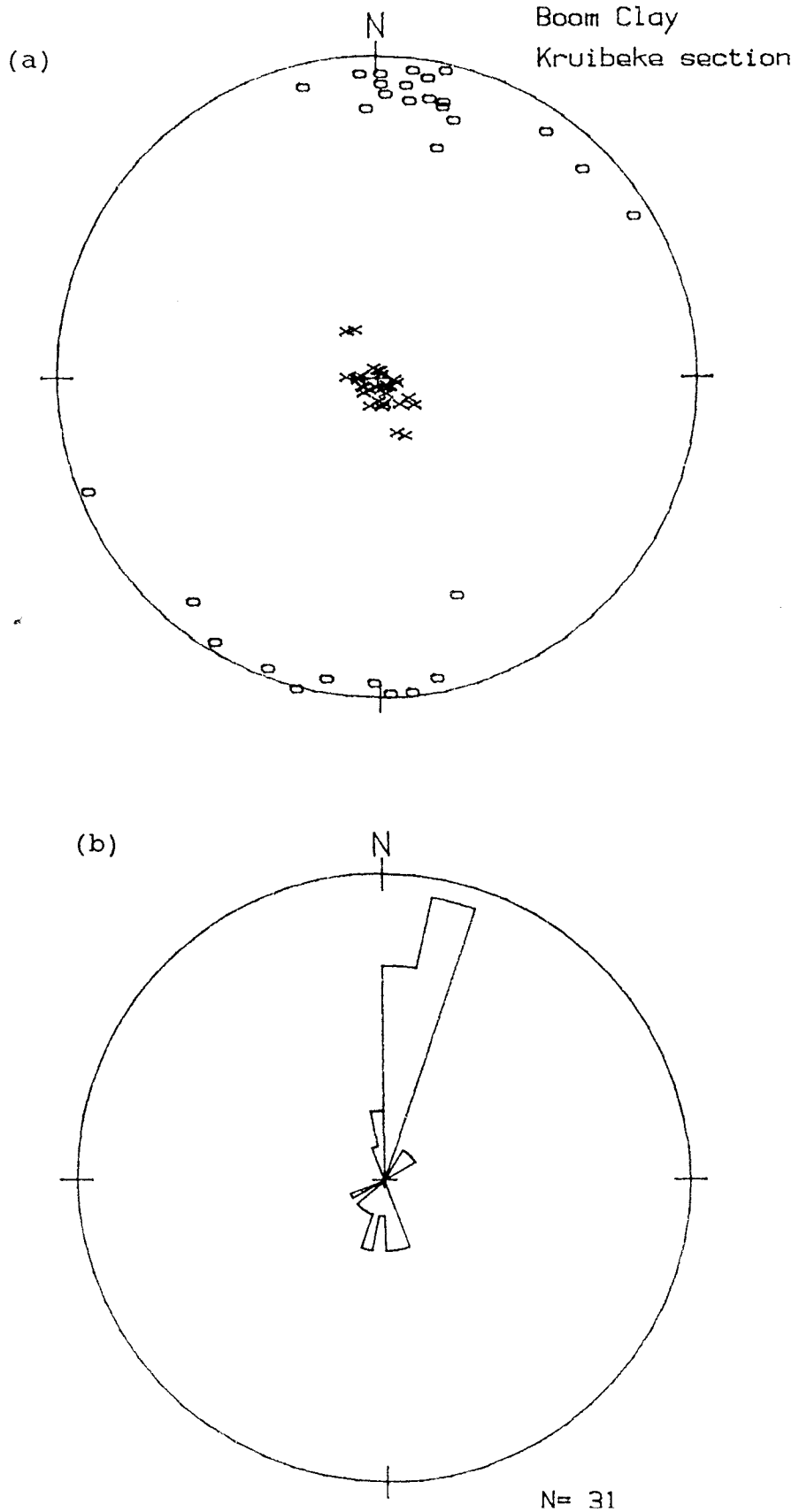

Fig.8.2.7 Magnetic fabric results from the Kruibeke section of the Boom Clay Formation, Northwest Belgium. Symbols and conventions as in Figs.8.2.3 and 8.2.4.

§8.3 Significance of the magnetic fabric results for depositional environment in these areas.

Fig.8.3.1 relates the statistical distributions of k_{max} directions to the sampling locations in the Wessex Formation along the southern coast of England. As noted earlier, the Isle of Wight section shows a k_{max} trend towards the southwest while at Durdle Door the k_{max} trend is towards the southeast. As the two intervening localities (Mupe Bay and Worbarrow Bay) the trends are NW-SE. The data for the Isle of Wight section can be compared with the results of Stewart (1978), who identified a NE-SW palaeocurrent direction for the Wessex Formation. No previously reported palaeocurrent directions have been found for the Durdle Door area. It is possible that at the far western edge of the Wessex basin the dominant flow direction was towards the southeast, carrying deposits into the basin, as indicated by the k_{max} trends for all three Dorset coast sections. These patterns conform with the observations of Stewart (1978), for the Worbarrow Bay section.

Fig.8.3.2 shows the combined magnetic fabric results for the Weald Clay Formation from different localities. A relatively complicated set of palaeocurrents indicated by the k_{max} grouping. The sampling localities are located in the middle of the Wealden Basin, which has a west-east elongated shape. Therefore, the east-west k_{max} trend at Langhurst appears to coincide with the elongated direction of the basin and may represent some palaeocurrent flow in this direction. On the other hand, according to Allen's (1954, 1975) model of the Weald Clay Formation there were many irregular sources of sedimentary materials flowing from the north towards the southeast or southwest into the basin (Fig.8.3.2b). Prentice (1962) also demonstrated that the palaeocurrent direction at the northern part of the Warnham brickwork pits had both southeast and southwest components, by means of groovecast orientation and other geological evidence. These sorts of palaeocurrent directions might represent seasonal flood events, which could produce a strong preferred orientation of the magnetic mineral grains, thus forming a strong lineation pattern on a very localised scale.

Fig.8.3.3 illustrates the palaeogeographic depositional model for

the North Sea area in the early Tertiary (Selley 1977). The magnetic fabric results from the Boom Clay Formation are plotted as a rose diagram, centred at the sampling locality. This locality is situated close to the southern edge of the basin and the k_{max} trend is closely parallel to the elongated direction of the southern part of the North Sea Basin. Consequently, this well-defined k_{max} direction appears to represent a relatively strong transport direction, running into the basin from the south, but with the sedimentary materials being relatively homogeneous compared with the continental depositional environment of the Wealden-Wessex Basin.

Although some wind-forming magnetic susceptibility anisotropy of sediments was reported (eg see Kukla *et al* 1988), in the depositional areas of southern England and northwest Europe no evidence has been found for this type of depositional environment. Thus, the magnetic fabric results discussed above are exclusively from hydaulically dynamic source.

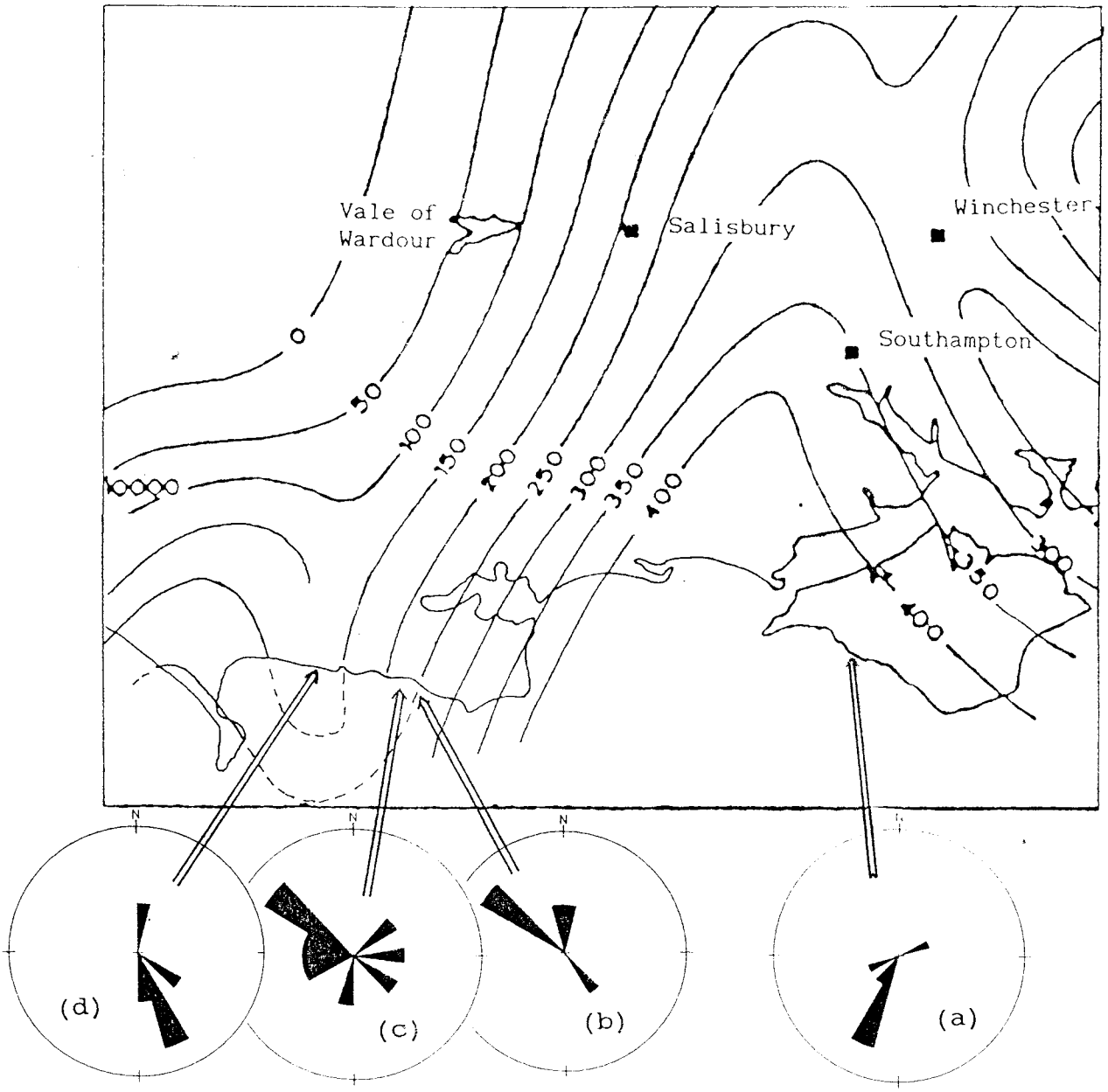

Fig. 8.3.1 Rose diagrams of K_{max} axes distributions for different localities along the southern coast of England, superimposed on the palaeotopographic model of the Wessex Basin for the Early Cretaceous stage, from Howitt (1964) (see Fig. 3.2.1). (a) Isle of Wight section, (b) Worbarrow Bay, (c) Mupe Bay and (d) Durdle Door. Symbols and conventions as in Figs. 3.2.1 and 8.2.4.

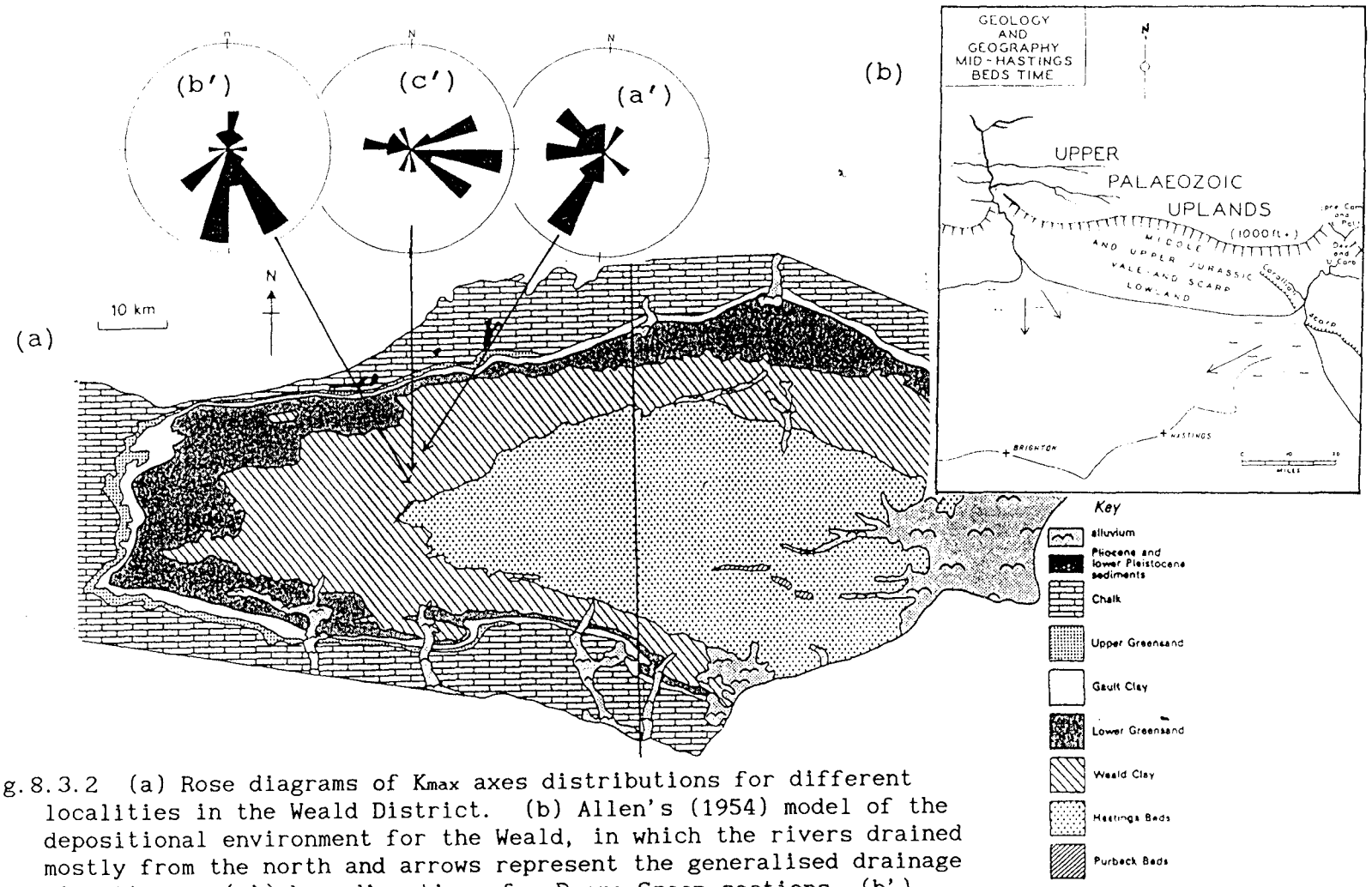

Fig. 8.3.2 (a) Rose diagrams of K_{max} axes distributions for different localities in the Weald District. (b) Allen's (1954) model of the depositional environment for the Weald, in which the rivers drained mostly from the north and arrows represent the generalised drainage directions. (a') k_{max} directions for Beare Green sections, (b') and (c') for the Langhurst sections (Weald Clay Formation). Symbols and conventions as in Fig. 8.2.4.

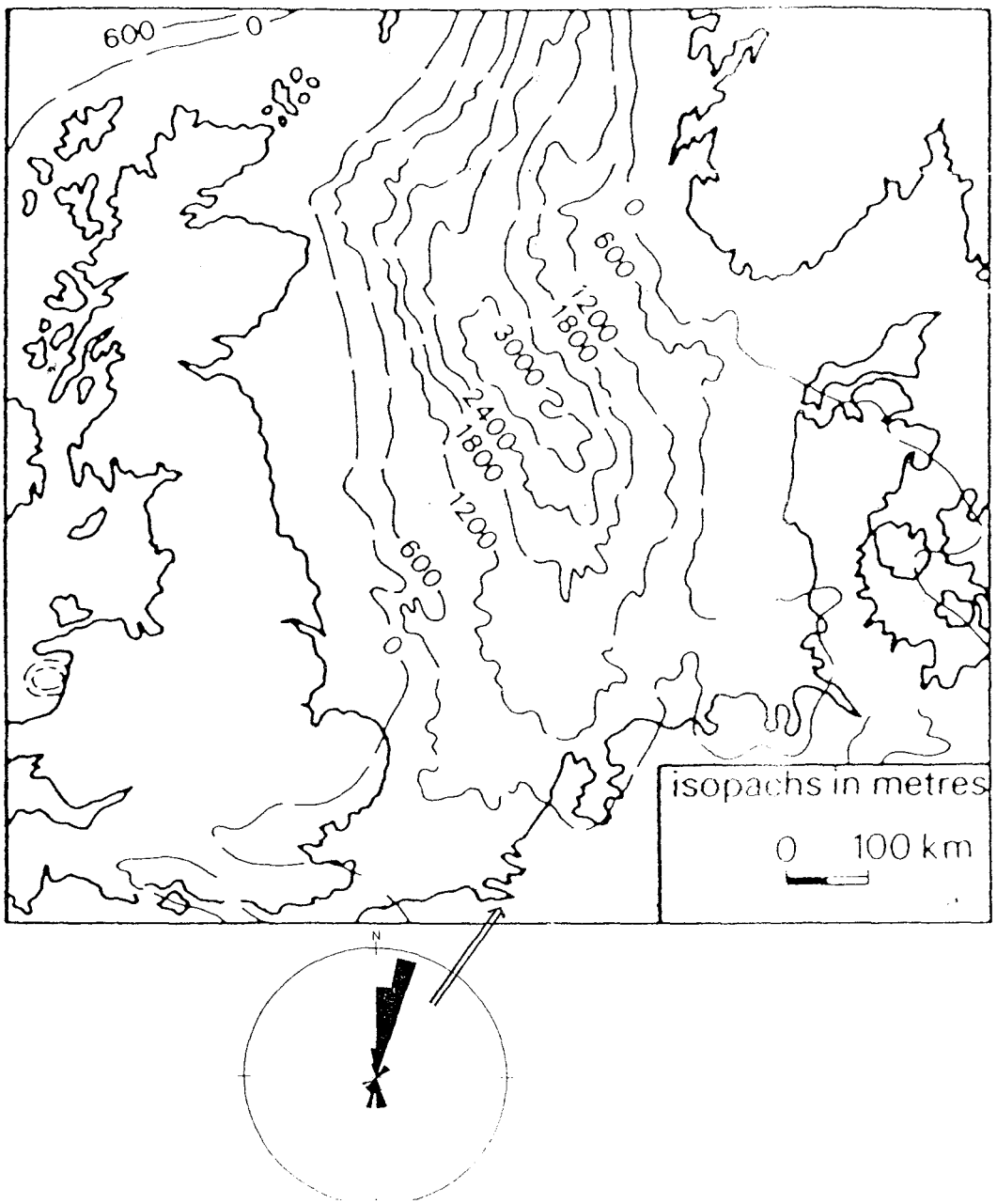

Fig. 8.3.3 K_{max} distribution for the Oligocene Boom Clay Formation, plotted with respect to the model of the North Sea depositional Basin during the Early Tertiary (Selley 1977). The k_{max} direction is parallel to the elongated direction of the basin and located at its southwestern margin.

CHAPTER IX CONCLUSIONS AND SUGGESTIONS FOR FURTHER WORK

§9.1 The Lower Cretaceous Wealden Beds of Southern and Southeast England

9.1.1) The Wessex Formation, Southern England.

The five best exposed sections of the Wessex Formation in Southern England have been fully investigated for both magnetostratigraphy and magnetic fabric. The magnetostratigraphic evidence gave well-correlated results throughout this formation, in which the Worbarrow Bay and Mupe Bay sections were the best exposed and revealed the expected magnetic polarity sequence for the Lower Cretaceous Chrons before Chron CM0 (which was previously identified within the Vectis Formation by Kerth & Hailwood, 1988). Therefore, the magnetic stratigraphy allows a refined estimate of the age of the beds to be made, based on a correlation of the observed polarity sequence with the Cretaceous polarity time scale of Kent & Gradstein (1985). Four reverse polarity events were revealed in the Worbarrow Bay section. Although some sampling gaps exist in the sequences measured, these should not lead to significant errors in the relative age determinations. The Mupe Bay section was almost a lateral duplicate of the upper part of the Worbarrow Bay section in its magnetostratigraphic characteristics. The other sections studied (the Compton-Hanover section on the Isle of Wight, the Lulworth Cove and Durdle Door sections in Dorset) all carried dominantly normal polarity magnetisations, as expected for their deposition during the long normal polarity interval between Chrons CM0 and CM1.

The Coarse Quartz Grit (CQG) layers present in the southern Dorset sections provide potentially important references for the correlation of these sections. However, it is demonstrated from the magnetostratigraphic data, that these layers generally occur at different stratigraphic levels in the different sections studied.

For correlation purposes, the NRM intensity values were found to be useful and they appear to offer greater potential for correlating the different sections than do the magnetic susceptibility values. The

latter had a much broader spectrum.

A suggestion for further work on the Wessex Formation of this area is that detailed thermal demagnetisation work should be done on samples from the vicinity of the CQG layers, at the Mupe Bay, Lulworth Cove and Durdle Door sections, to fully confirm that the isolated samples showing possible reverse polarity behaviour do not represent reversed events of significant duration.

9.1.2) The Weald Clay Formation, Southeast England.

The preliminary results for this formation make it clear that the characteristic magnetisation of these clay-rich sediments is suitable for magnetostratigraphic investigations. The reverse polarity event revealed in the Langhurst sections (Bed 2 of Thurrell *et al* 1968) indicates that the lower part of the formation at this locality must be older than Chron CM0 or CM1. A further full investigation of the Weald Clay Formation for magnetostratigraphic purposes is strongly recommended, not only utilising the available brickwork pit sections but also available borehole cores from this district.

The suggested major brickwork pits which should be sampled include Newdigate, Clock House, Warnham and South Water brickwork pits (see Fig.3.3.6a). Others distributed in the east and west of the area are also likely to yield important results, although some of them might have shorter available sections. This further work should extend to both the older and younger formations, eg the Hastings and the Atherfield Clay Formations. Borehole sections are likely to be an important source of information since good, continuous exposures in this area are rare.

§9.2 The Oligocene Beds of Southwest England and Northwest Belgium.

9.2.1) The Bovey Formation, Southwest England.

Although the magnetic intensities of samples from this formation were very weak, the overall magnetic polarity sequence yielded from the

three sections did give a clear pattern. The Borehole SD485 plays an important part in the correlation of the Longmarsh and John Acres Lane sections, which represent the main exposed bodies of the two sedimentary units (Southacre Clay and Lignite, Abbrook Clay and Sand) but with an incomplete boundary between them. Because of the lack of detailed biostratigraphic evidence for these sediments, the magnetic polarity sequences yielded for this formation can only be correlated in a preliminary way with the GPTS of Berggren *et al* (1985). Further work is necessary to extend the investigation to other relevant sections exposed in clay pits and to fully utilise other borehole cores (see Edwards 1976). The thermal demagnetisation procedure is recommended for the clay samples.

9.2.2) The Boom Clay Formation, Northwest Belgium.

The often erratic nature of the remanent magnetisation of samples from this remarkable formation made the determination of the magnetic polarity sequences relatively difficult. Some reasons have been put forward to explain these erratic characteristics, of which the most likely is believed to be the effects of secondary diagenetic processes that may have resulted in the formation of new magnetic minerals (Vandenberghe & Laga 1986). Pyrite (Fe_2S), in either crystalline or coating form, might be the major cause of the stable erratic magnetisation components which could not be completely removed by the a.f. demagnetisation technique used.

In spite of the above problems, the overall magnetic polarity patterns for the three quarry sections are relatively clear, except those in the upper part of the Kruibeke section, where a higher proportion of samples showed erratic behaviour. Combination of the preliminary magnetostratigraphic and very detailed biostratigraphic evidence made the correlation of this formation with the GPTS relatively straightforward. The main part of the formation, which has been assigned to nannofossil zone NP23, shows three well-defined normal polarity events, which can be correlated with some confidence to Chron C11 and the upper part of Chron C12.

Further work on these sections is strongly recommended, and the

investigation should be to extend to the Rupelian sections in the Winterwijk area (the Netherlands) and the Lower Rhine District (West Germany) (Van den Bosch & Hager 1984). It would be also valuable to study borehole sections which penetrate the Boom Clay and the overlying and underlying units in the Antwerp and surrounding area.

§9.3 Conclusions from magnetic fabric work

The best magnetic fabric results defined in present study were from the Weald Clay and Boom Clay Formations. The quality of the results is highly dependent on the magnetic mineral content of the samples, the magnetite-rich samples generally giving more reliable results.

All reliable magnetic fabric results from the present study, using both the LFTM and HFTM, demonstrated that the K_{max} directions can be related to the depositional environment models suggested by other authors. Different magnetic fabric characteristics have been observed for the continental and marine depositional facies, in which the former yield more complicated azimuthal K_{max} distributions, corresponding to the more complicated continental depositional environment, (reflecting, for example, seasonal fluctuations, intermittent connection with different depositional sources etc), compared with the apparently more uniform marine environment.

Further magnetic fabric investigations are recommended, particularly of the Weald Clay. However, the preliminary results reported have indicated that sampling deformation effects are likely to be minimised by cutting cubic specimens by scalpel, from oriented hand samples, rather than using the copper tube sampling method.

REFERENCES

Alvarez,W., Arthur,M.A., Fischer,A.G., Lowrie,W., Napoleone,G., Premoli Silva,I., & Roggenthen,W.M.,1977, Upper Cretaceous - Paleocene magnetic stratigraphy at Gubbio,Italy V.type section for the Late Cretaceous-Paleocene geomagnetic reversal time scale. Geol. Soc. Am. Bull., **88**, p.383-389.

Anderson,F.W. 1967. Ostracods from the Weald Clay of England. Bull. Surv. Gt. Britain. **27**. p.237-269.

Anderson,F.W.,1973. The Jurassic-Cretaceous transition: the non-marine ostracod faunas. in Casey,R. & Rawson,P.F. (ed) 1973, The Boreal Lower Cretaceous.

Anderson,J.G. 1983. Field geology in the British Isles — A guide to regional excursion. Published by Pergamon Press.

Anderton,R.,Bridges,P.H.,Leeder,M.R. & Sellwood,B.W., 1985. A dynamic stratigraphy of the British Isles — A study in crustal evolution. p.227-244

Allen,P., 1954. Geology and geography of the London-North Sea uplands in Wealden time Geol.Mag., **91**, p.498-508.

Allen,P., 1955. The age of the Wealden in north-western Europe. Gel. Mag., **92**, p.265-281.

Allen,P., 1959. The Wealden environment: Anglo-Paris Basin. Phil. Trans. R. Soc., B**242**, p.283-346.

Allen,P. 1965. L'age du Purbecko-Wealdien d'Angleterre. Mém.Bur.Rech. géol miniér. **34**, p.321-326.

Allen,P. 1967. Origin of the Hastings facies in north-western Europe. Proc.Geol.Ass. **78**, p.27-105.

Allen,P. 1975. Weald of the Weald: a new model. Proc.Geol.Ass., **86** (4), p.389-437.

Arkell,W.J. 1947. The geology of the country around Weymouth, Swanage, Corfe and Lulworth. Reprinted in 1978.

Banerjee,s.k., 1963. An attempt to observe the basal-plane anisotropy of hematite. Phil.Mag., **8**, p2119-2120.

Banerjee,s.k. and Stacey,F.D., 1967. The high-field torque-meter method of measuring magnetic anisotropy of rocks. in D.W. Collinson, K.M.Creer and S.K.Runcorn: Methods in Palaeomagnetism. Amsterdam. p.470-476.

Banner,F.T. & Blow,W.H., 1965. Progress in the planktonic foraminiferal biostratigraphy of the Neogene. Nature. London, **208**, p.1164-1166.

Bennison,G.M. & Wright,A.E. 1978. The Geological history of the

British Isles.

Berggren, W.A., 1965. Paleocene —— a micropalaeontologist's point of view. Bull.Am.Ass.Petrol.Geol., **49**, p.1473-1484.

Berggren, W.A. & Kent, D.V. & Flynn, J.J., 1985. Palaeogene geochronology and chronostratigraphy. in Snelling N.J. (ed) Geochronology and the geological record. Mem.Geol.Soc., no.10, Blackwell Scientific Publications, Oxford. p.141-195.

Beyrich, G., 1854. Ueberdie stellung deshessischen Tertiärbildunggen. Mber. Preuss. Akad. Wiss. p.640-666.

Bhatal, R.S. 1971. Magnetic anisotropy in rocks. Earth-Sci.Rev. **7**, p.227-253.

Blow, W.H., 1969. Late Middle Eocene to recent foraminiferal biostratigraphy. in Brönnimann, P. & Renz, H.H. (ed), Proc.first Intern.Conf.Planktonic Microfossils. Geneva, 1967. E.J.Brill, Leiden, p.199-422

Bolli, H.M., 1957. Planktonic foraminifera from the Oligocene-Miocene Cipero and Lengua Formations of Trinidad, B.W.I. Bull.US.natn.Mus., no.215, p.97-123.

Bolli, H.M., 1966. Zonation of Cretaceous to Pliocene marine sediments based on Planktonic Foraminifera. Boln, Inf.Asoc.Venerzol.Geol., Min.Petrol., **9**, no.1, p.3-32.

Boscoh, M.vanden, & Hager, H., 1984. Lithostratigraphic correlation of Rupelian deposits (Oligocene) in the Boom area (Belgium), the Winterswijk area (The Netherlands) and the lower Rhine district (F.R.G.). Meded.Werkgr.Tert Kwart.Geol., **21**(3), p.123-138.

Boswell,.G.H., 1929. Cretaceous. in Evans, J.W. *et al* (ed), Handbook of the geology of Great Britain —— A compilative work, 1929. p.383-396.

Boulter, M.C. & Wilkinson, G.C., 1977. A system of group names for some Tertiary pollen. Palaeonotology. **20**, p.559-579.

Bramlette, M.N. & Riedel, W.R., 1954. Stratigraphic value of discoasters and some other microfossils related to recent coccolithophores. J.Palaeont., **28**, p.385-403.

Bramlette, M.N. & Wilcoxon, J.A., 1967. Middle Tertiary calcareous nannoplankton of the Cipero Section. Trinidad, W.I., Tulane Stud. Geol., **5**(3), p.93-131.

Brian, D and Insole, A 1987. The Isle of Wight. Geologists' Association Guide No.**25**.

Brown, G.C. & Mussett, A.E. 1981. The inaccessible Earth. Published by George Allen & Unwin Ltd.

Casey, R. 1961. The stratigraphical palaeontology of the Lower Green Sand. Palaeontology. **3**, p.1-22.

Casey,R. and Gallois,R.W. 1973. The Sandringham Sands of Norfolk. Proc. Yorks. Geol. Soc., **40**, p.1-22.

Casey,R. and Rawson,P.F. 1973. (ed) The Boreal Lower Cretaceous. Geol. J1 Spec. Iss. 5, Seel House Press, Liverpool.

Cavelier,C. 1986. Correlations and biostratigraphic events at the Eocene-Oligocene boundary in France and in Europe. in "Terminal Eocene Events" (ed) Pomerol,C & Premoli-Silva,I., published by ELSEVIER, p.91-96.

Chan,L.S. and Alvarez,W., 1983. Magnetic polarity stratigraphy. Rev.Geophys.Space Phys. **21**, p.620-626.

Chandler,M.E.1957. The Oligocene flora of the Bovey Tracey lake basin, Devonshire. Bull.Br.Mus.Nat.Hist., **3**, p.71-123.

Channell,J.E.T., Ogg,J.G. & Lowrie,W., 1982. Geomagnetic polarity in the Early Cretaceous and Jurassic. Phil.Trans.R.Soc.London, **A**, **306**,p.137-146.

Chevallier,R., Mathieu,S., 1943. Propriétés magnétiques des proudres d'hematites-influence des dimensions des grains. Ann.Phys., **18**. p.258-288.

Collinson,D.W., 1965. Origin of remanent magnetisation and initial susceptibility of certain red sandstones. Geophys.J.R.Astr.Soc., **9**, p203-217.

Collinson,D.W. 1983. Methods in rock magnetism and palaeomagnetism. Published by Chapman and Hall.

Cox,A. 1975. The frequency of geomagnetic reversals and the symmetry of the non-dipole field. Rev.Geophys.Space Phys. **13**. p.35.

Cox,A. 1982. Magnetostratigraphic time scale. In Harland,W.B., Cox,A.V., LLewellyn,P.G., Pickton,C.A.G., Smith,A.G., and Walters, R.A., Geologic time scale. Cambridge University Press, Combridge. p.63-84.

Cox,A.V.,Doell,R.R., & Dalrymple,G.B., 1963. Geomagnetic polarity epochs and Pleistocene geochronometry. Nature. **198**, p.1049-1051.

Curry,D., Adams,C.G., Boutler,M.C., Dilley,F.C.,F.E., Funnell,B.M. & Wells,M.K. 1978. A correlation of Tertiary rocks in the British Isles. Geol.Soc.Lond.,Special Report no12.

Daley,B. and Insole,A. 1984. The Isle of Wight. Geol.Ass.Guide, **25**.

Daley,B.and Stewart,D.J. 1979. Week-end field meeeting: The Wealden Group in the Isle of Wight. Proc.Geol.Ass., **90** (2) p.51-54.

Dearman,W.R. 1963. Wrench faulting in Cornwall and south Devon. Proc.Geol.Ass., **74**, p.265-287.

Dodson,R., Dunn,J.R., Fuller,M., Williams,I., Ito,H., Schmidt,V.A. and

Wu Yu M., 1978, Palaeomagnetic record of a late Tertiary field reversal. Geophys.J., **53**, p373.

Dumont,M.A. 1849. Rapport sur la carte géologique du Royaume. Bull. Acad. Royale Belgique toume XVI partie, p.351-373.

Dunlop,D.J., 1979, On the use of Zijderveld vector diagrams in multi-component palaeomagnetic studies. Phys.Earth Planet.Int., **20**, p12-24.

Edwards,R.A. 1976. Tertiary sediments and structure of the Bovey Basin, south Devon. Proc.Geol.Ass., **87** (1) p.1-26.

Ellwood,B.B. 1984. Bioturbation: minimal effects on the magnetic fabric of some natural and experimental sediments. Earth and Planetary Science Letters. **67** p.367-376.

Elmore,R.D. & Van der voo,R. 1982. Origin of hematite and its associated remanence in the Copper Harbor Conglomerate (Keweenawan) upper Michigan. J.Geophys. Res., **87**, B13, p.10918-10928.

Evans,J.W., 1929. Handbook of geology of Great Britain —— A compilative work. ed. by J.W.Evans and C.J.Stubblefield. p.383-396.

Fasham,M.J.R. 1971. A gravity survey of the Bovey Tracey basin, Devon. Geol.Mag., **108**, p.119-130.

Galbrun,B. 1985. Magnetostratigraphy of the Berriasian stratype section (Berrias, France). Earth Planet. Sci. Lett., **74**, 130-136.

Gollois,R.W. 1965. British regional geology: The Wealden District. 4th edition. published by NERC Institute of Geological Sciences, 1965.

Gibbons,W., 1981. The Weald. Published by UNWIN PAPERBACKS.

Graham,J.W., 1949. The stability and significance of magnetism in sedimentary rocks. J.Geophy.Res. **54**, p.131.

Granar,L. 1958. Magnetic measurements on Swedish varved sediments. Arkif.F.Geofysik, **3**, p.1-40.

Gravenor,C.P., Symons,D.T.A. and Coyle,D.A. 1984. Errors in the anisotropy of magnetic susceptibility and magnetic remanence unconsolidated sediments produced by sampling methods. Geophys. Res. Letter. **1** (9) p.386-839.

Gulinck,M. 1965. Le passage du Bartonien au Rupélien dan la region Boom-Malines. Bull. Soc. belge Géol., Bruxelles, t.XXIV. p.115-119.

Hailwood,E.A. 1989. Magnetostratigraphy. The Geological Society special report No.19. Published by Blackwell Scientific Publications.

Hailwood, E.A. 1989. The role of magnetostratigraphy in the development

of geological time scales. Paleoceanography, **4**. no.1 page 1-18, Feb. 1989.

Hailwood,E.A., Bock,W., Costa,L., Dupeuble,P.A., Muller,C., & Schnitker,D. 1979. Chronology and biostratigraphy of northeast Atlantic sediments DSDP, Leg 48. In Montadert,L., Roberts,D.G. *et al.* Init.Rep.DSDP., **48**,Washington (US Govt, Printing Office), p.1119-1141.

Hailwood,E.A. and Sayre,W.O., 1979. Magnetic anisotropy and sediment transport directions in North Atlantic Early Cretaceous black shales Eeocene mudstones correlated on DSDP LEG48. Init. Rept. DSDP. Vol. XLVIII, Washington (US Govt.printing office).

Hallam,A.,Hancock,J.M.,LaBrecque,J.L.,Lowrie,W. & Channell,J.E.T. 1985. Jurassic and Cretaceous geochronology and Jurassic to Paleogene magnetostratigraphy. in Snelling,N.J. (ed), The chronology of the geological record. Published by Blackwell Scientific Publication, Oxford. p.118-140.

Halls,H.C. 1976. A least squares method to find a remanence direction from converging remagnetisation circles. Geophys.J.R.Astron.Soc., **45**,p.297-304.

Halls,H.C. 1978. The use of converging remagnetisation circles in palaeomagnetism. Phys.Earth Planet.Int., **16**, p.1-11.

Hamilton,N. 1967. Laboratory redeposition studies —— an appraisal of apparatus and technique. in D.W.Collinson, K.M.Creer and S.K. Runcorn (ed) "Methods in palaeomagnetism" Elsevier, Amsterdam. p.596-603.

Hamilton,N., Owens,W.H. and Rees,A.I. 1968. Laboratory experiments on the production of grain orientation in shearing sand. J.Geol., **76**, p465-472.

Hamilton,N. and Rees,A.I. 1970. The use of magnetic fabric palaeocurrent estimation. in S.K.Runcorn (ed) Palaeogeophysics. Oxford University Press. p.445-463.

Hedley,I.G. 1968. Chemical remanent magnetisation of the FeOH, Fe_2O_3 system. Phys.Earth Planet Ints. **1**, p.103-121.

Heirtzler,J.R., Dickson,G.O., Herron,E.M., Pitman,W.C.III and LeipichonX. 1968. Marine magnetic anomalies, geomagnetic field reversals and motions of the ocean floor and continents. J.Geophy.Res. **73**, p.2119.

Heller,F. 1980. Self-reversal of natural remanent magnetisation in the Olby-Laschamp lavas. Nature, **284**, no.5754, p334-335.

Henshaw,P.C. & Merrill,R.T. 1980. Magnetic and chemical changes in marine sediments. Rev. Geophys. Spac. Phys., **18**, no2, p.483-504.

Highley,D.E. 1976. The economic geology of the Weald. Proc.Geol.Ass., **86**, p.559-569.

Hoffman,K.A. 1988. Ancient magnetic reversals: clue to the geodynamo. Sci.Am., **285**, no.5, p.50-59.

Hooyberghs,H. 1983. Contribution to the study of planktonic Foraminifera in the Belgian Tertiary. Aardkindige Mededelingen, K.U.Leuven., V.Z.

Howitt,F. 1964. Stratigraphy and structure of Purbeck inliers of Sussex (England). Q.J.Geol.Soc. London, **120**, p.77-113

Hrouda,F. 1982. Magnetic anisotropy of rocks and its application in geology and geophysics. Geophysical Surveys **5** p.37-82.

Hrouda,F. and Janák,F. 1971. A study of the hematite fabric of some red sediments on the basis of their magnetic susceptibility anisotropy. Sediment. Geol., **6**, p.187-199.

Hughes,N.F. 1973. Palynological time correlation of English Wealden with boreal marine successions. *In:* Casey and Rawson (eds) 1973 The Boreal Lower Cretaceous. Liverpool.

Hughes,N.F. and McDougall,A.B. 1989. New Wealden correlation for the Wessex Basin. Proc.Geol.Ass., **100** (1), p.85-95.

Hughes,N.F. and Moody-Stuart,J.C. 1967. Proposed method of recording pre-Quaternary palynological data. Rev.Palaeobot.Palynol., **3**, p.347-358.

Institute of Geological Sciences, 1976. Geological maps of England and Wales, 1:50 000, Swanage. Sheet 343 and part of 342.

Institute of geological sciences, 1978. Gelogical maps of England and Wales, 1:50 000, Isle of Wight. Special sheet, drift edition, Sheets 344 & 345 and part of 330 & 331.

Ising,E. 1942. On the magnetic properties of varved clay. Arkiv. Astron. Fysik., **29A** (5) p.1-37.

Jacobs,J.A. 1984. Reversals of the Earth's magnetic field. Published by Adam Hilger Ltd.

Johnson,E.A., Murphy,T. & Torreson,O.W. 1984. Pre-history of the earth's magnetic field. Terr. Magn. Atomos. Elec., **53**, p.349-372.

Johnson,H.P., Kinoshita,H. & Merrill,R.T. 1975. Rock magnetism and palaeomagnetism of some North Pacific deep sea sediments. Geol. Soc. Am. Bull., **86**, p.412.

Kennedy,W.J. and MacDougall,J.D.S. 1969. Crustacean burrows in the Weald Clay (Lower Cretaceous) of southeastern England and their environmental significance. Palaeontology **12** part3 p.459-471.

Kennedy,W.J. & Odin,G.S. 1982. The Jurassic and Cretaceous time scale in 1981. in Odin,G.S.(ed) Numerical Dating in Stratigraphy. John Winley. Chichester. p.557-592.

Kent,D.V. & Gradstein,F.M. 1985. A Cretaceous and Jurassic

geochronology. Geol. Soc. Am. Bull., **96**. p.1419-1427.

Khan,M.A. 1962. Anisotropy of magnetic susceptibility of some igneous and metamorphic rocks. J.Geophy.Res., **67**, p.2873-2885.

King,R.F. 1955. Remanenet magnetism of artificially deposited sediments. Mon. Notice Roy. Astron. Soc. Geophys. Suppl., **1**, p.115-134.

Kirkaldy,J.F., 1958. Geology of the Weald. Geologists' Association Guides no.29.

Kerth,M. and Hailwood,E.A. 1988. Magnetostratigraphy of the Lower Cretaceous Vectis Formation (Wealden Group) on the Isle of Wight, southern England. J. Geol. Sco. London, **145**, p.351-360.

King,R.F. & Rees,A.I. 1962. The measurement of the anisotropy of magnetic susceptibility of rocks by the torque method. J. Geophys. Res., **67**, no.4, p.1565-1572.

Koci,A. 1985. Variations of the geomagnetic field at the time of reversals. Stud.Geophys.Geod., **29**, no.3, p.280-289.

Kukla,G.,Heller,F.,Liu,X.M.,Xu,T.C.,Liu,T.S. and An,Z.S. 1988. Pleistocene climates in China dated by magnetic susceptibility. Geology, **16**, p.811-814.

La Brecque,J.L., Kent,D.V. & Candy,S.C. 1977. Revised magnetic polarity time scale for Late Cretaceous and Cenozoic time. Geology. **5**, p.330-335.

La Brecque,J.L. 1985. Problems in magnetostratigraphic time-scale calibration. in Snelling,N.J.(ed) The Chronology of the geological record. Mem. Geol. Soc. Lond., Blackwell Scientific Publications, Oxford. p.125-131.

Larson,R.L. & Hilde,T.W.C. 1975. A revised time-scale of magnetic reversals for Early Cretaceous and Late Jurassic. J.Geophys.Re., **80**, p.2586-2594.

Larson,R.L. and Pitman,W.C. 1972. World wide correlation of Mesozoic magnetic anomalies and its implications. Bull.Geol.Soc.Am., **83**, p.3645.

Lowrie,W. and Alvarez,W. 1981. One hundred million years of geomagnetic polarity history. Geology, **9**, p.392-397.

Lowrie,W. and Alvarez,W. 1984. Lower Cretaceous magnetic stratigraphy in Umbrian pelagic limestone section. Earth Planet. Sci. Lett., **71**, p315-328.

Mankinen,E.A. and Dalrymple,.B. 1979. Revised geomagnetic polarity time scale for the interval 0-5 m.y.B.P., J.Geophys.Res., **84**, p.615-626.

Mardia,K.V. 1972. Statistics of directional data. Published by Academic Press INC.(London) Ltd.

Marechal,R. & de Breuck,W. 1979. Geologie. in Twintig eeuwen Valaanderen, **7**(1), p.13-45.

Martini,E. 1970. The Upper Eocene Brockenhurst Bed. Geol.Mag., **107**, p.225-228.

Martini,E. & Worsley,T. 1970. Standard Neogene calcareous nannoplakton zonation. Nature, London, **225** p.289-290.

Mason,R.G. 1958, A magnetic survey of the west coast of the united states between latitudes 32° and 36° N and longitudes 121° and 128° W. Geol.J.Roy.Astron.Soc, **1**, p.320-329.

Matuyama,M. 1929. On the direction of magnetism of basalt in Japan, Tyosen and Manchuria. Japan Acad.Proc., **5**, p.203-205.

McElhinny,M.W. 1964. Statistical significance of the fold test in palaeomagnetism. Geophys. J. Roy.Astron.Soc., **8**, p338-340.

McElhinny,M.W. 1973. Palaeomagnetism and plate tectonics. Published by Cambridge University Press 1973.

McFadden,P.L. 1980. The best estimate of Fisher's precision parameter κ. Geophys.J.R.Astr.Soc., **60**, p.397-407.

McFadden,P.L. & Jones,D.L. 1981. The fold test in palaeomagnetism. Geol.J.Roy.Soc., **67**, No.1, p53-58.

McFadden,P.L. 1990. A new fold test for palaeomagnetic studies. Revised version submitted to Geophys.J.Int.

Melville,R.V. & Freshney,E.C. 1982. British regional geology — The Hampshire Basin and adjoining areas. Fourth edition. Published by London Her Majesty's Stationery Office.

Meshcheryakov,G.A., Astaf'yev,V.V. & Marchenko,A.N. 1979. Multipole analysis of the global geomagnetic field for intervals of varying duration and secular variations of this field. Geomag.Aeron. (USSR), **19**, no.4, p.482-488.

Müller,C. 1970. Nannoplankton aus dem Mittel-Oligozän von Norddeutschland und Belgien. N.Jb.Geol. Paläont. Abh. **135**(1), p.82-101.

Nagata,T. 1953. Rock magnetism. Tokyo.

Obradovich,J.D. & Cobban,W.A. 1975. A timescale for the Late Cretaceous of the western interior of North America. in Caldwell,W.G.E.(ed) The Cretaceous system in the Western Interior of North America. Spec.Pap.Geol.Ass.Can., **13**, p.31-54.

Ogg,J.G. 1981. Sedimentology and palaeomagnetism of Jurassic pelagic limestones:"Ammonitico rossoslfacies". Unpublished Ph.D. thesis, Univ. of California, San Diego.

Ogg,J.G. 1983. Magnetostratigraphy of Upper Jurassic and Lower

Cretaceous sediments. DSDP Site 534 Western North Atlantic. in Sheridan,R.E. *et al* . Rep.DSDP, **76**, Washinton (US Govt. Printing Office), p.685-699.

Onstott,T.C. 1980. Application of the Bingham Distribution in paleomagnetic studies. J.Geophys.Res., **85**, no.B3, p.1500-1510.

Opdyke,N.D. 1972. Paleomagnetism of deep-sea cores. Rev Geophys.Space Phys. **10**, p.213-249.

Opdyke,N.D., Glass,B., Hays,J.D. & Foster,J. 1966. Paleomagnetic study of Antarctic deep-sea cores. Science, **154**, p.349-357.

Opdyke,N.D. & Henry,K.W. 1969. A test of the dipole Hypothesis. Earth Planet. Sci. Lett., **6**, p.138-151.

O'Reilly,W.O. 1984. Rock and mineral magnetism. Published by Blackie & Son Ltd.

Owens,W.H. 1974. Mathematical method studies on factors affecting the magnetic anisotropy of deformed rocks. Tectonophysics, **24**, p.115-131.

Packard,M. & Varian,R. 1954. Free nuclear induction in the Earth's magnetic field. Phys. Rev. Series 2, **93**, p.945-955.

Payne.M.A. and Verosub,K.L. 1982. The acquisition of post-depositional remenant magnetisation in a variety of natual sediments. Geophys. J.R.Astr.Soc., **68**, p.625-642.

Peddie,N.W. 1982. International Geomagnetic Reference Field: the third generation J. Geomag.Geoelec., **34**, p.309.

Piper,J.D.A. 1987. Palaeomagnetism and the continental crust. Published by Open University Press.

Piper,J.D.A. 1988. Paleaomagnetic database. Open University Press.

Porath,H. and Chamalaun,F.H. 1966. The magnetic anisotropy of hematite bearing rocks. Pure Appl.Geophys., **64**, p.81-88.

Pretice, .E. 1962. Some sedimentary structures from a Weald Clay Sandstone at Warnham Brickworks, Horsham, Sussex. Proc.Geol.Ass., **73**, p.171-185.

Rawson,P.F., Curry,D., Dilley,F.C., Hancock,J.M., Kennedy,W.J., Neale, J.W. and Worssam,B.C. 1978. A correlation of Cretaceous rocks in the British Isles. Geol.Soc.London, Special Report No.9.

Readman,P.W. and O'Reilly,W. 1972. Magnetic properties of oxidised titanomagnetites., J.Geomag.Geoelec., **24**, p.69-90.

Rees,A.I. 1966. The effect of depositional slopes on the anisotropy of magnetic susceptibility of laboratory deposited sands. J.Geol., **74**, p.856-867.

Rees,A.I. 1968. The production of preferred orientation in a

concentrated dispersion of elongated and flattened grains. J. Geol., **76**, p.457-465.

Rees, A. I. 1971. The magnetic fabric of a sedimentary rock deposited on a slope. J. Sediment Petrol., p.307-309.

Rees. A. I. & Woodall, W. A. 1975. The magnetic fabric of some laboratory-deposited sediments. Earth Planet. Sci. Lett. **25**, p.121-130.

Reeves, J.W. 1968. Subdivision of the Weald Clay in the north Surrey and Kent. Proc. Geol. Ass. **79** p.457-476.

Roth, P. H., 1970. Oligocene calcareous nannoplankton biostratigraphy. Eclog. Geol. Helv., **63**(3), p.799-881.

Roy, J. L., Lapointe, P. L. and Anderson, P. 1975. Paleomagnetism of the oldest red beds and the direction of Late Aphebian polar wander relative to Laurentia. Geophys. Res. Lett., **2**, p.537-540.

Sclater, J. G., Jarrard, R. D., McGowran, R. D. & Gardener, S. Jr. 1974. Comparison of the magnetic and biostratigraphic time scales since the late Cretaceous. In Von der Borch, C. C. *et al.* Init. Rep. DSDP. **22**, Washington (US Govt. Printing Office), p.381-386.

Selley, R.. 1976. The habit of North Sea oil. Proc. Geol. Ass., **87**, p.359-388.

Shaw, J. & Share, J. A. 1984. An automatic superconducting magnetometor and demagnetising system. Geophys. J. R. Astr. Soc., **78**, p.209-218.

Shcherbakov, V. P. & Shcherbakova, V. V., 1987. On the physics of acquisition of post-depositional remanent magnetisation. Phys. Earth Planet. Int., **46**. p.64-70.

Simpson, M.. 1985. The stratigraphy of the Atherfield Clay Formation (Lower Aptian, Lower Cretaceous) at the type and other localities in southern England. Proc. Geol. Ass., **96**, p.23-45.

Smith, A. G., Hurley, A. M. & Briden, J. C. 1981. Phanerozoic palaeocontinental world maps. Cambridge University Press.

Snelling, N. J. 1985. The chronology of the geological record.

Sprague, D. L. & Pollack, H. N. 1980. Heat flow in the Mesozoic and Cenozoic. Nature, **285**, No.5764, p393-395, Jun.5.

Stacey, F. D. 1960. Magnetic anisotropy of igneous rocks. J. Geophys. Res., **65**, no.8, p.2429-2442.

Stacey, F. D. 1963. The physical theory of rock magnetism. Phil. Mag. Supp. Adv. Phys., **12**, p.46-133.

Stephenson, A., Sadikun, S. and Potter. D. K. 1986. A theoretical and experimental comparison of the anisotropies of magnetic susceptibility and remanence in rocks and minerals. Geophys. J. R. astr. Soc., **84**. p 185-200.

Steurbaut,E. 1986. The Kallo Well and its key-position in establishing the Eo-Oligocene boundary in Belgium. in Pomerol & Premolin-Silva (ed) Terminal Eocene events. Amsterdam (Elsevier Publ.), p.97-100.

Steurbaut,E. & Herman,J. 1978. Biostratigraphie et poissons fossiles dela formation de L'Argile de Boom (Oligocene Moyen Du bassin Belge). Géobios, no.11, p297-325.

Stewart,D.J. 1978. The sedimentology and palaeoenvironment of the Wealden Group of the Isle of Wight, Southern England. unpublished Ph.D Thesis, Portsmouth Polytechnic.

Stewart,D.J. 1981. A meander-belt sandstone of the Lower Cretaceous of southern England. Sedimentology **28** p.1-20.

Stewart,D.J. 1983. Possible suspended-load channel deposits from the Wealden Group (Lower Cretaceous) of southern England. Spec. Publs. Int. Ass. Sediment. **6** p.369-384.

Stoner,E.C. 1945. The demagnetising factors for Ellipsoids. Phil.Mag., **36**, p.803-821.

Strangway,D.W., Larson,E.E. & Goldstein,M. 1968. A possible cause of high magnetic stability in volcanic rocks. J.Geophys.Re., **73**, p.3787-3795.

Tarling,D.H. 1983. Palaeomagnetism. Published by Chapman and Hall Ltd.

Theyes,F. & Hammond,S.R. 1974. Cenozoic magnetic time scale in deep-sea cores: completion of the Neogene. Geology, **2**, p.487-492.

Thurrell,R.G., Worssam,B.C. and Edmonds,E.A. 1968. Geology of the country around Haslemere. Mem.Geol.Surv.G.B.

Townsend,H.A. and Hailwood,E.A. 1985. Magnetostratigraphic correlation of Palaeogene sediments in the Hampshire and London Basin. southern U.K.. J. Geol. London, **142** p.957-982.

Valet,J.P., Laj,C. & Tucholka,P. 1986. High-resolution sedimentary record of a magnetic reversal. Nature. **322**, no.6074, p.27-32.

Vandenberghe,N. 1978. Sedimentology of the Boom Clay (Rupelian) in Belgium. Verhand. Kon. Acad. België, Wetensch, **40**(147).

Vandenberghe,N. 1981. Rupelian, Bulletin D'information, des Géologues Du Bassin De Paris. Stratotypes of Palaeogene stages. 1981, Mém. hors série N°2, ISSN 0374-1346, p.203-217.

Vandenberghe,N. & Laga,P. 1986. The septaria of the Boom Clay (Rupelian) in its type area in Belgium. Aardkundige Mededelingen, **3**, p.229-238.

Vandenberghe,N. & Van Echelpoel,E. 1982. Field Guide to the Rupelian stratotype.

Van der voo,R., Henry,S.G. and Pollack,H.N. 1978. On the significance

and utilisation of secondary magnetisations in red beds. Phys. Earth Planet. Int., **16**, p.12-19.

Van Hinte J.E. 1976. A Cretaceous time scale. Am. Assoc. Petrol. Geol. Bull., **60**, p.498-516.

Versub,K.L. 1977. Depositional and post depositional processes in the magnetisation of sediments. Rev. Geophys. Space Phys., **15**, no2, p.129-143.

Vlasov,A.Y. & Zvegintsev,A.G. 1969. On the self-reversal of rock magnetisation. IASPEI/IAGA (Programme and Abstracts), Madrid, Spain, Sep.1969, p189.

Windley,B.F. 1984. The evolving continents. 2nd edition, John Windley & Sons, Chichester.

Worssam,B.C. and Thurrell,R.G. 1966. Field meeting to an area north of Horsham, Sussex. Proc. Geol.Ass., **77** p.263-271.

Worssam,B.C. 1978. The stratigraphy of The Weald Clay. Rep. Inst. Geol. Sci., No.78/11. Institute of geological sciences, London.

Worssam,B.C. and Ivimey-Cook.H.C. 1971. The stratigraphy of the Geological Survey borehole at Warlingham, Surrey. Bull. Geol. Surv.G.B., No.36, p.1-146.

APPENDIX 1. MAGNETOSTRATIGRAPHIC RESULTS FROM ISLE OF WIGHT SECTION (LOWER CRETACEOUS)

SAMPLE No	STRATI. HEIGHT (meter)	COMPONENT 1 (before B.C) DEC	INC	COMPONENT 2 (after B.C) DEC	INC	RC/α95	DEMAG. RANGE mT/°C	MAGNETIC CHARACT. trend/sep	POLARI (N/R)	POLARI. SEQUENCE
	start from the boundary of Vectis Formation and Wessex Formation									
CB1.1	137.99							TREND	R	
1.2										
2.1a	134.99	293.2	59.9	313.5	47.6	8.6	25-35mT	SEP	N	
2.2a		358.3	65.7	356.8	47.1	.54/.99	10-35	SEP	N	
3.1a	132.74	3.2	70.6	3.5	48.8	.97/.99	10-35	SEP	N	
3.2a		5.4	72.6	4.5	50.8	.90/.99	200-400°C	SEP	N	
4.1	130.24	5.5	66.6	4.8	44.6	.96/1.0	10-35	SEP	N	
4.2		343.6	54.1	350.0	33.2	.97/.99	200-500	SEP	N	
5.1	127.24									
5.2a		24.5	65.2	11.5	46.1	.85/.99	10-35	SEP	N	
6.1a	125.78	354.6	66.8	354.4	45.8	.99/1.0	20-35	SEP	N	
6.2a		10.8	57.9	5.4	37.7	.79/.99	100-500	SEP	N	
7.1a	118.26	351.7	79.1	353.2	58.1	1.8	5-35	SEP	N	
7.1b		2.0	71.2	358.0	50.3	5.8	300-600	SEP	N	
7.2		36.8	71.0	22.6	54.5	.99/.99	300-600	SEP	N	
8.1a	117.26	16.9	60.7	13.3	42.9	.98/1.0	20-35	SEP	N	
8.2		9.1	58.9	8.2	40.9	.89/.99	200-400	SEP	N	
9.1	116.41	13.3	64.0	10.4	47.1	.83/.97	10-35	SEP	N	
10.1	115.41	42.0	71.0	25.5	55.0	0.3	10-35	SEP	N	
10.2		14.0	73.5	9.7	55.8	.90/.99	200-500	SEP	N	
11.1	109.43	1.1	66.4	3.1	48.5	.90/1.0	10-35	SEP	N	
11.2		341.6	70.1	352.6	53.1	.97/.99	100-500	SEP	N	
12.1	107.11	356.3	72.6	1.1	54.7	.28/.99	10-35	SEP	N	
12.2		356.6	62.2	359.9	44.4	6.0	100-500	SEP	N	
13.1	106.11	359.3	59.3	1.4	41.4	.93/.99	20-35	SEP	N	
13.2a		12.6	52.1	10.9	34.2	.99/.99	100-600	SEP	N	
14.1	103.41									
14.2								TREND	R	
*15.1	97.41									
15.1										
16.1	96.41									
16.2a		12.8	62.9	10.3	45.0	.98/.99	10-35	SEP	N	
16.2b		3.6	67.6	0.5	49.9	.11/.99	100-600	SEP	N	
17.1	90.26									
17.2a		353.8	64.3	358.3	46.6	0.7	10-35	SEP	N	
17.2b		347.6	70.3	356.0	53.1	.93/.99	200-600	SEP	N	
18.1	87.66									
18.2										
19.1	84.81	236.2	-36.0	228.7	-23.5	0.8	20-35	SEP	R	
19.2		257.5	-49.2	241.2	-41.0	3.5	100-600	SEP	R	
20.1	82.81	350.4	70.7	357.5	53.0	0.3	10-35	SEP	N	
20.2		357.8	67.4	1.1	49.5	.64/1.0	200-500	SEP	N	
21.1	77.34	1.6	68.6	3.4	50.6	3.5	100-600	SEP	N	
21.2										
22.1a	75.84	321.2	58.1	334.9	43.8	.99/.99	200-500	SEP	N	
22.2a		19.6	47.0	16.6	29.4	3.3	100-500	SEP	N	
23.1	74.00	22.3	71.1	14.6	53.6	.96/.99	200-600	SEP	N	
23.2										
24.1	72.69	19.3	66.3	14.0	48.6	5.4	100-500	SEP	N	

SAMPLE No	STRATI. HEIGHT (meter)	COMPONENT 1 (before B.C) DEC	INC	COMPONENT 2 (after B.C) DEC	INC	RC/α_{95}	DEMAG. RANGE mT/°C	MAGNETIC CHARACT. trend/sep	POLARI. (N/R)	POLARI. SEQUENCE
CB24.2										
25.1	71.53	3.8	56.1	4.4	38.1	.98/1.0	100-400	SEP	N	
25.2a		15.9	57.8	12.9	40.0	.97/.99	100-600	SEP	N	
26.1	69.27	344.9	67.3	2.2	48.8	.70/.99	200-500	SEP	N	
26.2		0.3	66.3	2.2	48.4	.70/.99	200-400	SEP	N	
27.1	66.47									
27.2										
28.1	65.52	35.7	58.1	26.5	41.8	.94/.99	200-600	SEP	N	
28.2		36.5	62.4	25.7	46.0	12.7	100-500	SEP	N	
29.1	64.06	359.2	71.5	348.8	55.8	.71/.98	100-500	SEP	N	
29.2		337.7	53.5	345.6	37.8	.91/.96	100-500	SEP	N	
30.1a	59.56	346.3	62.4	353.3	45.3	.96/.99	200-500	SEP	N	
30.2		354.3	69.1	0.4	52.6	.10/.97	100-600	SEP	N	
60.1	56.56	36.0	52.1	28.4	35.9	.97/.99	200-500	SEP	N	
60.2		356.9	67.8	0.7	49.9	.20/.99	200-500	SEP	N	
59.1	55.06	3.8	66.6	5.0	49.6	.91/.97	300-500	SEP	N	
59.2		356.1	64.4	0.2	46.6	.04/.99	200-500	SEP	N	
58.1a	53.64	340.8	52.4	347.3	35.7	.99/.99	300-400	SEP	N	
58.2		336.8	55.6	345.2	39.2	.98/.99	300-500	SEP	N	
57.1	51.73	334.9	67.9	347.7	51.7	.85/.99	200-500	SEP	N	
57.2		350.8	64.0	356.4	46.4	.73/1.0	300-500	SEP	N	
56.1	50.41									
56.2										
55.1a	49.38	302.4	50.7	317.3	40.8	.99/.98	100-500	SEP?	N?	
55.2		310.4	42.0	319.7	33.9	.98/.86	100-500	SEP	N	
54.1	47.89	25.7	-14.7	28.5	-31.5	.99/.99	200-600	SEP	/	
54.2		6.2	45.9	6.0	28.1	.89/.98	300-500	SEP	N	
53.1a	46.89	24.2	58.4	18.5	41.1	.99/.99	100-500	SEP	N	
53.2a		338.8	49.3	334.7	33.5	.93/.95	200-500	SEP	N	
52.1	40.90	348.7	64.9	353.5	48.7	.49/.96	200-500	SEP	N	
52.2		353.6	67.3	358.6	49.5	4.3	100-500	SEP	N	
51.1	39.26	337.3	59.1	346.6	42.9	.97/.98	200-500	SEP	N	
51.2a		3.2	60.5	4.1	42.8	.73/.98	100-500	SEP	N	
50.1	36.81	335.8	60.8	345.8	44.7	.97/.99	100-500	SEP	N	
50.2		351.6	62.1	356.1	45.5	.69/.96	200-500	SEP	N	
49.1	34.34	352.8	60.0	357.0	42.6	.42/.98	100-500	SEP	N	
49.2		355.6	68.0	359.8	51.2	.09/.97	200-500	SEP	N	
48.1	32.28	335.1	65.3	347.2	49.0	.96/.99	100-500	SEP	N	
48.2										
47.1	30.38	337.6	60.1	347.2	44.1	.96/.98	100-400	SEP	N	
47.2		342.7	58.9	350.1	42.0	.97/.99	100-500	SEP	N	
46.1	28.54							TREND	R?	
46.2		346.1	64.7	352.6	41.3	.98/.97	200-500	SEP	N	
45.1	26.72	348.1	66.2	355.4	48.9	.55/.99	300-500	SEP	N	
45.2		2.5	58.2	0.1	40.4	.13/.99	100-500	SEP	N	
44.1a	24.97	351.0	65.1	356.8	47.5	.92/.99	300-500	SEP	N	
44.2		349.9	59.8	355.3	42.9	.66/.97	100-400	SEP?	N?	
43.1a	22.95	1.5	62.7	2.7	45.5	.55/.97	300-500	SEP	N	
43.2a		3.5	48.6	4.0	30.9	.75/.97	100-500	SEP	N	
42.1	21.95	343.8	64.5	352.2	47.8	.71/.98	100-500	SEP?	N?	
42.2		341.0	62.5	350.1	46.8	.89/.96	100-500	SEP	N	

SAMPLE No	STRATI. HEIGHT (meter)	COMPONENT 1 (before B.C) DEC	INC	COMPONENT 2 (after B.C) DEC	INC	RC/α_{95}	DEMAG. RANGE mT/°C	MAGNETIC CHARACT. trend/sep	POLARI. (N/R)	POLARI. SEQUENCE
CB41.1	19.90	341.2	68.1	351.6	51.1	2.2	100-500	SEP	N	
41.2		357.8	68.2	1.3	50.3	.47/.99	100-500	SEP	N	
40.1	16.90	358.4	72.0	2.0	54.2	.90/.99	200-400	SEP	N	
40.2		240.5	67.5	289.5	71.3	6.6	200-500	SEP	N	
39.1a	14.95						100-500	SEP	N	
39.2							100-500	SEP	N	
38.1a	13.25						100-500	SEP	N	
38.2		10.2	66.8	7.7	53.0	.43/.92	100-500	SEP	N	
37.1	11.01	4.6	60.4	5.0	42.5	.98/.99	200-500	SEP	N	
37.2		354.4	62.9	358.5	45.4	.85/.99	200-500	SEP	N	
36.1	9.71	40.1	61.7	25.1	54.1	.95/.89	100-400	SEP	N	
36.2							100-500	TREND	R?	
35.1a	8.17	201.2	-56.7	196.7	-39.1	1.8	300-500	SEP	R	
35.2		25.7	71.7	16.4	54.5	.99/.99	300-600	SEP	N	
34.1	6.7	15.9	60.7	12.5	42.9	.99/.99	300-600	SEP	N	
34.2a		207.6	-55.3	201.5	-38.2	.99/.99	300-500	SEP	R	
33.1a	4.7	358.9	69.7	358.1	52.1	.54/.99	100-500	SEP	N	
33.2a		158.8	-53.3	166.1	-36.8	6.4	300-500	SEP	R	
32.1	2.5	354.6	55.3	357.9	37.7	.81/.99	200-600	SEP	N	
32.2		357.1	61.2	359.9	43.4	.05/.99	100-400	SEP	N	
31.1	base of	341.9	73.6				100-500	SEP	N	
31.2	section	344.2	60.0	351.3	42.9	5.8	100-600	SEP	N	

Supplementary work within the interval around the Compton Grange Sandstone.

SAMPLE No	STRATI. HEIGHT (meter)	COMPONENT1 (before B.C) DEC	INC	COMPONET2 (after B.C) DEC	INC	RC/α_{95}	DEMAG. RANGE mT/°C	MAGNETIC CHARACT. trend/sep	POLARI. (N/R)	POLARI. SEQUENCE
CB61.1a	6.4	265.0	59.9	295.3	54.1	1.4	35mT	SEP	N	
62.1a	5.3	251.0	46.7	275.3	47.8	6.4	35	SEP	N	
63.1a	4.0	342.2	78.0	349.5	58.2	0.4	35	SEP	N	
64.1a	2.9	297.7	67.9	322.1	52.4	2.3	35	SEP	N	
65.1a	2.1	319.0	47.3	326.8	32.6	9.0	35	SEP	N	
66.1a	1.6	299.5	55.2	315.2	40.5	2.8	35	SEP	N	
*67.1a	0.0	17.3	81.4	351.6	49.5	10.1	35	SEP	N	
68.1a	-0.9	310.5	73.2	331.1	55.5	0.1	35	SEP	N	
69.1a	-2.1						35	TREND	N	
70.1	-10.1	358.0	59.4	355.6	39.0	4.1	35	SEP	N	
71.1	-11.93	355.9	67.6	353.5	47.7	2.1	35	SEP	N	
72.1	-13.3	348.2	75.0	349.2	55.0	0.9	35	SEP	N	
73.1	-14.5	258.1	82.6	329.6	69.0	0.8	35	SEP	N	

Note: 1) * represents the reference point at which the supplementary section correlates with the original one at the base of Compton Grange Sanstone.
2) Black thick line represent the normal polarity and blank the reverse. Thick dot line are opposite polarity within the background polarity sequence.
3) B.C.: Bedding correction.
4) N and R represent Normal and Reverse polarity.
5) Bold face letters represent samples subjected to thermal demagnetisation.
6) Rc is the regression value for straight line fit (horizontal/vertical projection respectively and α_{95} is used for calculation of characteristic direction for the last few demagnetisaion steps if they do not show a good straight line as the field or temp. is increase.

APPENDIX 2. MAGNETOSTRATIGRAPHIC RESULTS FROM WORBARROW BAY SECTION (LOWER CRETACEOUS)

SAMPLE No	STRATI. HEIGHT (m)	CHARACTERISTIC COMPONENT(F.C.) DEC	INC	COMPONENT(B.C.) DEC	INC	Rc/α_{95}	TEMPERATURE OR AF LEVEL °C/mT	TREND /SEP	POLARI.	POLARITY SEQUENCE
	top of the section, ≤ 10m to the base of the Lower GreenSand.									
WW119.1a	353.4	3.3	63.4	350.8	34.1	.80/.99	35	SEP	N	
119.2a		324.4	62.0	323.2	44.6	.92/.92	35	SEP	N	
118.1a	351.2						35	TREND	R?	
118.2		311.7	83.3	338.7	54.3	9.6	35	SEP	N	
117.1	341.5									
117.2a		7.4	57.9	358.4	29.2	5.9	35	SEP	N	
117.2b		11.6	55.2	1.4	27.4	.20/.98	35	SEP	N	
116.1	338.0	9.3	3.5	350.9	58.6	.81/.94	35	SEP	N	
116.2a		25.2	72.1	357.3	51.7	.25/.95	35	SEP	N	
115.1	334.5									
115.2a							35	TREND	N?	
115.2b		302.2	58.3	319.8	32.9	20.1	35	SEP	N	
	gap~15-30m									
114.1	314.5							-	-	
114.2								-	-	
113.1a	312.9	357.2	65.9	351.1	36.2	1.4	35	SEP	N	
113.2a		25.7	74.0	0.2	46.7	1.7	35	SEP	N	
112.1a	311.1	102.9	35.6	67.4	47.9	16.4	35	SEP	N	
112.2a		222.2	57.9	276.3	61.3	12.5	35	SEP	N?	
111.1a	306.9	316.1	53.4	326.3	25.7	9.8	35	SEP	N	
111.2a		308.7	50.5	320.6	24.3	8.6	35	SEP	N	
110.1	304.4	319.8	70.8	334.0	42.2	.99/.99	35	SEP	N	
110.2a		286.1	72.4	322.1	48.4	9.3	35	SEP	N	
109.1	301.2							-	-	
109.2a		329.9	58.4	335.5	30.5	.98/.94	35	SEP?	N?	
108.1a	298.1	357.3	68.9	350.2	40.8	.94/.97	35	SEP	N	
108.2a		263.9	81.9	329.9	57.8	5.0	35	SEP	N	
107.1	294.3	11.6	81.6	350.8	52.7	.82/.99	35	SEP	N	
107.2		335.8	78.3	337.3	52.2	.95/.98	35	SEP	N	
106.1	290.8	140.0	84.8	343.2	58.1	.98/.99	35	SEP	N	
106.2a		136.7	73.0	359.0	57.5	.20/.98	35	SEP	N	
105.1	287.8	109.9	72.0	22.9	65.8	0.5	35	SEP	N	
105.2a		102.5	73.9	18.5	63.6	0.8	35	SEP	N	
104.1a	284.0	29.6	73.3	1.8	47.2	.48/.99	35	SEP	N	
104.2a		141.5	82.5	354.4	62.4	.97/.99	35	SEP	N	
103.1a	281.0	159.1	83.2	346.7	66.7	0.2	35	SEP	N	
103.2a		84.0	32.3	64.6	31.9	2.7	35	SEP	N	
	gap~10-15m									
102.1a	271.0	263.9	80.9	328.2	57.4	6.0	35	SEP	N	
102.2a							35	/	/	
101.1a	269.6	155.2	60.9	60.1	85.1	6.9	35	SEP	N	
101.2a		181.5	76.7	334.0	71.5	.52/.98	35	SEP?	N??	
100.1a	266.6	78.1	74.8	13.9	57.4	8.8	35	SEP	N	
100.2a		45.2	69.6	11.0	46.5	18.9	35	SEP	N	
	gap~6m									
99.1a	260.6	159.6	63.5	17.7	85.6	14.5	35	SEP	N	
99.2a		292.5	84.2	336.7	56.1	8.7	35	SEP	N	
98.1a	258.6						35	TREND	R?	
98.2a		207.8	53.7	258.8	66.2	29.4	35	SEP?	N?	
97.1a	255.6	82.6	54.0	44.9	47.7	14.6	35	SEP	N	
97.2a		228.5	72.1	314.8	55.9	.94/.95	35	SEP	N	

SAMPLE No	STRATI. HEIGHT (m)	CHARACTERISTIC COMPONENT(F.C.) DEC	INC	COMPONENT(B.C.) DEC	INC	Rc/α_{95}	TEMPERATURE OR AF LEVEL °C/mT	TREND /SEP	POLARI.	POLARITY SEQUENCE
96.1a	253.4	6.6	65.7	355.8	36.7	13.2	35	SEP	N	
96.2a		16.7	76.7	355.4	48.2	10.4	35	SEP	N	
95.1	252.2							-	-	
95.2		83.0	84.8	352.3	62.9	16.7	35	SEP	N	
	gap~8m									
94.1a	244.2	317.5	-72.5	189.9	-62.7	.37/.97	35	SEP	R	
94.2a		137.7	5.0	132.7	31.2	11.1	35	/	/	
93.1a	241.0	169.8	72.0	337.8	77.7	0.9	35	SEP	N	
93.2a		90.3	73.9	17.6	60.3	0.3	35	SEP	N	
92.1a	238.8						35	TREND	N?	
92.2a							35	TREND	N?	
91.1a	235.8	90.1	-26.0	101.0	-15.2	9.7	35	SEP	R	
91.2a		152.0	-65.7	158.4	-36.1	26.7	35	SEP	R	
90.1a	232.6	345.7	69.7	345.3	39.7	0.8	35	SEP	N	
90.2a		275.9	52.8	301.0	35.5	16.2	35	TREND	N	
65.1a	225.6	310.3	-15.4	300.3	-38.4	.99/.98	35	/	/	
65.2a		183.2	81.0	337.4	68.3	21.6	35	SEP	N	
64.1a	223.6	171.3	-66.5	168.1	-36.5	1.0	35	SEP	R	
64.2a		148.6	-52.5	154.2	-23.2	1.0/1.0	35	SEP	R	
63.1a	221.1	178.3	-66.8	171.5	-37.2	0.8	35	SEP	R	
63.2a		88.2	48.2	54.6	46.2	6.0	35	SEP	N	
62.1a	219.1						35	TREND	R?	
62.2a							35	TREND	R?	
61.1	217.6	317.2	-52.3	269.1	-72.9	11.9	35	SEP	R	
61.2							35	TREND	/	
60.1a	215.6	133.3	-1.3	129.9	23.9	9.4	35	/	/	
60.2a							35	TREND	R	
59.1a	213.6	160.6	17.1	159.5	46.8	.68/.88	35	/	/	
59.2a							35	TREND	N?	
58.1a	212.6						35	TREND	R?	
58.2							35	TREND	N?	
57.1	210.1	218.6	-57.2	196.9	-34.9	.99/.99	35	TREND	N	
57.2a		208.7	-47.3	195.6	-23.0	.97/.99	35	SEP	N	
	gap ~17m									
56.1a	193.1	103.4	-39.8	118.2	-21.8	.99/.99	35	SEP	R	
56.2a		197.1	-45.1	188.3	-18.3	7.2	35	SEP	R	
55.1	192.6						35	TREND	R	
55.2a							35	TREND	R	
54.1a	187.6	331.2	66.1				35	SEP	N	
54.2a		323.2	64.4	333.7	35.3	.99/.99	35	SEP	N	
53.1a	182.6						35	TREND	N	
53.2a		206.8	-48.5	193.8	-23.7	6.1	35	SEP	R	
52.1a	178.6	324.1	62.4	333.6	33.5	7.6	35	SEP	N	
52.2		334.1	69.0	339.9	39.2	6.1	35	SEP	N	
51.1a	176.1	11.7	46.8	3.9	19.0	10.9	35	SEP	N	
51.2a							35	TREND	N	
50.1a	174.1	61.0	42.0	40.7	29.4	3.4	35	SEP	N	
50.2a		278.2	67.6	314.5	46.5	7.8	35	SEP	N	
49.1a	172.9(?)						35	TREND	N	
49.2a		183.6	74.5	342.5	71.7	.42/.94	35	SEP	N	
2.1a	170.9	78.1	53.6	34.8	33.2	.99/.99	35	SEP	N	
2.1b		76.3	41.5	47.3	29.6	.99/.97	35/**450**	SEP **SEP**	N **N**	
2.2a							35	TREND	R??	

SAMPLE No	STRATI. HEIGHT (m)	CHARACTERISTIC COMPONENT(F.C.) DEC	INC	COMPONENT(B.C.) DEC	INC	Rc/α_{95}	TEMPERATURE OR AF LEVEL °C/mT	TREND /SEP	POLARI.	POLARITY SEQUENCE
2.2b		79.9	54.5	33.7	33.0	14.9	35	SEP	N	
3.1a	169.9	74.5	28.9	58.1	13.0	9.4	35	SEP	N	
3.1b		85.1	62.0	41.0	36.7	22.6	**450**	**SEP**	**N**	
3.2a		59.4	66.7	15.4	30.7	28.6	35	SEP	N?	
4.1a	168.3	350.1	65.9	352.3	21.8	.72/.89	35	SEP	N?	
4.1b							**500**	**TREND**	**N?**	
4.2a							35	TREND	R	
4.2b		356.1	49.5	352.2	4.0	.44/.35	35	SEP	N?	
5.1a	167.8	338.3	67.1	344.9	22.1	.99/.97	35	SEP	N	
5.1b							35	/	/	
5.2a							35	TREND	R?	
5.2b		298.8	61.6	329.9	25.7	.90/.95	30	SEP	N?	
6.2a	167.2	36.1	77.0	0.4	33.1	.17/.99	35	SEP	N	
6.2b		349.7	64.4	350.5	18.0	.95/.92	35/**500**	SEP/**TREND**	N **N??**	
7.1	166.4	359.4	63.4	354.3	15.7	.99/.99	35/**600**	SEP/**SEP**	N **N**	
7.2a							35	TREND	N	
7.2b		70.6	32.5	49.4	14.9	16.0	35	SEP	N	
8.1a	163.9						35	TREND?	N?	
8.1b		321.1	73.5	341.1	27.2	1.0/.99	35/**600**	SEP	N **N**	
9.1a	163.4	338.6	59.6	343.9	12.3	.98/.96	65/**550**	SEP/**SEP**	N **N**	
9.2a		319.1	62.0	343.8	22.7	.99/.99	35	SEP	N	
10.1a	162.7	211.0	72.6	331.6	53.8	.96/.99	35	SEP	N	
10.2a		1.1	62.0	355.4	14.4	.60/.69	35	SEP	N	
10.2b		39.4	-51.2	112.8	-55.5	11.8	**500**	**SEP**	**R**	
11.1a	161.9	339.9	47.8	342.6	0.4	2.9	65/**600**	SEP	N? **N?**	
11.1b		320.7	40.5	328.2	-3.2	.97/.72	35	SEP	N?	
12.1	160.8	303.1	37.2	314.7	-0.1	9.0	35/**500**	SEP /	N??/	
12.2		63.3	66.3	20.7	36.4	.97/.98	35	SEP	N	
13.1							-	-	-	
13.2	155.9	11.7	71.2	359.2	26.2	.15/.96	65/**500**	SEP**trend**	N **R?**	
14.1a	154.0	309.2	-79.4	180.6	-49.5	7.9	35	SEP	R	
14.2a		174.3	-60.2	172.1	-12.3	1.2	35	SEP	R	
14.2b		131.9	-74.0	158.0	-32.5	.99/.97	**600**	**SEP**	**R**	
16.1a	150.0	163.4	66.3	351.4	45.7	.68/.94	35	SEP	N	
16.1b		251.5	78.6	334.6	42.6	3.8	35	SEP	N	
16.2a		165.1	60.0	357.7	71.7	26.0	35	SEP	N	
16.2b							**550**	/	/	
15.1a	148.2	188.2	-54.0	180.7	-7.2	2.5	35	SEP	R	
15.1b		178.3	-74.4	172.5	-26.5	4.3	**550**	**SEP**	**R**	
15.2a		177.5	3.2	182.0	50.6	5.0	35	SEP	/	
15.2b		105.3	-61.5	141.3	-25.8	87.1	35	SEP	R	
17.1	147.4	338.3	75.0	346.8	27.5	.97/.99	35	SEP	N	
17.2a		336.1	67.9	339.2	30.5	.91/.92	35	SEP	N	
17.2b							**550**	**TREND**	**R??**	
18.1a	146.2	23.1	23.5	21.7	-17.6	3.0	35	SEP	N?	
18.1b							35	TREND	N	
18.2a							35	TREND	R	
18.2b							35	TREND	R	
18.2c							**500**	/	/	
18.2d							35	SEP	/	
19.1	144.2	289.5	48.9	313.6	15.3	14.9	35	SEP	N?	
19.2a							35	TREND	R	
19.2b							35	TREND	R	

SAMPLE No	STRATI. HEIGHT (m)	CHARACTERISTIC COMPONENT(F.C.) DEC	INC	COMPONENT(B.C.) DEC	INC	Rc/α_{95}	TEMPERATURE OR AF LEVEL °C/mT	TREND /SEP	POLARI.	POLARITY SEQUENCE
20.1a	142.0						35	TREND	R	
20.1b		5.9	69.8	5.4	23.6	.41/.95	35	SEP	N	
20.2							35	TREND	R	
21.1a	139.9						35	TREND?	R?	
21.1b							**500**	**TREND**	**R**	
21.2a							35	TREND?	R?	
22.1a	138.4	311.1	48.0	325.0	6.3	8.2	35	SEP	N?	
22.1b							35	TREND	R	
22.2a							35	TREND	R	
22.2b		47.3	-51.6	114.4	-50.6	17.0	**550**	**SEP**	**R**	
23.1	133.7						20	TREND	R	
23.2							35	TREND	R	
24.1a	131.7	159.3	85.0	351.3	46.8	30.6	35	SEP	N?	
24.1b		307.1	-50.6	228.5	-59.6	25.1	35	SEP	R	
24.2a							35	TREND?	R?	
24.2b							35	TREND	R??	
25.1a	130.0						35	TREND	R	
25.1b							**550**	**TREND**	**R?**	
25.2		174.1	69.0	346.7	62.8	45.1	35	SEP	N	
26.1a	126.4	33.9	78.6	359.5	33.6	.40/.99	35	SEP	N	
26.1b		49.7	64.9	14.6	27.6	.98/.98	**550**	**SEP**	**N**	
26.2a		355.8	82.8	350.8	35.2	1.0/.99	35	SEP	N	
27.1a	124.9	344.3	-6.4	340.4	-54.1	6.2	35	SEP	/	
27.1b		334.1	16.8	332.5	-29.3	4.6	35/**550**	/ /	/ /	
27.2a							35	TREND	R	
27.2b		6.2	62.2	357.7	15.0	6.2	35	SEP	N	
28.1a	121.4	291.8	61.8	323.9	23.8	15.2	35	SEP	N?	
28.1b							**450**	**TREND**	**N**	
28.2a		235.2	55.6	301.6	46.7	18.1	35	SEP?	N?	
29.1a	119.5	19.5	71.8	359.8	25.7	1.9	65	SEP	N	
29.1b		49.3	81.5	359.5	37.6	.16/.99	**600**	**SEP**	**N**	
29.2		11.6	72.0	357.2	25.0	1.4	40	SEP	N	
30.1a	115.5	341.3	64.1	346.1	16.3	.99/.99	35	SEP	N	
30.1b							**500**	**/**	**/**	
30.2		179.0	83.5	352.7	47.1	.69/.99	35	SEP	N	
31.1	114.0	45.0	48.4	24.5	13.1	.96/.93	35	SEP	N	
31.2		47.7	62.2	16.2	24.3	.88/.99	35/**500**	SEP/**SEP**	N **N**	
32.1	112.3	337.6	60.4	343.7	12.9	1.6	35	SEP	N	
32.2		359.9	53.4	355.9	5.8	1.6	50/**600**	SEP	N? **N**	
33.1a	111.4	66.5	38.5	44.5	21.6	.98/.89	35	SEP	N	
33.1b							35	TREND	R	
33.2a							35	TREND	R?	
33.2b		56.8	52.0	27.5	20.5	.96/.99	35	SEP	N	
34.1	110.3	122.2	46.1	56.3	55.9	7.1	35	SEP	N	
34.2		139.9	60.8	23.6	63.8	0.9	35/**600**	SEP	N **N**	
35.1a	109.0	56.8	70.4	6.0	38.6	.67/.98	35	SEP	N	
35.2a		74.3	77.5	6.1	39.6	0.4	35	SEP	N	
35.2b		118.5	63.2	354.6	42.9	.59/.99	**600**	**SEP**	**N**	
36.1	108.1	263.5	75.7	331.4	39.5	7.7	35/**400**	SEP /**SEP**	N **N**	
37.1a	106.1	15.7	81.6	354.4	34.3	4.7	35	SEP	N	
37.1b							**500**	**TREND**	**N**	
37.2a		346.1	54.6	356.2	20.6	.30/.74	35	SEP	N	
38.1a	104.7	34.8	67.4	7.3	24.5	6.8	35	SEP	N	

SAMPLE No	STRATI. HEIGHT (m)	CHARACTERISTIC COMPONENT(F.C.) DEC	INC	COMPONENT(B.C.) DEC	INC	Rc/α_{95}	TEMPERATURE OR AF LEVEL °C/mT	TREND /SEP	POLARI.	POLARITY SEQUENCE
38.1b		349.7	62.8	349.8	14.8	24.6	**500**	**SEP**	**N**	
38.2a		146.5	35.3	92.3	70.5	8.9	35	SEP	N	
38.2b		186.7	59.7	325.4	69.4	5.2	35	SEP	N	
39.1a	103.6	208.1	-62.4	187.5	-18.8	2.1	35	SEP	R	
39.2a		154.3	-52.2	160.4	-5.1	0.3	35	SEP	R	
40.1	102.7	168.5	-39.2	168.8	8.7	1.1	35	SEP?	R	
40.2		227.6	-66.9	193.1	-28.3	.93/.99	35	SEP	R	
	up to site 40									
46.1a	97.7	39.7	46.1	22.3	8.7	.99/.96	35	SEP	N	
46.1b		64.5	68.1	15.3	33.1	32.5	**400**	**SEP?**	**N**	
46.2a							35	TREND?	R?	
47.1a	95.5						35	TREND	R	
47.1b							**350**	**TREND**	**R?**	
47.2a							35	TREND	R??	
47.2b							35	TREND	R	
48.1a	93.3	102.0	78.1	5.6	45.4	1.8	60	SEP	N	
48.1b		143.5	11.3	12.1	42.3	.88/.99	**600**	**SEP**	**N**	
48.2		100.1	79.5	3.8	44.7	0.9	35	SEP	N	
	continued nearly at the same place (or ~20m below site 48 ?)									
66.1a	93.3	175.3	61.8	342.6	69.8	11.2	35	SEP	N	
66.2a		312.4	58.9	330.9	15.6	16.1	35	SEP	N	
67.1a	87.3	140.3	65.2	17.2	60.7	2.7	35	SEP	N	
67.2		129.5	63.8	22.8	58.0	0.4	35	SEP	N	
68.1a	83.3	219.1	73.8	330.3	51.0	1.2	35	SEP	N	
68.2a		212.9	29.9	254.8	53.6	1.1	35	/	/	
69.1a	79.3(?)	312.5	-88.0	171.6	-43.5	1.6	35	SEP	R	
69.2a		253.9	-67.7	197.7	-36.1	2.7	35	SEP	R	
70.1a	76.2						35	TREND	N	
70.2a		163.0	41.8	79.5	84.7	45.7	35	TREND	N	
	gap ~8m									
71.1a	68.2						35	TREND	R	
71.2a		0.8	64.6	354.5	17.4	.87/.97	35	SEP	N	
72.1a	66.6	4.7	65.2	356.2	18.2	.41/.97	35	SEP	N	
72.2a		25.8	64.0	5.7	19.8	8.4	35	SEP	N	
73.1a	65.6	154.2	4.2	354.2	42.0	.69/.98	35	SEP	N	
73.2a		335.4	68.5	344.3	21.0	10.4	35	SEP	N	
74.1a	63.4						35	TREND	N?	
74.2a		167.1	46.5	13.2	85.0	29.1	35	SEP?	N	
75.1a	58.4						35	TREND	N	
75.2a		249.7	75.9	330.9	42.9	14.5	35	SEP	N	
76.1a	55.4(?)	50.5	58.3	19.6	22.1	8.6	35	SEP	N	
76.2a							35	TREND	R?	
	gap~14m									
77.1	41.4	195.3	83.7	346.0	47.5	0.6	35	SEP	N	
77.2		184.2	77.9	345.0	53.5	0.5	35	SEP	N	
78.1a	38.9	187.7	58.1	321.4	70.3	20.9	35	SEP	N	
78.2a		357.4	-46.7	124.3	-82.8	16.7	35	SEP	R	
79.1a	37.8						35	TREND	R	
79.2							35	TREND	R?	
80.1a	35.8(?)						35	TREND?	R?	
80.2							35	TREND	R?	
	gap~19m									
81.1a	16.8	242.3	-58.5	203.8	-26.9	6.9	35	SEP	R	

SAMPLE No	STRATI. HEIGHT (m)	CHARACTERISTIC COMPONENT(F.C.) DEC	INC	COMPONENT(B.C.) DEC	INC	Rc/α_{95}	TEMPERATURE OR AF LEVEL °C/mT	TREND /SEP	POLARI.	POLARITY SEQUENCE
81.2a		146.7	48.0	51.5	72.5	2.5	35	SEP	N	
82.1a	15.2						35	TREND	R?	
82.2a							35	TREND	R	
83.1a	13.5						35	SEP	N	
83.2a							35	SEP	R	
84.1a	11.7						35	TREND	R?	
84.2a		102.0	26.6	72.5	33.3	16.7	35	SEP?	N	
85.1a	8.7	146.6	29.3	106.3	67.2	6.2	35	SEP	N?	
85.2a							35	TREND	N	
86.1a	6.4						35	TREND	R?	
86.2a							35	TREND	N?	
87.1a	4.2	322.3	59.5	335.9	14.0	7.1	35	SEP	N	
87.2a		287.9	44.4	309.7	12.7	7.5	35	SEP	N	
88.1a	2.0m	301.5	56.4	323.5	17.4	.99/.96	35	SEP	N	
88.2a		331.7	38.4	331.9	-3.6	.92/.16	35	TREND	N	
89.1a	base of						35	SEP	N	
89.2	section						35	TREND	N	

Note: F.C.: field correction data. Other symbols and conventions as in Appendix 1.

APPENDIX 3. MAGNETOSTRATIGRAPHIC RESULTS FROM MUPE BAY SECTION (LOWER CRETACEOUS)

SAMPLE No	STRATI. HEIGHT (m)	CHARACTERISTIC COMPONENT(F.C.) DEC	INC	COMPONENT(B.C.) DEC	INC	Rc/α_{95}	TEMPERATURE OR AF LEVEL °C/mT	TREND /SEP	POLARI.	POLARITY SEQUENCE
	top of section, ~7.5m below the Lower GreenSand									
MP1.1a	225.2						35	/	/	
1.2a							35	/	/	
2.1a	224.3	126.7	9.2	90.3	32.6	37.4	35	SEP?	N?	
2.2a		187.5	36.9	346.9	48.6	.54/.99	35	SEP	N	
	slump~19.3m									
3.1a	205.0	192.2	45.8	354.8	53.4	.18/.99	35	SEP	N	
3.2a		165.4	44.8	26.9	51.4	9.5	35	SEP	N	
4.1a	200.6	244.0	68.3	34.5	51.5	.60/.84	35	SEP	N	
4.2a		217.2	50.3	332.7	32.9	.90/.95	35	SEP	N	
5.1a	198.8	159.6	82.8	8.1	16.4	0.3	35	SEP	N	
5.2		228.4	48.9	331.5	22.6	.99/.83	35	SEP?	N?	
6.1a	197.3	341.0	31.4	329.4	-38.2	.44/.67	35	SEP	N?	
6.2a		238.1	38.0	314.7	34.8	15.2	35	SEP	N	
7.1a	196.2	271.3	84.6	356.8	13.1	9.5	35	SEP	N	
7.2a		161.0	45.5	30.6	48.9	15.6	35	SEP	N	
8.1a	191.7			340.4	23.8	0.3	35	SEP	N	
8.2a		351.0	64.4	358.8	-14.8	0.9	35	SEP	N??	
9.1a	190.7	184.1	38.0	6.3	61.9	26.6	35	SEP	N?	
9.2a		192.5	29.6	346.3	69.1	14.0	35	SEP	N	
10.1a	188.8	184.4	50.7	7.6	41.8	.41/.90	35	SEP?	N?	
10.2a		185.8	38.9	3.6	61.0	18.0	35	SEP	N	
11.1	186.5	158.3	60.3	21.0	34.1	.98/.97	35	SEP	N	
11.2a							35	TREND?	R??	
12.1	184.7	118.6	73.5	33.5	-10.4	.91/.77	35	SEP	N	
12.2a		339.8	19.0	324.4	-51.8	23.7	35	SEP	/	
13.1a	183.1	90.9	72.1	22.8	8.2	13.5	35	SEP	N?	
13.2a		75.7	-51.9	146.8	-19.6	19.9	35	SEP	R	
14.1	181.6	187.9	55.2	2.6	44.6	1.3	35	SEP	N	
14.2		83.0	50.0	43.9	0.1	9.2	35	SEP	N?	
15.1	180.1	25.9	1.3	52.6	-62.7	.61/.60	35	SEP	/	
15.2		15.3	-26.7	156.0	-70.5	20.5	35	SEP	R	
16.1a	178.3	200.3	40.2	343.2	56.8	0.6	35	SEP	N	
16.2		199.9	13.6	290.5	74.9	2.1	35	SEP	N	
17.1a	176.9	13.6	24.9	18.9	-54.0	14.5	35	SEP	/	
17.2a							35	TREND	N?	
18.1	175.9	331.0	38.8	334.1	-31.8	20.7	35	SEP	/	
18.2a		109.1	-21.3	118.7	9.2	6.5	35	SEP	/	
19.1	174.1	286.6	79.1	354.2	7.6	4.7	35	SEP	N	
19.2		40.8	-60.7	165.1	-32.7	4.9	35	SEP	R	
	gap~7.5m									
20.1a	166.6						35	TREND?	N?	
20.2a		41.3	-30.4				35	SEP	R?	
21.1	165.1						35	TREND	N??	
21.2a							35	TREND	/	
22.1	163.7	19.5	43.0	18.0	-35.3	9.4	35	SEP	/	
22.2		234.2	69.2	348.0	22.9	12.9	35	SEP	N	
23.1a	162.2	200.0	56.0	353.1	40.9	.92/.97	35	SEP	N	
23.2a		173.0	38.3	23.7	59.6	7.0	35	SEP	N	

SAMPLE No	STRATI. HEIGHT (m)	CHARACTERISTIC COMPONENT(F.C.) DEC	INC	COMPONENT(B.C.) DEC	INC	Rc/α_{95}	TEMPERATURE OR AF LEVEL °C/mT	TREND /SEP	POLARI.	POLARITY SEQUENCE
24.1a	160.9						35	TREND	N	
24.2a		198.1	38.3	353.1	52.5	.41/.88	35	SEP	N	
25.1a	160.4						35	SEP?	N?	
25.2							35	TREND	/	
26.1	159.5	188.1	42.5	0.6	57.3	1.4	35	SEP	N	
26.2a		192.1	39.7	354.0	59.6	2.2	35	SEP	N	
27.1a	158.0	177.7	53.4	11.2	46.1	6.7	35	SEP	N	
27.2a		175.2	-18.8	166.5	59.5	13.3	35	SEP	/	
28.1a	157.1	145.0	85.7	7.7	13.2	5.8	35	SEP	N	
28.2a		140.7	42.0	47.3	39.7	14.7	35	SEP	N	
29.1	155.8						35	TREND?	R??	repeat
29.2	as MP30	83.0	-10.5	97.6	-15.8	40.6	35	SEP?	R	MP30
30.1a	155.8	356.6	-36.2	199.7	-62.6	2.4	35	SEP	R	
30.2a		348.9	-33.2	215.0	-62.4	1.0	35	SEP	R	
31.1a	154.7						35	TREND	N	
31.2a							35	TREND	N?	
32.1	151.2	202.2	50.2	348.7	47.2	27.6	35	SEP	N	
32.2		169.6	29.1	39.7	66.0	12.2	35	SEP	N	
33.1	148.3	190.3	41.7	357.4	57.9	0.8	35	SEP	N	
33.2a		351.7	31.9	352.2	-18.9	.19/.59	35	SEP	/	
34.1a	145.8	200.2	79.0	1.9	20.5	16.0	35	SEP	N	
34.2a							35	TREND	N?	
	gap~10.6m									
35.1a	135.2	207.2	30.4	322.9	60.8	29.5	35	SEP	N	
35.2a		324.5	7.4	322.3	5.5	.80/.17	35	SEP	N	
36.1a	133.1	20.3	-28.9	149.8	-66.2	3.7	35	SEP	R	
36.2		354.5	-65.9	190.3	-33.5	14.9	35	SEP	R	
37.1a	132.6						35	TREND	R?	
37.2a		237.3	63.9	342.4	24.8	12.6	35	SEP	N	
38.1a	129.0	227.7	-77.6	193.3	-0.8	5.2	35	SEP	R?	
38.2a		18.3	24.6	25.3	-52.9	12.8	35	SEP	/	
39.1a	127.4	191.4	49.4	358.4	50.2	0.7	35	SEP	N	
39.2a		166.3	48.4	23.7	48.5	2.3	35	SEP	N	
40.1a	126.0	15.6	-50.4	174.7	-48.6	9.9	35	SEP	R	
40.2a		25.2	-62.4	173.6	-35.5	22.7	35	SEP	R	
41.1a	124.2	149.9	78.8	11.7	19.0	1.4	35	SEP	N	
41.2a		146.9	73.6	15.8	22.6	1.2	35	SEP	N	
42.1a	122.0	220.4	53.3	341.1	34.6	.75/.94	35	SEP	N	
42.2a		100.3	55.6	39.9	11.2	12.3	35	SEP	N	
43.1a	121.0	180.5	83.3	5.5	16.6	16.4	35	SEP	N	
43.2a		154.5	65.7	18.9	30.4	7.0	35	SEP	N	
44.1a	120.0	286.2	60.7	336.3	3.3	3.4	35	SEP	N	
44.2a		256.6	42.6	316.9	20.6	6.6	35	SEP	N	
45.1	118.0	335.0	58.7	344.8	-19.5	5.9	35	SEP	/	
45.2		2.5	78.3	4.5	-1.6	4.7	35	SEP	N?	
46.1	115.7	47.2	-42.8	144.3	-40.7	4.0	35	SEP	R	
46.2a		36.6	-42.2	149.8	-47.5	0.3	35	SEP	R	
47.1a	113.9	224.8	15.0	286.5	50.8	11.2	35	SEP	N	
47.2a		202.6	54.6	351.0	43.2	0.2	35	SEP	N	
48.1a	112.7	197.8	64.2	358.2	34.9	11.5	35	SEP	N	
48.2a		170.2	20.9	55.8	72.1	41.5	35	SEP??	N?	

SAMPLE No	STRATI. HEIGHT (m)	CHARACTERISTIC COMPONENT(F.C.) DEC	INC	COMPONENT(B.C.) DEC	INC	Rc/α_{95}	TEMPERATURE OR AF LEVEL °C/mT	TREND /SEP	POLARI.	POLARITY SEQUENCE
49.1	108.9	141.4	59.7	27.9	28.0	.99/.95	35	SEP	N	
49.2		124.1	-37.7	139.0	15.8	17.0	35	TREND	/	
50.1	106.6	133.4	-78.1	175.7	-2.5	1.8	35	SEP	R?	
50.2							35	TREND	N?	
51.1a	103.6						35	TREND	N?	
51.2a							35	/	/	
52.1a	100.8	164.5	47.6	27.0	47.7	.91/.99	35	SEP	N	
52.2		357.9	60.7	1.3	-19.0	11.8	35	SEP	/	
53.1	98.7	202.3	45.3	345.2	51.6	0.7	35	SEP	N	
53.2		197.9	15.4	299.8	76.2	0.8	35	SEP	N	
54.1a	96.7	243.2	29.6	303.8	32.4	18.5	35	SEP	N	
54.2a							35	/	/	
55.1a	94.0	155.2	44.7	35.9	46.8	19.0	35	SEP	N	
55.2a							35	TREND	N	
56.1a	92.5	347.9	29.0	342.6	-47.6	3.6	35	SEP	/	
56.2a		143.9	36.0	53.3	44.6	15.7	35	TREND	N	
57.1a	90.7	293.5	52.3	329.5	-3.0	7.3	35	SEP	N??	
57.2a		217.3	-9.4	244.9	52.4	14.4	35	SEP	/	
58.1	89.2	241.7	41.7	317.3	30.3	.93/.99	35	SEP	N	
58.2							35	TREND?	R??	
59.1	84.8	173.5	50.1	15.7	48.7	.89/.99	35	SEP	N	
59.2a							35	TREND	R?	
60.1a	83.3	243.6	77.6	354.0	16.2	9.7	35	SEP?	N?	
60.2		204.9	35.9	333.7	48.9	.99/.86	35	SEP	N	
61.1	81.9	249.1	48.5	324.1	24.4	24.7	35	SEP	N	
61.2		285.4	-32.4	243.8	-14.1	11.5	35	SEP	R	
62.1a	80.1						35	TREND	R	
62.2				160.1	-9.9	15.5	35	SEP?	R	
63.1a	78.9						35	TREND?	N?	
63.2		284.6	-20.1	256.3	-12.3	11.1	35	SEP	R	
64.1	76.9	350.8	60.0	357.6	-17.5	.94/.93	35	SEP	/	
64.2a		318.8	43.6	330.8	-21.9	14.1	35	SEP	/	
65.1	75.0						35	TREND?	N?	
65.2		328.4	-54.7	214.9	-23.1	.89/.81	35	SEP??	R?	
	gap~9m									
66.1	65.5						35	TREND	R	
66.2		304.5	-22.6	254.4	-31.0	14.9	35	SEP	R?	
	slump~5m									
67.1a	60.0						35	TREND	R?	
67.2							35	TREND	R?	
68.1a	57.0						35	TREND	R	
68.2		214.5	49.8	342.8	38.8	.84/.93	35	SEP	N	
69.1	54.4						35	TREND?	R?	
69.2		162.5	46.1	28.8	49.0	34.5	35	SEP	N	
70.1	52.9						35	TREND	N??	
70.2		208.9	59.1	349.7	37.6	5.1	35	SEP	N	
71.1	51.7	323.2	59.6	340.6	-9.9	.91/.89	35	SEP	/	
71.2a		267.4	41.8	315.8	12.2	6.9	35	SEP	/	
72.1	50.3	193.7	45.9	352.4	48.2	.76/.92	35	SEP?	N	
72.2		267.9	62.4	336.9	12.0	7.8	35	SEP	N	
73.1a	49.6	244.1	51.5	328.2	26.7	9.2	35	SEP	N	

SAMPLE No	STRATI. HEIGHT (m)	CHARACTERISTIC COMPONENT(F.C.) DEC	INC	COMPONENT(B.C.) DEC	INC	Rc/α_{95}	TEMPARETURE OR AF LEVEL °C/mT	TREND /SEP	POLARI.	POLARITY SEQUENCE
73.2		182.0	56.8	6.7	41.4	.96/.97	35	SEP	N	
74.1	48.2	196.0	72.8	355.1	19.0	.49/.91	35	SEP?	N?	
74.2		340.7	37.0	340.4	-37.6	25.2	35	SEP	/	
75.1	46.7	216.5	56.3	343.5	37.5	0.5	35	SEP	N	
75.2a		205.2	47.8	344.5	48.5	0.5	35	SEP	N	
76.1a	45.7	193.8	37.9	350.5	60.9	2.6	35	SEP	N	
76.2a		157.7	55.7	24.5	39.5	12.4	35	SEP	N	
	slump~3m									
77.1a	42.2	191.5	45.3	357.1	54.1	7.6	35	SEP	N	
77.2							35	TREND	N	
	gap~6m									
78.1	35.7	230.9	37.3	316.3	40.5	0.4	35	SEP	N	
78.2a		218.6	37.2	322.5	49.2	5.3	35	SEP	N	
	gap~10m									
79.1	25.2	298.7	-34.1	241.8	-25.1	12.4	35	SEP	R	
79.2a		15.3	-58.3	177.8	-41.0	8.2	35	SEP	R	
80.1a	24.1	45.2	42.7	36.8	-25.6	30.9	35	SEP	/	
80.2							35	TREND	R?	
81.1	22.6						35	TREND	R??	
81.2a							35	SEP	/	
82.1	20.9	35.7	-24.2	119.0	-58.3	16.4	35	SEP	R	
82.2							35	TREND	R?	
83.1	19.8	23.0	-60.0	173.6	-38.2	35.5	35	SEP	R	
83.2							35	TREND?	R?	
84.1	18.9	236.2	-13.2	251.4	34.0	16.0	35	SEP	/	
84.2a							35	TREND?	R?	
85.1	17.6	356.1	43.3	357.0	-36.0	9.8	35	SEP	/	
85.2		319.9	-29.1	243.8	-43.7	17.6	35	SEP	R	
86.1	16.5	17.2	-0.2	56.9	-74.4	24.4	35	SEP	R??	
86.2a		149.7	-81.1	180.1	-3.0	7.3	35	SEP	R?	
87.1	14.7	89.3	-51.1	145.4	-11.2	10.0	35	SEP	R	
87.2							35	TREND	R	
88.1a	13.7						35	SEP??	R??	
88.2a		320.1	-35.9	235.0	-41.8	16.7	35	SEP	R	
89.1	12.1	335.9	-8.2	275.9	-61.3	20.7	35	TREND	R?	
89.2a		192.8	30.3	346.4	68.3	44.1	35	SEP	N	
90.1	3.6	240.7	-47.5	220.1	14.2	0.4	35	SEP	/	
90.2a		278.6	-44.3	231.6	-8.9	.99/.97	35	SEP	R	
91.1	base of						35	TREND	N	
91.2	section						35	TREND?	N??	

APPENDIX 4. MAGNETOSTRATIGRAPHIC RESULTS FROM LULWORTH COVE SECTION (LOWER CRETACEOUS)

SAMPLE No	STRATI. HEIGHT (m)	CHARACTERISTIC COMPONENT(F.C.) DEC	INC	CHARACTERISTIC COMPONENT(B.C.) DEC	INC	Rc/α_{95}	TEMPERATURE OR AF LEVEL mT	TREND /SEP	POLARI.	POLARITY SEQUENCE
	The Lower GreenSand section, which is just below the Chalk, on the east to central side of the bay									
LC16.1a	204.5?						35	TREND	N?	
16.2a							35	TREND	N??	
17.1	202.5	342.7	57.7	353.6	-23.9	12.6	35	SEP	/	
17.2a							35	TREND	N?	
18.1a	201.1	179.5	62.6	12.3	31.6	5.3	35	SEP	N	
18.2							35	TREND	N	
19.1a	198.9	2.0	-19.7	207.1	-67.4	21.1	35	SEP	/	
19.2a							35	TREND	N	
20.1a	195.4						35	TREND	/	
20.2b		182.2	41.6	15.1	53.0	11.2	35	SEP	N	
21.1a	189.0	216.9	73.6	359.6	19.1	27.9	35	SEP?	N	
21.2a							35	TREND	N??	
22.1a	181.5	338.8	24.2	325.1	-49.2	14.8	35	SEP	/	
22.2b		131.2	24.3	72.3	32.2	14.8	35	SEP?	N	
	18m gap of slumping									
23.1a	162.8	207.7	71.3	1.2	22.5	18.6	35	SEP	N	
23.2b		250.3	-68.0	208.1	5.3	.94/.99	35	SEP	/	
	10m gap of slumping									
24.1a	152.7						35	TREND	N	
24.2b		168.9	41.2	30.3	49.8	11.8	35	SEP	N	
	12m gap of slumping									
25.1a	140.3	50.4	16.2	70.2	-42.9	6.5	35	SEP	/	
25.2b		13.6	29.3	16.6	-55.1	19.0	35	SEP	/	
26.1a	138.9	22.9	43.7	21.9	-39.4	22.0	35	SEP	/	
26.2b		214.6	42.3	339.6	45.7	35.7	35	SEP?	N	
27.1	136.1						35	TREND?	N?	
27.2		135.3	70.2	24.2	16.6	14.9	35	SEP	N	
28.1a	132.0	119.1	16.9	81.6	21.6	21.2	35	TREND	N	
28.2b							35	TREND	N?	
29.1a	127.1						35	TREND	N??	
29.2b							35	TREND	N	
30.1a	121.1	145.8	57.2	32.0	29.9	11.7	35	SEP	N	
30.2b		321.8	-14.8	262.1	-43.6	20.9	35	SEP?	R	
31.1a	113.3						35	TREND	N?	
31.2b							35	TREND	/	
32.1a	111.7	97.4	54.4	43.6	3.7	4.3	35	SEP	N	
32.2b		144.3	-12.2	120.0	43.3	10.8	35	SEP	N??	
33.1	108.6	116.0	34.6	63.1	17.6	16.5	35	SEP	N	
33.2		147.9	3.4	98.6	49.9	34.2	35	SEP?	N?	
34.1a	103.6						35	TREND	R?	
34.2		340.1	27.3	329.7	-47.9	18.8	35	SEP	/	
35.1a	97.60	2.3	34.5	1.0	-47.9	.36/.99	35	SEP	/	
35.2a		15.3	-11.3	139.5	-80.3	8.2	35	SEP	R??	
36.1a	95.30	156.2	63.2	24.5	26.6	.88/.98	35	SEP	N	
36.2b							35	TREND	N	
37.1a	93.10	41.5	44.4	29.6	-28.9	.83/.88	35	SEP	/	
37.2							35	TREND	N?	

SAMPLE No	STRATI. HEIGHT (m)	CHARACTERISTIC COMPONENT(F.C.) DEC	INC	COMPONENT(B.C.) DEC	INC	Rc/α_{95}	TEMPERATURE OR AF LEVEL mT	TREND /SEP	POLARI.	POLARITY SEQUENCE
	9m gap of slumping, the lower section is possibly within the Wessex Formation									
38.1a	84.10	136.6	64.9	28.6	20.0	13.0	35	SEP	N	
38.2a		224.8	24.8	311.2	49.4	21.7	35	SEP?	N	
39.1a	82.10	205.9	62.5	358.4	30.9	1.5	35	SEP	N	
39.2a		169.8	63.4	17.2	30.0	0.9	35	SEP	N	
40.1a	80.10	158.4	41.8	37.9	43.2	.91/.96	35	SEP	N	
40.2a		195.8	50.9	1.1	43.6	5.6	35	SEP	N	
41.1	79.10	189.9	62.1	6.9	32.8	1.1	35	SEP	N	
41.2		148.8	43.9	41.6	36.5	.97/.96	35	SEP	N	
42.1	78.10									
42.2a		167.1	50.4	21.5	39.7	.82/.96	35	SEP	N	
42.2b		179.1	49.9	15.8	44.2	.98/.99	35	SEP	N	
43.1a	77.10	184.7	69.6	6.2	20.8	.58/.91	35	SEP	N	
43.2a		160.7	44.5	34.9	43.8	12.3	35	SEP	N	
44.1	69.30	99.7	83.1	14.8	5.1	12.0	35	SEP?	N?	
44.2a		162.1	-24.0	148.1	51.5	16.8	35	SEP	/	
45.1	67.20									
45.2		145.6	66.2	21.9	18.5	.90/.92	35	SEP	N	
46.1a	63.60	168.8	34.2	36.8	55.6	.99/.99	35	SEP	N	
46.2		159.5	34.6	45.9	50.3	1.4	35	SEP	N	
	22m gap of slump									
47.1a	41.60	148.1	56.9	33.3	24.6	.96/.90	35	SEP?	N?	
47.2a		150.8	49.8	34.7	31.0	.97/.91	35	SEP	N	
48.1a	35.60						35	TREND	/	
48.2		297.2	-15.6	263.1	-19.8	16.5	35	TREND	N?	
49.1	34.00	351.3	-40.7	208.2	-51.3	.99/.99	35	SEP	R	
49.2a							35	TREND?	R?	
50.1a	31.30						35	TREND	R	
50.2a							35	TREND	R?	
	To the top of Quartz Grit is ~ 10m									
	Within the Quartz Grit.									
1.1	21.30	141.5	24.6	67.2	40.6	.94/.94	35	SEP	N	
1.2		233.4	45.9	331.6	33.2	41.3	35	SEP	N	
2.1a	15.30	172.7	40.8	27.3	6.0	.93/.31	35	SEP	N	
2.2b							35	TREND	/	
3.1a	12.10	64.0	14.0	78.2	-31.2	23.4	35	SEP?	/	
3.2a							35	TREND	N	
4.1	11.75						35	TREND	R?	
4.2a		281.8	-42.3	223.2	-1.6	.96/.46	35	SEP?	R?	
5.1	11.45	332.0	56.3	347.4	-21.9	6.9	35	SEP	/	
5.2a		189.7	39.5	5.6	55.3	22.3	35	SEP	N	
6.1	9.65									
6.2a							35	TREND	R?	
6.2b							35	TREND	R?	
7.1	7.35?									
7.2a		111.8	83.1	14.7	6.6	28.8	35	SEP	N?	
7.2b							35	TREND	R?	
8.1a	5.35?	119.9	-10.2	110.8	20.5	12.8	35	SEP	/	
8.2a		126.9	8.0	73.7	30.8	.29/.32	35	TREND?	N	

SAMPLE No	STRATI. HEIGHT (m)	CHARACTERISTIC COMPONENT(F.C.) DEC	INC	COMPONENT(B.C.) DEC	INC	Rc/α_{95}	TEMPERATURE OR AF LEVEL °C/mT	TREND /SEP	POLARI.	POLARITY SEQUENCE
9.1a	3.35	49.0	81.1	13.8	-1.7	0.9	35	SEP	N	
9.2a							35	TREND	N	
10.1a	2.70						35	TREND	R	
10.2a		242.2	42.5	322.3	27.7	.93/.99	35	SEP?	N	
11.1a	2.05						35	TREND	N?	
11.2a		314.8	37.2	323.3	-24.9	13.2	35	SEP	/	
12.1	1.50	8.3	79.6	8.0	-5.3	11.6	35	SEP	N??	
12.2a		105.3	49.6	48.4	8.5	14.1	35	SEP?	N	
13.1a	1.15	196.8	67.7	5.3	11.7	.55/.74	35	SEP	N	
13.2a		190.3	66.9	6.9	28.0	2.2	35	SEP	N	
14.1a	0.65	198.4	58.9	1.3	20.6	.27/.80	35	SEP	N	
14.2a		332.7	73.6	0.1	5.4	.12/.87	35	SEP	N	
15.1a		353.2	69.9	2.8	-14.3	1.3	35	SEP	N??	
15.2a		123.2	48.9	47.2	20.1	12.2	35	SEP	N	
	base of section, slump follows.									

APPENDIX 5. MAGNETOSTRATIGRAPHIC RESULTS FROM DURDLE DOOR SECTION (LOWER CRETACEOUS)

SAMPLE No	STRATI. HEIGHT (m)	CHARACTERISTIC COMPONENT(F.C.) DEC	INC	CHARACTERISTIC COMPONENT(B.C.) DEC	INC	Rc/α_{95}	TEMPERATURE OR AF LEVEL mT	TREND /SEP	POLARI.	POLARITY SEQUENCE
	top of the section,~21m to lower boundary of chalk									
	the distance between Marls & Lower Greensands is not able to measure.									
DD44.1a	58.47						35	SEP?	R	
44.2a							35	SEP	/	
43.1a	57.37	55.1	67.6	19.1	-17.2	5.4	35	SEP	/	
43.2a		121.0	27.1	57.0	24.7	24.7	35	SEP	N	
42.1	56.37	154.3	22.2	41.7	52.9	20.7	35	SEP	N	
42.2a		51.2	79.0	10.9	-11.3	.79/.98	35	SEP	/	
41.1	54.27									
41.2							35	TREND?	N??	
40.1a	51.47	185.6	-17.4	203.3	76.4	51.4	35	SEP?	N?	
40.2a							35	TREND	N	
39.1	47.87						35	TREND	/	
39.2a							35	TREND	/	
38.1	40.07	181.5	73.1	359.5	11.8	8.5	35	SEP	N	
38.2a		199.1	49.8	345.4	32.7	3.0	35	SEP	N	
37.1a	38.37						35	TREND	N	
37.2		159.2	41.7	19.9	39.5	45.6	35	SEP?	N	
36.1a	36.07	220.9	53.4	337.9	19.1	.92/.89	35	SEP	N	
36.2							35	TREND	/	
35.1	34.77						-	-	-	
35.2							35	TREND	N??	
34.1	33.37						35	TREND	N	
34.2							35	TREND	R?	
33.1	32.27	11.6	34.7	18.5	-58.3	26.0	35	SEP	/	
33.2		342.1	-67.7	186.9	-16.1	13.2	35	SEP	R	
32.1a	31.17						35	TREND	N?	
32.1b		188.1	-62.6	184.4	32.0	89.5	35	SEP	/	
32.2										
31.1a	30.47	209.1	58.4	344.0	22.3	65.7	35	SEP	N	
31.2a		344.2	-47.5	193.0	-35.6	27.1	35	SEP	R	
30.1	28.87	137.6	52.0	26.6	22.5	5.8	35	SEP	N	
30.2		167.3	28.1	19.4	54.6	16.7	35	SEP	N	
29.1	26.97						35	TREND	N	
29.2										
28.1a	25.87						35	TREND?	N??	
28.1b							35	TREND	N	
28.2										
27.1a	24.87						35	TREND	N?	
27.2		186.5	3.4	333.7	75.0	21.1	35	SEP	N	
26.1a	23.87	28.4	-8.0	121.4	-56.4	17.1	35	SEP	R?	
26.2		154.7	22.7	36.7	48.9	28.7	35	SEP?	N?	
25.1a	22.87	19.2	59.2	12.4	-38.6	16.1	35	SEP	/	
25.2a		18.4	-21.1	149.8	-53.9	85.6	35	TREND	R?	
24.1	21.97	288.9	-18.8	247.4	-14.2	20.0	35	SEP?	R?	
24.2		128.0	50.2	31.4	14.7	15.8	35	SEP	N	
23.1	21.12									
23.2							35	TREND	N?	
22.1a	20.37	4.7	62.9	2.7	-36.9	12.1	35	SEP	/	
22.2							35	SEP	N?	

SAMPLE No	STRATI. HEIGHT (m)	CHARACTERISTIC REMANENT COMPONENT(F.C.) DEC	INC	COMPONENT(B.C.) DEC	INC	Rc/α_{95}	TEMPERATURE OR AF LEVEL mT	TREND /SEP	POLARI.	POLARITY SEQUENCE
21.1a	19.37	326.9	66.8	344.0	-38.6	13.3	35	SEP	/	
21.2a							35	SEP	/	
20.1	18.52	119.3	42.9	39.8	5.9	21.2	35	SEP	N	
20.2a		209.1	21.1	323.6	39.9	14.3	35	SEP	N	
19.5.1		203.7	48.4	343.6	18.2	8.6	35	SEP	N	
19.5.2a		254.6	57.3	328.2	-8.8	5.7	35	SEP	N??	
19.1	16.52	224.5	44.0	327.9	12.7	.99/.89	35	SEP	N	
19.2a		176.1	31.3	4.1	38.5	14.3	35	SEP	N	
18.1a	14.72	163.5	59.1	8.4	9.6	9.1	35	SEP	N?	
18.2		182.0	30.1	357.6	39.7	25.8	35	SEP	N	
17.1a	13.72	204.7	23.6	329.8	40.0	33.3	35	SEP	N	
17.2		171.5	27.8	10.0	41.4	15.2	35	SEP	N	
16.1a	12.92						35	TREND	N?	
16.2a		160.6	20.8	26.0	44.9	15.3	35	SEP	N	
15.1a	11.92						35	TREND	N	
15.2a		140.4	-20.0	97.6	52.9	23.3	35	SEP	N	
14.1a	11.12	314.3	-0.9	250.4	-40.6	24.7	35	TREND	N??	
14.2a		346.3	1.2	217.0	-66.9	59.9	35	SEP	N	
13.1a	10.37	142.0	49.5	23.6	13.0	12.9	35	TREND	/	
13.2		33.8	56.5	26.1	-45.6	13.8	35	SEP	/	
12.1	9.57						35	TREND	/	
12.2a		8.2	59.4	6.8	-39.7	.44/.89	35	SEP	/	
11.1a	8.92	74.7	47.7	45.6	-24.7	28.4	35	SEP	/	
11.2		334.5	46.0	327.1	-56.6	30.0	35	TREND?	N??	
10.1	8.22									
10.2										
9.1a	7.65	13.8	27.0	56.5	-75.3	.96/.96	35	SEP	/	
9.2							35	TREND	N??	
8.1	7.1									
8.2							35	TREND	N	
7.1a	5.3	14.5	-33.5	165.2	-34.6	36.4	35	SEP	R?	
7.2		356.1	4.6	194.3	-74.1	22.0	35	SEP	R	
6.1	4.65						35	TREND	N	
6.2		116.0	13.6	67.2	18.6	14.5	35	SEP	N	
5.1	4.0	198.7	36.7	342.6	30.5	13.2	35	SEP	N	
5.2							35	TREND	N?	
4.1a	3.45	357.7	45.2	356.2	-64.6	22.1	35	SEP	/	
4.2a							35	TREND	N??	
3.1	3.0						35	TREND	R?	
3.2a		297.0	34.0	298.2	-33.0	15.8	35	SEP	R??	
2.1a	2.2	0.6	49.2	0.8	-60.7	8.0	35	SEP	/	
2.1b		345.6	32.9	340.6	1.2	.99/.09	35	SEP	/	
2.2a							35	TREND	N	
1.1	0.0	43.9	35.9	57.9	-48.7	2.8	35	SEP	R??	
1.2a		36.1	-6.5	123.0	-45.6	8.5	35	SEP	R	

base of section, ~7m to Purbeck sandstone

APPENDIX 6. MAGNETOSTRATIGRAPHIC RESULTS FROM THE WEALD CLAY SECTIONS (LANGHURST, WARNHAM; LOWER CRETACEOUS)

SAMPLE No	STRATI. HEIGHT (m)	CHARACTERISTIC COMPONENTS DEC	INC	Rc/α_{95}	TEMPERATURE OR AF LEVEL mT	TREND /SEP	POLARI.	POLARITY SEQUENCE
top of the section								
LG19.1	11.25	179.1	-13.8	.13/.98	35	TREND	R	
19.2		162.8	-26.2	.99/1.0	35	SEP	R	
18.1a	10.68	8.0	71.9	.99/.96	35	SEP	N	
18.2a		6.2	77.5	.34/.97	35	SEP	N	
17.1a	10.00	2.6	67.5	.33/1.0	35	SEP	N	
17.2a		353.6	57.7	.58/.98	35	SEP	N	
16.1a	9.15	145.1	-56.7	.95/.99	35	SEP	R	
16.2a		160.9	-52.2	.99/.97	35	SEP	R	
15.1	8.80	5.0	56.4	.30/.98	35	SEP	N	
15.2a		344.8	62.4	1.0/.98	35	SEP	N	
14.1a	8.06	344.8	39.1	1.0/1.0	35	SEP	N	
14.2a		340.6	48.9	.99/.99	35	SEP	N	
13.1a	7.42				35	TREND	N?	
13.2a					35	TREND	N?	
12.1a	6.90	19.8	67.9	.56/.95	35	SEP	N	
12.2a					35	TREND	N	
11.1a	6.16	57.0	74.1	.81/.83	35	SEP	N	
11.2		44.4	79.6	.74/.89	35	SEP	N	
10.1a	5.37	152.4	-40.9	1.0/1.0	35	SEP	R	
10.2a		168.0	-49.7	.79/.99	35	SEP	R	
9.1	4.60	41.9	48.6	.99/.99	35	SEP	N	
9.2a		320.2	77.1	.97/.86	35	SEP	N?	
8.1	3.80	1.2	51.5	.30/.95	35	SEP	N	
8.2a		338.4	60.0	.46/.76	35	SEP	N	
7.1	3.42				35	SEP	N?	
7.2a		347.3	57.7	.75/.98	35	SEP	N	
6.1	2.66	170.6	-15.1	.44/.40	35	SEP	R	
6.2a		164.6	-24.8	1.0/1.0	35	TREND	R	
5.1a	2.20	153.8	-37.4	.99/.99	35	SEP	R	
5.1b					35	TREND	R	
5.2		25.9	56.9	.90/.99	35	SEP	N	
4.1a	1.60	239.9	-33.0	.95/.67	35	SEP	R	
4.1b					35	TREND	R	
4.2a		193.7	-25.4	1.0/.84	35	SEP	R	
4.2b					35	TREND	R	
3.1a	0.94	171.6	-41.0	.94/.98	35	SEP	R	
3.1b					35	SEP	R	
3.2a		175.3	-27.7	.76/.99	35	SEP	R	
3.2b					35	SEP	R	
2.1a	0.44	172.2	-51.2	.88/.99	35	SEP	R	
2.1b					35	TREND	R	
2.2a		166.6	-42.0	.99/.99	35	SEP	R	
2.2b					35	SEP	R	
1.1	0.00	169.8	-8.8	.92/.88	35	SEP	R	
1.2a					35	TREND	R	
1.2b					35	TREND	R	
base of the northeast section in the pit								

SAMPLE No	STRATI. HEIGHT (m)	CHARACTERISTIC COMPONENTS DEC	INC	Rc/α_{95}	TEMPERATURE OR AF LEVEL mT	TREND /SEP	POLARI.	POLARITY SEQUENCE
	top of the southwest section							
LG35.1a	7.81	19.6	81.4	.82/.97	35	SEP	N	
35.2a		7.1	57.1	1.0/1.0	35	SEP	N	
34.1	7.41	322.8	61.7	.96/.98	35	SEP	N	
34.2a		328.5	51.6	.98/.99	35	SEP	N?	
33.1a	7.0	143.8	-56.5	.51/.75	35	SEP	R	
33.2a					35	SEP?	N?	
33.2b					35	SEP?	N?	
32.1a	6.42				35	TREND	R	
32.2a		212.8	-31.7	.98/.82	35	SEP	R	
31.1a	6.25	198.0	-27.9	.98/.99	35	SEP	R	
31.2a					35	TREND	R	
30.1	5.26				35	TREND	R?	
30.2a					35	TREND	R	
29.1a	4.58	182.8	-44.1	.44/.99	35	SEP	R	
29.2		172.0	-21.6	.65/.99	35	SEP	R	
28.1a	4.00				35	SEP?	R?	
28.2a		179.2	-46.7	.40/10	35	SEP	R	
27.1a	3.05	193.8	-51.4	.97/.99	35	SEP	R	
27.2								
26.1	2.84				35	TREND	N	
26.2a					35	SEP?	R?	
25.1a	2.10	180.2	-26.1	1.0/1.0	35	TREND	R	
25.2a		184.2	-34.7	.38/.99	35	SEP	R	
24.1	1.50	166.2	-33.1	.99/.98	35	SEP	R	
24.2					35	TREND	R	
23.1a	1.33	148.8	-13.4	.99/.98	35	SEP	R	
23.2		142.9	-41.1	.98/.95	35	SEP	R	
22.1a	0.84				35	SEP?	R??	
22.2a					35	TREND	N	
21.1	0.47	177.0	-36.7	.55/.99	35	SEP	R	
21.2								
20.1	0.00	182.8	-14.3	.36/.99	35	SEP	R	
20.2a		184.8	-17.1	.79/.99	35	SEP	R	
	base of the southwest section							

APPENDIX 7. MAGNETOSTRATIGRAPHIC RESULTS FROM LONGMARSH QUARRY, BOVEY TRACEY.

SAMPLE No	STRATI. HEIGHT (m)	CHARACTERISTIC COMPONENT(after B.C) DEC	INC	Rc or α_{95}	MAX. TEMPERATURE OR AF LEVEL (^{o}C /mT)	SEP or TREND?	POLARITY	POLARITY SEQUENCE
	top of section							
LM1.1a	34.6	343.8	34.6	.99/.99	35mT	SEP	N	
1.1b		5.7	19.3	6.7	35	SEP	N	
1.2a		19.3	-11.6	0.6	20	/	/	
1.2b		354.4	11.1	1.3	35	SEP	N	
2.1a	34.2				35	TREND	R	
2.2a					35	TREND?	R	
2.2b		326.9	41.2	8.0	35	SEP	N	
3.1a	33.2				35	/	I?	
3.1b		138.2	-51.5	22.9	35	SEP	R	
3.2a		103.8	-20.6	13.7	20	SEP?	R	
4.1	31.9	172.2	-33.8	8.2	35	SEP	R	
4.2					20	TREND	R	
5.1	29.3	168.6	-17.3	10.1	35	SEP?	R	
5.2					35	TREND	R	
6.1a	26.8				35	TREND	R	
6.2a					35	TREND?	R??	
6.2b		143.4	-43.4	.78/.99	35	SEP	R	
7.1a	26.1	319.3	48.1	8.0	35	SEP	N	
7.1b		17.9	78.6	14.5	35	SEP	N	
7.2a		92.3	-30.5	9.0	35	SEP	R	
7.2b		209.4	-41.7	11.8	15	SEP	R	
8.1a	25.3				35	/	/	
8.1b		178.2	-58.4	29.9	35	SEP	R	
8.2a					35	TREND	R?	
8.2b					35	TREND	R?	
9.1a	24.5				35	SEP??	R	
9.1b					35	TREND	R	
9.2a		194.2	-71.6	19.2	35	SEP	R	
10.1a	22.8	180.5	-36.6	14.4	35	SEP	R	
10.2a		255.1	-61.7	6.1	35	SEP	R	
11.1a	21.7	330.6	-79.4	14.4	35	SEP	R??	
11.2a		222.0	-77.3	12.9	35	SEP	R	
12.1a	20.9	161.2	-55.8	.82/.97	35	SEP?	R	
13.1a	19.1	160.1	-57.0	20.4	35	SEP	R	
14.1a	18.0				35	TREND	N?	
14.1b					35	TREND	N?	
14.2a					20	TREND?	R??	
14.2b								
15.1a	15.7				35	TREND	N	
15.2a		173.3	-71.6	.48/.99	20	SEP	R	
16.1a	15.0				35	TREND	R?	
16.2a		180.8	-48.5	.91/.99	20	SEP	R	
17.1a	12.3				35	TREND	R	
17.1b					35	SEP	N?	
17.2a					35	TREND	R	
18.1a	11.0				35	TREND	R?	
18.2a					35	/	/	
18.2b		25.0	22.4	20.2	15	SEP??	N??	
19.1a	10.4	51.0	70.6	13.6	35	SEP	N	
19.2a		271.0	22.0	23.5	35	SEP??	N	

SAMPLE No	STRATI. HEIGHT (m)	CHARACTERISTIC COMPONENT(after B.C) DEC	INC	Rc or α_{95}	MAX. TEMPERATURE OR AF LEVEL (°C /mT)	SEP or TREND?	POLARITY	POLARITY SEQUENCE
20.1a	9.2				35	TREND	N?	
20.2a		274.5	25.4	30.9	35	SEP	N	
21.1a	7.5	26.4	58.2	4.5	35	SEP	N	
21.2a					35	SEP	N	
22.1a	6.5				35	TREND	R	
22.1b		48.4	42.4	11.8	35	SEP	N	
22.2a		353.9	30.3	8.1	35	SEP	N	
23.1a	6.0				35	/	/	
23.1b					35	TREND?	N??	
23.2a					35	TREND	N	
24.1a	4.6	4.5	50.3	6.9	35	SEP	N	
24.2a		279.7	22.8	8.4	35	SEP	N	
25.1	3.7				35	TREND?	R?	
25.2a		341.6	82.9	19.7	35	SEP?	N	
25.2b		27.7	76.4	10.9	35	SEP	N?	
26.1	1.6				35	TREND	R?	?
26.2a		14.1	50.3	32.4	35	TREND	N	
26.2b					35	TREND	R	
27.1a	section	339.0	34.1	5.7	35	SEP	N	
27.2a	base	340.2	42.0	20.2	35	SEP	N	

APPENDIX 8. MAGNETOSTRATIGRAPHIC RESULTS FROM JOHN ACRES LANE QUARRY, BOVEY TRACEY (OLIGOCENE)

SAMPLE No	STRATI. HEIGHT (m)	CHARACTERISTIC COMPONENT(after B.C) DEC	INC	Rc or α_{95}	MAX. TEMPERATURE OR AF LEVEL (°C /mT)	SEP or TREND?	POLARITY	POLARITY SEQUENCE
	top of section							
JA34.1	37.6	154.1	-61.5	2.5	35	SEP	R	
34.2	top of	158.3	-56.8	1.1	35	SEP	R	
33.1a	36.7	206.6	-50.5	18.5	35	SEP	R	
33.2a					35	TREND	R	
33.2b					35	TREND	R	
32.1a	34.5				35	TREND?	R??	
32.1b					35	/	/	
32.2					35	/	/	
31.1a	33.3				35	TREND	R	
31.1b					35	TREND	R?	
31.2a					35	TREND	R??	
30.1	32.2	242.9	-78.0	9.6	35	SEP	R	
30.2a		169.0	-61.4	.39/.92	35	SEP	R	
29.1a	31.5				35	TREND	R	
29.2a					35	TREND	R?	
29.2b					35	TREND	R	
28.1a	30.6				35	TREND	R?	
28.2a					35	TREND	R?	
28.2b					35	/	/	
27.1a	29.1				35	SEP??	N?	
27.1b					35	TREND	N	
27.2a					35	TREND	R?	
26.1	28.2				35	/	/	
26.2					35	TREND	N	
25.1a	27.0				35	TREND	R?	
25.1b		243.3	63.7	15.2	35	/	/	
25.2a					35	TREND?	N?	
25.2b		65.5	85.0	4.1	35	SEP	N	
24.1a	26.3				35	TREND	R?	
24.1b					35	TREND	R	
24.2a					35	TREND	R	
24.2b					35	TREND	R??	
23.1a	25.8				35	TREND	R??	
23.1b					35	TREND	N?	
23.2a					35	TREND	R?	
23.2b					35	/	/	
22.1a	25.1				35	TREND	N?	
22.1b					35	TREND	N?	
22.2a					35	/	/	
22.2b		345.5	47.3	32.8	35	SEP??	N?	
21.1a	24.5	3.5	58.1	3.8	35	SEP	N	
21.1b		350.0	50.1	13.1	25	SEP	N	
21.2a		326.5	11.7	9.2	35	SEP	N	
21.2b		338.5	57.2	4.4	35	SEP	N	
20.1a	22.8				35	SEP	I?	
20.1b					25(65)	TREND	N?	
20.2a					35	SEP	I?	
19.1	20.9	44.8	64.3	18.4	35	SEP	N	
19.2a					35	SEP	N	

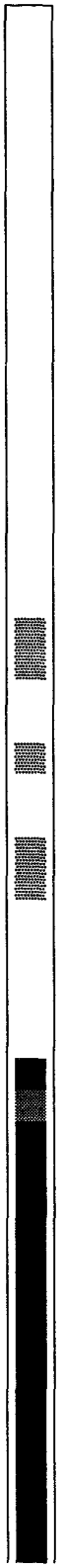

SAMPLE No	STRATI. HEIGHT (m)	CHARACTERISTIC COMPONENT(after B.C) DEC	INC	Rc or α_{95}	MAX. TEMPARETURE OR AF LEVEL (°C /mT)	SEP or TREND?	POLARITY	POALRITY SEQUENCE
19.2b					35	TREND	N??	
18.1a	20.5	349.9	53.5	9.6	25	SEP	N	
18.1b		22.6	59.1	12.0	35	SEP?	N	
18.2a					35	TREND	N	
18.2b					35	TREND	R	
17.1a	20.0				25	SEP??	R?	
17.1b		183.1	-77.9	26.2	35	SEP	R	
17.2a					35	TREND	R	
17.2b					35	TREND	R	
16.1a	19.5				25	/	/	
16.1b					35	TREND?	R?	
16.2a					35	TREND	R	
16.2b					35	TREND	R??	
15.1	19.1				35	/	/	
15.2a					35	/	/	
15.2b					35	TREND	R	
14.1	18.6				35	TREND	R??	
14.2					35	TREND	R	
13.1	15.9				35	TREND?	R?	
13.2					35	TREND	R	
12.1a	12.2				35	SEP	I	
12.1b					35	SEP	I	
12.2a					35	TREND	R	
12.2b		157.7	-21.5	12.6	35	SEP	R	
11.1a	10.9	310.1	45.9	10.6	35	SEP	N	
11.1b		350.2	20.9	8.5	35	SEP	N	
11.2a					35	SEP	I	
11.2b					35	TREND	R	
10.1a	9.9				35	/	/	
10.1b					35	TREND?	N	
10.2a					35	TREND	R	
10.2b					35	TREND	R	
9.1a	7.9				35	TREND	R	
9.1b					35	TREND	R?	
9.2		333.0	40.9	21.7	35	SEP	N	
8.1a	6.2	36.6	35.1	9.6	35	SEP	N	
8.1b					35	SEP	R	
8.2					35	TREND	R	
7.1a	4.9				35	TREND	R	
7.1b					35	TREND	R?	
7.2		24.2	30.9	13.2	35	SEP	N	
6.1a	3.4	81.6	-67.1	22.8	35	SEP	R	
6.1b					35	TREND	R	
6.2a		311.2	41.5	12.1	25	SEP	N	
6.2b		344.5	40.4	17.1	35	SEP	N	
5.1a	2.2	55.2	49.7	13.8	35	SEP	N	
5.1b					35	TREND	R	
5.2a					25	TREND	R	
5.2b		278.2	47.6	21.4	35	TREND	R?	
4.1a	1.5	230.8	-45.2	20.7	35	SEP	R	
4.1b					35	TREND	R	
4.2a					35	SEP	I	

SAMPLE No	STRATI. HEIGHT (m)	CHARACTERISTIC COMPONENT(after B.C) DEC INC Rc or α_{95}	MAX. TEMPARETURE OR AF LEVEL (°C /mT)	SEP or TREND?	POLARITY	POALRITY SEQUENCE
4.2b			35	TREND	R	
3.1a	1.0		15	SEP	N	
3.1b			35	SEP	I	
3.2a			35	TREND	R	
3.2b			35	TREND	N	
2.2a	0.6		25	TREND	R?	
2.2b			35	TREND	R	
1.1			35	TREND	R	
1.2a	base of	section	35	TREND	R	
1.2b			35	TREND	R	

APPENDIX 9. MAGNETOSTRATIGRAPHIC RESULTS FROM BOREHOLE SD485, BOVEY TRACEY (OLIGOCENE)

SAMPLE No	BORE-HOLE DEPTH(m)	CHARACTERISTIC COMPONENT DEC	INC	Rc or α_{95}	MAX. TEMPERATURE OR AF LEVEL (°C /mT)	SEP or TREND?	POLARITY	POLARITY SEQUENCE
	highest level of sampling in the borehole							
BB37a	11.2	296.2	18.5	8.0	35mT	SEP	N	
37b*					300°C	TREND	**R**	
40a*	12.2	49.2	41.3	31.1	300	SEP?	**N**	
40b		26.7	38.8	22.0	35	SEP	N	
41a	12.5	72.5	65.7	25.7	35	SEP	N	
41b*					300	TREND	**N**	
43a*	13.1	213.1	-32.8	51.6	300	SEP?	**R?**	
43b		238.8	33.1	16.4	35	SEP	N	
45a*	13.7				300	/	/	
45b		162.7	43.6	17.1	35	SEP	N	
46a*	14.0				300	TREND	**R?**	
46b					35	TREND	R	
50a*	15.2				300	/	/	
50b		288.6	-50.1	10.0	35	SEP?	R	
52a	15.8				20	TREND	R?	
52b*					250	TREND	**R??**	
56/1a	17.0				20	TREND	R	
56/2a*					300	TREND	**R**	
56/2b		293.7	-66.9	12.2	35	SEP	R	
58a*	17.7				300	TREND	**R**	
58b					35	TREND	R?	
60a	18.3				20	SEP??	R?	
60b*					300	/	/	
64a	19.5				35	TREND?	N??	
64b*					250	TREND	**R?**	
65a*	19.8				300	TREND	**R??**	
65b		265.8	-50.7	12.9	35	SEP	R	
67a*	20.4				250	/	/	
67b		253.4	-46.3	23.6	35	SEP	R	
75a	22.8				35	TREND	R?	
75b*					250	TREND	**R??**	
79a*	24.1				300	SEP?	**R**	
79b					35	TREND	R	
87a*	26.5				300	/	/	
87b					35	TREND	R??	
88a	26.8	259.4	38.6	18.8	35	SEP?	N?	
88b*		281.5	51.4	45.7	250	SEP	**N?**	
90a*	27.4				300	TREND	**N**	
90b		6.4	41.3	7.7	35	SEP	N	
91a*	27.7				300	TREND	**N**	
91b		241.4	34.9	19.3	35	SEP	N	
93a	28.3	281.1	19.0	22.8	35	SEP?	N	
93b*					300	TREND	**N**	
94a	28.6	308.9	61.6	.60/.77	35	SEP	N	
94b*					200	SEP??	**N?**	
99a*	30.2				200	TREND	**N**	
99b		216.1	-52.8	14.3	35	SEP	R	
100	30.5				200	TREND	**R**	

SAMPLE No	STRATI. HEIGHT (m)	CHARACTERISTIC COMPONENT DEC	INC	Rc or α_{95}	MAX. TEMPERATURE OR AF LEVEL ($^{\circ}$C/mT)	SEP or TREND?	POLARITY	POLARITY SEQUENCE
106a*	32.3				300	TREND	**R**	
106b		145.7	31.0	14.2	35	SEP	N	
109/1a	33.2	235.4	52.1	11.1	15	SEP	N	
109/1b*		219.8	79.0	8.7	300	SEP	**N**	
109/2a		268.4	43.9	10.1	20	SEP	N	
109/2b		88.9	48.0	7.3	35	SEP	N	
110/1a*	33.5	143.6	83.5	12.0	35	SEP	N	
110/1b		263.7	55.9	7.1	300	SEP	**N**	
110/2a		247.1	24.7	6.3	35	SEP	N	
112a	34.1	244.7	47.6	11.5	35	SEP	N	
112b*					300	/	/	
114a*	34.7				300	TREND	**N**??	
114b					30	/	/	
116a	35.3	306.5	31.9	39.1	35	SEP?	N	
116b*					300	TREND	**R**?	
118a	36.0				35	TREND	R?	
118b		203.0	-50.6	14.2	35	SEP	R	
120a	36.6				35	SEP?	N	
120b					35	/	/	
122a	37.2	239.0	21.0	14.4	35	SEP	N	
122b		184.4	-20.6	25.8	35	SEP	R?	
124a	37.8	269.0	34.8	13.3	35	SEP	N	
124b		234.2	-36.7	11.6	35	SEP	R	
126a	38.4				35	/	R?	
126b					35	/	/	
130a	39.6				35	TREND	R	
130b					35	SEP??	R?	
132a	40.2	196.1	55.7	15.0	35	SEP	N?	
132b					35	TREND	R?	
135a	41.1	295.5	-41.5	21.4	35	SEP	R	
135b					35	SEP	R?	
137a	41.7				35	TREND	R	
137b					35	TREND	R	
139a	42.3				35	TREND?	R	
139b					35	TREND	R	
140a	42.7				35	SEP??	R?	
140b		106.2	-33.4	10.9	35	SEP	R	
144a	43.9	62.5	-59.4	14.7	35	SEP	R	
144b		106.9	-52.0	9.5	35	SEP	R	
147a	44.8				35	TREND	R	
147b		254.9	-46.9	15.9	35	SEP	R	
149a	45.4				35	TREND	R	
149b		317.7	-55.3	18.7	35	SEP	R	
151a	46.0	288.3	-55.1	.39/.76	35	SEP	R	
151b		60.8	-38.8	8.0	35	SEP	R	
154a	46.9				35	TREND	R	
154b		182.9	-32.5	17.8	35	SEP	R	
157a	47.8	186.2	-53.3	15.2	35	SEP	R	
157b		221.2	-56.2	.95/.92	35	SEP	R	
161a	49.0				35	SEP?	N?	

SAMPLE No	STRATI. HEIGHT (m)	CHARACTERISTIC COMPONENT DEC	INC	Rc or α_{95}	MAX. TEMPERATURE OR AF LEVEL (°C/mT)	SEP or TREND?	POLARITY	POLARITY SEQUENCE
161b		279.1	-36.7	.75/.80	35	SEP	R	
164a	50.0				20	SEP	I?	
164b					35	TREND	N?	
167a	50.9	40.5	46.6	35.3	35	SEP	N	
167b					35	SEP?	N?	
171a	52.1	208.2	58.4	.26/.63	35	SEP	N	
171b					35	TREND	R	
174a	53.0				35	TREND	N	
174b					35	SEP	N?	
177a	53.9	243.0	45.4	23.5	35	SEP	R	
177b					35	TREND?	N?	
180a	54.8	347.8	16.9	.99/.99	35	SEP	N	
180b	bottom				35	SEP?	R?	

Note: * represents those samples with thermal demagnetisation.

APPENDIX 10. MAGNETOSTRATIGRAPHIC RESULTS FROM St.NIKLAAS QUARRY, BOOM CLAY FORMATION (OLIGOCENE)

SAMPLE No	STRATI. HEIGHT (m)	CHARACTERISTIC COMPONENTS DEC	INC	Rc/α_{95}	TEMPERATURE OR AF LEVEL °C/mT	TREND /SEP	POLARI.	POLARITY SEQUENCE
	top of the section							
SN30.1	9.98				35	TREND	R?	
30.2					35	SEP?	/	
29.1a	9.15				35	TREND	R?	
29.1b					35	TREND	R	
28.1	8.82	183.6	-60.7	1.0/1.0	35	SEP	R	
28.2		171.6	-37.8	1.0/1.0	35	SEP	R	
27.1a	8.50	157.7	-43.6	.88/.88	35	SEP	R	
26.1	8.17	312.1	43.7	.62/.31	35	SEP?	N?	
26.2		184.5	-12.0	.64/.97	35	SEP	R	
25.1a	7.84				35	TREND	R	
25.1b					35	TREND?	R?	
24.1	7.52				35	SEP?	R	
24.2					35	TREND	R?	
23.1a	7.19				35	TREND	R?	
22.1	6.86				35	TREND	R	
22.2		324.0	68.1	.61/.91	35	SEP	N	
21.1a	6.54				35	TREND	R?	
20.1	6.21	18.3	32.9	.99/.93	35	SEP	N	
20.2					35	TREND	N??	
19.1a	5.88				35	TREND	R?	
18.1	5.56				35	TREND	R	
18.2		120.4	-38.8	13.7	35	SEP	R	
17.1a	5.23	67.8	64.6	18.8	35	SEP	N	
16.1	4.90	14.0	45.1	.61/.96	35	SEP	N	
16.2		44.7	45.2	.62/.63	35	SEP	N	
15.1	4.58	340.0	50.4	.66/.92	35	SEP	N	
14.1	4.25				35	TREND	R?	
14.2					35	SEP	/	
13.1	3.92	288.7	26.2	.92/.53	35	SEP	N	
13.2					35	TREND	N?	
12.1a	3.60				35	TREND	R	
11.1	3.27				35	TREND	R	
11.2					35	SEP	/	
10.1a	2.94				35	SEP?	N?	
9.1	2.61				35	TREND	R	
9.2					35	TREND	R	
8.1a	2.29	140.4	-58.2	.72/.94	35	SEP	R	
7.1	1.96				35	TREND	N	
7.2					35	TREND	R?	
6.1a	1.63	130.8	-56.3	56.8	35	SEP	R	
5.1a	1.31				35	TREND	R?	
5.2		111.6	-42.0	14.1	35	SEP	R	
4.1	0.98	154.8	-72.7	.97/.92	35	SEP	R	
3.2	0.65				35	TREND	R	

SAMPLE No	STRATI. HEIGHT (m)	CHARACTERISTIC COMPONENTS DEC	INC	Rc/α_{95}	TEMPERATURE OR AF LEVEL °C/mT	TREND /SEP	POLARI.	POLARITY SEQUENCE
2.1	0.27				35	SEP	/	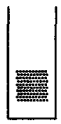
1.1a	0.00	171.0	-48.3	.41/.92	35	SEP	R	
1.2		78.4	63.1	29.1	35	SEP	N	
base of St.Niklaas section								

APPENDIX 11. MAGNETOSTRATIGRAPHIC RESULTS FROM STEENDORP QUARRY, BOOM CLAY FORMATION (OLIGOCENE)

SAMPLE No	STRATI. HEIGHT (m)	CHARACTERISTIC COMPONENTS DEC	INC	Rc/α_{95}	TEMPERATURE OR AF LEVEL °C/mT	TREND /SEP	POLARI.	POLARITY SEQUENCE
	top of section							
SD12.1	5.92	84.3	-36.4	11.5	35	SEP	R?	
11.1a	5.24				35	TREND	R	
10.1a	4.65				35	SEP	/	
10.1b					35	TREND	R	
9.1	4.07				35	TREND	N?	
9A.1a		122.6	-54.9	47.9	35	SEP?	R	
8.1a	3.49				35	SEP	R??	
7.1	2.91				35	TREND	R	
6.1a	2.62				35	TREND	R?	
5.1	2.33	357.6	27.0	20.5	35	SEP?	N?	
4.1a	2.04	22.9	3.2	.94/.88	35	SEP	N?	
3.1a	1.75				35	TREND	N	
2.1a	1.45	349.5	40.4	1.0/1.0	35	SEP?	N	
1.1a					35	TREND	N?	
1.1b		48.2	33.4	.72/.70	35	SEP	N	
	base of Steendorp section							

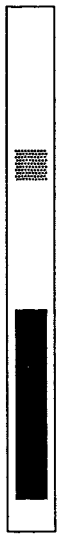

APPENDIX 12. MAGNETOSTRATIGRAPHIC RESULTS FROM KRUIBEKE QUARRY, BOOM CLAY FORMATION (OLIGOCENE)

SAMPLE No	STRATI. HEIGHT (m)	CHARACTERISTIC COMPONENTS DEC	INC	Rc/α_{95}	TEMPERATURE OR AF LEVEL °C/mT	TREND /SEP	POLARI.	POLARITY SEQUENCE
	top of the Boom Clay Formation							
KB81.1	29.37							
81.2		103.2	-13.5	16.0	35	SEP	R	
80.2	29.00				35	TREND	R	
79.2	28.63	320.5	50.5	.80/.92	35	SEP	N	
78.1					35	TREND?	R?	
77.2	27.89				35	/	/	
76.1	27.52	5.4	12.8	.25/.48	35	SEP	N	
75.1	27.15				35	TREND	R	
74.1	26.78				35	TREND?	R?	
73.2	26.41				35	TREND?	R?	
72.1	26.04							
71.2	25.67				35	TREND	R?	
70.2	25.31				35	TREND?	R??	
69.2	24.94	197.0	-27.3	.58/.89	35	SEP	R	
68.2	24.54	254.5	-29.5	27.1	35	SEP	R	
67.2	24.20	81.9	40.7	7.1	35	SEP	N	
66.1	23.83	98.8	-27.0	20.6	35	SEP	R	
65.1	23.46				35	TREND	R?	
64.1	23.09				35	TREND	R	
63.1	22.75				35	TREND?	R?	
62.1	22.35				35	SEP	/	
61.1	21.98				35	SEP	/	
60.1	21.61				35	SEP	/	
59.1	21.24				35	TREND	R	
58.1	20.87	10.4	40.3	.68/.97	35	SEP	N	
57.1a	20.50				35	TREND?	R??	
57.1b					35	TREND?	R	
56.1a	20.13				35	SEP	/	
56.1b					35	SEP	/	
55.1	19.76				35	TREND	R	
54.1	19.40	314.4	48.7	.84/.69	35	SEP	N	
53.1a	19.03				35	TREND	R	
52.1a	18.66	273.6	32.2	8.7	35	SEP	N	
52.1b					35	TREND?	R?	
51.1	18.29	194.8	-30.4	.52/.88	35	SEP	R	
50.1	17.92	199.5	-26.4	.52/.99	35	SEP	R	
49.1	17.56				35	TREND?	R	
48.1	17.18				35	TREND	R	
47.1a	16.81	310.8	24.9	.98/.99	35	SEP	N?	
47.1b		323.6	11.0	.89/.18	35	SEP	N?	
46.1a	16.44				35	TREND	R?	
46.1b					35	TREND	R	
45.1	16.07				35	TREND	N	
	base of upper part of Kruibeke section							

SAMPLE No	STRATI. HEIGHT (m)	CHARACTERISTIC COMPONENTS DEC	INC	Rc/α_{95}	TEMPERATURE OR AF LEVEL °C/mT	TREND /SEP	POLARI.	POLARITY SEQUENCE
	top of lower part of Kruibeke				section			
KB44.1	16.07				35	TREND	R	
43.1a	15.86				35	TREND	R?	
43.1b					35	TREND	R	
42.1a	15.15				35	TREND?	R??	
42.1b					35	TREND	R	
41.1a	14.78				35	TREND	R	
41.1b					35	TREND	R	
40.1a	14.41	324.2	-78.6	20.6	35	SEP?	R	
40.1b					35	TREND	R	
39.1a	14.04				35	SEP	/	
39.1b		230.9	-36.7	.98/.98	35	SEP	R	
38.1a	13.67				35	TREND	R	
38.1b					35	TREND	R	
37.1a	13.30				35	TREND	R?	
37.1b					35	SEP	/	
36.1a	12.93				35	TREND	R?	
36.1b					35	TREND	N?	
35.1a	12.56	342.2	48.8	.44/.78	35	SEP	N	
35.1b		11.0	11.0	.51/.86	35	SEP	N	
34.1a	12.19	15.1	72.2	.28/.88	35	SEP	N	
34.1b					35	SEP	N	
33.1	11.82	292.6	33.6	.90/.79	35	SEP	N	
32.1a	11.45	285.7	30.7	.99/.98	35	SEP	N	
32.1b					35	SEP	/	
31.1	11.08	297.9	52.1	.86/.76	35	SEP	N	
30.1b	10.71	323.9	49.5	.99/.96	35	SEP?	N	
29.1a	10.34				35	TREND?	R?	
29.1b		355.1	31.8	.47/.82	35	SEP?	N	
28.1	9.97	303.2	39.6	.98/.99	35	SEP	N	
27.1	9.60	100.6	70.9	13.8	35	SEP	N	
26.1	9.24	104.6	53.1	.94/.85	35	SEP	N	
25.1a	8.87	140.2	-42.1	.96/.99	35	SEP	R	
25.1b		10.2	1.4	.99/.88	35	SEP	N?	
24.1a	8.47				35	TREND?	R?	
24.1b					35	TREND	N?	
23.1a	8.13				35	TREND	R	
23.1b					35	TREND	R??	
22.1a	7.76	278.9	24.8	8.0	35	SEP	N	
22.1b		287.3	14.3	12.0	35	SEP	N	
21.1a	7.39	178.8	-13.7	.19/.87	35	SEP	R	
21.1b		221.6	-18.0	1.0/.98	35	SEP	R	
20.1b	7.02				35	SEP	/	
19.1a	6.65				35	TREND?	R	
19.1b					35	SEP?	N?	
18.1a	6.28				35	SEP	/	
18.1b					35	SEP	/	

SAMPLE No	STRATI. HEIGHT (m)	CHARACTERISTIC COMPONENTS DEC	INC	Rc/α_{95}	TEMPERATURE OR AF LEVEL °C/mT	TREND /SEP	POLARI.	POLARITY SEQUENCE
17.1a	5.91				35	TREND	R?	
17.1b					35	SEP	/	
16.1a	5.54				35	TREND	R?	
16.1b					35	SEP	R??	
15.1b	5.17				35	TREND	R	
14.1a	4.80				35	SEP	/	
14.1b					35	SEP	/	
13.1a	4.43	133.2	-68.5	.98/.73	35	TREND?	R??	
13.1b					35	SEP	/	
12.1	4.06	55.5	34.9	.98/.74	25	SEP	N	
12.2a		351.0	39.8	.59/.92	35	SEP	N	
12.2b		291.8	20.8	11.6	35	SEP	N	
11.1b		334.4	80.7	15.3	35	SEP	N	
10.1	3.33							
10.2								
9.1	2.96							?
9.2								
8.1	2.59							
8.2								
7.1a	2.22	4.6	31.7	.42/.72	35	SEP	N	
7.1b					35	SEP	/	
6.1a	1.85				35	SEP	/	
6.1b		11.7	45.6	.45/.93	35	SEP	N	
5.1b	1.48				35	SEP	/	
4.1a	1.11	337.0	63.6	.96/.97	35	SEP	N	
3.1a	0.74				35	TREND?	N?	
3.1b					35	SEP	/	
2.1a	0.37				35	SEP	/	
2.1b					35	TREND	R?	
1.1b	0.00				35	TREND	R	
	base of lower part of Kruibeke section							

APPENDIX 13. Computer sub-programme for the great circle fitting which is named "G.CIR/INTS" within a main programme "REMSTERO4" (modified mainly from the programme "DEVIAT") as a sub-function. The computer language used for this programme is BASIC language for the HP-86 computer (Hewlett-Packard). The presented programme gives the main calculation for the intersections yielded from great circles for each demagnetised sample, but some sub-functions, such as data reading, data selection and field and bedding correction, will utilize other sub-functions from the main programme.

```
5360 ! !! ********* SUB GREAT CIRCLE FITTING & INTERSECTIONS" ********
5370 J=1 @ L1=1
5380 CLEAR @ DISP "THIS FUNCTION DETERMINE GREAT CIRCLES & THEIR INTERSECTIONS
                   FROM DIRECTIONAL TRENDS, MAXIMUM IS 100 SAMPLES.  "
5390 DISP "INPUT DATA FROM DISK, at least 2 samples must be input"
5400 DISP "WHAT POLARITY DO YOU CALCULATE?  N/R" @ INPUT PO$
5410 IF PO$="N" THEN CM=1 ELSE CM=2
5420 DISP " INPUT CHARACTERISTIC DIR.FOR MEAN INTERS. e.g using mean SEP D=  , I=
 ." @ INPUT D6,I6
5430 IF CM=2 THEN D5=D6-180 @ I5=90-ABS (I6) ELSE I5=90-I6 @ D5=D6
5440 DISP "INPUT SAMPLE NO. " @ INPUT F1$
5450 NAME$(L1)=F1$
5460 GOSUB 860 ! input data from disk
5470 GOSUB 3430 ! edit data (erase some irregular data)
5480 GOSUB 4120 ! field / bedding correction
5490 CLEAR
5500 DISP "WHICH SET OF DATA DO YOU USE FOR GREAT CIRCLE & INTERSECTIONS? "
5510 DISP "WRT SAMPLE: 2; FIELD CORRECTED: 5; BEDDING CORRECTED: 7" @ INPUT CH
5520 FOR I=1 TO N
5530 G(I+1,J)=E(I,CH) @ G(I+1,J+1)=E(I,CH+1)
5540 NEXT I
5550 G(1,J)=N
5560 DISP "INPUT ANY MORE DATA FROM DISK?  Y/N " @ INPUT T$
5570 IF T$="Y" THEN J=J+2 @ L1=L1+1 @ GOTO 5440
5580 M=J+1 ! the last column
5590 ! ******  SUB CALCULATE POLE   DIRECTION FOR G.C. PLANE" *****
5600 DISP "CALCULATING POLE DIRECTIONS FOR GREAT CIRCLE PLANES..."
5610 K=1
5620 FOR J=1 TO M-1 STEP 2
5630 DISP "CALCULATING SAMPLE ";NAME$(K)
5640 N=G(1,J) @ II=1
5650 FOR I=2 TO N+1
```

```
5660 NC(I-1,1)=COS (G(I,J))*COS (G(I,J+1))
5670 NC(I-1,2)=SIN (G(I,J))*COS (G(I,J+1))
5680 NC(I-1,3)=SIN (G(I,J+1)) !  x,y,z components for each vector
5690 NEXT I
5700 FOR I=1 TO N-1
5710 FOR L=1 TO N-I
5720 X=NC(I,2)*NC(I+L,3)-NC(I,3)*NC(I+L,2)
5730 Y=NC(I,3)*NC(I+L,1)-NC(I,1)*NC(I+L,3)
5740 Z=NC(I,1)*NC(I+L,2)-NC(I,2)*NC(I+L,1)
5750 ND(II,1)=ATN2 (Y,X)
5760 IF ND(II,1)<0 THEN ND(II,1)=ND(II,1)+360
5770 H1=SQR (X*X+Y*Y)
5780 ND(II,2)=ATN2 (Z,H1) !  ND: pole directions for each trend
5781 GOTO 5790
5782 PRINT ND(II,1);ND(II,2)
5790 II=II+1
5800 NEXT L
5810 NEXT I
5820 N1=(N*N-N)/2
5830 ! ******  FISHER STATISTICS FOR NORMALS OF FITTING PLANES *****
5840 DISP "  CALCULATING FISHER STATS FOR NORMAL DIRECTION OF"
5850 DISP "  GREAT CIRCLE PLANES"
5860 FOR I=1 TO N1
5870 DI(I,1)=ND(I,1) @ DI(I,2)=ND(I,2)
5880 NEXT I
5890 PRINT "    FISHER MEAN OF FITTING PLANE FOR ";NAME$(K) @ SY=0
5900 N=N1 @ GOSUB 4990 @ PRINT @ PRINT @ PRINT @ CLEAR ! fisher statistics
5910 DISP "       CONTINUED AND PLEASE WAITING....."
5920 WN(K,1)=COS (MD111)*COS (MI111) ! md111 & mi111: mean pole direction
5930 WN(K,2)=SIN (MD111)*COS (MI111)
5940 WN(K,3)=SIN (MI111) ! WN: all mean pole directions for all trends
5950 K=K+1
5960 NEXT J
```

```
5970 ! *******  SUB CALCULATE INTERSECTIONS *******
5980 L=1 @ K=K-1
5990 FOR I=1 TO K-1
6000 FOR J=1 TO K-I
6010 AA=WN(I,2)*WN(I+J,3)-WN(I,3)*WN(I+J,2)
6020 BB=WN(I,3)*WN(I+J,1)-WN(I,1)*WN(I+J,3)
6030 CC=WN(I,1)*WN(I+J,2)-WN(I,2)*WN(I+J,1)
6040 DI(L,1)=ATN2 (BB,AA)
6050 IF DI(L,1)<0 THEN DI(L,1)=DI(L,1)+360
6060 H1=SQR (AA*AA+BB*BB)
6070 DI(L,2)=ATN2 (CC,H1)
6080 X11=COS (DI(L,1))*COS (DI(L,2))
6090 Y11=SIN (DI(L,1))*COS (DI(L,2))
6100 Z11=SIN (DI(L,2))
6110 Z15=X11*COS (D5)*SIN (I5)+Y11*SIN (D5)*SIN (I5)+Z11*COS (I5)
6120 IF CM=1 AND Z15>0 THEN GOTO 6160 ELSE GOTO 6130
6130 IF CM=2 AND Z15<0 THEN GOTO 6160 ELSE GOTO 6140
6140 DI(L,1)=DI(L,1)-180 @ IF DI(L,1)<0 THEN DI(L,1)=DI(L,1)+360
6150 DI(L,2)=-DI(L,2) ! DI: all intersections from all trends
6160 L=L+1
6170 NEXT J
6180 NEXT I
6190 N=L-1
```

APPENDIX 14. MAGNETIC FABRIC RESULTS FOR SAMPLES FROM WESSEX FORMATION

ISLE OF WIGHT SECTION

SAMPLE No	Kmax DEC	Kmax INC	Kmin DEC	Kmin INC	q	∑G%	Lineation L%	Foliation F%	Anis. Deg. h
CB4.1	71	-10	278	-78	0.147	-8.5	21.3	134.3	113.1
9.1	197	-18	340	-68	0.277	73.4	13.6	42.3	51.0
12.1	218	-19	353	-64	0.462	-11.2	38.6	64.4	95.0
13.1	196	-6	51	-82	0.283	14.7	9.3	28.3	35.5
43.1b	240	-6	80	-84	0.253	145.8	25.6	88.7	95.5
55.1b	204	-14	81	-65	0.705	-138.9	14.7	13.5	28.5

WORBARROW BAY SECTION

SAMPLE No	Kmax DEC	Kmax INC	Kmin DEC	Kmin INC	q	∑G%	Lineation L%	Foliation F%	Anis. Deg. h
WW2.1a	307	-3	211	-68	0.06	-43.8	6.4	109.5	86.3
4.1a	356	-14	158	-76	0.14	-138.7	15.0	98.1	88.6
5.1a	10	-8	120	-69	0.36	-89.8	26.4	60.1	77.9
81.1a	139	-4	323	-86	0.58	-38.1	25.4	31.3	55.6

MUPE BAY SECTION

SAMPLE No	Kmax DEC	Kmax INC	Kmin DEC	Kmin INC	q	∑G%	Lineation L%	Foliation F%	Anis. Deg. h
MP1.1a	43	-6	216	-84	0.33	-49.7	28.9	72.3	88.5
3.1a	126	-4	24	-71	0.75	65.5	29.4	24.1	54.5
6.1a	240	-5	100	-84	0.13	-134.1	3.7	28.2	29.6
10.1a	277	-5	21	-69	0.08	-64.5	10.4	120.6	95.6
21.1	193	-13	319	-68	0.08	-64.5	6.7	78.8	69.1
36.1a	97	-3	331	-85	0.28	-68.3	20.2	61.4	71.8
54.1	294	-13	67	-71	0.19	-135.7	10.5	50.4	53.9
67.1a	316	-21	149	-68	0.23	-105.5	18.2	69.5	75.0
82.1	302	-3	205	-65	0.16	-106.3	16.7	94.9	88.4

DURDLE DOOR SECTION

SAMPLE No	Kmax DEC	Kmax INC	Kmin DEC	Kmin INC	q	∑G%	Lineation L%	Foliation F%	Anis. Deg. h
DD9.1a	12	-1	105	-80	0.38	76.3	17.0	35.6	49.6
11.1a	120	-4	356	-82	0.74	-91.6	21.1	18.0	44.1
13.1a	178	-11	38	-76	0.45	17.1	12.7	21.8	26.6
14.1a	157	-4	53	-75	0.53	-106.3	23.6	32.7	43.3
17.1a	152	-7	39	-72	0.60	4.5	12.0	13.8	24.3

APPENDIX 15. MAGNETIC FABRIC RESULTS FOR SAMPLES FROM THE WEALD CLAY FORMATION

BEARE GREEN SECTION

SAMPLE No	Kmax DEC	Kmax INC	Kmin DEC	Kmin INC	q	∑G%	Lineation L%	Foliation F%	Anis. Deg. h
SH1.2	354	-3	117	-84	0.07	65.7	0.5	8.1	8.5
3.1	195	-1	304	-86	0.12	56.3	1.3	10.2	11.3
6.2	206	-1	109	-81	0.14	62.2	1.2	7.4	8.4
7.1	215	-5	344	-82	0.15	46.7	1.7	10.6	12.0
8.2	333	-2	228	-80	0.07	18.2	1.0	13.9	14.4
10.1	37	-2	212	-88	0.10	63.7	1.0	9.9	10.6
11.1	265	-7	127	-80	0.11	16.3	0.9	7.6	8.4
12.1	284	-0	61	-89	0.12	51.6	0.6	4.8	5.4
13.2	236	-7	82	-82	0.08	42.3	0.6	7.9	8.4
14.1	313	-10	79	-73	0.09	10.3	0.4	4.2	4.7
15.1	201	-5	68	-82	0.24	43.3	1.1	4.2	5.4
16.1	300	-6	143	-84	0.17	59.1	1.0	5.2	6.2
16.2	137	-0	46	-82	0.14	30.2	0.9	6.2	7.1
17.1	276	-12	99	-78	0.12	55.9	1.0	8.0	8.9

BLOCK SAMPLE

SAMPLE No	Kmax DEC	Kmax INC	Kmin DEC	Kmin INC	q	∑G%	Lineation L%	Foliation F%	Anis. Deg. h
B2.2	209	-13	10	-76	0.14	-25.2	1.8	12.2	13.6
2.4	212	-3	309	-69	0.06	35.9	0.7	12.7	13.0
3.2	225	-8	26	-82	0.06	11.2	0.6	10.9	11.2
3.3	192	-10	331	-76	0.08	1.9	1.0	12.4	13.0
3.6	234	-12	64	-78	0.07	-4.0	0.9	12.6	13.1
4.1	226	-10	28	-79	0.08	24.2	0.8	10.6	11.2

LANGHURST SECTIONS

SAMPLE No	Kmax DEC	Kmax INC	Kmin DEC	Kmin INC	q	∑G%	Lineation L%	Foliation F%	Anis. Deg. h
northwest section									
LG1.2a	31	-3	130	-73	0.144	-12.9	0.8	5.1	5.9
2.1a	141	-1	41	-85	0.14	-4.9	0.5	3.5	4.0
2.2a	185	-5	27	-84	0.09	8.5	0.6	5.8	6.3
3.1a	86	-17	283	-72	0.25	-42.4	0.2	0.7	0.9
3.2a	342	-2	122	-87	0.12	33.9	0.4	3.6	4.0
4.1a	160	-1	61	-83	0.08	24.8	0.5	5.7	6.2
4.2a	19	-4	133	-81	0.17	35.7	0.8	4.4	5.2
5.1a	152	-1	59	-76	0.15	22.7	0.8	5.3	6.1
5.2	56	-2	314	-82	0.06	38.9	0.4	6.4	6.8
7.1	140	-12	19	-67	0.10	-29.1	0.5	5.3	5.8
7.2a	222	-5	114	-75	0.23	13.8	1.1	4.4	5.5
8.2a	190	-10	33	-79	0.07	-11.5	0.2	3.9	4.1
9.1	190	-10	27	-80	0.13	21.5	0.7	5.5	6.2
10.1a	322	-5	75	-77	0.16	-10.2	0.2	1.3	1.6
10.2a	277	-8	50	-78	0.17	24.9	0.1	0.9	1.1
11.2	190	-7	317	-78	0.07	4.1	0.7	10.0	10.4
13.1a	189	-3	301	-83	0.12	53.9	0.4	3.3	3.7
14.1a	10	-2	260	-84	0.08	7.6	0.3	4.5	4.3
15.1	141	-8	28	-72	0.06	-4.1	0.2	4.1	4.4
15.2a	125	-0	32	-84	0.09	42.0	0.3	3.4	3.7
16.2a	166	-4	53	-79	0.07	-5.3	0.2	2.7	2.9
17.2a	360	-4	104	-76	0.09	4.7	0.3	3.4	3.7
18.2a	148	-5	16	-83	0.39	20.9	0.7	1.4	2.1
19.1	227	-4	351	-84	0.07	-40.9	0.2	2.6	2.8
19.2	228	-27	84	-58	0.09	-7.8	0.2	2.5	2.7
southeast section									
20.2a	127	-5	278	-85	0.09	56.7	0.7	8.1	8.6
21.1	94	-2	227	-87	0.14	29.0	1.1	7.3	8.3
22.1a	98	-10	239	-77	0.08	20.8	0.8	9.7	10.3
22.2a	283	-3	169	-82	0.14	37.6	1.6	10.7	12.1
23.2	171	-4	309	-84	0.06	46.1	0.7	10.9	11.2
24.1	125	-7	349	-81	0.18	55.6	1.4	7.2	8.5
25.1a	90	-15	222	-68	0.14	11.5	0.8	5.0	5.9
25.2a	98	-7	221	-76	0.13	0.0	0.7	5.4	6.1
26.1	279	-3	21	-76	0.11	59.2	0.3	2.7	3.0
26.2a	123	-4	9	-80	0.06	52.1	0.2	3.1	3.3
28.2a	305	-4	57	-79	0.25	-15.8	1.3	4.7	6.0
30.1	255	-4	123	-84	0.09	-14.2	0.7	7.2	7.8
31.1a	45	-5	176	-83	0.09	-34.9	0.5	5.5	6.0
31.2a	202	-3	333	-85	0.14	5.8	0.5	3.5	4.1
33.1a	105	-6	233	-80	0.12	18.5	0.6	5.4	6.0
33.2a	101	-1	197	-79	0.08	-17.6	0.5	6.0	6.2
34.2a	72	-6	180	-71	0.17	-55.5	1.3	7.1	8.4
35.1a	60	-8	240	-82	0.13	57.4	0.3	2.1	2.4
35.2a	67	-11	186	-68	0.19	7.3	0.4	2.1	2.6

APPENDIX 16. MAGNETIC FABRIC RESULTS FOR SAMPLES FROM BOOM CLAY FORMATION

KRUIBEKE SECTION

SAMPLE No	Kmax DEC	Kmax INC	Kmin DEC	Kmin INC	q	∑G%	Lineation L%	Foliation F%	Anis. Deg. h
KB1.1b	174	-1	274	-83	0.09	9.3	0.19	2.11	2.3
2.1b	357	-3	239	-84	0.14	50.2	0.26	1.68	1.9
3.1a	13	-1	122	-86	0.173	33.4	0.60	3.21	3.8
3.1b	181	-3	18	-87	0.14	20.7	0.53	3.63	4.1
4.1a	346	-4	124	-85	0.15	29.5	0.34	2.02	2.3
5.1b	1	-3	243	-84	0.22	44.6	0.44	1.80	2.2
6.1b	190	-3	2	-87	0.27	30.4	0.73	2.30	3.0
7.1a	17	-10	196	-80	0.19	53.2	0.75	3.50	4.2
7.1b	45	-5	217	-85	0.24	46.7	0.81	2.99	3.8
8.1b	6	-5	150	-84	0.16	59.3	0.93	5.22	6.1
10.b	10	-3	142	-86	0.11	51.7	0.42	3.53	3.9
11.1b	15	-17	160	-70	0.27	24.3	0.89	2.82	3.7
14.1a	1	-5	255	-83	0.19	60.0	0.80	3.68	4.4
14.1b	178	-1	280	-84	0.11	43.9	0.46	3.94	4.4
16.1a	169	-3	273	-79	0.14	57.2	0.67	4.40	5.0
16.1b	7	-8	165	-81	0.15	49.5	0.67	3.94	4.6
17.1a	14	-7	138	-78	0.14	42.1	0.71	4.64	5.3
17.1b	14	-8	177	-82	0.14	41.9	0.58	3.82	4.4
18.1a	7	-2	120	-85	0.09	28.1	0.46	5.05	5.4
19.1a	11	-7	125	-74	0.22	41.8	1.16	4.71	5.8
19.1b	195	-0	102	-83	0.27	29.0	1.66	5.20	6.8
20.1b	10	-3	187	-87	0.11	37.9	0.51	4.36	4.8
21.1b	35	-4	266	-83	0.21	51.2	0.99	4.13	5.1
22.1a	2.	-7	121	-77	0.12	40.1	0.46	5.07	5.6
23.1a	220	-6	327	-70	0.46	21.3	1.81	3.02	4.8
23.1b	160	-19	335	-71	0.154	53.4	0.64	3.85	4.4
24.1b	358	-10	171	-80	0.19	53.3	0.55	2.57	3.1
26.1	249	-2	41	-81	0.18	38.3	0.45	2.16	2.6
28.1	201	-2	93	-84	0.14	38.2	0.58	3.80	4.3
29.1b	212	-2	340	-86	0.27	41.6	1.06	3.30	4.3